

---

## CONTENTS

---

<i>Chapter 1 Magnetic Circuits .....</i>	1
1.1 Introduction.....	1
1.2 Ampere's Law of Force.....	1
1.3 The Magnetic Field $B$ .....	3
1.4 The Electric Field.....	4
1.5 The Vector Potential $A$ .....	5
1.6 Concept of Magnetic Flux .....	6
1.7 Ampere's Law .....	8
1.8 Magnetic Field Intensity .....	10
1.9 Boundary Conditions for $B$ and $H$ .....	15
1.10 Faraday's Law.....	18
1.11 Induced Electric Field Due to Motion .....	19
1.12 Permeance, Reluctance and the Magnetic Circuit .....	20
1.13 Example 1.1 .....	25
1.14 Multiple Circuit Paths.....	26
1.15 General Expression for Reluctance.....	27
1.16 Inductance .....	30
1.17 Magnetic Field Energy.....	31
1.18 The Problem of Units.....	34
1.19 Magnetic Paths Wholly in Iron .....	37
1.20 Magnetic Materials .....	40
1.21 Example 1.2 .....	41
1.22 Magnetic Circuits with Air Gaps .....	45
1.23 Example 1.3 .....	47
1.24 Example 1.4 Calculation for Series-Parallel Iron Paths.....	49
1.25 Multiple Winding Magnetic Circuits .....	50
1.26 Magnetic Circuits Applied to Electrical Machines.....	52
1.27 Effect of Excitation Coil Placement .....	54

---

---

## CONTENTS

---

<i>Chapter 2 The MMF and Field Distribution of an AC Winding</i>	59
2.1     MMF and Field Distribution of a Full Pitch Winding.....	59
2.2     Fractional Pitch Winding for Two Pole Machine .....	62
2.3     Distributed Windings .....	65
2.4     Concentric Windings.....	73
2.5     Effect of Slot Openings.....	79
2.6     Fractional Slot Windings .....	80
2.7     Winding Skew .....	84
2.8     Pole Pairs and Circuits Greater than One .....	88
2.8 <i>MMF Distribution for Three Phase Windings</i> .....	88
2.10    Concept of an Equivalent Two Phase Machine.....	92
2.11    References.....	93

<i>Chapter 3 Main Flux Path Calculations Using Magnetic Circuits</i> .....	95
3.1     The Main Magnetic Circuit of an Induction Machine .....	95
3.2     The Effective Gap and Carter's Coefficient .....	97
3.3     The Effective Length.....	101
3.4     Calculation of Tooth and Slot Reluctance .....	105
3.5     Example #1 - Tooth <i>MMF</i> Drop .....	109
3.6     Calculation of Core Reluctance .....	116
3.7     Example #2 - <i>MMF</i> Drop Over Main Magnetic Circuit .....	125
3.8     Magnetic Equivalent Circuit .....	137
3.9     Flux Distribution in Highly Saturated Machines .....	139
3.10    Calculation of Magnetizing Reactance .....	144
3.11    Example #3 - Calculation of Magnetizing Inductance .....	149
3.12    References.....	153

---

## CONTENTS

---

<i>Chapter 4 Use of Magnetic Circuits in Leakage Reactance Calculations</i>	155
4.1 Components of Leakage Flux in Induction Machines .....	155
4.2 Specific Permeance .....	157
4.3 Slot Leakage Permeance Calculations .....	160
4.4 Slot Leakage Inductance of a Single Layer Stator Winding.....	167
4.5 Slot Leakage of Two Layer Windings.....	169
4.6 Slot Leakage Inductances of a Double Cage Rotor Winding .....	172
4.7 Slot Leakage Inductance of a Double Layer Stator Winding .....	174
4.8 End-Winding Leakage Inductance .....	180
4.9 Stator Harmonic or Belt Leakage .....	188
4.10 Zigzag Leakage Inductance .....	192
4.11 Example #4 - Calculation of Leakage Inductances .....	199
4.12 Effective Resistance and Inductance per Phase of Squirrel Cage Rotor .....	207
4.13 Fundamental Component of Rotor Air Gap MMF .....	212
4.14 Rotor Harmonic Leakage Inductance .....	215
4.15 Calculation of Mutual Inductances .....	219
4.16 Example #5 - Calculation of Rotor Leakage Inductance per Phase..	227
4.17 Skew Leakage Inductance.....	228
4.18 Example #6 - Calculation of Skew Leakage Effects.....	231
4.19 References.....	233
<i>Chapter 5 Calculation of Induction Machine Losses</i> .....	215
5.1 Introduction.....	215
5.2 Eddy Current Effects in Conductors .....	216
5.3 Calculation of Stator Resistance .....	227
5.4 Example #7 - Calculation of Stator and Rotor Resistance.....	230
5.5 Rotor Parameters of Irregularly Shaped Bars .....	240

---

---

## CONTENTS

---

5.6	Core Losses Due To Fundamental Flux Component .....	244
5.7	Stray Load and No Load Losses .....	247
5.8	Calculation of Surface Iron Losses Due to Stator Slotting .....	254
5.9	Calculation of Tooth Pulsation Iron Losses .....	268
5.11	Friction and Windage Losses .....	277
5.12	Example #8 - Calculation of Iron Loss Resistances .....	278
<i>Chapter 6 Principles of Design</i> .....		315
6.1	Introduction.....	315
6.2	Design Factors .....	315
6.3	Standards for Machine Construction .....	317
6.4	Main Design Features .....	321
6.5	The $D_{is}^2 L$ Output Coefficient .....	332
6.6	The $D_{os}^2 L$ Output Coefficient.....	331
6.7	Power Loss Density .....	343
6.8	The $D_{os}^{2.5} L$ Sizing Equation .....	344
6.9	Choice of Magnetic Loading .....	345
6.9.1	Maximum Flux Density in Iron.....	345
6.9.2	Magnetizing Current.....	347
6.10	Choice of Electric Loading .....	348
6.10.1	Voltage Rating .....	348
6.10.3	Performance Under Stalled Conditions .....	350
6.11	Practical Considerations Concerning Stator Construction.....	355
6.11.1	Random Wound vs. Formed Coil Windings.....	356
6.11.2	Delta vs. Wye Connection .....	357
6.11.3	Lamination Insulation.....	358
6.11.4	Selection of Stator Slot Number.....	358
6.11.5	Choice of Dimensions of Active Material for NEMA Designs.....	359
6.11.6	Selection of Wire Size .....	360
6.10.7	Selection of Air Gap.....	362
6.11	Rotor Construction.....	363

---

## CONTENTS

---

6.11.1	Slot Combinations to Avoid .....	364
6.11.2	Rotor Heating During Starting or Under Stalled Conditions.....	365
6.12	Effect of Machine Performance by a Change in Dimension .....	366
6.13	References.....	370

## LIST OF SYMBOLS

Symbol	Meaning	Page Number First Used
		A
$a$	unit vector .....	4
$A$	magnetic potential (vector) .....	6
		B
$B$	magnetic flux density (vector) .....	3
$b_{1/3}$	breadth of slot 1/3 of the way from narrow portion .....	101
$B_{gl}$	peak fundamental air gap flux density .....	117
$B_m$	flux density midway down the tooth .....	
$B_{mr}$	flux density at the mid point of the rotor tooth .....	131
$b_o$	slot opening .....	97
$b_{or}$	rotor slot opening .....	126
$B_r$	flux density at the root of a tooth .....	107
$B_{rr}$	flux density at the root of the rotor tooth .....	131
$B_s$	flux density in the slot .....	105
$B_{tr}$	flux density at the top of the rotor tooth .....	131
$B_g$	flux density in the gap.....	62
$B_t$	flux density at the top of the tooth.....	107
		C
$C$	contour bound surface S .....	7
$C$	number of parallel circuits .....	88
$C_{tr}$	loss coefficient .....	287
$C_p$	heat capacity of conductor .....	351
$\cos\phi_{gap}$	power factor as measured from the gap (neglecting stator iron and copper losses) .....	325
		D
$D_{is}$	inner diameter of stator core .....	124
$D_{os}$	outer diameter of stator core .....	331
$D_{or}$	outer diameter of the rotor punching .....	124

## LIST OF SYMBOLS

<b>Symbol</b>	<b>Meaning</b>	<b>Page Number First Used</b>
$d_{cr}$	depth of rotor core .....	119
$d_{cs}$	depth of stator core .....	119
$d_e$	penetration constant .....	286
$d_s$	slot depth .....	101
$d_{sr}$	depth of rotor slot .....	124
$d_{ss}$	depth of one stator slot .....	124
<b>E</b>		
$E$	electric field intensity.....	4
$e_b$	induced voltage in a rotor bar .....	209
<b>F</b>		
$F$	magnetomotive force (MMF) .....	23
$\mathcal{F}_{cr}$	rotor core <i>MMF</i> drop .....	96
$\mathcal{F}_{cs}$	stator core <i>MMF</i> drop .....	96
$\mathcal{F}_g$	air gap <i>MMF</i> drop .....	96
$\mathcal{F}_p$	<i>MMF</i> per pole .....	62
$\mathcal{F}_{p1}$	peak <i>MMF</i> drop for one pole .....	96
$\mathcal{F}_{ph}$	<i>MMF</i> drop per pole for harmonic $h$ .....	63
$\mathcal{F}_{t(ave)}$	<i>MMF</i> drop over the entire length of a tooth .....	108
$\mathcal{F}_{tr}$	rotor tooth <i>MMF</i> drop .....	96
$\mathcal{F}_{ts}$	stator tooth <i>MMF</i> drop .....	96
$F$	Force .....	1
<b>G</b>		
$g_e$	equivalent gap including effect of flux fringing .....	99
$g$	mechanical gap .....	60
$g_e'$	equivalent gap including effect of fringing and saturation	148

## LIST OF SYMBOLS

Symbol	Meaning	Page Number First Used
<b>H</b>		
$h$	harmonic index .....	63
$H$	magnetic field intensity.....	14
$H_m$	field intensity at the mid point of a tooth .....	108
$H_{mr}$	field intensity at the mid point of one rotor tooth .....	132
$H_r$	field intensity at the narrowest section of tooth .....	108
$H_{rr}$	field intensity at the root of one rotor tooth .....	132
$H_t$	field intensity at the widest section of a tooth .....	108
$H_{t(ave)}$	average field intensity over the entire length of a tooth .	108
$H_{tr}$	field intensity at the top of one rotor tooth .....	132
$H_{tr(ave)}$	average value of field intensity over one rotor tooth .....	132
<b>I</b>		
$i_a, i_b, i_c$	instantaneous current in phases a, b, and c .....	91
$i_b$	current in a rotor bar .....	209
$i_e$	current in an end ring segment .....	209
$I_m$	peak ac current .....	91
$I_{mr}$	peak ac rotor bar current.....	220
$I_{ms}$	peak ac stator current .....	222
$I_s$	rms stator current .....	224
$I_1$	rms stator current per phase .....	273
<b>J</b>		
$J$	current density .....	3
$J_{ms}$	surface polarization current .....	13
$J_m$	volumetric polarization current.....	13
$J_s$	surface current density .....	16
<b>K</b>		
$k_c$	Carter factor .....	99

## LIST OF SYMBOLS

Symbol	Meaning	Page Number First Used
$k_{cu}$	copper space factor .....	337
$k_{dh}$	distribution factor for $h^{th}$ harmonic .....	70
$k_{hys}$	Steinmetz coefficient .....	269
$k_i$	lamination space factor .....	106
$k_h$	winding factor for $h^{th}$ harmonic .....	87
$K_p$	factor to include the effect of slot leakage flux on saturation of the core .....	120
$K_{pfr}$	pole face loss factor .....	289
$k_{ph}$	pitch factor for $h^{th}$ harmonic .....	64
$k_{sh}$	skew factor for $h^{th}$ harmonic .....	87
$k_{\chi h}$	slot opening factor factor for the $h^{th}$ harmonic .....	80
$K_{s(rms)}$	RMS surface current density .....	325

### L

$l_s$	stator physical length including ducts .....	61
$l_e$	stator equivalent length including effect of fringing due to ducts .....	103
$l_{is}$	length of the stator iron not including ducts .....	103
$L$	inductance .....	30
$L_{ST}$	slot leakage inductance of coil side in top of slot .....	178
$L_{ITB}$	mutual inductance between slot leakage components of top and bottom coil .....	178
$L_{IB}$	slot leakage inductance of coil side in bottom of slot.....	178
$L_{sl}$	slot leakage inductance including effects of mutual coupling between bottom and top coil sides .....	180
$L_{slm}$	mutual component of slot leakage .....	178
$L_b$	inductance of one rotor bar .....	209
$L_{be}$	equivalent value of bar inductance including the effect of end ring inductance. ....	212
$l_{cs}$	length of the path of one pole pitch as measured	

## LIST OF SYMBOLS

Symbol	Meaning	Page Number First Used
	at the midpoint of the stator core .....	141
$l_e$	effective axial length of stator or rotor (including fringing) .....	103
$L_e$	end winding leakage inductance .....	181
$L_e'$	inductance of one end ring segment .....	209
$l_e$	axial length (general) .....	97
$l_{ew}$	length of end winding corresponding to end winding leakage inductance .....	181
$L_{h/phase}$	harmonic leakage inductance of the rotor per phase .....	219
$l_i$	physical axial length of the stator iron (not including air ducts and fringing) .....	178
$L_{lk}$	leakage inductance arising from belt leakage .....	190
$L_{lr}'$	rotor leakage inductance referred to the stator turns and phases .....	259
$L_{lz}$	zig zag leakage inductance per phase .....	196
$l_o$	axial length of one air duct .....	104
$L_{phase}$	slot leakage inductance of one phase .....	168
$L_{slot}$	slot leakage inductance of a single slot .....	167
$L_{sts}$	self component of slot leakage .....	178
$L_{zz/s}$	zig zag leakage inductance per phase .....	196

### M

$m$	magnetic dipole moment .....	11
$MMF$	magnetomotive force .....	23
$M$	magnetic polarization vector.....	12

### N

$N$	number of turns .....	20
$N_1$	total number of turns of one phase.....	59
$N_s$	number of series connected turns for one phase .....	148

## LIST OF SYMBOLS

Symbol	Meaning	Page Number First Used
<b>O</b>		
$\mathcal{O}$	contour bounding surface $S$ .....	1
<b>P</b>		
$P$	number of poles .....	72
$p_e$	eddy current power loss per unit volume .....	268
$P_h$	hysteresis loss per unit volume .....	269
$p_i$	eddy current plus hysteresis loss per unit volume .....	269
$P_{r(surf)}$	surface power loss .....	288
$\mathcal{P}$	permeance .....	24
$p$	specific permeance .....	159
$P_{ew}$	specific permeance corresponding to end winding leakage inductance .....	181
<b>Q</b>		
$q$	number of coils in a phase belt (slots/pole/phase) .....	65
<b>R</b>		
$R$	distance between two points .....	4
$r_{is}$	radius of inner stator surface .....	4
$\mathcal{R}$	reluctance .....	24
$R_{be}$	equivalent value of bar resistance including the effect of end ring resistance .....	212
$R_e$	resistance of one rotor end ring segment .....	209
$R_b$	resistance of one rotor bar .....	261
$r_p$	resistance of the $p^{th}$ layer of a rotor bar .....	261
$\mathcal{R}_t$	reluctance of one tooth .....	108
$r_{sl}$	resistance of the slot portion of conductor.....	343

## LIST OF SYMBOLS

Symbol	Meaning	Page Number First Used
	<b>S</b>	
$S_1, (S_2)$	total number of stator (rotor) slots .....	72
$S$	surface area .....	7
	<b>T</b>	
$t_e$	air space between adjacent coils in the end winding region .....	182
$t_m$	rotor tooth width at the midpoint of the tooth .....	131
$t_o$	tooth thickness .....	98
$t_t$	tooth width at the tooth top .....	126
$t_r$	tooth width at the tooth bottom (tooth root) .....	126
	<b>V</b>	
$V$	volume .....	4
$V_{gap}$	voltage at the gap as viewed by one rotor bar .....	263
$V_m$	air gap voltage across the magnetizing inductance .....	152
	<b>W</b>	
$W_m$	magnetic field energy.....	31
$W$	equivalent span of a distributed winding .....	70
$W_{ave}$	average energy stored in stator rotor tooth region .....	196
	<b>X</b>	
$X_1$	total stator leakage reactance .....	120
$X_m$	magnetizing reactance per phase .....	120
	<b>Z</b>	
$Z$	arc length occupied by the $q$ coils in a phase belt .....	69

## LIST OF SYMBOLS

Symbol	Meaning	Page Number First Used
Greek Symbols		
$\alpha$	inverse of the skin depth .....	244
$\alpha$	skew angle .....	86
$\gamma$	pitch angle .....	62
$\nabla$	gradient vector .....	4
$\nabla^2$	laplacian .....	9
$\nabla \times$	curl operator.....	4
$\nabla \cdot$	divergence operator.....	6
$\epsilon_0$	permittivity of free space .....	4
$\epsilon$	permittivity.....	4
$\Phi$	magnetic flux .....	7
$\Phi_c$	magnetic flux in the core .....	119
$\Phi_g$	flux crossing the air gap .....	120
$\Phi_{tr}$	flux in one rotor tooth .....	132
$\Phi_{cs}$	flux in the stator core .....	120
$\eta_{gap}$	efficiency as measured at the gap (not including stator copper and iron losses.....	325
$\lambda_{ms}$	total air gap flux linkages of one phase .....	147
$\lambda_p$	flux linkages per pole.....	147
$\mu$	permeability .....	14
$\mu_0$	permeability of free space .....	3
$\theta$	angular position along the air gap .....	60
$\omega_e$	stator applied angular frequency .....	91
$\omega_{rm}$	mechanical angular speed in radians per second .....	211
$\rho$	charge density .....	4
$\sigma$	conductivity .....	19
$\tau_p$	pole pitch .....	64
$\tau_r$	rotor slot pitch .....	125
$\tau_s$	stator slot pitch .....	97

# Chapter 1

## Magnetic Circuits

### 1.1 Introduction

Our knowledge of magnetic phenomena is literally as old as science itself. According to the Greek philosopher Aristotle, the attractive power of magnets was known even at that time. However, it was not until the sixteenth century that experimental work on magnetism began in earnest. Notable among scientists active at that time were the work of Gilbert who discovered the earth's magnetism, Volta who developed the voltaic cell and Oersted who related the magnetic field to the flow of current. However, it is the work of Biot and Savart, Ampere and finally Faraday upon which the modern theory of magnetism is based. In their experiments, the force on a current carrying wire due to the flow of current in another wire was carefully measured and forms the experimental basis for the entire theory of magnetism.

### 1.2 Ampere's Law of Force

Using modern notation, the experiments of these pioneers can be expressed compactly in a single vector equation. With reference to Fig. 1.1, let  $O_1$  and  $O_2$  be two very thin closed conducting current loops in which steady (DC) currents flow. The coordinates along the loop  $O_1$  can be designated by  $x_1, y_1, z_1$  and the coordinates along the second loop  $O_2$  as  $x_2, y_2, z_2$ . The arc length along the loop  $O_1$  and  $O_2$  are denoted as vector quantities  $dl_1$  and  $dl_2$  respectively. From the experiments of Biot, Savart and Ampere, the differential force exerted on small piece of loop 2 carrying current  $I_2$  due to the current  $I_1$  in a small piece of loop 1 can be expressed as

$$d\mathbf{F}_{21} = \left(\frac{\mu_0}{4\pi}\right) \frac{I_2 dl_2 \times [I_1 dl_1 \times \mathbf{a}_{r12}]}{R^2} \quad (1.1)$$

where

$$R = \sqrt{(x_2 - x_1)^2 + (y_2 - y_1)^2 + (z_2 - z_1)^2}$$

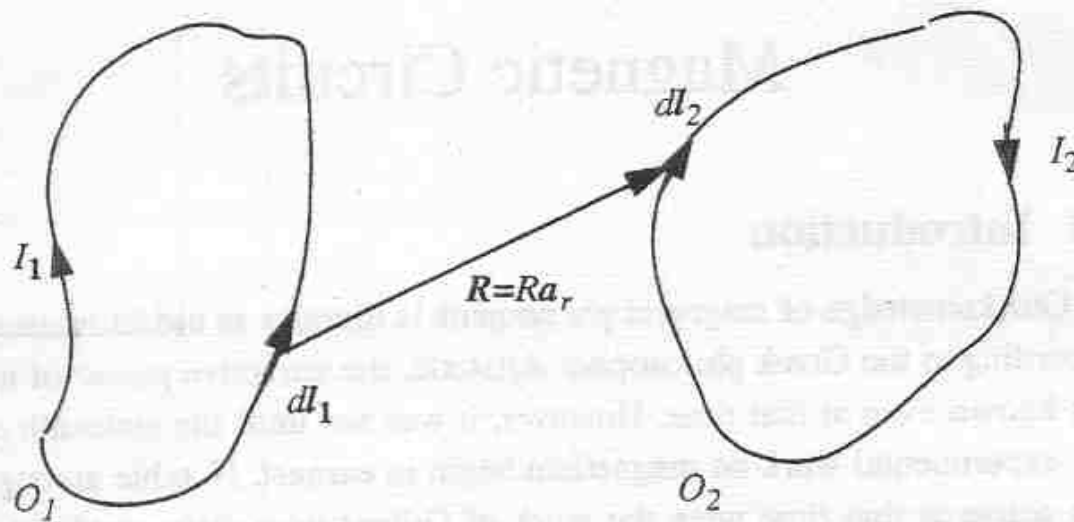


Figure 1.1 Illustration of Biot-Savart's law

and  $\alpha_{r12}$  is a unit vector pointing from  $dl_1$  to  $dl_2$ . Essentially this force acts to align the two differential elements (i.e. make  $dl_1$  and  $dl_2$  co-linear). This expression can be integrated around coil 2 to find the total force exerted on coil 2 due to the differential current element in coil 1 as

$$dF_{21} = \frac{\mu_0}{4\pi} \oint_{O_1} \oint \frac{I_2 dl_2 \times (I_1 dl_1 \times \alpha_{r12})}{R^2} \quad (1.2)$$

To find the total force on wire 2 we can integrate a second time to form what is called Biot-Savart's Law or, alternatively, Ampere's Law of Force,

$$F_{21} = \frac{\mu_0}{4\pi} \oint_{O_2 O_1} \oint \frac{I_2 dl_2 \times (I_1 dl_1 \times \alpha_{r12})}{R^2} \quad (1.3)$$

When the force  $F_{21}$  is measured in newtons and the currents are in amperes with the tests made in a vacuum the proportionality constant  $\mu_0$  is equal to  $4\pi \cdot 10^{-7}$  newtons per ampere squared (eventually defined as henries per meter).

Thus the proportionality constant  $\mu_0$ , is called the *permeability of free space*, and ultimately has the units of inductance per unit length. It can be shown that reciprocity holds, that is  $F_{12} = -F_{21}$

### 1.3 The Magnetic Field $B$

One of the great philosophical contributions of mathematics to science was the use of so-called “fields” to explain action at a distance, a concept justly troubling to these early researchers. Upon examination of Eq. (1.3), we can define the magnetic field  $B$  acting at a point on circuit 2 as

$$\mathbf{B}_{21} = \frac{\mu_0}{4\pi} \oint_{O_1} \frac{I_1 d\mathbf{l}_1 \times \mathbf{a}_{r12}}{R^2} \quad (1.4)$$

whereupon, the force equation, Eq. 1.3, becomes the much simpler “*BII*” form,

$$\mathbf{F}_{21} = \oint_{O_2} I_2 d\mathbf{l}_2 \times \mathbf{B}_{21} \quad (1.5)$$

In contrast to Eq. (1.3), this formulation evaluates the force on a current loop in terms of the interaction of this current with a *magnetic field B*. Note that there is now no restriction on the value of  $\mathbf{a}_{r12}$  and  $R$  in Eq. (1.4). That is, these quantities need not be concerned with the distance between two current elements on the two circuits. Hence,  $B$  is well defined everywhere in space and thereby constitutes what is called a *vector field*.

One of the advantages of the field formulation is that when  $B$  is known, the relation permits one to evaluate what would be the force exerted on a current carrying conductor placed anywhere in the  $B$  field without consideration as to what are the system of currents actually giving rise to this field.

An alternative expression for  $B$  can be obtained if the current loops cannot be considered to have negligibly small cross-sectional areas, that is

$$\mathbf{B}_{21} = \frac{\mu_0}{4\pi} \int_V \frac{\mathbf{J} \times \mathbf{a}_{r12}}{R^2} dV \quad (1.6)$$

where  $\mathbf{J}$  is the vector current density in amperes/meter<sup>2</sup>.

## 1.4 The Electric Field

In a manner similar to the magnetic field discussion above, the force impressed on one electric charge by another located some distance away can be described by a *electric field* acting directly on the charge. In integral form, assuming a continuous swarm of charges the field is expressed as

$$\mathbf{E}_{21} = \frac{1}{4\pi\epsilon} \int_V \frac{\mathbf{a}_{R12}\rho(V)}{R^2} dV \quad (1.7)$$

where  $\rho$  is the charge density in coulombs/meter<sup>3</sup>,  $R$  is the distance from the differential charge  $\rho dV$  to the point at which  $E$  is evaluated,  $\mathbf{a}_R$  is the corresponding unit vector,  $\epsilon = \epsilon_r\epsilon_0$  is the permittivity of the material and  $\epsilon_r$  is the relative permittivity. The unit vector  $\mathbf{a}_{R12}$  again points from the location of the charge, point 1, to the point at which  $E$  is to be evaluated, point 2. The electric field is usually given in units of volts per meter whereupon,  $\epsilon_0 = (1/36\pi)*10^{-9}$  coulombs per volt meter (farad per meter). Finally, when the electric field exists inside a conducting material the presence of the field establishes a current according to Ohm's Law, i.e.

$$\mathbf{J} = \sigma \mathbf{E} \quad (1.8)$$

It can be easily shown that the following result is an identity

$$\frac{\mathbf{a}_{r12}}{R^2} = -\nabla\left(\frac{1}{R}\right) \quad (1.9)$$

where  $\nabla$  is the gradient operator defined by

$$\nabla = \frac{\partial}{\partial x} \mathbf{a}_x + \frac{\partial}{\partial y} \mathbf{a}_y + \frac{\partial}{\partial z} \mathbf{a}_z$$

From the form of the definition of  $E$ , Eq. (1.7), and by using Eq. (1.9) and the vector identity  $\nabla \times \nabla(1/R) = 0$  it can be readily shown that

$$\nabla \times \mathbf{E} = 0 \quad (1.10)$$

if  $\rho$  is not time dependant.

From Stoke's Theorem Eq. (1.10) has the property that

$$\int_S (\nabla \times \mathbf{E}) \cdot d\mathbf{S} = \oint_O \mathbf{E} \cdot d\mathbf{l} = 0 \quad (1.11)$$

where  $O$  bounds the surface area  $S$ . Equation (1.11) essentially implies that the line integral of  $\mathbf{E}$  between any two points is independent of path resulting in the electrical field being conservative. That is, no energy is lost or gained in moving a charged particle around a closed path in an electromagnetic field produced by static (non-moving charges) or by steady currents. In a practical sense this statement implies that if a conductor is placed in a steady field, no current will flow in the conductor in the steady state.

## 1.5 The Magnetic Vector Potential $A$

The expression for magnetic field can be further simplified by introducing the concept of the magnetic vector potential. Using Eq. (1.9), Eq. (1.6) can be written as

$$\mathbf{B}_{21} = \frac{\mu_0}{4\pi} \int_V \mathbf{J} \times \nabla \left( \frac{1}{R} \right) dV \quad (1.12)$$

The vector differential operator affects only the variables at the point at which  $\mathbf{B}_{21}$  is evaluated while the integral is taken over the region for which the current density  $\mathbf{J}$  is defined. However, if  $f$  is a scalar function of  $x$ ,  $y$  and  $z$ , from the vector identity

$$\nabla \times (f\mathbf{v}) = f\nabla \times \mathbf{v} + \nabla f \times \mathbf{v} \quad (1.13)$$

then

$$\nabla \times \left( \frac{\mathbf{J}}{R} \right) = \left( \frac{1}{R} \right) \nabla \times \mathbf{J} + \nabla \left( \frac{1}{R} \right) \times \mathbf{J} \quad (1.14)$$

The first term on the right hand side of Eq. (1.14) is clearly zero by virtue of Eq. (1.10) (assuming that the current distribution is not time dependent as we have assumed or if the frequency is sufficiently low as is typically the case with electrical machines). Thus Eq. (1.12) becomes

$$\mathbf{B}_{21} = \nabla \times \frac{\mu_0}{4\pi} \int_V \mathbf{J} dV \quad (1.15)$$

The curl operation can be brought outside of the integral since the two operations are independent, i.e. the integral is taken over the volume containing  $\mathbf{J}$  while the differential operator operates at the point defining  $\mathbf{B}_{12}$ . The field  $\mathbf{B}_{12}$  has now been defined by the curl of a function we can designate as  $A$ ,

$$\mathbf{B} = \nabla \times A \quad (1.16)$$

which can be formally defined as

$$A = \frac{\mu_0}{4\pi} \int_V \mathbf{J} dV \quad (1.17)$$

The subscript "12" on  $\mathbf{B}$  has now been dropped for simplicity. The quantity  $A$  is called the *magnetic vector potential* and must be formally evaluated by decomposing the integrand into components along the three coordinates. That is, for the  $x$  component of  $A$ ,

$$A_x = \frac{\mu_0}{4\pi} \int_V J_x dV \quad (1.18)$$

and so forth for  $A_y$  and  $A_z$ . Note that the vector potential in the  $x$  direction is caused only by the current distribution in the  $x$  direction. Hence, the problem of computing the magnetic field  $\mathbf{B}$  has been reduced to solving three decoupled scalar integrals.

## 1.6 Concept of Magnetic Flux

It has been determined that the magnetic field  $\mathbf{B}$  can be expressed in terms of the curl of an auxiliary vector potential function  $A$ . However, the divergence of the curl of any function is always zero, that is

$$\nabla \cdot (\nabla \times A) = 0$$

in which case it is evident that the divergence of  $\mathbf{B}$  must be identically zero.

$$\nabla \cdot \mathbf{B} = 0 \quad (1.19)$$

If Eq. (1.19) is integrated over a volume we have,

$$\int_V \nabla \cdot \mathbf{B} dV = 0 \quad (1.20)$$

Whereupon, from 'Gauss' Theorem we have the result that

$$\int_V \nabla \cdot \mathbf{B} dV = \oint_S \mathbf{B} \cdot d\mathbf{S} = 0 \quad (1.21)$$

In many cases it is advantageous to think of a vector field as the "flow" of a quantity and in the case of the magnetic field, as suggested from Eq. (1.21), it is useful to think of  $\mathbf{B}$  as a density of flow of "something" per unit area. In the SI system of units we have agreed to term this "something" as *magnetic flux* with units *webers*. Consequently when the webers/unit area are integrated over a closed surface the total amount enclosed is identically zero. For an arbitrary surface  $S$  bounded by a closed contour  $O$  as shown in Fig. 1.1, the total magnetic flux  $\Phi$  passing through the surface  $S$  is expressed by

$$\Phi = \int_S \mathbf{B} \cdot d\mathbf{S} \quad (\text{webers}) \quad (1.22)$$

The flux which passes through the surface  $S$  is said to link the contour  $O$  and is generally referred to as the *flux linkage* of the contour. The flux which links a contour  $O$  may also be expressed in terms of the vector potential  $\mathbf{A}$ . Since  $\mathbf{B}$  is the curl of  $\mathbf{A}$  we can write

$$\Phi = \int_S \mathbf{B} \cdot d\mathbf{S} = \int_S \nabla \times \mathbf{A} \cdot d\mathbf{S}$$

This expression can be transformed to a contour integral by using Stoke's Theorem, in which case,

$$\Phi = \int_S \nabla \times \mathbf{A} \cdot d\mathbf{S} = \oint_O \mathbf{A} \cdot d\mathbf{l} \quad (1.23)$$

This expression is sometimes more convenient to evaluate than Eq. (1.22) and will be particularly useful when we investigate finite element analysis later in this text.

## 1.7 Ampere's Law

Ampere's Law forms the fundamental basis upon which we begin all machine design. While often presented as a separate Law to that of Biot and Savart, its basis is, in actuality, embedded in the definition of the magnetic field  $\mathbf{B}$ . Upon taking the curl of  $\mathbf{B}$  as defined by Eq. (1.6), and replacing the curl-curl operator by the equivalent expression, the gradient of the divergence minus the Laplacian, we obtain

$$\nabla \times \mathbf{B} = \nabla \times \nabla \times \frac{\mu_0}{4\pi} \int_V \frac{\mathbf{J}}{R} dV \quad (1.24)$$

$$= \frac{\mu_0}{4\pi} \int_V \left[ \nabla \nabla \cdot \frac{\mathbf{J}}{R} - \mathbf{J} \nabla^2 \left( \frac{1}{R} \right) \right] dV \quad (1.25)$$

The differential operators have been taken behind the integral since these operators are taken with respect to the point at which  $\mathbf{B}$  is desired whereas the integral is taken over the region where the current density  $\mathbf{J}$  exists.

The first term in Eq. (1.25) can be written alternatively as

$$\int_V \nabla \nabla \cdot \frac{\mathbf{J}}{R} dV = \nabla \int_V \nabla \cdot \frac{\mathbf{J}}{R} dV$$

where the gradient operator has been brought out from under the integral sign since the gradient and integral operations can again be interchanged. However from Gauss' Theorem, this integral can be replaced by the expression

$$\nabla \int_V \nabla \cdot \frac{\mathbf{J}}{R} dV = -\nabla \oint_S \frac{\mathbf{J}}{R} \cdot d\mathbf{S} \quad (1.26)$$

The minus sign appears in this expression since the divergence operator is taken with respect to the point defining  $\mathbf{B}$  whereas the integral is taken over the

volume defining the current density  $\mathbf{J}$ . However, the surface  $S$  describes the outer surface of the conductor over which a net current clearly is not escaping. Thus the dot product  $\mathbf{J} \cdot d\mathbf{S}$  is zero on this surface and the first term in Eq. (1.25) is therefore zero.

The expression for the curl of  $\mathbf{B}$  reduces to

$$\nabla \times \mathbf{B} = -\frac{\mu_0}{4\pi} \int_V \mathbf{J} \nabla^2 \left( \frac{1}{R} \right) dV \quad (1.27)$$

where  $\nabla^2 = (\nabla \bullet \nabla)$  is the Laplacian operator. That is,

$$\nabla^2 = \frac{\partial^2}{\partial x^2} + \frac{\partial^2}{\partial y^2} + \frac{\partial^2}{\partial z^2}$$

where the set  $(x, y, z)$  denotes the point at which  $\mathbf{B}$  is defined. Also  $R$  is the distance from the point where  $\mathbf{B}$  is evaluated to the differential element  $dV$  locating  $\mathbf{J}$ . In a similar manner we can define the set  $(x', y', z')$  as denoting the point at which the differential volume  $dV$  is defined and the corresponding Laplacian operator

$$\nabla' = \frac{\partial^2}{\partial (x')^2} + \frac{\partial^2}{\partial (y')^2} + \frac{\partial^2}{\partial (z')^2}.$$

By formal differentiation it can be shown that the expression  $\nabla^2(1/R)$  is identically zero everywhere except at the point of singularity, namely where  $R \rightarrow 0$ . At the point of singularity the points  $(x, y, z)$  and  $(x', y', z')$  coincide so that  $\nabla^2(1/R) = \nabla'^2(1/R)$  where the prime indicates differentiation with respect to the prime variables. Since  $\nabla^2$  is equivalently written as  $\nabla \bullet \nabla$ , Eq. (1.27) can also be written as

$$\nabla \times \mathbf{B} = -\lim_{R \rightarrow 0} \frac{\mu_0}{4\pi} \int_V \mathbf{J} \nabla' \cdot \nabla' \left( \frac{1}{R} \right) dV \quad (1.28)$$

which, by Gauss' Theorem becomes,

$$\nabla \times \mathbf{B} = -\lim_{R \rightarrow 0} \frac{\mu_0}{4\pi} \oint_S \mathbf{J} \nabla' \left( \frac{1}{R} \right) dS \quad (1.29)$$

The differential surface area in spherical coordinates is  $a_n(R^2 \sin\theta d\phi d\theta)$  where  $a_n$  is the unit normal to the surface  $dS$ . However, the gradient of  $1/R$  is equal to  $-a_n/R^2$  so that the integral becomes

$$\nabla \times \mathbf{B} = \lim_{R \rightarrow 0} \frac{\mu_0}{4\pi} \oint_S J \sin\theta d\phi d\theta \quad (1.30)$$

Since the radius of the small sphere approaches zero, the current density vector  $J$  can be removed from the integrand since it becomes a constant. The remaining integral can now be evaluated as simply  $4\pi$ . Eq. (1.24) finally reduces to *Ampere's Law*

$$\nabla \times \mathbf{B} = \mu_0 \mathbf{J} \quad (1.31)$$

The integral form for Ampere's Law can be obtained by integrating Eq. (1.31) over an arbitrary finite open surface which includes the region where the current density  $J$  is flowing, whereupon,

$$\int_S (\nabla \times \mathbf{B}) \cdot d\mathbf{S} = \mu_0 \int_S \mathbf{J} \cdot d\mathbf{S} \quad (1.32)$$

The right hand side of Eq. (1.32) is clearly proportional to the current  $I$  flowing through the surface  $S$ . With the use of Stoke's Theorem, the left hand side can be altered to the form

$$\int_S (\nabla \times \mathbf{B}) \cdot d\mathbf{S} = \oint_C \mathbf{B} \cdot d\mathbf{l} \quad (1.33)$$

where the path  $C$  corresponds to the outer edge of the surface  $S$ . Thus, the integral form of Ampere's Law is,

$$\oint_C \mathbf{B} \cdot d\mathbf{l} = \mu_0 I \quad (1.34)$$

## 1.8 Magnetic Field Intensity

Thus far, we have been concerned with the behavior of the magnetic field in a vacuum. When dealing with material bodies, orbiting electrons of each individual atom can be considered as a current loop. With an external magnetic

field the orbiting atoms are randomly disposed so that they do not produce, themselves, a magnetic field (except for permanent magnets). The presence of the magnetic field influences the orbits of the individual atoms creating what is called a *magnetic dipole moment m*. Its dipole moment is defined as equal to the product of the area of the circular loop defined by the orbiting times the magnitude of the circulating current and with a direction perpendicular to the plane of the loop in the direction of a right hand screw. That is, if the current loop is located in the  $x,y$  plane and orbiting in a counterclockwise direction as shown in Figure 1.2, the magnetic dipole moment is defined by,

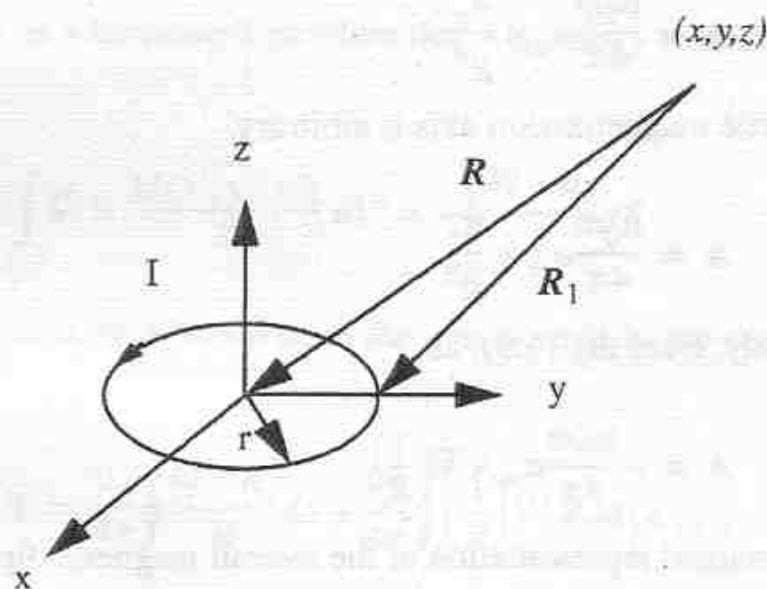


Figure 1.2 The magnetic dipole

$$m = \pi r^2 I a_z \quad (\text{amps/square meter})$$

The vector potential for this small electric circuit is,

$$A = \frac{\mu_0 I}{4\pi} \oint_{R_1} \frac{dl}{R} \quad (1.35)$$

If  $R^2$  is much greater than  $r^2$  then

$$\frac{1}{R_1} \approx \frac{1}{R} \left( 1 + \frac{rx}{R^2} \cos \phi' + \frac{ry}{R^2} \sin \phi' \right) \quad (1.36)$$

Eq. (1.35) then integrates to yield

$$\mathbf{A} = \frac{\mu_0 I r^2}{4R^3} (-ya_z + xa_y) \quad (1.37)$$

However,

$$\mathbf{a}_z \times \mathbf{R} = \mathbf{a}_z \times (xa_x + ya_y + za_z) = -ya_z + xa_y$$

so that the vector potential can be expressed in vector form as

$$\mathbf{A} = \frac{\mu_0 m}{4\pi} \mathbf{a}_m \times \frac{\mathbf{a}_r}{R^2} \quad (1.38)$$

In general if the magnetization axis is arbitrary,

$$\mathbf{A} = \frac{\mu_0 m}{4\pi} \mathbf{a}_m \times \frac{\mathbf{a}_r}{R^2} \quad (1.39)$$

or, alternatively, from Eq. (1.9), as

$$\mathbf{A} = -\frac{\mu_0 m}{4\pi} \mathbf{a}_m \times \nabla \left( \frac{1}{R} \right) \quad (1.40)$$

A mathematical representation of the overall magnetic dipole moment of a finite body can be obtained by multiplying  $m\mathbf{a}_m$  by the number of atoms per unit volume  $N$  to obtain the *magnetic polarization vector*  $\mathbf{M}$

$$\mathbf{M} = N\mathbf{m} = Nm\mathbf{a}_m \quad (\text{amps/meter}) \quad (1.41)$$

so that we can write in place of (1.40),

$$\mathbf{A}(x, y, z) = -\frac{\mu_0}{4\pi} \int_V \mathbf{M}(x', y', z') \times \nabla \left( \frac{1}{R} \right) dV' \quad (1.42)$$

where  $\mathbf{M}$  is considered here as varying within the body (i.e. a function of  $(x', y', z')$ ) and  $R$  represents the distance between the external point  $(x, y, z)$  and the internal point  $(x', y', z')$ . Now,

$$\mathbf{M} \times \nabla \left( \frac{1}{R} \right) = -\mathbf{M} \times \nabla' \left( \frac{1}{R} \right)$$

and

$$\mathbf{M}(x', y', z') \times \nabla' \left( \frac{1}{R} \right) = \left( \frac{1}{R} \right) \nabla' \times \mathbf{M}(x', y', z') - \nabla' \times \frac{\mathbf{M}(x', y', z')}{R} \quad (1.43)$$

Eq. (1.42) can now be written as

$$\mathbf{A} = -\frac{\mu_0}{4\pi} \int_V \left( \frac{1}{R} \right) \nabla' \times \mathbf{M}(x', y', z') dV' + \frac{\mu_0}{4\pi} \int_V \nabla' \times \frac{\mathbf{M}(x', y', z')}{R} dV' \quad (1.44)$$

It is shown as a homework problem that a corollary to Stoke's Theorem is the fact that,

$$\int_V \nabla' \times \frac{\mathbf{M}(x', y', z')}{R} dV' = - \oint_C \frac{\mathbf{M} \times \mathbf{a}_n}{R} dS \quad (1.45)$$

for any vector field  $\mathbf{M}$  wherein  $\mathbf{a}_n$  is the unit normal to the surface  $dS$ . Thus, finally,

$$\mathbf{A} = \frac{\mu_0}{4\pi} \oint_S \frac{\mathbf{M} \times \mathbf{a}_n}{R} dS + \frac{\mu_0}{4\pi} \int_V \left( \frac{1}{R} \right) \nabla' \times \mathbf{M}(x', y', z') dV' \quad (1.46)$$

If one compares this expression of the vector potential with that for true currents, it is apparent that we can interpret the term  $\mathbf{M} \times \mathbf{a}_n$  as an equivalent surface polarization current  $J_{ms}$ . Similarly, the curl of the magnetization vector  $\nabla \times \mathbf{M}$  as an equivalent volumetric polarization current  $J_m$ . The expression for vector potential becomes

$$\mathbf{A} = \frac{\mu_0}{4\pi} \left( \oint_C \frac{J_{ms}}{R} dS + \int_V \frac{J_m}{R} dV \right) \quad (1.47)$$

Note that this equation again generates three "decoupled" equations involving only  $x, y$  and  $z$  components of  $\mathbf{A}, J_{ms}$  and  $J_m$  respectively.

Consider now the magnetic flux density at any point within a material body having both true current  $\mathbf{J}$  and polarization current  $\mathbf{J}_m$ . From Eq. (1.12),

$$\mathbf{B} = \nabla \times \left( \frac{\mu_0}{4\pi} \int_V \frac{J_m + J}{R} dV \right) \quad (1.48)$$

In Section 1.7 it was shown that  $\nabla \times \mathbf{B} = \mu_0 \mathbf{J}$ . In an analogous manner it is evident that with polarization currents,

$$\nabla \times \mathbf{B} = \mu_0 (J + J_m) \quad (1.49)$$

Since the volumetric polarization current  $J_m$  is equal to the curl of the magnetization  $M$ , this expression can be written as

$$\nabla \times \left( \frac{\mathbf{B}}{\mu_0} - \mathbf{M} \right) = \mathbf{J} \quad (1.50)$$

in which the vector on the left hand side of the equation  $\mathbf{B}/\mu_0 - \mathbf{M}$  has as its source only the true currents  $\mathbf{J}$ . It is therefore useful to define the *magnetic field intensity*  $H$  as

$$\mathbf{H} = \frac{\mathbf{B}}{\mu_0} - \mathbf{M} \quad (\text{amps/meter}) \quad (1.51)$$

from which we can establish that

$$\mu = \frac{\mu_0}{1 - \mu_0 \left( \frac{\mathbf{M}}{\mathbf{B}} \right)} \quad (1.52)$$

in which case

$$\mathbf{B} = \mu \mathbf{H} \quad (1.53)$$

or, alternatively,

$$\mathbf{B} = \mu_r \mu_0 \mathbf{H} \quad (1.54)$$

where  $\mu_r = \mu/\mu_0$  is defined as the *relative permability*. The differential form for Ampere's Law is finally obtained, namely

$$\nabla \times \mathbf{H} = \mathbf{J} \quad (1.55)$$

Since  $\nabla \cdot \mathbf{H} = -\nabla \cdot \mathbf{M}$ , the divergence of the magnetic field intensity is not zero as is the case for the divergence of  $\mathbf{B}$ . The magnetic field intensity is also sometimes called the *magnetic potential gradient*.

Starting with Eq. (1.55), and applying Stoke's Theorem, provides us with the usual integral form of Ampere's Law

$$\int_S (\nabla \times \mathbf{H}) \cdot d\mathbf{S} = \oint_C \mathbf{H} \cdot d\mathbf{l} = \int_S \mathbf{J} \cdot d\mathbf{S} = I \quad (1.56)$$

where  $I$  is the total current enclosed by the path defined by  $C$ . If current  $I$  is confined to a conductor and flows  $N$  times through the loop  $C$ ,  $I$  is replaced by  $NI$  in Eq. (1.56).

## 1.9 Boundary Conditions for $B$ and $H$

In the derivation of the differential form for Ampere's Law, points within the material were specified and not points on the boundary where an additional polarization current component exists,  $\mathbf{J}_{ms}$ . Hence, for points on the boundary the results obtained must be modified to take account of this current which results from a discontinuity in the magnetization vector  $\mathbf{M}$ . Consider now an interface between two material bodies with permeability  $\mu$  different from  $\mu_0$  as illustrated in Figure 1.3. Let  $H_{1t}$  and  $H_{2t}$  be the components of  $\mathbf{H}$  tangent to the

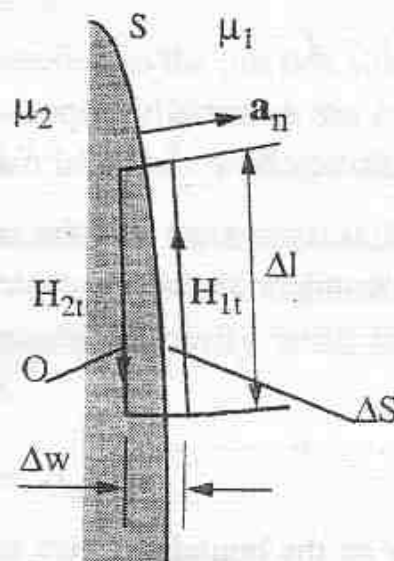


Figure 1.3 Determination of boundary condition for the tangential component of  $\mathbf{H}$

interface surface in the material body and air respectively. We have, from Eq.

(1.55) that  $\nabla \times \mathbf{H} = \mathbf{J}$ . If the path  $O$  is chosen as shown in Figure 1.3, the integral form for Ampere's Law gives,

$$\int_{\Delta S} (\nabla \times \mathbf{H}) \cdot d\mathbf{S} = \oint_{\Delta O} \mathbf{H} \cdot d\mathbf{l} = \int_{\Delta S} \mathbf{J} \cdot d\mathbf{S} \quad (1.57)$$

where  $\Delta O$  is the outer contour of the surface  $\Delta S$ . Since no physical current is enclosed, these expressions are equal to zero. If we shrink  $\Delta w$  to a negligibly small value, then  $H_{t1}\Delta l - H_{t2}\Delta l = 0$  so that,

$$H_{t1} = H_{t2} \quad (1.58)$$

which states, in effect, that the tangential components of  $\mathbf{H}$  must be continuous across a boundary not carrying a true surface current  $J_s$ . It is clear that if the boundary supports a physical current surface current  $J_s$ , then Eq. (1.58) must be replaced with

$$H_{t1} - H_{t2} = J_s \quad (1.59)$$

where positive current is taken in the direction made by a right hand screw when rotated in the direction defined by the path  $O$ . In vector form, the equivalent expression is written as,

$$\mathbf{a}_n \times (\mathbf{H}_1 - \mathbf{H}_2) = \mathbf{J}_s \quad (1.60)$$

Although true surface currents are essentially impossible, Eq. (1.59) is often used to approximate physical situations in electrical machine design.

As a corollary to Eq. (1.58) it is apparent that the tangential components of  $\mathbf{B}$  are discontinuous across a boundary separating materials with different permeabilities, that is

$$\frac{B_{t1}}{\mu_1} = \frac{B_{t2}}{\mu_2} \quad (1.61)$$

when no surface currents flow on the boundary.

The behavior of the normal components of  $\mathbf{B}$  and  $\mathbf{H}$  can also be determined as shown in Figure 1.4. In this case, we have, from Eq. (1.18)

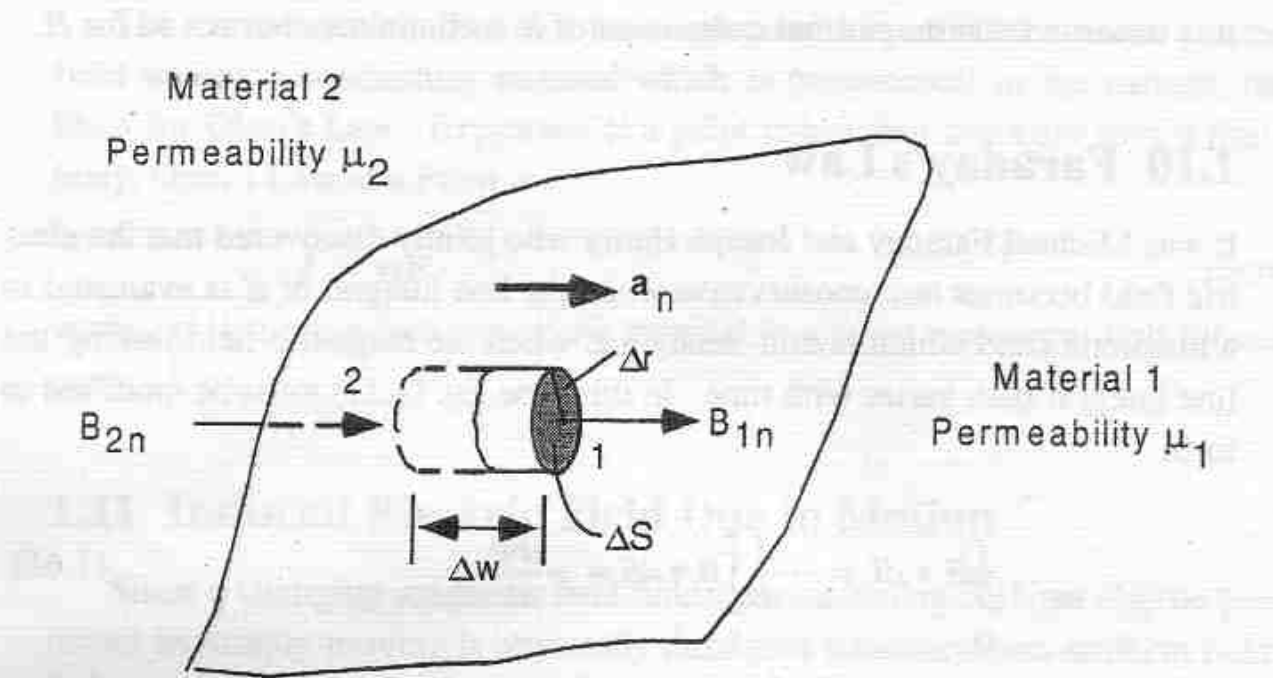


Figure 1.4 Determination of the boundary condition for the normal component of  $\mathbf{B}$

$$\oint_S \mathbf{B} \cdot d\mathbf{S} = 0$$

If we apply this expression to the pill box shape of Figure 1.4 then

$$B_{n1}\Delta S - B_{n2}\Delta S = (B_{n1s} + B_{n2s})(\pi\Delta r\Delta w)$$

where  $B_{n1}$ ,  $B_{n2}$  pertains to the top and bottom of the pill box and  $B_{n1s}$  and  $B_{n2s}$  pertains to the sides of the pillbox in materials 1 and 2 respectively. If the sides of the pillbox are made arbitrarily small then  $B_{n1}\Delta S = B_{n2}\Delta S$ , or finally across any boundary,

$$B_{n1} = B_{n2} \quad (1.62)$$

In vector form we can say that,

$$\mathbf{a}_n \cdot (\mathbf{B}_1 - \mathbf{B}_2) = 0 \quad (1.63)$$

The corresponding boundary condition for  $\mathbf{H}$  is clearly

$$\mu_1 H_{n1} = \mu_2 H_{n2} \quad (1.64)$$

It is observed that the normal component of  $B$  is continuous but not so for  $H$ .

## 1.10 Faraday's Law

It was Michael Faraday and Joseph Henry who jointly discovered that the electric field becomes non-conservative when the line integral of  $E$  is evaluated in a magnetic field which is non-steady, i.e. when the magnetic field linking the line integral path varies with time. In this case Eq. (1.11) must be modified to form

$$\oint_O E \bullet dl = - \frac{d}{dt} \int_S B \bullet dS = - \frac{d\Phi}{dt} \quad (1.65)$$

where  $O$  bounds surface  $S$ . In a practical sense this expression shows that an additional electric field is produced by a time changing magnetic field and consequently a voltage is produced in a closed short circuited coil when placed in this field. The strength of this voltage is proportional to the time rate of change of flux linking the coil and, in turn, induces a current in the conducting loop. The negative sign indicates that the voltage is directed in such a manner so as to produce a current which produces a consequent magnetic field which reduces the net flux linking the loop.

The differential form of Eq. (1.65) may be obtained by using Stoke's Theorem to replace the line integral by a surface integral so that,

$$\oint_O E \bullet dl = \int_S \nabla \times E \bullet dS = - \frac{d}{dt} \int_S B \bullet dS$$

or

$$\int_S \left( \nabla \times E + \frac{dB}{dt} \right) \bullet dS = 0$$

from which,

$$\nabla \times E = - \frac{dB}{dt} \quad (1.66)$$

The current which flows in the conducting loop creates also an electric field within a conducting material which is proportional to the current, the basis for Ohm's Law. Expressed at a point rather than averaged over a finite body, Ohm's Law at a Point is

$$J = \sigma E \quad (1.67)$$

where,  $\sigma$  is the conductivity of the material in ampere meters per volt (ohms/meter)<sup>-1</sup>.

## 1.11 Induced Electric Field Due to Motion

Since a changing magnetic field linking a conducting coil can also be produced by simply moving it physically through a stationary, non-uniform field, Eq. (1.65) is equally valid for this condition as well. Movement of the coil through the field, however, produces an accompanying phenomenon, the Lorentz force which states that moving charges in a magnetic field experience a force proportional to the velocity of the charge and the strength of the magnetic field according to the equation,

$$\mathbf{F} = q\mathbf{v} \times \mathbf{B} \quad (1.68)$$

The force is seen acting in a direction perpendicular to both  $v$  and  $B$ . This force is proportional to the electric field since,

$$\frac{\mathbf{F}}{q} = \mathbf{E} = \mathbf{v} \times \mathbf{B} \quad (1.69)$$

The corresponding field, in turn induces a voltage in the coil resulting in current flow according to Ohm's Law, Eq. (1.67). This induced voltage is typically called the *Electromotive Force* (a misnomer since this quantity is a voltage and not a force but is only derived from a force). Note from Figure 1.5 that this voltage is in such a direction so as to produce a current which resists any change in the flux linking the coil. The degree to which this is accomplished depends upon the resistance of the coil. If superconducting, flux linking the coil will not change at all. The interrelationship between the force on moving coil and the resulting current (or vice versa) is the key component for the principle of *electromechanical energy conversion*.

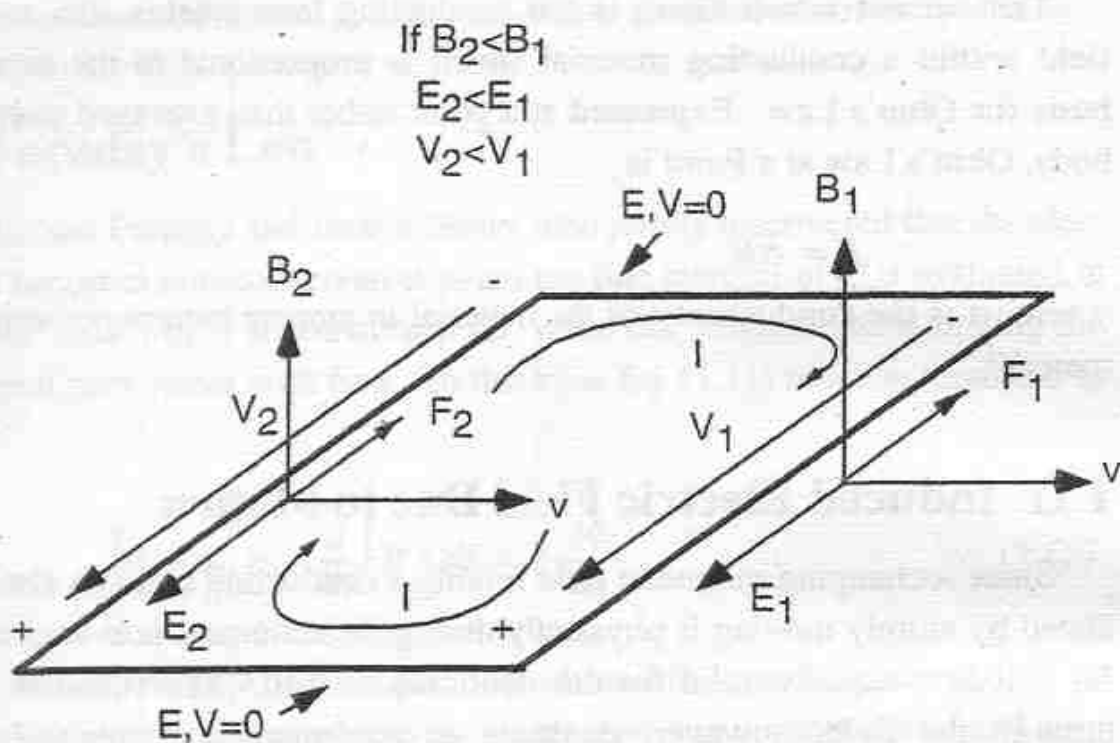


Figure 1.5 Induced voltage in a coil moving in a direction so as to increase the flux linking the coil. Force assumed to be impressed on a negative charge (electron).

## 1.12 Permeance, Reluctance and the Magnetic Circuit

The solution to the general magnetostatic boundary-value problem involving conduction currents in the presence of magnetic material is very difficult to obtain. Fortunately, applications involving electric machine design allow for good approximate solutions to be obtained. The analysis procedure parallels that of dc circuits which are composed of series and parallel resistors. Consider, for example, the field in the region of a toroid with a rectangular cross section wound with  $N$  turns as illustrated in Figure 1.6.

Due to symmetry the magnetic field intensity has only a circumferential component. At any point in the core  $x$  meters from its center, the magnetic potential gradient is

$$H = \frac{NI}{2\pi x} \quad (1.70)$$

The flux density at the distance  $x$  is therefore

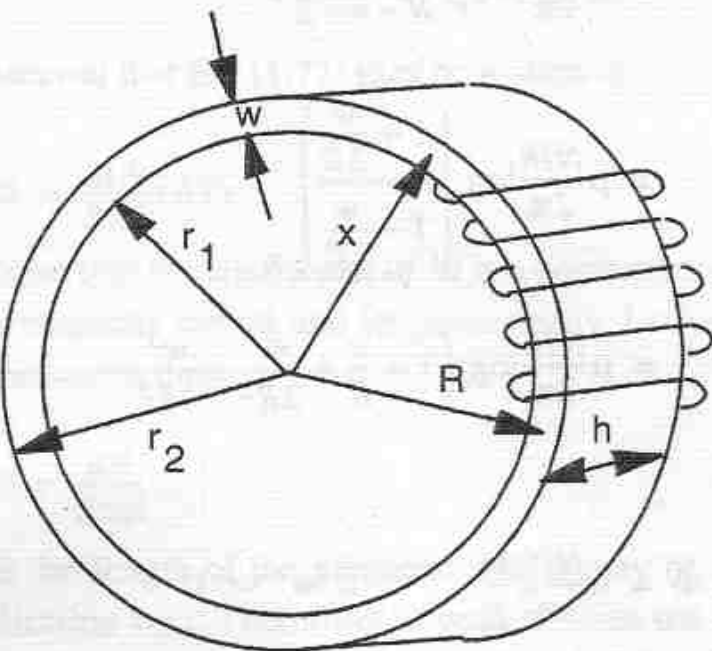


Figure 1.6 Flux distribution of a toroid with a rectangular cross section

$$B = \mu H = \frac{\mu NI}{2\pi x} \quad (1.71)$$

However the flux density at any point is equal to  $d\Phi/dA$ . The total flux over a cross sectional area ( $h dx$ ) is

$$d\Phi = BdA = Bh dx = \mu \frac{NIhdx}{2\pi x} \quad (1.72)$$

The total flux over the area  $A$  is given by

$$\begin{aligned} \Phi &= \int_{r_1}^{r_2} \mu \frac{NIhdx}{2\pi x} \\ &= \mu \frac{NIh}{2\pi} \log_e(r_2/r_1) \end{aligned} \quad (1.73)$$

$$= \mu \frac{NIh}{2\pi} \log_e \left( \frac{R + w/2}{R - w/2} \right)$$

$$= \mu \frac{NIh}{2\pi} \log_e \left( \frac{1 + \frac{w}{2R}}{1 - \frac{w}{2R}} \right)$$

$$= \mu \frac{NIh}{2\pi} \log_e \left( 1 + \frac{w}{R} + \frac{w^2}{2R^2} + \frac{w^3}{4R^3} + \dots \right)$$

so that finally,

$$\Phi = \mu \frac{NI}{2\pi} h \frac{w}{R} \quad \text{if } w/r \ll 1 \quad (1.74)$$

When  $w/R = 0.2$  then the natural log of the expansion  $1 + w/R + w^2/R^2 + \dots$  is equal to  $w/R$  to within 0.3%. Therefore for cases where the core width is small in comparison with the mean radius  $R$ , we can assume the flux density to be uniform. Thus

$$\Phi = \frac{\mu NIhw}{2\pi R} \quad (1.75)$$

By assuming the core width  $w$  small compared with  $R$ , we can assume that  $H$  is constant at all points of the toroid and equal to its value at the center. In this case from Eq. (1.74)

$$\frac{\mu NI}{2\pi R} = B \quad (1.76)$$

and

$$hw = A$$

Therefore

$$\Phi = \frac{\mu NI}{2\pi R} A \quad (= BA) \quad (1.77)$$

Note that we have purposely chosen a square toroid for this example. The case of a circular toroid reduces in the same manner but the exact solution involves Bessel Functions. It is useful noting that in this book we will use the symbol  $A$

for both vector potential and cross-sectional area, hopefully without much confusion.

It can be observed that Eq. (1.77) may be written as

$$\Phi = \frac{\mu A}{2\pi R} (NI) \quad (1.78)$$

where  $A = hw$ . Note that the coefficient of  $NI$  is a constant depending upon the geometry of the magnetic circuit and its permeability. Let us define this constant as the permeance  $\mathcal{P}$ , thus

$$\mathcal{P} = \frac{\mu A}{2\pi R} \quad (1.79)$$

Since  $2\pi R$  is the length of the magnetic path it may be replaced for purposes of generalization by  $l$ . Therefore, in general when the flux is uniformly distributed over a constant cross-sectional area,

$$\mathcal{P} = \frac{\mu A}{l} \quad (1.80)$$

where  $\mathcal{P}$  is called the permeance and is given in units of *webers per ampere turn or henries*.

It is also useful to define the quantity

$$\mathcal{F} = \int_O H \cdot dl \quad (1.81)$$

The quantity  $\mathcal{F}$  is called the magnetomotive force (*MMF*) which has *MKS* units of ampere turns. When the closed path  $O$  encloses a circuit of  $N$  turns carrying  $I$  amperes, it is clear from Ampere's Law that

$$\mathcal{F} = NI \quad (1.82)$$

Therefore, in general, we can write that the flux in a magnetic circuit can be expressed as

$$\Phi = \mathcal{P}\mathcal{F} \quad (1.83)$$

In almost all practical cases the permeance  $\mathcal{P}$  is not so easy to find. Therein lies the art and science of electrical machine design. When the flux density var-

ies over the cross sectional area the differential form of Eq. (1.83) is often useful. In this case

$$d\Phi = \mathcal{F} d\mathcal{P}$$

where

$$d\mathcal{P} = \frac{\mu dA}{l}$$

The total permeance is found by taking

$$\mathcal{P} = \int_0^A \mu \frac{dA}{l} \quad (1.84)$$

where  $l$  is frequently a function of  $A$ .

In the case of our example rectangular toroid,  $dA = hdx$  and  $l = 2\pi x$ . Eq. (1.84) becomes

$$\mathcal{P} = \int_{r_1}^{r_2} \mu \frac{h dx}{(2\pi x)}$$

whereupon,

$$\mathcal{P} = \frac{\mu h}{2\pi} \log_e \left( \frac{r_2}{r_1} \right)$$

directly.

The reciprocal of permeance also has great utility in magnetic circuit analysis. Formally, by definition

$$\mathcal{R} = 1/\mathcal{P} \quad (1.85)$$

and if the cross-sectional area  $A$  and the permeability are constants independent of the length of the circuit,

$$\mathcal{R} = \frac{l}{\mu A} \quad (1.86)$$

The quantity reluctance carries units of ampere turns per weber. In the MKS unit system this corresponds to inverse henries  $h^{-1}$ . In these notes we will use  $h^{-1}$  as the preferred unit to avoid confusion with the time unit (seconds). We will often find the reluctance a more useful quantity in our analysis of electrical machines.

### 1.13 Example 1.1

- Find the reluctance of a toroid of square cross section and radius  $R$  to the center of the core. The core is designed such that  $\mu = 1 \cdot 10^{-4}$ ,  $R = 50$  and  $a = 2$  cm. Refer to Figure 1.7. The reluctance  $R$  is given by

$$\begin{aligned} \mathcal{R} &= \frac{L}{\mu A} \\ &= \frac{2\pi(0.5)}{1 \cdot 10^{-4}(0.02)^2} \\ &= 7.85 \cdot 10^7 (h^{-1}) \end{aligned}$$

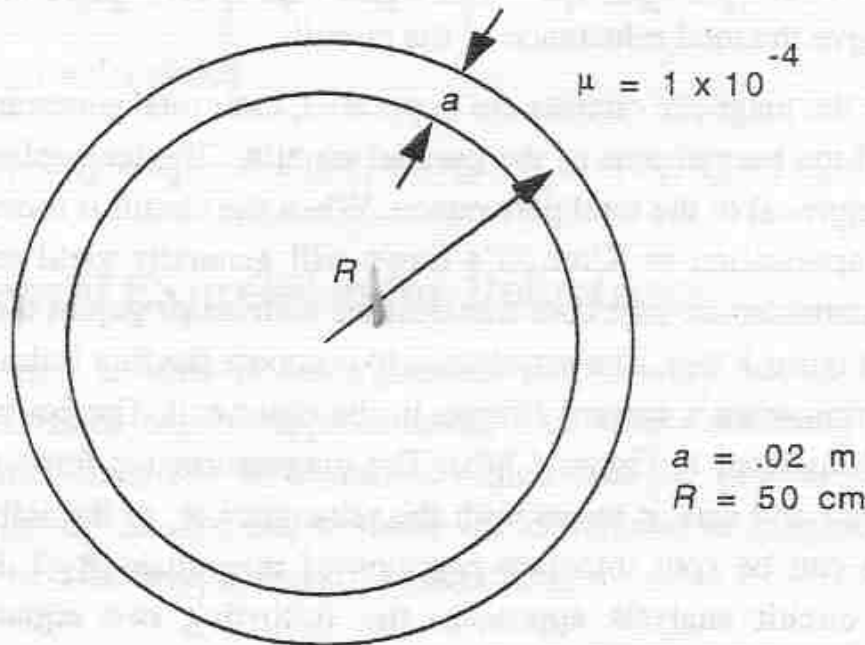


Figure 1.7 Square toroid for Example 1.1.

2. The toroid has 1570 ampere turns uniformly wound around its core. What is the value of the flux inside the toroid?

$$\Phi = \mathcal{F}/\mathcal{R}$$

$$= \frac{1570}{7.85 \cdot 10^7} = 2 \cdot 10^{-5} \quad \text{webers}$$

3. What is the flux density in the core of the toroid?

$$B = \frac{\Phi}{A} = \frac{2 \cdot 10^{-5}}{(0.02)^2} = 0.05 \quad \text{webers/m}^2$$

## 1.14 Multiple Circuit Paths

When the same flux is set up in a magnetic circuit made of the same material but with parts of different cross sections or when the parts of the circuit are of materials of different permeabilities but of the same or different cross sections, the flux can be found by finding the reluctance of the different parts, adding them to give the total reluctance of the circuit, and finally dividing the magnetomotive force by the total reluctance. As in the case of the resistances of an electric circuit, the reluctances in a magnetic circuit when in series are added to give the total reluctance of the circuit.

When the magnetic circuits are in parallel, their total permeance is equal to the sum of the permeances of the parallel circuits. The total reluctance is simply the reciprocal of the total permeance. When the circuit is more complicated the usual application of Kirchoff's Laws will generally yield an answer. For example, consider the iron core transformer with an air gap in the center leg as shown in Figure 1.8(a). The problem is to compute the flux linkage for the coil with  $N_2$  turns when a current  $I$  flows in the other coil. The equivalent magnet circuit is illustrated in Figure 1.8(b). The magnetomotive force  $N_1 I$  is applied to the circuit and acts in series with the reluctance  $\mathcal{R}_1$  of the left side leg. The reluctance can be split into two portions of magnitude  $\mathcal{R}_1/2$ . Following the usual dc circuit analysis approach, the following two equations may be obtained,

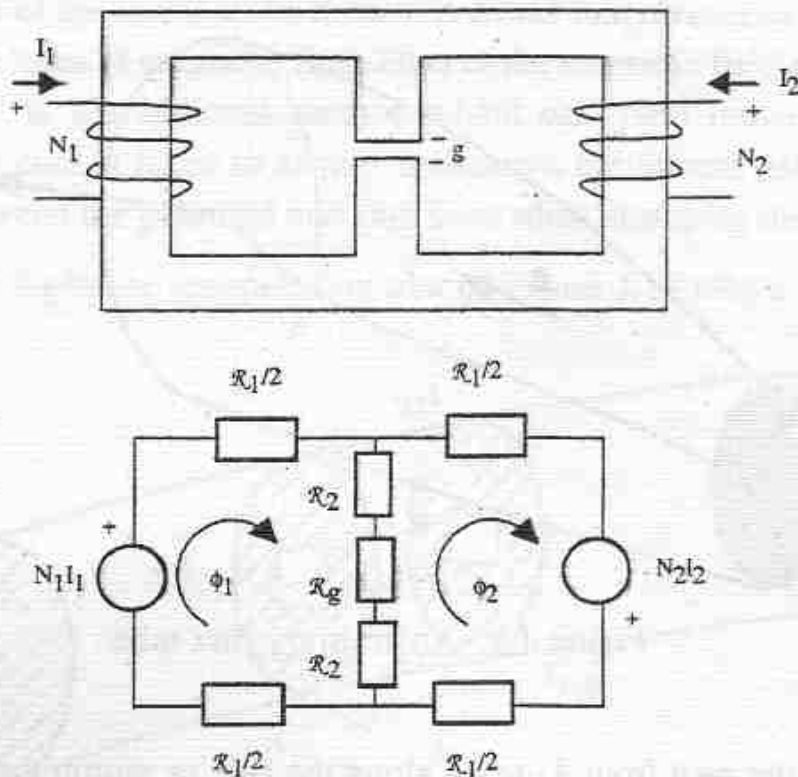


Figure 1.8 A type of iron core transformer and its equivalent magnetic circuit

$$N_1 I_1 = \Phi_1 (\mathcal{R}_1 + 2\mathcal{R}_2 + \mathcal{R}_g) - \Phi_2 (2\mathcal{R}_2 + \mathcal{R}_g)$$

$$N_2 I_2 = \Phi_2 (\mathcal{R}_1 + 2\mathcal{R}_2 + \mathcal{R}_g) - \Phi_1 (2\mathcal{R}_2 + \mathcal{R}_g)$$

Upon solving for  $\Phi_2$  yields

$$\Phi_2 = [N_1 I_1 (2\mathcal{R}_2 + \mathcal{R}_g) + N_2 I_2 (\mathcal{R}_1 + 2\mathcal{R}_2 + \mathcal{R}_g)] / [\mathcal{R}_1 (\mathcal{R}_2 + 4\mathcal{R}_2 + 2\mathcal{R}_g)].$$

## 1.15 General Expression for Reluctance

Assume now a body of homogeneous permeability but of an arbitrary shape. If flux lines can be approximated, flux tubes containing a specified number of flux lines can be identified which take the general shape of the sketch of Figure 1.9. We can evaluate the difference of magnetic potential between the two faces  $A_1$  and  $A_2$  by again taking

$$\int_{l_{12}} \mathbf{H} \cdot d\mathbf{l} = \mathcal{F}_1 - \mathcal{F}_2$$

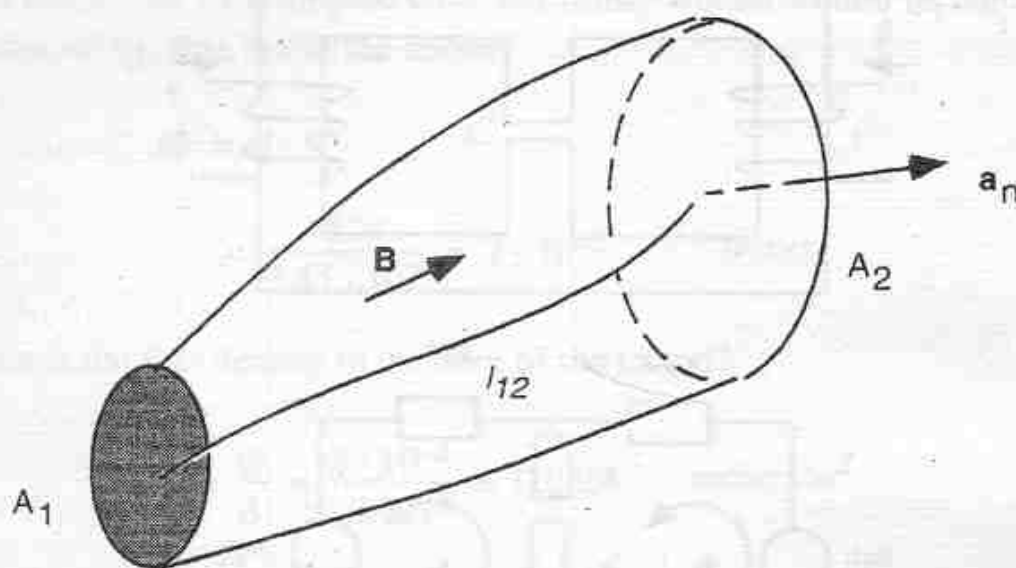


Figure 1.9 An arbitrary flux tube

where  $l_{12}$  is the path from  $A_1$  to  $A_2$  along the side or within the flux tube. The flux which is confined within the flux tube is

$$\int_A \mathbf{B} \cdot d\mathbf{S} = \Phi$$

where  $A$  is the area  $A_1$ ,  $A_2$  or any cross sectional area across the flux tube. By definition, the reluctance between the two surfaces  $A_1$  and  $A_2$  is

$$R = \frac{\int_A \mathbf{H} \cdot d\mathbf{l}}{\mu \int_A \mathbf{H} \cdot d\mathbf{S}} \quad (1.87)$$

Although this expression is rather simple in form, the integrals cannot be established easily since the location of the flux lines must be known before the integrals can be carried out. Evaluation of the reluctance can be made more accurate if the cross section of the flux tubes are considered as curvilinear squares or rectangles. That is, it is assumed that the corners of the cross sectional area of a flux tube is always 90 degrees but the sides of the rectangles are allowed to be curved lines. This behavior of the cross sectional area is a natural

consequence of the fact that the lines of constant magnetic potential are at right angles to the lines of magnetic flux. Plots of the magnetic field using "curvilinear squares" is a traditional method which can yield remarkably accurate results when care is taken to always maintain a curvilinear (right angle) relationship between the potential and flux lines when sketching the field plot.

Consider the more accurate flux plot of Figure 1.10 where two equipotential surfaces  $S_i$  and  $S_{i+1}$  are identified. Let the potential difference between these surfaces be  $\Delta\mathcal{F}_i$ . The region between  $S_i$  and  $S_{i+1}$  can be decomposed into a number of more elementary flow tubes of length  $\Delta l_i$  and cross section  $\Delta A_j$ .

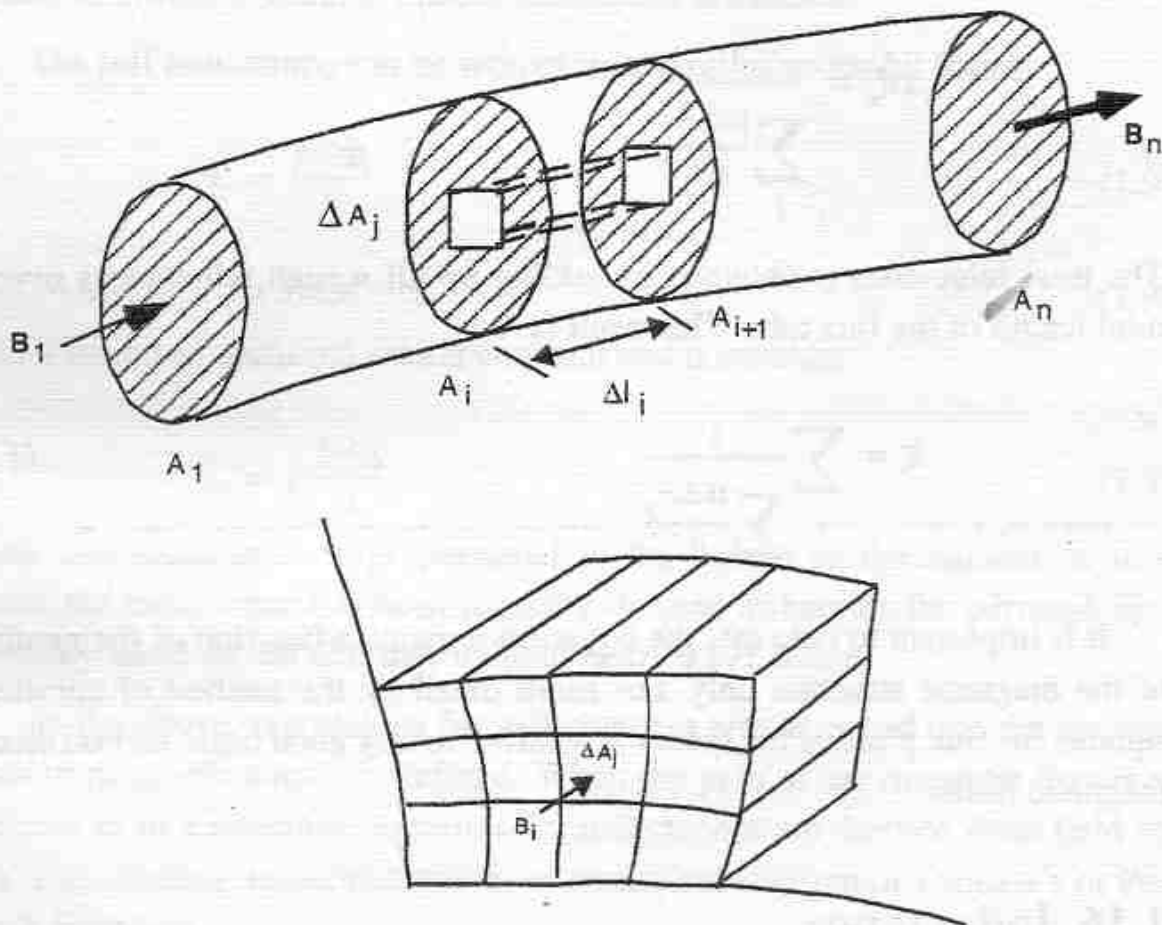


Figure 1.10 Orthogonal curvilinear squares used to portray magnetic flux tube

tial surfaces  $S_i$  and  $S_{i+1}$  are identified. Let the potential difference between these surfaces be  $\Delta\mathcal{F}_i$ . The region between  $S_i$  and  $S_{i+1}$  can be decomposed into a number of more elementary flow tubes of length  $\Delta l_i$  and cross section  $\Delta A_j$ . The reluctance of an arbitrary elementary flow tube is

$$\mathcal{R}_i = \frac{\Delta\mathcal{F}_i}{\Delta\Phi_i} = \frac{\Delta l_i}{\mu \Delta A_i}$$

Since permeances add directly in parallel, the total permeance between surfaces  $S_i$  and  $S_{i+1}$  is

$$\Delta P_i = \sum_j \frac{\mu \Delta A_j}{\Delta l_i}$$

The corresponding reluctance is

$$\Delta R_i = \frac{1}{\sum_j \frac{\mu \Delta A_j}{\Delta l_i}}$$

The total reluctance is obtained by adding up all  $n$  such reluctances over the total length of the flux tube. The result is

$$R = \sum_i \frac{1}{\sum_j \frac{\mu \Delta A_j}{\Delta l_i}} \quad (1.88)$$

It is important to note that the equation remains a function of the geometry of the magnetic structure only. For more detail on the method of curvilinear squares for flux plotting the reader is referred to any good basic text on electromagnetic fields.

## 1.16 Inductance

In most practical cases the magnetic flux links the a number of circuit loops or "turns" in which case one defines the flux linkage  $\lambda$  as,

$$\lambda = N\Phi \quad (1.89)$$

The inductance of a coil is defined as "the number of flux linkages in weber turns per ampere of current flowing in the coil". Flux linkages per ampere is formally defined as a *henry*. Interpreted in mathematical form

$$L = \frac{\lambda}{I} = \frac{N\Phi}{I} \quad (\text{flux linkages/ampere or henries}) \quad (1.90)$$

where

$L$  is the inductance in henries

$N$  is the number of turns of the coil

$\Phi$  is the flux in webers linking the turns

$I$  is the current in the turns in amperes

If the current  $I$  and flux  $\Phi$  correspond to the same circuit, then the resulting inductance is termed self inductance. When the current  $I$  and flux  $\Phi$  correspond to different circuits, mutual inductance is defined.

The self inductance can be written in several other useful forms

$$L = \frac{N^2\Phi}{F} \quad (1.91)$$

$$= N^2\mathcal{P} \quad (1.92)$$

and if the cross sectional area is constant and  $\mu$  constant

$$L = \mu \frac{N^2 A}{l} \quad (1.93)$$

Note that inductance is proportional to the square of the number of turns. Since the inductance has been formally defined as henries the permeability  $\mu$  formally takes on the alternate units of *henries per meter*.

In the above expressions for inductance it was assumed that the magnetic path or magnetic circuit is defined. When the path of the magnetic flux is not defined as in a solenoid, formulas for inductances are derived from field theory, flux plotting, experimentation, or numerical solution of Laplace's or Poisson's Equation.

## 1.17 Magnetic Field Energy

Utilizing the magnetic field energy is often a convenient method of determining the inductance. The energy stored in a magnetic field can be expressed as

$$W_m = \frac{1}{2} \int_V (B \cdot H) dV \quad (1.94)$$

since, also,

$$W_m = \frac{1}{2} L I^2 \quad (1.95)$$

then, when  $B$  and  $H$  arise from the same current

$$L_{self} = \frac{1}{l^2} \int_V (B \cdot H) dV \quad (1.96)$$

Alternative forms of Eq. (1.96) are useful. In machine analysis it is frequently possible to assume that the field intensity and flux density are only radially directed in the air gap and that they vary only circumferentially. Furthermore, since  $H = B/\mu$ , then if  $\mu \rightarrow \infty$ ,  $H$  can be assumed as zero in the iron. Alternatively the relatively small MMF drop in the iron can be corrected by appropriately increasing the MMF in the gap. If  $\theta$  denotes the angular measure in the circumferential direction,  $r$  the radial direction and  $z$  the axial direction, after performing integration in the radial and axial directions, Eq. (1.96) can be written as

$$L_{self} = \frac{grl}{I^2} \int_0^{2\pi} B(I, \theta) H(I, \theta) d\theta \quad (1.97)$$

where  $g$  is the gap measured in the radial direction,  $r$  the mean gap radius,  $l$  is the length resulting from integrating in the  $z$  direction and the explicit dependence of  $B$  and  $H$  on the current  $I$  and circumferential measure  $\theta$  are explicitly shown. From Eqs. (1.55) and (1.81) we can write this equation as either

$$L_{self} = \frac{rl}{I} \int B(I, \theta) \frac{\mathcal{H}(I, \theta)}{I} d\theta \quad (1.98)$$

or

$$L_{self} = \mu_o \frac{rl}{g} \int \left[ \frac{\mathcal{H}(I, \theta)}{I} \right]^2 d\theta \quad (1.99)$$

Since the gap  $g$  is comprised of air, the  $MMF$  must vary linearly with current so that it can be expressed as the product of current times a second function which only depends upon  $\theta$ . Thus the self inductance can be obtained from either

$$L_{self} = \frac{rl}{l} \int B(I, \theta) N(I, \theta) d\theta \quad (1.100)$$

or the expression,

$$L_{self} = \mu_o \frac{rl}{g} \int N(\theta)^2 d\theta \quad (1.101)$$

The new quantity  $N(\theta) = \mathcal{F}(I, \theta)/I$  is called the *winding function* and is frequently employed in the analysis of ac machines.

The field representation of stored energy can also be used to calculate mutual inductance. When  $B$  and  $H$  arise from currents in two different circuits,

$$W_m = \frac{1}{2} \int_V (\mathbf{B}_1 + \mathbf{B}_2) \cdot (\mathbf{H}_1 + \mathbf{H}_2) dV \quad (1.102)$$

However, it is also true from circuit theory that

$$W_m = \frac{1}{2} L_1 I_1^2 + L_{12} I_1 I_2 + \frac{1}{2} L_2 I_2^2 \quad (1.103)$$

Comparing Eqs. (1.102) and (1.103), the terms involving the mutual inductance can be equated whereupon,

$$L_{12} I_1 I_2 = \frac{1}{2} \int_V (\mathbf{B}_1 \cdot \mathbf{H}_2 + \mathbf{B}_2 \cdot \mathbf{H}_1) dV \quad (1.104)$$

When the  $B$ 's and  $H$ 's are colinear, exist only in the gap and are only a function of  $\theta$ , Equation (1.104) clearly reduces to

$$L_{12} = \mu_o \frac{rl}{g} \int_0^{2\pi} N_1(\theta) N_2(\theta) d\theta \quad (1.105)$$

where,  $(B_1/\mu_o)g = H_1 g = \mathcal{F}_1$ ,  $(B_2/\mu_o)g = H_2 g = \mathcal{F}_2$  and

$$N_1(\theta) = \frac{\mathcal{F}_1(\theta)}{I_1}; \quad N_2(\theta) = \frac{\mathcal{F}_2(\theta)}{I_2}$$

When the flux density produced by one of the two windings is known the following expression for  $L_{12}$  is also convenient.

$$L_{12} = \frac{rl}{I_1 V} \int B_1(\theta) \cdot N_2(\theta) d\theta \quad (1.106)$$

## 1.18 The Problem of Units

One of the facts of life concerning electromagnetic design of an electric machine is inconsistency regarding physical units. This inconsistency is a consequence of the long history associated with this discipline. In practice three unit systems are used based around the MKS (or SI) system (Europe and elsewhere), the CGS unit system (small transformers, permanent magnet or PM machines and small subfractional horsepower (HP) machines) and the English unit system (fractional HP machines and above in the U.S.). The English unit system is a throw back to our use of inches and pounds whereas the CGS system came into use via the physicists. Clearly, the MKS system is the unit system for the future. However, in view of the tremendous work done in the past incorporating the other unit it is important to be equally familiar with all three sets of units.

In this course we will typically derive a particular relationship using SI units and then convert the result, if desired, to the other units. As an example, consider the *constituent equation* for magnetic materials.

$$B(w/m^2) = \mu_r \mu_o (h/m) H(A/m) \quad (1.107)$$

Multiplying this equation by  $10^4$  and substituting explicitly for  $\mu_o$

$$10^4 B(w/m^2) = \mu_r [4\pi \cdot 10^{-3} H(A/m)] \quad (1.108)$$

If we define

$$B(g) = 10^4 B(w/m^2) \quad (1.109)$$

and

$$H(oe) = 4\pi \cdot 10^{-3} H(A/m) \quad (1.110)$$

then in CGS units

$$B(g) = \mu_r H(oe) \quad (1.111)$$

where the new units of  $B$  and  $H$  are the gauss and the oersted respectively.

Consider now the possibility of converting this equation to English units. Let us multiply Eq. (1.107) by  $10^8$ . The result is

$$10^8 B(w/m^2) = 10^8 \mu_r \mu_o (h/m) H(A/m) \quad (1.112)$$

We will define a new unit of flux called the maxwell or line such that

$$1 \text{ weber} = 10^8 \text{ lines or maxwells} \quad (1.113)$$

Making this substitution in Eq.(1.112), and explicitly substituting for

$$B\left(\frac{\text{lines}}{m^2}\right) = \mu_r (40\pi) H(A/m) \quad (1.114)$$

Now

$$B\left(\frac{\text{lines}}{m^2}\right) = B\left(\frac{\text{lines}}{in^2}\right) \left(\frac{1 \text{ in}}{2.54 \text{ cm}}\right)^2 \left(\frac{100 \text{ cm}}{m}\right)^2 \quad (1.115)$$

and

$$H(A/m) = H(A/(in)) \left(\frac{1 \text{ in}}{2.54 \text{ cm}}\right) \left(\frac{100 \text{ cm}}{m}\right) \quad (1.116)$$

so that in the English system,

$$B\left(\frac{\text{lines}}{in^2}\right) = \mu_r 40\pi \left(\frac{2.54}{100}\right)^2 \left(\frac{100}{2.54}\right) H\left(\frac{A}{in}\right)$$

$$B\left(\frac{\text{lines}}{in^2}\right) = \mu_r \left(\frac{4\pi}{10}\right) 2.54 H\left(\frac{A}{in}\right) \quad (1.117)$$

The quantity  $(4\pi/10)2.54 = 3.192$  is sometimes called the "free space" permeability in the English system.

A similar development can be carried out for the magnetic circuit equation, Eq. (1.83), that is

$$\Phi(\text{web}) = \mathcal{P}(\text{henries}) \mathcal{F}(A \cdot t) \quad (1.118)$$

Multiplying both sides by  $10^8$  and making use of Eqs. (1.113) and (1.80)

$$\begin{aligned}\Phi(\text{lines}) &= (10^8)(4\pi \cdot 10^{-7})\mu_r \frac{A(m^2)}{l(m)} \mathcal{F}(A \cdot t) \\ &= 40\pi\mu_r \mathcal{F}(A \cdot t) \frac{A(m^2)}{l(m)}\end{aligned} \quad (1.119)$$

Now

$$A(m^2) = A(cm^2) \left( \frac{1m}{100cm} \right)^2$$

$$l(m) = l(cm) \left( \frac{1m}{100cm} \right)$$

so that Eq. 1.40 becomes

$$\Phi(\text{lines}) = 0.4\pi\mu_r \frac{A(cm^2)}{l(cm)} \mathcal{F}(A \cdot t) \quad (1.120)$$

In the CGS system the gilbert is defined as

$$\mathcal{F}(\text{gilberts}) = 0.4\pi \mathcal{F}(A \cdot t)$$

so that in the CGS system the magnetic circuit equation, Eq. (1.120), becomes

$$\Phi(\text{maxwells}) = \mu_r \frac{A(cm^2)}{l(cm)} \mathcal{F}(\text{gilberts}) \quad (1.121)$$

In the English system we must convert lengths to inches,

$$\Phi(\text{maxwells}) = \frac{(0.4\pi)\mu_r A(in^2)}{(2.54)l(in)} \mathcal{F}(A \cdot t) \quad (1.122)$$

The key equations in magnetic circuit analysis in the three systems are summarized in the Table 1.1. The reader should get to know these equations well. In order to help sort out the various conversion factors between the three systems, "flow charts" for the important variables are provided in Figure 1.11.

Constit. Eq.	MKS (SI) Units	CGS Units	English Units
	$B = \mu_o \mu_r H$	$B = \mu_r H$	$B = \mu_o \mu_r H$
Magnetic Ohm's Law	$\Phi = \mu_o \frac{\mu_r A}{l} \mathcal{F}$	$\Phi = \frac{\mu_r A}{l} \mathcal{F}$	$\Phi = \mu_o \frac{\mu_r A}{l} \mathcal{F}$
Faraday's Law	$v = N \frac{d\Phi}{dt}$	$v = N \frac{d\Phi}{dt} \cdot 10^{-8}$	$v = N \frac{d\Phi}{dt} \cdot 10^{-8}$
Free Space Permeability	$\mu_o = 4\pi \cdot 10^{-7}$	$\mu_o = 1$	$\mu_o = \frac{4\pi}{10} \cdot 2.54$ $= 3.192$
	$B$ in webers/m <sup>2</sup> $H$ in A.turns/m $\Phi$ in webers $\mathcal{F}$ in A.turns	$B$ in gauss $H$ in oersteds $\Phi$ in lines(maxwells) $\mathcal{F}$ in gilberts	$B$ in lines/in <sup>2</sup> $H$ in A.turns/in $\Phi$ in lines $\mathcal{F}$ in A.turns

TABLE 1.1. Comparison of magnetic circuit equations with various systems of units

## 1.19 Magnetic Paths Wholly in Iron

The analogies between the electric circuit and the magnetic circuit seem to indicate, upon first consideration, that the Ohm's law type of relationship among *MMF*, flux and reluctance or permeance ought to provide a straightforward method for solving magnetic circuit problems. However, the problem is much more difficult than the simple examples thus far considered. The direct application of the method is made difficult in practice by the relatively large flux leakage encountered in magnetic circuit problems and by the dependence of the reluctance of a ferromagnetic material upon the flux density, i.e., the problem is nonlinear.

In general solution of magnetic circuit problems are solved to resolve two key questions: (a) the determination of the *MMF* required to produce a desired flux or flux density in a specified part of a structure, (b) the determination of the flux or flux density produced at specified places in a magnetic structure

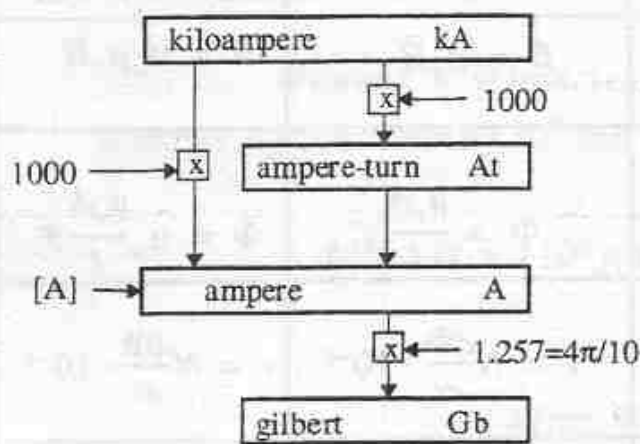
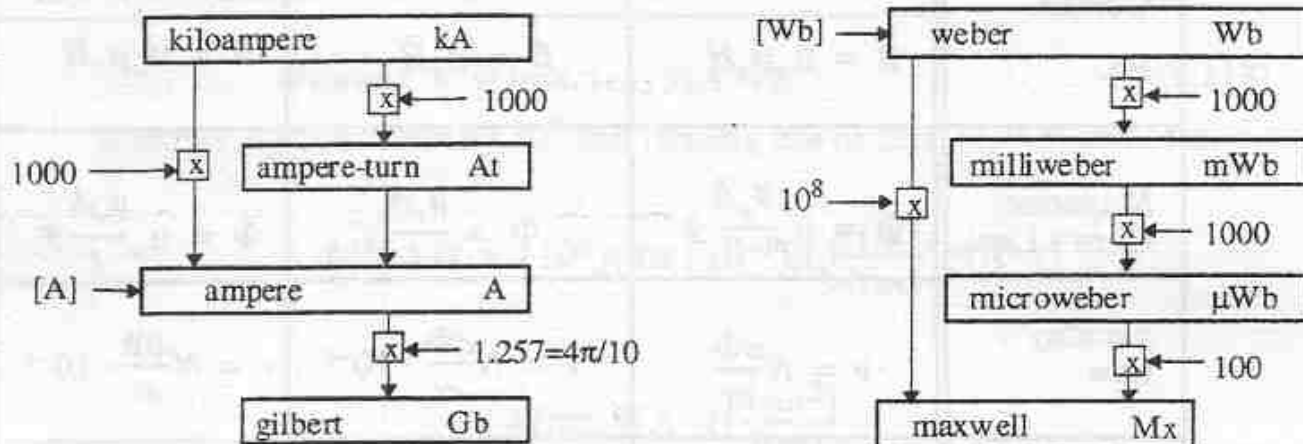
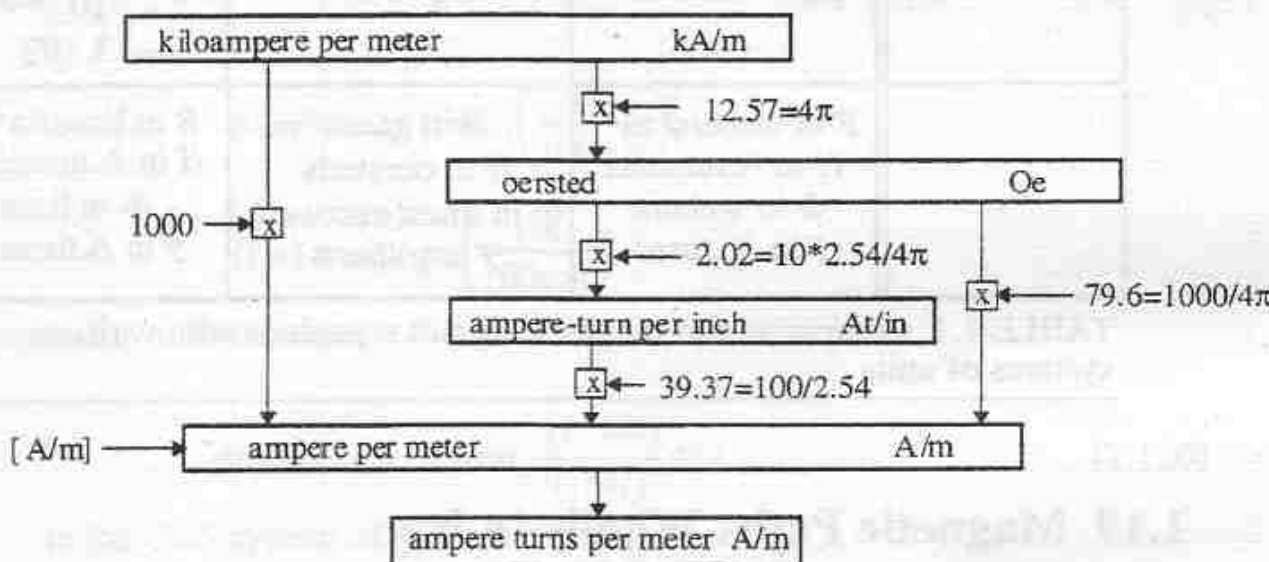
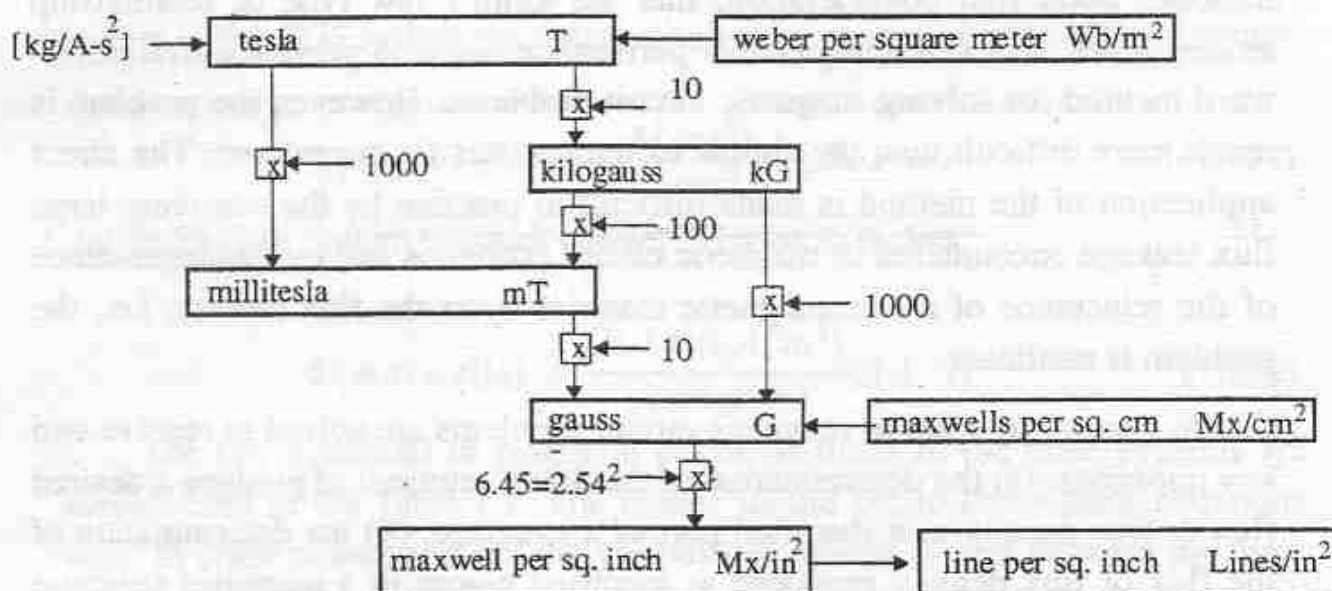
**MAGNETOMOTIVE FORCE****MAGNETIC FLUX****MAGNETIC FIELD STRENGTH****MAGNETIC FLUX DENSITY**

Figure 1.11 Conversion factors for magnetic field quantities

brought about by *MMFs* impressed at various places throughout the structure. Strictly speaking, the magnetic circuit method of analysis does not yield flux densities except as averages of total fluxes over the cross-sectional areas of the circuit, the exact determination of the flux distribution is a field problem.

When the problem is to determine the *MMF* required to produce a desired total flux or flux density, that is, the calculation as in (a) the procedure is direct, provided that the leakage flux is neglected or estimated. In each portion of a series magnetic path having a cross-sectional area  $A$ , the average value of flux density  $B$  is equal to the ratio of the total flux  $\Phi$  to the area  $A$ . The value of magnetizing force  $H$  required to establish this value of  $B$  is determined as a curve of  $B$  plotted as a function of  $H$  for the particular material. This value of  $H$  is then multiplied by the length of that portion of the path for which  $B$  is assumed constant, to give the magnetic potential difference  $\mathcal{F}_{ab}$  between the ends of that portion of the path, that is

$$\mathcal{F}_{ab} = Hl_{ab} \quad (1.123)$$

where the distance  $a$  to  $b$  is the length of path of uniform material and cross-sectional area. If the path includes portions of different kinds of ferromagnetic material, the value of  $H$  for each material is multiplied only by the length of path in that material to give the magnetic potential difference for that portion of the path. The sum of the magnetic potential differences for all such portions of paths  $a-b$ ,  $b-c$ ,  $c-d$  etc. taken around the series circuit gives the total *MMF* required, that is

$$\mathcal{F} = \mathcal{F}_{ab} + \mathcal{F}_{bc} + \mathcal{F}_{cd} + \dots + \mathcal{F}_{na} \quad (1.124)$$

If the construction of the circuit is such that the average flux density differs markedly from the extremes of flux density on the cross-sectional more elaborate magnetic circuits must be employed.

When the problem is to determine the total flux or flux density produced by *MMFs* impressed at various places, that is, the calculation as in (b) above, the procedure is not so straightforward even if leakage fluxes are neglected. In certain simple combinations of paths, graphical methods are applicable. These are illustrated in the examples to follow. In complicated combinations of paths, a successive-approximation methods leads rapidly to a solution. For such problems the *MMF* required to produce an assumed value of flux  $\Phi_1$ , is first calculated. If the calculated *MMF* does not approach the assumed impressed value

within limits, a second trial value  $\Phi_2$  is chosen, greater or less by the amount required to equal the magnetic potential drop produced by the assumed flux  $\Phi_1$ . After a few iterations a solution is easily obtained. A Newton-Raphson iteration procedure using a digital computer is convenient for this purpose.

## 1.20 Magnetic Materials

Historically, electric motors have been constructed from magnetic steels usually in the form of thin laminations, electrical conductors (either copper or aluminum), insulation for the conductors and slots, high tensile strength steel for shafts and steel or copper alloys for bearings. The laminations used in most general purpose motors have been "common iron" or low carbon steel. Although low in cost, this material typically produces machines of only modest efficiency. More recently, high efficiency motors often feature higher quality silicon steels at a correspondingly higher cost. The percent of silicon in the steel has a beneficial effect in reducing losses in the steel but at the same time tends to reduce the saturation flux density. The percent of silicon in motor steels typically range from 1% to 3.25%. The corresponding losses range from 0.6 watt per pound of core for the 3.25% steel to 1.0 watt per pound for the 1% silicon steel at a flux density of 15,000 gauss (1.5 tesla). Nickel alloys, such as permalloy, have low losses but are very expensive and have low saturation flux density. The cobalt alloys such as Supermendur (49% iron, 49% cobalt and 2% vanadium) have peak flux densities over 20,000 gauss, but are also very expensive (\$7 to \$8 per pound) and have higher losses.

When the magnetic structure is assembled by means of stacking laminations punched from thin sheet material, the volume occupied by the stacked laminations does not truly represent the volume of iron that supports the magnetic flux. A region whose permeability is that of air exists between the laminations because of the presence of irregularities in the laminations or due to a thin coat of insulating varnish applied to avoid circulating current flow between laminations (eddy currents). In order to allow for this effect, the effective cross-sectional area of iron is equal to the cross-sectional area of the stack times a factor called *the stacking factor*. The stacking factor, defined as the ratio of the cross sectional area of the iron to the cross sectional area of the stack, ranges between about 0.95 and 0.90 for lamination thickness between 0.025 inch and 0.014 inch (25 and 14 mil) respectively. For thinner laminations, for example 1 mil to 5 mil thick, the stacking factor can be in the range

of 0.4 to 0.75. Thinner laminations than 14 mil are generally not used unless iron loss is a severe problem. This choice typically occurs when the machine operates at high frequencies, for example an aircraft generator.

A new group of alloys has already been developed grouped under the generic title of amorphous metal alloys. These materials represent a new state of matter for electromagnetic materials, the so called amorphous or non-crystalline state. Ordinary window glass is a typical example of an amorphous material. Some of these new amorphous alloys have magnetic properties which surpass the properties of conventional alloys. Thus, they appear to be a potentially useful new class of soft magnetic material. These alloys contain about 80% ferritic elements such as iron, nickel and cobalt, and 20% glasseous elements such as silicon, phosphorous, boron, and carbon. A good example of an amorphous alloy having 80% iron and 20% boron by atomic weight is Fe80B20 (Allied Chemical's *Metglass*). Major advantages of amorphous metal include low cost (0.30 per pound vs. 0.50 for silicon steel), very low core loss (one fifth that of the best silicon steels), low annealing temperature and high tensile strength. Unfortunately, this new material has not yet been successfully used in a large scale because the high tensile strength also makes the material difficult to punch. Also, amorphous materials are presently only available in thicknesses of 1 to 2 mils (0.001" to 0.002") which results in a poor stacking factor and creates problems during assembly.

## 1.21 Example 1.2

The magnetic structure shown in Figure 1.12 is similar to that of a core type transformer. The core is made of 29 gage (14 mil) fully processed steel. The  $B$ - $H$  curve for this material is shown in Figure 1.13. The sheets are stacked into a 3 inch stack. The stacking factor is 0.91. The exciting winding has 200 turns. Compute the current required in the exciting winding to produce a maximum core flux density of 1.2 Tesla. Leakage flux is to be neglected.

*Solution.*

The cross-sectional area of the iron portion of legs  $x$  is  $2 \times 3 \times 0.91 = 5.46 \text{ in}^2$  and of the legs  $y$  is  $1.5 \times 3 \times 0.91 = 4.1 \text{ in}^2$ .

- The maximum flux density will clearly occur in the  $y$  member having the smallest cross section. If  $B_y = 1.2 \text{ Tesla}$  then in the  $x$  leg  $B_x = 1.2 \times 4.1 / 5.46 = 0.9 \text{ T}$ .

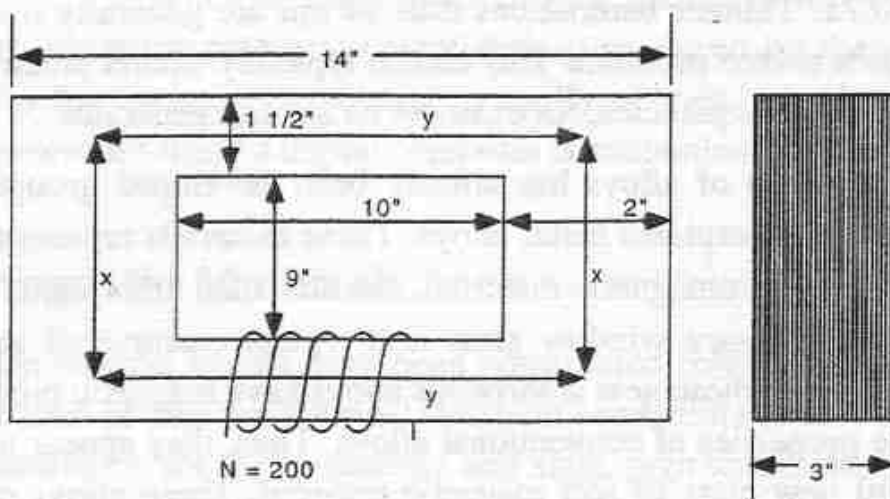


Figure 1.12 Core type transformer structure with two different cross-sectional areas

- From Figure 1.13 the magnetizing force is  $2.9 \text{ Oe}$  or  $5.8 \text{ A.t/in}$  for legs  $y$  and  $1.4 \text{ Oe}$  or  $2.85 \text{ A.t/in}$  for legs  $x$ .
- The mean length of the flux paths in Figure 1.12 is estimated as  $21 \text{ in}$  for the two  $x$  legs and  $24 \text{ in}$  for the two  $y$  legs.
- The sum of the  $MMFs$  acting on the two  $y$  legs is  $5.8 \times 24 = 140 \text{ A.t.}$  and for the  $x$  legs  $2.85 \times 21 = 60 \text{ A.t.}$  The total ampere-turns for the entire magnetic circuit is therefore  $140 + 60 = 200 \text{ A.t.}$
- The excitation current required to produce a flux density of  $1.2 \text{ T}$  in the transformer core is thus  $200/200 = 1.0 \text{ A.}$
- The flux in the core is clearly  $\Phi = B_y \times A_y = 1.2 \times 3 \times 1.5 \times 0.91 \times (0.0254)^2 = 3.17 \text{ mWb}$
- The saturated inductance is then  $L = N\Phi/i = 200 \times 3.17 \times 10^{-3} / 1.0 = 0.63 \text{ H}$

When a specified  $MMF$  acts on a core, the inverse problem of calculating the fluxes is not simple. Let us assume that the results of the previous calculations is not known and that the core is excited with  $200 \text{ A.t.}$  In this case it is necessary to estimate the probable magnetic potential difference between the ends of each core portion.

- Since the cross-sectional area of the  $y$  legs is much smaller than that of the  $x$  legs, the flux density is much larger in the  $y$  legs and would consume the major part of the  $MMF$  drop. As a first approximation, all the  $MMF$  is assumed to drop along the  $y$  legs. The resulting potential gradient is therefore  $200/24 = 8.3 \text{ A.t./in}$  or  $4.1 \text{ Oe}$ .

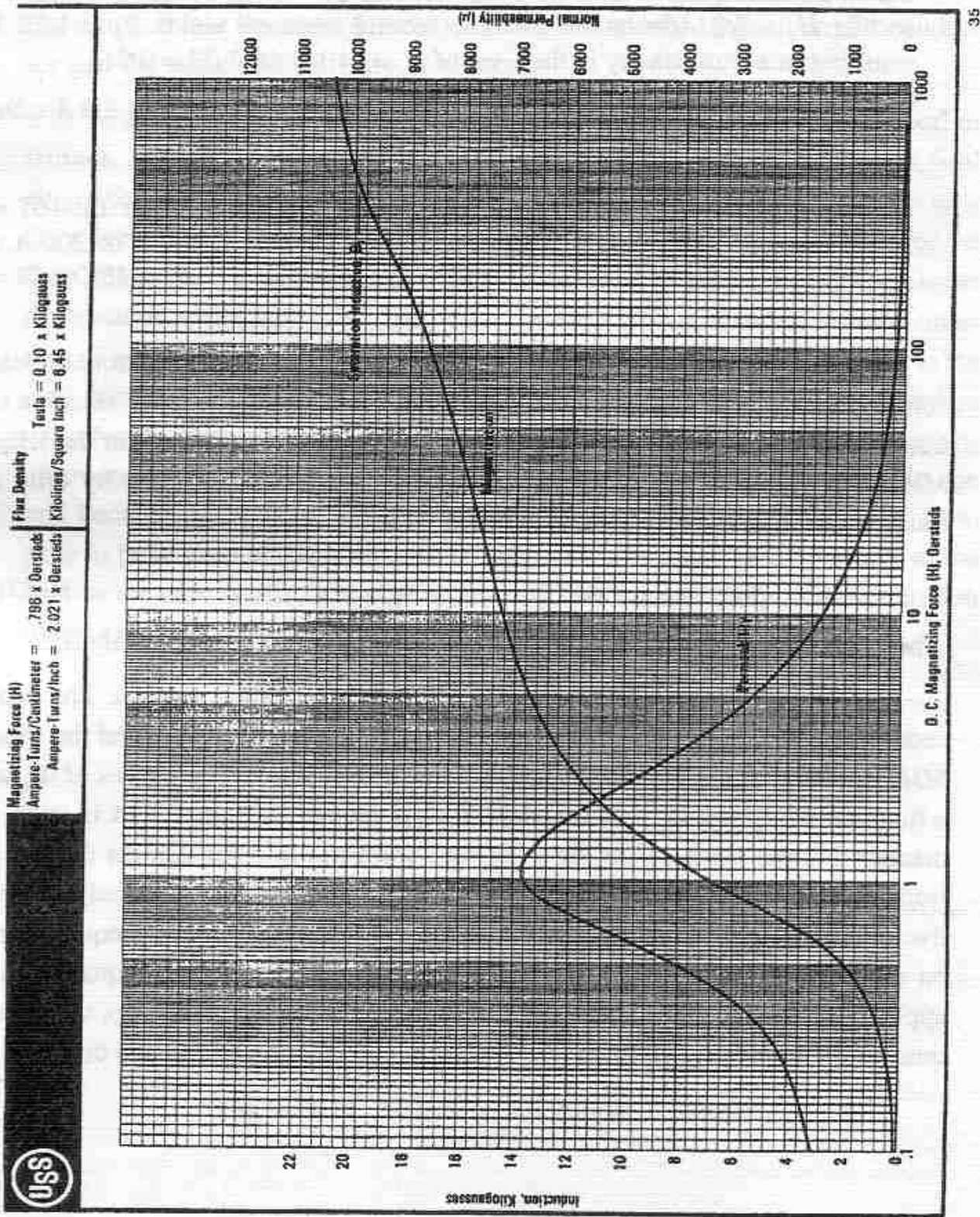


Figure 1.13 B-H curves for 29 Gage M27 fully processed steel

- From Figure 1.13 the flux density in the  $y$  legs is then about  $1.3\text{ T}$ . By proportionality, the flux density in the  $x$  legs is  $(4.1/5.46)1.3 = 0.97\text{ T}$ . Again from Figure 1.13 the  $x$  legs require an  $MMF$  of  $1.6 \times 2.021 \times 21 = 68\text{ A.t.}$  The  $MMF$  required by the entire circuit is  $200 + 68 = 268$  which is, of course, too much  $MMF$  to satisfy Ampere's Law.
- As a second approximation the  $MMF$  drops in the  $x$  and  $y$  legs can be estimated by taking ratios. For the  $y$  legs assume  $\mathcal{F}_y = (200/268)200 = 149\text{ A.t.}$  so that  $H_y = 6.2\text{ A/in}$  or  $3.1\text{ Oe}$ . The second iteration yields  $B_y = 1.22\text{ T}$  resulting in a flux density in the  $x$  leg of  $B_x = (4.1/5.46)1.22 = 0.91$ .
- The corresponding field intensity in the  $x$  leg becomes  $1.45\text{ Oe}$  or  $2.9\text{ A.t./in.}$
- The  $MMF$  drop in the  $x$  legs of  $2.9 \times 21 = 61\text{ A.t.}$
- The total  $MMF$  drop around the circuit is now estimated to be  $149 + 61 = 210\text{ A.t.}$  which is now just slightly greater than the correct value of  $200\text{ A.t.}$  As a third iteration it is now possible to assume that  $\mathcal{F}_y = (149/210)149 = 106\text{ A.t.}$

Note that the method oscillates about the correct solution. But nonetheless converges rapidly if implemented on a digital computer since the  $B-H$  curve is a simple monotonically increasing function. The iteration method for the  $y$  leg  $MMF$  can be made less oscillatory by changing the new estimate by only a fraction of the error from the last iteration by using the algorithm,

$$\mathcal{F}_i = \mathcal{F}_{i-1} + \lambda(\mathcal{F}_{i-1(calc)} - \mathcal{F}_{i-1}) \quad (1.125)$$

The quantity  $\lambda$  is an acceleration factor which can be taken as roughly 0.5.

For simpler problems one can also resort to a graphical method. The procedure is to first determine the relationship between the total flux and the total  $MMF$  for each of the two nonlinear portions of the circuit. The curves of  $\Phi_x$  as a function of  $\mathcal{F}_x$  and  $\Phi_y$  as a function of  $\mathcal{F}_y$  is plotted in Figure 1.14 in such a manner that the abscissa for the  $x$  leg runs from left to right and for the  $y$  leg from right to left. The plot for the  $y$  legs, turned end for end, is called a negative magnetization curve and its origin is put at the point where  $\mathcal{F}$  equals 200 on the plot for the  $x$  legs. The point 200 is chosen because it is equal to the applied  $MMF$ . Since the same total flux is present in both legs  $x$  and  $y$ , the solution for the impressed value of  $200\text{ A.t.}$  is the intersection of the two curves.

## 1.22 Magnetic Circuits with Air Gaps

Because electrical machines involve magnetic circuits in relative rotation an air gap must exist between the stator and rotor. In addition other air gaps frequently occur because of limitations inherent in the construction. Air gaps are often introduced into iron-core inductors in order to make the inductance of the element essentially independent of the current in the coil throughout its working range, but at the same time to make the inductance larger than if the inductor had the same coil and only an air core.

When an air gap is inserted in a magnetic circuit, the flux spreads out, or fringes, around the gap as shown by the sketch of Figure 1.15 and the flux density in the gap assumes a nonuniform distribution. The flux that terminates near the edges of the gap is called the fringing flux. Because of the spreading of the flux, the apparent reluctance of the gap is not that of an air space of the same dimensions as the gap. Since the permeability of iron is several thousand times that of air the reluctance of even a short air gap is usually large compared to the iron portion of the circuit. Relatively large magnetic potentials may therefore exist between iron parts not immediately near the gap. For example, in a synchronous machine the main flux that traverses the gap fringes at the pole tips and because of the large reluctance of the air gap considerable flux goes from pole to pole, pole leakage flux. This flux is often as much as 25 per cent of the flux in the core of the field pole and contributes considerably to the saturation of the pole body.

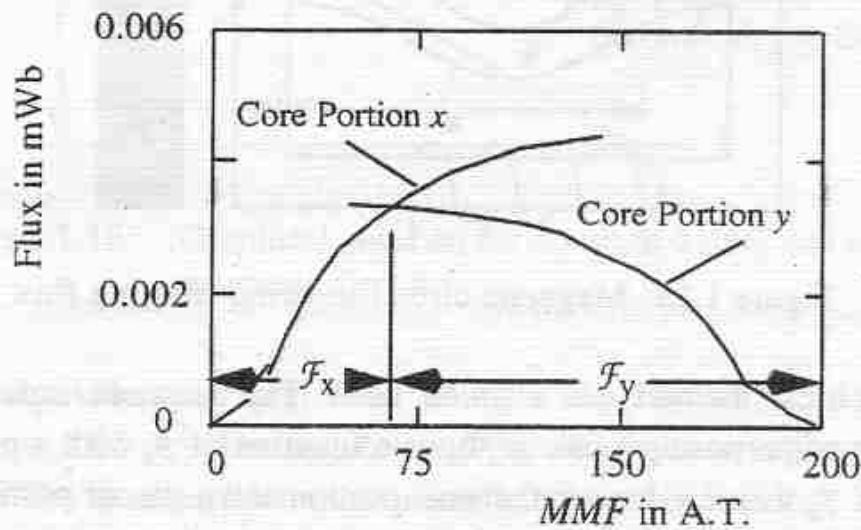


Figure 1.14 Graphical solution of Example 1.2

When the air gap is short compared with its cross-sectional dimensions and has parallel faces, the fringing effect can be incorporated into the analysis by the use of simple correction factors. If the cross-sectional dimensions of the core are the same on both sides of the gap, the equivalent gap is assumed to have a length  $g$  equal to the actual air gap, but to have an equivalent cross-sectional area

$$A = (a + g)(b + g) \quad (1.126)$$

where  $a$  and  $b$  are the cross-sectional dimensions of the core faces. If one of the faces of the gap has a cross-sectional dimension much larger than the corresponding dimensions of the other, a correction of  $2g$  should be used. Experience has shown that these rules give satisfactory results if the correction applied does not exceed about 1/5 of the physical cross-section.

If the total *MMF* applied is known a successive approximation solution can again be used. The first approximation can be obtained by considering that all the ampere-turns are required to overcome the reluctance of the air gap. A

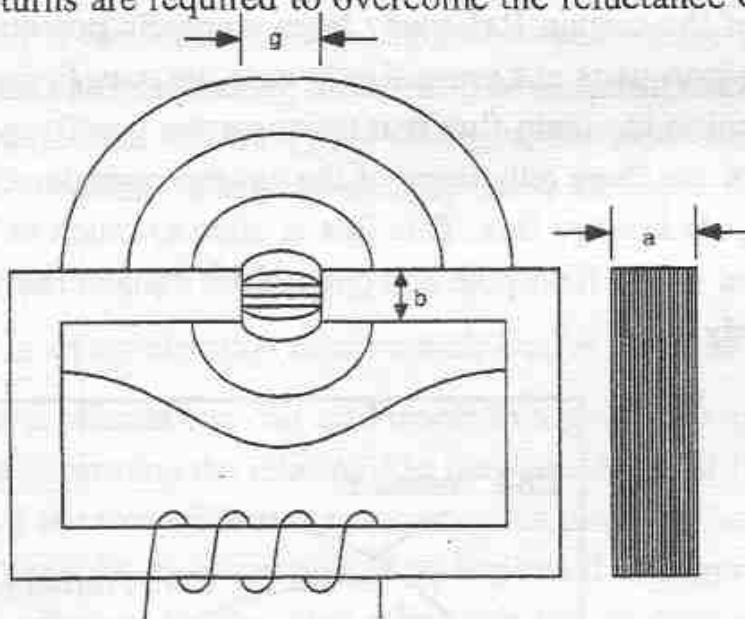


Figure 1.15 Magnetic circuit showing fringing flux

direct graphical method can also be used. The required solution is again obtained by superposing a plot of  $\Phi_s$  as a function of  $\mathcal{F}_s$  with a plot of  $\Phi_a$  as a function of  $\mathcal{F}_a$  where  $s$  denotes the steel portion and  $a$  the air portion of the flux path. The construction is shown in Figure 1.16 where  $\mathcal{F}_t$  denotes the total impressed *MMF*. Note that the ordinate intersection of the air gap line is readily determined since

$$\Phi_a = \frac{\mathcal{F}_a}{R_a} = \frac{\mu_0 A}{g} \mathcal{F}_a \quad (1.127)$$

The intersection of the negative air gap line with the saturation characteristic of the steel for all values of  $\mathcal{F}_t$  will generate the flux vs. *MMF* characteristics for the overall device, i.e., the “sat curve”. The net saturation curve can be readily visualized as the sum of the iron and air saturation curves at each value of flux. Figure 1.18 shows such a construction.

### 1.23 Example 1.3

A magnetic structure similar to Figure 1.15 is made of 29 gage sheet steel laminations 0.014 in. thick stacked 2 in. thick. Dimension  $b$  is 2.5 in. The air gap length  $g$  is 0.10 in. The mean length of the steel part of the circuit is 30 in. Find the resultant flux if the applied *MMF* is 1400 A.t.

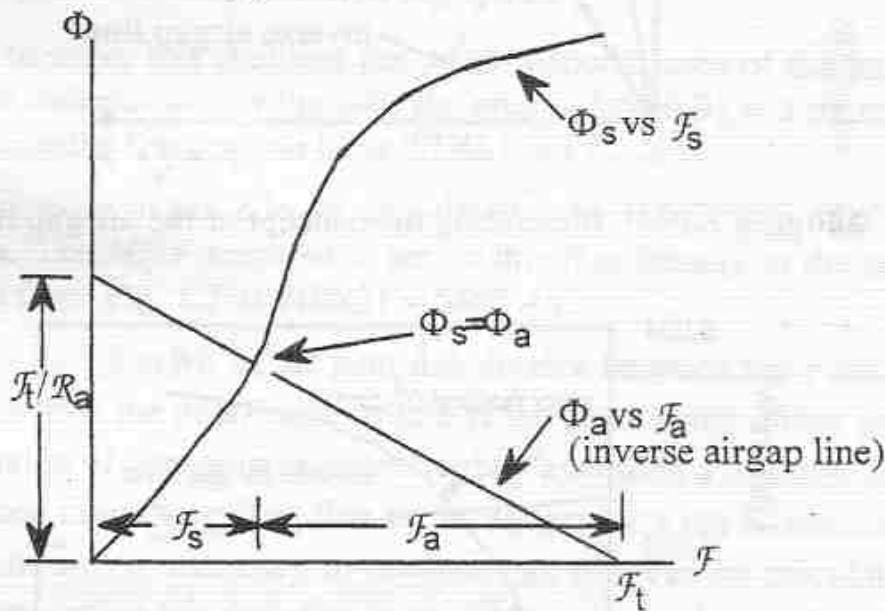


Figure 1.16 Graphical solution for combined steel and air magnetic circuit

The equivalent air gap area, using a 2g correction is  $(2.0 \times 0.91 + 0.2)(2.5 + 0.2) = 5.45 \text{ in}^2$ . The negative air gap line intersects the abscissa at  $\mathcal{F} = 1400 \text{ A.t}$ . The intersection on the ordinate is found by solving

$$\phi_a = (\mu_0) \frac{A}{l} \mathcal{F}_a \quad (1.128)$$

or

$$\Phi_a = 4\pi \cdot 10^{-7} \left( \frac{5.45}{0.1} \right) \frac{1}{39.37} (1400) = 2.44 \text{ mWb} \quad (1.129)$$

The saturation curve for the iron is found by neglecting the MMF drop of the gap. A plot of the steel saturation curve and the negative air gap line is shown in Figure 1.18. The point of intersection of the two curves is read as 2.2 mWb.

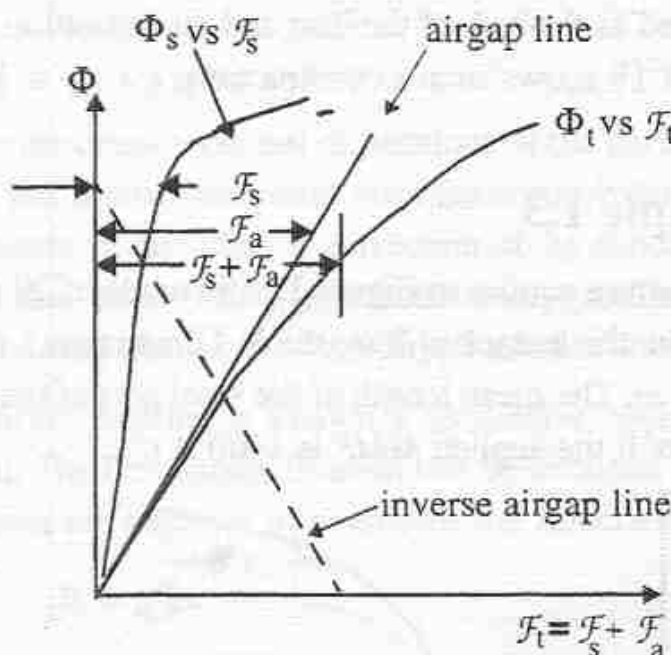


Figure 1.17 Illustrating the concept of the air gap line

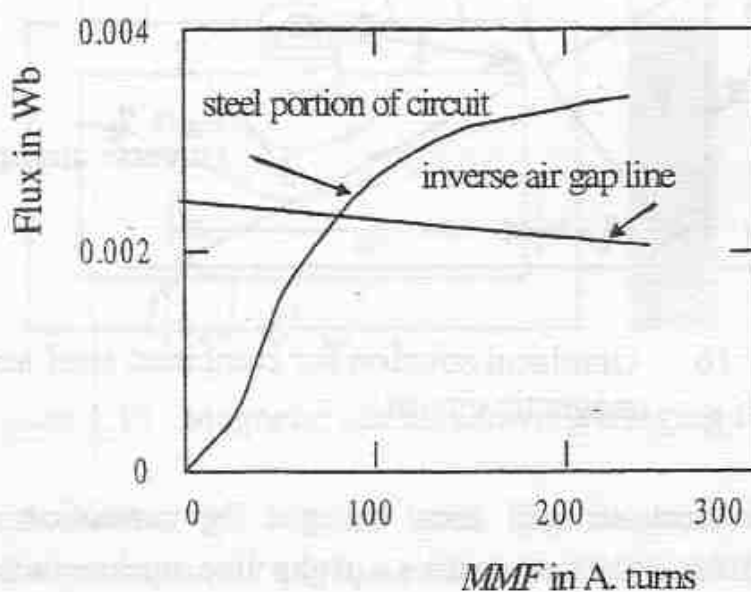


Figure 1.18 Graphical solution of Problem 1.3

## 1.24 Example 1.4 Calculation for Series-Parallel Iron Paths

A type of core construction used frequently for certain transformers in which a relatively small magnetic coupling between primary and secondary coils is desired is shown in Figure 1.19. This type of geometry will also be used in our subsequent analysis of a machine for calculating the flux entering the core through both the tooth and the slot. Because of the non-linearities of the core material the fraction of the total flux by-passed through the leg  $y$  varies with the amount of magnetic saturation.

For illustration, assume a flux of  $3.8 \text{ mWb}$  is set up in the leg  $x$  by a coil wound around this leg. The ampere-turns required is to be calculated. The magnetic material is again fully processed steel, 14 mil thick. The stacking factor is 0.91. The paths  $axb$  and  $azb$  are assumed to have a mean length of 21 in. The mean length of core in the center leg is 8 in.

- In order to solve this problem the cross-sectional area of the core and air gap is first calculated. For the core the area is  $2 \times 2 \times 0.91 = 3.64 \text{ in}^2$ . For the air gap including fringing we have  $2.1 \times 2.1 = 4.41 \text{ in}^2$ .
- The flux density in the  $x$  leg is calculated to be  $0.00380 / (3.64 \times 0.0254^2) = 1.62 \text{ Tesla}$ . The MMF required to set up this flux density in the path  $axb$  is calculated from Fig. 1.7 as  $260 \times 21 = 5462 \text{ A.t.}$

The total flux of  $3.8 \text{ mWb}$  in the path  $axb$  divides between the  $z$  and  $y$  legs in such a manner that the MMF from  $a$  to  $b$  is the same using either path  $azb$  or  $ayb$ . The division of flux must be calculated by assuming a tentative flux distribution and then correcting. The flux in the air gap or  $y$  leg is assumed so that the MMF from  $a$  to  $b$  necessary to produce this flux can be calculated. Since this MMF also acts on leg  $z$  the flux in the  $z$  leg is now calculated and added to the flux assumed to exist in the  $y$  leg. The result is compared to the assumed total value of flux and if the result differs the amount of flux assumed in the air gap is corrected accordingly. The procedure continues iteratively until convergence occurs.

- For example, let us assume that  $0.80 \text{ mWb}$  of flux exists in the  $y$  leg of the transformer. The corresponding value of flux density in the  $y$  leg iron is  $0.00080 / (3.64 \times 0.0254^2) = 0.34 \text{ Tesla}$ . Since this is a relatively small value of flux density the MMF drop in the iron can be neglected relative to the drop in the air.

- The MMF consumed in the air gap is from Eq. (1.83) as  $(0.0008)(0.1)/(2+0.1)^2 = 568 \text{ A.t}$ . This MMF drop acts on the z leg producing a magnetizing force of  $568/21 = 27 \text{ A.t./in}$  which from the data of Figure 1.13 establishes a flux density of 1.47 Tesla.
- The corresponding flux in the z leg is then  $(1.47)(3.276)(0.0254^2)$  or 3.1 mWb. The total flux in the two legs is 3.9 mWb which is somewhat more than the specified value of 3.8 mWb.
- If necessary, a second trial is now made using the value  $0.8 \times 3.8 / 3.9 = 0.78$  as the value of flux assumed to flow in the y leg. The procedure proceeds iteratively to about 0.72 mWb in the y leg and 3.08 mWb in the z leg.
- The MMF drop in the y leg is now computed to be 511 A.t resulting in a total MMF drop around the path xaybx corresponds to the ampere turns required to produce 3.8 mWb in the x leg, namely  $\text{MMF} = 5462 + 511 = 5973 \text{ A.t.}$

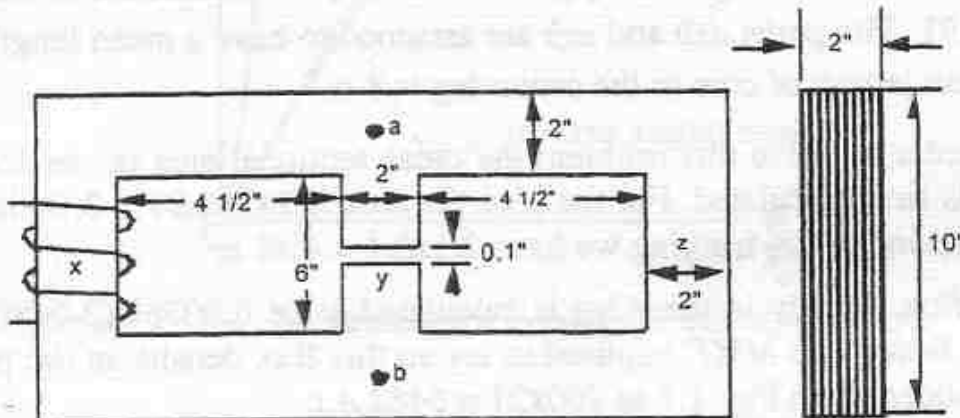


Figure 1.19 Magnetic circuit with series-parallel paths

## 1.25 Multiple Winding Magnetic Circuits

In many cases the magnetic circuit includes the effect of two or more sources of MMF. This was, for example, the case when we examined the transformer of Section 1.14. This is also typically the case in many electrical machines which have not only a excitation component but also a separate load component typically on different members of the machine. When the iron is allowed to saturate the problem not now so simple.

The basic issue can be demonstrated by the simple electromagnet shown in Figure 1.20. This device can be represented by the equivalent magnetic circuit shown in Figure 1.21. In this case the MMF drop from point a to point b can be written in terms of three equations, namely

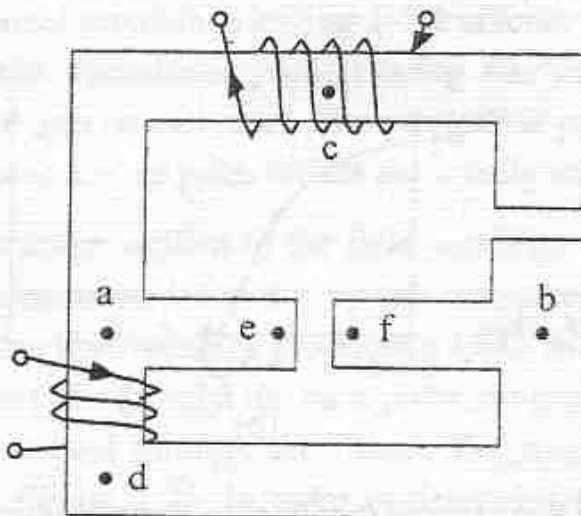


Figure 1.20 Electromagnetic with two sources of excitation

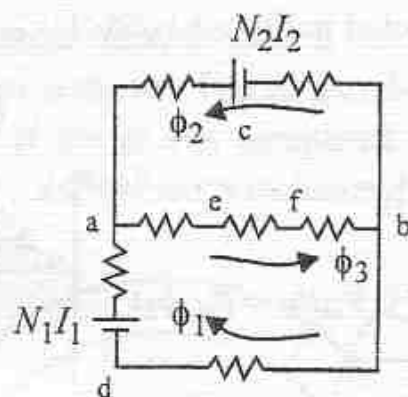


Figure 1.21 Equivalent magnetic circuit of Figure 1.20

$$\mathcal{F}_{ab}(\phi_1) = N_1 I_1 - \mathcal{R}_{adb}(\phi_1) \phi_1 \quad (1.130)$$

$$\mathcal{F}_{ab}(\phi_2) = N_2 I_2 - \mathcal{R}_{acb}(\phi_2) \phi_2 \quad (1.131)$$

$$\mathcal{F}_{ab}(\phi_3) = \mathcal{R}_{defb}(\phi_3) \quad (1.132)$$

where

$$\phi_1 + \phi_2 = \phi_3 \quad (1.133)$$

Three *MMF* vs. flux curves can be constructed as shown in Figure 1.22.

Clearly,  $\mathcal{F}_{ab}(\phi_1) = \mathcal{F}_{ab}(\phi_2)$ . If both  $\phi_1$  and  $\phi_2$  are plotted versus  $F_{ab}$  then the flux  $\phi_3$  can be determined for every value of  $\mathcal{F}_{ab}$ . The resulting con-

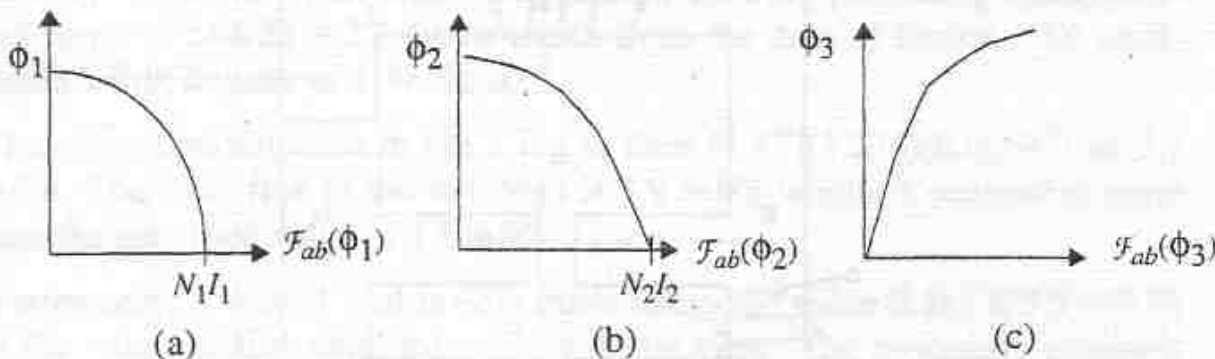


Figure 1.22  $MMF$  vs. flux curves for the three magnetic paths (a) lower member, (b) upper member, (c) middle member

construction is shown in Figure 1.23(a). The actual solution is the point where the  $MMF$  as determined by this curve matches the  $MMF$  as determined by the function  $F_{ab}(\phi_3)$  as computed in Figure 1.22(c).

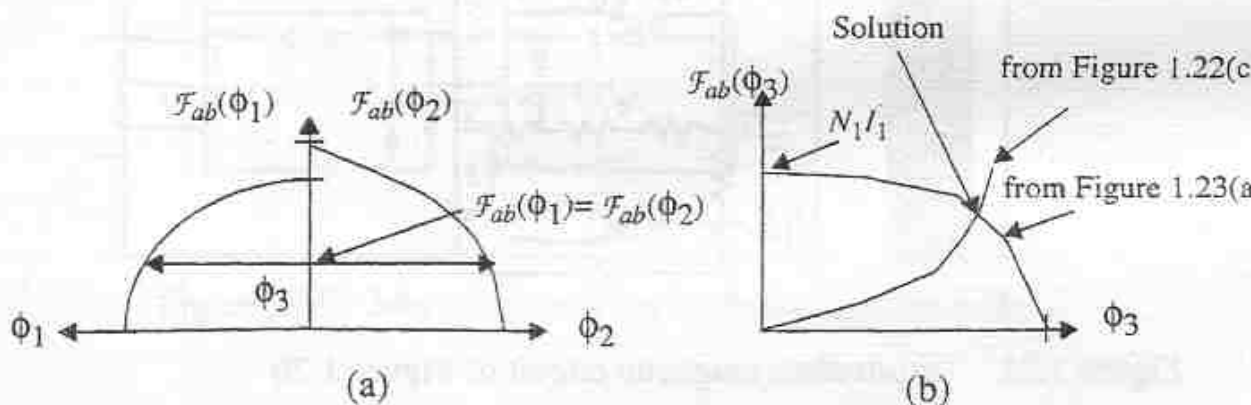


Figure 1.23 Graphical solution of the dual excitation problem

## 1.26 Magnetic Circuits Applied to Electrical Machines

Although the methods and simplifying assumptions outlined in the preceding sections yield results of reasonable accuracy for simple geometries, electrical machines present a considerably more complicated problem. Nonetheless, the basic principles which have been discussed form the basis for analysis and design of any machine structure. For illustration, Figure 1.24 shows that magnetic circuit of a typical two pole DC machine. The center-slotted member is the rotor which carries the rotor winding in the slots. It is usually assembled

from laminated steel punchings having 1-3% silicon. The outer member is the field structure, the cylindrical portion being the yoke or frame which frequently is of cast iron or cast steel. The protruding portions of the field structure of *salient poles* are the poles which are usually made of laminated steel.

With a DC voltage applied to the field windings the steady state value of field current is determined entirely by the resistance of the circuit. For the polarity shown, the field winding produces a *MMF* in the direction to establish a flux from left to right through the field poles, air gaps and armature. The flux path is then completed through the frame. The magnetic circuit is redrawn schematically in Figure 1.25. In order to determine the portions of the magnetic circuit whose properties predominate, a graph of the relative *MMF* of various points around the circuit is sketched in Figure 1.26. The *MMFs* are given with respect to an arbitrary point at the center of the yoke, point *a*. The magnetic potential drop from *a* to *b* is shown as a negatively sloped line in Figure 1.26. From *b* to *c* similar conditions hold but since the material is different a slightly different slope is shown. The air gap *d-e* offers a very large *MMF* drop relative to the iron. If the plot is completed for the remainder of the path, returning to the point *a*, the total reluctance drop is found to equal twice the *MMF* drop from *a* to *f*.

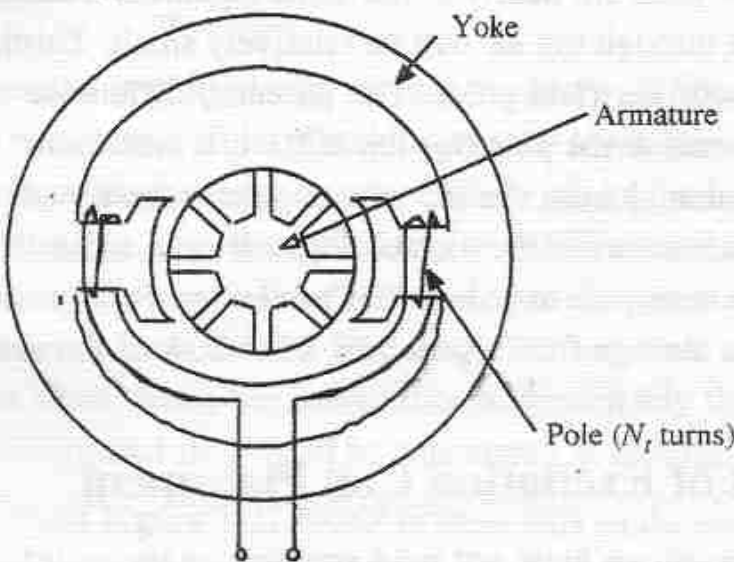


Figure 1.24 Magnetic circuit of a dc machine

For the drop from *a* to *f* to exist, an equal and opposite rise in *MMF* must exist somewhere in the circuit. The required potential rise is established by the *MMF* of the field windings, the magnitude of the contribution being the same as the *MMF* drop from *a* to *f* for each of the two field windings. The upper

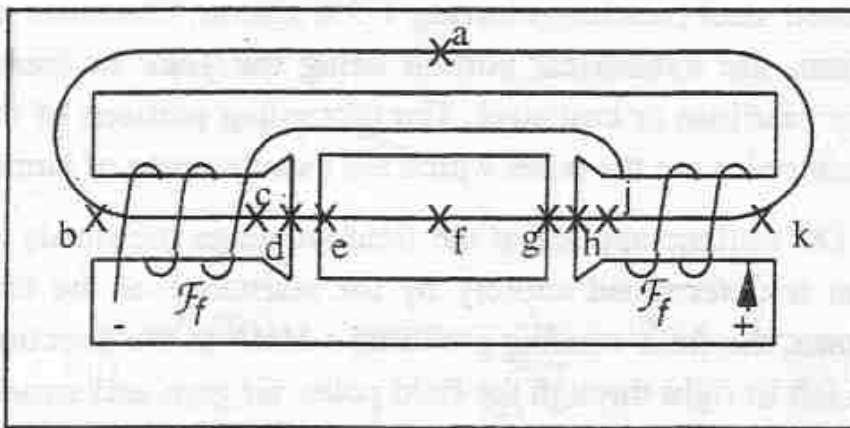


Figure 1.25 Simplified magnetic equivalent circuit corresponding to Figure 1.24

curve of Figure 1.26 shows the rise in potential given by the windings. The nett *MMF* curve shows the sum of the rises and drops at each point in the circuit and thus gives the actual *MMF* at each point with respect to point *a*.

Several important points can be deduced from Figure 1.26. First note that the points *a* and *f* are at the same potential and the *MMF* from *f* to *a* and *a* to *f* are mirror images of each other. Therefore it can be deduced that all calculations can be made on a "per pole" basis. Second, the resultant curve shows that all points on the yoke are nearly at the same potential. Therefore, the leakage flux from *b* to *k* through the air will be relatively small. Third, the same is not true for the tips of the field poles. The potential difference through the pole body increases until at the pole tips the *MMF* is a maximum. In particular, the difference in potential from the top of one pole to the tip of the other is  $2N_f I$ . Since the distance between the tops of adjacent pole shoes is relatively small, the leakage flux from pole to pole is likely to be appreciable. Indeed, even for a good design this leakage flux is generally 10 to 20% of the useful flux.

## 1.27 Effect of Excitation Coil Placement

Up to this point we have not paid attention to the exact placement of the coil core making up an inductor. In practice the location of the exciting coil has a considerable effect on the overall losses as well as the exact value of the inductance obtained. Consider again the simple air gapped core of Figure 1.15. Figure 1.27 shows three cases in which the coil is placed a) on the limb farthest from the gap, b) on the limb with the gap and c) on the upper and lower limbs. In each case the *MMF* is plotted from point *a* to point *f* as identified in the fig-

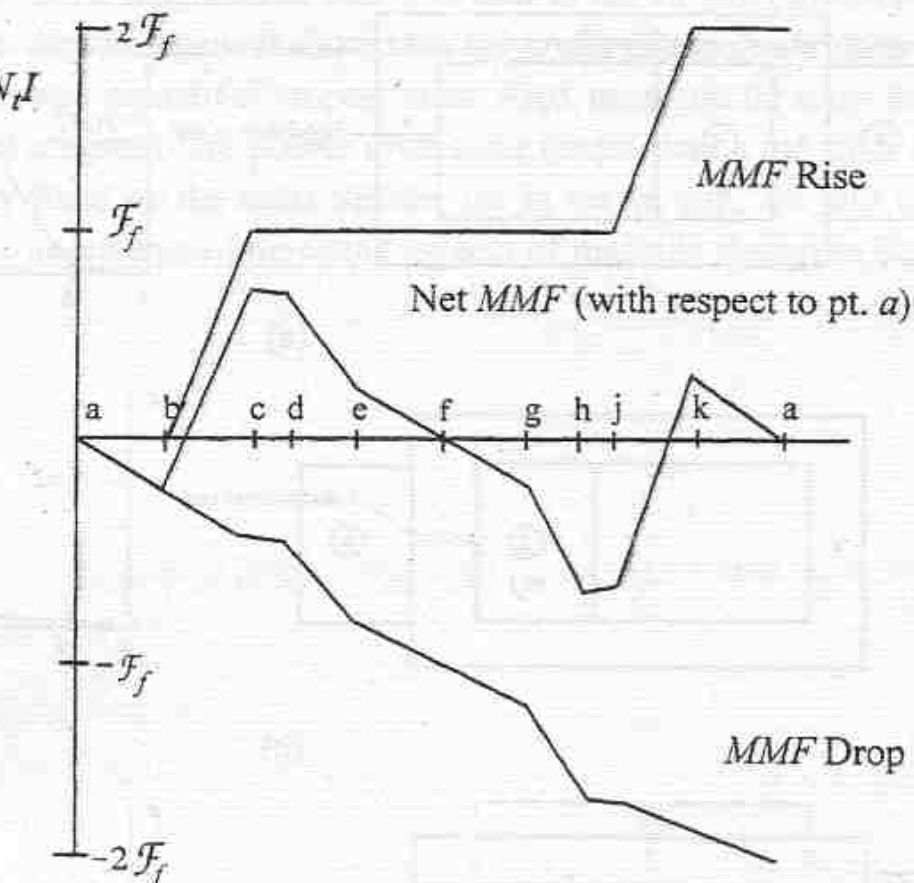


Figure 1.26 Magnetic potential drops and rises in a two pole dc machine

ure. The potential is plotted with respect to point  $a$ . While the remainder of the flux path is not plotted (from  $f$  back to  $a$  in the lower portion of the core), it is identical (mirror image) to the upper half. In case (a) where the coil is on the side away from the gap, the difference in MMF potential between the upper half of the core and the lower half is large over the distance  $c$  to  $d$  resulting in a large flux passing from the top limb to the bottom limb which closes through the left hand limb. Since the useful flux is presumably the flux in the air gap region, this additional flux could be considered as leakage flux.

In case (b) of Figure 1.27 MMF is large only in the region near the air gap ( $d$  to  $e$ ) resulting in "leakage" flux concentrated in this region. Clearly, if the purpose of the inductor design is create a specified amount of flux in the air gap region, then this design would wind up being the smallest and lightest since most of the iron path does not have to support these additional leakage flux lines. Unfortunately, this option is often not a good choice since heating of the copper conductors around the air gap will occur due to eddy current effects. We will have more to say concerning this feature in Chapter 5.

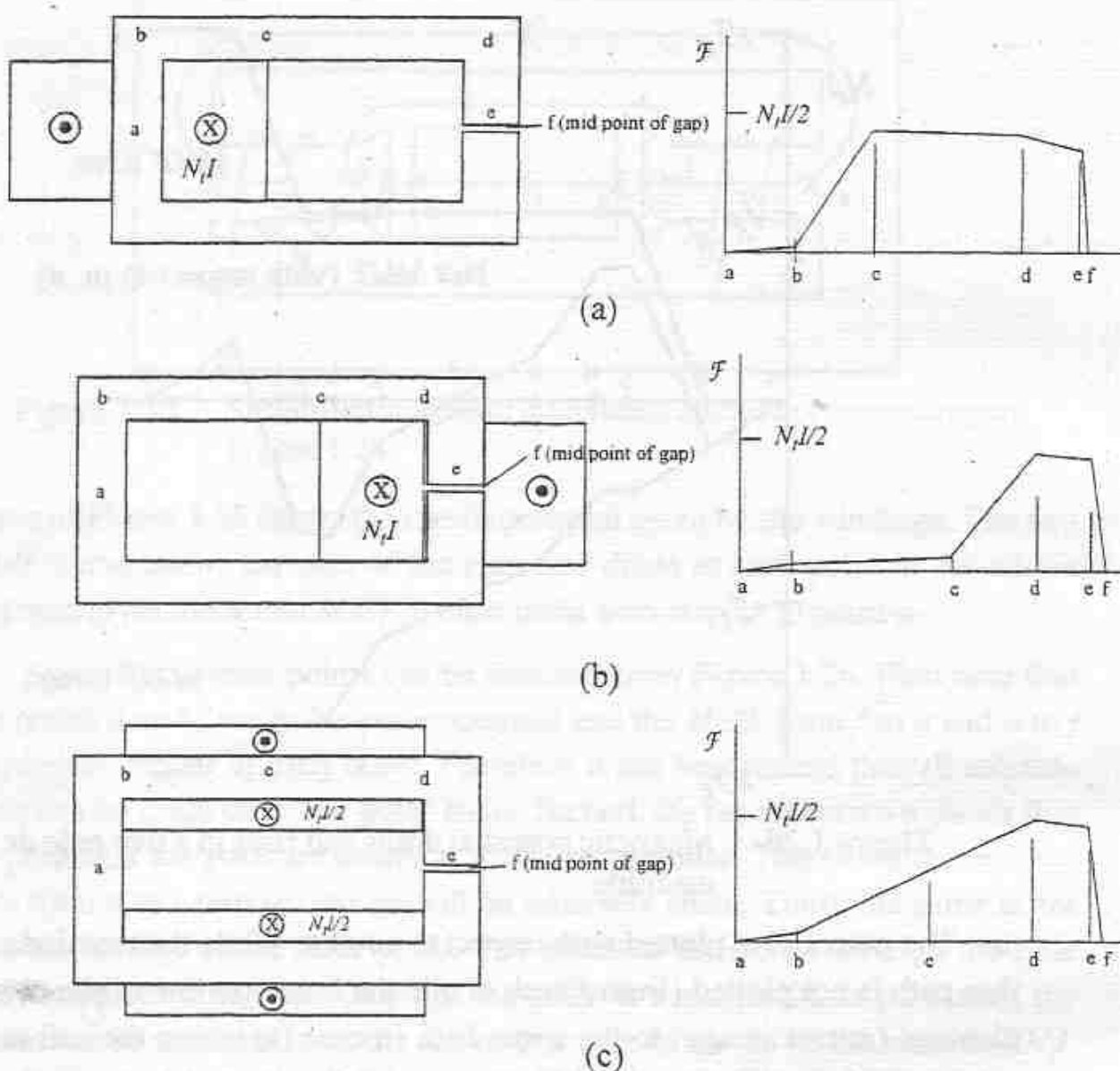


Figure 1.27. Three different methods of winding a simple gapped core. *MMF* potential plotted with respect to point *a*

With case (c) a compromise can be reached concerning these additional flux lines. Since the *MMF* in this case increases linearly over the entire length of the upper and lower limbs, the overall average difference in potential is decreased resulting in leakage flux lines somewhere between cases (a) and (b).

Although a poor choice for inductor design, case (b) clearly does produce the desirable effect of creating a maximum number of flux lines in the air gap. This result is also a valid and important observation in the design of electrical machines where the process of creating a maximum amount of flux line in the air gap for a given amount of ampere turns is of critical importance. The design of case (b) teaches us that it is important to design machine in which the copper

exciting the main magnetic circuit is as near to the air gap (largest reluctance) as possible. Hence, many shallow slots are preferable to fewer deep slots containing the same amount of ampere turns. Also, magnets far away from the air gap (buried magnets) are poorer in creating torque than a machine with magnets simply fixed on the rotor surface, i.e. in the air gap. We will have much more to say about these interesting aspects of machine design in future chapters.

## The Effect of Pole Number on AC Winding

### Effect of Pole Number on AC Winding

The number of poles per pole pair is an important factor in determining the performance of a motor. Pole pairs are usually denoted by the letter  $p$ . The number of pole pairs is given by the formula:

$$p = \frac{N}{2} \quad (1)$$

where  $N$  is the total number of slots in the machine. The number of slots per pole pair is given by the formula:

$$s = \frac{N}{2p} \quad (2)$$

The number of slots per pole pair is also known as the slot distribution. The slot distribution is determined by the number of slots per pole pair, the number of pole pairs, and the number of phases.

The number of slots per pole pair is determined by the number of slots per pole pair, the number of pole pairs, and the number of phases. The slot distribution is determined by the number of slots per pole pair, the number of pole pairs, and the number of phases. The slot distribution is determined by the number of slots per pole pair, the number of pole pairs, and the number of phases.

(resistive losses) are present in each of the iron laminations and generate heat which must be dissipated by air cooling or water cooling, depending on the ambient temperature and the cooling techniques used with respect to the heat generation.

Figure 14.1 shows a cross-sectional view of a typical magnetic core. The core consists of two main parts, the primary and secondary windings, and the magnetic core. The magnetic core is made of thin iron laminations stacked together to form a closed magnetic circuit. The primary winding is wound around the primary coil, and the secondary winding is wound around the secondary coil.

The magnetic core is made of thin iron laminations stacked together to form a closed magnetic circuit. The primary winding is wound around the primary coil, and the secondary winding is wound around the secondary coil.

The magnetic core is made of thin iron laminations stacked together to form a closed magnetic circuit. The primary winding is wound around the primary coil, and the secondary winding is wound around the secondary coil.

The magnetic core is made of thin iron laminations stacked together to form a closed magnetic circuit. The primary winding is wound around the primary coil, and the secondary winding is wound around the secondary coil.

The magnetic core is made of thin iron laminations stacked together to form a closed magnetic circuit. The primary winding is wound around the primary coil, and the secondary winding is wound around the secondary coil.

The magnetic core is made of thin iron laminations stacked together to form a closed magnetic circuit. The primary winding is wound around the primary coil, and the secondary winding is wound around the secondary coil.

The magnetic core is made of thin iron laminations stacked together to form a closed magnetic circuit. The primary winding is wound around the primary coil, and the secondary winding is wound around the secondary coil.

The magnetic core is made of thin iron laminations stacked together to form a closed magnetic circuit. The primary winding is wound around the primary coil, and the secondary winding is wound around the secondary coil.

The magnetic core is made of thin iron laminations stacked together to form a closed magnetic circuit. The primary winding is wound around the primary coil, and the secondary winding is wound around the secondary coil.

The magnetic core is made of thin iron laminations stacked together to form a closed magnetic circuit. The primary winding is wound around the primary coil, and the secondary winding is wound around the secondary coil.

The magnetic core is made of thin iron laminations stacked together to form a closed magnetic circuit. The primary winding is wound around the primary coil, and the secondary winding is wound around the secondary coil.

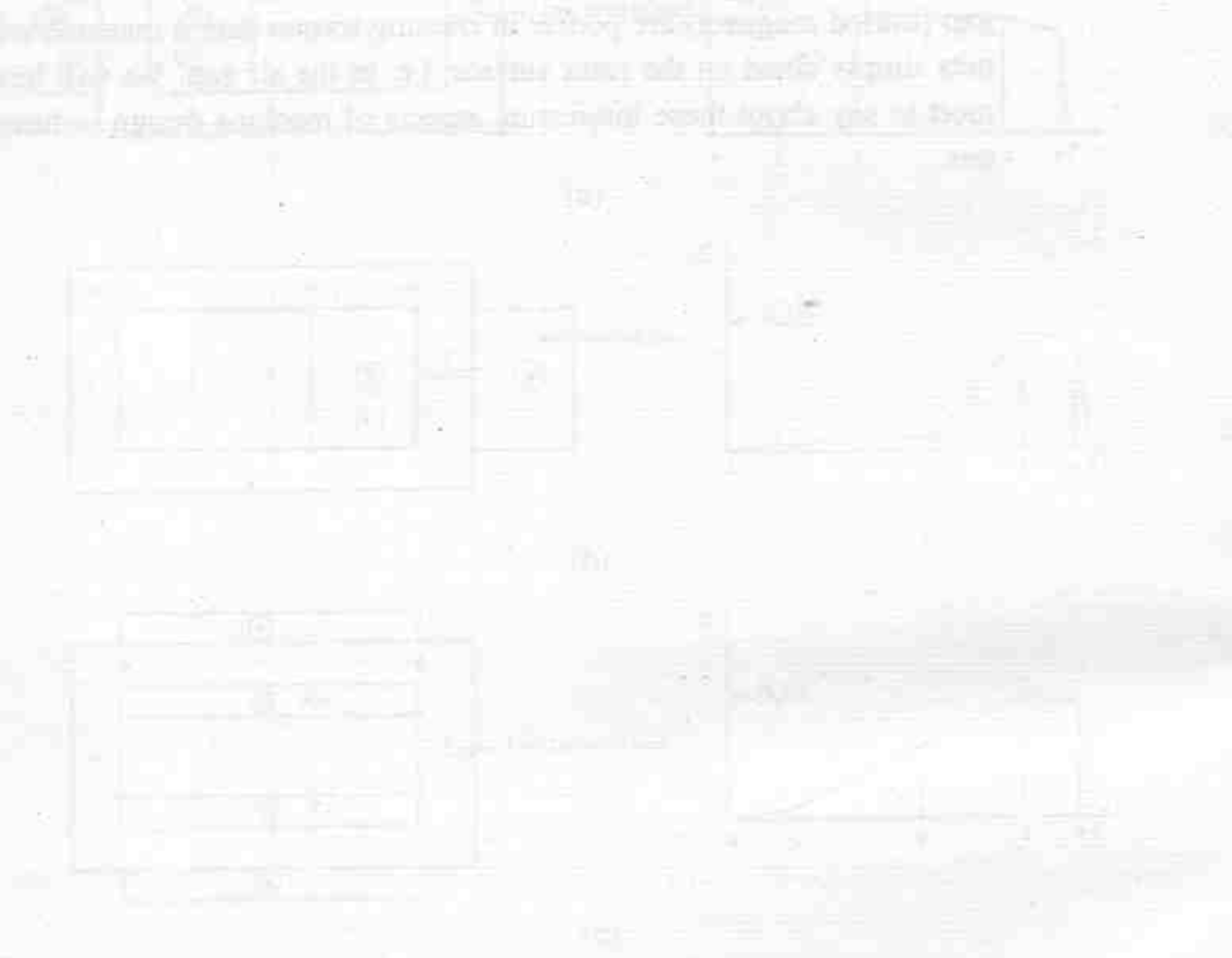


Figure 14.1 Cross-sectional view of a magnetic core showing primary and secondary windings.

which will be addressed in the next section, may also affect the core loss. However, since the MMF is not zero, it is known that the initial hysteresis and eddy current losses, the overall energy efficiency is proportional to the core thickness as follows:  $\text{loss} \propto \text{core thickness}^2$ .

To reduce the core loss, the design has to take into account the magnetic field effect of core loss minimization. This can be done by increasing the core thickness and the magnetic flux density. In addition, the core loss can be reduced by using a magnetomotive force of 1000 Amperes per meter. This design objective is to ensure that the magnetic flux density is high enough to provide a high magnetic field strength. The magnetic field strength is defined as the product of the magnetic flux density and the magnetic permeability. The magnetic permeability is defined as the ratio of the magnetic flux density to the magnetic field strength. The magnetic permeability is given by the formula:

## Chapter 2

# The *MMF* and Field Distribution of an AC Winding

### 2.1 *MMF* and Field Distribution of a Full Pitch Winding

In this Chapter we will first consider the “forcing function” to the magnetic field of a typical ac machine, namely the stator *MMF*. To begin, a single-phase full-pitch winding having one slot per pole is assumed. Figure 2.1 shows a schematic representation of such a winding. The directions of the current are shown for a single instant of time. We will assume that the length of the air gap along the surface of the armature is constant. Figure 2.1 shows also the direction of the lines of force (flux lines) produced by the current carrying conductors. The only lines of force possible are those which are linked with one coil. No lines of force are possible which are linked with two coils at the same time because the *MMF* of such lines is zero. Since all flux lines enclose  $N_t I$  ampere turns, the *MMF* corresponding to each field line is also  $N_t I$ , where  $N_t$  is the total number of turns with which the lines of force are linked. Since every line of force consists of two symmetrical parts taking opposite directions in the air gap, teeth and core the *MMF* can be divided into two portions corresponding to single crossings of the gap, i.e., corresponding to one-half the path of the magnetic circuit (one magnetic pole).

The line integral of the magnetic field intensity  $H$  along a closed path is equal to the ampere-turns *MMF* linking this path. In general the integral has to be divided into a sum corresponding to the stator core, rotor core, stator teeth, rotor teeth and the air gap. However, assuming no saturation in the iron, the field intensity in the iron is very small and can be neglected. Taking the path defined as loop 1 in Figure 2.1 in a clockwise direction.

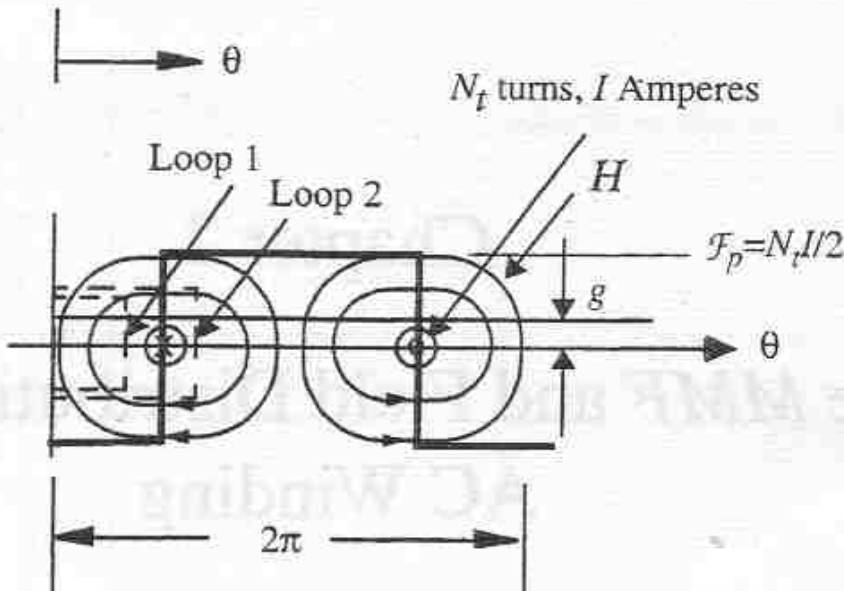


Figure 2.1 MMF and field intensity of a full pitched coil as a function of position along the air gap

$$\oint \mathbf{H} \cdot d\mathbf{l} = 0 \quad (2.1)$$

Since the gap is small the field intensity can be assumed constant over the portion of the path leading from the stator to the rotor resulting in,

$$[H(0) - H(\theta)]g = 0 \quad (2.2)$$

or

$$H(0) = H_1(\theta) \quad 0 \leq \theta < \frac{\pi}{2} \quad (2.3)$$

where  $H(0)$  and  $H_1(\theta)$  represent the field in the gap encountered when traversing the two vertical sides of the test loop #1. While we are not able to solve for the field intensity, Eq. (2.3) indicates that it is uniformly constant over the region where  $0 < \theta < \pi/2$  since the same result will be obtained over any path which closes before encircling any current.

Upon taking loop 2 clockwise,

$$\oint \mathbf{H} \cdot d\mathbf{l} = N_t I \quad (2.4)$$

which yields

$$[H(0) - H_2(\theta)]g = N_t I \quad \frac{\pi}{2} \leq \theta < 3\frac{\pi}{2} \quad (2.5)$$

where  $H_2(\theta)$  is constant over the region since  $H(0)$  and  $N_t I$  are clearly constant. Finally if we integrate over a closed path that crosses the gap vertically upward where  $\theta = 0$  and return across the gap where  $3\pi/2 < \theta < 2\pi$  then, again

$$[H(0) - H(\theta)]g = 0 \quad \frac{3\pi}{2} < \theta < 2\pi \quad (2.6)$$

However from Gauss' Law

$$\oint_S \mathbf{B} \cdot d\mathbf{S} = 0$$

If this integral is taken over a cylinder passing through the air gap whose top and bottom are outside the region of the machine, the portion of the integral associated with the regions outside the air gap proper can be neglected where-upon,

$$\int_{airgap surface} \mu_o H(\theta) l_s r_{is} d\theta = 0$$

where  $l_s$  is the length of the machine (gross length of the iron stack) and  $r_{is}$  is the radius of the inner stator surface. Since both  $H_1(\theta)$  and  $H_2(\theta)$  are constant, this integral becomes,

$$[H_1(\theta) + H_2(\theta)]\pi l_s r_{is} = 0$$

so that

$$H_2(\theta) = -H_1(\theta) \quad (2.7)$$

and, from Eq. (2.5),

$$H_1(\theta)g = \frac{N_t I}{2} \quad (2.8)$$

Since the quantity  $H_1(\theta)g$  represents the magnetic potential between the stator and rotor surfaces at the point  $\theta$  along the air gap it is useful to define

$$\mathcal{F}_p = H_1 g \quad (2.9)$$

so that

$$B_g = \frac{\mu_0 \mathcal{F}_p}{g} \quad (2.10)$$

$\mathcal{F}_p$  corresponds to the *MMF* of one half the magnetic circuit, that is, the *MMF* of one pole of a complete two pole magnetic circuit. Equation (2.10) indicates that, for the idealized situation we are considering, the shape of the flux density curve is essentially proportional to the *MMF* at every point in the gap.

If the origin for the measure of angular distance along the air gap periphery is taken instead as the point where the winding is located ( $\theta = \pi/2$  in Figure 2.1) the square wave can be expanded in a Fourier series in which all cosine terms and even sine terms are zero. The result is

$$\mathcal{F}_p = \left(\frac{4}{\pi}\right)\left(\frac{N_t I}{2}\right) \left[ \sin\theta + \frac{1}{3}\sin 3\theta + \frac{1}{5}\sin 5\theta + \dots \right] \quad (2.11)$$

## 2.2 Fractional Pitch Winding for Two Pole Machine

When the span of the coil sides of an individual coil is less than the pole pitch, the winding as a whole is said to be a fractional pitch winding. Such windings are extensively used for the reason that the *MMF* wave form is more nearly sinusoidal than with full pitch windings, and because of the saving in copper and the greater stiffness of the coils due to the shorter end connections. The latter reason is especially important in the case of two pole high speed turbo-alternators because of stresses produced in the end connections under short circuit conditions.

Fractional pitch windings are ordinarily of the two layer lap wound type, although single layer lap windings are also used. The use of fractional pitch makes it possible to use a number of slots which is not an exact multiple of the number of poles, thus tending to suppress pulsations of flux as the teeth move relative to the pole faces and so largely eliminate tooth ripple in the voltage waveform.

As a simple example consider the *MMF* distribution of the fractional pitch winding of Figure 2.2 in which the coil of  $N_t$  turns of Figure 2.1 has been split into two coils and both have been moved back and forth (pitched) by a net electrical angle  $\gamma$ . The amplitude of the corresponding *MMF* distribution for

the  $h^{\text{th}}$  harmonic is readily calculated in electrical radians (as opposed to mechanical radians) as

$$\begin{aligned}\mathcal{F}_{ph} &= \frac{2}{\pi} \left[ \int_0^{\gamma/2} 0 \sin h\theta d\theta + \int_{\gamma/2}^{(\pi-\gamma/2)} \frac{N_t I}{2} \sin h\theta d\theta + \int_{(\pi-\gamma/2)}^{\pi} 0 \sin h\theta d\theta \right] \\ &= \left( \frac{4}{\pi} \right) \left( \frac{N_t I}{2} \right) \frac{\cosh \frac{\gamma}{2}}{h} \quad (h \text{ odd})\end{aligned}$$

Hence the fractional pitch, rectangular distribution of Figure 2.2 can be represented by the series

$$\mathcal{F}_p = \sum_{h=1, 3, 5, \dots}^{\infty} \mathcal{F}_{ph} \sin h\theta$$

$$\mathcal{F}_p = \frac{4N_t I}{\pi} \left[ \cos \frac{\gamma}{2} \sin \theta + \frac{1}{3} \cos \frac{3\gamma}{2} \sin 3\theta + \frac{1}{5} \cos \frac{5\gamma}{2} \sin 5\theta + \dots \right] \quad (2.12)$$

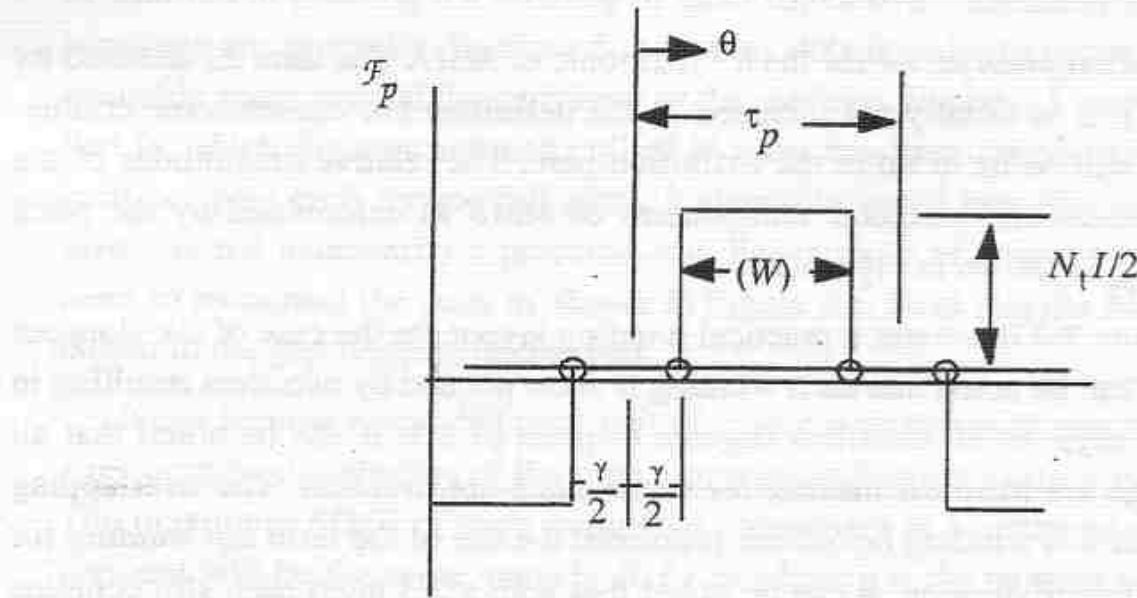


Figure 2.2 MMF distribution of a coil with fractional pitch

Upon comparing Eq.(2.12) with Eq. (2.11), the additional factor introduced by short pitching the winding is clearly, for the  $h^{\text{th}}$  harmonic,

$$k_{ph} = \cos \frac{h\gamma}{2} \quad (h \text{ odd}) \quad (2.13)$$

It is conventional to write the series of Eq.(2.12) in a slightly different form. If  $\tau_p$  denotes the length of one pole pitch measured along the air gap periphery and  $W$  is the actual width of the coil then is

$$\gamma = \frac{\tau_p - W}{\tau_p} \pi = \pi \left( 1 - \frac{W}{\tau_p} \right) \quad (2.14)$$

and

$$\cos \frac{h\gamma}{2} = \cos \left[ h \left( \frac{\pi}{2} - \frac{W\pi}{\tau_p 2} \right) \right] = \sin \frac{h\pi}{2} \sin h \left( \frac{W\pi}{\tau_p 2} \right) \quad (h \text{ odd})$$

so that

$$\mathcal{F}_{ph} = \frac{4}{\pi} \left( \frac{N_t I}{2h} \right) \sin \frac{h\pi}{2} \sin \left[ h \left( \frac{W}{\tau_p} \right) \frac{\pi}{2} \right] \quad (2.15)$$

The quantity

$$k_{ph} = \sin \left[ \frac{hW}{\tau_p} \left( \frac{\pi}{2} \right) \right] \sin \left( \frac{h\pi}{2} \right) \quad (h \text{ odd}) \quad (2.16)$$

is called the *pitch factor* for the  $h^{\text{th}}$  harmonic of *MMF*. The term  $\pm 1$  denoted by  $\sin(h\pi)/2$  is usually not included in the definition but causes some confusion. It will be included in the definition here. The relative magnitudes of the fundamental and harmonic components of *MMF* as determined by the pitch factor  $k_{ph}$  is shown in Figure 2.3.

Figure 2.4 illustrates a practical winding layout for the case of six slots per pole. It can be noted that each winding is short pitched by two slots resulting in a pitch angle of 60 electrical degrees or pitch of 2/3. It can be noted that all windings are identical making for economical construction. The overlapping nature of this winding layout has prompted the use of the term *lap winding* for this coil configuration. It can be noted that with a 2/3 pitch each slot contains coil sides belonging to different phases, which has an effect upon the leakage reactance of the winding and also upon the resultant *MMF* of the winding.

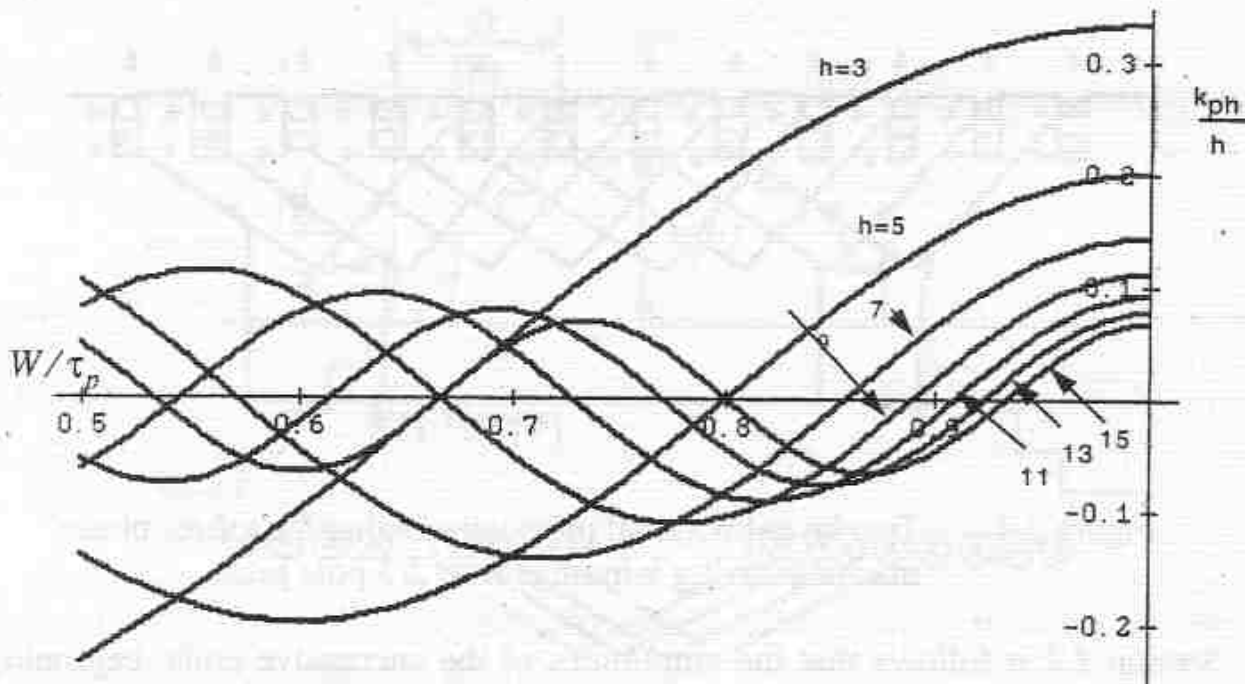


Figure 2.3 Pitch factor for harmonics  $h = 3, 5, 7 \dots 15$  as a function of per unit coil pitch  $W/\tau_p$

## 2.3 Distributed Windings

In addition to pitching the winding in order to remove undesirable harmonics, windings are generally distributed in several slots in order to better utilize the available space around the periphery of the machine. Figure 2.5 shows a situation in which the concentrated coil of  $N_t$  turns has been distributed into four coils per pole each having full pitch. It should be noted here that the winding layout is not necessarily a practical one. For purpose of analysis it is convenient to reconnect the coils as shown in Figure 2.6. Note that the *MMF* distribution in the gap remains unchanged.

It can be now noted that each pair of coils connected as shown contributes a rectangular distribution of the type discussed in Section 2.2 (see Figure 2.2). The maximum *MMF* of each individual component is a rectangular distribution and will be the same, namely  $N_t I / 2q$  where  $q$  is the number of coils per pole (four in this case). The  $q$  coils are said to comprise a *phase belt* and is a key parameter for the representation of a winding layout. Note that the displacement of each coil with respect to its neighbor is again taken to be  $\gamma$ . From

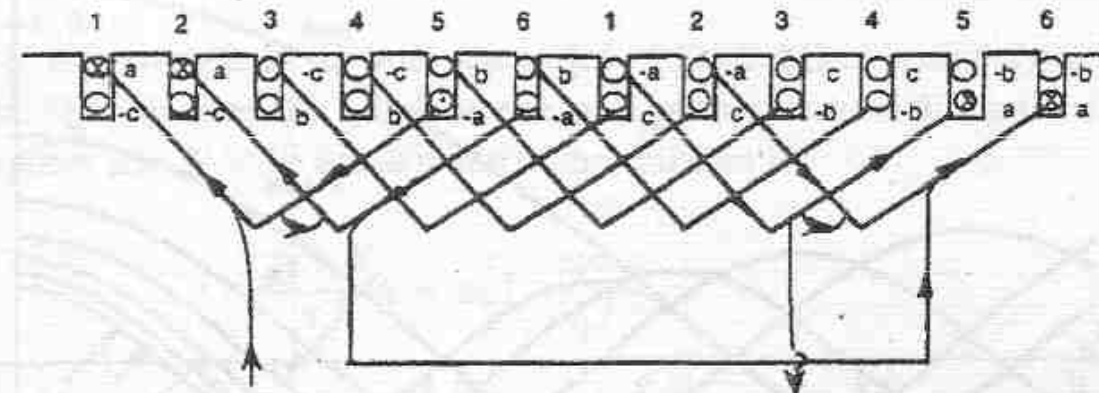


Figure 2.4 Two layer fractional pitch lap winding for a three phase machine having windings with 2/3 pole pitch

Section 2.2 it follows that the amplitudes of the successive coils, beginning with the outer coil, are, respectively,

Coil	Amplitude of $h^{\text{th}}$ Harmonic	
1 (outer)	$\frac{4}{\pi} \left( \frac{N_t I}{2q} \right) \frac{\cos\left(\frac{h\gamma}{2}\right)}{h}$	
2	$\frac{4}{\pi} \left( \frac{N_t I}{2q} \right) \frac{\cos\left(\frac{3h\gamma}{2}\right)}{h}$	(2.17)
3	$\frac{4}{\pi} \left( \frac{N_t I}{2q} \right) \frac{\cos\left(\frac{5h\gamma}{2}\right)}{h}$	
•	•	
•	•	
$q$ (inner)	$\frac{4}{\pi} \left( \frac{N_t I}{2q} \right) \frac{\cosh[\gamma/2 + (q-1)\gamma]}{h}$	

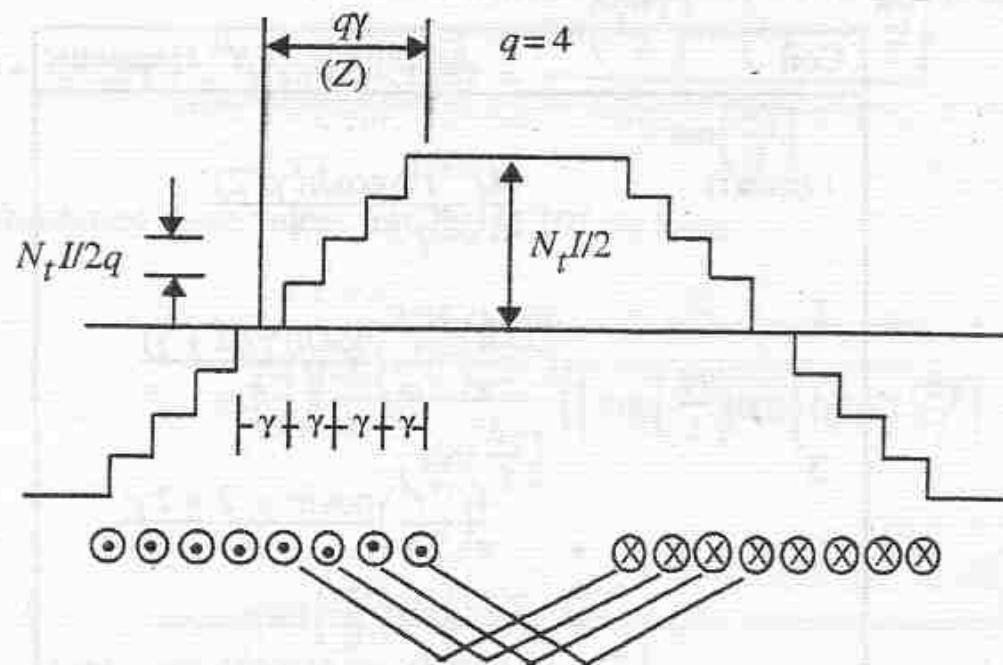


Figure 2.5      Distributed winding having four coils in a phase belt

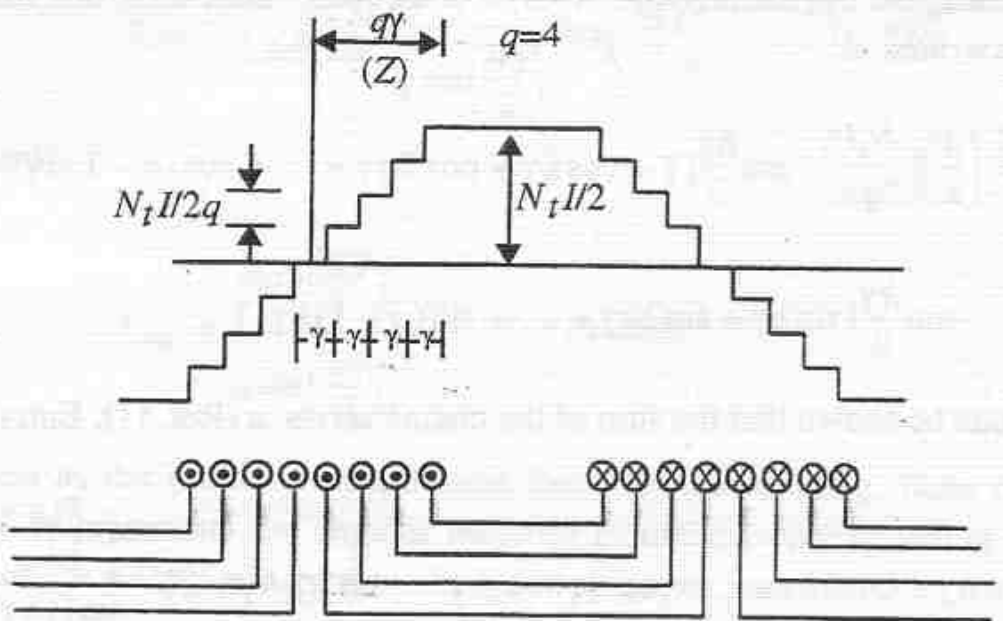


Figure 2.6      Distributed winding viewed as four coils of different pitch per pole

The  $q$  amplitudes can be written in the form

Coil	Amplitude of $h^{th}$ Harmonic
1 (outer)	$\frac{4}{\pi} \left( \frac{N_t I}{2q} \right) \frac{\cosh(\gamma/2)}{h}$
2	$\frac{4}{\pi} \left( \frac{N_t I}{2q} \right) \frac{\cosh(\gamma/2 + \gamma)}{h}$
3	$\frac{4}{\pi} \left( \frac{N_t I}{2q} \right) \frac{\cosh(\gamma/2 + 2\gamma)}{h}$
•	•
•	•
$q$ (inner)	$\frac{4}{\pi} \left( \frac{N_t I}{2q} \right) \frac{\cosh[\gamma/2 + (q-1)\gamma]}{h}$

The net amplitude of the  $h^{th}$  harmonic is found by summing the  $q$  terms. After using the trig identity  $\cos(A+B) = \cos A \cos B - \sin A \sin B$ , this summation can be written as

$$\begin{aligned} \mathcal{F}_{ph} &= \left( \frac{4}{\pi} \right) \left( \frac{N_t I}{2q h} \right) \left\{ \cos \frac{h\gamma}{2} [1 + \cosh h\gamma + \cos 2h\gamma + \dots + \cos(q-1)h\gamma] \right. \\ &\quad \left. - \sin \frac{h\gamma}{2} [\sin h\gamma + \sin 2h\gamma + \dots + \sin(q-1)h\gamma] \right\} \end{aligned} \quad (2.19)$$

It can be shown that the sum of the cosine series is (Ref. [1], Entry 420.2),

$$1 + \cosh h\gamma + \cos 2h\gamma + \dots + \cos(q-1)h\gamma = \sin[(qh\gamma)/2] \frac{\cos \left[ \frac{(q-1)n\gamma}{2} \right]}{\sin[(h\gamma)/2]} \quad (2.20)$$

and that the sum of the sine series is (Ref. [1], Entry 420.1),

$$\sin h\gamma + \sin 2h\gamma + \dots + \sin (q-1)h\gamma = \frac{\sin\left(\frac{qh\gamma}{2}\right)\sin\left[(q-1)\frac{h\gamma}{2}\right]}{\sin\left(\frac{h\gamma}{2}\right)} \quad (2.21)$$

Substituting these values into Eq. (2.19) we have

$$\begin{aligned} \mathcal{F}_{ph} &= \left(\frac{4}{\pi}\right)\left(\frac{N_p I}{qh}\right) \frac{\sin\left(\frac{hq\gamma}{2}\right)}{\sin\left(\frac{h\gamma}{2}\right)} \left\{ \left[ \cos\left(\frac{h\gamma}{2}\right) \cos\left[(q-1)\frac{h\gamma}{2}\right] \right. \right. \\ &\quad \left. \left. - \sin\left(\frac{h\gamma}{2}\right) \sin\left[\frac{(q-1)h\gamma}{2}\right] \right] \right\} \end{aligned} \quad (2.22)$$

which reduces to

$$\mathcal{F}_{ph} = \left(\frac{4}{\pi}\right)\left(\frac{N_p I}{2h}\right) \frac{\sin\left(\frac{hq\gamma}{2}\right)}{q \sin\left(\frac{h\gamma}{2}\right)} \cos\left(\frac{hq\gamma}{2}\right) \quad (h \text{ odd}) \quad (2.23)$$

The quantity

$$k_{dh} = \frac{\sin\left(\frac{hq\gamma}{2}\right)}{q \sin\left(\frac{h\gamma}{2}\right)} \quad (h \text{ odd}) \quad (2.24)$$

is defined as the harmonic distribution factor of the winding. Note that the quantity  $q\gamma$  represents the angular measure in radians corresponding to that portion of the air gap occupied by the  $q$  coil sides per phase belt.

It is convenient to let  $Z$  denote the arc length occupied by the  $q$  coils of the winding group. Then, if  $\tau_p$  denotes one pole pitch

$$q\gamma = \frac{Z}{\tau_p} \pi \quad (2.25)$$

$$\gamma = \frac{Z\pi}{\tau_p q}$$

The distribution factor for the  $h^{th}$  harmonic then can also be written as

$$k_{dh} = \left(\frac{1}{q}\right) \frac{\sin\left(\frac{hz\pi}{\tau_p 2}\right)}{\sin\left(\frac{hz\pi}{\tau_p 2q}\right)} \quad (h \text{ odd}) \quad (2.26)$$

Consider now the cosine term in Eq. (2.23). Examining Figure 2.5 it is apparent that the angle  $q\gamma/2$  is the equivalent pitch of the coil which is now considered to be distributed over  $q$  slots. Again it is convenient to let

$$\frac{q\gamma}{2} = \left(1 - \frac{W}{\tau_p}\right) \frac{\pi}{2} \quad (2.27)$$

where  $W$  is the equivalent span of the distributed winding. The cosine term becomes

$$\cos\left(\frac{hq\gamma}{2}\right) = \sin\left(\frac{hW\pi}{\tau_p 2}\right) \sin\left(h\frac{\pi}{2}\right) \quad (2.28)$$

which is recognized as the pitch factor for the  $h^{th}$  harmonic, which has already been defined by Eq. (2.16). The final expression for the  $h^{th}$  harmonic of MMF corresponding to the coil of Figure 2.4 becomes

$$\mathcal{F}_{ph} = \frac{4N_t I}{\pi 2h} k_{ph} k_{dh} \quad (h \text{ odd}) \quad (2.29)$$

where  $k_{ph}$  and  $k_{dh}$  are given by Eqs. (2.16) and (2.26) respectively.

In most case, winding distributions are nearly always symmetrical if the number of slot per pole per phase is two or greater. This is usually the case for three phase machines having six poles or less ranging up to several hundred horsepower. Hence, the harmonic components of the MMF distribution of the winding can typically be written as the product of a distribution factor times a

pitch factor times the harmonic component of *MMF* for a full pitch coil in which all the turns are concentrated in one slot.

In principle, phase belts spanning any portion of a pole pitch are possible. Unless used for a special purpose such as for two speed motors, phase belts greater than one pole pitch are considered as impractical since the end turn length is excessive. However, practical considerations for accommodating symmetrical phase groups result in  $60^\circ$  and  $120^\circ$  phase belts the most practical for three phase system and  $90^\circ$  and  $180^\circ$  the best for two phase systems. Table 2.1 shows the distribution factor for the fundamental component of *MMF* for these four phase belts. Note that the difference between two coils or slots per phase belt and a continuous or infinite number of slots is relatively small, particularly for the  $60^\circ$  phase belt. Considerably more voltage is generated by the  $60^\circ$  phase belt compared to the  $120^\circ$  belt and hence is the most widely used winding configuration.

Slots or Coils per Phase Belt $q$	Phase Belt in Electrical Degrees			
	$60^\circ$	$90^\circ$	$120^\circ$	$180^\circ$
1	1.000	1.000	1.000	1.000
2	0.966	0.924	0.866	0.707
3	0.960	0.911	0.844	0.667
4	0.958	0.906	0.837	0.654
5	0.957	0.904	0.833	0.648
$\infty$	0.955	0.900	0.827	0.636

TABLE 2.2 Fundamental winding distribution factor  $k_{d1}$  for four typical phase belts.

Distribution factors for the first 26 harmonics of *MMF* of three phase windings with 60 phase belts is given in Table 2.2. Note that the distribution factors of the harmonics decrease much more rapidly with increasing values of  $c$  than does the distribution factor of the fundamental. The distribution factor for the fundamental is always positive. The distribution factor of a harmonic can be negative which means that the harmonic is in phase opposition to the fundamental. Note also that in the table of distribution factors some harmonics

have the same amplitude as the corresponding fundamental component. These harmonics,  $h_k$ , are called *slot harmonics*. From Table 2.2 their orders are

$$h_k = 6kq \pm 1 \quad (2.30)$$

$$= 2kmq \pm 1 \quad (2.31)$$

$$= \frac{2kS_1}{P} \pm 1 \quad (2.32)$$

where  $S_1$  represents the total number of stator winding slots,  $P$  is the number of poles,  $q$  is the number of slots/pole/phase, and  $m$  is the number of phases ( $m=3$  in this case). The analysis applies equally well to a wound rotor winding distribution in which case  $S_1$  is replaced by  $S_2$ . The slot harmonics which correspond to  $k = 1$  (slot harmonics of the first order) are amongst the most troublesome resulting in noise as well as contributing to "stray losses", a subject which will be treated in more detail in Chapter 5.

TABLE 2.4 Harmonic distribution factors for a winding with  $60^\circ$  phase belt.

<i>k<sub>dh</sub></i> - Harmonic Distribution Factors						
<i>h</i>	<i>q=2</i>	<i>q=3</i>	<i>q=4</i>	<i>q=5</i>	<i>q=6</i>	<i>q=∞</i>
1	0.966	0.960	0.958	0.957	0.957	0.955
3	0.707	0.667	0.654	0.646	0.644	0.636
5	0.259	0.217	0.205	0.200	0.197	0.191
7	-0.259	-0.177	-0.158	-0.149	-0.145	-0.136
9	-0.707	-0.333	-0.270	-0.247	-0.236	-0.212
11	-0.966	-0.177	-0.126	-0.110	-0.102	-0.087
13	-0.966	0.217	0.126	0.102	0.092	0.073
15	-0.707	0.667	0.270	0.200	0.172	0.127
17	-0.259	0.960	0.158	0.102	0.084	0.056
19	0.259	0.960	-0.205	-0.110	0.084	-0.059
21	0.707	0.667	-0.654	-0.247	-0.172	-0.091
23	0.966	0.217	-0.958	-0.149	-0.092	-0.041
25	0.966	-0.177	-0.958	0.200	0.102	-0.038

TABLE 2.4 Harmonic distribution factors for a winding with  $60^\circ$  phase belt.

$h$	$k_{dh}$ - Harmonic Distribution Factors					
	$q=2$	$q=3$	$q=4$	$q=5$	$q=6$	$q=\infty$
27	0.707	-0.333	0.654	0.646	0.236	0.071
29	0.259	-0.177	-0.205	0.957	0.145	0.033
31	-0.259	0.217	0.158	0.957	-0.197	-0.031
33	-0.707	0.667	0.270	0.646	-0.644	-0.058
35	-0.966	0.960	0.126	0.200	-0.957	-0.027
37	-0.966	0.960	-0.126	-0.149	-0.957	0.026
39	-0.707	0.667	-0.270	-0.247	-0.644	0.049
41	-0.259	0.217	-0.158	-0.110	-0.197	0.023
43	0.259	-0.177	0.205	0.102	0.145	-0.022
45	0.707	-0.333	0.654	0.200	0.236	-0.042
47	0.966	-0.177	0.958	0.102	0.102	-0.020
49	0.966	0.217	0.958	-0.110	-0.092	0.019
51	0.707	0.667	0.654	-0.247	-0.172	0.038

## 2.4 Concentric Windings

Although lap windings are historically the configuration of choice, they are used today only for large ac machines over a few hundred horsepower having coils made from copper bars (*form wound coils*) where manual insertion of the coils into the slots still predominates. For smaller machines the coils are made from copper wire, *random wound coils*, which is more amenable to factory automation. However, the overlapping nature of the lap wound construction make machine insertion of the coils difficult. An alternative to a lap winding is the concentric coils arrangement shown in Figure 2.7. In this case, the coils are nested in such a manner that the entire phase group can be inserted in slots in one operation.

Calculation of the winding factor for concentric windings proceeds in much the same manner as for lap windings. The amplitude of the  $h^{\text{th}}$  harmonic is, in this case, found by summing  $3q$  terms since the concentrated winding

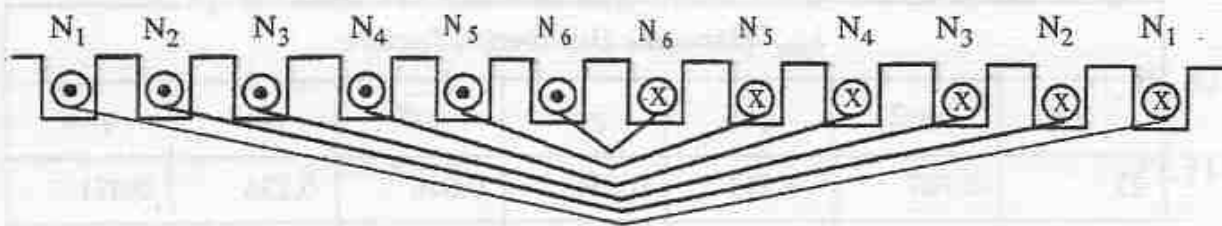


Figure 2.7 Concentric winding arrangement having a  $180^\circ$  phase belt (one phase only shown)

can, in general span one pole pitch ( $3q$  slots per pole). From a similar process as used to obtain Eq. (2.19)

$$\begin{aligned} \mathcal{F}_{ph} = & \left(\frac{4}{\pi}\right)\left(\frac{I}{2h}\right)\{\cos\frac{h\gamma}{2}[N_1 + N_2\cosh h\gamma + N_3\cos 2h\gamma + \dots + N_{3q}\cos 3qh\gamma] \\ & - \sin\frac{h\gamma}{2}[N_2\sinh h\gamma + N_3\sin 2h\gamma + \dots + N_{3q}\sin 3qh\gamma]\} \end{aligned} \quad (2.33)$$

By normalizing to the total number of turns  $N_t = N_1 + N_2 + \dots + N_{3q}$ , this result can be written as,

$$\begin{aligned} \mathcal{F}_{ph} = & \left(\frac{4}{\pi}\right)\left(\frac{N_t I}{2h}\right)\{\cos\frac{h\gamma}{2}\left[\frac{N_1}{N_t} + \frac{N_2}{N_t}\cosh h\gamma + \frac{N_3}{N_t}\cos 2h\gamma + \dots + \frac{N_{3q}}{N_t}\cos 3qh\gamma\right] \\ & - \sin\frac{h\gamma}{2}\left[\frac{N_2}{N_t}\sinh h\gamma + \frac{N_3}{N_t}\sin 2h\gamma + \dots + \frac{N_{3q}}{N_t}\sin 3qh\gamma\right]\} \end{aligned} \quad (2.34)$$

The  $h^{th}$  harmonic winding factor for concentrated windings is therefore,

$$\begin{aligned} k_{ch} = & \cos\frac{h\gamma}{2}\left[\frac{N_1}{N_t} + \frac{N_2}{N_t}\cosh h\gamma + \frac{N_3}{N_t}\cos 2h\gamma + \dots + \frac{N_{3q}}{N_t}\cos 3qh\gamma\right] \\ & - \sin\frac{h\gamma}{2}\left[\frac{N_2}{N_t}\sinh h\gamma + \frac{N_3}{N_t}\sin 2h\gamma + \dots + \frac{N_{3q}}{N_t}\sin 3qh\gamma\right] \end{aligned} \quad (2.35)$$

Figure 2.7 shows the case where the coil sides of the windings of one phase occupy all of the slots of the machine ( $180^\circ$  phase belt). In general the lap windings can be inserted in any number of slots per pole. Assuming an integer number for  $q$  the concentrated winding phase belts can take on values of  $60(n/q)$ ,  $n = 1, 2, \dots, 3q$ . For example when  $q = 1$ , then 60, 120 and  $180^\circ$  are possible. When  $q = 2$ , then 30, 60, 90, 120, 150 and  $180^\circ$  phase belts can be obtained, and so forth. When phase belts between 120 and  $180^\circ$  is chosen, a fraction of the slots contain coils from two phase while the remainder contain coils from three phases. Conversely, when a phase belt between 60 and  $180^\circ$  is used some of the coils contain windings from one phase while the remainder contain windings from two phases. If a phase belt of  $120^\circ$  is chosen all of the slots contain windings from two phases. Hence, it is configuration that can be easily wound and is frequently encountered.

The presence of the winding ratios  $N_1/N_t$ ,  $N_2/N_t$ , etc. clearly opens the door for selecting these ratios in an optimal manner so as to minimize the harmonic content in the resulting *MMF* waveform. This work has been carried out in Ref. [2] by minimizing the total harmonic distortion given by

$$THD = \sqrt{\sum_{h=2}^{\infty} \mathcal{F}_{ph}^2} \quad (2.36)$$

Table 2.5 to Table 2.8 show optimal winding patterns for  $120^\circ$  phase belt windings with values of  $q$  ranging from 2 to 5 and for values of  $N_t$  ranging from 4 to 30. The numbers in the table show the number of turns over  $180^\circ$  progressing left to right from the interpolar axis to the polar axis. For example in the first row with  $N_t = 4$  the number of turns of Coil #1 of Figure 2.7 (containing  $N_1$  turns) is zero, the turns of Coil #2 is zero, Coil #3 is 2, Coil #4 is 2, Coils #5 and #6 are again zero. The distribution of turns in the other phases are appropriately phase shifted by plus or minus  $120$  electrical degrees.

**Table 2.5 Optimal Number of Turns for Concentric Windings with 120° Phase Belts and with  $q = 2$**

$N_t$	$N_1$	$N_2$	$N_3$	$N_4$	$N_5$	$N_6$	$k_{c1}$	THD
4	0	0	2	2	0	0	1.0	0.5010
5	0	1	2	1	1	0	0.8928	0.4327
6	0	1	2	2	1	0	0.9107	0.3894
7	0	1	2	3	1	0	0.9234	0.3595
8	0	1	3	3	1	0	0.9330	0.3595
9	0	1	3	4	1	0	0.9405	0.3762
10	0	1	4	4	1	0	0.9464	0.3894
11	0	1	4	4	2	0	0.9269	0.3515
12	0	2	4	4	2	0	0.9107	0.3894
13	0	2	5	4	2	0	0.9176	0.3732
14	0	2	5	5	2	0	0.9234	0.3595
15	0	2	6	5	2	0	0.9285	0.3494
16	0	2	6	6	2	0	0.9330	0.3595
17	0	2	6	7	2	0	0.9369	0.3684
18	0	2	7	7	2	0	0.9405	0.3762
19	0	3	7	7	2	0	0.9295	0.3515
20	0	3	7	7	3	0	0.9196	0.3684
21	0	3	8	7	3	0	0.9234	0.3595
22	0	3	8	8	3	0	0.9269	0.3515
23	0	3	9	8	3	0	0.9301	0.3529
24	0	3	9	9	3	0	0.9330	0.3595
25	0	4	9	9	3	0	0.9250	0.3560

**Table 2.6 Optimal Number of Turns for Concentric Windings with 120° Phase Belts and with  $q = 3$**

$N_t$	$N_1$	$N_2$	$N_3$	$N_4$	$N_5$	$N_6$	$N_7$	$N_8$	$N_9$	$k_{c1}$	THD
6	0	0	0	2	2	2	0	0	0	0.9598	0.3223
7	0	0	1	2	2	1	1	0	0	0.9073	0.1948
8	0	0	1	2	2	2	1	0	0	0.9114	0.2330
9	0	0	1	2	3	2	1	0	0	0.9212	0.1995
10	0	0	1	3	3	2	1	0	0	0.9231	0.1964
11	0	0	1	3	3	3	1	0	0	0.9246	0.2135
12	0	0	1	3	4	3	1	0	0	0.9309	0.2133
13	0	0	2	3	4	3	1	0	0	0.9182	0.1739
14	0	0	2	3	4	3	2	0	0	0.9073	0.1948
15	0	0	2	3	5	3	2	0	0	0.9135	0.2011
16	0	0	2	4	5	3	2	0	0	0.9151	0.1758
17	0	0	2	4	5	4	2	0	0	0.9166	0.1806
18	0	0	2	4	6	4	2	0	0	0.9212	0.1995
19	0	0	2	5	6	4	2	0	0	0.9222	0.1865
20	0	0	2	5	6	5	2	0	0	0.9231	0.1964
21	0	0	3	5	6	5	2	0	0	0.9156	0.1906
22	0	0	3	5	6	5	3	0	0	0.9088	0.2053
23	0	0	3	5	7	5	3	0	0	0.9127	0.1806
24	0	0	3	6	7	5	3	0	0	0.9139	0.1832
25	0	0	3	6	7	6	3	0	0	0.9149	0.1973

**Table 2.7 Optimal Number of Turns for Concentric Windings with 120° Phase Belts and with  $q = 4$**

$N_t$	$N_1$	$N_2$	$N_3$	$N_4$	$N_5$	$N_6$	$N_7$	$N_8$	$N_9$	$N_{10}$	$N_{11}$	$N_{12}$	$k_{c1}$	THD
9	0	0	0	0	2	3	2	2	0	0	0	0	0.9697	0.3379
10	0	0	0	1	1	3	3	1	1	0	0	0	0.9464	0.2636
11	0	0	0	1	2	3	3	1	1	0	0	0	0.9451	0.2082
12	0	0	0	1	2	3	3	2	1	0	0	0	0.9440	0.1760
13	0	0	0	2	2	3	3	2	1	0	0	0	0.9329	0.1611
14	0	0	0	2	2	3	3	2	2	0	0	0	0.9234	0.1838
15	0	0	0	2	2	4	3	2	2	0	0	0	0.9285	0.1567
16	0	0	0	2	2	4	4	2	2	0	0	0	0.9330	0.1838
17	0	0	0	2	2	4	5	2	2	0	0	0	0.9370	0.2075
18	0	0	0	2	2	5	5	2	2	0	0	0	0.9405	0.1658
19	0	0	0	2	3	5	4	3	2	0	0	0	0.9364	0.2067
20	0	0	0	2	3	5	4	3	2	0	0	0	0.9396	0.1706
21	0	0	0	2	3	5	5	3	2	0	0	0	0.9241	0.1712
22	0	0	1	2	3	5	5	3	2	1	0	0	0.9100	0.1749
23	0	0	1	2	3	5	5	4	2	1	0	0	0.9109	0.1596
24	0	0	1	2	4	5	5	4	2	1	0	0	0.9118	0.1456
25	0	0	1	2	4	5	5	4	3	1	0	0	0.9074	0.1332

**Table 2.8 Optimal Number of Turns for Concentric Windings with 120° Phase Belts and with  $q = 5$**

$N_t$	$N_1$	$N_2$	$N_3$	$N_4$	$N_5$	$N_6$	$N_7$	$N_8$	$N_9$	$N_{10}$	$N_{11}$	$N_{12}$	$N_{13}$	$N_{14}$	$N_{15}$	$k_{c1}$	THD
12	0	0	0	0	1	2	2	3	2	1	1	0	0	0	0	0.9393	0.1440
13	0	0	0	0	1	2	2	3	2	2	1	0	0	0	0	0.9373	0.1526
14	0	0	0	0	1	2	3	3	2	2	1	0	0	0	0	0.9402	0.1326
15	0	0	0	0	1	2	3	3	3	2	1	0	0	0	0	0.9427	0.1262

**Table 2.8 Optimal Number of Turns for Concentric Windings with 120° Phase Belts and with  $q = 5$**

$N_r$	$N_1$	$N_2$	$N_3$	$N_4$	$N_5$	$N_6$	$N_7$	$N_8$	$N_9$	$N_{10}$	$N_{11}$	$N_{12}$	$N_{13}$	$N_{14}$	$N_{15}$	$k_{cl}$	THD
16	0	0	0	1	1	2	3	3	3	2	1	0	0	0	0	0.9256	0.1106
17	0	0	0	1	1	2	3	3	3	2	1	1	0	0	0	0.9106	0.1257
18	0	0	0	1	2	2	3	3	3	2	1	1	0	0	0	0.9049	0.0963
19	0	0	0	1	2	22	3	3	2	2	2	1	0	0	0	0.8999	0.1011
20	0	0	0	1	2	2	3	4	3	2	2	1	0	0	0	0.9049	0.0934
21	0	0	0	1	2	2	3	4	3	2	2	1	0	0	0	0.9053	0.0899
22	0	0	0	1	2	3	3	4	3	3	2	1	0	0	0	0.9057	0.1031
23	0	0	0	1	2	3	4	4	3	3	2	1	0	0	0	0.9088	0.0805
24	0	0	0	1	2	3	4	4	4	3	2	1	0	0	0	0.9117	0.0832
25	0	0	0	1	2	3	4	5	4	3	2	1	0	0	0	0.9152	0.0882

## 2.5 Effect of Slot Openings

Although it has been assumed to this point that the *MMF* changes abruptly when each coil is encountered when traversing the inner surface of the stator, the slot opening has filtering effect on the *MMF*. While the exact variation of *MMF* across an open slot is difficult to determine, the effect is well approximated by assuming that the *MMF* varies linearly across the slot as shown in Figure 2.8 for a single concentrated coil. Any *MMF* harmonic  $h$  can now be represented by the Fourier coefficient,

$$\mathcal{F}_{ph} = \left( \frac{4}{\pi} \right) \frac{N_r I}{2} \left[ \int_0^{\chi/2} \frac{\theta}{(\frac{\chi}{2})} \sin h\theta d\theta + \int_{\chi/2}^{\pi/2} \sin h\theta d\theta \right] \quad (2.37)$$

which when solved becomes, assuming only odd harmonics,

$$\mathcal{F}_{ph} = \left( \frac{4}{\pi} \right) \left( \frac{N_r I}{2h} \right) \frac{\sin \left( \frac{h\chi}{2} \right)}{\left( \frac{h\chi}{2} \right)} \quad (2.38)$$

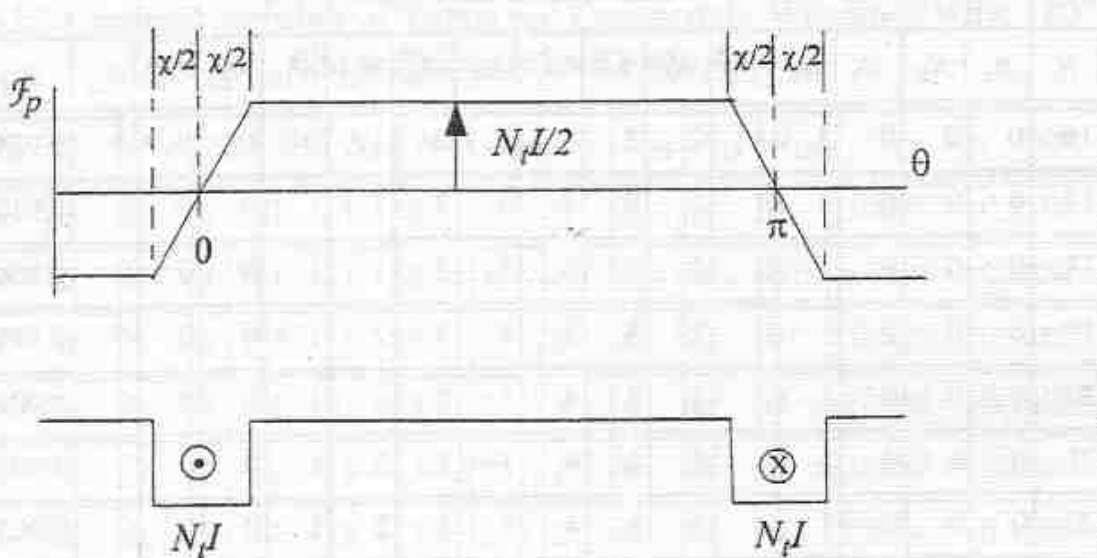


Figure 2.8 Concentrated full pitch coil including the effects of slot opening.

The added factor, the *slot opening factor*, can be defined as

$$k_{\chi h} = \frac{\sin\left(\frac{h\chi}{2}\right)}{\left(\frac{h\chi}{2}\right)} \quad (2.39)$$

Since this term is common to all coils, it simply becomes a coefficient in the final expression for *MMF* harmonics. With slot opening accounted for, the *MMF* harmonics, previously given by Eq. (2.29), can be altered to form,

$$\mathcal{F}_{ph} = \left(\frac{4}{\pi}\right) \left(\frac{N_t I}{2h}\right) k_{ph} k_{dh} k_{\chi h} \quad (h \text{ odd}) \quad (2.40)$$

## 2.6 Fractional Slot Windings

From the previous section it is clear that it is desirable to increase  $q$ , the number of slots per pole per phase to as large a value as possible so as to reduce the slot harmonic frequency. An increase in  $q$  implies a corresponding increase in the number of slots for a machine with a specified number of poles. In some cases where the pole number is large, a value of even  $q=2$  cannot be reached

without the number of slots reaching a prohibitively large number for the machine rating. Rather than select a value of  $q=1$  resulting in strong slot harmonics at the fifth and seventh harmonic, a fractional value of  $q$  can be chosen. In some cases, for example in very large water wheel generators, values of  $q$  less than even unity is often chosen.

Although the number of slots of a fractional slot winding arrangement is not a multiple of the number of poles, it must be multiple of the number of phases in order to maintain phase symmetry. In the case of a three phase machine, this constraint stipulates that the number of slots must be at least a multiple of three. Consider, for example, a three phase winding for a 10 pole machine. In this case the machine must have at least 30 slots ( $q=1$ ) to maintain phase symmetry. If we desire  $q=2$  this would imply that the machine must have 60 slots, too large a number for most small machines. Instead if we pick 42 stator slots, then  $q=42/(3 \cdot 10) = 7/5$  slots per pole per phase. Thus, there are  $(7/5) \cdot 3 = 21/5$  slots per pole; suggesting that the winding arrangement must fit into 21 slots distributed over 5 poles and that the winding pattern will begin to repeat after five poles are wound. The fact that  $q = 7/5$  implies that the slots occupied by one of the phases over consecutive poles must alternate in some manner between 2 and 1 slots occupied per pole. For example the pattern 2,1,1,2,1 can potentially satisfy this requirement as can the pattern 1,1,2,2,1.

In order to determine which one of several possible patterns is most desirable it is first necessary to choose the pitch of the winding which is assumed to be the same for all coils. For this example, the phase shift in electrical degrees between slots is  $10 \cdot 180/42 = 42 \frac{6}{7}^\circ$ . Hence, if the coil spans four slots the pitch angle in electrical degrees is  $180 - 4 \cdot (42 \frac{6}{7}) = 8 \frac{4}{7}^\circ$  which is probably the best choice. The pitch factor for the fundamental component of the winding becomes, from Eq. (2.13),

$$k_{p1} = \cos\left(\frac{8.57}{2}\right) = 0.997 \quad (2.41)$$

Since the winding pattern repeats after 21 slots, a sketch of the first 21 slots of the machine can be constructed as shown in Figure 2.9 with the first coil of one of the three phases inserted in slots 1 and 5 (coil short pitched by  $4 \frac{2}{7}^\circ$  and spanning four slots). This coil is designated as coil #1.

Coil #1 can now be considered as the reference coil and a second coil inserted in slots 2 and 6. If it is assumed that these coils are excited by a sinu-

sinoidal 10 pole travelling wave in the air gap, the voltage induced in this second coil can be considered to be phase shifted (phase delayed) by  $42\frac{6}{7}^\circ$  from coil #1. These sinusoidal induced voltages can be expressed as phasors as shown in Figure 2.10. Proceeding now with a third coil placed in slots 3 and 7, the voltage induced in this coil will lag the voltage induced in coil #1 by  $85\frac{5}{7}^\circ$ . It is possible to now proceed with all such coils placed in slots 4-8, 5-9,..., until 21-25. The 21 phasors form the phasor diagram of Figure 2.10.

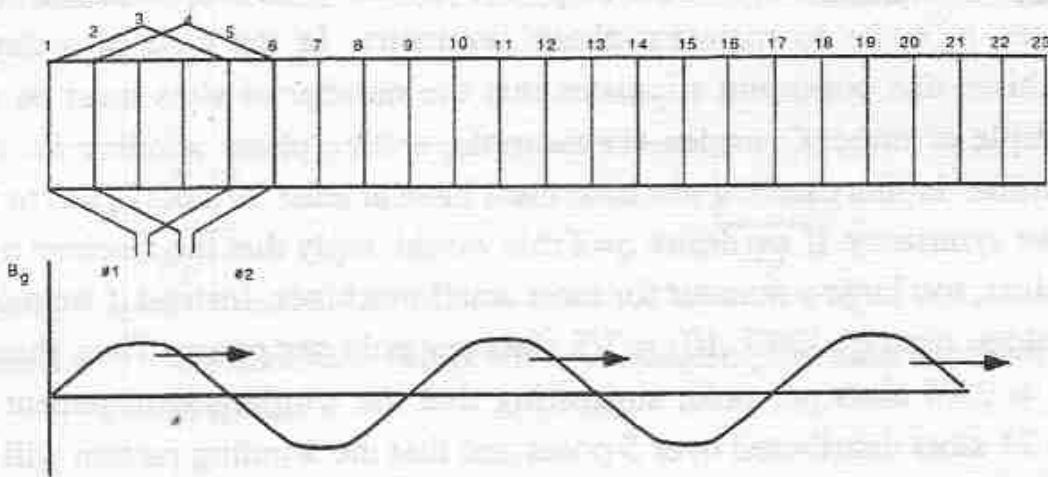


Figure 2.9 Showing first 21 slots of machine with first and second coils inserted in slots 1 and 5 and also 2 and 6

It is now possible to collect all of the coil voltages which are intended to contribute to one of the three phases, say phase *a*. If we consider coil #1 to be associated with phase *a*, then all of the coils encountered clockwise over the next 60 degrees can be claimed for phase *a*. This includes coils #1, 18, 10, 2 and 19. In addition, if we reverse the polarity of coils 6 and 14 we can also claim these for phase *a* making a total of 7 of the 21 coils (as required for one phase of the three phase system). Phase *b* can now be made up of coils 4, 5, -8, -9, 13, -17 and 21. Phase *c* is made up of coils -3, 7, -11, -12, 15, 16, and -20. (The minus signs indicate the reversal of the polarity of the coil). Figure 2.12 shows the winding layout of the three phases over the five pole, 21 slot portion of the machine. The winding pattern for the remaining 5 poles is, of course, identical. Note that each slot is occupied by two coils sides. Even though the coils are taken from different poles it can be said that the winding forms an equivalent  $60^\circ$  phase belt distributed over 7 slots ( $\gamma=8\frac{4}{7}^\circ$ ). The distribution factor is therefore

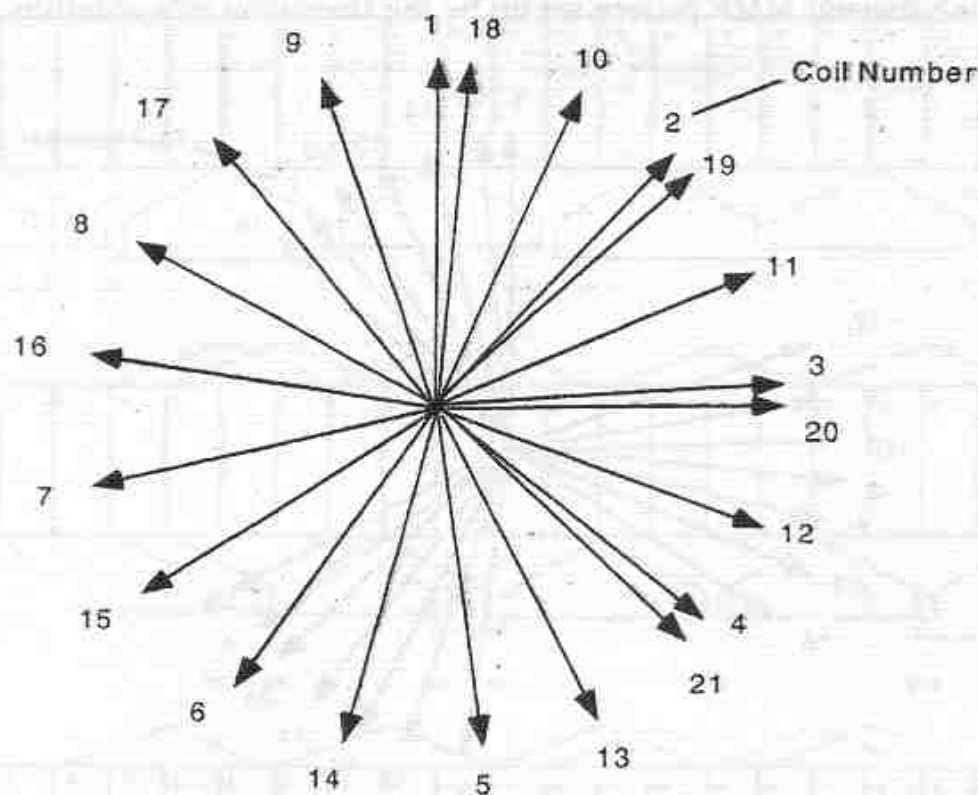


Figure 2.10 Showing EMF of the 21 Coils inserted in slots 1-5, 2-6, 3-7,...,21-25.

$$k_{dl} = \frac{\sin\left(7 \cdot \frac{60}{7 \times 2}\right)}{7 \sin\left(\frac{60}{7 \times 2}\right)} = 0.956 \quad (2.42)$$

The product of the pitch and distribution factor for this winding layout is consequently,

$$k_{p1} k_{dl} = 0.997 \times 0.956 = 0.953 \quad (2.43)$$

Similar results can be shown to apply for the other odd winding harmonics. It is important to mention however, that when the approach is used for machines in which induced currents can flow on the other member, i.e. squirrel cage induction and synchronous machines with amortisseur windings during starting. These additional losses will be caused by the fractional slot approach as

the short circuited bars progressively moves through the magnetic field set up by the unbalanced *MMF* pattern set up by the fractional slot winding.

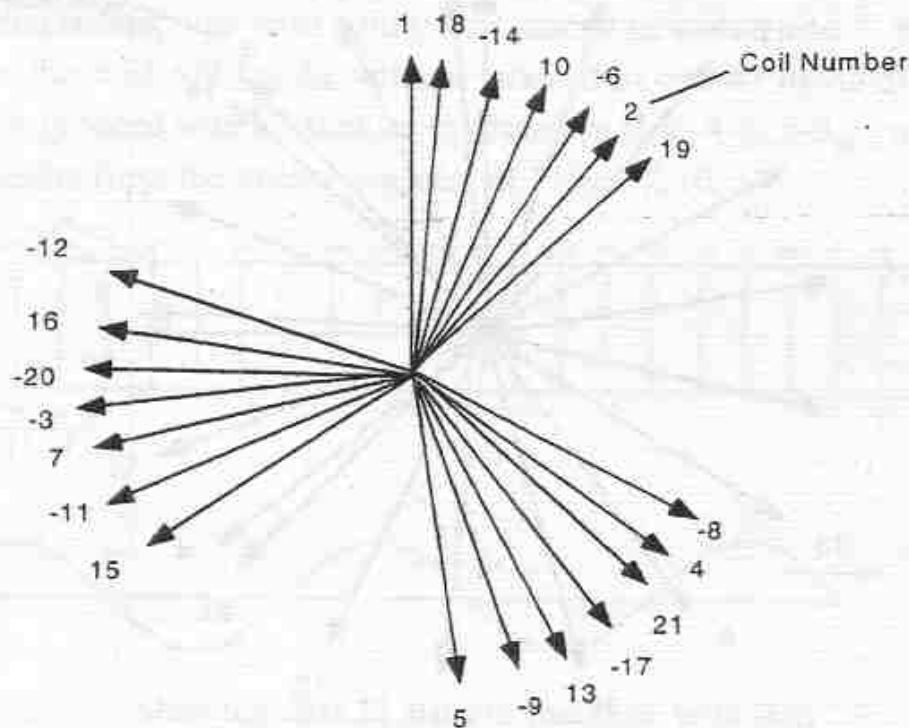


Figure 2.11 EMFs of coils making up the three phases after reversing the polarities of coils to obtain "60° phase belts".

## 2.7 Winding Skew

While pitching and distributing the winding has the effect of reducing the harmonics, substantial harmonics typically remain primarily associated with the slot harmonics. Such harmonics of higher order can be further reduced by "skewing" the winding. Skewing is invariably done to the rotor of a squirrel cage induction machine in order to reduce the so-called cogging or subsynchronous torques which occur without skewing. In addition, the stator slots are sometimes skewed in smaller salient pole synchronous generators or the poles in larger slow speed salient pole generators. In this case the skewing also reduces the flux variation in the fringing of the flux at the pole tips due to the slots entering and leaving the poles which leads to acoustic noise problems.

In order to illustrate the effect of skew let us again consider a single full-pitch concentrated coil having one slot per pole. In this case the slot is con-

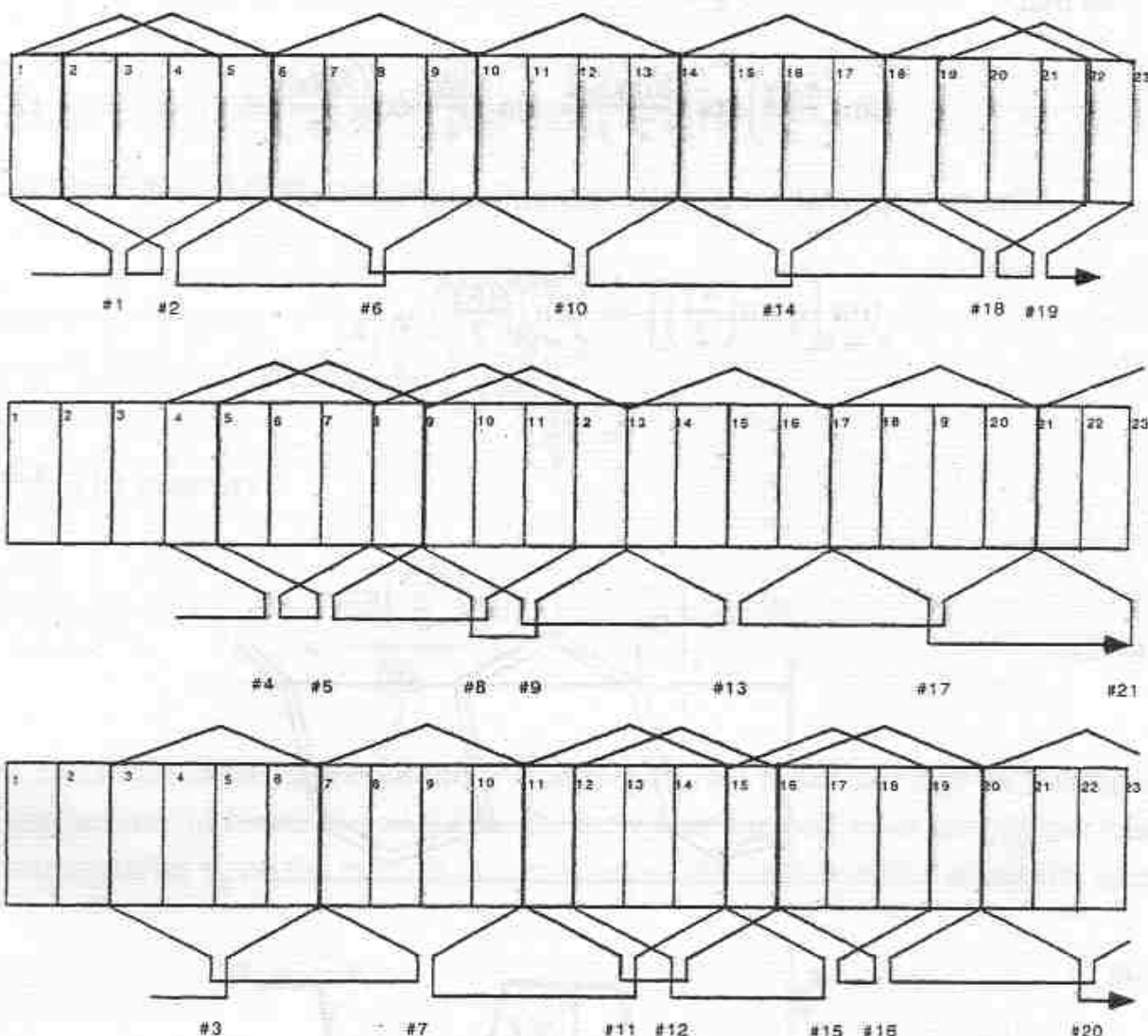


Figure 2.12 Winding layout of the three phases over the first five poles

structed so that the winding is twisted circumferentially in the slot of "skewed" by an angle  $\alpha$ . The corresponding *MMF* acting in the gap becomes dependent on the axial position. However "on the average" the effective *MMF* is again a rectangular function but with sloping sides as shown. The harmonic components of the resulting *MMF* can again be calculated by means of Fourier Series. However, with proper interpretation, the harmonic coefficients can be obtained directly from Eq. (2.23). In particular, note that as the number of slots (coil sides)  $q$  approach infinity the resulting shape assumes the continuous function of Figure 2.13. Although  $q$  becomes infinite, it is clear that the product  $q\gamma$  remains constant. In particular,

$$q\gamma = \alpha/2 \quad (2.44)$$

so that

$$\sin\left(\frac{ha\gamma}{2}\right)\cos\left(\frac{hq\gamma}{2}\right) = \sin\left(\frac{h\alpha}{4}\right)\cos\left(\frac{h\alpha}{4}\right) \quad (2.45)$$

Also, as  $\gamma$  approaches zero the denominator becomes

$$\begin{aligned} \lim_{\gamma \rightarrow 0} \left[ q \sin\left(\frac{h\gamma}{2}\right) \right] &= \lim_{\gamma \rightarrow 0} \left( \frac{qh\gamma}{2} \right) \\ &= \frac{h\alpha}{4} \end{aligned} \quad (2.46)$$

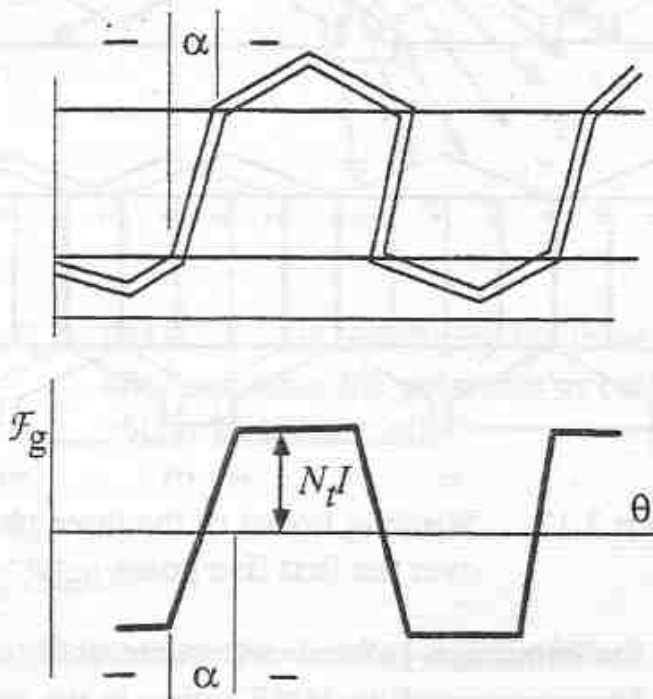


Figure 2.13 Concentrated full pitch coil skewed by a skew angle  $\alpha$

Hence, as the number of slots tend to infinity Eq. (2.23) becomes

$$\mathcal{F}_{ph} = \left(\frac{4}{\pi}\right) \left(\frac{N_t I}{2h}\right) \frac{\sin\left(\frac{h\alpha}{4}\right)\cos\left(\frac{h\alpha}{4}\right)}{\frac{h\alpha}{4}} \quad (2.47)$$

However

$$\sin\left(\frac{h\alpha}{4}\right)\cos\left(\frac{h\alpha}{4}\right) = \frac{1}{2}\sin\left(\frac{h\alpha}{2}\right)$$

so that Eq. (2.47) reduces to

$$\mathcal{F}_{ph} = \frac{4}{\pi} \left( \frac{N_t I}{2h} \right) \frac{\sin\left(\frac{h\alpha}{2}\right)}{\left(\frac{h\alpha}{2}\right)} \quad (2.48)$$

The quantity

$$k_{sh} = \frac{\sin\left(\frac{h\alpha}{2}\right)}{\frac{h\alpha}{2}} \quad (2.49)$$

is called the *skew factor* for the  $h^{th}$  harmonic. This result can also be written in another useful form. If we let  $Z$  be the arc which the coil sides occupy per pole and again let  $\tau_p$  be the pole pitch measured on the surface of the armature, then

$$\alpha = \frac{Z}{\tau_p} \pi \quad (2.50)$$

and  $k_{sh}$  can be expressed as

$$k_{sh} = \frac{\sin\left[h\left(\frac{Z}{\tau_p}\right)\frac{\pi}{2}\right]}{h\left(\frac{Z}{\tau_p}\right)\frac{\pi}{2}} \quad (2.51)$$

The *MMF* for a distributed, fractional pitch winding with skew can again be computed by considering these effects separately. The combined effect can then be obtained by taking the product of the four winding factors.

$$\mathcal{F}_{ph} = \frac{4N_t I}{\pi 2h} k_{ph} k_{dh} k_{\chi h} k_{sh} \quad (2.52)$$

The product

$$k_h = k_{ph} k_{dh} k_{\chi h} k_{sh} \quad (2.53)$$

is often termed simply the *winding factor*.

## 2.8 Pole Pairs and Circuits Greater than One

Thus far, *MMF* distributions for two pole, single circuit machines have been discussed. The actual number of electrical poles, however, depends upon design considerations which will be discussed later. This number is nearly always greater than two, since two pole machines are particularly wasteful of stator conductors due to large return paths at the end of the machine (end windings). A bulky end winding also results in a machine with high leakage reactance which is often an undesirable design. Also, because of the large amount of flux per pole, the amount of core material that must be used in the stator tends to increase. Finally, it is also difficult to find sufficient room in the rotor of the machine to contain the large flux per pole. In general, for a  $P$  pole machine, with  $N_t$  total turns and with all poles connected in series, the *MMF* for the  $h^{\text{th}}$  harmonic, Eq. (2.52), becomes

$$\mathcal{F}_{ph} = \frac{4}{\pi} \left( \frac{N_t I}{P} \right) \frac{k_{ph} k_{dh} k_{\chi h} k_{sh}}{h} \quad (2.54)$$

As a final complication, phase windings are often not all connected in series to form one continuous path for each phase. Practical considerations such as limited wire diameters often require that two or more poles be connected in parallel rather than in series in order to achieve the required number of turns with the wire diameters available. The number of parallel circuits must always result in equal voltage across each circuit in order to avoid circulating currents. In order to avoid this problem, the ratio of poles to circuits must clearly be an integer. The final general expression for the  $h^{\text{th}}$  harmonic of a  $P$  pole,  $C$  circuit winding is

$$\mathcal{F}_{ph} = \frac{4}{\pi} \left( \frac{N_t I}{CP} \right) \frac{k_{ph} k_{dh} k_{\chi h} k_{sh}}{h} \quad h = 1, 3, 5, 7, \dots \quad (2.55)$$

where the current  $I$  is now taken to be the net current into the  $C$  circuits, that is, the current for each circuit is  $I/C$ .

## 2.9 MMF Distribution for Three Phase Windings

When the machine is excited with three symmetrically wound coils the net *MMF* acting on the magnetic circuits of the machine is the superposition of the three *MMFs* of the individual coils. Assuming that the three coils are wound

identically but physically placed in the machine at  $120^\circ$  intervals, the MMFs of the three windings  $a, b, c$  be written as

$$\mathcal{F}_a = \frac{4}{\pi} \left( \frac{N_t i_a}{CP} \right) \sum_{h \text{ odd}} k_h \frac{\sin \frac{P}{2} h \theta}{h} \quad (2.56)$$

$$\mathcal{F}_b = \frac{4}{\pi} \left( \frac{N_t i_b}{CP} \right) \sum_{h \text{ odd}} k_h \frac{\sin h \frac{P}{2} \left( \theta - \frac{4\pi}{3P} \right)}{h} \quad (2.57)$$

$$\mathcal{F}_c = \frac{4}{\pi} \left( \frac{N_t i_c}{CP} \right) \sum_{h \text{ odd}} k_h \frac{\sin h \frac{P}{2} \left( \theta + \frac{4\pi}{3P} \right)}{h} \quad (2.58)$$

where

$$k_h = k_{ph} k_{dh} k_{\chi h} k_{sh}$$

With the aid of trig identities, Eqs. (2.56) to (2.58) can also be written in the form

$$\mathcal{F}_a = \frac{4}{\pi} \left( \frac{N_t i_a}{CP} \right) \sum_{h \text{ odd}} k_h \frac{\sin [(hP\theta)/2]}{h} \quad (2.59)$$

$$\mathcal{F}_b = \frac{4}{\pi} \left( \frac{N_t i_b}{CP} \right) \sum_{h \text{ odd}} k_h \left[ \frac{\sin [(hP\theta)/2]}{h} \cos \frac{2h\pi}{3} - \frac{\cos [(hP\theta)/2]}{h} \sin \frac{2h\pi}{3} \right] \quad (2.60)$$

$$\mathcal{F}_c = \frac{4}{\pi} \left( \frac{N_t i_c}{CP} \right) \sum_{h \text{ odd}} k_h \left[ \frac{\sin [(hP\theta)/2]}{h} \cos \frac{2h\pi}{3} + \frac{\cos [(hP\theta)/2]}{h} \sin \frac{2h\pi}{3} \right] \quad (2.61)$$

The three MMFs can be summed to form

$$\begin{aligned}\mathcal{F}_a + \mathcal{F}_b + \mathcal{F}_c &= \frac{4}{\pi} \left( \frac{N_t}{CP} \right) \sum_{h \text{ odd}} \frac{k_h}{h} \left( i_a + i_b \cos \frac{2h\pi}{3} + i_c \cos \frac{2h\pi}{3} \right) \sin [(hP\theta)/2] \\ &\quad + \left( i_c \sin \frac{2h\pi}{3} - i_b \sin \frac{2h\pi}{3} \right) \cos [(hP\theta)/2]\end{aligned}\tag{2.62}$$

Now

$$\cos \frac{2h\pi}{3} = -1/2 \quad \text{for } h = 1, 5, 7, 11, \dots$$

$$\cos \frac{2h\pi}{3} = 1 \quad \text{for } h = 3, 9, 15, \dots$$

$$\sin \frac{2h\pi}{3} = \frac{\sqrt{3}}{2} \quad \text{for } h = 1, 7, 13, \dots$$

$$\sin \frac{2h\pi}{3} = -\frac{\sqrt{3}}{2} \quad \text{for } h = 5, 11, \dots$$

$$\sin \frac{2h\pi}{3} = 0 \quad \text{for } h = 3, 9, 15, \dots$$

Let us assume that the machine has no neutral return, then

$$i_a + i_b + i_c = 0 \tag{2.63}$$

Equation (2.66) reduces to the form

$$\begin{aligned}\mathcal{F}_a + \mathcal{F}_b + \mathcal{F}_c &= \frac{4}{\pi} \left( \frac{N_t}{CP} \right) \sum_{h=1, 5, 7, 11, \dots} \frac{k_h}{h} \left[ \left( \frac{3i_a}{2} \right) \sin [(hP\theta)/2] \right. \\ &\quad \left. + \frac{\sqrt{3}}{2} (\pm 1) (i_c - i_b) \cos [(hP\theta)/2] \right]\end{aligned}\tag{2.64}$$

where

$$(\pm 1) = 1 \quad \text{for } h = 1, 7, 13, \dots$$

and

$$(\pm 1) = -1 \quad \text{for } h = 5, 11, 17, \dots$$

Note that the third harmonic components have been eliminated if the machine has no neutral return.

Consider now the special case of balanced sinusoidal currents, that is

$$i_a = I_m \cos \omega_e t \quad (2.65)$$

$$i_b = I_m \cos \left( \omega_e t - \frac{2\pi}{3} \right) \quad (2.66)$$

$$i_c = I_m \cos \left( \omega_e t + \frac{2\pi}{3} \right) \quad (2.67)$$

It can be shown that

$$\frac{\sqrt{3}}{2}(i_c - i_b) = -\frac{3}{2}I_m \sin \omega_e t \quad (2.68)$$

Equation (2.64) can now be written in the form

$$\begin{aligned} \mathcal{F}_a + \mathcal{F}_b + \mathcal{F}_c &= \left(\frac{3}{2}\right)\left(\frac{4}{\pi}\right)\left(\frac{N_t I_m}{CP}\right) \sum_{h=1, 5, 7, \dots} \frac{k_h}{h} [\sin((hP\theta)/2) \cos \omega_e t \\ &\quad - (\pm 1) \cos((hP\theta)/2) \sin \omega_e t] \end{aligned} \quad (2.69)$$

which reduces to

$$\begin{aligned} \mathcal{F}_a + \mathcal{F}_b + \mathcal{F}_c &= \frac{3}{2}\left(\frac{4}{\pi}\right)\left(\frac{N_t I_m}{CP}\right) \left[ \sum_{h=1, 7, 13, \dots} \frac{k_h}{h} \sin\left(\frac{hP\theta}{2} - \omega_e t\right) \right. \\ &\quad \left. + \sum_{h=5, 11, 17, \dots} \frac{k_h}{h} \sin\left(\frac{hP\theta}{2} + \omega_e t\right) \right] \end{aligned} \quad (2.70)$$

Hence balanced, sinusoidal operation of a machine with a practical winding distribution containing odd harmonic results in an *MMF* which produces positively and negatively rotating *MMFs* in the machine. Each of these *MMFs* are of constant amplitude and rotate in the forward direction for  $h = 1, 7, 13, 19, \dots$  and in the negative direction for  $h = 5, 11, 17, \dots$ . The harmonic components corresponding to  $h = 3, 9, \dots$  are not present if the machine has no neutral return, i.e.,

no zero sequence component. It is important to note that the amplitude of each *MMF* harmonic is  $3/2$  times the amplitude of the *MMF* for an individual phase. The *MMFs* corresponding to  $n$  greater than one are called the *space harmonics* of the machine winding. The velocity of rotation of these *MMFs* can be found by differentiating the argument of the sine function. Hence the velocity of the  $n$ th harmonic of *MMF* is

$$\frac{d\left(\frac{hP\theta}{2} - \omega_e t\right)}{dt} = \left(\frac{hP}{2}\right) \frac{d}{dt} - \omega_e$$

or

$$\frac{d\theta}{dt} = \frac{2\omega_e}{hP} \quad (2.71)$$

so that the synchronous mechanical speed for each harmonic is an integer fraction of the speed of rotation of the fundamental component of *MMF*.

## 2.10 Concept of an Equivalent Two Phase Machine

It is interesting to note that the form of Eq. (2.70) has implications concerning modeling of three phase machines. In particular since the coefficient of the bracketed term is precisely  $3/2$  greater than the coefficient of an individual phase, Eqs. (2.56) to (2.58), it is possible to replace the physical three phase windings by an equivalent two phase winding which results in the same instantaneous *MMF* in the gap of the machine. The form of the equivalent winding can be discerned if we examine the form of Eq. (2.64) which is a general expression for the instantaneous *MMF* in the gap for arbitrary values of currents  $i_a$ ,  $i_b$  and  $i_c$ . Note that, in effect, the *MMF* has at this point been decomposed into orthogonal components since the arguments of the angle  $\phi$  involve  $\sin n\phi$  and  $\cos n\phi$ . Although the concept can be extended to machines with a neutral, that does not concern us here. Hence, if we assume no neutral return, Eq. (2.64) results. If a three-halves factor is taken out of the square bracket there results

$$\mathcal{F}_a + \mathcal{F}_b + \mathcal{F}_c =$$

$$\left(\frac{3}{2}\right)\left(\frac{4}{\pi}\right)\left(\frac{N_t}{CP}\right) \sum_{h=1, 5, 7, 11\dots} \left[ i_a \frac{k_h}{h} \sin \frac{hP\theta}{2} + \frac{1}{\sqrt{3}}(i_c - i_b)(\pm 1) \frac{k_h}{h} \cos \frac{hP\theta}{2} \right] \quad (2.72)$$

Equation suggests that if we define two fictitious currents  $i_{qs}$  and  $i_{ds}$

$$i_{qs} = i_a \quad (2.73)$$

$$i_{ds} = \frac{1}{\sqrt{3}}(i_c - i_b) \quad (2.74)$$

which flow through winding distributions

$$N_{qs}(\theta) = \left(\frac{6}{\pi CP}\right) \sum_{h=1, 5, 7, 11\dots} \frac{k_h}{h} \sin \frac{hP\theta}{2} \quad (2.75)$$

and

$$N_{ds}(\theta) = \left(\frac{6}{\pi CP}\right) \sum_{h=1, 5, 7, 11\dots} (\pm 1) \left(\frac{k_h}{h}\right) \cos \frac{hP\theta}{2} \quad (2.76)$$

then the instantaneous MMF in the gap will remain unchanged. This concept forms the basis of *d-q* axis theory which we study in quite some detail in other course. We will make use of this concept later in our analysis of synchronous machines.

## 2.11 References

- [1] H.B. Dwight, "Tables of Integrals and Other Mathematical Data", 4th Ed, MacMillan, 1961.
- [2] Sang-Baeck Yoon, "Optimization of Winding Turns for Concentric Windings with 180 and 120 degree phase belts", Report, Univ. of Wisconsin, 24 May, 1999.

in the air gap between the two main magnetic poles. As the main magnetic flux density increases by following the magnetic path from one pole to the other, the total magnetomotive force per phase is increased due to the increase in the current in the primary winding. This is in accordance with the law of conservation of energy.

The total magnetomotive force per phase is given by the sum of the magnetomotive forces produced by the primary and secondary windings, assuming that the leakage fluxes due to the air gap are negligible.

$$M.M.F. = \frac{N_p}{R_p} + \frac{N_s}{R_s}$$

where  $N_p$  and  $N_s$  are the number of turns in the primary and secondary windings respectively, and  $R_p$  and  $R_s$  are the resistance of the primary and secondary windings respectively.

It is evident that the total magnetomotive force per phase is proportional to the primary current and the ratio of the primary to the secondary current is given by the ratio of the primary to the secondary resistance.

It is also evident that the total magnetomotive force per phase is proportional to the primary current and the ratio of the primary to the secondary current is given by the ratio of the primary to the secondary resistance.

It is also evident that the total magnetomotive force per phase is proportional to the primary current and the ratio of the primary to the secondary current is given by the ratio of the primary to the secondary resistance.

It is also evident that the total magnetomotive force per phase is proportional to the primary current and the ratio of the primary to the secondary current is given by the ratio of the primary to the secondary resistance.

It is also evident that the total magnetomotive force per phase is proportional to the primary current and the ratio of the primary to the secondary current is given by the ratio of the primary to the secondary resistance.

It is also evident that the total magnetomotive force per phase is proportional to the primary current and the ratio of the primary to the secondary current is given by the ratio of the primary to the secondary resistance.

It is also evident that the total magnetomotive force per phase is proportional to the primary current and the ratio of the primary to the secondary current is given by the ratio of the primary to the secondary resistance.

It is also evident that the total magnetomotive force per phase is proportional to the primary current and the ratio of the primary to the secondary current is given by the ratio of the primary to the secondary resistance.

It is also evident that the total magnetomotive force per phase is proportional to the primary current and the ratio of the primary to the secondary current is given by the ratio of the primary to the secondary resistance.

It is also evident that the total magnetomotive force per phase is proportional to the primary current and the ratio of the primary to the secondary current is given by the ratio of the primary to the secondary resistance.

It is also evident that the total magnetomotive force per phase is proportional to the primary current and the ratio of the primary to the secondary current is given by the ratio of the primary to the secondary resistance.

It is also evident that the total magnetomotive force per phase is proportional to the primary current and the ratio of the primary to the secondary current is given by the ratio of the primary to the secondary resistance.

# Chapter 3

## Main Flux Path Calculations Using Magnetic Circuits

### 3.1 The Main Magnetic Circuit of an Induction Machine

We are now in a position to calculate the fluxes and *MMF* drops in the main magnetic circuit of an induction machine. It has been shown in Chapter 2 that a balanced, sinusoidal set of currents results in an infinite series of constant amplitude, rotating *MMFs*. It can be shown that torque varies with the square of current, the corresponding higher harmonic fluxes produce negligible average torque. These harmonics interact with the main fundamental component of flux to produce primarily pulsating components of torque. Hence, these unwanted components of flux can be relegated to the category of "leakage" fluxes. In general, the higher space harmonics of flux within the machine are said to produce belt leakage and the corresponding inductance is termed the *belt leakage inductance*. We will have more to say regarding leakage inductances in Chapter 4.

If only the fundamental components of *MMF* are considered, the fluxes produced by balanced sinusoidal stator currents form symmetrical flux paths within the machine. For purposes of illustration, Figure 3.1, shows the situation for a four pole machine. The peak fundamental *MMF* per pole is given from Eq. (2.70) as

$$\mathcal{F}_{p1} = \frac{3}{2} \left( \frac{4}{\pi} \right) \left( \frac{N_t}{CP} \right) k_{p1} k_{d1} k_{s1} k_{\chi1} I_m \quad (3.1)$$

where  $k_{p1}$ ,  $k_{d1}$ ,  $k_{s1}$  and  $k_{\chi1}$  are the pitch, distribution, skew and slot opening factors for the fundamental component of *MMF* respectively,  $N_t / C$  is the number of series connected turns of the  $C$  circuits and  $I_m$  is the peak current per phase which is equal to the peak line current in the case of a wye connected machine.

It can be observed from Figure 3.1 that the flux for each circuit traverses two rotor teeth, two stator teeth, two air gaps, a portion of the stator core and finally a portion of the rotor core. For the present we will neglect the possibility of flux bypassing the teeth and passing through the slot on its way to the core. It is convenient to write Ampere's Law for this case as

$$2\mathcal{F}_{p1} = 2\mathcal{F}_{ts} + 2\mathcal{F}_{tr} + 2\mathcal{F}_g + \mathcal{F}_{cs} + \mathcal{F}_{cr} \quad (3.2)$$

where the subscript *ts* denotes the stator tooth drop, *tr* the rotor tooth drop, *cs* the stator core drop, *cr* the rotor core drop and *g* the *MMF* drop across the gap. In Chapter 1 it was assumed that the exciting ampere turns were concentrated in one portion of the core. However, in the case of an electrical machine the exciting *MMF* is distributed along the magnetic path. Also, the presence of slots along both the stator and rotor surfaces make the correction for the effect of the air gap considerably more complicated than in the case of a rectangular core. Nonetheless, the same principles set forth in Chapter 1 can be applied with proper attention to these effects. For this purpose it is useful to consider in detail each of the three key areas of the magnetic circuit, the air gap, the teeth and the core.

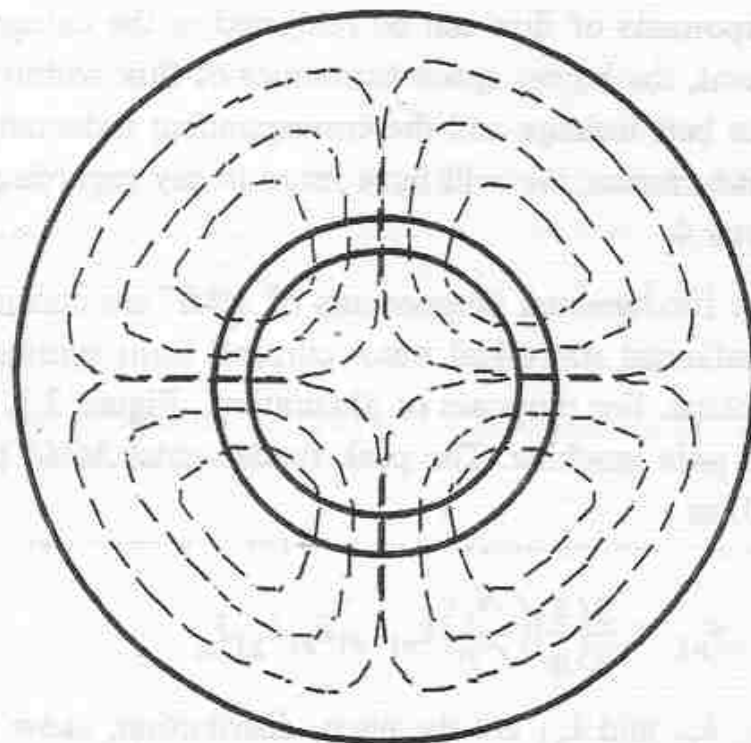


Figure 3.1 Flux distribution in a four pole machine

### 3.2 The Effective Gap and Carter's Coefficient

Although the permeability of the gap region is constant, it is bounded on either side by iron surfaces which, far from being smooth, are indented with slots in the circumferential direction and by cooling ducts in the axial direction. Rather than use more complicated expressions for reluctance it is conventional to derive equivalent values of cross sectional area and length and to continue to use the same expression derived in Chapter 1 for a magnetic path of uniform cross section.

In order to explain how the permeance of the air paths between a smooth iron surface and a slotted surface may be calculated, the flux lines will, for simplicity, be assumed to follow the paths indicated in Figure 3.2. The tooth is drawn, for convenience, with parallel sides and the magnetic lines entering the sides of the tooth are assumed to follow a path consisting of a straight portion of length  $g$  equal to the actual air gap, and a circular arc of radius  $r$  as indicated in the figure. Consider a portion of the air gap  $l_e$  inches long axially (i.e., in a direction normal to the plane of the section shown). Note that the permeance over the slot pitch of width  $\tau_s$  is made up of two parts a) the permeance  $P_1$  between the unslotted surface and the top of the tooth, and b) the permeance  $2P_2$  where  $P_2$  is the permeance between the unslotted surface and one side of the tooth.

In SI units the permeance  $P_1$  is simply

$$P_1 = \mu_o(\tau_s - b_o) \frac{l_e}{g} \quad \text{henries (H)} \quad (3.3)$$

The permeance of any small section of thickness  $dr$  and depth  $l_e$  meters in the region over the slot is

$$dP_2 = \frac{\mu_o l_e dr}{g + \left(\frac{\pi r}{2}\right)} \quad \text{henries (H)} \quad (3.4)$$

Hence, the total permeance over one side of the tooth is

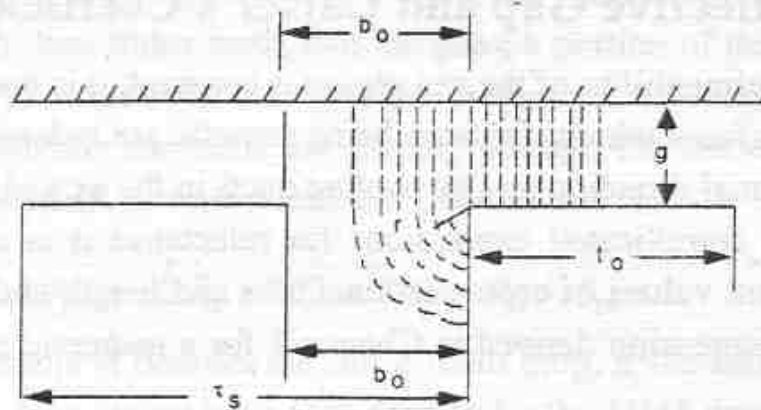


Figure 3.2 Approximate shape of flux lines entering a slotted armature

$$\begin{aligned}
 P_2 &= \frac{2\mu_o}{\pi} \int_0^{b_o/2} \frac{l_e dr}{\frac{2g}{\pi} + r} \\
 &= \frac{2\mu_o l_e}{\pi} \log_e \left[ \frac{g + \frac{\pi b_o}{4}}{g} \right]
 \end{aligned} \tag{3.5}$$

The total effective permeance of both the slot and tooth is therefore

$$\begin{aligned}
 P_g &= P_1 + 2P_2 \\
 &= \mu_o l_e \left\{ \frac{\tau_s - b_o}{g} + \frac{4}{\pi} \log_e \left[ 1 + \frac{\pi b_o}{4g} \right] \right\}
 \end{aligned} \tag{3.6}$$

The effective reluctance is the reciprocal of this quantity.

It is now possible to suppose that the actual slotted surface can be replaced by an equivalent unslotted surface having the same cross-section but with a modified "equivalent" gap. Equating the permeance of the equivalent unslotted surface to the actual permeance

$$\frac{\mu_o \tau_s l_e}{g_e} = \mu_o l_e \left\{ \frac{\tau_s - b_o}{g} + \frac{4}{\pi} \log_e \left[ 1 + \frac{\pi b_o}{4 g} \right] \right\} \quad (3.7)$$

Equation (3.7) can now be solved for the equivalent gap  $g_e$  as

$$g_e = \frac{\tau_s}{\frac{\tau_s - b_o}{g} + \frac{4}{\pi} \log_e \left[ 1 + \frac{\pi b_o}{4 g} \right]} \quad (3.8)$$

Alternatively, a so-called *Carter factor* can be defined such that

$$g_e = k_c g \quad (3.9)$$

where

$$k_c = \frac{\tau_s}{\tau_s - b_o + \frac{4g}{\pi} \log_e \left[ 1 + \frac{\pi b_o}{4 g} \right]} \quad (3.10)$$

The equation that we have derived assumes that the flux is evenly distributed along the side of the tooth to the depth  $b_o / 2$ . In reality the flux density is nonuniform with the highest flux density near the surface of the tooth and drops off as the flux penetrates into the tooth. A more exact formula, obtained by conformal mapping which takes account of the fact that the flux lines do not exactly follow the paths assumed in Figure 3.2, is given by

$$k_c = \frac{\tau_s}{\tau_s - \frac{2b_o}{\pi} \left\{ \tan^{-1} \frac{b_o}{2g} - \frac{g}{b_o} \log_e \left[ 1 + \left( \frac{b_o}{2g} \right)^2 \right] \right\}} \quad (3.11)$$

It can be shown that for large  $b_o / g$  this equation can be approximated by

$$k_c = \frac{\tau_s}{\tau_s - b_o + \frac{4g}{\pi} \log_e \left[ \frac{b_o}{2g} \right]} \quad (3.12)$$

Note that this result is remarkably similar to our previous result. In many cases a simple approximation to Eq. (3.11) suffices.

$$k_c \approx \frac{\tau_s}{\frac{b_o^2}{\tau_s - \frac{(5g + b_o)}{}}}$$
 (3.13)

The approximation is within 10% for  $b_o/g$  between one and infinity.

The effective gap  $g_e$  can be as much as 70 to 80 per cent greater than  $g$  for machines with open slots. For most practical machines however,  $g_e$  is generally found to be 15 to 25 per cent larger than  $g$ . If there are slot openings on both sides of the air gap, it can be shown that the effective gap length is found by multiplying the actual gap by the product of the two Carter factors, each calculated separately from either Eq. (3.11) or (3.12). That is, the effective gap for a doubly slotted machine is

$$k_c = k_{cs} k_{cr}$$
 (3.14)

where  $k_{cs}$  and  $k_{cr}$  are the Carter factors for the stator and rotor slotting respectively.

Thus far, the calculation of air gap permeance has been based on the assumption of infinite iron permeability. Consider now Figure 3.3(a) which illustrates the case of highly saturated tooth. Note that as the tooth saturates there will be more and more flux passing directly from the gap to the bottom of the slot in addition to the flux lines directed to the side of the tooth as previously calculated from Figure 3.2. A closer approximation to the actual conditions which exist in a saturated tooth may be obtained by assuming a parallel field in the slot superimposed on the field of Figure 3.2 as illustrated in Figure 3.3(b) and Figure 3.3(c). The resultant field in the slot and air gap will then be a closer approximation to that of Figure 3.3(a). With small values of tooth flux density the *MMF* between the tooth tops and the bottom of the slots will be small and only a few flux lines will pass from the pole face into the armature core without entering the teeth. With higher tooth densities, however the *MMF* to overcome the increasing tooth reluctance becomes larger and larger and more flux will be diverted into the parallel path and pass directly to the bottom of the slot.

The permeance of the slot portion of a single tooth pitch is simply

$$P_s = \frac{\mu_0 l_e b_{1/3}}{g/2 + d_s} \quad (3.15)$$

where  $b_{1/3}$  is the breadth of the slot taken 1/3 of the way from the narrow portion of the slot and  $d_s$  is the slot depth. This value of  $b$  is used to partially account for cases in which the slot is not exactly rectangular. Most often this condition occurs with rotor slots which often have a trapezoidal or "coffin" shape. In large machines the shape of the stator slot is rectangular with the tooth being non-uniform due to the cylindrical geometry. However, in small random wound machines the reverse is typically true and the same breadth factor can be used. It can be observed that only half the gap has been used in Eq. (3.14) with the other half of the gap being used to calculate the permeance of the corresponding rotor (or stator) tooth. The magnetic equivalent circuit for the region of one tooth is given in Figure 3.4. Note that the equivalent circuit is given in terms of reluctances which are simply the inverse of the permeances in this section. The tooth reluctance  $\mathcal{R}_t$  is as yet unknown.

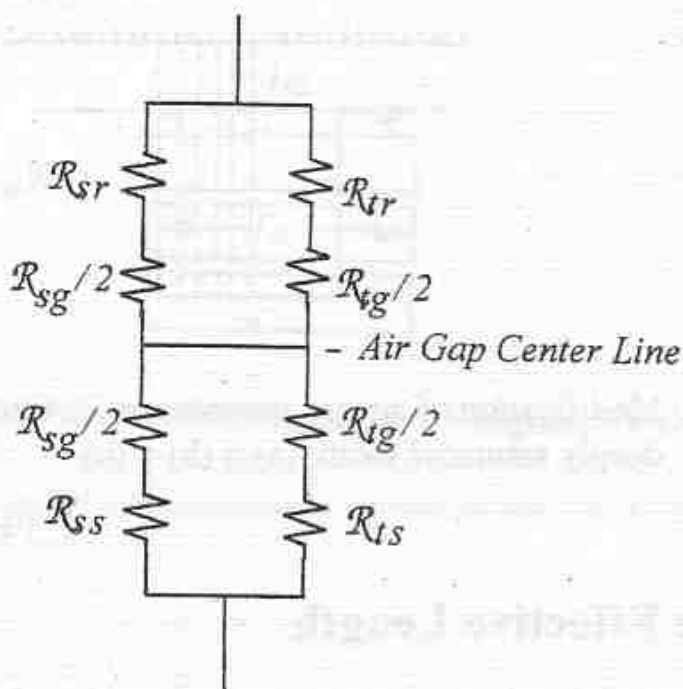


Figure 3.4 Magnetic circuit for region of one stator and rotor tooth

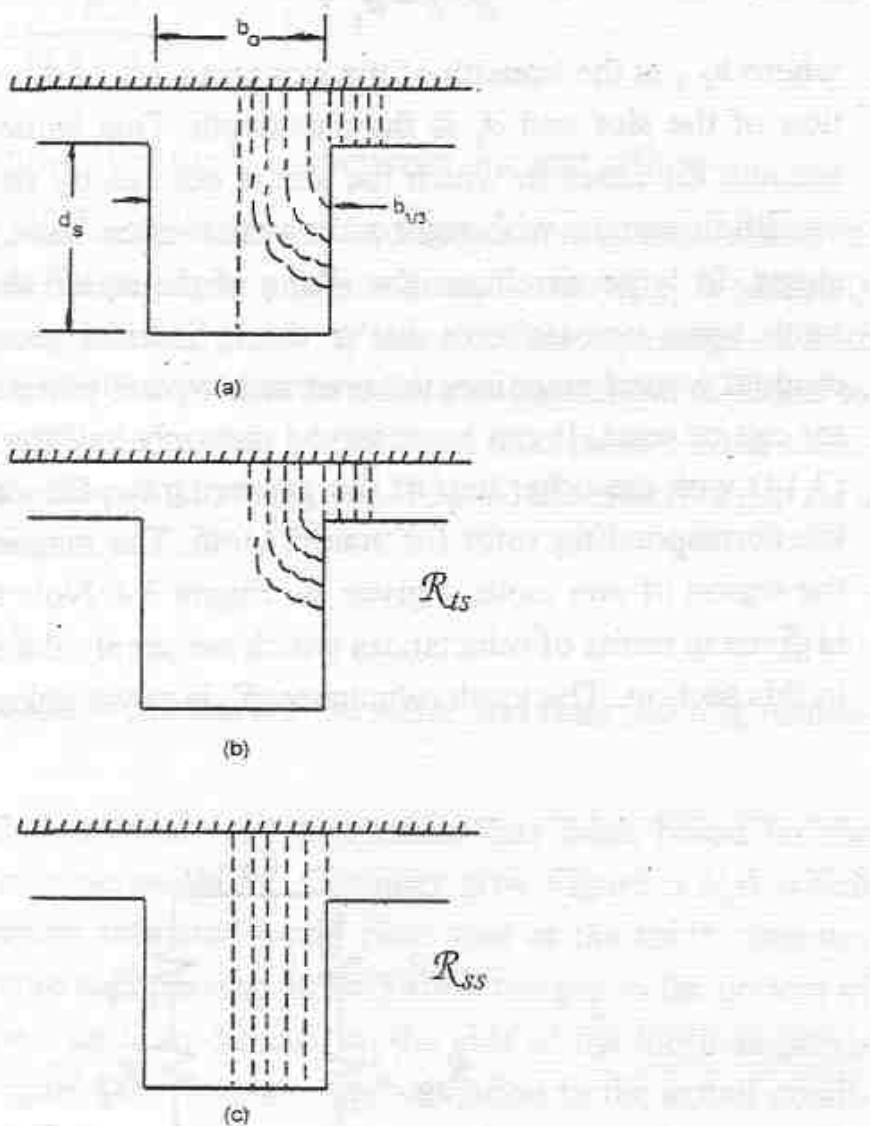


Figure 3.3 Modification of air gap permeance for finite iron permeability for deeply saturated tooth. (a)  $\equiv$  (b) + (c)

### 3.3 The Effective Length

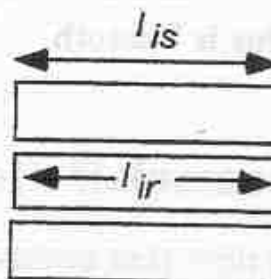
The presence of slots to accommodate windings is only one type of disturbance in the stator and rotor air gap surfaces. Another type of slotting occurs in machines with cooling ducts spaced along the core length. When forced ventilation is used, a fan or centrifugal blower is attached at one end of the rotor. The cooling action is assisted by either radial ventilating ducts spaced along the air gap or by axial ducts which are constructed by punching holes in the core area of the laminations. Since the thermal conductivity of a lamination is

from forty to fifty times greater in the direction parallel to the plane of the laminations than in a direction perpendicular to this plane axial air ducts are often preferred. However, radial ventilation must often be used in machines with long core lengths due to the difficulty in supplying the central parts of the core with cool air. When radial ducts are employed, duct widths are typically 3/8 to 1/2 inches. In order to maintain adequate cooling the spacing of the core ducts do not generally exceed 6 inches.

The approach to incorporating the effect of radial ducts is similar to that for slotting and can be readily derived. The following approximate equations can be used to calculate the effective length of a machine without ducting. The effective length as calculated from these equations is used together with the effective gap, Eq. (3.8), to calculate the permeance of an equivalent machine with smooth iron surfaces in both the circumferential and longitudinal directions.

### 1. Stator and Rotor Same Length, No Ducts

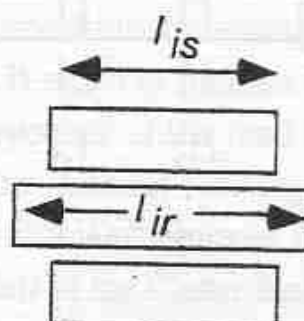
$$l_e = l_i + 2g; \quad l_{is} = l_{ir}$$



### 2. Stator and Rotor with Slightly Different Core Lengths, No Ducts

$$l_e = \frac{l_{is} + l_{ir}}{2} \quad (l_{is} \neq l_{ir})$$

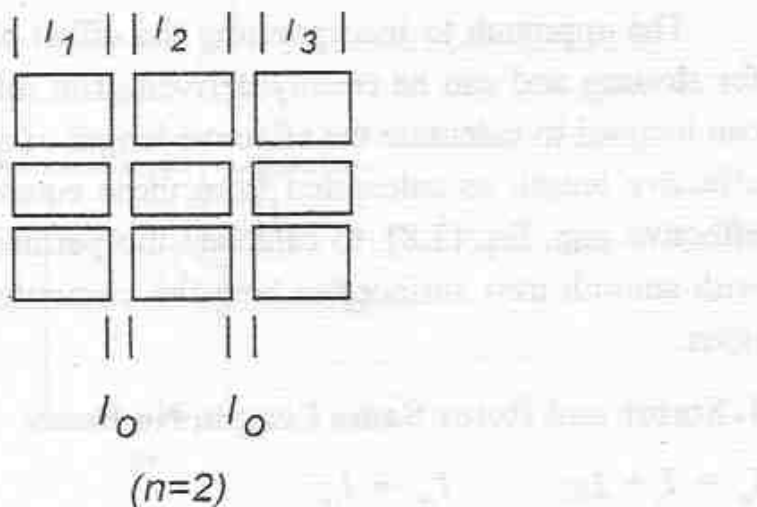
if  $l_{is} < l_e < l_{is} + 8g$



### 3. Stator and Rotor with Same Stack Length, Same Number of Ducts

$$l_e = l_i + 2g + nl_o \left[ \frac{5}{5 + \frac{2l_0}{g}} \right]$$

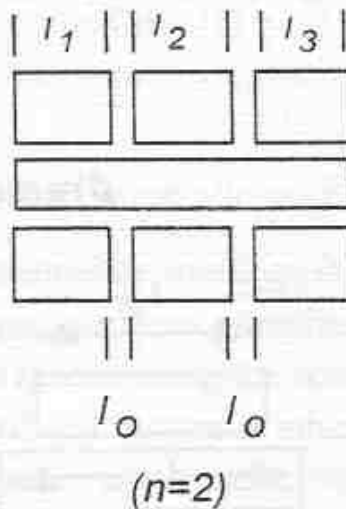
where  $l_i = l_1 + l_2 + l_3 + \dots + l_{n-1}$



### 4. Stator Has $n$ Ducts, Rotor is Smooth

$$l_e = l_i + 2g + nl_o \left[ \frac{5}{5 + \frac{l_0}{g}} \right]$$

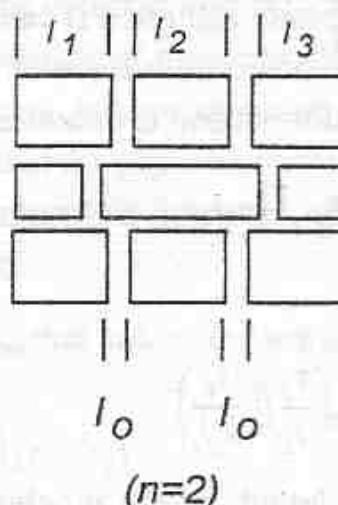
where  $l_i = l_1 + l_2 + l_3 + \dots + l_{n+1}$



### 5. Stator and Rotor Have $n$ Ducts But Are Not Aligned

$$l_e = l_i + 2g + nl_o \left[ \frac{5}{5 + \frac{l_o}{g}} \right]$$

where  $l_i = l_1 + l_2 + l_3 + \dots + l_{n+1}$



### 3.4 Calculation of Tooth Reluctance

Thus far we have concerned ourselves only with the air portion of the magnetic circuit. It is now time to calculate the permeance of a typical stator (or rotor) tooth. Since the iron permeance is assumed to be nonlinear the calculation of this quantity depends upon a knowledge of the actual flux density in the tooth. For low flux densities in the iron (up to 1.6 tesla) the tooth density is readily computed by assuming that all of the flux passes through the tooth. That is to say, practically all the flux entering the armature over one tooth pitch will pass into the core through the root of the tooth. This component of flux is accounted for by the Carter factor. For densities exceeding 1.6 tesla and even for lower values when the depth of slot is small in relation to the air gap, the calculations should take account of a component of the total flux which goes straight from the gap to the bottom of the slot without entering the teeth as discussed in Section 3.3. Since the Carter Coefficient assumes that the slot is infinitely deep, these flux lines are not included in the Carter factor.

It is useful to define the following symbols:  $B_{g,ave}$  = the average gap flux density along the centerline of the air gap over one slot pitch;  $B_{g1}$  = the peak fundamental component of air gap flux density at the centerline of the air gap;  $B_m$  = the flux density of the tooth at the point mid-way down the tooth;  $B_{gt}$  the gap flux density at the just above the surface (top) of a tooth;  $B_t$  the flux density just below the surface of the tooth,  $B_r$  the flux density at the root of the tooth (where the flux enters the stator or rotor core).

When the tooth is not greatly saturated it can simply be assumed that all of the flux over one slot pitch enters the surface of the tooth. In this case the flux entering the core from the slot portion is essentially neglected. Then,

$$B_t k_i t_i l_i = B_{g,ave} \tau_s l_e \quad (3.16)$$

or

$$B_t = B_{g,ave} \left( \frac{\tau_s}{t_i} \right) \left( \frac{l_e}{k_i l_i} \right) \quad (3.17)$$

where  $l_i$  denotes the axial length of the machine excluding ducts (length of iron) and  $k_i$  takes into account the insulation space between the laminations. The factor  $k_i$  has a value between 0.87 for 0.014 inch (14 mil) laminations and 0.93 for 0.025 inch (25 mil) laminations.

The assumption that each tooth has uniform cross-section throughout its length can only be justified when the diameter of the machine is very large in relation to the slot depth or when the teeth are intentionally designed to have parallel sides. More often stator and rotor slots have considerable taper which results in the top or the root of the tooth saturating first depending upon whether the tooth is associated with the stator or rotor. When tooth taper is appreciable the flux density at three points in the tooth; namely at the top, at the center and at the root of the tooth must be calculated and the corresponding field intensities found from the iron  $B$ - $H$  curves. The net or average field intensity is then computed approximately by Simpson's rule.

In order to simplify the calculations the assumption is made that the total flux in the tooth remains unaltered throughout all tooth cross sections. The tooth is considered as having a total length (or depth)  $d_s$  with corresponding width  $t_t$  at the top, a width  $t_m$  midway down the tooth and a width  $t_r$  at the root of the tooth. See Figure 3.5. The flux density at the top of the tooth nearest the

air gap and at the root of the tooth is found by simple ratios from knowing the flux density at the mid point of the tooth  $B_m$ .

The numerical value of  $B_m$ , measured at the mid point of the tooth with the highest flux density, is a key to a successful design since it can be used as a measure of the flux loading in the teeth which typically has the highest flux density in the machine. By selecting a number of values for  $B_m$ , the corresponding values of  $B_{g1}$  can be obtained for a particular type of magnetic material. Alternatively  $B_{g1}$  can be selected and  $B_m$  calculated (approximated). It is important to note that knowledge of the peak fundamental component of flux density  $B_{g1}$  is approximate at this point since the permeability varies from tooth to tooth so that the exact air gap flux density distribution is non-sinusoidal. The estimate can be improved however when the true variation in flux density has been determined.

Assuming a value for  $B_m$  one has, at the top and root of the tooth

$$B_t = B_m \frac{\left(\frac{1}{2}\right)(t_t + t_r)}{t_t} \quad (3.18)$$

$$B_r = B_m \frac{\left(\frac{1}{2}\right)(t_t + t_r)}{t_r} \quad (3.19)$$

Simpson's rule states that an approximation to the integral of a function  $y(x)$  over a measure  $x$  is

$$\int_0^x y(x) dx = \frac{\Delta x}{3} \{ (y(0) + 4y(\Delta x) + 2y(2\Delta x) + \dots) \\ 4y[(n-1)\Delta x] + y(n\Delta x) \} \quad (3.20)$$

where

$$\Delta x = x/n$$

and  $n$  is an even number. In our case we wish to compute

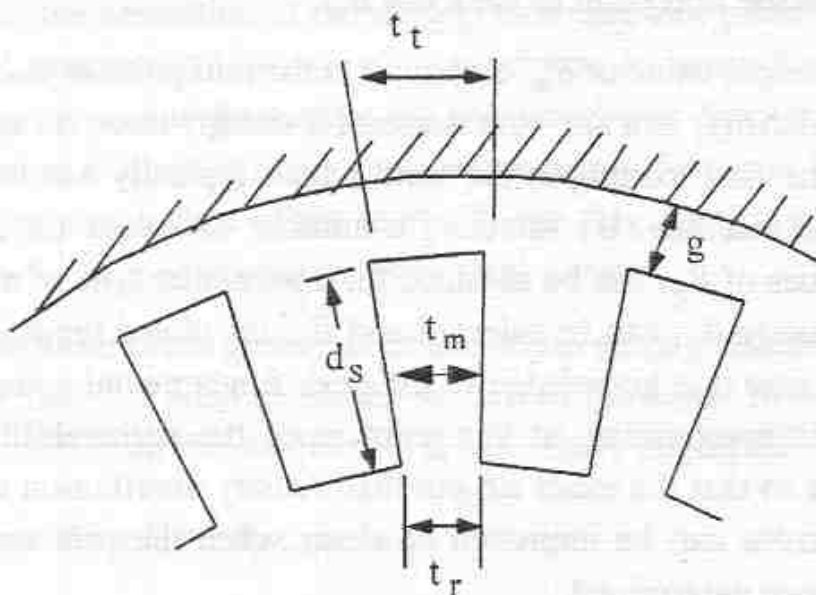


Figure 3.5 Illustrating *MMF* calculations for tapered teeth.

$$H_{t(\text{ave})} = \frac{1}{d_s} \int_0^{d_s} H_t(l) dl$$

If we let  $n = 2$  in Eq. (3.20) then

$$H_{t(\text{ave})} = \frac{1}{d_s} \left( \frac{d_s}{2} \right) \left( \frac{1}{3} \right) [H_t(0) + 4H_t(d_s/2) + H_t(d_s)]$$

or

$$H_{t(\text{ave})} = \frac{1}{6} [H_t(0) + 4H_t(d_s/2) + H_t(d_s)] \quad (3.21)$$

If the three values of  $H$  are replaced by  $H_r$  for the value at the root, by  $H_m$  at the center section and by  $H_t$  at the top section of the tooth, Simpson's approximation becomes

$$H_{t(\text{ave})} = \frac{1}{6} H_t + \frac{2}{3} H_m + \frac{1}{6} H_r \quad (3.22)$$

The total *MMF* drop in the tooth is then readily computed as

$$\mathcal{F}_{t(\text{ave})} = \left[ \frac{1}{6}H_t + \frac{2}{3}H_m + \frac{1}{6}H_r \right] d_s \quad (3.23)$$

The values of  $H_t$ ,  $H_m$  and  $H_r$  are determined from the non-linear  $B$ - $H$  curve of the material by entering the curve for the flux densities  $B_t$ ,  $B_m$ , and  $B_r$  and reading  $H_t$ ,  $H_m$  and  $H_r$  from the curve.

The reluctance associated with the toothed region is

$$\mathcal{R}_t = \frac{\mathcal{F}_{t(\text{ave})}}{\Phi_t} \quad (3.24)$$

where

$$\Phi_t = B_t k_i l_i t_t = B_m t_m k_i l_i \quad (3.25)$$

Hence

$$\mathcal{R}_t = \frac{\mathcal{F}_{t(\text{ave})}}{B_m t_m k_i l_i} \quad (3.26)$$

A repeated calculation of  $\mathcal{R}_t$  over all expected values of  $B_m$  results in one of the desired nonlinear elements in the per pole magnetic circuit. A similar calculation can be carried out for the other slotted element, i.e., the stator (or rotor). With ordinary cold rolled steel the peak value of  $B$  typically should not normally exceed 1.7 Teslas (roughly 110 kilolines/in<sup>2</sup>) in the stator or 1.8 T (115 Kl/in<sup>2</sup>) in the rotor teeth. For silicon steels the maximum values are 1.6 and 1.7 Teslas respectively.

### 3.5 Example #1 - Tooth MMF Drop

Let us now attempt to calculate the *MMF* drop in the air gap and rotor slots over one tooth pitch. For purposes of analysis the dimensions of Figure 3.6 are assumed. The thickness of the laminations is assumed to be 0.014" ( $k_i = 0.87$ ). The material is low carbon steel,  $B$ - $H$  curves of which is given in Figure 1.12. From Figure 3.6 we can deduce that

$$\tau_s = 0.922" \quad l_i = 8.4"$$

$$b_o = 0.4" \quad l_o = 0.5"$$

$$d_s = 1.4" \quad g = 0.1"$$

$$t_t = 0.522" \quad t_r = 0.405"$$

The first step in the analysis is to calculate the effective values of length, width and depth. From the equation corresponding to case #4 in Section 3.3,

$$l_e \approx 2g + l_i + nl_0 \left[ \frac{5}{5 + \frac{l_0}{g}} \right]$$

where  $l_o$  is the duct opening and  $l_i$  is the length of the iron stack. From this equation we obtain

$$\begin{aligned} l_e &= 0.2 + 8.4 + 2 \cdot 0.5 \left[ \frac{5}{5 + \frac{0.5}{0.1}} \right] \\ &= 9.1" \end{aligned}$$

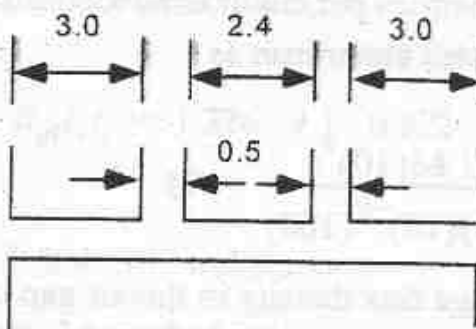
From Eq. (3.11) we have

$$\begin{aligned} k_c &= \frac{\tau_s}{\tau_s - \frac{2b_o}{\pi} \left\{ \tan^{-1} \left( \frac{b_o}{2g} \right) - \frac{g}{b_o} \left( \log_e \left[ 1 + \left( \frac{b_o}{2g} \right)^2 \right] \right) \right\}} \\ &= \frac{0.922}{0.922 - \left( \frac{2 \cdot 0.4}{3.1416} \right) \left\{ \tan^{-1} \left( \frac{0.4}{2 \cdot 0.1} \right) - \frac{0.1}{0.4} \log_e \left[ 1 + \left( \frac{0.4}{2 \cdot 0.1} \right)^2 \right] \right\}} \\ &= 1.24 \end{aligned}$$

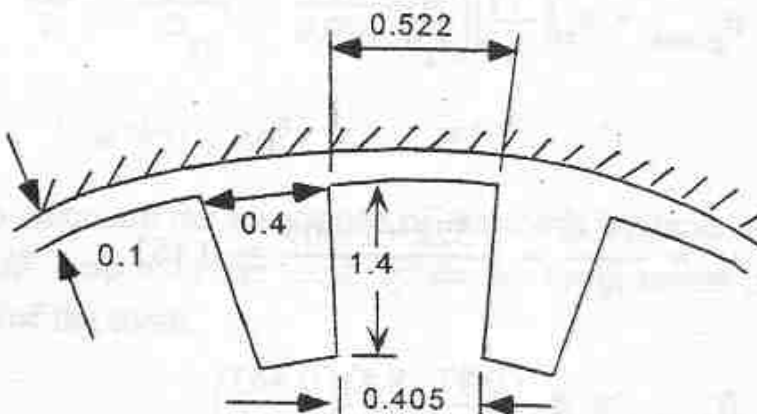
so that

$$g_e = k_c g = 0.124"$$

Let us now calculate the MMF drops for a value of 1.86 tesla (120 kilo-lines/in<sup>2</sup>) at the midpoint of the tooth. It should be noted that this value of flux density results in a quite saturated condition at the root of the tooth and certainly is at the upper end for conventional design. However, this case was chosen merely as an example of a highly saturated machine. We will ultimately



(a) Core Detail Showing Ducts



(b) Rotor Slot Detail

Figure 3.6 Core and slot dimensions for calculation of air gap and rotor slot *MMF*. All dimensions in inches.

find that the voltage required to supply this amount of flux density is greater than the rated value. From the iron  $B$ - $H$  curves in the Chapter 1, Fig. 1.12, one can find that corresponding to

$$B_m = 1.86 \text{ T}$$

one has, for low carbon steel

$$H_m = 200 \text{ Oe} \times 0.796 \text{ At/cm/Oe} = 160 \text{ ampere-turns/cm}$$

The constituent equation is (Ch. 1, Sec. 1.8)

$$B_m = (4\pi 10^{-9}) \mu_i H_m$$

when  $\mu_o$  is expressed in henries per cm. It is now possible to obtain the relative permeability of the saturated stator iron as

$$\mu_i = \frac{1.86(10)^4}{(4\pi)(10)^{-9}(160)} = 93$$

An estimate for the average flux density in the air gap corresponding to 1.86 T at the mid point of the tooth is consequently,

$$B_{g, ave} = B_m \left( \frac{k_t l_t}{l_e} \right) \left( \frac{t_m}{\tau_s} \right)$$

where

$$t_m = \frac{t_t + t_r}{2} = \frac{0.522 + 0.405}{2} = 0.463$$

$$B_{g, ave} = B_m \left( \frac{0.87 \cdot 8.4}{9.1} \right) \left( \frac{0.463}{0.922} \right) \\ = B_m(0.410)$$

$$B_{g, ave} = 0.751 \text{ T}$$

The flux density in the air gap over the tooth is

$$B_{gt} = \frac{k_t l_t t_t}{l_e t_m} B_m = \frac{0.87 \cdot 8.4}{9.1} \cdot \frac{0.464}{0.522} \cdot 1.86 \\ = 1.326 \text{ T}$$

Assuming that the flux density varies linearly from  $B_g$  at the gap center line to  $B_{gt}$  at the surface of the slot, the corresponding MMF drop in half the gap over the tooth is

$$\frac{\mathcal{F}_{gt}}{2} = \frac{B_{gt} + B_g \left( \frac{g_e}{2} \right)}{2\mu_o} = \frac{1.326 + 0.751}{4\pi \cdot 10^{-7}} \cdot \frac{0.124}{4} \left( \frac{2.54}{100} \right) \\ = 1,303 \text{ ampere-turns}$$

The flux passing through the tooth is,

$$\begin{aligned}\Phi_t &= B_{gt} l_e t_t = 1.326 \cdot 9.1 \cdot 0.522 \cdot \left(\frac{2.54}{100}\right)^2 \\ &= 0.00406 \text{ webers}\end{aligned}$$

The reluctance over the toothed region is

$$\begin{aligned}\frac{\mathcal{R}_{gt}}{2} &= \frac{\mathcal{F}_{gt}/2}{\Phi_{gt}} = \frac{1,303}{0.00406} \\ &= 321 \times 10^3 \text{ H}^{-1}\end{aligned}$$

In order to calculate the reluctance of the tooth we have we must first calculate the *MMF* drop over the tooth. Since the tooth tapers linearly from the top to the root of the tooth

$$B_r = B_m \left( \frac{0.5(0.522 + 0.405)}{0.405} \right) = 2.13 \text{ T.}$$

From the *B-H* curve we obtain

$$H_r = 1353 \text{ ampere-turns/cm}$$

which is, in reality, off the scale of Figure 1.13 so that the root of the tooth is deeply saturated.

Again, by taking ratios, the flux density at the top of the tooth is

$$B_t = B_m \left( \frac{0.5(0.522 + 0.405)}{0.522} \right) = 1.652 \text{ T.}$$

whereupon we arrive at the result that

$$H_t = 47.8 \text{ ampere-turns/cm}$$

The average *MMF* drop along the tooth is now computed from Simpson's Rule (Eq. (3.22))

$$\begin{aligned}
 H_{t(ave)} &= \frac{H_t}{6} + \frac{2H_m}{3} + \frac{H_r}{6} \\
 &= \frac{1}{6}(47.8) + \frac{2}{3}(160) + \frac{1}{6}(1353) \\
 &= 340 \quad \text{ampere-turns/cm}
 \end{aligned}$$

Hence, the average *MMF* drop down the length of the tooth is

$$\begin{aligned}
 \mathcal{F}_{t(ave)} &= H_{t(ave)} d_s \\
 &= (340)(1.4)2.54 \\
 &= 1,208 \quad \text{ampere-turns}
 \end{aligned}$$

so that the reluctance of the rotor tooth is

$$\begin{aligned}
 \mathcal{R}_t &= \frac{\mathcal{F}_{t(ave)}}{\Phi_r} = \frac{1208}{4.06} \times 10^3 \\
 &= 297 \times 10^3 \quad \text{H}^{-1}
 \end{aligned}$$

Note that this value is nearly equal to the air gap portion of the reluctance. While abnormally high in this case, it is clear that the *MMF* drops in the iron cannot be neglected even when the flux density in the iron reaches a mildly saturated value. The magnetic circuit of the gap, tooth and slot is given in Figure 3.7.

The effects of saturation are often calculated approximately by computing the flux density and corresponding field intensity at a point 1/3 the distance from the narrowest part of the tooth (1/3 the way from the root of the tooth in our example above) given the maximum flux density in the air gap. If we assume the same value of air gap flux density and the approximate expression for tooth flux, we have, for a point 1/3 the way from the root of the tooth of Figure 3.6 and neglecting the effect of finite permeability, either

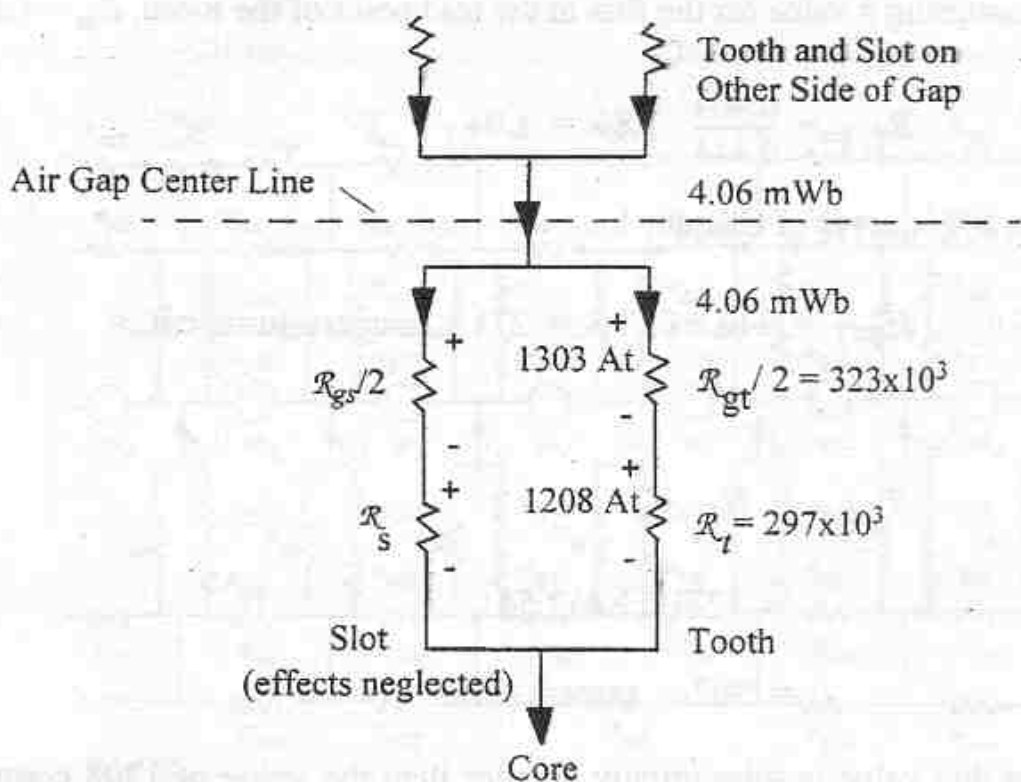


Figure 3.7 Magnetic equivalent circuit for gap slot and tooth configuration of Figure 3.6 for  $B_m = 1.86 \text{ T}$  ( $120 \text{ KI/in}^2$ )

$$B_{1/3} = \frac{B_g}{\left(\frac{k_i l_i}{l_e}\right) \left[\frac{t_{1/3}}{\tau_s}\right]} \quad (3.27)$$

or

$$B_{1/3} = \left(\frac{t_m}{t_{1/3}}\right) B_m \quad (3.28)$$

depending upon whether  $B_g$  or  $B_m$  has been assumed and where  $t_{1/3}$  is the tooth width at the point  $1/3$  of the way from the root of the tooth. The width  $t_{1/3}$  is readily found to have a value

$$t_{1/3} = t_r + \frac{1}{3}(t_t - t_r)$$

$$= 0.405 + \frac{1}{3}(0.522 - 0.405)$$

$$= 0.444''$$

Hence, assuming a value for the flux at the mid point of the tooth,  $B_m = 1.86 \text{ T.}$ ,

$$B_{1/3} = \frac{0.464}{0.444} \cdot 1.86 = 1.94 \quad \text{T}$$

From the  $B$ - $H$  curves of Chapter 1,

$$H_{1/3} = 340 \times 0.796 = 271 \quad \text{ampere-turns/cm}$$

so that

$$\begin{aligned} \mathcal{F}_{t(\text{ave})} &= H_{1/3} d_s \\ &= (271)(1.4)2.54 \\ &= 962 \quad \text{ampere-turns} \end{aligned}$$

Note that this value is substantially smaller than the value of 1208 computed previously. While not suitable for high saturation conditions the estimate improves considerably when the iron is only mildly saturated. However, since a more detailed approach using three or even 5, 7 or more subdivisions along a tooth involves negligible computer power, the simplified approach is rarely justified.

### 3.6 Calculation of Core Reluctance

The process of computing tooth permeances as a function of gap flux density over one tooth span has now been completed. The remaining task in solving the complete magnetic circuit is to evaluate the *MMF* drop in the core or "back iron" portion of the circuit. Figure 3.8 shows the magnetic equivalent circuit for a machine with only six stator and rotor slots per pole. (In general the stator and rotor slot numbers must be unequal. The case of unequal slot numbers will be discussed later). Note that a "flux tube" can be identified for each pair of slots and the core portion of the machine supports all such flux tubes in a pole. The flux in the outermost flux tube splits equally between a north and an adjacent south pole (see Figure 3.1). Note that an even number of slots result in one tooth per pole that is essentially supporting no flux at any instant. That is to say, since the *MMF* distribution is symmetrical, when there are an even number of "steps" in the *MMF* per half cycle the center "step" *MMF* must be

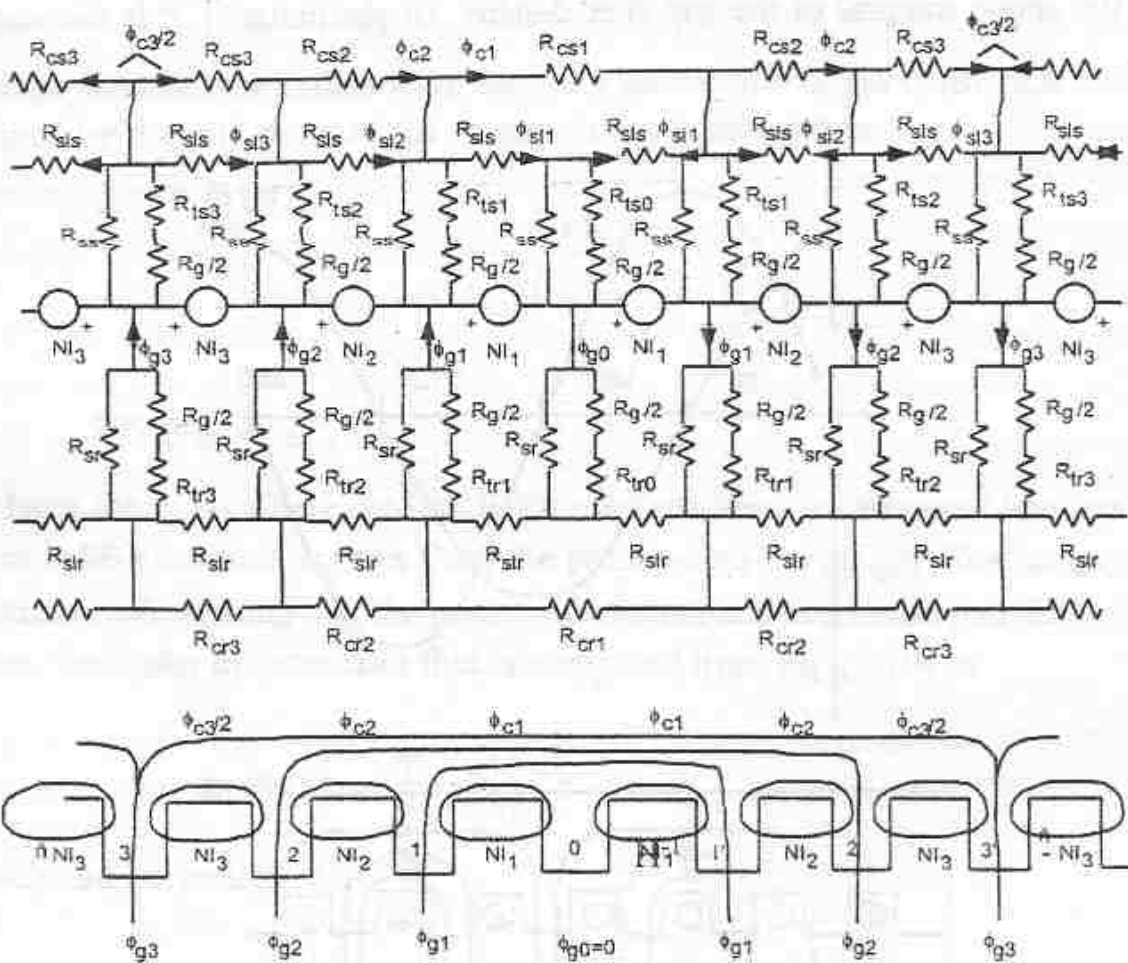


Figure 3.8 Magnetic equivalent circuit for an induction machine with six stator and rotor slots per pole including slot leakage flux effects

zero. When an odd number of slots per pole are used, all of the teeth are excited at any instant.

The *MMF* drop in the core portion can best be computed by using the outermost flux tube (teeth 3 and 3'). However the problem remains complicated by the fact that the three magnetic circuits represented by the flux tubes corresponding to the gap fluxes,  $\Phi_{g1}$ ,  $\Phi_{g2}$ , and  $\Phi_{g3}$  are not independent since the magnetic material in the core area is nonlinear. In addition, leakage flux paths exist (designated in this example by  $\Phi_{sl1}$ ,  $\Phi_{sl2}$ , and  $\Phi_{sl3}$ ) which close their path through the rotor core. Hence, the *MMF* drop in each of the three core reluctances is a function of the flux density in the core which involves the total flux flowing in all three magnetic circuits taken simultaneously. Nonetheless, the problem can still be solved if we assume that we know the flux density in the gap and that it is sinusoidal.

Note from Figure 3.9 that if the gap flux density is sinusoidal then the flux density in the core area is co-sinusoidal, that is to say the core flux density is the space integral of the gap flux density. In particular if  $P$  is the number of

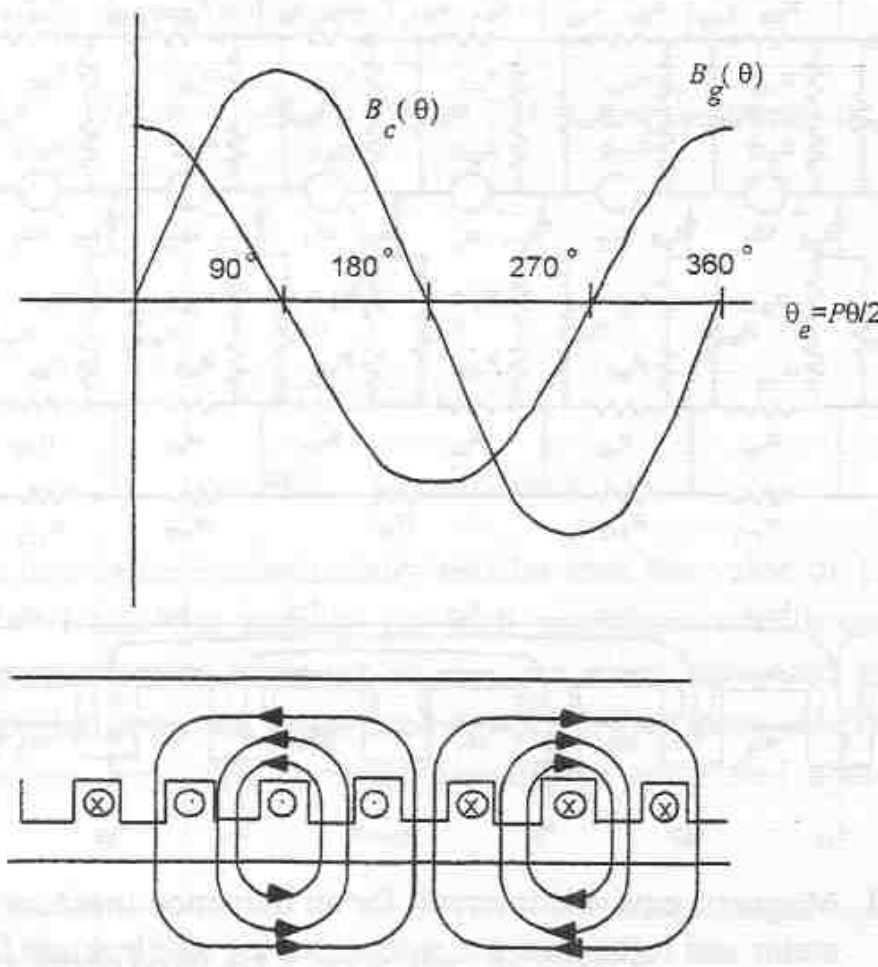


Figure 3.9 Gap and core flux density as a function of electrical angle along the gap

poles then the spatial distribution of flux density in the air gap can be written as

$$B_g(\theta) = B_{g1} \cos\left(\frac{P\theta}{2}\right)$$

where  $\theta$  is an angular circumferential measure around the air gap. From Figure 3.9 it can be noted that the core flux is zero at the point where the air gap flux density is a maximum ( $\theta = 0^\circ$ ). The total flux entering the core as a result of air gap flux from the point  $\theta = 0^\circ$  to an arbitrary point  $\theta$  is

$$\Phi_c(\theta) = \int_0^\theta B_{g1} \cos\left(\frac{P\theta}{2}\right) r l_e d\theta \quad (3.29)$$

where  $r$  denotes the radius from the rotor center line to the cylindrical surface defined by the mid point of the air gap. In particular, when

$$\frac{P\theta}{2} = \pi/2$$

or

$$\theta = \pi/P$$

we have the point where the flux in the core reaches a maximum. Note that this point is 90 electrical degrees from the point where the air gap flux density is a maximum. Assuming that the peak fundamental and maximum gap flux are the same, the stator or rotor core flux is computed from Eq. (3.29) as

$$\Phi_c(90^\circ) = \frac{2}{P} l_e r B_{g1}$$

which can be written as

$$\Phi_c(90^\circ) = \left(\frac{\tau_p}{2} l_e\right) \left(\frac{2}{\pi} B_{g1}\right) \quad (3.30)$$

Note that the quantity  $2B_{g1}/\pi$  is the average value of flux density per pole and that  $\tau_p l_e/2$  is the area through which the half the air gap flux passes on its way to the stator or rotor core. Half the total flux finds its way in each direction in the core as shown in Figure 3.9. The flux density in the core at the point  $\theta = \pi/P$  (90 electrical degrees) is found by taking the flux given by Eq. (3.30) and dividing by the cross sectional area of the core. The result is

$$\begin{aligned} B_c(90^\circ) &= \frac{\Phi_c(90^\circ)}{d_c k_i l_i} \\ &= \frac{l_e (\tau_p/2)}{d_c k_i l_i} \left(\frac{2B_{g1}}{\pi}\right) \end{aligned} \quad (3.31)$$

where  $d_c$  ( $d_{cs}$  or  $d_{cr}$ ) is the depth of the core (stator or rotor) and  $k_i$  and  $l_i$  are the appropriate values for either the stator or rotor. The flux in other points of the core can be found in a similar manner.

As noted in Figure 3.8, the total flux in the core results from both the gap flux which closes its path through the core and also a leakage component which does not enter the gap but also closes its path through the core. The flux in any portion of the core is dependent upon the sum of the gap flux plus the leakage flux. Leakage flux calculations are the subject of the next chapter. However the essential effect of leakage on the core flux must be dealt with here in the main flux calculation. In particular, the leakage flux component which is represented in Figure 3.8 is termed the *slot leakage* flux. It is stated in Refs. 1 and 2 that the total stator leakage flux can be estimated from the equation

$$X_1 = \frac{(P/100)X_m}{1 - \frac{P}{100}} \quad (3.32)$$

when the machine is unsaturated and by

$$X_1 = \frac{1.5(P/100)X_m}{1 - 1.5\frac{P}{100}} \quad (3.33)$$

when the machine is saturated. In Eqs. (3.32) and (3.33),  $X_m$  represents the reactance corresponding to the air gap flux (i.e. magnetizing reactance) and  $X_1$  denotes the total stator leakage reactance. In general, the slot leakage reactance is only a portion of the total stator leakage reactance. Assuming that the slot leakage makes up 1/2 of the total, we can write that,

$$\Phi_{cs} = \left( \frac{X_m + X_1/2}{X_m} \right) \left( \frac{\Phi_g}{2} \right) \quad (3.34)$$

where  $\Phi_{cs}$  denotes the flux in the stator core measured at the point of maximum core flux and  $\Phi_g$  denotes the flux crossing the air gap over one pole pitch. Substituting Eq. (3.33) into Eq. (3.34) it can be readily determined that

$$\Phi_{cs} = \frac{1 + K_p}{2K_p} \Phi_g \quad (3.35)$$

where  $\Phi_{cs}$  and  $\Phi_g$  denote the core and gap flux respectively and

$$K_p = 1 - \frac{1.5P}{100}.$$

Hence, to include the effect of slot leakage flux, Eq. (3.30) must be written as,

$$\Phi_{cs}(90^\circ) = \left(\frac{\tau_p l_e}{2}\right) \left(\frac{2B_{g1}}{\pi}\right) \frac{1 + K_p}{2K_p} \quad (3.36)$$

The flux density in the core at the same point is

$$B_{cs}(90^\circ) = \frac{\tau_p (l_e/2)}{d_{cs} k_{is} l_{cs}} \left(\frac{2B_{g1}}{\pi}\right) \frac{1 + K_p}{2K_p} \quad (3.37)$$

The same factor applies to estimating the flux and flux density at other points in the core. It can be similarly shown that the peak flux density in the rotor is

$$B_{cr}(90^\circ) = \frac{\tau_p (l_e/2)}{d_{cr} k_{ir} l_{cr}} \left(\frac{2B_{g1}}{\pi}\right) \frac{3K_p - 1}{2K_p} \quad (3.38)$$

A similar correction factor can be used to account for the effects of rotor leakage flux on saturation of the rotor core.

The  $B$ - $H$  curves can now be used in conjunction with Simpson's Rule to find the resulting  $MMF$  drop in the core similar to the approach taken for tooth saturation. Before we take this step, however, it is useful to pause to consider what happens to the air gap flux as the teeth begin to saturate. Clearly the teeth with the highest flux density will saturate first so that the flux distribution will begin to assume a "flattened" sine wave with peak value  $B_{g,max}$  as shown in Figure 3.10. Note that the amplitude of the fundamental component,  $B_{g1}$ , will be somewhat greater than  $B_{g,max}$ . Let us now consider what would happen if we assumed a value  $B_{g1}$  for teeth 3 and 3' and compute the  $MMF$  around the magnetic circuit on this basis. The resulting computation would clearly be in error on the high side since the flux in the teeth 3 and 3' of Figure 3.8 would certainly be too high. On the other hand if we assume a sinusoidal distribution with amplitude  $B_{g,max}$  the  $MMF$  drop around the magnetic circuit will be too small since the flux density in the core portion will not be computed accurately and hence the  $MMF$  drop in the core will be in error.

This apparent dilemma can be resolved if we pause to consider that the flattening of the sine wave of air gap flux density is produced primarily by a third harmonic component. Note from Figure 3.10 that the actual waveform and the

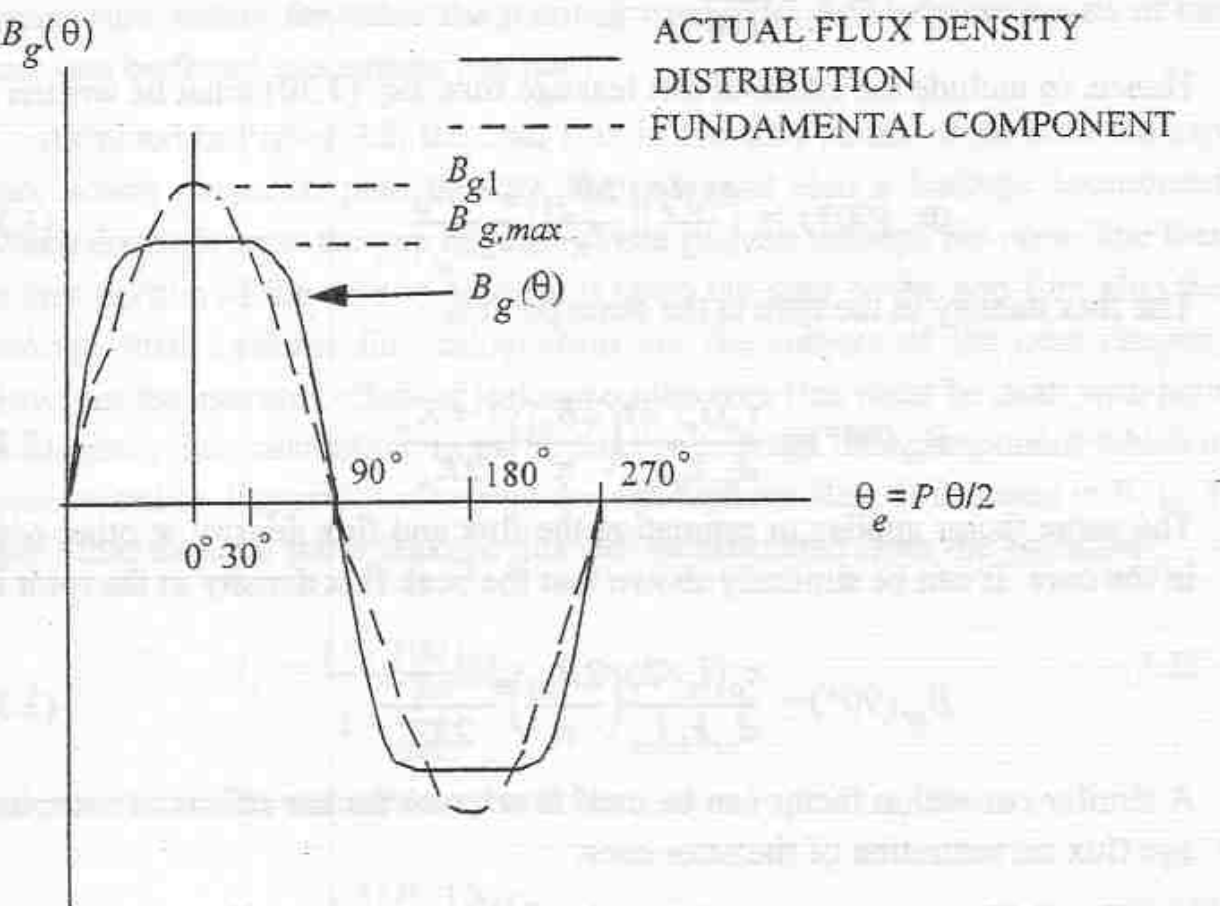


Figure 3.10 Actual and fundamental component of air gap flux density vs. electrical angle around the gap. Effect of slotting neglected.

fundamental component are equal very near  $30^\circ$ . The value is exactly  $30^\circ$  if the fifth, seventh etc. harmonics are neglected. If we assume that the harmonics vary as inverse integers, that is  $1/3$  for the third,  $1/5$  fifth,  $1/7$  seventh, etc. a more accurate value of this intersection is about  $37^\circ$ . In practice, values anywhere from zero to  $38.3^\circ$  might be obtained depending upon the relative content of the third, fifth and seventh harmonic and their relative polarity (phase shift). It has been shown by Lee [2] that a value of  $30^\circ$  is reasonable choice for practical machines.

Since the apparent and actual flux density are equal at a  $37^\circ$  point on the flux density angular distribution, the MMF drops in the teeth centered around this point will be nearly correct if we assume an average value of flux density for this tube equal to  $(\sqrt{3}/2)B_{g1}$ . Hence the proper flux tube to use corresponds to slots 2 and 2' in Figure 3.8. (It should be mentioned that the choice of six slots per pole was intentional. The argument is valid for any number of

slot per pole since the *MMF* pattern can always be rotated so that the  $60^\circ$  point is properly centered over a tooth.) The "ripple" in the flux density wave due to slotting is a type of leakage which will be calculated separately later. It is important to note that even though we have eliminated the effect of the third harmonic on the computation of tooth *MMF*, we have not eliminated its effect in the core calculation. Generally, the core flux density is much lower than the tooth flux density so that the extra core flux due to the third harmonic does not result in an appreciable change in core *MMF* drop. If this is not the case, an iterative solution must be resorted to in order to converge on the proper solution. The proper procedure to follow in such a case is left to the interested reader [3].

The computation of *MMF* drops in the main magnetic circuit of an induction machine now proceeds as follows:

- 1) Assuming a fundamental component of flux density amplitude  $B_{g1}$ , the corresponding value at a point  $30^\circ$  from the maximum is computed as

$$B_g(30^\circ) = B_{g1}(30^\circ) = \frac{\sqrt{3}}{2} B_{g1} \quad (3.39)$$

- 2) The corresponding tooth flux density is calculated by means of Eq. (3.17).
- 3) The *MMF* drop in the tooth and gap is computed.
- 4) Using  $B_{g1}$  one can calculate the flux density at points in both the stator and rotor core where  $\theta = 30^\circ, 60^\circ$  and  $90^\circ$ . For the stator core the quantity,  $B_{cs}(90^\circ)$  is readily derived from Eq. (3.37). The values of core flux density at  $30^\circ$  and  $60^\circ$  are easily seen to be

$$\begin{aligned} B_{cs}(60^\circ) &= B_{cs}(90^\circ) \cos 30 \\ &= \frac{\sqrt{3}}{2} B_{cs}(90^\circ) \end{aligned} \quad (3.40)$$

$$\begin{aligned} B_{cs}(30^\circ) &= B_{cs}(90^\circ) \cos(60^\circ) \\ &= 0.5 B_{cs}(90^\circ) \end{aligned} \quad (3.41)$$

Similar expressions apply for the rotor core.

5) The corresponding values of field intensity  $H$  can be read from the  $B$ - $H$  curves of the magnetic material being used. For common steel the peak core flux density should be limited to 1.2 T and 1.4 T in the stator and rotor cores respectively. For silicon steels the values should be reduced by approximately 10%.

6) Simpson's rule can now be used to find the average  $MMF$  drop over the core span from  $\theta = 30^\circ$  to  $\theta = 150^\circ$  for both the stator and rotor. In particular, Simpson's rule for the average value of a function  $H$  over a length  $l$  using five equidistant points is

$$H_{c(ave)} = \left(\frac{1}{l_c}\right)\left(\frac{l}{4}\right)\left(\frac{1}{3}\right)[H_c(30^\circ) + 4H_c(60^\circ) + 2H_c(90^\circ) + 4H_c(120^\circ) + H_c(150^\circ)] \quad (3.42)$$

From symmetry we have the following relationships

$$H_c(150^\circ) = H_c(30^\circ)$$

$$H_c(120^\circ) = H_c(60^\circ)$$

So that Eq. (3.42) reduces to

$$H_{c(ave)} = \frac{1}{6}H_c(30^\circ) + \frac{2}{3}H_c(60^\circ) + \frac{1}{6}H_c(90^\circ) \quad (3.43)$$

The procedure is done for both stator  $H_{cs(ave)}$  and rotor core  $H_{cr(ave)}$ .

7) The mean length of path through the stator core over one pole pitch is computed as

$$l_{cs} = \frac{\pi(D_{is} + 2d_{ss} + d_{cs})}{P} \quad (3.44)$$

where  $D_{is}$  is the inner diameter of the stator core,  $d_{ss}$  is the depth of one stator slot and  $d_{cs}$  is the radial depth of the stator core as measured from the bottom of a stator slot to the outer radius of the stator core.

For the rotor

$$l_{cr} = \frac{\pi(D_{or} - 2d_{sr} - d_{cr})}{P} \quad (3.45)$$

where  $d_{sr}$  is the depth of the rotor slots and  $D_{or}$  is the outer diameter of the rotor punching, i.e.

$$D_{or} = D_{is} - 2g \quad (3.46)$$

8) The *MMF* drop over the stator and rotor core can now be computed as

$$\mathcal{F}_{cs(ave)} = H_{cs(ave)} \left( \frac{2}{3} l_{cs} \right) \quad (3.47)$$

and

$$\mathcal{F}_{cr(ave)} = H_{cr(ave)} \left( \frac{2}{3} l_{cr} \right) \quad (3.48)$$

9) The *MMF*'s can now be summed to find the impressed *MMF* per pole at the  $30^\circ$  point, that is

$$2\mathcal{F}_p(30^\circ) = 2\mathcal{F}_g(30^\circ) + 2\mathcal{F}_{ts}(30^\circ) + 2\mathcal{F}_{tr}(30^\circ) + \mathcal{F}_{cs(ave)} + \mathcal{F}_{cr(ave)} \quad (3.49)$$

10) The actual value of *MMF* corresponding to the peak of assumed sine wave of flux density is

$$2\mathcal{F}_p(0^\circ) = \frac{2}{0.8} \mathcal{F}_p(37^\circ) \quad (=2\mathcal{F}_p \text{ in Eq. 3.1}) \quad (3.50)$$

### 3.7 Example #2 - MMF Drop Over Main Magnetic Circuit

A certain 250 HP, 8 pole, 2400 volt, 60 Hz induction machine has the following constants and dimensions (in inches):

Stator OD = $D_{os} = 32"$	Gross Core Length = $10"$
Stator ID = $D_{is} = 24.08"$	Number of Opposing Stator
Rotor OD = $D_{or} = 24"$	and Rotor Ducts = 4
Rotor ID = $D_{ir} = 17.5"$	Width of Stator and Rotor Ducts = $3/8"$
No. of Stator Slots = $S_1 = 120$	Lamination Thickness = $0.025"$
No. of Rotor Slots = $S_2 = 97$	Type of Steel = 3% Silicon Steel

From this data we can deduce the following information

Gap =  $g = 0.04"$  Length of Stator and Rotor Stack =  $l_{is} = l_{ir} = 8.5"$

Stacking Factor (Stator and Rotor) =  $k_{is} = k_{ir} = 0.93$

Pole Pitch Measured at the Air Gap =  $\tau_p = 9.456"$

Stator Slot Pitch =  $\tau_s = 0.630"$

Rotor Slot Pitch =  $\tau_r = 0.770"$

Details of the stator and rotor slot shapes are given in Figure 3.11. From this figure and the above information we can establish the following. For the stator:

Depth of Slot =  $d_{ss} = 2.2"$

Depth of Core =  $d_{cs} = 1.76"$

Tooth Width at Top =  $t_{ts} = 0.256"$

Tooth Width at Root =  $t_{rs} = 0.369"$

Slot Opening =  $b_{os} = 0.374"$

For the rotor:

Depth of Slot =  $d_{sr} = 0.67"$

Depth of Core =  $d_{cr} = 2.58"$

Tooth Width at Top =  $t_{tr} = 0.392"$

Tooth Width at Root =  $t_{rr} = 0.348"$

Slot Opening =  $b_{or} = 0.09"$

Finally, the effective length of the stator (and rotor in this case) is obtained from Case 3 of Section 3.3. The relevant equation is, repeating

$$l_e = l_{is} + 2g + nl_o \left( \frac{\frac{5}{2l_o}}{5 + \frac{g}{2l_o}} \right)$$

from which

$$\begin{aligned} l_e &= 8.5 + 2(0.04) + \frac{5(4)(0.375)}{5 + 2\frac{(0.375)}{0.04}} \\ &= 8.5 + 0.08 + 0.316 = 8.896'' \end{aligned}$$

Let us now determine the *MMF* per pole necessary to produce a fundamental component of air gap flux density of 0.775 T (50,000 lines/in<sup>2</sup>). In this case the flux which travels straight down the slot will be neglected.

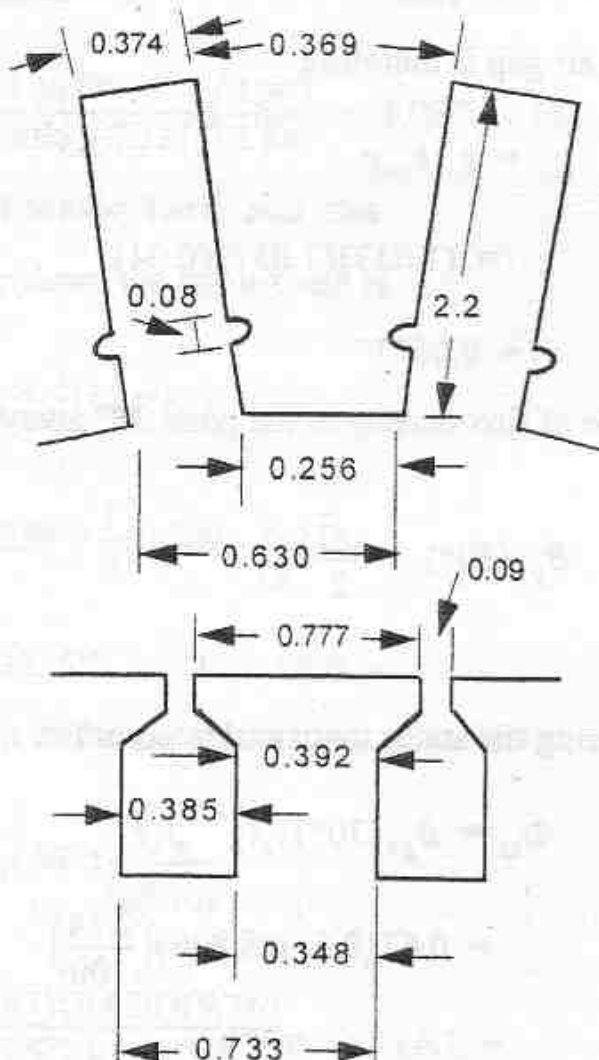


Figure 3.11 Details of the stator and rotor slot shapes for 250 HP induction machine

#### **MMF and Reluctance of Air Gap**

From Eq. (3.11), Carter's coefficient for the stator slots is

$$k_{cs} = \frac{0.63}{0.63 - 0.238(1.36 - 0.107(3.129))}$$

$$= 1.6327$$

Carter's coefficient for the rotor slots is

$$k_{cr} = \frac{0.777}{0.777 - 0.0573(0.844 - 0.444(0.818))}$$

$$= 1.037$$

The effective air gap is therefore

$$g_e = k_{cs} k_{cr} g$$

$$= (1.633)(1.037)(0.04)$$

$$= 0.0677''$$

The amplitude of flux density at the point 30° away from the maximum is

$$B_{g1}(30^\circ) = \frac{\sqrt{3}}{2} B_{g1}$$

$$= 0.67 \text{ T}$$

The flux entering the stator tooth at this point is

$$\Phi_{ts} = B_{g1}(30^\circ) \tau_s l_e$$

$$= 0.67(0.63)(8.896) \left(\frac{2.54}{100}\right)^2$$

$$= 2.43 \text{ mWb}$$

The *MMF* necessary to overcome the air gap is therefore

$$\mathcal{F}_g(30^\circ) = \frac{B_{g1}(30^\circ)}{\mu_0} g_e$$

$$\mathcal{F}_g(30^\circ) = \frac{(0.67)(0.0677)2.54}{(4\pi 10^{-7}) \frac{100}{100}}$$

$$= 919 \text{ ampere-turns}$$

The air gap reluctance referred to one stator tooth is

$$\mathcal{R}_{gs} = \frac{g_e}{\mu_o l_e \tau_s} = \frac{0.0677}{(\mu_o)(8.896)(0.63)} \left( \frac{100}{2.54} \right) = 3.786 \times 10^5 \text{ H}^{-1}$$

or referred to one rotor tooth

$$\mathcal{R}_{gr} = \frac{g_e}{\mu_o l_e \tau_r} = \frac{0.0677}{(\mu_o)(8.896)(0.777)} \left( \frac{100}{2.54} \right) = 3.0979 \times 10^5 \text{ H}^{-1}$$

### MMF and Reluctance of Stator Tooth and Slot

The tooth width mid-way down the stator tooth is

$$\begin{aligned} t_{ms} &= t_{ts} + \frac{1}{2}(t_{rs} - t_{ts}) \\ &= 0.256 + \frac{1}{2}(0.369 - 0.256) \\ &= 0.3125'' \end{aligned}$$

The flux density at the top of the stator tooth is

$$\begin{aligned} B_{ts} &= B_{g1}(30^\circ) \frac{\tau_s l_e}{t_{ts} k_{is} l_{is}} \\ &= \frac{(0.67)(0.630)(9.36)}{(0.2572)(0.93)(8.5)} \\ &= 1.86 \text{ T} \end{aligned}$$

Note that this result indicates that the teeth are highly saturated. The "dimples" in the stator teeth to accommodate the slot wedge will probably not appreciably affect the answer under such conditions. The possibility of this constriction producing premature saturation under reduced flux conditions should normally be examined carefully.

Since the flux density at the top of the tooth is known, the corresponding flux densities at the mid point and at the root of the tooth are found from the following ratios

$$B_{ms} = \frac{B_{ts} t_{ts}}{t_{ms}}$$

$$= \frac{(1.86)(0.256)}{(0.3125)}$$

$$= 1.52 \text{ T.}$$

$$B_{rs} = \frac{B_{ts} t_{ts}}{t_{rs}}$$

$$= \frac{(1.86)(0.256)}{(0.369)}$$

$$= 1.29 \text{ T.}$$

The corresponding values of field intensity are

$$H_{ts} = 327.6 \text{ At/in}$$

$$H_{ms} = 27.8 \text{ At/in}$$

$$H_{rs} = 12.4 \text{ At/in}$$

Hence the average field intensity along the stator tooth is

$$H_{ts(ave)} = \frac{1}{6} H_{ts} + \frac{2}{3} H_{ms} + \frac{1}{6} H_{rs}$$

$$= 75 \text{ At/in}$$

and the corresponding average MMF drop in the stator tooth is

$$\mathcal{F}_{ts(ave)} = H_{ts(ave)} d_{os}$$

$$= (75)(2.2)$$

$$= 165 \text{ At}$$

The reluctance of the stator tooth is computed as

$$\mathcal{R}_{ts} = \frac{\mathcal{F}_{ts(\text{ave})}}{\Phi_{ts}} = \frac{165}{0.00255}$$

$$= 6.8 \times 10^4 \quad \text{H}^{-1}$$

### MMF and Reluctance of Rotor Tooth and Slot

For simplicity the rotor slot will be considered as an open slot having the constant width  $b_o = 0.385$ . The error caused by this assumption will be negligible since it is expected that the flux density in the rotor tooth will be smallest at this point. This assumption should be checked later and if necessary a correction made for the *MMF* drop down the overhang section.

The tooth width at the midpoint of the tooth are

$$t_{mr} = t_{tr} - \frac{1}{2}(t_{tr} - t_{rr})$$

$$= 0.392 - \frac{1}{2}(0.392 - 0.348)$$

$$= 0.370''$$

Using the uncorrected value of air gap flux density, the flux density at the top of the rotor tooth is

$$B_{tr} = B_{g1}(30^\circ) \frac{\tau_r l_e}{t_{tr} k_{tr} l_{ir}}$$

$$= (0.67) \frac{(0.777)(8.896)}{(0.392)(0.93)(8.5)}$$

$$= 1.48 \quad \text{T}$$

From this result we obtain

$$B_{mr} = B_{tr} \frac{t_{tr}}{t_{mr}}$$

$$= 1.48 \frac{(0.392)}{0.370}$$

$$= 1.57 \text{ T}$$

$$B_{rr} = B_{or} \frac{t_{tr}}{t_{rr}}$$

$$= 1.48 \frac{(0.392)}{0.348}$$

$$= 1.67 \text{ T}$$

Using the  $B$ - $H$  curves for 2.6% silicon steel the corresponding field intensities are

$$H_{tr} = 23 \text{ At/in}$$

$$H_{mr} = 35.9 \text{ At/in}$$

$$H_{rr} = 79.3 \text{ At/in}$$

Hence,

$$H_{tr(ave)} = \frac{1}{6}H_{tr} + \frac{2}{3}H_{mr} + \frac{1}{6}H_{rr}$$

$$= 41 \text{ At/in}$$

Note that  $H_{tr}$  is relatively small so that its contribution to the average MMF drop is minor. For example, if  $H_{tr}$  is half as large (23 At/in) then the corresponding  $H_{tr(ave)}$  is 41 At/in, a difference of only 5%. The assumption that the rotor slot overhang can be neglected is therefore justified.

The MMF drop in the rotor teeth is computed from

$$\mathcal{F}_{tr(ave)} = H_{tr(ave)} d_{or}$$

$$= (41)(0.67)$$

$$= 27.5 \text{ At}$$

The flux in the rotor tooth is

$$\begin{aligned}\Phi_{tr} &= B_{g1}(30^\circ)\tau_r l_e \\ &= (0.67)(0.777)(8.896)\left(\frac{2.54}{100}\right)^2 \\ &= 2.97 \text{ mWb}\end{aligned}$$

The reluctance of the rotor tooth is

$$\begin{aligned}\mathcal{R}_{tr} &= \frac{\mathcal{F}_{tr(ave)}}{\Phi_{tr}} \\ &= \frac{27.5}{0.0031} \\ &= 9.26 \times 10^3 \text{ H}^{-1}\end{aligned}$$

The *MMF* drop across the tooth and half the gap is assumed equal to the slot *MMF* or

$$\begin{aligned}\mathcal{F}_{sr} &= \mathcal{F}_{tr(ave)} + \frac{1}{2}\mathcal{F}_{gr} \\ &= 27.5 + \frac{919}{2} \\ &= 487 \text{ At}\end{aligned}$$

### **MMF and Reluctance of Stator Core**

The maximum flux in the stator core is obtained from Eq. (3.30) as

$$\begin{aligned}\Phi_{cs} &= \left(\frac{2}{\pi}B_{g1}\right)\left(\frac{\tau_p}{2}l_e\right) \\ &= \left(\frac{2}{\pi}0.775\right)\left(\frac{9.456}{2}\right)(8.896)\left(\frac{2.54}{100}\right)^2 \\ &= 13.4 \text{ mWb}\end{aligned}$$

The peak fundamental component of flux density in the core is therefore, from Eq. (3.31),

$$\begin{aligned} B_{cs}(90^\circ) &= \frac{\Phi_{cs}(90^\circ)}{d_{cs} k_{is} l_{is}} \\ &= \frac{0.0134}{(1.76)(0.93)(8.5)} \left( \frac{100}{2.54} \right)^2 = 1.49 \text{ T} \end{aligned}$$

The corresponding values of core flux density points  $30^\circ$  and  $60^\circ$  from the maximum are

$$B_{cs}(60^\circ) = \frac{\sqrt{3}}{2} B_{cs}(90^\circ)$$

$$= 1.29 \text{ T}$$

$$B_{cs}(30^\circ) = \frac{1}{2} B_{cs}(90^\circ)$$

$$= 0.746 \text{ T}$$

From the  $B$ - $H$  curves the field intensities at the same three points in the stator core are

$$H_{cs}(90^\circ) = 23.7 \text{ ampere-turns/inch}$$

$$H_{cs}(60^\circ) = 12.5 \text{ ampere-turns/inch}$$

$$H_{cs}(30^\circ) = 5.6 \text{ ampere-turns/inch}$$

The average value of  $H$  over the stator core portion of the flux path is

$$\begin{aligned} H_{cs(\text{ave})} &= \frac{1}{6} H_{cs}(90^\circ) + \frac{2}{3} H_{cs}(60^\circ) + \frac{1}{6} H_{cs}(30^\circ) \\ &= 13.2 \text{ At/in} \end{aligned}$$

The length of one pole pitch at the center line of the stator core can be computed from the equation

$$l_{cs} = \frac{\pi(D_{os} - d_{cs})}{P}$$

$$= \frac{\pi}{8}(32 - 1.76)$$

$$= 11.875''$$

The *MMF* drop over the stator core is therefore

$$\mathcal{F}_{cs(ave)} = H_{cs(ave)} \left( \frac{2}{3} l_{cs} \right)$$

$$= (13.2) \left( \frac{2}{3} \right) (11.875)$$

$$= 104.6 A \cdot t$$

The effective core reluctance of the flux tube corresponding to the tooth and slot in question must be equal

$$\mathcal{R}_{cs} = \frac{\mathcal{F}_{cs(ave)}}{\Phi_{cs}}$$

$$= \frac{104.6}{0.0134}$$

$$= 7.8 \times 10^3 \text{ H}^{-1}$$

### **MMF and Reluctance of Rotor Core**

Since leakage flux has been neglected, the flux per pole in the rotor core is the same as in the stator core. That is

$$\Phi_{cr} = 13.4 \text{ mWb}$$

The peak fundamental component of flux density in the core is

$$B_{cr}(90^\circ) = \frac{\Phi_{cr}}{k_{ir} l_{ir} d_{cr}}$$

$$= \frac{0.0134}{(0.93)(8.5)(2.58)} \left( \frac{100}{2.54} \right)^2 \\ = 1.02 \text{ T}$$

Hence

$$B_{cr}(60^\circ) = \frac{\sqrt{3}}{2} B_{cr}(90^\circ)$$

$$= 0.88 \text{ T}$$

$$B_{cr}(30^\circ) = \frac{1}{2} B_{cr}(90^\circ)$$

$$= 0.51 \text{ T}$$

From the material  $B-H$  curves

$$H_{cr}(90^\circ) = 7.7 \text{ ampere-turns/inch}$$

$$H_{cr}(60^\circ) = 6.6 \text{ ampere-turns/inch}$$

$$H_{cr}(30^\circ) = 3.8 \text{ ampere-turns/inch}$$

from which we obtain

$$H_{cr(\text{ave})} = \frac{1}{6} H_{cr}(90^\circ) + \frac{2}{3} H_{cr}(60^\circ) + \frac{1}{6} H_{cr}(30^\circ) \\ = 6.3 \text{ ampere-turns/inch}$$

The length of one pole pitch at the center of the rotor core cross section is

$$l_{cr} = (\dot{D}_{ir} + d_{cr}) \frac{\pi}{P}$$

$$= (17.5 + 2.85) \frac{\pi}{8}$$

$$= 7.885''$$

Hence

$$\begin{aligned}\mathcal{F}_{cr(ave)} &= H_{cr(ave)} \left( \frac{2}{3} l_{cr} \right) \\ &= (6.3) \left( \frac{2}{3} \right) (7.885) = 33.2 \text{ At}\end{aligned}$$

and

$$\begin{aligned}\mathcal{R}_{cr} &= \frac{\mathcal{F}_{cr(ave)}}{\Phi_{cr}} \\ &= \frac{33.2}{0.0134} \\ &= 2.48 \times 10^3 \text{ H}^{-1}\end{aligned}$$

The total *MMF* drop around the magnetic circuits is obtained by summing up the individual *MMF* drop around the entire magnetic circuit comprised of two air gaps, two stator and rotor teeth, the stator core and the rotor core. The required *MMF* per pole at the  $30^\circ$  point needed to produce the specified air gap flux density is

$$\begin{aligned}2\mathcal{F}_p(30^\circ) &= 2\mathcal{F}_g + 2\mathcal{F}_{tr} + 2\mathcal{F}_{ts} + \mathcal{F}_{cr} + \mathcal{F}_{cs} \\ &= 2(919) + 2(27.5) + 2(165.4) + 33.2 + 104.6 \\ \mathcal{F}_p(30^\circ) &= 1181 \text{ ampere-turns}\end{aligned}$$

The corresponding value of *MMF* per pole at the maximum value of air gap flux density of approximately 0.775 Tesla (50 Klines/in<sup>2</sup>) is

$$\begin{aligned}\mathcal{F}_p(0^\circ) &= \mathcal{F}_{p1} = \frac{2}{\sqrt{3}} \mathcal{F}_p(30^\circ) \\ &= 1364 \text{ ampere-turns}\end{aligned}$$

### 3.8 Magnetic Equivalent Circuit

Figure 3.12 shows an equivalent circuit of the per pole magnetic circuit for the 250 HP example of Section 3.7. Note that since the slot pitch of the stator and rotor teeth are not equal the reluctance of one-half the air gap, differs on the two sides of the gap. Conceptual problems seems to arise since a different amount of flux "flows" in the stator and rotor sides of the equivalent circuit. However, it is important to remember that the width of the stator and rotor teeth are typically not identical.

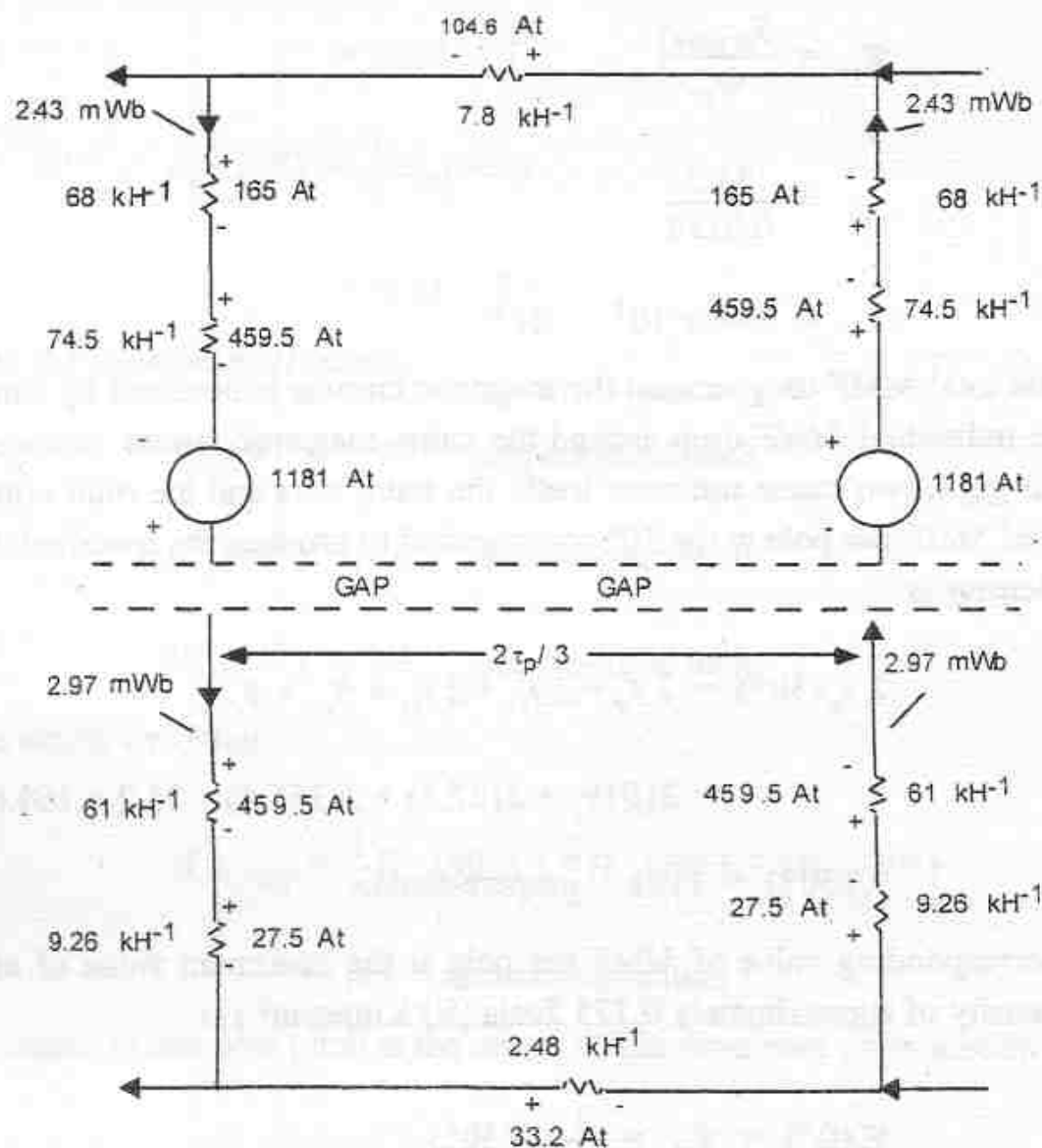


Figure 3.12 Magnetic equivalent circuit of one pole of 250 hp induction machine for a peak fundamental flux density of 0.775 Tesla

This conceptual difficulty can be eliminated if we replace the actual rotor slots and teeth by "equivalent" slots and teeth which produce the same *MMF* drop as the actual rotor teeth but carry the same flux as the stator teeth. However, this degree of complexity for the purpose of achieving a simpler equivalent circuit is generally not necessary.

The concept of an equivalent circuit is potentially as powerful a concept in magnetic circuit analysis of electric machines as it traditionally has been in electric circuit analysis. However, the approach has not been widely adopted. Rather, hybrid solutions such as that outlined in Section 3.8 are more popular primarily due to the long history of this subject and the unavailability, until recently, of powerful digital computer solution algorithms. Clearly, the desired answer is best obtained if we simply establish the reluctance of the four non-linear elements of Figure 3.12 (stator core, rotor core, stator tooth and rotor tooth) as a function of the flux through the reluctance and then turn the work over to a standard non-linear algebraic equation solver. Although there is almost an urgent need to keep the complexity of the computations at a minimum with traditional methods this is clearly not the case if we employ an equivalent circuit solution on a digital computer. Indeed, circuits of nearly any complexity can be set up with relative ease and problems encountered with indentations or overhangs in the teeth and core (so studiously avoided in Section 3.8) can be handled without much difficulty.

### 3.9 Flux Distribution in Highly Saturated Machines

In general, the saturable portion of the magnetic circuit of an induction machine consists of the stator teeth, rotor teeth, stator core and rotor core. Depending upon the design, any one of these elements or any combination of them can be placed in deep saturation. When a sinusoidal *MMF* is applied, the resultant air gap flux density may be either *flat-topped* as shown in Figure 3.10 or *peaked* depending upon whether the teeth or cores are more highly saturated. It is rather evident that saturation of the stator and rotor teeth are the cause of the flattening of the air gap flux density wave. Peaked waves, on the other hand can occur when the core saturates. If the core is saturated, the distribution of flux density along the circumference of the core is essentially constant. Since the flux in the cores is the space integral of the flux in the air gap, the derivative of the square wave produces a peaked (approaching a "pulse") flux density wave in the air gap of the machine. In most practical machines,

however, the teeth are more saturated than the cores so that the air gap flux density wave is nearly always flat topped. In this case, the *MMF* drop due to the harmonic flux in the core can be neglected.

When the machine is highly saturated, the easiest way to calculate core ampere turns is illustrated in Figure 3.13. If the flux density waveform in the

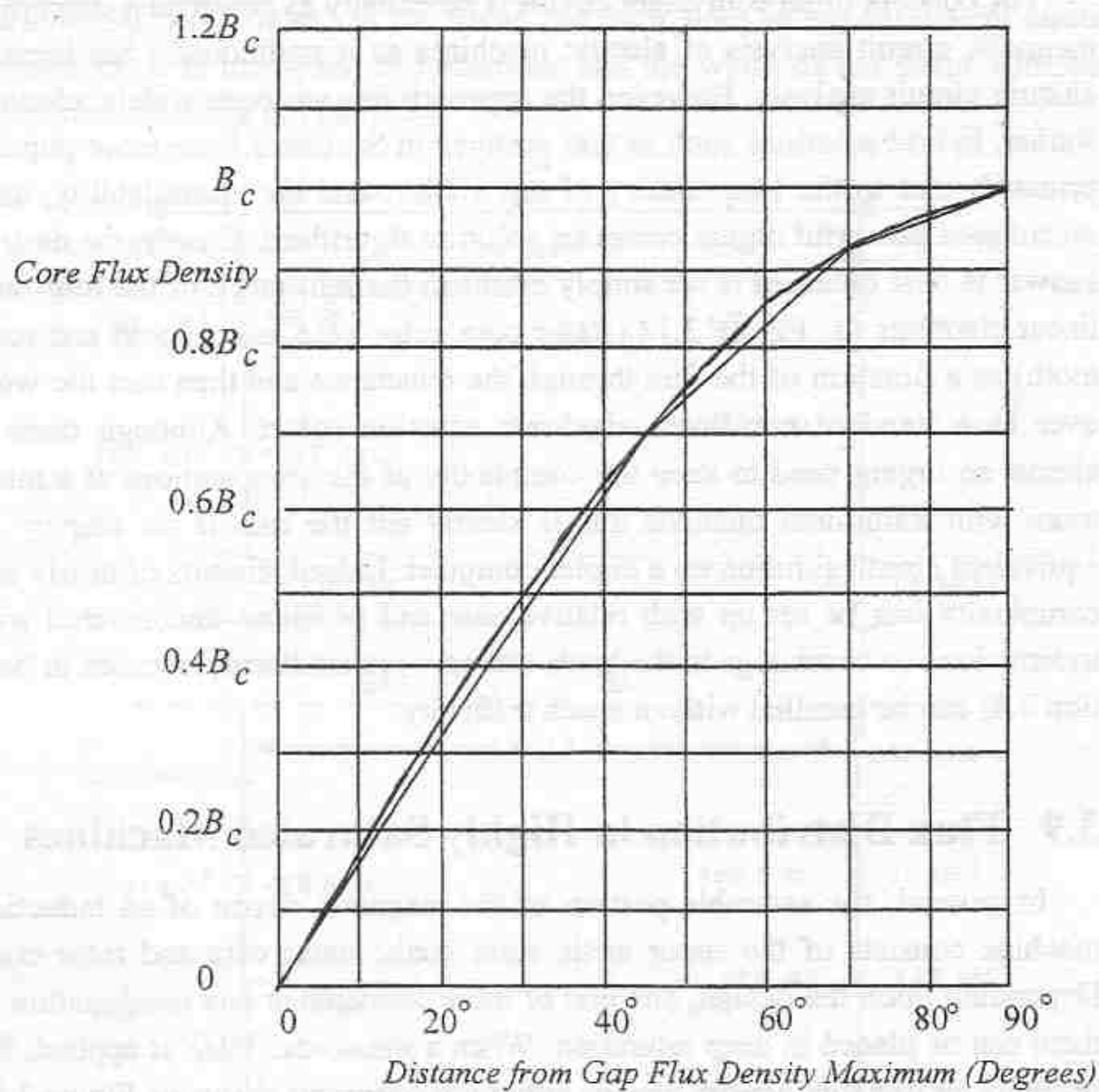


Figure 3.13 Stator or rotor core flux density distribution showing three segment linear approximation

core remains sinusoidal the curve can be approximated by three straight lines as shown with terminal points  $0^\circ$ ,  $45^\circ$ ,  $70^\circ$  and  $90^\circ$ . In each of the three sections, the flux density variation is assumed to be linear. As in calculating the ampere turns of a tapered tooth, the ampere turns drop for each section can be determined by using Simpson's rule. Alternatively, the effective flux density

one-third from the high-density end can be determined and then using the appropriate *dc* magnetization curve for the steel at this point. The three effective core densities in Figure 3.14 are  $B_c \sin 30^\circ = 0.5B_c$ ,  $B_c \sin 61.67^\circ = 0.88B_c$  and  $B_c \sin 83.3^\circ = 0.983B_c$ , where  $B_c$  is an assumed maximum core flux density which is not sufficiently large so as to deeply saturate the core and make the sinusoidal distribution of core flux density assumption invalid. If  $H_{30}$  denotes the field intensity at the 30 degree point (1/3 of the way from the flux density at the 45 degree point), and  $H_{61.7}$  and  $H_{83.3}$  are the corresponding magnetic field intensities for the other two straight line segments then the core ampere turns drop over the interval from  $0^\circ$  to  $45^\circ$  is

$$\mathcal{F}_{c(0-45)} = \frac{1}{2} \left( \frac{l_c}{2} \right) H_{30} \quad (3.51)$$

Over the interval  $0^\circ$  to  $70^\circ$

$$\mathcal{F}_{c(0-70)} = \frac{1}{2} \left( \frac{l_c}{2} \right) H_{30} + \frac{5}{18} \left( \frac{l_c}{2} \right) H_{61.7} \quad (3.52)$$

and over the interval from  $0^\circ$  to  $90^\circ$

$$\mathcal{F}_{c(0-90)} = \frac{1}{2} \left( \frac{l_c}{2} \right) H_{30} + \frac{5}{18} \left( \frac{l_c}{2} \right) H_{61.7} + \frac{2}{9} \left( \frac{l_c}{2} \right) H_{83.3} \quad (3.53)$$

where  $l_c$  is the total length of the path of one pole pitch as measured at the midpoint of the core. The same procedure can be used to determine both the stator and the rotor core drop. Typical resulting curves for both core *MMF* drops are plotted in Figure 3.14.

The *MMF* producing the air gap flux density at any location  $\theta$  between  $0^\circ$  and  $90^\circ$  is then, from Ampere's Law,

$$\mathcal{F}_{gt}(\theta) = \mathcal{F}_{p1} \cos \theta - \mathcal{F}_{cs}(\theta) - \mathcal{F}_{cr}(\theta) \quad (3.54)$$

where  $\mathcal{F}_{cs}(\theta)$  and  $\mathcal{F}_{cr}(\theta)$  are obtained from Figure 3.14,  $\mathcal{F}_{gt}(\theta)$  is the total *MMF* drop in the stator tooth, rotor tooth and air gap at the point corresponding to  $\theta$  and  $\mathcal{F}_{p1}$  is defined by Eq. (3.1).

In general, while the flux density in the stator and rotor cores can be considered as nearly sinusoidal, the saturation of the teeth make the air gap flux usually flat-topped (unless the core is more saturated rather than the teeth in which case the gap flux density is peaked). Including only the possibility of the

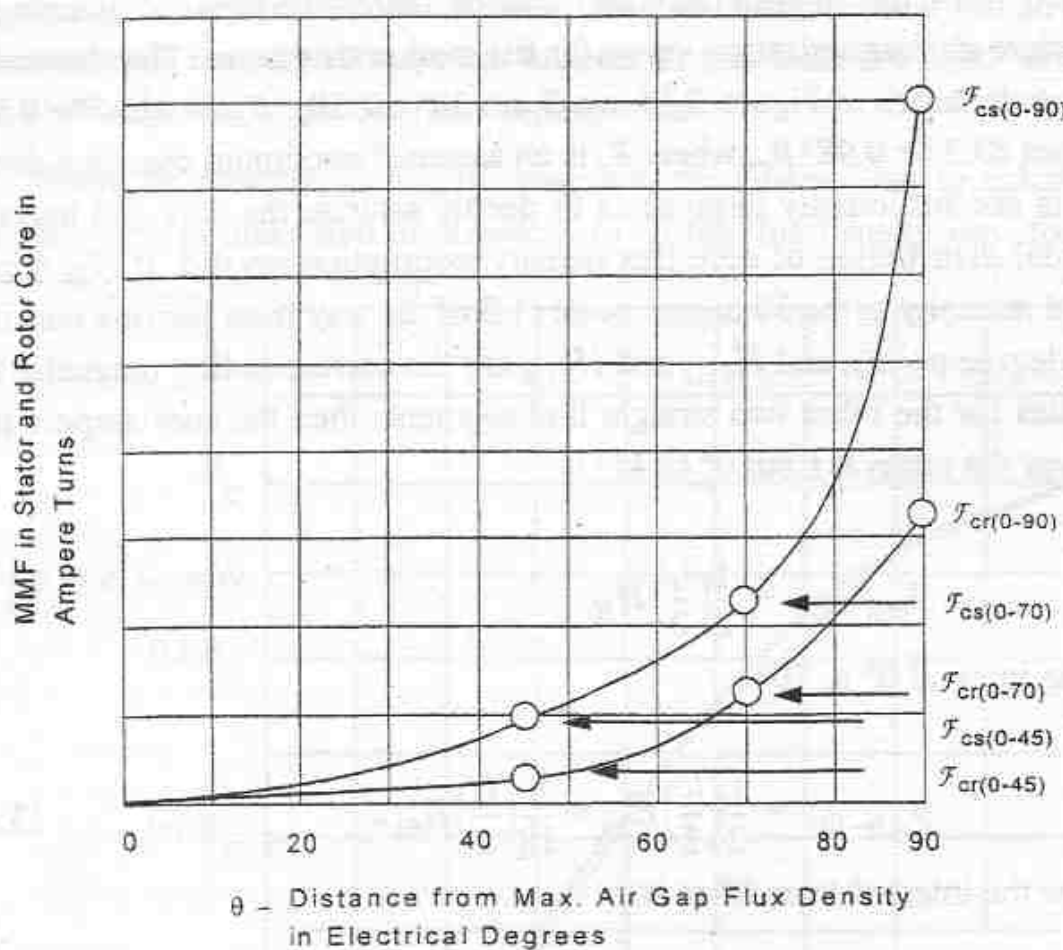


Figure 3.14 Typical plot of core ampere turns vs. angular position relative to maximum air gap flux density

first, third, fifth and seventh harmonics, the flux density in the gap can be expressed as

$$B_g(\theta) = B_{g1} \cos \theta + B_{g3} \cos 3\theta + B_{g5} \cos 5\theta + B_{g7} \cos 7\theta \quad (3.55)$$

When  $\theta = 0^\circ$ , Eq. becomes

$$B_g(0) = B_{g1} + B_{g3} + B_{g5} + B_{g7}$$

When  $\theta = 30^\circ$ ,

$$B_g(30^\circ) = \frac{\sqrt{3}}{2} B_{g1} + 0 \cdot B_{g3} - \frac{\sqrt{3}}{2} B_{g5} - \frac{\sqrt{3}}{2} B_{g7}$$

and when  $\theta = 60^\circ$ ,

$$B_g(60^\circ) = \frac{1}{2}B_{g1} - B_{g3} + \frac{1}{2}B_{g5} + \frac{1}{2}B_{g7}$$

These three equations can now be solved for  $B_{g1}$  as

$$B_{g1} = \frac{1}{3}[B_g(0) + \sqrt{3}B_g(30^\circ) + B_g(60^\circ)] \quad (3.56)$$

An iterative process can now be used to determine the solution.

- First a value of  $B_m$  is selected. The corresponding value of  $B_{g,max}$  can be determined from Eq. (3.17).
- The corresponding values of  $B_{cs}$  and  $B_{cr}$  are obtained from Eqs. (3.37) and (3.38):
- Since the harmonics in the air gap are assumed to not affect the MMF drop in the cores, the MMF drop in the stator and rotor cores are thereby fixed and curves similar to Figure 3.13 can be established.
- Since the amplitude of the flat-topped flux density  $B_{g,max}$  must lie between  $B_{g1}$  and, perhaps  $0.7B_{g1}$ , a representative value is guessed, for example  $B_{g1} = B_{g,max}/0.9$ .
- The MMF per pole is then calculated from Eq. (3.54) by adding the MMF necessary to carry the fundamental component of flux in the cores plus the MMF needed to drive the gap flux corresponding to  $B_{g,max}$  through the gap plus the stator and rotor teeth. That is, setting Eq. (3.54) equal to the MMF per pole,

$$\mathcal{F}_{p1} = \mathcal{F}_{gt}(0) + \mathcal{F}_{cs}(0-90) + \mathcal{F}_{cr}(0-90) \quad (3.57)$$

- The flux densities at the 30 and 60 degree points are then determined by first calculating the MMF available at these points to establish the air gap flux. For example,

$$\mathcal{F}_{gt}(30^\circ) = \mathcal{F}_{p1} \cos(30^\circ) - \mathcal{F}_{cs}(30^\circ) - \mathcal{F}_{cr}(30^\circ) \quad (3.58)$$

where  $\mathcal{F}_{cs}$  and  $\mathcal{F}_{cr}$  are the core MMF drops obtained from Figure 3.14.

- The corresponding air gap flux densities  $B_g(30^\circ)$  and  $B_g(60^\circ)$  are then calculated.
- Equation (3.56) is then solved and compared with the guessed value of  $B_{g1}$ . If the result does not match, a new factor relating  $B_{g,max}$  and  $B_{g1}$  is guessed, for example  $B_{g,max} = 0.85B_{g1}$ . The iteration continues until a match is obtained within 1%. Usually only three or four iterations will do sufficiently well.

- Having obtained the correct value of  $B_g(\theta)$ , the saturation harmonics at no load can now be computed in the same manner as used to compute the first harmonic. The result is

$$B_{g3} = \frac{1}{3}[2B_g(60^\circ) - B_g(0^\circ)] \quad (3.59)$$

$$B_{g5} = \frac{1}{5}[2B_g(72^\circ) - 2B_g(36^\circ) + B_g(0^\circ)] \quad (3.60)$$

$$B_{g7} = \frac{1}{7}[2B_g(77.1^\circ) - 2B_g(51.4^\circ) + 2B_g(25.7^\circ) - B_g(0^\circ)] \quad (3.61)$$

If the saturation harmonics are sufficiently large they could affect the core flux density making the initial assumption of a sinusoidally distributed core flux density invalid. In this case a new curve of core flux vs. position along the stator and/or rotor core periphery, similar to Figure 3.13 can be determined. This new curve will have a “peaked” rather than “flattened” shape compared to a sine wave. That is, the peak core flux density will be slightly greater than the initial value assumed at the beginning of the calculation procedure. The process of calculating the core *MMF* drop can now be repeated with the new function of core flux density and iteration used until convergence is obtained.

While the determination of these “saturation harmonics” are not necessary to determine our fundamental task, that of calculating the magnetizing reactance, they are important contributors to stray losses which will be determined in Chapter 5.

### 3.10 Calculation of Magnetizing Reactance

Although we have nearly finished our solution for the main magnetic circuit of the induction machine it is an interesting fact that we have yet to define the exact distribution of windings in the stator slots and therefore we have yet to specify the voltage and current supplied to the machine. Let us now assume that the winding distribution in the stator slots have been specified so that the fundamental component of impressed *MMF* is known. That is, at the center line for each of the  $P$  poles of the machine, Eq. (3.1) prevails and

$$\mathcal{F}_{p1} = \left(\frac{3}{2}\right)\left(\frac{4}{\pi}\right)\left(\frac{k_1 N_t}{CP}\right) I_m \quad (3.62)$$

where

$$k_1 = k_{p1} k_{d1} k_{\chi 1} k_{s1} \quad (3.63)$$

Since the MMF  $\mathcal{F}_{p1}$  is assumed known and the winding distribution fixes the pitch, distribution and skew factors as well as the total turns, poles and circuits, the corresponding maximum current per phase is readily computed.

The remaining task is to relate the air gap flux density in the gap to the flux linking the winding and thereby to the terminal voltage. In general, the MMF is sinusoidal so that

$$\mathcal{F}_p(\theta) = \mathcal{F}_{p1} \cos\left(\frac{P\theta}{2}\right) \quad (3.64)$$

where  $\theta$  is the circumferential angle measured along the stator periphery and represents the distance away from the maximum defined by Figure 3.10.

Recall from Chapter 2 that the net stator MMF distribution is made up of three MMF distributions, one for each of the three stator phases  $a$ ,  $b$  and  $c$  which are physically displaced around the air gap by 120 electrical degrees. When harmonics are neglected these three phase MMF's are also sinusoidal. For purposes of convenience let the axis of phase  $a$  coincide with the positive peak value of MMF  $F_p$ . Then the phase  $a$  current is also a maximum and the corresponding MMF distribution of phase  $a$  is, from Eq. (2.55)

$$\mathcal{F}_a(\theta) = \frac{4}{\pi} \left(\frac{k_1 N_t}{CP}\right) I_m \cos\left(\frac{P\theta}{2}\right) \quad (3.65)$$

where  $I_m/C$  is amplitude of the current in each of the  $C$  circuits.

We have also established that if MMF impressed by all three phase currents is given by Eq. (3.62) then the flux density has the identical variation in the air gap or,

$$B_g(\theta) = B_{g1} \cos\left(\frac{P\theta}{2}\right) \quad (3.66)$$

The phase  $a$  turns linked by the flux density  $B_g(\theta)$  over one pole of the machine inherently takes into account the fact that the machine is excited by

three phase currents and therefore includes the mutual coupling between phases. The calculation must also take into account the partial linkages caused by the sinusoidal winding distribution. For this purpose, the magnetizing inductance is most easily calculated by first computing the magnetic energy stored in the gap of one pole corresponding to the air gap flux linking one phase (flux linkage per pole per phase). In terms of the gap magnetic flux density and magnetic field of phase  $a$ ,

$$W_{fp} = \frac{1}{2} \int_{\text{one pole}} (B_g \cdot H_a) dV \quad (3.67)$$

Upon specifying that  $B$  and  $H$  are radially directed, taking the dot product and noting that the field intensity of one of the three phases is

$$H_a = \left(\frac{2}{3}\right) \frac{\mathcal{F}_{p1}}{g} \cos\left(\frac{P\theta}{2}\right)$$

then, since  $B_g$  and  $H_a$  are only functions of  $\theta$ , the integral reduces to

$$W_{fp} = \left(\frac{1}{2}\right) B_{g1} \left(\frac{4}{\pi}\right) \left(\frac{k_1 N_t I_m}{CP}\right) \left(\frac{D_{is}}{2}\right) l_e \int_{-\frac{\pi}{P}}^{\frac{\pi}{P}} \cos^2\left(\frac{P\theta}{2}\right) d\theta \quad (3.68)$$

Eq. (3.68) works out to,

$$W_{fp} = 2B_{g1} \frac{k_1 N_t I_m}{CP^2} \left(\frac{D_{is}}{2}\right) l_e \quad (3.69)$$

Eq. (3.69) can also be written as

$$W_{fp} = \frac{1}{2} \left(\frac{k_1 N_t}{P}\right) \left(\frac{I_m}{C}\right) \left(\frac{2}{\pi} B_{g1}\right) (\tau_p l_e) \quad (3.70)$$

where the pole pitch

$$\tau_p = \frac{\pi D_{is}}{P}$$

The left hand pair of product terms in Eq. (3.70) can be recognized as the *MMF per pole* while the right hand pair of terms corresponds to the average value of flux density per pole times the cross sectional area of one pole through which this flux density passes.

Since  $I_m/C$  is equivalent to the current in coils making up one of the poles, the magnetic energy stored per pole can also be written as,

$$W_{fp} = \frac{1}{2} \lambda_p \left( \frac{I_m}{C} \right)^2 \quad (3.71)$$

Thus

$$\lambda_p = \left( \frac{k_1 N_t}{P} \right) \left( \frac{2}{\pi} B_{gl} \right) (\tau_p l_e) \quad (3.72)$$

The total flux linking each of the  $P$  poles of the entire winding is the same as the flux linking any one of the poles. The total flux linkages are found by multiplying the flux linkages per pole by the number of poles connected in series, that is

$$\begin{aligned} \lambda_{ms} &= \frac{P}{C} \lambda_p \\ &= \left( \frac{k_1 N_t}{C} \right) \left( \frac{2}{\pi} B_{gl} \right) (\tau_p l_e) \end{aligned} \quad (3.73)$$

The magnetizing inductance per phase is, by definition, found by taking the ratio of the flux linkages per winding phase to the current in the phase. Hence, by use of Eqs. (3.73) and (3.62) the magnetizing inductance is

$$\begin{aligned} L_{ms} &= \frac{\lambda_{ms}}{I_m} \\ &= \frac{\left( \frac{3}{2} \right) \left( \frac{4}{\pi} \right) \frac{k_1^2 N_t^2}{C^2 P} \left( \frac{2}{\pi} B_{gl} \right) (\tau_p l_e)}{\mathcal{F}_{p1}} \end{aligned} \quad (3.74)$$

The number of turns connected in series can be defined to be

$$N_s = \frac{N_t}{C} \quad (3.75)$$

so that in terms of the total number of series connected turns

$$L_{ms} = \left(\frac{3}{2}\right) \left(\frac{8}{\pi^2}\right) \frac{k_1^2 N_s^2}{P} (\tau_p l_e) \left(\frac{B_{g1}}{\mathcal{F}_{p1}}\right) \quad (3.76)$$

For purposes of analysis it is frequently convenient to define another equivalent gap  $g'_e$  which now takes into account the MMF drops in the iron portion of the magnetic circuit. If all of the MMF drop is now assumed to occur over this equivalent gap length, then from Ampere's Law

$$\frac{B_{g1}}{\mu_o} g'_e = \mathcal{F}_{p1} \quad (3.77)$$

Hence,

$$g'_e = \frac{\mu_o \mathcal{F}_{p1}}{B_{g1}} \quad (3.78)$$

Substituting this result in Eq. (3.76)

$$L_{ms} = \left(\frac{3}{2}\right) \left(\frac{8}{\pi^2}\right) \frac{k_1^2 N_s^2}{P} \mu_o \frac{\tau_p l_e}{g'_e} \quad (3.79)$$

Equation (3.79) has many alternative forms. In terms of the diameter  $D_{is}$ , we can also write  $L_{ms}$  as

$$L_{ms} = \left(\frac{3}{2}\right) \left(\frac{8}{\pi}\right) \left(\frac{k_1 N_s}{P}\right)^2 \mu_o \frac{D_{is} l_e}{g'_e} \quad (3.80)$$

If we recall that the fundamental component (effective number) of series connected turns is

$$N_{se} = \frac{4}{\pi} k_1 \frac{N_t}{C} = \frac{4}{\pi} k_1 N_s \quad (3.81)$$

then

$$L_{ms} = \frac{3}{2} \left(\frac{1}{2}\right) \left(\frac{N_{se}}{P}\right)^2 \mu_o \frac{\pi D_{is} l_e}{g'_e} \quad (3.82)$$

Or, finally, in terms of the radius  $r$  measured along the surface of the gap,

$$L_{ms} = \frac{3}{2} \left( \frac{N_{se}}{P} \right)^2 \mu_o \pi \frac{rl_e}{g_e'} \quad (3.83)$$

This equation is the form typically found in the derivation of machine  $d-q$  parameters using the approach of winding functions.

### 3.11 Example #3 - Calculation of Magnetizing Inductance

The 250 HP induction machine in Example #2 has the following additional information supplied for the stator winding

Phase Connection	Y
Circuits	1
Coil Pitch in Slots	12
Coil Sides per Phase Belt	5
Coil Sides/Slot	2
Conductors/Coil Side	6

From the previous example we know that the total number of stator slots is 120 and that there are 8 poles. Hence the number of stator slots per pole is

$$\text{Stator Slots/Pole} = S_1 / P = 120/8 = 15$$

The pitch of the winding is defined as

$$\text{Pitch} = W / \tau_p$$

However, this ratio is more easily computed by simply taking the ratio of slots corresponding to the coil pitch and pole pitch, i.e.

$$\text{Pitch} = \text{Slots per Coil Pitch} / \text{Slots per Pole Pitch} = 12/15 = 0.8$$

From this result we obtain from Eq. (2.15), the pitch factor for the fundamental component of MMF

$$k_{p1} = \sin\left(\frac{W\pi}{\tau_p 2}\right) \\ = \sin(0.8\pi)/2 = 0.951$$

Since five of the fifteen slots per pole are occupied by coil sides of the same phase winding ( $q=5$ ) the phase belt in per unit of a pole pitch  $Z/\tau_p$  can also be computed by taking the appropriate ratio of slots,

$$Z/\tau_p = (\text{Slots per Phasebelt})/(\text{Slots per Pole}) = 5/15 = 1/3$$

Hence, from Eq. (2.25) or Table 2.1 the distribution factor is

$$k_{d1} = \frac{1}{q} \frac{\sin\left(\frac{Z}{\tau_p}(\pi/2)\right)}{\sin\left(\frac{Z}{\tau_p}\frac{\pi}{2q}\right)} = \frac{1}{5} \frac{\sin(\pi/6)}{5 \sin(\pi/30)}$$

$$k_{d1} = \left(\frac{1}{5}\right) \frac{0.5}{0.1045} \\ = 0.9567$$

The slot opening factor is determined from

$$k_{\chi 1} = \frac{\sin(\chi/2)}{(\chi/2)}$$

where

$$\chi = \frac{b_{os}}{\tau_p} 180 = \frac{0.374}{9.456} 180 = 7.12^\circ$$

whereupon

$$k_{\chi 1} = \frac{\sin(3.56^\circ)}{3.56 \cdot \frac{\pi}{180}} = 0.9993$$

The effects of the slot opening on the fundamental component of MMF is clearly negligible except for open slot machines with a small number of slots per pole per phase and is frequently neglected calculations of this type.

Since the skew of the stator winding is not supplied it is assumed unskewed. Therefore

$$k_{s1} = 1.0$$

The overall winding factor for the stator winding of the machine is

$$\begin{aligned} k_1 &= k_{p1} k_{d1} k_{\chi 1} k_{s1} \\ &= (0.951) (0.9567)(0.9993) (1.0) = 0.91 \end{aligned}$$

The total number of series connected turns per phase can be found from the following.

$$\begin{aligned} \text{Turns/Phase/Circuit} &= (\text{coils/phase belt}) (\text{turns/coil})(\text{poles}) / (\text{circuits}) \\ &= (5)(6)(8)/(1) \end{aligned}$$

$$N_t / C = N_s = 240$$

Hence, the maximum current in each phase corresponding to 1364 A-t is

$$\begin{aligned} I_m &= \frac{\mathcal{F}_{p1}}{\left(\frac{3}{2}\right)\left(\frac{4}{\pi}\right)\left(\frac{k_1 \cdot N_s}{P}\right)} \\ &= \frac{1364}{\left(\frac{3}{2}\right)\left(\frac{4}{\pi}\right)\left(\frac{(0.91)(240)}{8}\right)} \\ &= 26.16 \text{ Amps pk} \end{aligned}$$

The magnetizing inductance per phase can be found conveniently from Eq. (3.74) as

$$\begin{aligned} L_{ms} &= \left(\frac{3}{2}\right)\left(\frac{4}{\pi}\right) \frac{k_1^2 N_s^2}{P} \frac{\left(\frac{2}{\pi} B_{g1}\right)(\tau_p l_e)}{\mathcal{F}_{p1}} \\ &= \left(\frac{3}{2}\right)\left(\frac{4}{\pi}\right) \frac{(0.91)^2 (240)^2}{(8)} \frac{\left(\frac{2}{\pi}(0.775)(9.456)(8.896)\right)}{1364} \times \left(\frac{2.54}{100}\right)^2 \\ &= 0.224 \text{ Henries} \end{aligned}$$

It was mentioned earlier that the actual gap  $g$  can be replaced by an equivalent gap which incorporates both the fringing of the flux due to the stator and rotor teeth and ducts and also allows for the saturation of the teeth and core. For our sample problem this value is obtained from Eq. (3.78) as

$$\begin{aligned} g_e' &= \frac{\mu_o F_{p1}}{B_{g1}} \\ &= \frac{(\mu_o)(1364)}{0.775}(39.37) \\ &= 0.0870'' \end{aligned}$$

Note that this equivalent gap is essentially twice as large as the actual gap of 0.04 inches.

It should now be recalled that the computation of magnetizing inductance was launched by assuming an arbitrary value of air gap flux density of 50,000 lines per inch<sup>2</sup>. In practice, this value is near the upper limit of air gap flux density for this machine and it is of interest to investigate the corresponding value of voltage drop in the per phase equivalent circuit. If the machine is excited by 60 Hz, the voltage across the air gap can be readily calculated as

$$\begin{aligned} V_m &= \omega_e L_m I_m \\ &= (377)(0.224)(26.16) \\ &= 2209 \text{ Volts Peak} \end{aligned}$$

Neglecting leakage inductance the corresponding RMS line-to-line voltage is approximately

$$V_{l-l} \approx \frac{\sqrt{3}}{\sqrt{2}} V_m = 2700 \text{ Volts RMS}$$

Hence, the particular case we have studied corresponds to a 12% overexcited condition since the rated voltage of the machine is stated to be 2400 V.

Often, an accurate calculation of the magnetic circuit is desired only for the rated voltage condition. In this case the approximate flux density in the gap can be calculated from Eq. (3.72) as

$$B_{g1} = \frac{\frac{\pi}{2} \lambda_p}{\left(\frac{k_1 N_s}{P}\right) (\tau_p I_e)} \quad (3.84)$$

where

$$\lambda_p = \left(\frac{C}{P}\right) \left(\frac{V_{l-l}}{\omega_e}\right) \frac{\sqrt{2}}{\sqrt{3}} \quad (3.85)$$

Hence

$$B_{g1} = \frac{\frac{\pi}{2} \sqrt{2} \frac{V_{l-l}}{\omega_e}}{(k_1 N_s)(\tau_p I_e)} \quad (3.86)$$

In the case of the example 250 HP machine we obtain the result that at rated line-to-line voltage

$$B_{g1} = \frac{\frac{\pi}{2} \sqrt{2} 2400}{(0.91)(240)(9.456)(8.896)} \times \left(\frac{100}{2.54}\right)^2 \\ = 0.689 \text{ T}$$

### 3.12 References

- [3] C.G. Veinott, "Theory and Design of Small Induction Motors", (book), McGraw-Hill Book Co., Inc., New York, N.Y., 1959.
- [4] C.H. Lee, "Saturation Harmonics of Polyphase Induction Machines", AIEE Transactions, Oct. 1961, pp. 597-603.
- [5] B.J. Chalmers and R. Dodgson, "Waveshapes of Flux Density in Polyphase Induction Motors Under Saturated Conditions", IEEE Trans. on Power Apparatus and Systems, vol. PAS-90, no. 2, March/April, 1971, pp. 564-569.

These calculations can then be repeated in an iterative manner until the flux densities within the magnetic circuit reach a steady state condition. The steady-state solution is obtained when the flux density in the air gap no longer changes.

### Example 1

Consider the magnetic circuit shown in Fig. 10.1. The air gap has a width of 0.002 in. and a flux density of 1000 G. The core has a cross-sectional area of 0.001 in.<sup>2</sup>.

The reluctance of the air gap is given by Eq. (10.1) as

$$\text{Reluctance} = \frac{\text{Flux}}{\text{Flux Density}} = \frac{1000}{1000} = 1 \text{ Vs/A}$$

The reluctance of the core is given by Eq. (10.2) as

$$\text{Reluctance} = \frac{\text{Flux}}{\text{Flux Density}} = \frac{1000}{1000} = 1 \text{ Vs/A}$$

The total reluctance of the magnetic circuit is given by Eq. (10.3) as

$$\text{Total Reluctance} = \text{Reluctance}_{\text{air gap}} + \text{Reluctance}_{\text{core}}$$

The total flux in the magnetic circuit is given by Eq. (10.4) as

$$\text{Total Flux} = \text{Flux Density} \times \text{Cross-Sectional Area}$$

The total flux in the magnetic circuit is given by Eq. (10.5) as

$$\text{Total Flux} = \text{Flux Density} \times \text{Cross-Sectional Area}$$

The total flux in the magnetic circuit is given by Eq. (10.6) as

$$\text{Total Flux} = \text{Flux Density} \times \text{Cross-Sectional Area}$$

The total flux in the magnetic circuit is given by Eq. (10.7) as

The total flux in the magnetic circuit is given by Eq. (10.8) as

The total flux in the magnetic circuit is given by Eq. (10.9) as

The total flux in the magnetic circuit is given by Eq. (10.10) as

The total flux in the magnetic circuit is given by Eq. (10.11) as

The total flux in the magnetic circuit is given by Eq. (10.12) as

The total flux in the magnetic circuit is given by Eq. (10.13) as

The total flux in the magnetic circuit is given by Eq. (10.14) as

The total flux in the magnetic circuit is given by Eq. (10.15) as

The total flux in the magnetic circuit is given by Eq. (10.16) as

The total flux in the magnetic circuit is given by Eq. (10.17) as

The total flux in the magnetic circuit is given by Eq. (10.18) as

The total flux in the magnetic circuit is given by Eq. (10.19) as

The total flux in the magnetic circuit is given by Eq. (10.20) as

The total flux in the magnetic circuit is given by Eq. (10.21) as

The total flux in the magnetic circuit is given by Eq. (10.22) as

The total flux in the magnetic circuit is given by Eq. (10.23) as

The total flux in the magnetic circuit is given by Eq. (10.24) as

# Chapter 4

## Use of Magnetic Circuits in Leakage Reactance Calculations

### 4.1 Components of Leakage Flux in Induction Machines

It is important to recall that torque production in any electrical machine involves the interaction of the air gap flux with the rotor *MMF*. We are now equipped to calculate the air gap flux and associated air gap inductance for practical machine geometries. To a first order of approximation this quantity is a function of the applied voltage and hence does not vary widely over a change in mechanical load. The second quantity, namely the rotor *MMF*, varies with rotor (and therefore stator) current and hence has a much more dominant role in torque production. The stator and rotor currents, are, in turn, primarily a function of the leakage reactances of the machine. In particular, key performance characteristics such as breakdown torque, starting torque and inrush current are nearly independent of magnetizing inductance but depend critically upon the leakage inductances. In addition, the key electromagnetic time constants are dependent almost solely upon the leakage inductances (together with the resistances) of the machine.

In general, five principle components of leakage flux can be identified for induction machines.

1. *Slot Leakage Flux.* Slot leakage flux is shown in Figure 4.1. Note that this component of flux crosses the slot from one tooth to the next, linking with that portion of the conductors below it by returning through the core portion of the punching.

2. *End Winding Leakage Flux.* The overhang or end winding portion of a winding produces a distinctly different component of leakage flux whose magnetic circuit is entirely in air. Nonetheless this component forms an appreciable portion of the leakage inductance since 55-75% of the copper of a two phase stator winding is located in the end winding region. Corresponding values for

4, 6 and 8 pole machines are 49-68%, 43-60% and 39-52% respectively. The complexity of the flux paths associated with practical winding arrangements call for very complex mathematical models. As a result, empirical correction factors are sometimes employed for better accuracy.

*3. Harmonic or Belt Leakage Flux.* This flux is due to the fact that the primary and secondary *MMF* distributions are not, in general, the same. Since the corresponding harmonic fluxes do not couple both stator and rotor equally, the net result is that they produce a form of leakage flux.

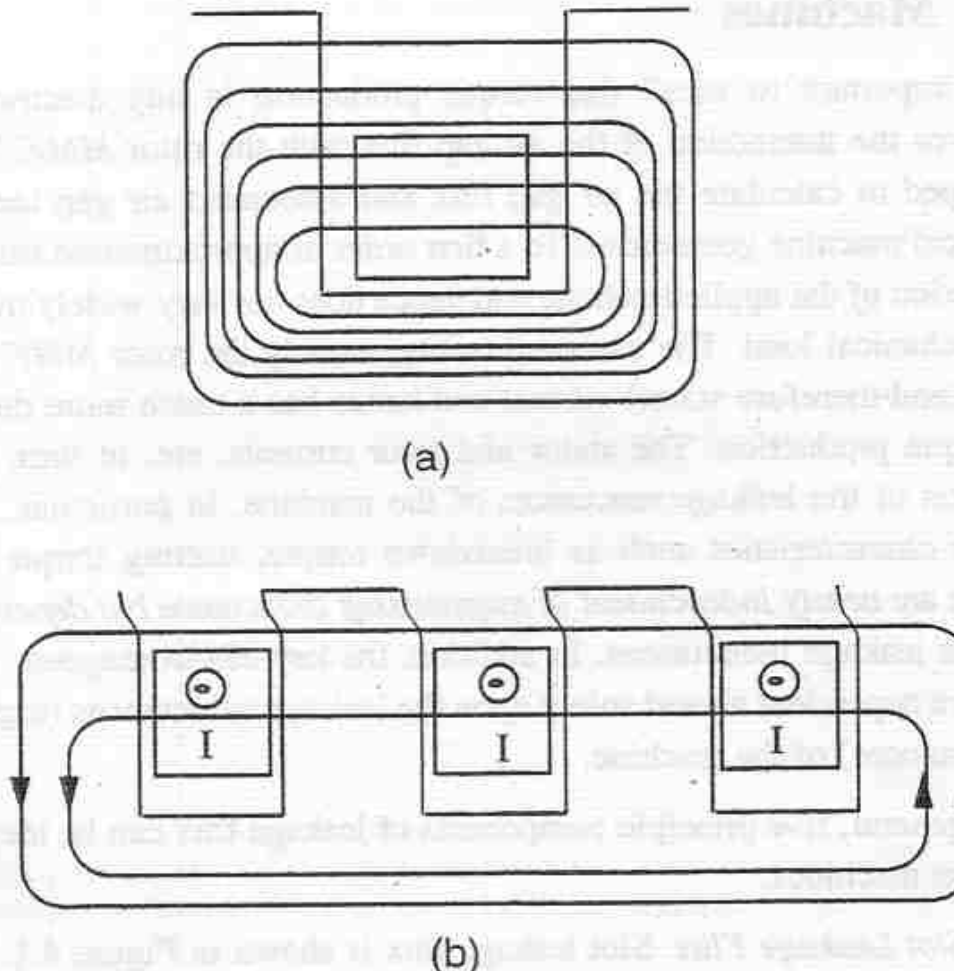


Figure 4.1      Slot leakage flux (a) in an isolated slot, (b) in a phase belt of three slots.

*4. Zigzag Leakage Flux.* This component of leakage flux passes across the air gap from one tooth to another in a zigzag fashion as shown in Figure 4.2. It can be observed that the magnitude of this flux depends upon the length of the air gap and the relative instantaneous positions of the tooth tips.

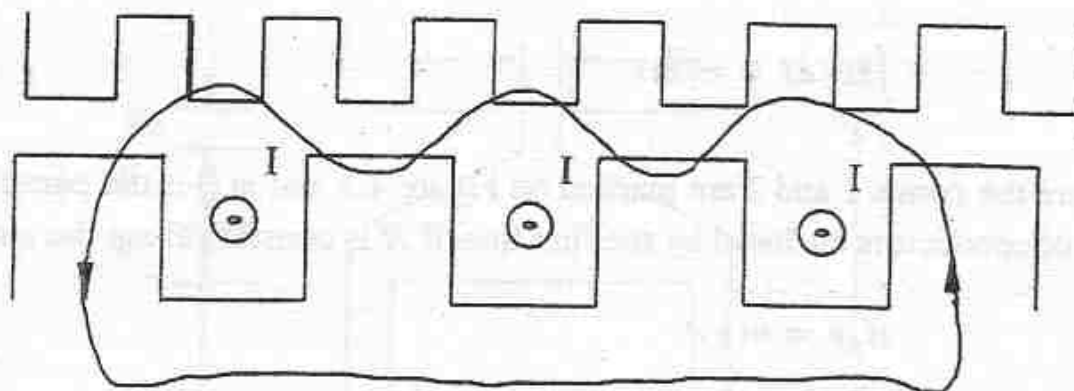


Figure 4.2 Zigzag leakage over one phase belt

*5. Skew Leakage Flux.* The skew leakage flux is present only when the stator or rotor windings are skewed. Skewing, in essence, results in a decrease in the amount of air gap flux coupling both the stator and rotor windings for a given amplitude of air gap flux. The result has the same effect as an increase in stator leakage flux and therefore is regarded as a type of leakage.

## 4.2 Specific Permeance

The leakage flux distribution in a practical machine is clearly a three dimensional problem. Nonetheless, by taking a cross section of the machine sufficiently remote from the ends, it is possible to reduce the problem to a two dimensional one. The flux which is forced across a slot is driven by the current which flows in the slot itself. By Ampere's Law the *MMF* supplied by the current in the slot is consumed by an *MMF* drop in the iron plus the drop in air across the slot. Since the slot width is extremely large, many times larger than the air gap of the machine, the per cent *MMF* drop in the iron is a small percentage of the drop even if the tooth is entering saturation. Hence, to a very good approximation we can frequently neglect the iron drop in our calculation. The permeance of the flux paths can now be found by summing up all tubes of flux of length and cross-sectional area  $l_{es} dx$  where  $l_{es}$  is the effective length of the machine for stator slot leakage flux and includes the "bowing out" of the slot leakage fluxes near stator based air ducts and at the end of the machine.

As an illustration of the computation of slot leakage flux, consider a flux line passing through an arbitrary point in the conductor as shown in Figure 4.3. Ampere's Law states

$$\int_1^2 \mathbf{H} \cdot d\mathbf{l} = n(x)I \quad (4.1)$$

where the points 1 and 2 are marked on Figure 4.3 and  $n(x)$  is the partial number of conductors enclosed by the flux line. If  $H$  is constant along the path 1-2

$$H_y y = n(x)I \quad (4.2)$$

or

$$\frac{B_y y}{\mu_o} = n(x)I \quad (4.3)$$

The differential flux passing through a differential area  $l_e dx$  centered about the path 1-2 is

$$d\Phi = B_y l_e dx = \mu_o \frac{n(x) I l_e dx}{y} \quad (4.4)$$

The flux linkages enclosed by the flux  $d\Phi$  is

$$d\lambda = n(x) d\Phi = \mu_o n(x)^2 I \frac{l_e dx}{y} \quad (4.5)$$

$$d\lambda = \mu_o n_s^2 I \left[ \frac{n(x)}{n_s} \right]^2 \frac{l_e dx}{y} \quad (4.6)$$

When  $n_s$  is the total number of conductors or "turns" in the slot. The differential inductance associated with the flux path is

$$dL = \frac{d\lambda}{I} = \mu_o n_s^2 \left[ \frac{n(x)}{n_s} \right]^2 \frac{l_e dx}{y} \quad (4.7)$$

Since by definition

$$dL = n_s^2 d\Phi \quad (4.8)$$

The effective differential permeance over the path 1-2 is

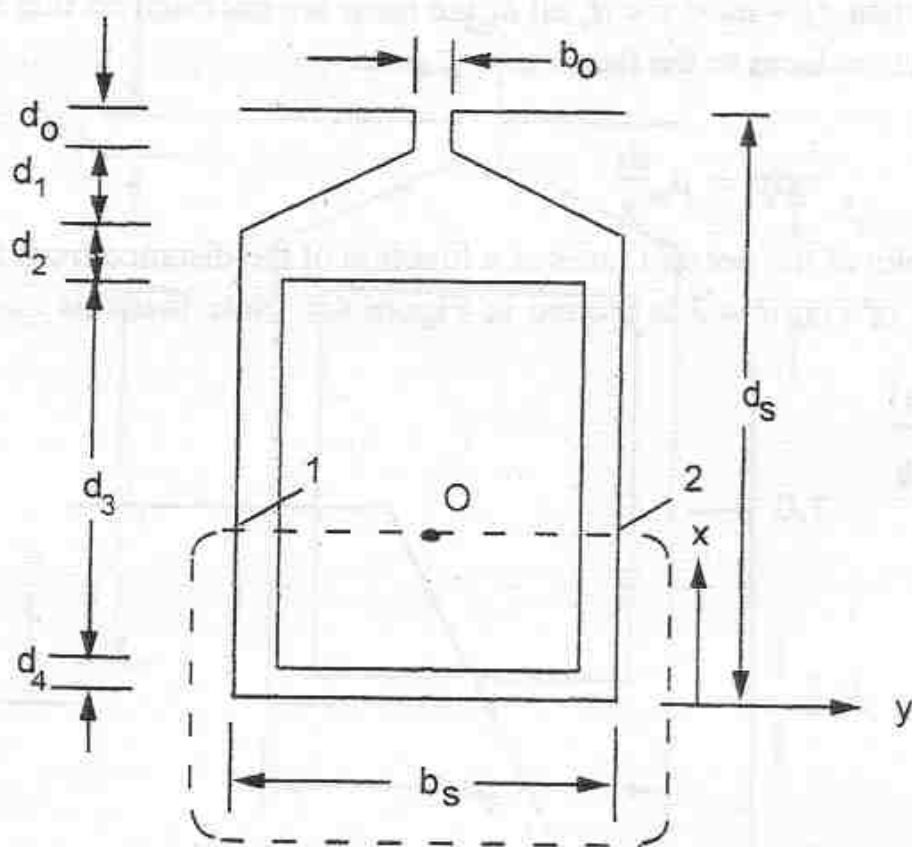


Figure 4.3 Determination of slot leakage

$$dP = \mu_o \left[ \frac{n(x)}{n_s} \right]^2 l_e dx / y \quad (4.9)$$

It can be observed that throughout this analysis the effective length  $l_e$  has been carried along simply as a constant. For this reason it is convenient to define a two dimensional permeance, or *specific permeance*, obtained by dividing Eq. (4.9) by the effective length, or

$$dp = \mu_o \left[ \frac{n(x)}{n_s} \right]^2 dx / y \quad (4.10)$$

The total specific permeance is found by integrating Eq. (4.10) over the slot depth in question or

$$P = \mu_o \int \left[ \frac{n(x)}{n_s} \right]^2 dx / y \quad (4.11)$$

Note that when  $0 < x < d_4$  the current enclosed by a tentative flux path is zero so that the flux below the conductor in the slot is exactly zero. Alterna-

tively when  $d_4 + d_3 < x < d_s$ , all of the turns are enclosed so that  $n(x) = n_s$  and Eq. (4.11) reduces to the form

$$dp = \mu_o \frac{dx}{y} \quad (4.12)$$

A plot of the per unit turns as a function of the distance from the bottom of the slot of Figure 4.3 is plotted in Figure 4.4. Note that this quantity can be

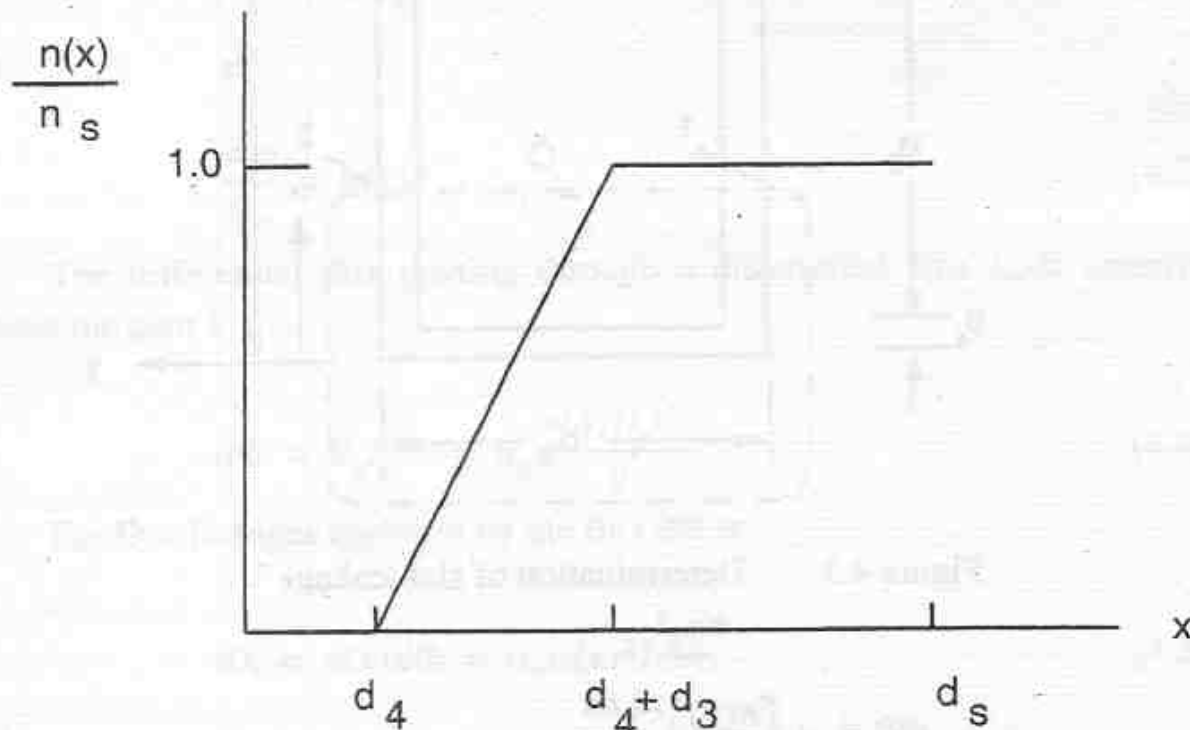


Figure 4.4 Plot of per unit turns vs. distance from bottom of slot corresponding to slot of Figure 4.3

viewed as a normalized turns function similar to the winding function defined in Chapter 1.

### 4.3 Slot Leakage Permeance Calculations

Let us consider first the simple slot shape with semi-closed slot opening shown in Figure 4.5. This shape is probably the most popular configuration for induction machine stator slots. Note that for  $d_4 < x < d_3 + d_4$  the typical tube of flux links with a portion  $(x - d_4)/d_3$  of the total conductors. Hence, by Eq. (4.11) the specific permeance for this portion of the slot is

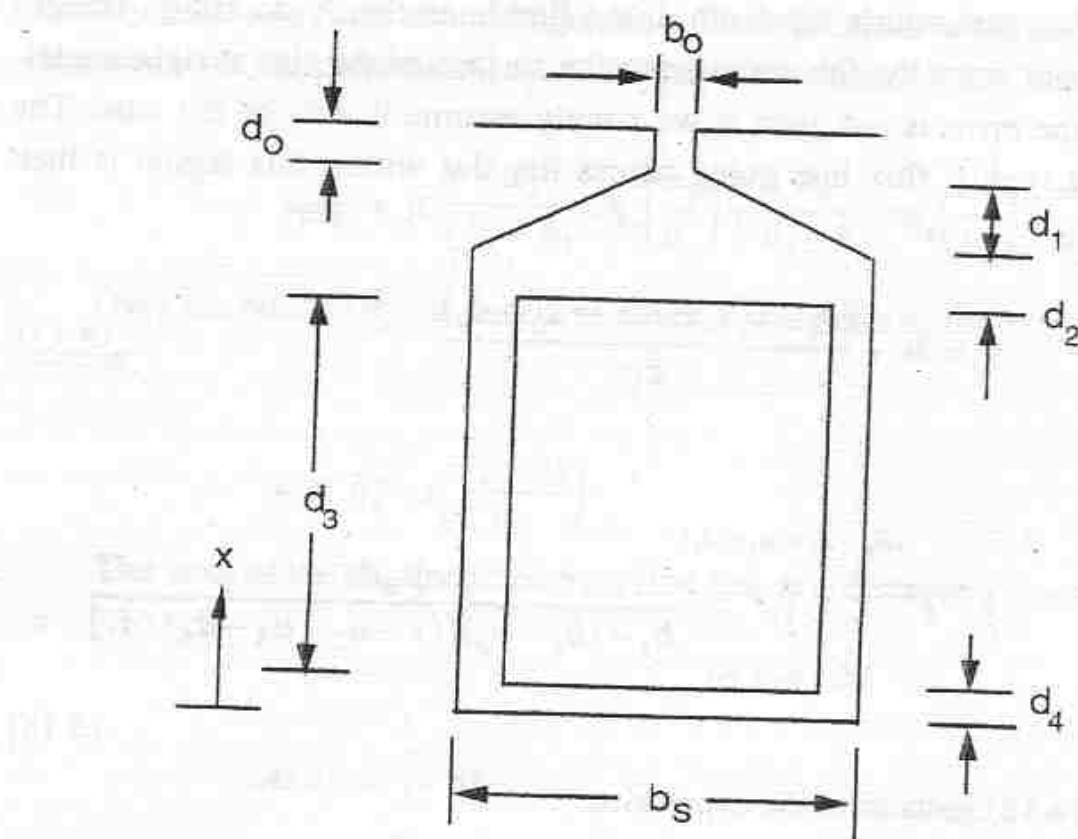


Figure 4.5      Semi-closed slot with parallel sides

$$P_3 = \mu_o \int_{d_4}^{(d_3 + d_4)} \left( \frac{x - d_4}{d_3} \right)^2 \frac{dx}{b_s} \quad (4.13)$$

which reduces to

$$P_3 = \mu_o \frac{d_3}{3b_s} \quad (4.14)$$

For the paths within the depths  $d_2$  and  $d_o$  the specific permeances are clearly

$$P_2 = \mu_o \frac{d_2}{b_s} \quad (4.15)$$

$$P_0 = \mu_o \frac{d_o}{b_s} \quad (4.16)$$

For a flux path within the depth  $d_1$  the flux lines clearly do not go straight across the slot since the flux must leave the surface of the slot at right angles. However, the error is not great if we simply assume this to be the case. The length of a typical flux line going across the slot within this region is then given by

$$y = b_s - \frac{(b_s - b_o)(x - d_2 - d_3 - d_4)}{d_1} \quad (4.17)$$

and thus

$$p_1 = \int_{(d_4 + d_3 + d_2)}^{(d_4 + d_3 + d_2 + d_1)} \frac{\mu_o dx}{b_s - (b_s - b_o)[(x - d_2 - d_3 - d_4)/d_1]} \quad (4.18)$$

Equation (4.18) reduces to the expression

$$p_1 = \frac{\mu_o d_1}{b_s - b_o} \log_e \left( \frac{b_s}{b_o} \right) \quad (4.19)$$

Since the four leakage paths are in parallel the specific permeance for the whole slot is simply the sum of the four individual permeance so that

$$p_s = \mu_o \left[ \frac{d_3}{3b_s} + \frac{d_2}{b_s} + \frac{d_1}{b_s - b_o} \log_e \left( \frac{b_s}{b_o} \right) + \frac{d_o}{b_o} \right] \quad (4.20)$$

It is important to mention that we have assumed uniform distribution of current over the slot. In the case of a stator winding this is nearly always the case since the stator coils are invariably many turns of wire so that the current in the slot is forced to be evenly distributed. However, for rotor slots only one conductor occupies the slot and eddy currents may reduce the specific permeance to a smaller value depending upon the depth of the slot and the frequency of the flux reversals within the slot. A further discussion of this phenomena, called *deep bar effect*, will be deferred to Chapter 5.

As a second, more difficult, example of specific permeance calculation consider the tapered or "coffin shaped" slot shown in Figure 4.6. This shape is

widely used as a rotor slot configuration. From previous work the specific permeance over the portions  $d_2$ ,  $d_1$ , and  $d_o$  have the value

$$p_{012} = \mu_o \left[ \frac{d_2}{b_2 - b_1} \log_e \left( \frac{b_2}{b_1} \right) + \frac{d_1}{b_1 - b_o} \log_e \left( \frac{b_1}{b_o} \right) + \frac{d_o}{b_o} \right] \quad (4.21)$$

Over the portion  $d_3$  the length of a tube of flux at a distance  $x$  from the bottom is

$$y = b_s - x \left( \frac{b_s - b_2}{d_3} \right) \quad (4.22)$$

The area of the bar encircled by a flux line at a distance  $x$  from the bottom is

$$\begin{aligned} A(x) &= \int_0^x y \, dx \\ &= \int_0^x \left[ b_s - \frac{(b_s - b_2)}{d_3} x \right] dx \\ &= x \left[ b_s - \frac{b_s - b_2}{d_3} \frac{(b_s - y)}{(b_s - b_2)} \frac{d_3}{2} \right] \\ &= \frac{x(y + b_s)}{2} \end{aligned} \quad (4.23)$$

The total area occupied by the conductor is

$$\begin{aligned} A_c &= A(x) \Big|_{x=d_3, y=b} \\ &= d_3 \frac{(b_s + b_2)}{2} \end{aligned} \quad (4.24)$$

Hence the fraction of the total turns enclosed by the flux line is

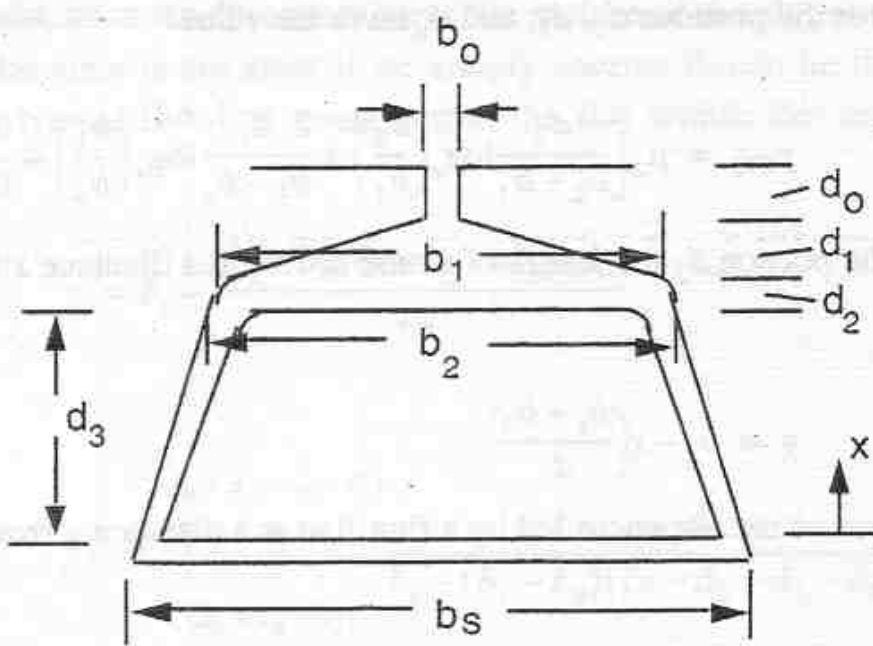


Figure 4.6 Tapered semi-closed "coffin-shaped" slots

$$\frac{n(x)}{n_s} = \frac{A(x)}{A_c} = \frac{[x(y + b_s)]/2}{[d_3(b_s + b_2)]/2} \quad (4.25)$$

$$= \frac{y + b_s}{b_2 + b_s} \left( \frac{x}{d_3} \right)$$

The specific permeance of the conductor occupied region is, from Eq. (4.11),

$$p_3 = \mu_o \int_0^{a_3} \left( \frac{y + b_s}{b_2 + b_s} \right)^2 \left( \frac{x}{d_3} \right)^2 \frac{dx}{y} \quad (4.26)$$

which yields ultimately

$$p_3 = \mu_o \frac{d_3}{b_s} \left[ \frac{\beta^2 - \frac{\beta^4}{4} - \log_e \beta - \frac{3}{4}}{(1 - \beta)(1 - \beta^2)^2} \right] \quad (4.27)$$

where

$$\beta = \frac{b_2}{b_s}$$

The total permeance of the coffin shaped slot is simply the sum of  $p_{012}$  and  $p_3$  defined respectively by Eqs. (4.21) and (4.27).

As a final example let us consider the circular slot of Figure 4.7. Again this is a widely used configuration for rotor slots particularly in larger machines where copper rods are inserted in the slots and soldered together at each end of the rotor to form a squirrel cage. The specific permeance of the slot opening is, almost by inspection

$$p_0 = \frac{\mu_o h_o}{b_o}$$

Over the circular portion, the length of an infinitesimal tube of flux at a distance  $x$  from the bottom of the slot can be expressed as

$$y = 2r \sin \alpha \quad (4.28)$$

where

$$\alpha = \cos^{-1} \left( \frac{r-x}{r} \right) \quad (4.29)$$

or,

$$x = r - r \cos \alpha$$

so that

$$dx = r \sin \alpha d\alpha \quad (4.30)$$

The area of the segment of the circle below the tube of flux is

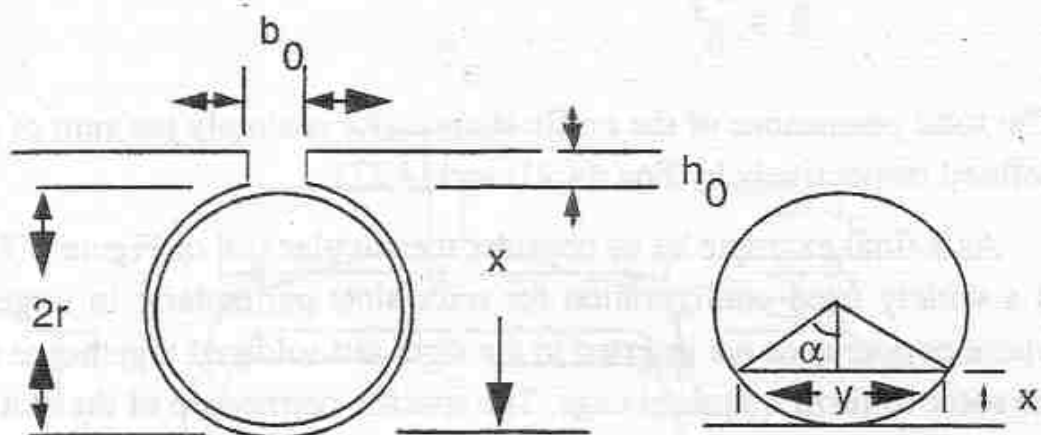


Figure 4.7 Circular slot

$$\begin{aligned}
 A(x) &= \int_{\alpha}^x y \, dx \\
 &= \int_{\alpha}^x 2r \sin \alpha \, d\alpha \\
 &= \frac{r^2}{2} (2\alpha - \sin 2\alpha)
 \end{aligned} \tag{4.31}$$

Hence, the portion of conductors producing flux in the infinitesimal strip is

$$\begin{aligned}
 \frac{n(x)}{n_s} &= \frac{A(x)}{A_c} = \frac{\frac{r^2}{2}(2\alpha - \sin 2\alpha)}{\pi r^2} \\
 &= \frac{\alpha - \frac{1}{2}\sin 2\alpha}{\pi}
 \end{aligned} \tag{4.32}$$

The specific permeance of the circular part of the slot is

$$p_c = \mu_o \int_0^{\pi} \left( \frac{\alpha - \frac{1}{2}\sin 2\alpha}{\pi} \right)^2 \frac{r \sin \alpha}{2r \sin \alpha} d\alpha$$

$$= \frac{\mu_o}{2\pi^2} \int_0^\pi \left( \alpha - \frac{1}{2} \sin 2\alpha \right)^2 d\alpha$$

which reduces to

$$p_s = \mu_o \left( \frac{\pi}{6} + \frac{5}{16\pi} \right) \quad (4.33)$$

so that, for the entire slot

$$p_s = \mu_o \left( 0.623 + \frac{h_o}{b_o} \right) \quad (4.34)$$

#### 4.4 Slot Leakage Inductance of a Single Layer Winding

In many machines only one coil side occupies each of the stator slots. In such cases the slot leakage inductance associated with only one coil side is clearly

$$L_{slot} = n_s^2 l_e p_s \quad (4.35)$$

where the specific permeance  $p_s$  has been calculated for the slot shape in question. Recall that the quantity  $n_s$  is the number of series-connected conductors in the slot. If we assume that the machine is connected as three phase and assume  $S$  total stator slots then the inductance associated with one stator phase belt of a three phase machine is

$$\begin{aligned} L_{phase\ belt} &= qL_{slot} = \left( \frac{S}{3P} \right) L_{slot} \\ &= \frac{S}{3P} n_s^2 l_e p_s \end{aligned} \quad (4.36)$$

The inductance of one circuit is the inductance per phase belt times the number of phase belts connected in series

$$\begin{aligned}
 L_{circuit} &= \frac{P}{C} L_{phasebelt} \\
 &= \frac{S}{3C} n_s^2 l_e p_s
 \end{aligned} \tag{4.37}$$

The inductance per phase is the parallel combination of  $C$  circuit inductances

$$L_{phase} = L_{circuit}/C = \frac{S}{3C^2} n_s^2 l_e p_s \tag{4.38}$$

The total number of series connected stator turns  $N_s$  is related to the number of series connected conductors per slot by

$$\begin{aligned}
 \text{series connected turns/phase/circuit} &= N_s = N_t/C \\
 &= \frac{(\text{turns/coil side})(\text{coil sides/slot})(\text{slots})}{(\text{phases})(\text{circuits})}
 \end{aligned}$$

or, for a single layer stator, three phase machine

$$\begin{aligned}
 N_s &= \frac{(n_c/2)[(1)S_1]}{3 \cdot C} \\
 &= \frac{n_c S_1}{6C}
 \end{aligned} \tag{4.39}$$

With a single layer the total number of conductors in one slot  $n_s$  is equal to  $n_c$  so that,

$$n_s = \frac{6CN_s}{S_1} \tag{4.40}$$

Hence, the slot inductance per phase can be written in the form

$$\begin{aligned}
 L_{phase} &= \frac{S_1}{3} \frac{36N_s^2}{S_1^2} l_e p_s \\
 &= 12N_s^2 l_e \frac{p_s}{S_1}
 \end{aligned} \tag{4.41}$$

When the number of phases differs from three it is immediately apparent that

$$L_{phase} = 4N_s^2 l_e \frac{mp_s}{S} \quad (4.42)$$

where  $m$  denotes the number of phases. While expressly written for the stator slot leakage the solution for a wound rotor winding is clearly similar. It is important to take note that the leakage inductance is inversely proportional to the number of slots so that the leakage inductance is minimized by increasing the number of slots to as large a value as possible.

## 4.5 Slot Leakage of Two Layer Windings

It has already been noted that two layer windings are very extensively employed in both induction and synchronous machines. Figure 4.8 shows a

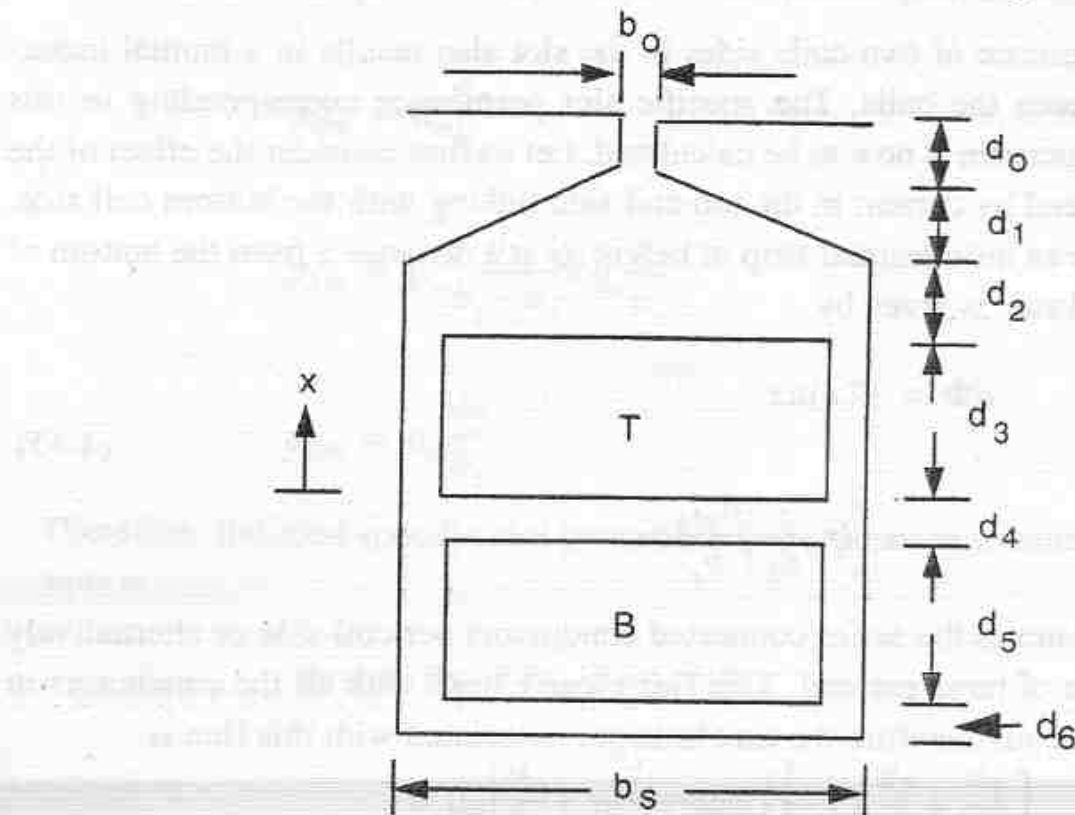


Figure 4.8 Semi-closed slot with double layer winding

typical parallel sided slot indicating  $T$  as the top coil side and  $B$  as the bottom coil side. Since the return portion of coil  $T$  will be in the bottom of another slot and vice versa for  $B$ , the total inductance of the coils will be made up of the

inductances of one top and one bottom side slot inductance. In cases where coils  $T$  and  $B$  are members of the same phase the total inductance will also include a term which is twice the mutual inductance between the top and bottom coil sides. If coils  $T$  and  $B$  are not members of the same phase then they are mutually coupled and a mutual inductance term exists.

From previous work it can be readily established that the specific slot permeance of the top coil side is

$$P_T = \mu_o \left[ \frac{d_3}{3b_s} + \frac{d_2}{b_s} + \frac{d_1}{b_s - b_o} \log_e \left( \frac{b_s}{b_o} \right) + \frac{d_o}{b_o} \right] \quad (4.43)$$

The specific slot permeance of the bottom coil side is

$$P_B = \mu_o \left[ \frac{d_5}{3b_s} + \frac{d_2 + d_3 + d_4}{b_s} + \frac{d_1}{b_s - b_o} \log_e \left( \frac{b_s}{b_o} \right) + \frac{d_o}{b_o} \right] \quad (4.44)$$

The presence of two coils sides in the slot also results in a mutual inductance between the coils. The specific slot permeance corresponding to this mutual inductance is now to be calculated. Let us first consider the effect of the flux produced by current in the top coil side linking with the bottom coil side. The flux in an infinitesimal strip of height  $dx$  at a distance  $x$  from the bottom of the top coil side is given by

$$d\Phi = \mathcal{F}(x)dx \quad (4.45)$$

$$= \left( I n_c \frac{x}{d_3} \right) \frac{\mu_o l_e}{b_s} dx$$

where  $n_c$  denotes the series connected conductors per coil side or alternatively the number of turns per coil. This flux clearly links with all the conductors in the bottom coil, therefore the flux linkages associated with this flux is

$$d\lambda_{3m} = \mu_o n_c^2 I \frac{l_e}{b_s d_3} \frac{x}{d_3} dx$$

The total flux linkages corresponding to the mutual flux is

$$\lambda_{3m} = \int_0^{d_3} d\lambda_{3m}$$

$$= \mu_o n_c^2 I l_e \frac{d_3}{2b_s} \quad (4.46)$$

The specific permeance associated with the conductor portion for the mutual flux is therefore

$$p_{3m} = \mu_o \frac{d_3}{2b_s} \quad (4.47)$$

In the non-conductor portion, the flux is produced by all the conductors in the top coil side and the flux so produced links with all the conductors in the bottom coil side. Therefore, previously derived expressions can be used for the regions involving  $d_o$ ,  $d_1$  and  $d_2$ . The relevant specific permeances are

$$p_{0m} = \mu_o \frac{d_o}{b_o}$$

$$p_{1m} = \mu_o \frac{d_1}{b_s - b_o} \log_e \frac{b_s}{b_o}$$

$$p_{2m} = \mu_o \frac{d_2}{b_s}$$

Therefore, the total specific slot permeance corresponding to mutual flux linkages is

$$P_{TB} = p_{0m} + p_{1m} + p_{2m} + p_{3m}$$

$$= \mu_o \left[ \frac{d_o}{b_o} + \frac{d_1}{b_s - b_o} \log_e \left( \frac{b_s}{b_o} \right) + \frac{d_2}{b_s} + \frac{d_3}{2b_s} \right] \quad (4.48)$$

Since the reciprocity holds even for the case of a non-linear magnetic circuit the flux linking coil  $T$  due to the current in coil  $B$  will be identical to the reverse case that we have calculated. Clearly the corresponding permeance terms are equal so that

$$P_{TB} = P_{BT}$$

It is an interesting exercise to verify this result by assuming a differential flux in coil  $B$  and finding the flux linkages in  $T$  in the manner outlined above.

## 4.6 Slot Leakage Inductances of a Double Cage Winding

One frequent design modification of an induction motor involves the use of a double rotor cage construction as shown in Figure 4.9. By proper design of the

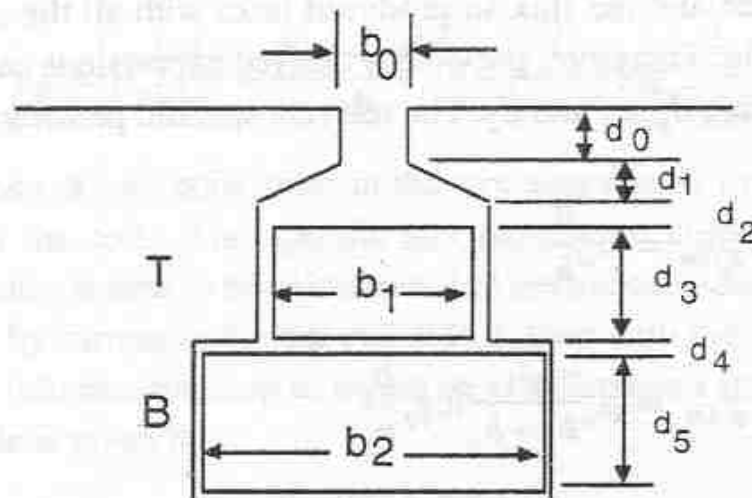


Figure 4.9 Double cage rotor bar construction

cage the relative distribution of currents between the top and bottom bar can be controlled, thereby reducing starting currents without appreciably sacrificing behavior near rated speed. A more thorough discussion of this phenomenon will be given in Chapter 5. In general, as the frequency of flux exciting the slot increases, the current in the bar is forced to flow primarily in the top bar. Hence, the parameters associated with this bar fixes the characteristic of the rotor circuit during the starting condition when the rotor slip frequency is high (i.e. equal to the excitation frequency). When the motor is operating near its rated speed condition the slip frequency is low so that the total cross sectional area associated with the two bar fixes characteristics of the rotor circuit. Since

it is desirable that the starting current remain low a small top bar of relatively small cross section is implied as indicated in Figure 4.9.

The permeances of the top and bottom bar of Figure 4.9 can be easily deduced from Eqs. (4.43), (4.44) and (4.47) by analogy. For a double rotor cage with rectangular bars we have

$$P_T = \mu_o \left[ \frac{d_3}{3b_1} + \frac{d_2}{b_1} + \frac{d_1}{b_1 - b_o} \log_e \left( \frac{b_1}{b_o} \right) + \frac{d_o}{b_o} \right] \quad (4.49)$$

$$P_B = \mu_o \left[ \frac{d_5}{3b_2} + \frac{d_2 + d_3 + d_4}{b_2} + \frac{d_1}{b_2 - b_o} \log_e \left( \frac{b_2}{b_o} \right) + \frac{d_o}{b_o} \right] \quad (4.50)$$

$$P_{TB} = \mu_o \left[ \frac{d_3}{2b_1} + \frac{d_2}{b_1} + \frac{d_1}{b_1 - b_o} \log_e \left( \frac{b_1}{b_o} \right) + \frac{d_o}{b_o} \right] \quad (4.51)$$

The leakage fluxes which link the top and bottom bars are clearly

$$\lambda_T = L_T i_T + L_{TB} i_B \quad (4.52)$$

$$\lambda_B = L_{TB} i_T + L_B i_B \quad (4.53)$$

where  $L_T = l_{er} p_T$ , etc. and  $l_{er}$  is the equivalent length for rotor slots. Equations (4.52) and (4.53) suggest the equivalent circuit of one rotor bar shown in Figure 4.10. The associated bar resistances are also shown. Without additional frequency dependent effects the resistances of the top and bottom bars,  $r_T$  and  $r_B$  are calculated in the conventional manner. That is, for example

$$r_T = \rho \frac{l_{br}}{d_3 b_1} \quad (4.54)$$

where  $\rho$  is the resistivity of the conductor in  $\Omega \text{ in}$  and  $l_{br}$  is the length of the rotor bar. It is interesting to note that this equivalent circuit results in negative inductance elements. For example

$$L_T - L_{TB} = -\mu_o l_{er} \left[ \frac{d_3}{6b_1} \right]$$

This anomaly should not concern us here since the resulting loop equations which describe the flux linkages of the two circuits ultimately generate positive inductance coefficients.

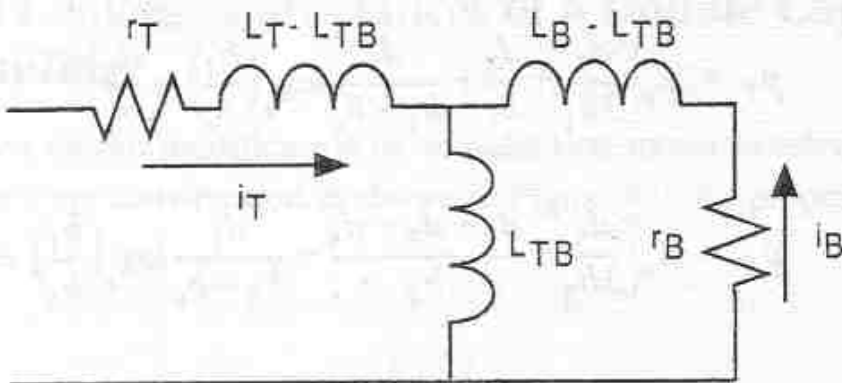


Figure 4.10 Equivalent circuit for double bar arrangement

## 4.7 Slot Leakage Inductance of a Double Layer Winding

In cases where the pitch of the winding is unity each slot will be occupied only by coil sides associated with the same phase. The corresponding leakage inductance for one slot or, alternatively, for one coil side will be given by

$$L_{slot} = n_c^2 l_e (p_T + p_B + 2p_{TB}) \quad (4.55)$$

The corresponding inductance per phase for a  $P$  pole,  $C$  circuit stator winding is

$$L_{phase} = \frac{S_1}{3C^2} n_c^2 l_e (p_T + p_B + 2p_{TB})$$

It can be noted that due to the two layer winding, the number of conductors per coil side  $n_c$  is one-half the number of conductors per slot  $n_s$ . It is useful to continue to express the slot inductance in terms of the number of conductors per slot rather than per coil. Equation (4.55) can also be written in the form

$$L_{phase} = \frac{S_1}{3C^2} n_s^2 l_e \left( \frac{p_T + p_B + 2p_{TB}}{4} \right) \quad (4.56)$$

The quantity

$$(p_T + p_B + 2p_{TB})/4$$

can be considered as the effective specific permeance per slot. If we define

$$p_s = \frac{1}{4}(p_T + p_B + 2p_{TB})$$

then

$$L_{phase} = \frac{S_1}{3C^2} n_s^2 l_e p_s \quad (4.57)$$

It can be again shown that the conductors per slot are related to the series connected number of turns per phase by

$$N_s = \frac{n_s S_1}{6C}$$

so that

$$L_{phase} = 12N_s^2 l_e \frac{p_s}{S_1} \quad (4.58)$$

which has the same form as Eq. (4.41).

It should be recalled that the above expression for slot leakage inductance is valid only when the pitch is unity. Let us now consider the more practical case in which the pitch is less than one. Figure 4.11 shows a typical situation for a machine with a 60° phase belt in which the pitch lies between 2/3 and unity. Note that just as many coil sides are on the bottom and on the top of the slot as for the case where the pitch is unity. Hence, that portion of the slot leakage inductance per phase associated with the coil sides in the bottom of the slots can be written by analogy with Eq. (4.38) as

$$L_{IB} = \frac{S_1}{3C^2} n_c^2 l_e p_B$$

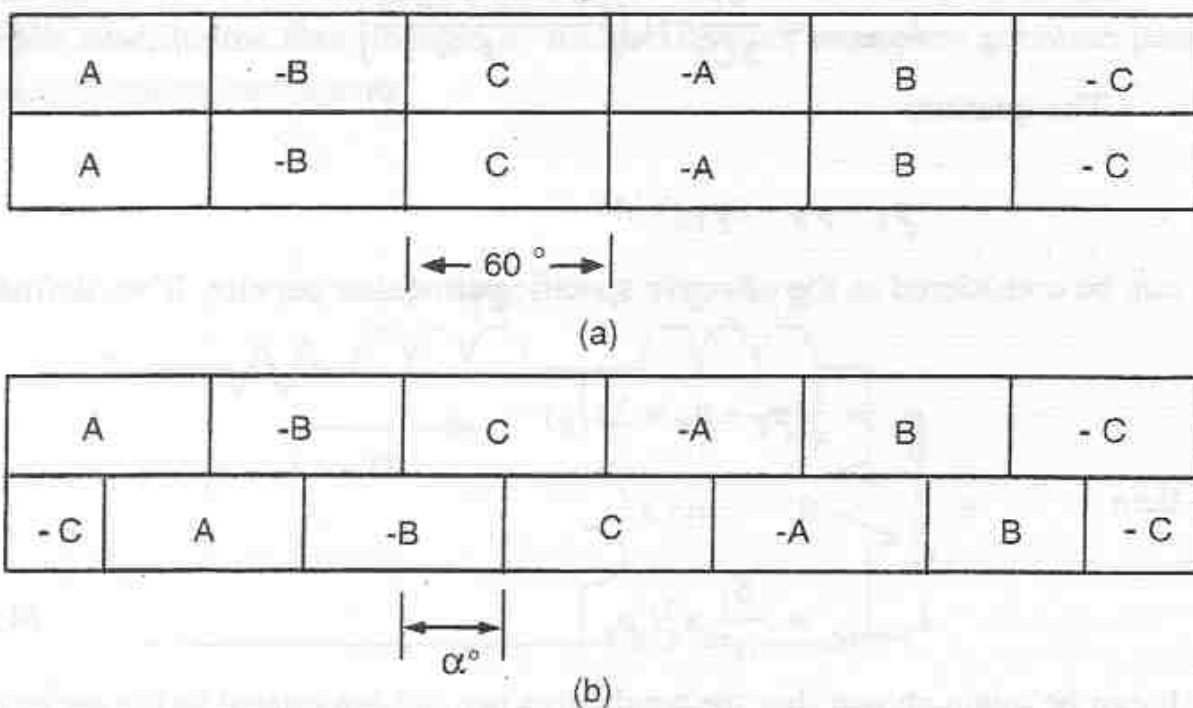


Figure 4.11 Winding distribution for (a) full pitch, (b) fractional pitch winding,  $2/3 < p < 1$ , where  $p = 1 - \alpha/180^\circ$

$$= \frac{S_1}{3C^2} n_s^2 l_e \left( \frac{p_B}{4} \right) \quad (4.59)$$

That portion of the leakage inductance associated with coil sides in the top of the slots is

$$L_{IT} = \frac{S_1}{3C^2} n_s^2 l_e \left( \frac{p_T}{4} \right) \quad (4.60)$$

Note that the mutual inductance from coil sides of the same phase in the top and bottom of the slots has not decreased. Clearly when the pitch  $p$  is unity the result will be the same as Eq. (4.48), and when  $p = 2/3$  this term will be zero. Hence when  $2/3 < p < 1$ , the leakage inductance due to mutual coupling is

$$\begin{aligned} L_{ITB} &= \frac{S_1}{3C^2} n_s^2 l_e \left[ \left( \frac{3p-2}{4} \right) p_{TB} \right] \\ &= 12N_s^2 \frac{l_e}{S_1} \left[ \left( \frac{3p-2}{4} \right) p_{TB} \right] \end{aligned} \quad (4.61)$$

$$= L_{IM}(3p - 2) \quad (4.62)$$

where

$$L_{IM} = 12N_s^2 \frac{l_e}{S_1} \left( \frac{p_{TB}}{4} \right) \quad (4.63)$$

Since the stator is symmetrically wound the "self" component of leakage flux for all three phases is

$$\begin{aligned} L_{sls} &= [L_{IT} + L_{IB} + 2L_{ITB}] \\ &= \frac{S_1}{3C^2} n_s^2 l_e \left[ \frac{p_T}{4} + \frac{p_B}{4} + \frac{p_{TB}}{2}(3p - 2) \right] \\ &= 12N_s^2 \frac{l_e}{S_1} \left[ \frac{p_T}{4} + \frac{p_B}{4} + \frac{p_{TB}}{2}(3p - 2) \right] \end{aligned} \quad (4.64)$$

Note that Eq. (4.64) is an extended definition of slot leakage corresponding to Eq. (4.42) which includes the effect of non-unity pitch. A stator slot with equivalent length  $l_e$  and slots  $S$  is assumed in Eq. (4.64).

When the pitch  $p$  is not equal to unity it is apparent that there now exists a mutual coupling term between the three phases due to slot flux. This term is zero when  $p = 1$  and reaches a maximum when  $p = 2/3$ . By analogy with previous work it is not difficult to verify that the proper expression for the mutual component of leakage inductance between any two phases is

$$\begin{aligned} L_{slm} &= -\frac{S_1}{3C^2} n_s^2 l_e p_{TB} \frac{(3 - 3p)}{4} \\ &= -12N_s^2 \frac{l_e}{S_1} p_{TB} \frac{(3 - 3p)}{4} \end{aligned} \quad (4.65)$$

$$= -L_{IM}(3 - 3p) \quad (4.66)$$

Note the presence of the negative sign which arises because the currents in the two coil sides are in opposition.

When  $1/3 < p < 2/3$  it can be verified from Figure 4.11 that the inductance  $L_{TB}$  remains at zero while the mutual inductance increases to a positive maximum. When  $0 < p < 1/3$  the inductance  $L_{TB}$  decreases to a negative maximum while the mutual inductance decreases to zero.

It is clear that in general the self and mutual leakage components of slot flux can be expressed by

$$L_{sls} = L_{lT} + L_{lB} + 2k_s(p)L_{IM} \quad (4.67)$$

$$L_{slm} = k_m(p)L_{IM} \quad (4.68)$$

where  $L_{lT}$  and  $L_{lB}$  are calculated for the case of unity pitch, that is

$$L_{lT} = 3N_s^2 l_e \frac{p_T}{S_1} \quad (4.69)$$

$$L_{lB} = 3N_s^2 l_e \frac{p_B}{S_1} \quad (4.70)$$

and

$$L_{IM} = 3N_s^2 l_e \frac{p_{TB}}{S_1} \quad (4.71)$$

The quantities  $k_s$  and  $k_m$  are called the slot factors. When  $2/3 < p < 1$  the slot factors are given by

$$k_s = 3p - 2 \quad (4.72)$$

$$k_m = 3p - 3 \quad (4.73)$$

When  $1/3 < p < 2/3$

$$k_s = 0 \quad (4.74)$$

$$k_m = 3(1 - 2p) \quad (4.75)$$

When  $0 < p < 1/3$

$$k_s = 3p - 1 \quad (4.76)$$

$$k_m = 3p \quad (4.77)$$

The slot factors  $k_s$  and  $k_m$  are plotted versus the pitch  $p$  in Figure 4.12. It is

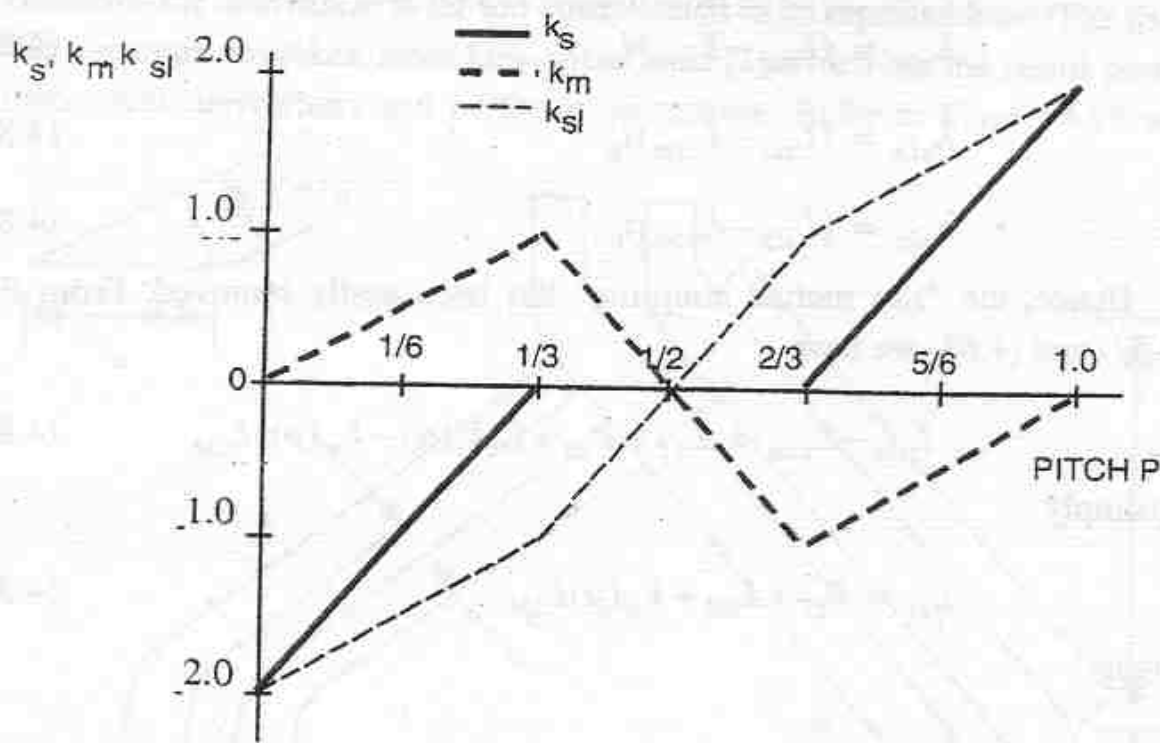


Figure 4.12 Slot factors for self and mutual components of slot leakage for leakage flux versus winding pitch for  $60^\circ$  phase belts

a useful exercise to calculate the slot factors for machines with other phase belts, for example with  $120^\circ$  phase belts.

The fact that the three phases have been shown to be mutually coupled suggests that the proper expressions for the slot leakage flux linkages of the three phase windings are

$$\lambda_{sla} = L_{s1s}i_a + L_{s1m}i_b + L_{s1m}i_c \quad (4.78)$$

$$\lambda_{s1b} = L_{s1m}i_a + L_{s1s}i_b + L_{s1m}i_c \quad (4.79)$$

$$\lambda_{s1c} = L_{s1m}i_a + L_{s1m}i_b + L_{s1s}i_c \quad (4.80)$$

Note that this type of coupling is not normally present in the usual per phase induction machine equivalent circuit. Hence, it is important to resolve this apparent inconsistency. This difficulty is readily put to rest if we recall that when a machine is connected as a three phase machine without a neutral return,

$$i_a + i_b + i_c = 0$$

Substituting this expression in Eqs. (4.78), (4.79) and (4.80) we have

$$\lambda_{sla} = (L_{sls} - L_{slm})i_a \quad (4.81)$$

$$\lambda_{slb} = (L_{sls} - L_{slm})i_b \quad (4.82)$$

$$\lambda_{slc} = (L_{sls} - L_{slm})i_c \quad (4.83)$$

Hence, the "slot mutual coupling" has been easily removed. From Eqs. (4.67) and (4.68) we have

$$L_{sls} - L_{slm} = L_{lT} + L_{lB} + [2k_s(p) - k_m(p)]L_{lM} \quad (4.84)$$

or simply

$$L_{sl} = L_{lT} + L_{lB} + k_{sl}(p)L_{lM} \quad (4.85)$$

where

$$L_{sl} \stackrel{\Delta}{=} L_{sls} - L_{slm}$$

$$k_{sl}(p) \stackrel{\Delta}{=} 2k_s(p) - k_m(p)$$

References to Eqs. (4.72) to (4.77) verifies that for  $2/3 < p < 1$

$$k_{sl}(p) = 3p - 1 \quad (4.86)$$

for  $1/3 < p < 2/3$

$$k_{sl}(p) = 3(2p - 1) \quad (4.87)$$

for  $0 < p < 1/3$

$$k_{sl}(p) = 3p - 2 \quad (4.88)$$

The function  $k_{sl}(p)$  is also plotted in Figure 4.12.

## 4.8 End-Winding Leakage Inductance

As already mentioned the exact calculation of the end-winding leakage is very difficult since the effect of adjacent coils and adjacent phases on each other as well as the effect of the rotor and stator circuits on each other must be consid-

ered. Probably the most rigorous solution in the literature is that of Alger [1]. However the derivation is far too complicated to be repeated here. The following formulas are taken from Lawsuits-Gorki [2] which are the result partly of theoretical derivations and partly of experience. Refer to Figure 4.13 which

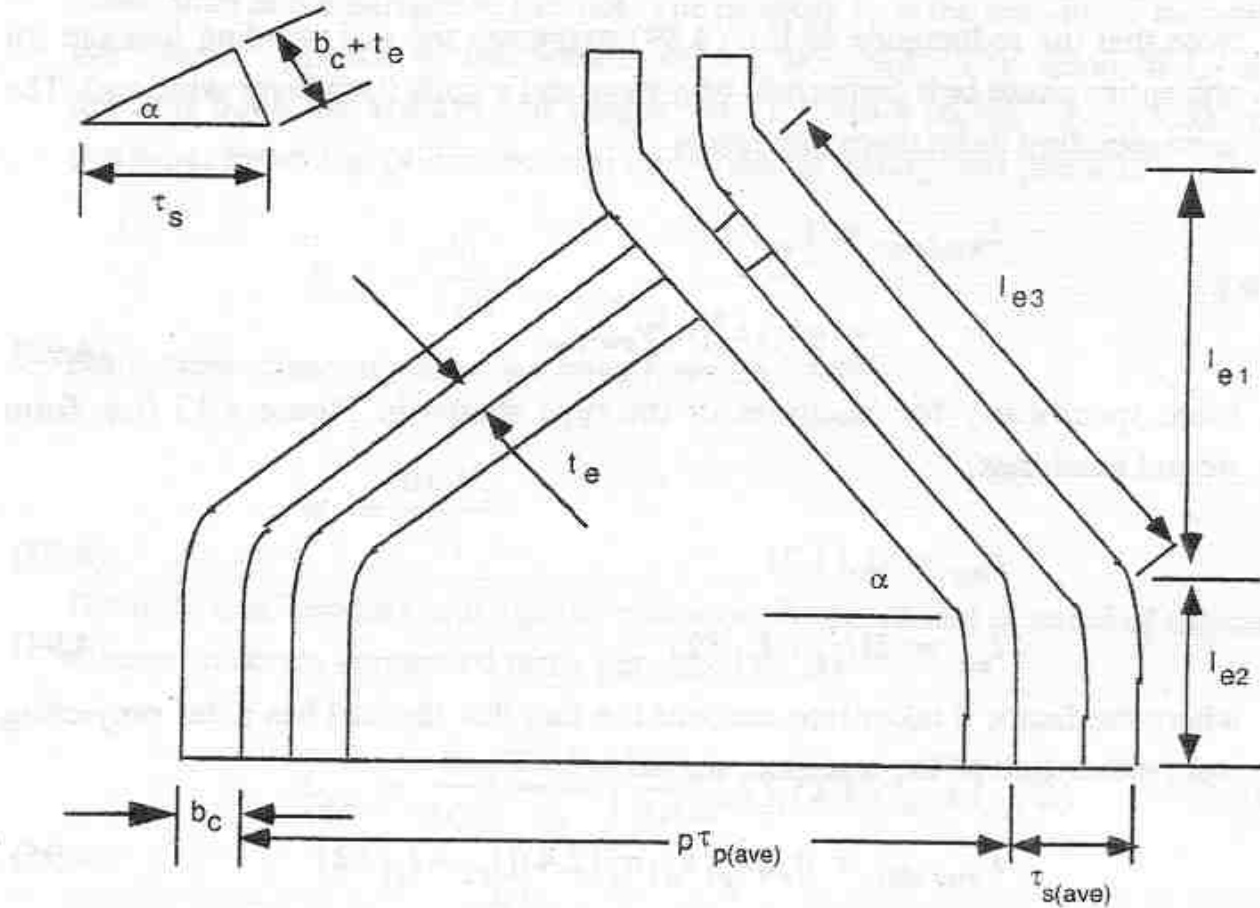


Figure 4.13 End winding configuration for form wound coils

illustrates an idealized portion of the end-winding region for the case of form wound coils. Figure 4.13 shows two coils of a phase belt having  $q$  slots per pole per phase. If all  $q$  coils were concentrated in one slot the end-winding leakage inductance of one side of the coil would be

$$L_{ew} = (qn_s)^2 p_{ew} l_{ew} \quad (4.89)$$

where  $p_{ew}$  and  $l_{ew}$  are the effective specific permeance and effective length which are as yet unspecified. When the coils are now spread over  $q$  slots

$$L_{ew} = (qk_{d1}n_s)^2 p_{ew} l_{ew} \quad (4.90)$$

and if each coil is now separated into two coils which are then pitched

$$\begin{aligned}
 L_{ew} &= (qk_{d1}k_{p1}n_s)^2 p_{ew} l_{ew} \\
 &= (qk_{d1}k_{p1}n_s)^2 p_{ew} l_{ew} \quad (4.91)
 \end{aligned}$$

Note that the inductance of Eq. (4.89) expresses the end winding leakage for one entire phase belt comprised of  $q$  slots and  $q$  coils (two layer winding). The corresponding inductance *per slot* is

$$\begin{aligned}
 L_{ew/slot} &= L_{ew}/q \\
 &= qk_{p1}^2 k_{d1}^2 n_s^2 p_{ew} l_{ew} \quad (4.92)
 \end{aligned}$$

More specifically for machines of the type shown in Figure 4.13 (i.e. form wound machines),

$$p_{ew} = \mu_o(1.2) \quad (4.93)$$

$$l_{ew} = 2(l_{e2} + l_{e1}/2) \quad (4.94)$$

where the factor 2 takes into account the fact that the coil has sides projecting from either side of the machine, so that

$$L_{ew/slot} = \mu_o q k_{p1}^2 k_{d1}^2 n_s^2 (2.4) [l_{e2} + l_{e1}/2] \quad (4.95)$$

The significance of  $l_{e1}$  and  $l_{e2}$  is seen from Figure 4.13. The method used in deriving Eq. (4.94) consists in treating the end-winding leakage as a revolving field in air. The presence of the iron is neglected in the derivation. Furthermore it is assumed that the flux is confined to radial planes and are arcs of circles. Note that the pitch of the winding starts off at  $k_{d1}$  at the surface of the end lamination of the stack but drops off to zero by the time it reaches the end of the coil. Hence, an effective length of  $l_{e1}/2$  is used in the formula. Clearly, the end winding field is not truly a two dimensional one but also spreads out axially. This effect was investigated experimentally by making approximate plots of the three dimensional field. The effect of axial flux, neglected in the idealized analysis, is accounted for by the constant 1.2.

Note the quantity  $t_e$  in Figure 4.13 which represents the air space between two insulated coil sides. In general, this quantity is controlled in order to provide insulation between adjacent coils. If  $t_e$  is fixed it can be shown that  $l_{e1}$  is related to  $t_e$  by

$$l_{e1} = \frac{P\tau_{p(ave)}(b_c + t_e)}{2\sqrt{\tau_{s(ave)}^2 - (b_c + t_e)^2}} \quad (4.96)$$

where  $\tau_{s(ave)}$  and  $\tau_{p(ave)}$  are the slot and pole pitches measured at the middle rather than at the surface of the slot. The quantity  $b_c$  is the breadth of the coil in the slot as opposed to the breadth of the slot itself. The value of  $l_{e2}$  also depends upon the voltage and ranges from 0.25 to 4 inches for a 13,200 volt machine. From Eq. (4.38) the total end-winding leakage per phase is

$$L_{ew} = \frac{S_1}{3C^2} L_{ew/slot} \quad (4.97)$$

For a three phase machine, we have from Eq. (4.40),

$$n_s = \frac{6CN_s}{S_1}$$

The total end-winding leakage per phase can be expressed in terms of the total number of series connected turns per phase  $N_s$  as

$$L_{ew} = \frac{S_1}{3C^2} \left( \frac{6CN_s}{S_1} \right)^2 \frac{S_1}{3P} k_{p1}^2 k_{d1}^2 (2.4)(l_{e2} + l_{e1}/2) \quad (4.98)$$

$$= 4\mu_o \frac{N_s^2}{P} k_{p1}^2 k_{d1}^2 (2.4)(l_{e2} + l_{e1}/2) \quad (4.99)$$

Another expression for end winding leakage can be obtained by using the method of images to replace iron of the machine adjacent to the end winding by the end turn portion on the opposite side of the machine as shown in Figure 4.14. It can be assumed that the flux produced by the axial component of end winding current can produce only transverse flux (flux in the plane of the flux lines within the machine) and vice versa. Consider first the axial component of end winding current. This portion can be segregated into two portions, that produced over the straight portion of the end winding  $l_{e2}$  and that over the slanted portion  $l_{e1}$ . From basic principles it is easily determined that the flux produced by the straight portion (including portions on both sides of the machine but only one turn) is

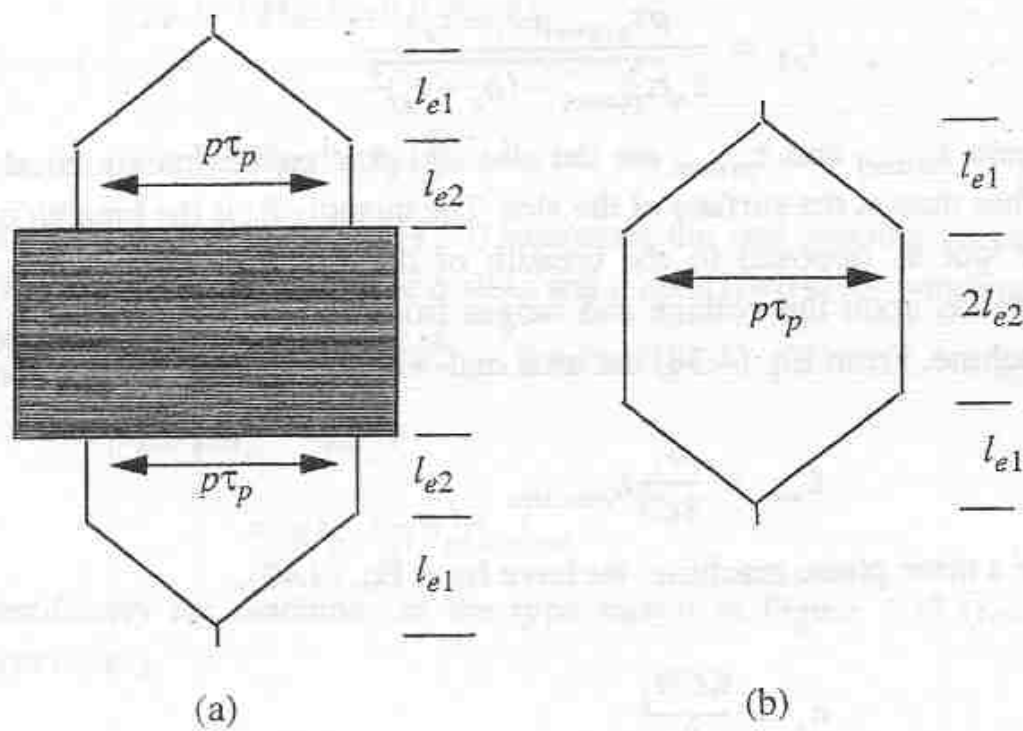


Figure 4.14 (a) Illustrating the end winding of typical coil, (b) simplified representation using the method of images

$$L_{ew1} = \frac{2\mu_o l_{e2}}{\pi} \log_e \left( \frac{p\tau_p}{R_1} \right) \quad (4.100)$$

where  $R_1$  is the radius of an equivalent circle of the same cross sectional area as the coil, i.e.,

$$R_1 = \sqrt{\frac{A_c}{\pi}}$$

The current flowing over the slanted portion can be subdivided into axial and circumferential components  $I_{ax}$  and  $I_{cir}$  as suggested in Figure 4.15 where,

$$I_{ax} = I \sin \alpha_o$$

and

$$I_{cir} = I \cos \alpha_o$$

and where

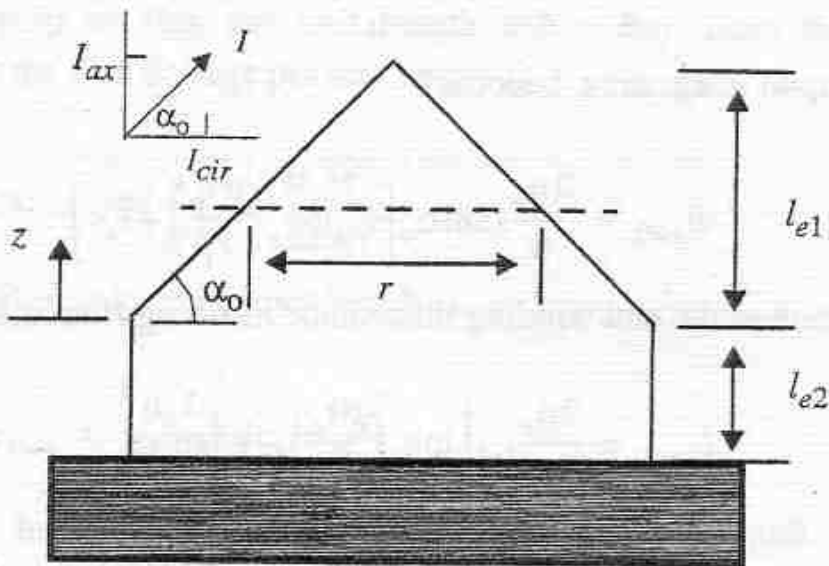


Figure 4.15 Subdivision of end winding current into axial and circumferential components.

$$\alpha_o = \tan^{-1} \left( \frac{2l_{e1}}{p\tau_p} \right)$$

If the slanted portion is sliced at an arbitrary point  $z$  from where the straight portion ends, the distance between the positive axially directed ( $z$  component) and negatively directed components of current can be expressed,

$$r = p\tau_p \left( 1 - \frac{z}{l_{e1}} \right)$$

The differential flux produced by a small increment of the  $z$  directed component of current over the slanted portion is (including slanted portions on both sides of the machine),

$$d\Phi_{ew2} = \frac{2\mu_o}{\pi} I \sin \alpha_o \log_e \left[ \frac{p\tau_p}{r_1} \left( 1 - \frac{z}{l_{e1}} \right) \right] dz$$

The total flux produced by this component of current is thus,

$$\Phi_{ew2} = \frac{2\mu_o}{\pi} I \sin \alpha_o \int_0^{l_{e1}} \log_e \left[ \frac{p\tau_p}{r_1} \left( 1 - \frac{z}{l_{e1}} \right) \right] dz$$

which, upon integrating, becomes

$$\Phi_{ew2} = \frac{2\mu_o}{\pi} I \sin \alpha_o \left[ l_{e1} \log_e \left( \frac{p\tau_p}{r_1} \right) - l_{e1} \right]$$

The portion of the end winding inductance resulting from this leakage flux is

$$L_{ew2} = \frac{2\mu_o}{\pi} l_{e1} \left[ \log_e \left( \frac{p\tau_p}{r_1} \right) - 1 \right] \sin \alpha_o \quad (4.101)$$

The flux produced by a differential component of circumferentially directed current is

$$d\Phi_{ew3} = \frac{2\mu_o}{\pi} I \cos \alpha_o \log_e \left( \frac{z + l_{e2}}{r_1} \right)$$

The total flux produced by the circumferential component is

$$\Phi_{ew3} = \frac{2\mu_o}{\pi} I \cos \alpha_o \int_0^{l_{e1}} \log_e \left( \frac{z + l_{e2}}{r_1} \right) dz$$

The corresponding inductance is, after some reduction

$$L_{ew3} = \frac{4\mu_o}{\pi} \cos \alpha_o \left\{ l_{e1} \left[ \log_e 2 \left( \frac{l_{e1} + l_{e2}}{r_1} \right) - 1 \right] + l_{e2} \log_e \left( \frac{l_{e1} + l_{e2}}{l_{e2}} \right) \right\} \quad (4.102)$$

A fourth and last component can be included to incorporate the flux linkages within the conductor itself. Using Amperes Law, the current enclosed in a circle of radius within the circular conductor of radius  $R$  is

$$\frac{B}{\mu_o} 2\pi r = I \left( \frac{r}{R} \right)^2 \quad (4.103)$$

where  $I$  is the total current in the conductor, or

$$B = \frac{\mu_o I}{2\pi R^2} r \quad (4.104)$$

A differential strip of flux per unit length  $d\Phi = Bdr$  lines the current  $I(r/R)^2$  so that the flux linkage per unit length is

$$d\lambda = d\Phi \left(\frac{r}{R}\right)^2 = \frac{\mu_o I r^3}{2\pi R^4} dr \quad (4.105)$$

so that the total flux linkage per unit length is

$$\lambda_{ew4} = \int_0^R \frac{\mu_o I r^3}{2\pi R^4} dr = \frac{\mu_o I}{8\pi} \quad (4.106)$$

whereupon,

$$L_{ew4} = \frac{\mu_o}{4\pi} \left( 2l_{e2} + \frac{p\tau_p}{\cos \alpha_o} \right) \quad (4.107)$$

The total end winding inductance is the sum of the four terms, modified by the turns per slot, distribution and pitch factors, poles and series connected turns to become,

$$L_{ew} = 4 \frac{k_{dl}^2 k_{p1}^2 N_s^2}{P} (L_{ew1} + L_{ew2} + L_{ew3} + L_{ew4}) \quad (4.108)$$

A formula for the self inductance per bar of the end-winding of a squirrel cage induction motor is also given in Liwschitz-Garik.<sup>1</sup> However, the origin as well as the reasoning behind the derivation is cloudy. Figure 4.16 illustrates the end-winding region for a squirrel cage machine. The corresponding equation for the end-winding inductance per end ring segment (per rotor slot pitch) for a three phase machine is

$$L_{ew} = \mu_o \left( \frac{4}{9} \right) [l_{be} + \kappa \tau_{pr(ave)}] \quad (4.109)$$

where

---

1. op.cit.

$l_{be}$  = length of the bar from end of core to start of the short circuiting ring

$\tau_{pr(ave)}$  = rotor pole pitch measured at the middle of the ring

$\kappa$  = 0.18 for  $P = 2$ , and 0.09 for  $P > 2$ .

It should be noted that since "empirical" constants have been incorporated into Eqs. (4.97) and (4.98) they must be used with caution since these equations assume English units.

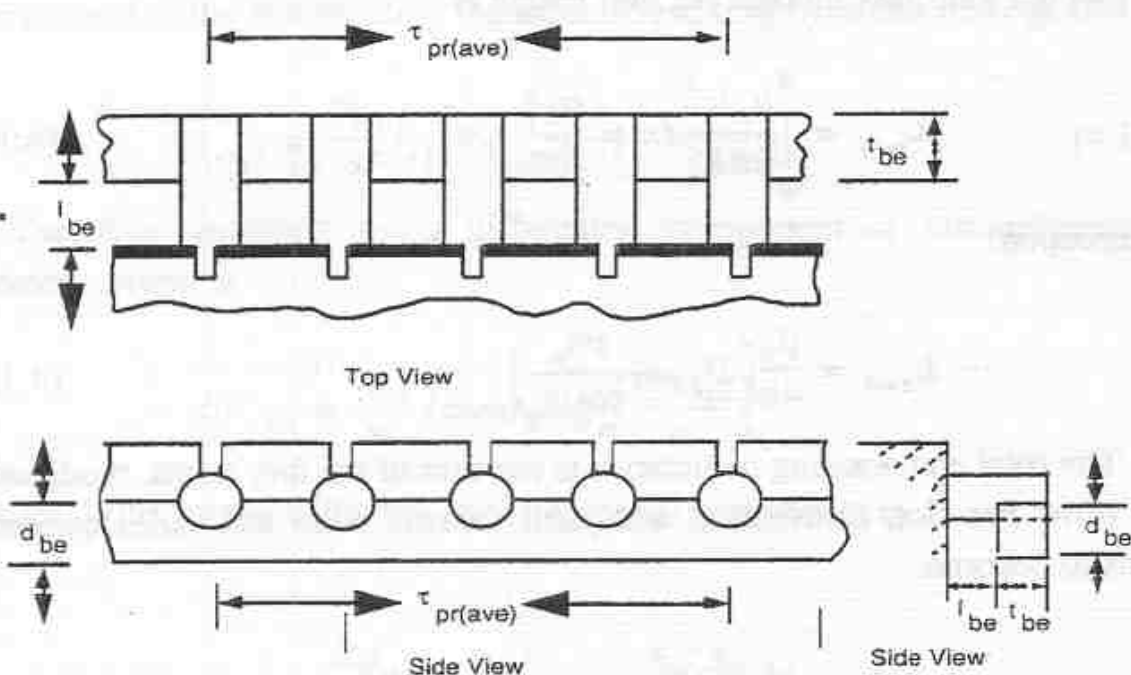


Figure 4.16 End winding configuration for squirrel-cage rotor construction

## 4.9 Stator Harmonic or Belt Leakage

Up to this point we have been successful in neglecting the harmonic components of flux in the air gap. However, we are aware that since the stator windings consist of coils placed in a finite number of slots, the shape of the flux wave is anything but sinusoidal. Clearly, these unwanted flux components must be accounted for in some manner and since they accomplish no useful work they may be considered as leakage components. In the analysis of these leakage components it is useful to distinguish between the effects of the harmonic components of MMF which arise because of the discrete number of stator coils and the effects of the stator slotting in which these coils are placed.

The first effect is said to produce *belt leakage inductance* while the second component, to be considered in the next section contributes to *zig zag leakage inductance*. Let us first consider the stator *MMF* produced by the stator windings. It has already been shown in Chapter 2 that any practical winding produces in the air gap, besides the main (fundamental) component of *MMF*, space harmonics which travel with different speeds with respect to the stator. The main flux wave induces a voltage across the air gap which along determines the useful power transferred to the rotor. However, the space harmonics also induce voltages in the stator winding. These voltages are of different magnitude but they are all of the same frequency since they all result from a fundamental component of stator current. Also they are all in phase which means that they all are purely reactive if they are not "shorted out" by opposing rotor currents.

From Chapter 2, Eq. (2.54) the  $h^{\text{th}}$  harmonic *MMF* in the gap corresponding to a  $P$  pole,  $C$  circuit winding is

$$\mathcal{F}_{ph} = \frac{34}{2\pi} \left( \frac{N_t}{CP} \right) \left( \frac{k_h}{h} \right) I_m \quad (4.110)$$

where

$$k_h = k_{ph} k_{dh} k_{sh} \quad (4.111)$$

The flux density in the air gap resulting from this impressed *MMF* is

$$B_{gh} = \frac{\mu_0 \mathcal{F}_{ph}}{g_e'} \quad (4.112)$$

where  $g_e'$  is the effective gap including the effects of saturation and is defined by Eq. (3.77).

The flux linkages coupling one pole of the  $hP$  pole *MMF* harmonic is found by determining the flux linking its corresponding fractional number of turns and then summing by integration, that is

$$\begin{aligned}\lambda_{ph} &= \int_0^{(2\pi)/(hP)} N_{ah}(h\phi) B_g(h\phi) l_e r d\phi \\ &= \frac{4}{\pi} \left(\frac{k_h N_t}{hP}\right) \int_0^{(2\pi)/(hP)} B_{gh} \cos^2\left(\frac{hP\phi}{2}\right) l_e r d\phi\end{aligned}$$

Recall for Chapter 1 that the winding function  $N_{ah}$  is simply the same as the MMF  $\mathcal{F}_{pn}$  per unit current. Upon integrating

$$\lambda_{ph} = \left(\frac{N_t}{P}\right) \left(\frac{k_h}{h^2}\right) \left(\frac{2B_{gh}}{\pi}\right) \tau_p l_e \quad (4.113)$$

The total series connected flux linkages of all  $hP$  poles is

$$\begin{aligned}\lambda_h &= \frac{hP}{C} \lambda_{ph} \\ &= \left(\frac{N_t}{C}\right) \left(\frac{k_h}{h}\right) \left(\frac{2B_{gh}}{\pi}\right) \tau_p l_e\end{aligned} \quad (4.114)$$

The inductance for the  $h^{th}$  harmonic of the MMF is found by substituting Eq. (4.110) and (4.112) into Eq. (4.114) and then dividing the result by the current in the stator winding  $I_m$ . The result is

$$L_h = \frac{3}{2} \left(\frac{8}{\pi^2}\right) \left(\frac{N_t^2}{C^2 P}\right) \left(\frac{k_h^2}{h^2}\right) \frac{\mu_o \tau_p l_e}{g_e'} \quad (4.115)$$

$$= \frac{3}{2} \left(\frac{8}{\pi^2}\right) \left(\frac{N_s^2}{P}\right) \left(\frac{k_h}{h}\right)^2 \frac{\mu_o \tau_p l_e}{g_e'} \quad (4.116)$$

Since the same current "flows through" all of the harmonic winding components, the inductances corresponding to each of the harmonics are in series. The total leakage inductance resulting from all of the harmonics of MMF is

$$L_{lk} = \frac{3}{2} \left(\frac{8}{\pi^2}\right) \left(\frac{N_s^2}{P}\right) \mu_o \frac{\tau_p l_e}{g_e'} \left[ \sum_{h=2}^{\infty} \left(\frac{k_h}{h}\right)^2 \right] \quad (4.117)$$

Comparison of this result with Eq. (3.78) indicates that Eq. (4.117) can be written in the compact form

$$L_{lk} = L_{ms} \left[ \frac{1}{k_1^2} \sum_{h=2}^{\infty} \left( \frac{k_h}{h} \right)^2 \right] \quad (4.118)$$

A plot of the term  $\sum \left( \frac{k_h}{h} \right)^2$  for the commonly used three phase  $60^\circ$  phase belt winding is given in Figure 4.17 for different numbers of slots per pole per phase  $q$  as the parameter. It can be seen from this figure that the harmonic leakage depends upon the number of slots per pole per phase and also on the pitch. The harmonic leakage decreases approximately with the square of  $q$ .

It is important to mention that the harmonic leakage is important only for wound rotor machines. When the induction machine is equipped with a squirrel cage the harmonics in the air gap produced by the non-fundamental components of MMF will each induce a component of rotor current which will tend to "short" the harmonic inductance. Although belt harmonic fluxes still remain in the gap, they are now very small being the summation of the harmonic stator fluxes and the opposing harmonic rotor fluxes. The problem is also much more complicated since the rotor resistance as well as reactance now enters the picture. The losses resulting from currents which flow in a squirrel cage rotor due to the harmonic stator fluxes are called belt harmonic losses and will be treated in Chapter 5. Although the losses produced by the belt harmonics are important the belt leakage inductance is normally neglected for squirrel cage machines.

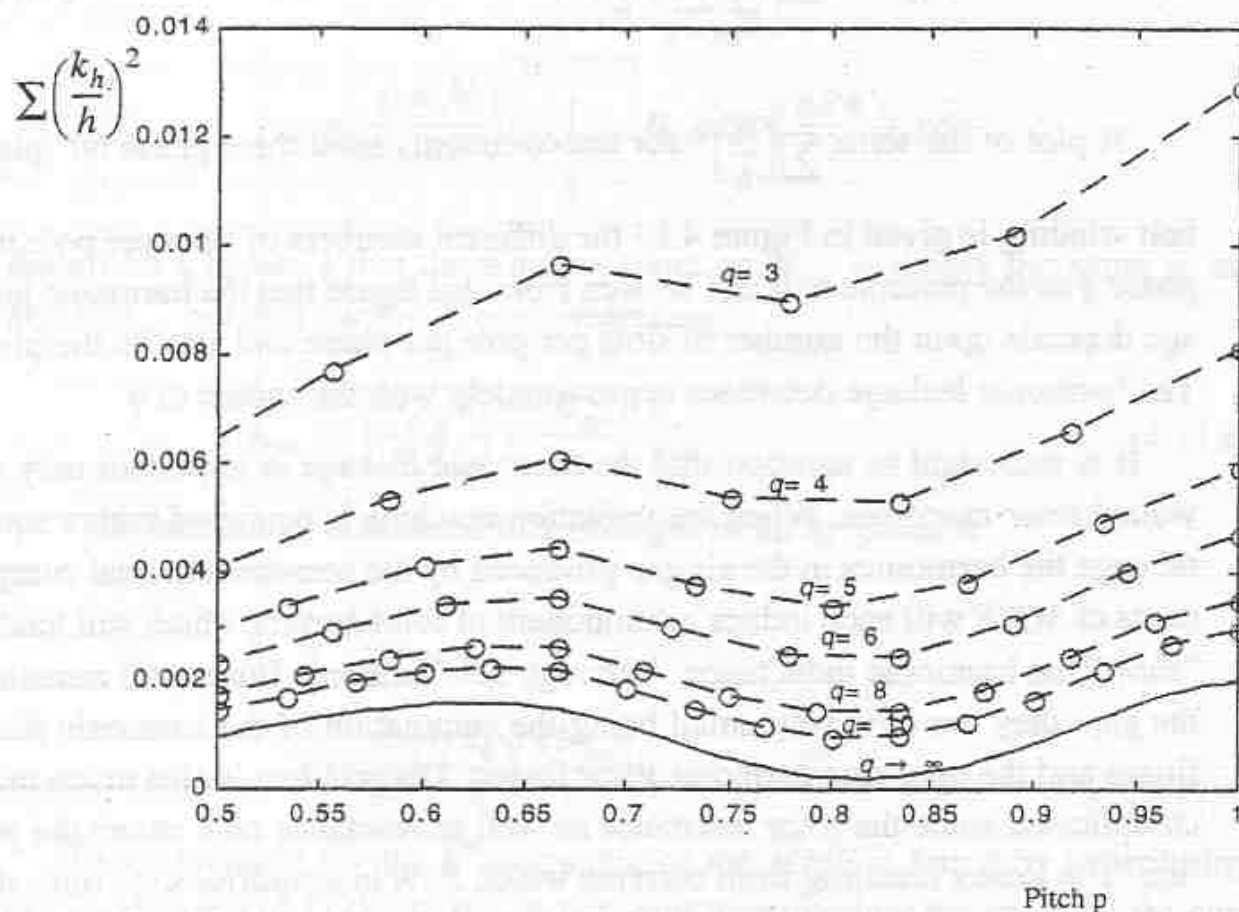


Figure 4.17 Belt leakage coefficient for integral slot windings and 60° phase belts. Note: for  $q = 2$  and  $p = 0.667, 0.833$  and  $1.0$ ,  $\sum(k_h/h)^2 = 0.199, 0.205$  and  $0.265$ .

## 4.10 Zigzag Leakage Inductance

Consider a symmetrical induction machine having  $n_s$  conductors per stator slot and  $n_r$  conductors per rotor slot. Assume that the rotor is arranged in such a position that the center line of one rotor tooth lines up with the center line of a stator tooth. Figure 4.18(a) indicates such a position. In general, the stator and rotor ampere turns tend to cancel much the same as a transformer. The difference between stator and rotor ampere turns sets up the air gap magnetic field which is rotating around the gap. If this difference component is discarded (the zig zag leakage for this component can be shown to be zero), then at this point the remaining stator and rotor ampere turns are equal and opposite. Hence the

*MMF* per unit length of the air gap induced by this component of stator current is the same as that induced by the rotor current. It follows that

$$\frac{n_s I_s}{\tau_s} = \frac{n_r I_r}{\tau_r} \quad (4.119)$$

Consider now line integral which encircles one stator and rotor slot which follows the center line of the rotor teeth as it crosses the air gap. The path taken corresponds to path *abca* in Figure 4.18(a). From Ampere's Law

$$\mathcal{F}_{ab} + \mathcal{F}_{cd} = n_s I_s - 2n_r I_r \quad (4.120)$$

From Eq. (4.119) this reduces to

$$\mathcal{F}_{ab} + \mathcal{F}_{cd} = n_s I_s \left(1 - \frac{(2\tau_r)}{\tau_s}\right) \quad (4.121)$$

Since the *MMF* is assumed to be sinusoidally varying, at least two of the stator teeth are clearly at (or near) zero *MMF*. If we assume that the tooth corresponding to point *a* is a zero potential point then so also is point *b* if Eq. (4.119) is assumed. Hence, we can write that

$$\mathcal{F}_{ab} = 0 \quad (4.122)$$

$$\mathcal{F}_{cd} = n_s I_s \left(\frac{\tau_s - 2\tau_r}{\tau_s}\right) \quad (4.123)$$

Note however that  $2\tau_r - \tau_s$  is the distance between the center lines of the stator and rotor teeth adjacent to the two teeth that are in alignment. If we define

$$2\tau_r - \tau_s = x \quad (4.124)$$

then

$$\mathcal{F}_{cd} = n_s I_s \frac{x}{\tau_s} \quad (4.125)$$

This is actually a general result which states that the magnetic potential difference between any two opposing teeth is equal to the *MMF* per stator slot times the ratio of the distance between the two tooth center lines to one stator slot pitch.

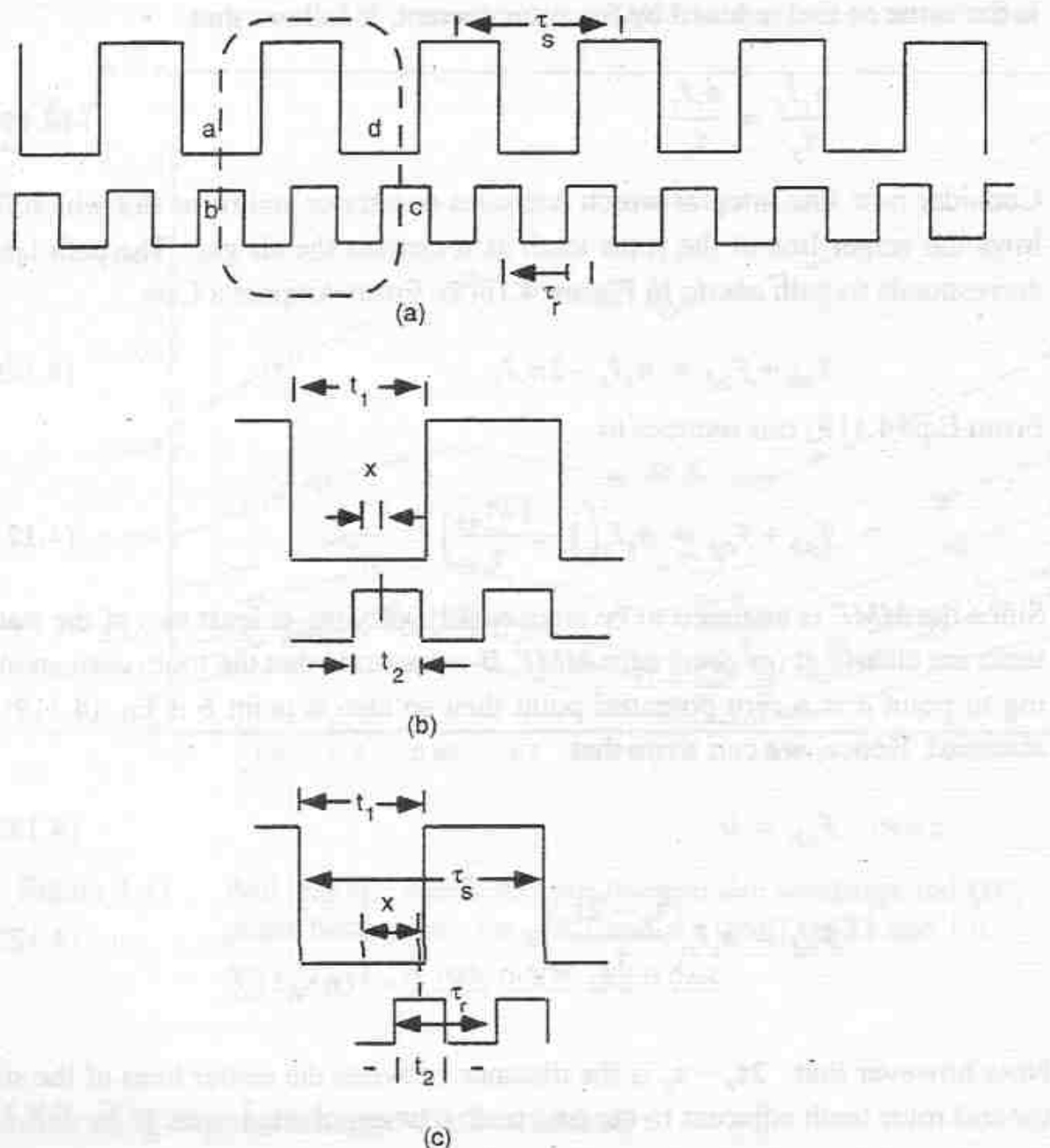


Figure 4.18 Illustrating calculation of zigzag leakage inductance

In general, as the rotor tooth moves through one stator slot pitch there are three regions to be considered (1) where the rotor tooth is entirely opposite the stator tooth and (2) partly opposite the stator slot, Figure 4.18(c), and (3) where the rotor tooth is entirely opposite the stator slot.

In the first region, that is where  $0 < x < (t_1 - t_2)/2$ , the MMF between the two teeth are, according to Eq. (4.125)

$$\mathcal{F}(x) = n_s I_s \frac{x}{\tau_s} \quad (4.126)$$

and the permeance is

$$\mathcal{P}(x) = \mu_o \frac{l_e t_2}{g_e} \quad (4.127)$$

Hence, the flux corresponding to zigzag leakage is

$$\Phi(x) = \mathcal{F}(x) \mathcal{P}(x) \quad (4.128)$$

or

$$\Phi(x) = \mu_o n_s I_s \frac{l_e t_2 x}{g_e \tau_s} \quad (4.129)$$

In the second region,  $(t_1 - t_2)/2 < x < (t_1 + t_2)/2$ . The MMF between the two teeth remain defined by Eq. (4.125). The permeance is

$$\mathcal{P}(x) = \frac{\mu_o l_e}{g_e} \left( \frac{t_1 + t_2}{2} - x \right) \quad (4.130)$$

so that

$$\Phi(x) = \mu_o n_s I_s \frac{l_e x}{g_e \tau_s} \left( \frac{t_1 + t_2}{2} - x \right) \quad (4.131)$$

In the third region,  $(t_1 + t_2)/2 < x < \tau_s/2$ . The MMF is again given by Eq. (4.125). The permeance in region three is assumed to be so small that it can be assumed as zero. The flux which flows between stator and rotor teeth due to zigzag leakage is therefore

$$\Phi(x) = \mathcal{F}(x) \mathcal{P}(x) = 0$$

A plot of the rotor tooth MMF with respect to the stator tooth MMF, the corresponding permeance per tooth and the resulting flux is given in Figure 4.19. It is clear that this type of behavior can be represented exactly only with an extremely complicated equivalent circuit. We are not particularly interested in the instantaneous behavior of this leakage mechanism but only in its gross effect. Hence, it is permissible to replace the actual situation by an equivalent one which produces the same average energy storage. In effect we define an equivalent inductance for zigzag leakage as

$$L_{(ll)/s} = \frac{W_{ave}}{\frac{1}{2}I_s^2} \quad (4.132)$$

where  $W_{ave}$  is the average energy stored in the stator-rotor tooth region during the motion from  $x = 0$  to  $x = \tau_s / 2$ . That is

$$\begin{aligned} W_{ave} &= \frac{2}{\tau_s} \int_0^{(t_1 - t_2)/2} (n_s I_s)^2 \left(\frac{x}{\tau_s}\right)^2 \mu_o \frac{l_e t_2}{g_e} dx \\ &\quad + \frac{2}{\tau_s} \int_{(t_1 - t_2)/2}^{(t_1 + t_2)/2} (n_s I_s)^2 \left(\frac{x}{\tau_s}\right)^2 \left(\mu_o \frac{l_e}{g_e}\right) \left(\frac{t_1 + t_2}{2} - x\right) dx \end{aligned} \quad (4.133)$$

Equation (4.133) works out to

$$W_{ave} = \frac{\mu_o l_e (n_s I_s)^2 t_1 t_2 (t_1^2 + t_2^2)}{12 g_e \tau_s^3} \quad (4.134)$$

so that the zigzag leakage inductance per slot is

$$L_{(zz)/s} = \frac{\mu_o l_e n_s^2 t_1 t_2 (t_1^2 + t_2^2)}{6 g_e \tau_s^3} \quad (4.135)$$

The corresponding specific permeance is clearly

$$p_{zz} = \frac{\mu_o t_1 t_2 (t_1^2 + t_2^2)}{6 g_e \tau_s^3} \quad (4.136)$$

Note that this result is independent of the value of current in the slots surrounding the stator and rotor teeth in question. Hence, the result is valid for any stator tooth and slot. The resulting zigzag inductance per phase is found in a manner analogous to Eqs. (4.38) to (4.41). For a three phase machine the result is

$$L_{lzz} = \frac{12 N_s^2}{S_1} l_e p_{zz} \quad (4.137)$$

At this point Eq. (4.137) is valid only for one layer windings. When the machine is wound with two layers, two types of slots exist, one type in which

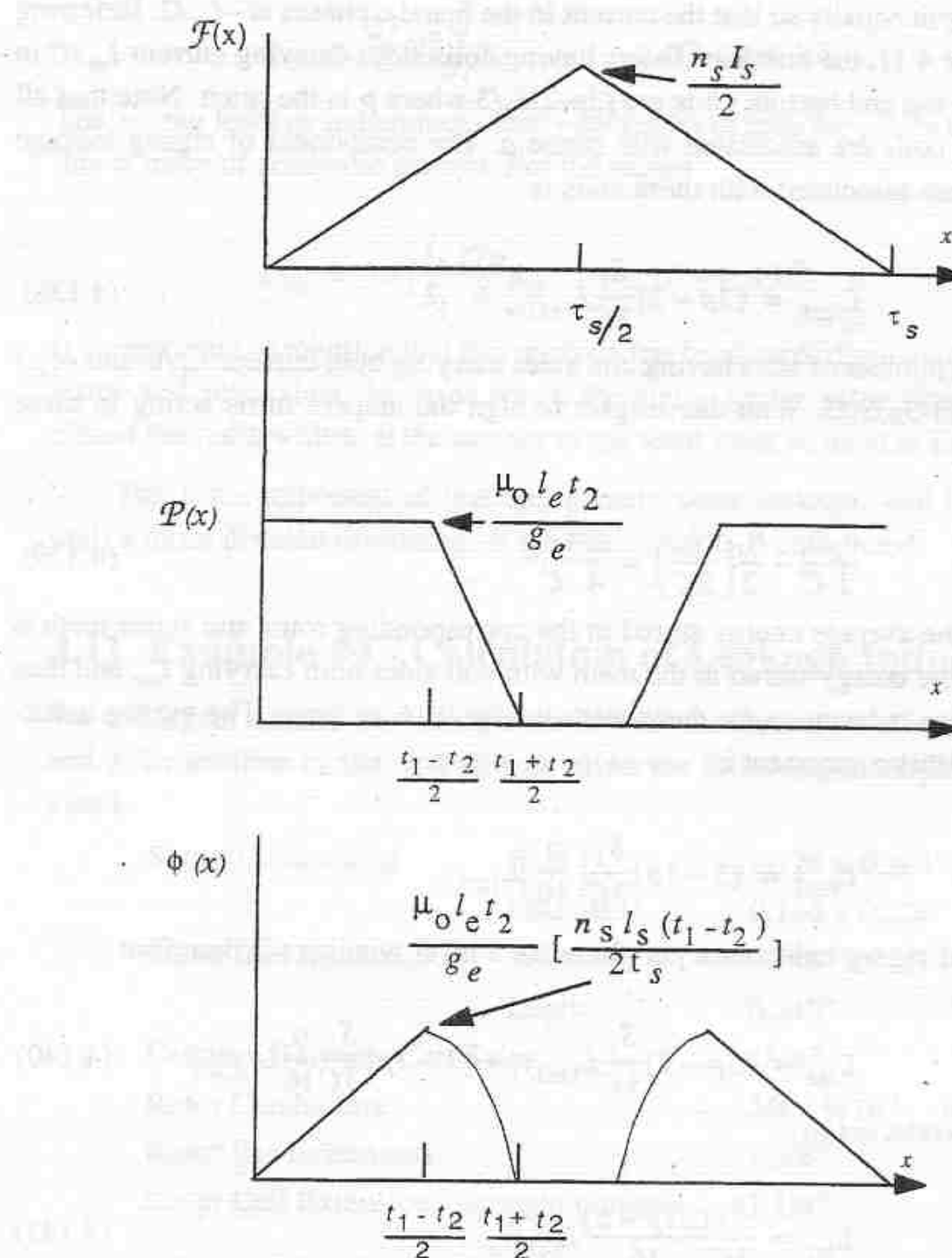


Figure 4.19 Zigzag permeance variation

the two coil sides are members of the same phase, and a second type in which the coil sides in the slot are members of different phases. Since the zigzag inductance is assumed to not vary with time let us choose for purposes of analysis the instant of time in which the current in phase  $a$  is a maximum  $I_m$ . If the machine is connected without a neutral return then the current in the other two

phases split equally so that the current in the *b* and *c* phases is  $-I_m/2$ . Referring in Figure 4.11, the number of slots having coil sides carrying current  $I_m/C$  in both the top and bottom coils are  $(3p-2)S_1/3$  where *p* is the pitch. Note that all of these coils are associated with phase *a*. The component of zigzag leakage inductance associated with these coils is

$$L_{lzz1} = (3p-2) \frac{S_1}{3C} L_{(zz)/s} \quad (4.138)$$

The number of slots having coil sides carrying both current  $I_m/C$  and  $-I_m/2C$  are  $(3-3p)S_1/3$ . With due respect to sign the ampere turns acting in these slots are

$$\frac{n_s I_m}{2C} - \frac{n_s}{2} \left( \frac{-I_m}{2C} \right) = \frac{3n_s I_m}{4C} \quad (4.139)$$

so that the average energy stored in the corresponding rotor and stator teeth is  $9/16$  of the energy stored in the teeth with coil sides both carrying  $I_m$ , and thus the zigzag inductance for these teeth is also  $9/16$  as large. The zigzag inductance of this component is

$$L_{lzz2} = (3-3p) \frac{S_1}{3C} \left( \frac{9}{16} \right) L_{(zz)/s}$$

The total zigzag inductance per phase for 2 layer windings is therefore

$$L_{lzz} = (3p-2) \frac{S_1}{3C} L_{(zz)/s} + (3-3p) \frac{S_1}{3C} \frac{9}{16} L_{(zz)/s} \quad (4.140)$$

which works out to

$$L_{lzz} = \frac{S_1}{3C} \frac{(21p-5)}{16} L_{(zz)/s} \quad (4.141)$$

$$= \frac{3N_s^2}{S_1} l_e \frac{(21p-5)}{4} p_{zz} \quad 2/3 < p < 1 \quad (4.142)$$

Note that the mutual coupling effect considered in Section 4.7 has been included as part of this analysis. Equation (4.141) is valid only for pitches greater or equal to  $2/3$ . When  $1/3 < p \leq 2/3$  the zigzag leakage inductance remains fixed at the value

$$L_{lzz} = \frac{27}{4} N_s^2 \frac{l_e}{S_1} p_{zz} \quad 1/3 < p < 2/3 \quad (4.143)$$

The zigzag leakage inductance clearly decreases to zero for  $p$  less than 1/3 but this is more of academic interest. For the record

$$L_{lzz} = 3N_s^2 \frac{l_e}{S_1} \frac{27p}{4} p_{zz} \quad 0 < p < 1/3 \quad (4.144)$$

It is important to mention that this analysis has been carried out assuming open stator and rotor slots. In cases where the stator and/or rotor slots are semi-closed the tooth widths at the surface of the teeth must be used in Eq. (4.135).

The last component of leakage, namely skew leakage, will be deferred until a more detailed discussion of the rotor circuits is completed.

## 4.11 Example #4 - Calculation of Leakage Inductances

We will again take as our example the 250 HP machine treated in Examples 2 and 3. In addition to the data already given the following information is provided.

Stator Conductors:	Bare	0.129 x 0.204"
	Insulated	0.146 x 0.220"
Stator Slot Insulation:	Width	0.145"
	Depth	0.240"
Distance Between Coil Sides		1/16"
Rotor Conductors:	3/8 x 9/16" bar	
Rotor Bar Extension:	1 5/8"	
Stator Coil Extension: (straight portion)	1 1/4"	

Using the above data the arrangement of conductors in a typical stator and rotor slot can be surmised. Details of stator and rotor slots after winding are shown in Figure 4.20. Note that the stator slot has three types of insulation: 1) insulation between conductors, 2) insulation between coil sides and 3) insulation to ground. The stator is usually heavily insulated since the potential to ground is generally high (2400 V in this case). The rotor is much less insulated since there is effectively only one turn per slot so that the potential to ground is

small. For smaller machines the insulation material used to isolate the rotor bars from the rotor laminations may be simply an oxide build up intentionally given to either the rotor bars or slots during a heat treatment process. In general, the total rotor cross section is selected to be in the range of 60-80% of the stator copper cross section for a squirrel cage machine and 85-90% for a wound rotor machine. The limiting factor is heating of the bars which limits the current density during starting to values typically on the order of  $60,000 \text{ A/in}^2$ . The corresponding values for the stator are in the range of  $35-50,000 \text{ A/in}^2$ , increasing with machine size. Figure 4.20 also shows details of the stator and rotor end winding regions.

### Stator Slot Leakage Inductance

From Figure 4.20 note that the clearance from the insulated conductors to the sides of the slot is

$$(0.376 - 0.220)/2 = 0.078''$$

We will assume that the same tolerance is allowed at the bottom of the slot. The distance  $d_6$  as defined by Figure 4.8 is equal to this distance plus one insulation thickness for the insulated stator conductor

$$d_6 = 0.078 + (0.146 - 0.129)/2 = 0.086''$$

The distance  $d_5$  measured from the start of the conductor of the bottom most conductor to the end of the conductor in the topmost conductor is

$$\begin{aligned} d_5 &= 5(0.146) + 0.129 \\ &= 0.859'' \end{aligned}$$

The distance  $d_4$  between coil sides is equal to the thickness of the coil side insulator plus twice the insulation thickness for one conductor

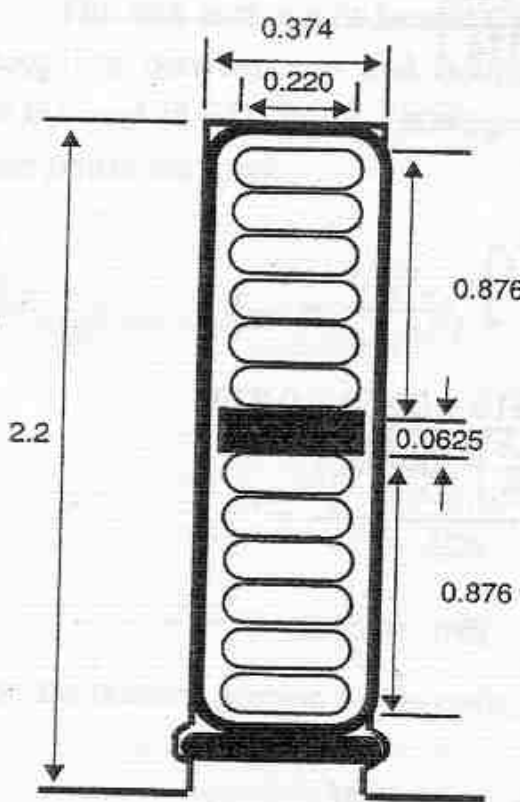
$$\begin{aligned} d_4 &= 0.0625 + (0.146 - 0.129) \\ &= 0.079'' \end{aligned}$$

The heights  $d_0$  and  $d_1$  are clearly zero for the case of an open slot. The height of the slot above the top coil side conductors is

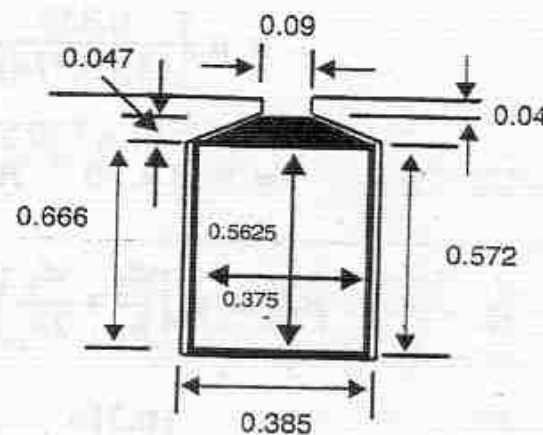
$$d_2 = d_s - d_6 - 2d_5 - d_4$$

$$= 2.2 - 0.0865 - 2(0.859) - 0.0625 - (0.146 - 0.129)$$

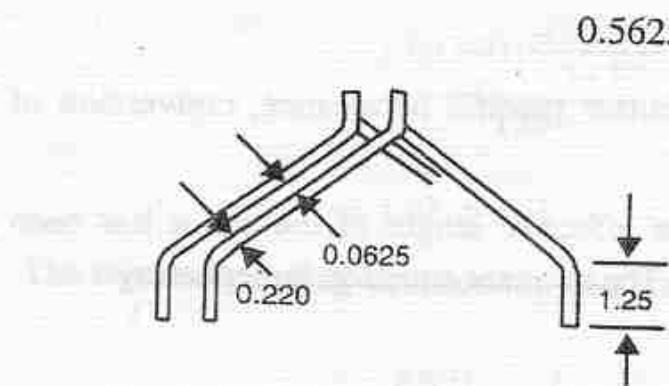
$$= 0.316''$$



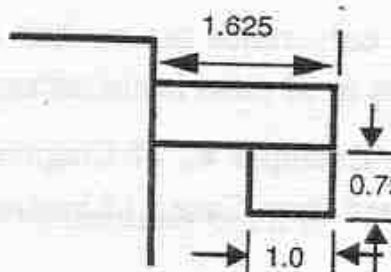
(a) Detail of Stator Slot



(b) Detail of Rotor Slot



(c) Detail of Stator End Winding



(d) Detail of Rotor End Winding

Figure 4.20 Detailed slot and end winding configurations for 250 hp machine

The specific permeances  $p_T, p_B, p_{TB}$  are

$$\begin{aligned} p_T &= \mu_o \left[ \frac{d_3}{3b_s} + \frac{d_2}{b_s} \right] \\ &= \mu_o \left[ \frac{0.859}{(3)(0.374)} + \frac{0.3862}{0.374} \right] \\ &= 2.027 \times 10^{-6} \text{ H/m} \end{aligned}$$

$$\begin{aligned} p_B &= \mu_o \left[ \frac{d_3}{3b_s} + \frac{d_2 + d_3 + d_4}{b_s} \right] \\ &= \mu_o \left[ \frac{0.859}{(3)(0.374)} + \frac{0.316 + 0.859 + 0.079}{0.374} \right] \\ &= 5.18 \times 10^{-6} \text{ H/m} \end{aligned}$$

$$\begin{aligned} p_{TB} &= \mu_o \left[ \frac{d_2}{b_s} + \frac{d_3}{2b_s} \right] \\ &= \mu_o \left[ \frac{0.316}{0.374} + \frac{0.859}{2(0.374)} \right] \\ &= 2.508 \times 10^{-6} \text{ H/m} \end{aligned}$$

Since only ratios are needed to calculate specific permeance, conversion of lengths to SI units is not necessary.

In Example #2 of Chapter 3, the effective length of the stator has been obtained from Case 3 of Section 3.3. The relevant equation is, repeating

$$l_{es} = l_{is} + 2g + n l_o \left( \frac{\frac{5}{2l_o}}{5 + \frac{2l_o}{g}} \right)$$

from which

$$l_e = 8.5 + 2(0.04) + \frac{5(4)(0.375)}{5 + 2 \frac{(0.375)}{0.04}}$$

$$= 8.5 + 0.08 + 0.316 = 8.896''$$

The slot leakage inductance per phase for the top, bottom and the mutual coupling between top and bottom coils can be obtained from Eqs. (4.59), (4.60) and (4.61). For the leakage inductance of the top portion of the coils of one phase we have

$$L_{IT} = \frac{3N_s^2 l_e}{S_1} p_T$$

$$= \frac{(3)(240)^2 \left(\frac{8.896}{39.37}\right)}{120} 2.013 \times 10^{-6}$$

$$= 0.6596 \text{ mH}$$

For the bottom portion of the coils,

$$L_{IB} = \frac{3N_s^2 l_e}{S_1} p_B$$

$$= \frac{(3)(240)^2 \left(\frac{8.896}{39.37}\right)}{120} 5.15 \times 10^{-6}$$

$$= 1.68 \text{ mH}$$

The mutual coupling between top and bottom coils for unity pitch is

$$L_{ITB} = \frac{6N_s^2 l_e}{S_1} p_{TB}$$

$$= \frac{6(240)^2 \left(\frac{8.896}{39.37}\right)}{120} 2.492 \times 10^{-6}$$

$$= 1.62 \text{ mH}$$

From Example #3 we have determined that the pitch of the stator coils is 0.8. From Eq. (4.86) the slot factor for mutual coupling is

$$k_{sl} = 3p - 1$$

$$= (3)(0.8) - 1$$

$$= 1.4$$

The total slot leakage inductance per phase is, from Eq. (4.85), therefore

$$\begin{aligned} L_{lsl} &= L_{lT} + L_{lB} + L_{lTB} \\ &= 0.655 + 1.68 + (1.4)(0.811) \\ &= 3.47 \text{ mH} \end{aligned}$$

### Stator End Winding Leakage Inductance

From the additional information that has been given, the length  $l_{e2}$  Figure 4.13 is 1.25". The spacing between adjacent coil sides in the slot is specified as 0.0625". If this minimum spacing is maintained in the end winding region then the quantity  $t_e$  in Figure 4.13 is also 0.0625". Hence from Eq. (4.96),

$$l_{e1} = \frac{p\tau_{p(ave)}(b_c + t_e)}{2\sqrt{\tau_{s(ave)}^2 - (b_c + t_e)^2}}$$

The pole pitch at the mid point of the stator slot is

$$\begin{aligned} \tau_{p(ave)} &= \frac{\pi}{P}(D_{is} + d_s) \\ &= \frac{\pi}{8}(24.08 + 2.2) = 10.32'' \end{aligned}$$

The slot pitch at the mid point of the stator slot is

$$\tau_{s(ave)} = \frac{P\tau_{p(ave)}}{S_1}$$

$$= \frac{8(10.32)}{120} = 0.688''$$

The length of the end winding extension over the diagonal region is therefore

$$l_{e1} = \frac{(0.8)(10.32)(0.22 + 0.0625)}{2\sqrt{0.688^2 - (0.22 + 0.0625)^2}}$$

$$= 1.859''$$

The stator end winding leakage inductance per phase is found from Eq. (4.99) as

$$L_{lew} = 4\mu_o \frac{N_s^2}{P} k_{p1}^2 k_{d1}^2 (1.25) \left( l_{e2} + \frac{l_{e1}}{2} \right)$$

$$= \frac{(4)(\mu_o)}{8} (240)^2 (0.91)^2 (2.4) \left( \frac{1.25 + 1.568/2}{39.37} \right)$$

$$= 2.1 \text{ mH}$$

### Belt Leakage Inductance

The belt leakage inductance is essentially zero since the machine is equipped with a squirrel cage rotor.

### Zigzag Leakage Inductance

The specific permeance corresponding to zigzag leakage flux is given by Eq. (4.136) as

$$p_{zz} = \frac{\mu_o t_{os} t_{or} (t_{os}^2 + t_{or}^2)}{6g_e \tau_s^3}$$

or

$$p_{zz} = \frac{(4\pi \times 10^{-7})(0.256)(0.392)(0.256^2 + 0.392^2)}{(6)(0.0664)(0.630)^3}$$

$$= 0.2775 \times 10^{-6} \text{ H/n}$$

Since the pitch is between unity and two-thirds, Eq. (4.142) applies and

$$\begin{aligned} L_{zz} &= \frac{12N_s^2}{S_1} l_{es} \frac{(21p - 5)}{16} p_{zz} \\ &= \frac{(12)(240^2)}{120} \left( \frac{8.896}{39.37} \right) \frac{[21(0.8) - 5]}{16} (27.17 \times 10^{-6}) \\ &= 0.368 \text{ mH} \end{aligned}$$

### Rotor Slot Leakage Inductance per Bar

As yet the rotor leakage inductances cannot be computed for an entire phase. The leakage associated with one rotor bar, however, can be computed from Eq. (4.20) as

$$\begin{aligned} p_{sl} &= \mu_o \left[ \frac{d_{3r}}{3b_{sr}} + \frac{d_{2r}}{(b_{sr} - b_{or})} \log_e \left( \frac{b_{sr}}{b_{or}} \right) + \frac{d_{or}}{b_{or}} \right] \\ &= (\mu_o) \left[ \frac{0.5625}{(3)(0.385)} + \frac{0.047}{(0.385 - 0.09)} \log_e \left( \frac{0.385}{0.09} \right) + \frac{0.040}{0.09} \right] \\ p_{sl} &= 1.461 \times 10^{-6} \text{ H/m} \end{aligned}$$

From Eq. (4.35) the slot leakage per bar is

$$\begin{aligned} L_b &= n_s^2 l_{er}' p_{sl} \\ &= (1)^2 \left( \frac{8.91}{39.37} \right) 1.559 \times 10^{-6} \\ &= 0.3527 \text{ } \mu\text{H/bar} \end{aligned}$$

Note that the quantity  $l_{er}'$  takes into account the slight additional length of the bar due to skew, i.e.

$$l_{er}' = \frac{l_{er}}{\cos\left(\frac{2\pi}{S_1}\right)} = \frac{8.896}{\cos\left(\frac{2\pi}{120}\right)} = 8.91$$

### Rotor End Winding Inductance per Bar

The end winding leakage inductance per segment of the end ring is obtained from Eq. (4.109) as

$$L_e = \mu_o \left( \frac{4}{9} \right) [l_{be} + k\tau_{pr(ave)}]$$

From Figure 4.20 the length of the bar extension from the surface of the core to the start of the end ring is

$$l_{be} = 1.625 - 1.0 = 0.625''$$

The rotor pole pitch measured at the middle of the end ring is

$$\begin{aligned} \tau_{pr(ave)} &= \frac{\pi}{P} [D_{or} - 2d_{sr} - d_{re}] = \frac{\pi}{8} [24 - 2(0.5625) - 0.75] \\ &= \frac{\pi}{8} (22.12) = 8.688'' \end{aligned}$$

$$\begin{aligned} L_e &= (4\pi 10^{-7}) \left( \frac{4}{9} \right) \frac{[0.625 + (0.09)(8.688)]}{39.37} \\ &= 0.01996 \text{ } \mu\text{H/end ring segment} \end{aligned}$$

The next task in the calculation of machine parameters is to relate the inductance bar per that we have just calculated to an expression which involves the rotor leakage inductance per phase. This is the topic of the next section.

## 4.12 Effective Resistance and Inductance per Phase of Squirrel Cage Rotor

We have shown that if the stator is excited with a sinusoidal set of stator voltages then the resulting currents produce an *MMF*, the fundamental component of which rotates about the air gap at synchronous speed. This fundamental

component of *MMF* produces a useful, torque producing air gap flux while the higher harmonics have been shown to result essentially in leakage components. The useful air gap flux density produced by this *MMF* has already been calculated in Chapter 3. It is now time to turn our attention to the induced rotor currents which clearly also exist since the rotating stator air gap flux density certainly also links rotor as well as stator circuits, thereby inducing currents in the rotor.

When the rotor is wound with discrete coils as is the case for wound rotor induction machines, the calculation of parameters proceeds in the same fashion as we have developed for stator windings. We will not discuss this case further. However, when the machine is equipped with a squirrel cage the problem is clearly quite different since the rotor currents do not flow in discrete coils but in shorted bars. Since the current in each of the  $S_2$  rotor slots is independent, a completely general solution would require  $S_2$  differential equations, one for each rotor mesh. Such a complicated solution is clearly impractical and it is useful to search for simpler equations which yet maintain the same effective behavior as the  $S_2$  rotor currents. Clearly, it is not necessary to retain all  $S_2$  currents since by symmetry, the currents induced under each stator pole will basically be the same. In addition, as the stator flux passes over the bars, the currents in adjacent bars will be nearly the same, differing only in the time phase related to the pitch of one rotor tooth.

For simplicity, let us assume that in response to the sinusoidally rotating *B* field, the current in each bar will vary sinusoidally. In general, the amplitude and speed of rotation of the stator *B* field is not fixed but can change in response to external influences such as line switching, load torque changes, etc. However, if the time constants of these changes are sufficiently small then the system can be assumed in the quasi-steady-state in which all of the rotor bars are of the same amplitude and that adjacent bars displaced in phase by the pitch of one rotor slot expressed in electrical radians, i.e. by the angle

$$\frac{\pi P}{S_2} = \frac{\pi \tau_r}{\tau_p} \quad (4.145)$$

where  $S_2$  is the number of rotor slots and  $P$  is the number of stator (and rotor) poles. It is apparent that the squirrel cage effectively represents a polyphase winding with as many phases  $m_2$  as there are slots per pole pair, i.e.  $m_2 = S_2/P$ . In general, this number need not be an integer and indeed integer

values are avoided in order to prevent the cogging torques previously described. We will assume here an integer value only for convenience in depicting the bar current distribution, illustrated in Figure 4.21 for the simple

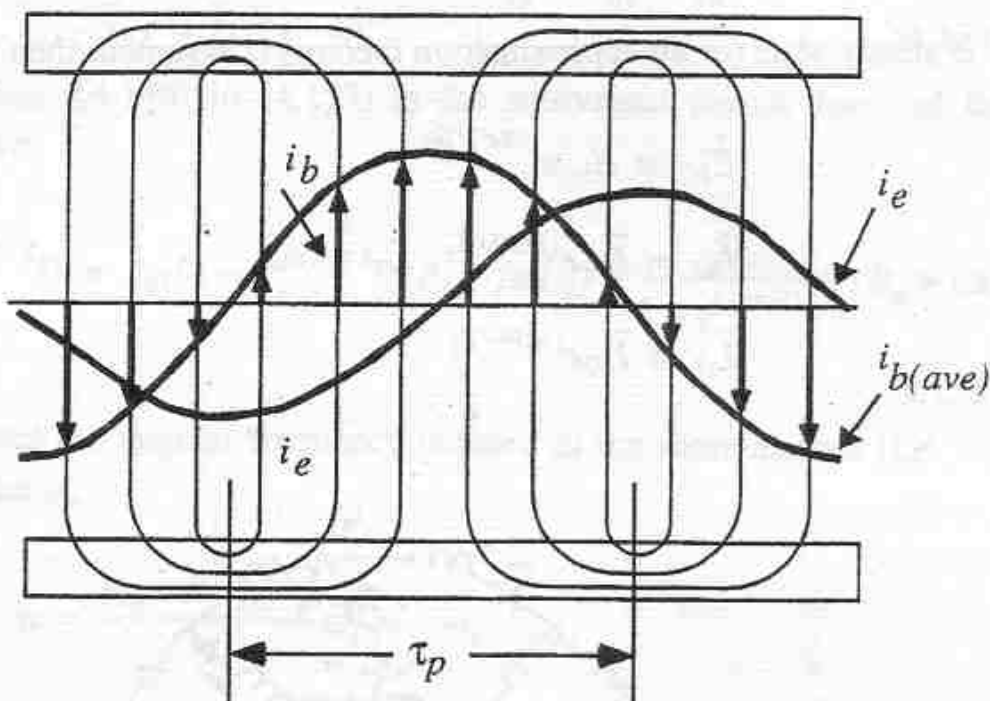


Figure 4.21 Current paths in squirrel cage rotor having six bars per pole case of six bars per pole.

The end ring segments between bars are clearly made up of the difference in current between two adjacent bars and therefore are also sinusoidal and phase displaced by an angle  $\alpha$  in the steady-state. If we let

$R_b, L_b$  = resistance and inductance of each bar

$R_e, L_e$  = resistance and inductance of each end ring segment

$i_b$  = current in the bars

$i_e$  = current in end ring segments

$e_b$  = induced voltage per bar

then the squirrel cage of the machine can be represented by the planar circuit of Figure 4.22. Applying Kirchoff's voltage law to mesh one we have

$$e_{b1} - e_{b2} = R_b(i_{b1} - i_{b2}) + L_b \frac{d}{dt}(i_{b1} - i_{b2}) + 2R_e i_{e1} + 2L_e \frac{di_{e1}}{dt}$$

(4.146)

and

$$i_{b1} + i_{e0} = i_{e1} \quad (4.147)$$

If steady-state (or an approximation thereof) is assumed, then in phasor form

$$\tilde{E}_{b2} = \tilde{E}_{b1} e^{(j\pi P)/S_2} \quad (4.148)$$

$$\tilde{I}_{b2} = \tilde{I}_{b1} e^{(j\pi P)/S_2} \quad (4.149)$$

$$\tilde{I}_{e1} = \tilde{I}_{e0} e^{(j\pi P)/S_2} \quad (4.150)$$

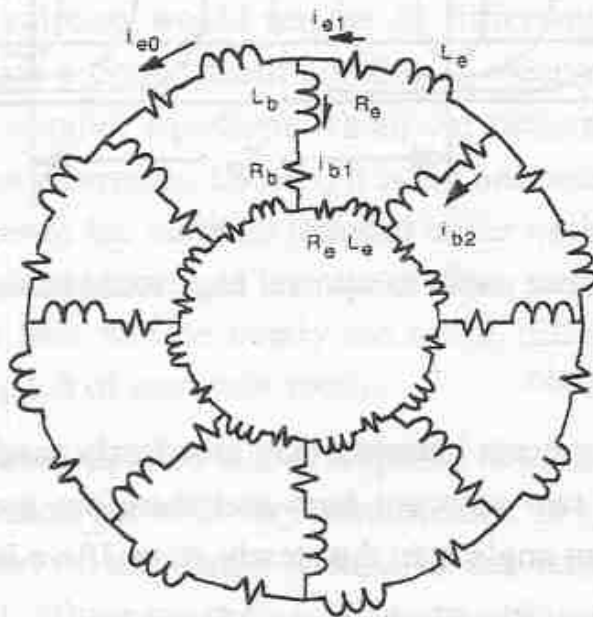


Figure 4.22 Meshes formed by squirrel cage with eight bars per pole pair

From Eqs. (4.147) and (4.150),

$$\tilde{I}_{b1} = \tilde{I}_{e1} - \tilde{I}_{e0} = \tilde{I}_{e1}(1 - e^{(-j\pi P)/S_2}) \quad (4.151)$$

or

$$\tilde{I}_{e1} = \frac{\tilde{I}_{b1}}{1 - e^{(-j\pi P)/S_2}} \quad (4.152)$$

and from Eqs. and (4.148)

$$\tilde{E}_{b1} - \tilde{E}_{b2} = \tilde{E}_{b1}(1 - e^{(j\pi P)/S_2}) \quad (4.153)$$

$$\tilde{I}_{b1} - \tilde{I}_{b2} = \tilde{I}_{b1}(1 - e^{(j\pi P)/S_2}) \quad (4.154)$$

Substituting Eqs. (4.148) to (4.153) in the equivalent phasor form of Eq. (4.146) we have

$$\tilde{E}_{b1}(1 - e^{(j\pi P)/S_2}) = \tilde{I}_{b1}(1 - e^{(j\pi P)/S_2})(R_b + j\omega L_b) + \frac{2\tilde{I}_{b1}}{1 - e^{(-j\pi P)/S_2}}(R_e + j\omega L_e) \quad (4.155)$$

where  $\omega$  denotes the angular frequency induced in the rotor meshes (i.e. slip frequency). That is,

$$\omega = \frac{\omega_e - P\omega_{rm}/2}{\omega_e} \omega_e = S\omega_e$$

where  $\omega_e$  and  $\omega_{rm}$  are the stator angular frequency of the stator current and rotor mechanical speed in radians per second respectively and  $S$  is the per unit slip

$$S = \frac{\omega_e - \omega_r}{\omega_e}$$

Equation (4.155) can be written as

$$\tilde{E}_{b1} = \tilde{I}_{b1}(R_b + j\omega L_b) + \frac{2\tilde{I}_{b1}}{(1 - e^{(j\pi P)/S_2})(1 - e^{(-j\pi P)/S_2})}(R_e + j\omega L_e) \quad (4.156)$$

But

$$(1 - e^{(j\pi P)/S_2})(1 - e^{(-j\pi P)/S_2}) = e^{\frac{j\pi P}{2S_2}} \left( e^{\frac{-j\pi P}{2S_2}} - e^{\frac{j\pi P}{2S_2}} \right) \left( e^{\frac{-j\pi P}{2S_2}} \right) \left( e^{\frac{j\pi P}{2S_2}} - e^{\frac{-j\pi P}{2S_2}} \right) \quad (4.157)$$

so that this term becomes

$$\begin{aligned}
 &= -\left( e^{\frac{j\pi P}{2S_2}} - e^{-\frac{j\pi P}{2S_2}} \right)^2 \\
 &= -\left[ 2j \sin\left(\frac{\pi P}{2S_2}\right) \right]^2 \\
 &= 4 \sin^2\left(\frac{\pi P}{2S_2}\right)
 \end{aligned} \tag{4.158}$$

Hence, the mesh equation reduces to

$$\tilde{E}_{b1} = \tilde{I}_{b1}(R_b + j\omega L_b) + \tilde{I}_{b1} \left[ \frac{R_e + j\omega L_e}{2 \sin^2(\pi P)/(2S_2)} \right] \tag{4.159}$$

Equation (4.159) shows that the effect of the end rings is to increase the bar resistance and inductance by an amount inversely proportional to the square of the sine of one-half the electrical angle between bars. It is useful to define quantities  $R_{be}$  and  $L_{be}$  as equivalent values of bar resistance and inductance. Then

$$R_{be} = R_b + \frac{R_e}{2 \sin^2[(\pi P)/(2S_2)]} \tag{4.160}$$

$$L_{be} = L_b + \frac{L_e}{2 \sin^2[(\pi P)/(2S_2)]} \tag{4.161}$$

This result implies that the mesh circuit of Figure 4.22 can be replaced by the equivalent circuit of Figure 4.23 where the resistance and inductance of the end rings have been absorbed into the rotor bar parameters. Because of the symmetry, the currents in this 8 mesh circuit can be solved by solving four meshes, one of which is shown.

## 4.13 Fundamental Component of Rotor Air Gap MMF

Consider now the fundamental component of the square wave air gap MMF set up by each one of these rotor meshes. If the machine has  $P$  poles rather than the simple two pole example of Figure 4.23, meshes such as those

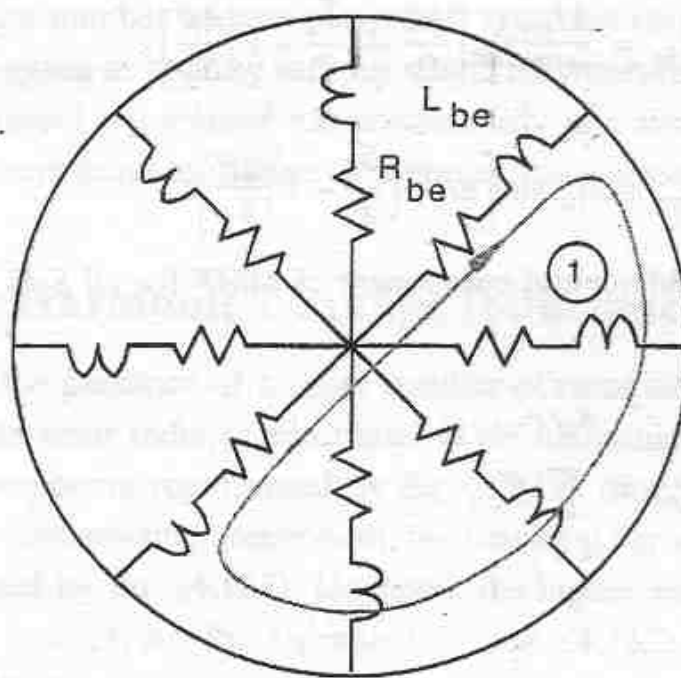


Figure 4.23 Equivalent eight mesh circuit obtained by absorbing effect of end ring into rotor bar parameters

shown exist for each pair of rotor poles. Hence, for mesh one and its companions in other pairs of rotor poles, we have

$$\mathcal{F}_{b1} = \frac{4i_{b1}}{\pi 2} \sin \frac{P\theta}{2} \quad 0 \leq \theta < 2\pi \quad (4.162)$$

where  $\theta$  is now the angular measure along the rotor surface,  $0 \leq \theta < 2\pi$ , and

$$i_{b1} = I_{rm} \sin \omega t \quad (4.163)$$

For the next successive mesh

$$\mathcal{F}_{b2} = \frac{4i_{b2}}{\pi 2} \sin \left( \frac{P\theta}{2} - \frac{\pi P}{S_2} \right) \quad (4.164)$$

where

$$i_{b2} = I_{rm} \sin \left( \omega t - \frac{\pi P}{S_2} \right) \quad (4.165)$$

This process continues until the  $S_2/P^{th}$  mesh for which

$$\mathcal{F}_{bn} = \frac{4}{\pi} \frac{i_{bn}}{2} \sin \left[ \frac{P\theta}{2} - \left( \frac{S_2}{P} - 1 \right) \frac{\pi P}{S_2} \right] \quad (4.166)$$

$$i_{bn} = I_{rm} \sin \left[ \omega t - \left( \frac{S_2}{P} - 1 \right) \frac{\pi P}{S_2} \right] \quad (4.167)$$

The total fundamental component of *MMF* for all  $S_2/2$  such rotor circuits is

$$\mathcal{F}_{pr} = \sum_{k=1}^{S_2/P} \mathcal{F}_{bn} \quad (4.168)$$

or,

$$\mathcal{F}_{pr} = \frac{2}{\pi} I_{rm} \sum_{k=1}^{S_2/P} \sin \left[ \omega t - (k-1) \frac{\pi P}{S_2} \right] \sin \left[ \frac{P\theta}{2} - (k-1) \frac{\pi P}{S_2} \right] \quad (4.169)$$

which can be written

$$\mathcal{F}_{pr} = \frac{1}{\pi} I_{rm} \left\{ - \sum_{k=1}^{S_2/P} \cos \left[ \omega t + \frac{P\theta}{2} - 2(k-1) \frac{\pi P}{S_2} \right] + \sum_{k=1}^{S_2/P} \cos \left( \omega t - \frac{P\theta}{2} \right) \right\} \quad (4.170)$$

The first summation adds to zero since it corresponds to a set of sine waves equally distributed in phase over  $P$  poles. Equation therefore reduces to

$$\mathcal{F}_{pr} = \left( \frac{1}{\pi} \right) \left( \frac{S_2}{P} \right) I_{rm} \cos \left( \omega t - \frac{P\theta}{2} \right) \quad (4.171)$$

Note that while  $S_2$  is necessarily an integer, the number of bars per pole  $S_2/P$  (rotor phases) need not be an integer. We have, for convenience, assumed an integer number of bars per pole in order to simplify the analysis. However, it can be shown that the result is the same for a fractional number of bars per pole.

A non-integer number of bars per pole is typically chosen to prevent sub-synchronous cogging or locking torques which may prevent the machine from reaching rated speed but instead run continuously at a small fraction of rated speed. We will have more to discuss concerning this phenomenon in Chapter 6.

## 4.14 Rotor Harmonic Leakage Inductance

Because of the presence of a finite number of rotor slots, the stator *MMF* impressed on the rotor induces additional *MMF* harmonics in addition to the fundamental component represented by Eq. (4.171). Since we are again concerned with the fundamental component, the temporal variation of the currents is again expressed by Eq. (4.167). However, the higher spatial harmonics are represented by multiplying the argument of Eqs. (4.162), (4.164), etc. by *h* where the *h*'s are the harmonic numbers which are to be determined. (As in Section 4.13, the values of *h* would equal 5, 7, 11, etc. if the number of bars per pole were an integer).

The *MMF* representing the additional spatial harmonic components produced by the rotor fundamental time harmonic component in the rotor bars can be written as

$$\mathcal{F}_{prh} = \frac{2}{\pi} \sum_h \sum_{k=1}^{S_2/P} I_{rh} \sin \left[ \omega t - (k-1) \frac{\pi P}{S_2} \right] \sin \left[ \frac{hP\theta}{2} - h(k-1) \frac{\pi P}{S_2} \right] \quad (4.172)$$

Using trigonometric identities, Eq. (4.172) can be expanded to form,

$$\mathcal{F}_{prh} = \frac{1}{\pi} \sum_h I_{rh} \left\{ \sum_{k=1}^{S_2/P} \cos \left[ \omega t - \frac{hP\theta}{2} + (k-1)\gamma_1 \right] - \cos \left[ \omega t + \frac{hP\theta}{2} - (k-1)\gamma_1 \right] \right\} \quad (4.173)$$

where

$$\gamma_1 = (h-1) \frac{\pi P}{S_2}$$

$$\gamma_2 = (h+1) \frac{\pi P}{S_2}$$

Expanding again the two cosine terms yields,

$$\begin{aligned} \mathcal{F}_{prh} = & \frac{1}{\pi} \sum_h I_{rh} \left\{ \cos\left(\omega t - \frac{hP\theta}{2}\right) \sum_{k=1}^{S_2/P} \cos(k-1)\gamma_1 - \sin\left(\omega t - \frac{hP\theta}{2}\right) \sum_{k=1}^{S_2/P} \sin(k-1)\gamma_1 \right. \\ & \left. - \cos\left(\omega t + \frac{hP\theta}{2}\right) \sum_{k=1}^{S_2/P} \cos(k-1)\gamma_2 - \sin\left(\omega t + \frac{hP\theta}{2}\right) \sum_{k=1}^{S_2/P} \sin(k-1)\gamma_2 \right\} \end{aligned} \quad (4.174)$$

However, from Ref. [8], entries 420.2 and 420.1,

$$\begin{aligned} \sum_{k=1}^q \cos(k-1)\alpha &= \frac{\sin\left(\frac{q\alpha}{2}\right)}{\sin\left(\frac{\alpha}{2}\right)} \cos\left[\frac{(q-1)\alpha}{2}\right] \\ \sum_{k=1}^q \sin(k-1)\alpha &= \frac{\sin\left(\frac{q\alpha}{2}\right)}{\sin\left(\frac{\alpha}{2}\right)} \sin\left[\frac{(q-1)\alpha}{2}\right] \quad \alpha \neq 0 \end{aligned}$$

Using these results in (4.174), after changing variables, yields

$$\begin{aligned} \mathcal{F}_{prh} = & \frac{1}{\pi} \sum_{h=1}^{\infty} I_{rh} \left\{ \frac{\sin\left[(h-1)\frac{\pi}{2}\right]}{\sin(\gamma_1/2)} \left[ \cos\left(\omega t - \frac{hP\theta}{2}\right) \cos\left(\frac{S_2-P}{2P}\gamma_1\right) - \sin\left(\omega t - \frac{hP\theta}{2}\right) \sin\left(\frac{S_2-P}{2P}\gamma_1\right) \right] \right. \\ & \left. - \frac{\sin\left[(h+1)\frac{\pi}{2}\right]}{\sin(\gamma_2/2)} \left[ \cos\left(\omega t + \frac{hP\theta}{2}\right) \cos\left(\frac{S_2-P}{2P}\gamma_2\right) + \sin\left(\omega t + \frac{hP\theta}{2}\right) \sin\left(\frac{S_2-P}{2P}\gamma_2\right) \right] \right\} \end{aligned} \quad (4.175)$$

where  $\gamma_1, \gamma_2 \neq 2n\pi$  and where  $n$  is an integer or zero.

Examining this result more carefully, it should first be noted that the coefficients of the expression within the curly brackets are zero for all odd  $h$ , and therefore the sum is identically zero for all the harmonics generated by the spatial distribution of the bars which are all odd due to the regular spacing of the rotor slots. On the other hand if  $\gamma_1 = 2n\pi$ , then  $\gamma_2 = 2n\pi + 2\pi(P/S_2)$  and Eq. (4.173) becomes

$$\mathcal{F}_{prh} = \frac{1}{\pi} \sum_h I_{rh} \left\{ \sum_{k=1}^{S_2/P} \cos \left[ \omega t - \frac{hP\theta}{2} + (k-1)2n\pi \right] - \cos \left[ \omega t + \frac{hP\theta}{2} - (k-1)(2n\pi + 2\pi \frac{P}{S_2}) \right] \right\} \quad (4.176)$$

which reduces to

$$\mathcal{F}_{prh} = \frac{S_2}{\pi P} \sum_h \left\{ I_{rh} \cos \left( \omega t - \frac{hP\theta}{2} \right) \right\}; \quad h = \frac{2nS_2}{P} + 1 \quad (4.177)$$

and  $n = 1, 2, \dots, \infty$ . Similarly, if  $\gamma_2 = 2n\pi$ , Eq. (4.175) reduces to

$$\mathcal{F}_{prh} = \frac{S_2}{\pi P} \sum_h \left\{ I_{rh} \cos \left( \omega t + \frac{hP\theta}{2} \right) \right\}; \quad h = \frac{2nS_2}{P} - 1 \quad (4.178)$$

For each value of  $n$ , the index  $h$  takes on two values given by both Eq. (4.177) and (4.178). For example if  $S_2 = 36$  and  $P = 2$  then when  $n = 1$ ,  $h = 35$  and 37. Note also that the fundamental component ( $h = 1$ ) is obtained from Eq. (4.177) by setting  $n = 0$ .

In order to determine the inductance associated with this component of MMF it is convenient to use the energy method employed in our study of zig-zag leakage reactance. We can state that the energy stored in the field arising from the MMF is defined by

$$W_f = \frac{1}{2} L_h I_{rm}^2 = \int_V \frac{1}{2} \mu_o \sum_h H_h^2 dV$$

The field energy associated with *one phase* of the  $S_2$  bar rotor winding is thus,

$$W_{f/phase} = \frac{1}{2(S_2/P)} \sum_h \frac{H_h^2}{(S_2/P)} dV$$

However,  $H_h g_e = \mathcal{F}_{prh}$  where  $\mathcal{F}_{prh}$  is the  $h^{th}$  component of the MMF defined by Eqs. (4.177) and (4.178). Twice the field energy per phase can be expanded to form

$$\frac{L_h I_{rm}^2}{(S_2/P)} = \int_V \frac{\mu_o}{(S_2/P)} \sum_h \left( \frac{S_2 I_{rh}}{\pi P g_e} \right)^2 \left[ \cos \left( \omega t \pm \frac{hP\theta}{2} \right) \right]^2 dV \quad (4.179)$$

where either the plus or minus sign applies in the cosine term depending upon whether Eq. (4.177) or (4.178) has been satisfied. Upon integrating out the radial and longitudinal components,

$$\frac{L_h I_{rm}^2}{(S_2/P)} = \int_0^{2\pi} \frac{\mu_o S_2}{P} \left( \sum_h \left( \frac{I_{rh}}{\pi g_e} \right)^2 \left[ \cos \left( \omega t \pm \frac{hP\theta}{2} \right) \right]^2 \right) \left( \frac{D_{or}}{2} \right) l_e g_e' d\theta \quad (4.180)$$

Upon carrying out the final integration it must be remembered either the plus or minus sign is attached to each value of  $h$  applies (not both). however since the cosine term is squared, the net result of each term in the summation ultimately does not depend upon the polarity of the phase angle  $hP\theta/2$ . Equation (4.180) reduces to

$$\frac{L_h I_{rm}^2}{(S_2/P)} = \frac{\mu_o S_2}{2P} \left[ \sum_h \left( \frac{I_{rh}}{\pi g_e} \right)^2 \right] D_{or} l_e g_e' \pi$$

which can be written as

$$\frac{L_h}{(S_2/P)} = \mu_o \left( \frac{D_{or} l_e}{\pi g_e} \right) \left( \frac{S_2}{2P} \right) \left[ \sum_h \left( \frac{I_{rh}}{I_{rm}} \right)^2 \right] \quad (4.181)$$

Recalling that

$$\pi D_{or} = P \tau_p$$

equation (4.181) can be expressed as

$$\frac{L_h}{(S_2/P)} = \mu_o \left( \frac{\tau_p l_e}{2\pi^2 g_e} \right) S_2 \left[ \sum_h \left( \frac{I_{rh}}{I_{rm}} \right)^2 \right] \quad (4.182)$$

Finally, if it can assumed that the harmonic currents in the bars decreases inversely with the harmonic order  $h$  then the belt harmonic leakage inductance per rotor phase can be written as

$$L_{h/\text{phase}} = \mu_0 \left( \frac{1}{2\pi^2} \right) \left( \frac{\tau_p l_e}{g_e} \right) S_2 \left[ \sum_h \left( \frac{1}{h^2} \right) \right] \quad (4.183)$$

where  $h$  is given by Eq. (4.177) and (4.178). The function  $\sum_h (1/h^2)$  is plotted in Figure 4.24 as a function of the number of slots per pole pair (rotor phases)  $2S_2/P$ . Note that the function is continuous, i.e. the number of slots per pole pair can take on non-integer values.

It is generally desirable to express Eq. (4.183) in terms of the inductance *per bar* rather than *per phase* since the calculation can be done at the same time as when calculating the slot and end leakage Eq. (4.161). Upon dividing Eq. (4.183) by the number of pole pairs, results in

$$L_{b(\text{har})} = \mu_0 \left( \frac{\tau_p l_e}{g_e} \right) \left( \frac{1}{\pi^2} \right) \left( \frac{S_2}{P} \right) \sum_{\substack{n=-\infty \\ (n \neq 0)}}^{\infty} \left( \frac{1}{\frac{2nS_2}{P} + 1} \right)^2 \quad (4.184)$$

where we have replaced the parameter  $h$  with the number  $n$  by the use of Eq. (4.177). The index  $n$  takes on all positive and negative values but excludes  $n = 0$ . Note that we have here used the effective gap  $g_e$  rather than  $g_e'$  since this leakage effect contributes flux components in the air gap but not appreciably in the iron paths of the machine.

Clearly the accuracy of this equation hinges upon how the actual harmonic current varies with frequency. While the higher harmonics in the stator MMF waveform also induce rotor currents which, in turn, result in leakage fluxes, this effect is usually relegated to those of a loss component. The subject of losses is treated in the next chapter.

## 4.15 Calculation of Mutual Inductances

The MMF given by Eq. (4.171) establishes a second flux density in the air gap which in turn links both itself as well as the stator windings. Let us now calculate the mutual coupling resulting from rotor currents linking one phase of the stator winding. Following the approach of Section 3.11 the air gap flux density corresponding to the rotor MMF, Eq. (4.171) is

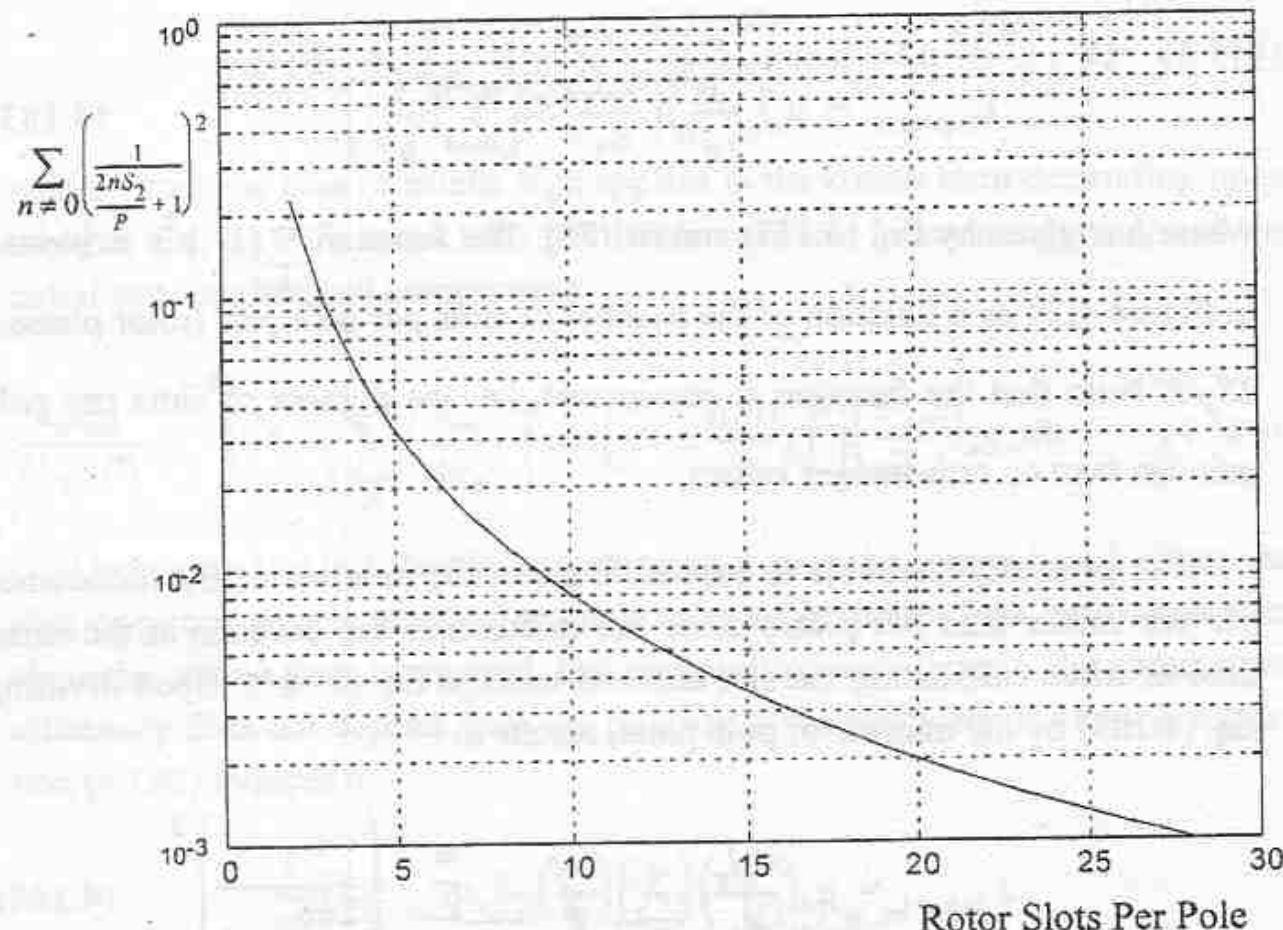


Figure 4.24 Harmonic leakage flux coefficient vs. number of rotor slots per pole  $S_2/P$

$$B_{gr} = \mu_o \frac{\mathcal{F}_{pr}}{g_e} \quad (4.185)$$

The flux linking one pole of one of the three stator phases due to all rotor phases is

$$\lambda_{psr} = \int_0^{(2\pi)/P} N_a(\theta) B_{gr}(\theta) l_e \left( \frac{D_{is}}{2} \right) d\theta \quad (4.186)$$

where, from previous work

$$N_a(\theta) = \frac{\mathcal{F}_a(\theta)}{(I_{mr}/C)} = \frac{4}{\pi} \left( \frac{k_1 N_t}{P} \right) \cos \left( \frac{P\theta}{2} \right) \quad (4.187)$$

Equation (4.186) becomes, upon substitution for  $B_{gr}(\theta)$  and  $\mathcal{F}_a(\theta)$ ,

$$\lambda_{psr} = \frac{4}{\pi} \left( \frac{k_1 N_t}{P} \right) \left( \frac{S_2}{\pi P} \right) \int_0^{(2\pi)/P} I_{rm} \cos \left( \frac{P\theta}{2} \right) \cos \left( \omega_e t - \frac{P\theta}{2} \right) \frac{\mu_o l_e}{g_e'} I_e \left( \frac{D_{is}}{2} \right) d\theta \quad (4.188)$$

Note that since the rotor is itself assumed to be rotating, the angular frequency of the rotating flux wave relative to the stator windings is assumed to be line frequency ( $\omega_e$ ).

The above expression reduces to

$$\lambda_{psr} = \frac{2}{\pi} \left( \frac{k_1 N_t}{P} \right) \left( \frac{S_2}{\pi P} \right) \left( \frac{\pi}{P} \right) \left( \frac{\mu_o l_e D_{is}}{g_e'} \right) I_{rm} \cos \omega_e t \quad (4.189)$$

or, if we introduce the pole pitch

$$\tau_p = \frac{\pi D_{is}}{P}$$

Eq. (4.189) becomes

$$\lambda_{psr} = \frac{2}{\pi^2} \left( \frac{k_1 N_t S_2}{P^2} \right) \left( \frac{\mu_o \tau_p l_e}{g_e'} \right) I_{rm} \cos \omega_e t \quad (4.190)$$

The total flux linking all series connected poles of one phase is

$$\begin{aligned} \lambda_{sr} &= \frac{P}{C} \lambda_{psr} \\ &= \frac{2}{\pi^2} \left( \frac{k_1 N_t S_2}{PC} \right) \left( \frac{\mu_o \tau_p l_e}{g_e'} \right) I_{rm} \cos \omega_e t \end{aligned} \quad (4.191)$$

The mutual inductance between stator and rotor phases is, by definition

$$L_{sr} = \frac{\lambda_{sr}}{I_{rm} \cos \omega_e t} \quad (4.192)$$

or

$$L_{sr} = \frac{2}{\pi^2} \left( \frac{k_1 N_s S_2}{P} \right) \left( \frac{\mu_o \tau_p l_e}{g_e'} \right) \quad (4.193)$$

where

$$N_s = \frac{N_t}{C}$$

This result can be compared with Eq. (3.78).

In a similar manner the flux set up by the stator *MMF* which couples one of the rotor phases can be calculated. In this case the total flux linking one of the  $S_2/P$  rotor meshes or phases is

$$\lambda_{rs} = \int_0^{(2\pi)/P} N_{b1}(\theta) B_{g1}(\theta) l_e \left( \frac{D_{or}}{2} \right) d\theta \quad (4.194)$$

where

$$N_{b1}(\theta) = \frac{2}{\pi} \sin \frac{P\theta}{2} \quad (4.195)$$

From Eq. (2.70), the *MMF* associated with the fundamental component of stator current of a three phase, *P* pole machine is

$$\mathcal{F}_{g1} = \frac{6k_1 N_s}{\pi P} I_{ms} \sin \left( \frac{P\theta}{2} - \omega_e t \right)$$

and, again

$$B_{g1} = \mu_o \frac{\mathcal{F}_{g1}}{g_e'}$$

Setting  $t = 0$  for convenience and upon solving we find that the flux linking one rotor circuit due to the stator *MMF* is

$$\lambda_{rs} = \int_0^{(2\pi)/P} \frac{2}{\pi} \sin \left( \frac{P\theta}{2} \right) \left[ \frac{\mu_o}{g_e'} \frac{6k_1 N_s}{\pi P} I_{ms} \sin \left( \frac{P\theta}{2} \right) \right] l_e \left( \frac{D_{or}}{2} \right) d\theta$$

so that

$$\lambda_{rs} = \frac{6}{\pi^2} \left( \frac{k_1 N_s}{P} \right) I_{ms} \left( \frac{\mu_o l_e \tau_p}{g_e'} \right) \quad (4.196)$$

Hence,

$$L_{rs} = \frac{6}{\pi^2} \left( \frac{k_1 N_s}{P} \right) \frac{\mu_o l_e \tau_p}{g_e} \quad (4.197)$$

The quantity  $L_{rs}$  expresses the mutual coupling resulting from the flux produced by all stator phases with one of the  $2S_2 / P$  rotor meshes assuming balanced excitation of all three stator phases. Note that this expression is quite different than  $L_{sr}$ , which expresses the coupling resulting from flux produced by all the rotor meshes linking one of the three stator phases.

The final inductance to be calculated is the magnetizing inductance of one of the rotor meshes (phases). This quantity is found by integrating the air gap flux density produced by all of the rotor meshes over one of the rotor meshes. In this manner the "mutual coupling" between any two rotor meshes is automatically taken into account.

For example, if we choose as reference the rotor phase defined by rotor bar  $b1$ , we have from Eq. (4.162)

$$\mathcal{F}_{b1} = \frac{4}{\pi} \left( \frac{i_{b1}}{2} \right) \sin \frac{P\theta}{2}$$

so that the *winding function* distribution is, from Eq. (1.101),

$$N_{b1}(\theta) = \frac{2}{\pi} \sin \frac{P\theta}{2} \quad (4.198)$$

The flux linkages which couple this  $P$  pole mesh arising from the air gap flux density  $B_{gr1}$  is

$$\lambda_{mr} = \int_0^{2\pi} N_{b1}(\theta) B_{gr1}(\theta) l_e \frac{D_{is}}{2} d\theta \quad (4.199)$$

which reduces to

$$\begin{aligned}
 \lambda_{mr} &= \int_0^{2\pi} \left[ \frac{2}{\pi} \sin\left(\frac{P\theta}{2}\right) \right] \left( \frac{\mu_o}{g_e'} \right) \left( \frac{S_2}{\pi P} \right) I_{rm} \cos\left(\omega_e t - \frac{P\theta}{2}\right) l_e \frac{D_{is}}{2} d\theta \\
 &= \frac{1}{\pi} \left( \frac{\mu_o l_e D_{is}}{g_e'} \right) \left( \frac{S_2}{P} \right) I_{rm} \sin(\omega_e t) \\
 &= \left( \frac{1}{\pi^2} \right) \left( \frac{S_2}{P} \right) \left( \frac{\mu_o \tau_p l_e}{g_e'} \right) I_{rm} \sin(\omega_e t)
 \end{aligned} \tag{4.200}$$

The magnetizing inductance associated with this flux linkage is

$$L_{mr} = \frac{\lambda_{mr}}{I_{rm} \sin(\omega_e t)}$$

or

$$L_{mr} = \left( \frac{1}{\pi^2} \right) \left( \frac{S_2}{P} \right) \frac{\mu_o \tau_p l_e}{g_e'} \tag{4.201}$$

We have now reached the point where we have established the total flux linking one of the stator phases as well as the flux which links one of the rotor meshes (phases). Since sinusoidal currents have been assumed in the rotor meshes, steady state operation with sine wave excitation is implied. The form of these equations on a "per phase" basis is, in phasor form

$$\tilde{\lambda}_s = L_{ls} \tilde{I}_s + L_{ms} \tilde{I}_s + L_{sr} \tilde{I}_r \tag{4.202}$$

$$\tilde{\lambda}_r = L_{lr} \tilde{I}_r + L_{mr} \tilde{I}_r + L_{rs} \tilde{I}_s \tag{4.203}$$

where  $L_{ls}$  is the leakage inductance associated with one of the stator phases and is the sum of the slot, end winding, belt and zigzag leakage inductances (Eqs. (4.85), (4.99), (4.118) and (4.141)) and  $L_{lr}$  is the leakage inductance of one rotor mesh (Eqs. (4.35), (4.109) and (4.161)). That is

$$L_{lr} = 2(L_{be} + L_{b(har)}) \tag{4.204}$$

The inductances  $L_{ms}$ ,  $L_{sr}$  and  $L_{mr}$  are fixed by Eqs. (3.78), (4.193) and (4.201) respectively. Substituting explicitly for  $L_{ms}$ ,  $L_{sr}$  and  $L_{mr}$  we have

$$\tilde{\lambda}_s = L_{ls}\tilde{I}_s + \frac{12(k_1N_s)^2}{\pi^2}P_m\tilde{I}_s + \frac{2k_1N_sS_2}{\pi^2}P_m\tilde{I}_r \quad (4.205)$$

$$\tilde{\lambda}_r = L_{lr}\tilde{I}_r + \frac{6k_1N_s}{\pi^2}P_m\tilde{I}_s + \frac{1}{\pi^2}\frac{S_2}{P}P_m\tilde{I}_r \quad (4.206)$$

where the permeance  $P_m$  is

$$P_m = \mu_o \frac{\tau_p l_e}{g_e}$$

Equation (4.205) can be manipulated so that the magnetizing inductance coefficient is the same for both components of current if we write it as

$$\tilde{\lambda}_s = L_{ls}\tilde{I}_s + \frac{12k_1^2N_s^2}{\pi^2}P_m \cdot \left( \tilde{I}_s + \frac{S_2}{6k_1N_s}\tilde{I}_r \right) \quad (4.207)$$

Recalling the turns ratio transformation of a transformer it is clear that the quantity  $S_2/(6k_1N_s)$  has the appearance of being a turns ratio transformation. However, the issue is more involved in this case since the number of phases of the stator and rotor are different. The term is more easily interpreted if it is written as

$$\frac{S_2}{6k_1N_s} = \frac{(S_2/P)(1/2)}{(3/P) k_1N_s} \quad (\text{Phases/pole})(\text{turns/phase}) \quad (4.208)$$

One can again define a modified value of rotor current, referred to stator turns as

$$\tilde{I}'_r = \frac{S_2}{6k_1N_s}\tilde{I}_r \quad (4.209)$$

Incorporating this modified value of current in the rotor flux linkage equation we have

$$\tilde{\lambda}_r = \frac{6k_1N_s}{S_2}(L_{be} + L_{b(har)})\tilde{I}'_r + \frac{6k_1N_s}{\pi^2}P_m\tilde{I}_s + \frac{6k_1N_s}{\pi^2P}P_m\tilde{I}'_r \quad (4.210)$$

The mutual inductance coefficient can now be made the same as in Eq. (4.207) if we multiply the entire equation by  $2k_1N_s$

$$2k_1N_s\tilde{\lambda}_r = \frac{12k_1^2N_s^2}{S_2}(L_{be} + L_{b(har)})\tilde{I}_r' + \frac{12k_1^2N_s^2}{\pi^2 P}\mathcal{P}_m(\tilde{I}_s + \tilde{I}_r') \quad (4.211)$$

If one now defines

$$\tilde{\lambda}'_r = \frac{k_1N_s}{(1/2)}\tilde{\lambda}_r \quad (4.212)$$

$$L_m = \frac{12k_1^2N_s^2}{\pi^2 P}\mathcal{P}_m \quad (4.213)$$

$$L_{lr'} = \frac{12k_1^2N_s^2}{S_2}(L_{be} + L_{b(har)}) \quad (4.214)$$

The stator and rotor flux linkage equations can now be expressed in the form

$$\tilde{\lambda}_s = L_{ls}\tilde{I}_s + L_m(\tilde{I}_s + \tilde{I}_r') \quad (4.215)$$

$$\tilde{\lambda}'_r = L_{lr'}\tilde{I}_r' + L_m(\tilde{I}_s + \tilde{I}_r') \quad (4.216)$$

The primed variables are interpreted as equivalent quantities referred to the stator turns by an effective turns ratio which includes not only the number of stator and rotor turns but also the number of stator and rotor phases.

In an analogous manner the voltage equation which describes the current in a given mesh, i.e. from Eq. (4.159)

$$\tilde{V}_{r1}(=0) = 2r_{be}\tilde{I}_r + j\omega\tilde{\lambda}_r \quad (4.217)$$

can be "transformed" to stator turns. The result is

$$\tilde{V}'_r(=0) = r'_r\tilde{I}'_r + j\omega\tilde{\lambda}'_r \quad (4.218)$$

where

$$\tilde{V}'_r = 2k_1N_s\tilde{V}_r \quad (4.219)$$

$$r'_r = \frac{12k_1^2N_s^2}{S_2}r_r \quad (4.220)$$

where  $r_r = 2r_{be}$  and  $\tilde{\lambda}'_r$  is defined above.

## 4.16 Example #5 - Calculation of Rotor Leakage Inductance per Phase

Using the results of the last section let us now attempt to establish the effect of the rotor leakage flux on a per phase rather than a per bar basis. Again the 250 HP machine will be used as the example. From Eq. (4.161) the effective leakage inductance per rotor mesh is

$$L_{lr} = 2(L_{be} + L_{b(har)}) \\ = 2L_b + \frac{L_e}{\sin^2 \frac{\pi P}{2S_2}} + 2L_{b(har)}$$

From Example #2 we have established that there are 97 rotor slots and eight poles. From Example #4 the slot leakage and the end winding leakages per bar are computed as

$$L_b = 0.3527 \mu\text{H}$$

$$L_e = 0.01996 \mu\text{H}$$

In addition the phase belt rotor inductance is, from Eq. (4.184),

$$L_{b(har)} = \mu_o \left( \frac{\tau_p l_e}{g_e} \right) \left( \frac{1}{\pi} \right) \left( \frac{S_2}{P} \right) \sum_{n=1}^{\infty} \left( \frac{1}{\frac{2nS_2}{P} + 1} \right)^2 \\ = \mu_o \left[ \left( \frac{9.456}{39.37} \right) \frac{8.896}{0.0677} \right] \left( \frac{1}{\pi^2} \right) \left( \frac{97}{8} \right) 0.006 \\ = 0.292 \mu\text{H}$$

The factor 0.006 is obtained from Figure 4.24. Hence the equivalent rotor phase inductance including the effect of the end ring current and harmonic leakage is

$$L_{lr} = 2 \left[ 0.3527 + \frac{0.01996}{2 \sin^2 \frac{8\pi}{2(97)}} + 0.292 \right] \times 10^{-6}$$

$$= 2.486 \text{ } \mu\text{H}$$

The rotor leakage per stator phase (referred to stator turns) is obtained from Eq. (4.214) as

$$L_{lr}' = \frac{12k_1^2 N_s^2}{S_2} L_{lr}$$

$$= \frac{(12)(0.91)^2 (240)^2}{(97)} (2.48) \times 10^{-6}$$

$$= 14.7 \text{ mH}$$

#### 4.17 Skew Leakage Inductance

Although the four types of leakage inductance previously discussed are unavoidable the skew leakage inductance occurs from an intentional twisting or "skewing" of either stator or rotor windings in the circumferential direction. Skewing serves to prevent undesirable pulsations of flux which are, in general, caused by the presence of space harmonics of *MMF*. These pulsations, if not sufficiently suppressed, may result not only in objectionable noise but also in appreciable negative torques produced by the locking effect between stator and rotor harmonic fluxes which rotate opposite to the direction of the main field. These negative torques, also called parasitic torques, if not minimized, would have the effect of producing pronounced dips in the torque-speed curves and interfere with the smooth acceleration of the rotor during the starting period. These dips could be so severe that they may even result in subsynchronous operation or "crawling."

The beneficial effects of skewing are, on the other hand, offset by an inevitable increase in the total leakage inductance of the motor, thereby reducing both the starting torque and the breakdown torque. The reasons for this increased leakage inductance may be understood by considering the coupling

that would occur between the stator and rotor without skewing, then introducing skewing and noting the effect on the rotating flux.

Without skewing, the equations which describe coupling between one of the stator phases, say the  $a$  phase and the corresponding rotor  $a$  phase are, from Eqs. (4.215) and (4.216)

$$\lambda_{as} = L_{ls} i_{as} + L_m (i_{as} + i_{ar}') \quad (4.221)$$

$$\lambda_{ar}' = L_{lr}' i_{ar}' + L_m (i_{as} + i_{ar}') \quad (4.222)$$

Note that we have already assumed that the rotor equation variables have been referred to the stator by the ratio of effective stator turns to rotor turns.

Let us now introduce a skewing of the stator or rotor windings (or both). Since the skew will affect only the mutual coupling between the stator and rotor the flux linkages with skew can be written

$$\lambda_{as} = L_{ls} i_{as} + L_m i_{as} + k_{s1} L_m i_{ar}' \quad (4.223)$$

$$\lambda_{ar}' = L_{lr}' i_{ar}' + k_{s1} L_m i_{as} + L_m i_{ar}' \quad (4.224)$$

Equations (4.221) and (4.222) can be written in the form

$$\lambda_{as} = L_{ls} i_{as} + L_m i_{as} + k_{s1}^2 L_m \frac{i_{ar}'}{k_{s1}} \quad (4.225)$$

$$k_{s1} \lambda_{ar}' = k_{s1}^2 L_{lr}' \frac{i_{ar}'}{k_{s1}} + k_{s1}^2 L_m \left( i_{as} + \frac{i_{ar}'}{k_{s1}} \right) \quad (4.226)$$

which in turn can be rearranged to the form

$$\lambda_{as} = L_{ls} i_{as} + (1 - k_{s1}^2) L_m i_{as} + k_{s1}^2 L_m \left( \frac{i_{ar}'}{k_{s1}} + i_{as} \right) \quad (4.227)$$

$$k_{s1} \lambda_{ar}' = k_{s1}^2 L_{lr}' \frac{i_{ar}'}{k_{s1}} + k_{s1}^2 L_m \left( i_{as} + \frac{i_{ar}'}{k_{s1}} \right) \quad (4.228)$$

If we define

$$\lambda_{ar}'' \triangleq k_{s1} \lambda_{as} \quad i_{ar}'' \triangleq \frac{i_{ar}'}{k_{s1}} \quad L_{lr}'' \triangleq k_{s1}^2 L_{lr}' \quad L_m'' \triangleq k_{s1}^2 L_m$$

then

$$\lambda_{as} = L_{ls} i_{as} + (1 - k_{s1}^2) L_m i_{as} + L_m'' (i_{ar}'' + i_{as}) \quad (4.229)$$

$$\lambda_{ar}'' = L_{lr}'' i_{ar}'' + L_m'' (i_{ar}'' + i_{as}) \quad (4.230)$$

The double primed quantities are referred rotor variables which include the effects of rotor skew. Note the presence of the extra term in the stator flux linkage equation proportional to  $(1 - k_{s1}^2)$ . The additional leakage caused by skewing is clearly

$$L_{lsk} = (1 - k_{s1}^2) L_m \quad (4.231)$$

$$= L_m \left\{ 1 - \left[ \frac{\sin(\alpha/2)}{\alpha/2} \right]^2 \right\} \quad (4.232)$$

If  $\alpha$  is sufficiently small then

$$\sin \alpha/2 = \frac{\alpha}{2} - \frac{1}{3!} \left( \frac{\alpha}{2} \right)^3$$

and

$$\left[ \frac{\sin \alpha/2}{\alpha/2} \right]^2 = \left[ 1 - \frac{\alpha^2}{24} \right]^2 \quad (4.233)$$

$$= 1 - \frac{\alpha^2}{12} + \frac{\alpha^4}{24^2}$$

$$= 1 - \frac{\alpha^2}{12}$$

so that approximately

$$L_{lsk} = \frac{\alpha^2}{12} L_m \quad (4.234)$$

In like manner the voltage equation for the rotor circuit can be written, for rotor phase  $a$ , as

$$k_{sl} v_{ar}' = k_{sl}^2 r_r' \left( \frac{i_{ar}'}{k_{sl}} \right) + \frac{d}{dt} \left( \frac{\lambda_{ar}'}{k_{sl}} \right) \quad (4.235)$$

which becomes

$$v_{ar}'' = 0 = r_r'' i_{ar}'' + \frac{d\lambda_{ar}''}{dt} \quad (4.236)$$

where

$$r_r'' = k_{sl}^2 r_r' \quad (4.237)$$

It is important to mention that the method we have used to incorporate skew leakage is not unique. In fact, it can be shown that if the effective number of turns in the mutual inductance is retained as  $k_{sl} N_s$  then a skew leakage term appears in the rotor equation by

$$L_{lsk} = L_m \frac{(1 - k_{sl}^2)}{k_{sl}} \quad (4.238)$$

If  $\sqrt{k_{sl}} N_s$  is used as the effective number of turns then equal values of skew inductance appear in both the stator and rotor equations. This approach is sometimes preferred (for example by Alger[6]). We will, however, lump the skew leakage term in the stator flux linkage equation.

#### 4.18 Example #6 - Calculation of Skew Leakage Effects

Again we will use the 250 HP machine of the previous examples. In Example #4 it was given that the rotor slots are skewed one stator slot pitch. Since there are 15 stator slots per pole the skew angle  $\alpha$  in degrees is 1/15 of 180° or

$$\alpha = \frac{180}{15} = 12^\circ$$

The inductance due to skew is found from Eq. (4.219)

$$L_{lsk} = L_m \left\{ 1 - \left[ \frac{\sin(\alpha/2)}{\alpha/2} \right]^2 \right\}$$

$$\begin{aligned}
 &= L_m \left\{ 1 - \left[ \frac{\sin(\pi/30)}{\pi/30} \right]^2 \right\} \\
 &= 0.224(1 - 0.9963) \\
 &= 0.818 \text{ mH}
 \end{aligned}$$

Because of skew it is important to remember that the magnetizing inductance and rotor leakage inductance must, in principle, be modified appropriately. When skew is considered

$$\begin{aligned}
 L_m'' &= k_{s1}^2 L_m \\
 &= (0.9963)(0.224) \\
 &= 0.223 \text{ mH}
 \end{aligned}$$

so that typically this modification can be neglected unless the skew is several slot pitches.

The total stator leakage inductance can be found as the sum of the slot, end winding, belt, zigzag and skew leakage inductances or

$$\begin{aligned}
 L_{ls} &= L_{lsl} + L_{lew} + L_{lb1} + L_{lzz} + L_{lsk} \\
 &= 3.47 + 2.10 + 0.0 + 0.368 + 0.818 \\
 &= 6.756 \text{ mH}
 \end{aligned}$$

For purposes of comparison it is useful to express the machine inductances in per unit form. The base impedance of a 250 hp, 2400 V, 60 Hz machine is

$$\begin{aligned}
 Z_b &= \frac{V_{llb}^2}{P_b} \\
 &= \frac{2400^2}{(746)(250)} = 30.88 \Omega
 \end{aligned}$$

Hence, the per unit values of stator leakage, rotor leakage and magnetizing reactance is

$$X_{ls(pu)} = \frac{\omega_e L_{ls}}{Z_b}$$

$$= \frac{(377)0.006756}{30.88} = 0.082$$

$$X_{lr(pu)}' = \frac{(377)(0.012)}{30.88} = 0.146$$

$$X_{m(pu)} = \frac{(377)(0.223)}{30.88} = 2.72$$

Note that the total per unit leakage reactance in per unit is  $0.082 + 0.159 = 0.241$ . For most practical designs this value is typically in the range 0.15 and 0.3 p.u. For well designed machines of this rating the magnetizing inductance is generally between 2.0 and 3.0 p.u.

## 4.19 References

- [6] P.L. Alger, "The Nature of Induction Machines", Gordon and Breach Publishers.
- [7] M. Liwschitz-Garik and C.C. Whipple, "Electric Machinery, Vol. 2 AC Machines", Van Nostrand Publishers 1946.
- [8] H.B. Dwight, "Tables of Integrals and Other Mathematical Data", 4th Ed. Macmillan, 1961.

The "Circuit 2" is reported independently by the following two papers: a) Design of a 1000-kVA three-phase transformer with no magnetic core, by H. G. Koenigsberger, Trans. AIEE, Vol. 52, p. 103, 1933; b) Design of a 1000-kVA three-phase transformer with no magnetic core, by H. G. Koenigsberger, Trans. AIEE, Vol. 52, p. 103, 1933.

The "Circuit 2" is reported independently by the following two papers: a) Design of a 1000-kVA three-phase transformer with no magnetic core, by H. G. Koenigsberger, Trans. AIEE, Vol. 52, p. 103, 1933; b) Design of a 1000-kVA three-phase transformer with no magnetic core, by H. G. Koenigsberger, Trans. AIEE, Vol. 52, p. 103, 1933.

and it is difficult to understand exactly what we have always meant by the 30% equivalent air gap length. The original literature does not provide any exact value of gap width, nor does it give any information concerning the air gap length. However, it is clear that the air gap length is much smaller than the air gap width, and probably less than 10% of the air gap width. This is supported by the following two papers: a) Design of a 1000-kVA three-phase transformer with no magnetic core, by H. G. Koenigsberger, Trans. AIEE, Vol. 52, p. 103, 1933; b) Design of a 1000-kVA three-phase transformer with no magnetic core, by H. G. Koenigsberger, Trans. AIEE, Vol. 52, p. 103, 1933.

The "Circuit 2" is reported independently by the following two papers: a) Design of a 1000-kVA three-phase transformer with no magnetic core, by H. G. Koenigsberger, Trans. AIEE, Vol. 52, p. 103, 1933; b) Design of a 1000-kVA three-phase transformer with no magnetic core, by H. G. Koenigsberger, Trans. AIEE, Vol. 52, p. 103, 1933.

The "Circuit 2" is reported independently by the following two papers: a) Design of a 1000-kVA three-phase transformer with no magnetic core, by H. G. Koenigsberger, Trans. AIEE, Vol. 52, p. 103, 1933; b) Design of a 1000-kVA three-phase transformer with no magnetic core, by H. G. Koenigsberger, Trans. AIEE, Vol. 52, p. 103, 1933.

The "Circuit 2" is reported independently by the following two papers: a) Design of a 1000-kVA three-phase transformer with no magnetic core, by H. G. Koenigsberger, Trans. AIEE, Vol. 52, p. 103, 1933; b) Design of a 1000-kVA three-phase transformer with no magnetic core, by H. G. Koenigsberger, Trans. AIEE, Vol. 52, p. 103, 1933.

The "Circuit 2" is reported independently by the following two papers: a) Design of a 1000-kVA three-phase transformer with no magnetic core, by H. G. Koenigsberger, Trans. AIEE, Vol. 52, p. 103, 1933; b) Design of a 1000-kVA three-phase transformer with no magnetic core, by H. G. Koenigsberger, Trans. AIEE, Vol. 52, p. 103, 1933.

The "Circuit 2" is reported independently by the following two papers: a) Design of a 1000-kVA three-phase transformer with no magnetic core, by H. G. Koenigsberger, Trans. AIEE, Vol. 52, p. 103, 1933; b) Design of a 1000-kVA three-phase transformer with no magnetic core, by H. G. Koenigsberger, Trans. AIEE, Vol. 52, p. 103, 1933.

The "Circuit 2" is reported independently by the following two papers: a) Design of a 1000-kVA three-phase transformer with no magnetic core, by H. G. Koenigsberger, Trans. AIEE, Vol. 52, p. 103, 1933; b) Design of a 1000-kVA three-phase transformer with no magnetic core, by H. G. Koenigsberger, Trans. AIEE, Vol. 52, p. 103, 1933.

# Chapter 5

## Calculation of Induction Machine Losses

### 5.1 Introduction

The final step in our complete description of the parameters of an induction machine is the calculation of its resistances. At first, this computation may appear to be almost a trivial task since the resistance of a wire of known length and having uniform cross section can be calculated from elementary circuit theory. Alas, nothing could be farther from the truth. The computation of losses is probably the most difficult and challenging aspect of machine design. In fact, the subject is much too lengthy to treat in detail here and we will be forced to discuss much of the subject in qualitative terms.

In general the power losses in an induction motor can be relegated to five elements

1. Stator copper loss
2. Rotor copper loss
3. Iron loss
4. Stray-load loss
5. Friction and windage loss

Aside from the friction and windage loss which accounts for mechanical losses, the losses of the machine arise from two basic phenomena; ohmic loss in the conductors (1 and 2 above) and magnetic loss in the laminations. The magnetic loss, in turn, consists of hysteresis loss which is a true magnetic loss and ohmic loss due to eddy currents (3 above). The fourth source of loss, namely stray load loss, lumps all of the electromagnetic losses which occur because the machine does not have a smooth air gap and sinusoidal winding distributions. The term is really a misnomer since this type of loss includes no-load as well as load losses. As can be imagined, this term is by far the most complex part of the loss picture.

Theoretically, it is possible to solve Maxwell's Equations and thus find the magnetic and electric fields at every point in the iron and conductor. It would then be a short step to accurately calculate all the electromagnetic losses. Until recently, this would be an impossible task. It remains, even in the age of high speed computers, a formidable assignment and has only recently been tackled. An alternate approach is to consider losses to be caused by separate, independent phenomena. Each phenomena is treated in a relatively simple manner physically. The physical parameters can then be reduced to a set of elements such as resistances and reactances to be used in an equivalent circuit. Unfortunately, the loss effects are not, in fact, independent since saturation makes the phenomena nonlinear. Correlation of any newly developed theory with test is also nearly impossible since it is possible, in general, to measure only the total or some aggregation of several loss components. Although some experimental work has been done on separately measuring several of the more important loss components, this work has generally not progressed to the point of being useful to the machine designer. Another difficulty arises because various authors have assigned different effects to the same equivalent circuit element. This conceptual problem is further complicated by the fact that the notation often does not distinguish between these differences.

## 5.2 Eddy Current Effects in Conductors

Although ohmic losses in conductors are basically easy to calculate, the problem is complicated by the fact that the current distribution in the conductors is often non-uniform. We have already considered the effect of slot leakage flux from current carrying conductors placed in the slots in Chapter 4. We have observed that more flux links with the conductor in the bottom of the slot than a conductor in the top portion of the slot. Thus, in effect, a higher voltage is induced in the bottom conductor resulting in a difference in potential between top and bottom conductors. If these two conductors are electrically insulated, the insulation medium will withstand this difference in potential. However, should these two conductors be connected together in parallel, this difference in potential drives a circulating current around the mesh formed by the two parallel conductors. These circulating currents are called eddy currents and they produce additional copper losses in the conductors which are known as eddy current losses. When this phenomenon acts to cause current flow near the surface of conductors it is also known by the term "skin effect".

Let us consider a solid conductor having a height  $d$  and width  $b$  lying in an open slot of depth  $d_s$  and width  $b_s$  as shown in Figure 5.1. Within the conductor, Ampere's Law states that

$$\nabla \times \mathbf{H} = \mathbf{J} \quad (5.1)$$

From the constituent equations we have, in SI units

$$\mathbf{H} = \frac{\mathbf{B}}{\mu_0} \quad (5.2)$$

and

$$\mathbf{J} = \mathbf{E}/\rho \quad (5.3)$$

Taking the curl of both sides of Eq. (5.1) we have

$$\nabla \times \nabla \times \left( \frac{\mathbf{B}}{\mu_0} \right) = \nabla \times \left( \frac{\mathbf{E}}{\rho} \right) \quad (5.4)$$

However from Faraday's Law in vector form

$$\nabla \times \mathbf{E} = -\frac{\partial \mathbf{B}}{\partial t}$$

In addition, an identity in vector algebra states that

$$\nabla \times \nabla \times \mathbf{V} = \nabla(\nabla \cdot \mathbf{V}) - \nabla^2 \mathbf{V}$$

where  $\mathbf{V}$  is any vector. Hence, Eq. (5.4) can be expressed as

$$\nabla(\nabla \cdot \mathbf{B}) - \nabla^2 \mathbf{B} = \frac{\mu_0}{\rho} \left( -\frac{\partial \mathbf{B}}{\partial t} \right) \quad (5.5)$$

Conservation of flux or Gauss' Law for magnetic fields states that

$$\nabla \cdot \mathbf{B} = 0$$

Hence, Eq. (5.5) reduces to

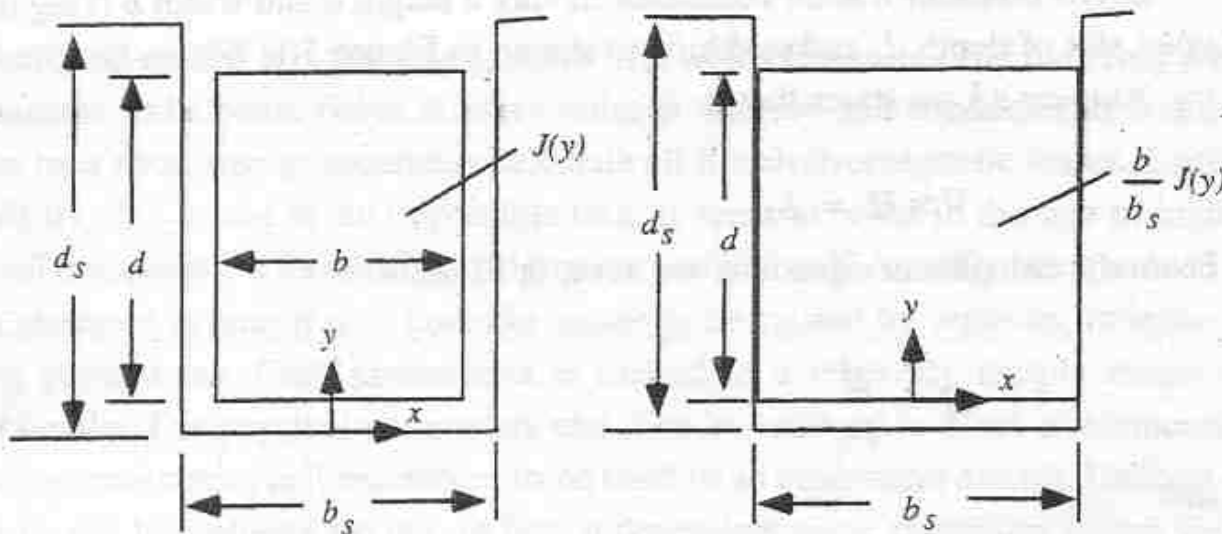


Figure 5.1 Rotor bar configuration and equivalent arrangement for purposes of analysis.

$$\nabla^2 B = \frac{\mu_0}{\rho} \frac{\partial B}{\partial t} \quad (5.6)$$

If it is again assumed that all flux lines go straight across the slot, then the magnetic flux density has only an  $x$  component which is a function only of the depth  $y$  as shown on Figure 5.1. Hence, for the fields within a rectangular slot the partial differential equation to be solved is

$$\frac{\partial^2 B_x}{\partial y^2} = \frac{\mu_0}{\rho} \frac{\partial B_x}{\partial t} \quad (5.7)$$

For fields outside the current carrying region one can assume that Eq. (5.7) reduces to

$$\frac{\partial^2 B_x}{\partial y^2} = 0 \quad (5.8)$$

since the current density  $J$  in this region is zero and the field in the region above the slot can be found by other means.

Simultaneous solution of Eqs. (5.7) and (5.8) is a difficult problem since the solutions in the two regions must be matched at the boundaries, i.e. at  $x = b_s/2$  and  $x = b/2$ . In the application in which have an interest, the space between the conductor and the walls of the slot are quite small. We will replace the

actual problem by an equivalent one in which the current is uniformly distributed lengthwise over the slot width and is reduced in magnitude such that the total current is the same in the slot. That is we will assume a current density

$$J_e = \left( \frac{b}{b_s} \right) J_a \quad (5.9)$$

With this value of current density we can now solve Eq. (5.7) over the entire slot width  $0 < y < b_s$ .

Since the excitation is sinusoidal, the response can also be assumed as sinusoidal in time, that is

$$B_x(x, y, t) = \operatorname{Re}[\tilde{B}_m(x, y)e^{j\omega t}]$$

and therefore

$$\frac{\partial B_x}{\partial t} = \operatorname{Re}[j\omega \tilde{B}_m(x, y)e^{j\omega t}]$$

Eq. 5.7 can be written in the form

$$\operatorname{Re}\left[ \frac{\partial^2}{\partial y^2} \tilde{B}_m(x, y) e^{j\omega t} \right] = \frac{\mu_o}{\rho} \operatorname{Re}[j\omega \tilde{B}_m(x, y) e^{j\omega t}] \quad (5.10)$$

If the real part of the bracketed quantity is assumed and the rotating complex time function  $e^{j\omega t}$  cancelled, Eq. (5.10) becomes

$$\frac{\partial^2 \tilde{B}_m}{\partial y^2} = \frac{j\omega \mu_o}{\rho} \tilde{B}_m \quad (5.11)$$

where the flux density  $B_m$  is complex.

The general solution to Eq. (5.11) is

$$\tilde{B}_m(x, y) = \tilde{P} \cosh(\gamma y) + \tilde{Q} \sinh(\gamma y) \quad (5.12)$$

where

$$\gamma = \sqrt{\frac{j\omega \mu_o}{\rho}} \quad (5.13)$$

Since  $B = 0$  when  $y = 0$ ,

$$\begin{aligned}\tilde{B}_m(x, 0) &= \tilde{P} \cosh(0) + \tilde{Q} \sinh(0) \\ 0 &= \tilde{P} \cdot 1 + \tilde{Q} \cdot 0\end{aligned}\quad (5.14)$$

Hence  $\tilde{P} = 0$ . Alternatively, when  $y = d$ , then all of the current is enclosed and

$$\frac{\tilde{B}_m(x, d)}{\mu_0} b_s = I_m$$

so that

$$\frac{\mu_0 I_m}{b_s} = \tilde{Q} \sinh(\gamma d)$$

and

$$\tilde{Q} = \frac{\mu_0 I_m}{b_s} \frac{1}{\sinh(\gamma d)} \quad (5.15)$$

The solution for the amplitude of the flux density in complex form is therefore

$$\tilde{B}_m = \frac{\mu_0 I_m}{b_s} \left[ \frac{\sinh(\gamma y)}{\sinh(\gamma d)} \right] \quad (5.16)$$

From Ampere's Law we have

$$\nabla \times \bar{H} = \bar{J} \quad (5.17)$$

which for our case reduces to the complex form

$$\frac{\partial}{\partial y} \tilde{H}_x = \tilde{J}_e \quad (5.18)$$

or since

$$\tilde{H}_x = \frac{\tilde{B}_m}{\mu_0}$$

we have

$$\tilde{J}_e = \frac{1}{\mu_0} \frac{\partial \tilde{B}_m}{\partial y} \quad (5.19)$$

Substituting Eq. (5.16) into Eq. (5.19) the equivalent current density in the slots is

$$\tilde{J}_e = \frac{\gamma I_m}{b_s} \left[ \frac{\cosh(\gamma y)}{\sinh(\gamma d)} \right] \quad (5.20)$$

Recall that the actual current density is related to the equivalent current density by

$$\tilde{J}_a = \frac{b_s}{b} \tilde{J}_e$$

so that the actual current density in the conductor is

$$\tilde{J}_a = \frac{\gamma I_m}{b} \left[ \frac{\cosh(\gamma y)}{\sinh(\gamma d)} \right] \quad (5.21)$$

The total voltage drop along the bar can be found from Ohm's Law and Faraday's Law since these two effects act simultaneously on any current filament in the bar. The total  $IR$  drop across the length of the bar at any height  $y$  is

$$\tilde{V}_R = \int_0^{l_i + nl_o} \tilde{E} \cdot dl$$

Note that we are using here the actual rotor length and therefore including that portion of the bar (corresponding to the ducts and end extensions) which are not embedded in iron. Defining  $l_b = l_i + nl_o$ ,

$$\tilde{V}_R = \rho \tilde{J}_a \int_0^{l_b} dl$$

or

$$\tilde{V}_R = \frac{\gamma \rho I_m l_b}{b} \left[ \frac{\cosh(\gamma y)}{\sinh(\gamma d)} \right] \quad (5.22)$$

Note that the resistive drop is a maximum at the top of the slot.

The total flux crossing the slot above the height  $y$  which therefore links the current below  $y$  is

$$\begin{aligned}\tilde{\phi}_m(y) &= \int_0^{l_e} \int_{-d}^d \tilde{B}_m dy dz \\ &= \frac{\mu_o I_m l_e}{\gamma b_s} \left[ \frac{\cosh(\gamma d) - \cosh(\gamma y)}{\sinh(\gamma d)} \right]\end{aligned}\quad (5.23)$$

The total  $IX$  drop across the length of the bar at any height  $y$  is therefore

$$\tilde{V}_L = \frac{\partial}{\partial t} \int_0^{l_e} \int_{-d}^d \tilde{B}_m dy dz$$

or in complex form

$$\tilde{V}_L = j\omega \tilde{\phi}_m$$

whereupon

$$\tilde{V}_L = \frac{j\omega \mu_o I_m l_e}{\gamma b_s} \left[ \frac{\cosh(\gamma d) - \cosh(\gamma y)}{\sinh(\gamma d)} \right]$$

Note that the reactive drop is zero at the top of the slot and a maximum at the bottom of the slot.

The total voltage drop along the bar at an arbitrary height  $y$  is clearly the sum of the inductive and resistive drop or

$$\begin{aligned}\tilde{V}_{bar} &= \tilde{V}_R + \tilde{V}_L \\ &= \frac{\gamma \rho I_m l_b}{b} \left[ \frac{\cosh(\gamma y)}{\sinh(\gamma d)} \right] + \frac{j\omega \mu_o I_m l_e}{\gamma b_s} \left[ \frac{\cosh(\gamma d) - \cosh(\gamma y)}{\sinh(\gamma d)} \right]\end{aligned}\quad (5.24)$$

But

$$\frac{j\omega \mu_o}{\gamma} = \frac{j\omega \mu_o}{\sqrt{(j\omega \mu_o)/\rho}}$$

$$\begin{aligned}
 &= \rho \sqrt{\frac{j\omega\mu_0}{\rho}} \\
 &= \rho\gamma
 \end{aligned} \tag{5.25}$$

and if

$$\frac{l_b}{b} \approx \frac{l_e}{b_s} \tag{5.26}$$

then,

$$\tilde{V}_{bar} = \frac{\gamma\rho I_m l_b}{b} \frac{\cosh(\gamma d)}{\sinh(\gamma d)} \tag{5.27}$$

Note that the total drop down the length of the bar is constant, which is to be expected since all of the current filaments are "connected" in parallel. While the assumption of Eq. (5.26) is rarely true, this result would have been an exact equality had we not made simplifying assumptions and solved the exact problem.

Assuming now an equality, Equation (5.27) can be written in terms of the dc resistance of the bar if we recall that

$$R_{DC} = \frac{\rho l_b}{bd} \tag{5.28}$$

Hence, the effective impedance of the bar is

$$\begin{aligned}
 \tilde{Z}_{bar} &= \frac{\tilde{V}_{bar}}{I_m} \\
 &= R_{DC} \left[ \frac{(\gamma d) \cosh(\gamma d)}{\sinh(\gamma d)} \right]
 \end{aligned} \tag{5.29}$$

The real portion of the impedance representing the ac resistance of the bar can be readily evaluated as

$$R_{AC} = \alpha d R_{DC} \left[ \frac{\sinh(2\alpha d) + \sin(2\alpha d)}{\cosh(2\alpha d) - \cos(2\alpha d)} \right] \tag{5.30}$$

where

$$\alpha = \sqrt{(\omega\mu_o)/(2\rho)}$$

The imaginary component of the impedance represents the reactance of the bar and is

$$X_{AC} = \alpha d R_{DC} \left[ \frac{\sinh(2\alpha d) - \sin(2\alpha d)}{\cosh(2\alpha d) - \cos(2\alpha d)} \right] \quad (5.31)$$

It is useful to consider the asymptotes of Eqs. (5.30) and (5.31) for very small and very large values of  $\alpha d$  (low and high values of frequency respectively). When  $\alpha d$  is small, Eqs. (5.30) and (5.31) become

$$R_{AC} \approx R_{DC} \left[ 1 + \frac{4}{45}(\alpha d)^4 - \frac{16}{4,725}(\alpha d)^8 + \dots \right] \quad (\alpha d < 1.5) \quad (5.32)$$

$$X_{AC} \approx \frac{2}{3}(\alpha d)^2 R_{DC} \left[ 1 - \frac{8(\alpha d)^4}{315} + \frac{32(\alpha d)^8}{31,185} \right] \quad (\alpha d < 1.5) \quad (5.33)$$

The coefficient in front of the bracket can be written as

$$\frac{2}{3}(\alpha d)^2 R_{DC} = \left( \frac{2}{3} \right) \left[ \sqrt{\frac{\omega\mu_o}{2\rho}} d \right]^2 \frac{\rho l_b}{d \cdot b}$$

$$= \frac{\omega\mu_o}{3} \frac{dl_b}{b} = \omega \left( \frac{\mu_o dl_b}{3b} \right)$$

$$\approx \omega \left( \frac{\mu_o dl_b}{3b} \right)$$

so that Eq. (5.33) becomes

$$X_{AC} \approx \omega L_{DC} \left[ 1 - \frac{8(\alpha d)^4}{315} + \frac{32(\alpha d)^8}{31,185} + \dots \right] \quad (\alpha d < 1.5) \quad (5.34)$$

Hence, as frequency is reduced the ac values of resistance and reactance tend toward their dc values.

If  $\alpha d$  is large Eqs. (5.30) and (5.31) can be approximated by

$$R_{AC} = \alpha d R_{DC} \quad (5.35)$$

and

$$X_{AC} = \alpha d R_{DC} = \frac{3\omega L_{dc}}{2 \alpha d} \quad (5.36)$$

Note that the resistance and reactance approach an equality as the frequency (or the bar depth) increases. The amplitude of the impedance increases as the square root of the frequency and the phase angle approaches  $45^\circ$ . Equation (5.35) can, by use of Eq. (5.28), be expressed in the form

$$\begin{aligned} R_{AC} &= \frac{\rho l_b}{bd} (\alpha d) \\ &= \rho \left( \frac{l_b}{b(1/\alpha)} \right) \end{aligned} \quad (5.37)$$

Hence, for sufficiently high frequencies, the ac resistance can be calculated in the same manner as for the dc resistance if one replaces the actual depth of the bar  $d$  by an equivalent depth  $1/\alpha$ . The quantity  $1/\alpha$  is called the *skin depth* and the fact that the current distributes itself unevenly over a conductor due to sinusoidal excitation is called the *skin effect*.

At  $75^\circ C$  the resistivity of copper is  $2.1 \cdot 10^{-6}$  ohm-cm. Hence the skin depth for a copper bar excited at 60 Hz can be computed as

$$\begin{aligned} 1/\alpha &= \sqrt{\frac{(2)(2.1 \cdot 10^{-6})}{(4\pi \cdot 10^{-9})(377)}} = 0.9416 \text{ cm} \\ &= 0.3707'' \end{aligned}$$

It is important to observe that since the reactance increases as the square root of frequency at high frequencies, then effectively the slot inductance actually decreases inversely with the square root of frequency. A plot of  $R_{AC}$ ,  $X_{AC}$  and  $L_{AC}$  normalized with respect to their dc values is given in Figure 5.2.

When the skin effect phenomenon occurs in the rotor it is usually referred to as the "deep bar effect". An improvement in the starting performance of a squirrel cage induction motor can actually be achieved if proper use is made of this phenomenon. In general, two general categories of rotors which utilize

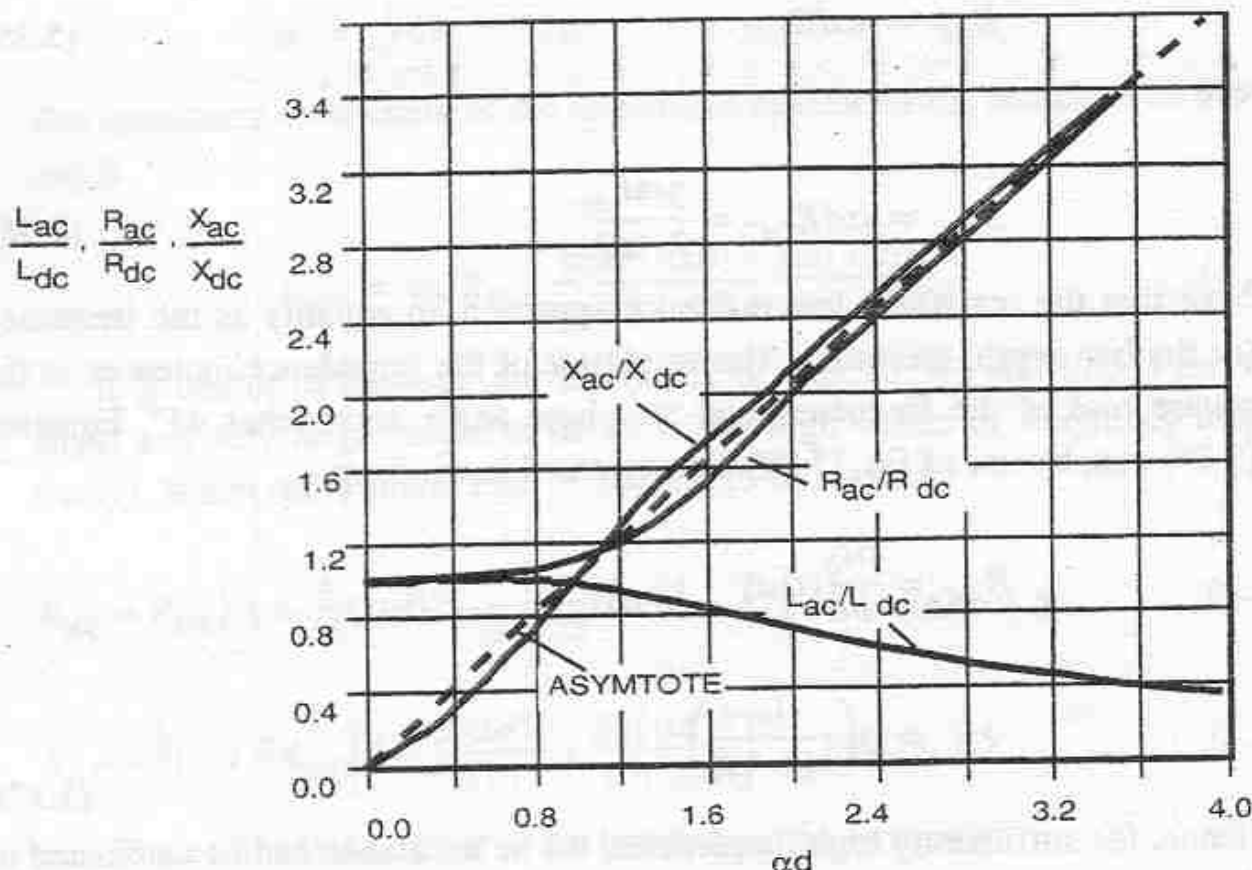


Figure 5.2 Sketch of normalized inductance, resistance and reactance of solid bar in a slot as a function of  $\alpha_d$

skin effect are used, the *deep bar rotor* in which a single bar is shaped to have a long bar depth (deep bar) and short width and the *double cage rotor* in which a second bar is located below the shallow bar near the surface. A variety of rotor bar shapes have been used over the years and are illustrated in Figure 5.3. The area of the deep bar as well as the area of the two or three bars belonging to a unit in the double cage rotor is chosen so that the  $I^2r$  losses at small slip do not exceed the amount permissible with respect to the desired efficiency and heat dissipation limit of the machine. Since the slip frequency is very low at normal speed and no skin effect occurs, the deep bar rotor and the double cage rotor behave at normal load just as the round bar or shallow bar rotor previously discussed. However, the behavior of both kinds of rotors is entirely different at high slips, for example at standstill where the frequency of the rotor currents is the same as the line frequency. In this case, the current density given by Eq. (5.20) may be thought of as the superposition of a uniform (average) current and a circulating current flowing in an additive fashion at the top of the bar and negatively at the bottom, directed in such a way as to oppose the time rate of change of slot leakage flux. The skin effect forces current to flow in the part of the conductor area which lies at the top of the slot and the effective

resistance is many times (usually three to four times) as large as the round bar or shallow bar rotor. In the case of the double bar rotor, the resistance of the top bar usually has a higher resistance than the bottom bar making the effective resistance at starting even larger if desired.

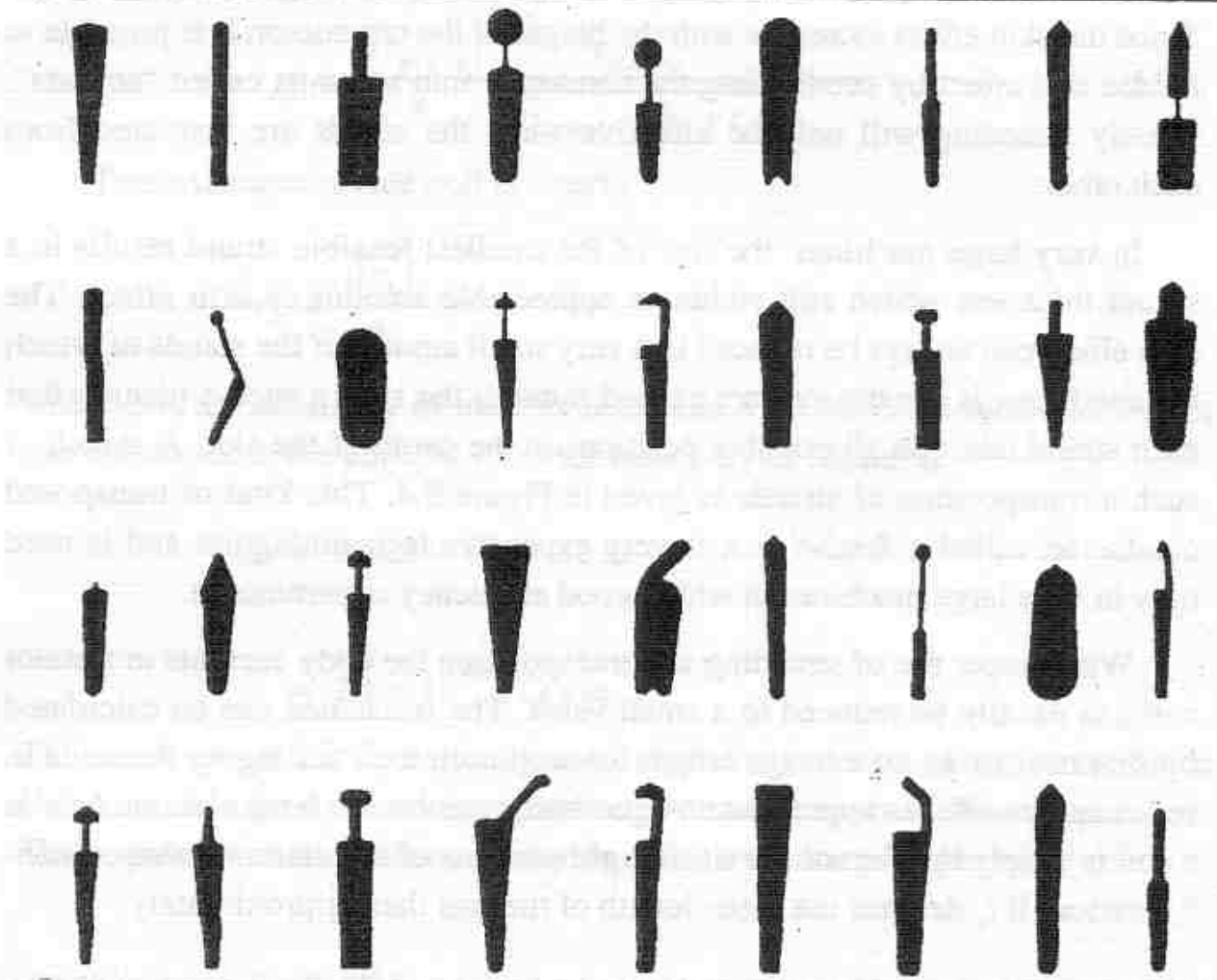


Figure 5.3 A variety of rotor shapes used to enhance skin effect

As the motor comes up to speed, the rotor frequency decreases and therefore the leakage reactance as well as the resistance of the rotor bar arrangement decreases and the influence of the skin effect becomes smaller. At low slips and at normal slip, the frequency of the rotor current is very small and the leakage reactance and resistance take on their dc values. The current is now uniformly distributed over the deep bar or divided in the ratio of the dc resistances of both cages in the case of the double cage rotor. The starting performance of a machine with considerable skin effect is therefore similar to that of the slip ring motor connected to an external resistance for starting.

### 5.3 Calculation of Stator Resistance

Although skin effect in the rotor bars is sometimes useful in the design of machines with high starting torque, the presence of skin effect in the stator conductors is always detrimental since it produces nothing but extra losses. Since the skin effect increases with the height of the conductor, it is possible to reduce this effect by subdividing the conductor into subunits called "strands". Clearly stranding will only be effective when the stands are insulated from each other.

In very large machines, the size of the smallest feasible strand results in a strand thickness which still yields an appreciable amount of skin effect. The skin effect can always be reduced to a very small amount if the stands of which the conductor is constructed are carried through the slot in such a manner that each strand takes on all possible positions in the depth of the slot. A sketch of such a transposition of strands is given in Figure 5.4. This kind of transposed conductor, called a *Roebel bar*, is very expensive to manufacture and is used only in very large machines in which good efficiency is paramount.

With proper use of stranding and transposition the eddy currents in a stator coil can usually be reduced to a small value. The resistance can be calculated by first estimating an average length for each coil, then adding up the coils in series and parallel as appropriate. A good estimate for the length of one turn in a coil is simply the sum of the six straight portions of the diamond shaped configuration. If  $l_c$  denotes the mean length of the coil then approximately

$$l_c = 2l_s + 4l_{e2} + 4l_{e3} \quad (5.38)$$

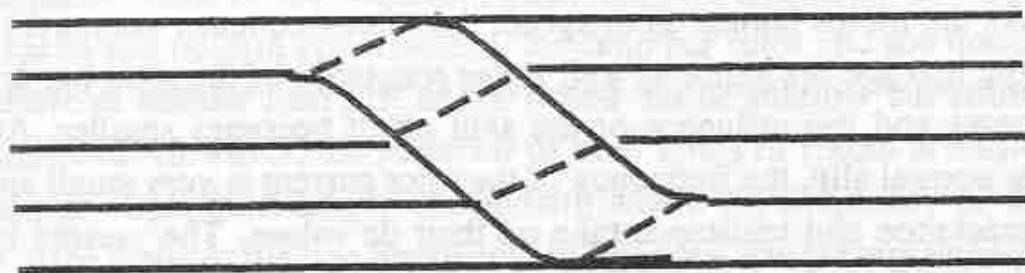


Figure 5.4      Roebel strand transposition.

where  $l_s$  is the length of the stator stack including ducts,  $l_{e2}$  is the straight extension of the coils beyond the stack, and  $l_{e3}$  is the diagonal portion of the end winding. By reference to Figure 4.13 it is readily verified that  $l_{e3}$  can be obtained from parameters already defined as

$$l_{e3} = \frac{P\tau_{p(ave)}}{2} \frac{\tau_{s(ave)}}{\sqrt{\tau_{s(ave)}^2 - (b_c + t_e)^2}} \quad (5.39)$$

The resistance of one coil is clearly

$$r_c = \frac{\rho n_c l_c}{A_c}$$

where  $\rho$  is the resistivity of the conductor and  $A_c$  is the cross-sectional area of one conductor in the coil. At 75°C the resistivity of copper is

$$\rho = 0.825 \times 10^{-6} \Omega \text{ in}$$

$$= 2.1 \times 10^{-6} \Omega \text{ cm}$$

The resistivity at 75°C is usually used for the calculation of resistance since U.S.A. standards are based on parameter measurements at this temperature. The resistance of the coils connected in series over one pole pitch is

$$r_p = \frac{S_1}{3P} r_c$$

If  $P/C$  poles are connected in series then the resistance of one parallel branch of a  $C$  branch circuit is

$$r_b = \frac{P}{C} r_p = \frac{S_1}{3C} r_c$$

The net resistance per phase is the resistance of these  $C$  circuits connected in parallel or

$$r_s = \frac{r_b}{C} = \frac{S_1}{3C^2} r_c \quad (5.40)$$

$$= \left( \frac{S_1}{3C^2} \right) \frac{\rho n_c l_c}{A_c} \quad (5.41)$$

Equation (5.41) can be written in a simpler form if we recall that for a two layer winding the number of turns per slot is twice the number of turns per coil. The number of turns per slot is related to the total number of turns for a three phase machine by Eq. (4.40),

$$n_s = \frac{6CN_s}{S_1}$$

Substituting these results into Eq. (5.41) we have the following alternative form for the resistance per phase

$$\begin{aligned} r_s &= \frac{S_1}{3C^2} \left( \frac{n_s}{2} \right) \frac{\rho l_c}{A_c} \\ &= \frac{S_1}{3C^2} \left( \frac{3CN_s}{S_1} \right) \frac{\rho l_c}{A_c} \\ &= \left( \frac{N_s}{C} \right) \rho \frac{l_c}{A_c} \end{aligned} \quad (5.42)$$

## 5.4 Example #7 - Calculation of Stator and Rotor Resistance

Again the 250 hp machine of the previous examples will be used. From information already provided, the following dimensions and constants can be determined which are necessary for the calculation of the stator resistance.

Total Number of Turns =  $N_t = 240$

Number of Circuits =  $C = 1$

Pitch =  $p = 0.8$

Pole Pitch Measured from the Slot Radial Midpoint =  $\tau_{p(ave)} = 10.324"$

Slot Pitch Measured from the Radial Midpoint of the

Slots =  $\tau_{s(ave)} = 0.688"$

Gross Core Length Including Ducts =  $l_i + nl_o = 10"$

Coil Extension (Section 4.11) =  $l_{e2} = 1.25"$

Spacing Between Coils (Figure 4.13) =  $t_e = 0.0625"$

Coil Thickness (Figure 4.13) =  $b_c = 0.220"$

Area of Coil (Section 4.11) =  $A_c = (0.129)(0.204)(0.97) = 0.02553 \text{ in}^2$

The factor 0.97 in the area of the conductor takes rounding of the corners into account. The length of the diagonal portion of the end winding is calculated from Eq. (5.39) as

$$l_{e3} = \frac{(0.8)(10.32)(0.688)}{\sqrt{(0.688)^2 - (0.0625 + 0.22)^2}} \\ = 4.527"$$

The mean length of a coil is therefore, from Eq. (5.38)

$$l_c = (2)(10) + (4)(1.25) + 4(4.527) \\ = 43.11"$$

The stator resistance is now obtained from Eq. (5.42) as

$$r_s = \frac{(0.825)(10^{-6})(240)(43.11)}{(1)(0.02553)} \\ = 0.334 \Omega @ 75^\circ\text{C}$$

The influence of skin effect may now be considered. From the discussion in Section 5.2, the skin depth in a copper bar at  $75^\circ$  with 60 Hz excitation is

$$1/\alpha = 0.3707"$$

so that

$$\alpha = 2.6976 \text{ in}^{-1}$$

Hence, in this example

$$\alpha d = (2.6976)(0.129) \\ = 0.348$$

Since  $\alpha d$  is much less than 1.5 we can use the approximation for the ac resistance, Eq. (5.32), so that

$$r_{s(AC)} \approx r_{s(DC)} \left[ 1 + \left( \frac{4}{45} \right) (\alpha d)^4 \right] = 0.334 [1 + 0.0014]$$

or

$$r_{s(AC)} = 0.335 \Omega \text{ (corrected for skin effect)}$$

As is usual, the impact of skin effect on the stator resistance is essentially negligible. Comparing the coefficient of Eq. (5.33) (i.e. 8/315) with the coefficient of Eq. (5.32) (i.e. 4/45) it can be concluded that the influence of skin effect on slot leakage inductance is much less than for resistance and can safely be neglected as well.

The following parameters are taken from Examples #3 and 4 and can be used to calculate the rotor resistance:

Actual Length Including Ducts	$l_b$	= 10"
Effective Rotor Length	$l_{er} = l_{es}$	= 8.896"
Bar Width	$b$	= 0.375"
Bar Depth	$d$	= 0.5625"
End Ring Area	$t_{be}$	= 1.0"
	$d_{be}$	= 0.75"
Rotor Bar Extension	$l_{be}$	= 0.625"
Avg. Rotor Pole Pitch	$\tau_{pr(av)}$	= 8.611"
Rotor Slots	$S_2$	= 97

From this information we can determine that the length of one rotor bar not including the portion over the end ring is

$$10 + 2(0.625) = 11.25"$$

In addition to this length we must include some portion of the part over the end ring since the current curves from the bar into the end ring over the distance  $t_{re}$ . If we take this value as  $(1/3)t_{be}$  then the total active length of the rotor bars including the slight additional length due to skew is

$$l_b = \frac{\left[ 11.25 + 2\left(\frac{1}{3}\right)(1) \right]}{\cos[(2\pi)/S_2]} = 11.94"$$

The resistance of one rotor bar is therefore

$$r_b = \frac{(11.94)(0.825) \times 10^{-6}}{(0.375)(0.5625)} = 46.7 \mu\Omega$$

The tooth pitch at the middle of the end ring can be obtained from  $\tau_{pr(ave)}$  as

$$\tau_{re(ave)} = \frac{P}{S_2} \tau_{pr(ave)}$$

$$= \frac{8}{97}(8.611) \\ = 0.71''$$

The resistance of the end ring portion over one rotor slot pitch is

$$r_e = \frac{\tau_{re(ave)} \rho}{t_{be} d_{be}} \\ = \frac{0.71(0.825 \times 10^{-6})}{1(0.75)} = 0.78 \times 10^{-6}$$

The effective bar resistance is therefore, from Eq. (4.156),

$$r_{be} = r_b + \frac{r_e}{2 \sin^2 \left( \frac{\pi P}{2 S_2} \right)} \\ = \left[ 46.7 + \frac{0.78}{2 \sin^2 \left( \frac{\pi \cdot 8}{2 \cdot 97} \right)} \right] \times 10^{-6} = (46.7 + 23.37) \times 10^{-6} \\ = 70.1 \mu\Omega$$

The resistance per rotor mesh is

$$r_r = 2r_{be} = 140.2 \mu\Omega$$

The rotor resistance referred to the stator is obtained from Eq. (4.204)

$$r'_r = \frac{12k_1^2 N_s^2}{S_2} r_r$$

$$= \frac{(12)(0.91)^2(240)^2}{97} 140.2 \times 10^{-6}$$

$$= 0.827 \Omega$$

Finally, we must remember to include the effects of skew. The coefficient needed to compensate for skew is the same as used for rotor leakage inductance. From Section 4.16 we have the result that

$$r''_r = k_{s1}^2 r'_r = (0.9963)^2(0.827)$$

$$= 0.82 \Omega$$

This value of resistance is valid over the full range of load conditions since near synchronous speed the frequency of the currents induced in the rotor bars is low. However, during starting, the frequency of the currents which flow in the rotor bars is 60 Hz and skin effect is a definite possibility. The possibility of skin effect can be evaluated by recalling that the value of  $\alpha d$  of a rotor bar is 1.52. Reference to Figure 5.2 indicates that skin effect will indeed be important for the starting condition.

Although some skin effect exists in the air portion of the current path the effect is less prominent than for the slot portion. Hence, we will approximate the actual situation by assuming that skin effect only takes place in the slot region and is dictated by the effective length corresponding to rotor slot leakage flux.

The dc resistance of the portion of the bar including the iron and the duct portions is

$$r_{b(DC)} = \frac{l_e \rho}{bd}$$

From previous work the effective length for rotor slots (not including ducts) is

$$l_{er} = 8.896''$$

so that, taking the ratio, the iron portion of the bar is

$$r_{bi(DC)} = \left( \frac{8.896}{11.94} \right) (46.7) \times 10^{-6}$$

$$= 34.79 \mu\Omega$$

Since  $\alpha d > 1.5$  the approximate formula, Eq. (5.32) will be inaccurate. The ac resistance computed from Eq.(5.30) is

$$\begin{aligned} r_{bi(AC)} &= (\alpha d) r_{b(DC)} \left[ \frac{\sinh(2\alpha d) + \sin(2\alpha d)}{\cosh(2\alpha d) - \cos(2\alpha d)} \right] \\ &= (1.517)(34.79) \left[ \frac{10.366 + 0.1074}{10.414 + 0.9942} \right] \times 10^{-6} \\ &= 48.45 \mu\Omega \end{aligned}$$

The effective resistance per rotor mesh will be equal to twice the sum of the resistance of the portion of the bar in the slots plus the resistance of the bar traversing the slot ducts and overhang plus the resistance due to the end rings.

$$r_r = 2 \left( r_{bi(AC)} + \frac{l_b - l_{er}}{l_b} r_{b(DC)} + \frac{r_e}{2 \sin^2 \left( \frac{\pi P}{2 S_2} \right)} \right)$$

$$\begin{aligned} r_r &= 2 \left[ 48.45 + \frac{11.94 - 8.896}{11.94} (34.79) + 23.37 \right] \times 10^6 \\ &= 167.5 \mu\Omega \end{aligned}$$

The corresponding value referred to the stator by the turns ratio and skew is

$$\begin{aligned} r_r'' &= \frac{(12)(0.91)^2(0.9963)^2(240)^2}{(97)(1)^2} (167.5) \times 10^{-6} \\ &= 0.981 \text{ (starting value)} \end{aligned}$$

Note that skin effect has increased the resistance at starting by approximately 39%. The skin effect, of course, varies continuously as the rotor comes up to speed so that the rotor resistance varies smoothly. For low values of  $\alpha d$  the ac resistance of the bar is related to the dc resistance by

$$r_{AC} \approx r_{DC} \left[ 1 + \frac{4}{45} (\alpha d)^4 \right] \quad (5.43)$$

If one defines

$$\alpha_o = \sqrt{\frac{2\pi \cdot 60\mu_o}{2\rho}} \quad (5.44)$$

then for any slip  $S$  the above equation for ac resistance can be written as

$$r_{AC} = r_{DC} \left[ 1 + \frac{4}{45} (\alpha_o d)^4 S^2 \right]$$

This equation can be solved in the form

$$\frac{r_{AC} - r_{DC}}{r_{DC}} = \frac{4}{45} (\alpha_o d)^4 S^2 \quad (5.45)$$

Hence, for low values of  $\alpha d$  the resistance varies with the square of the slip. The curve passes through the value 0.981 for  $S = 1$  and the point 0.82 for  $S = 0$ . A sketch of the rotor resistance as a function of slip is given in Figure 5.5.

When the skin effect is not large and follows essentially Eq. (5.45), it can be conveniently modeled in the per phase equivalent circuit as follows. The increase in rotor resistance above the dc value can, from Eq. (5.45), be expressed as,

$$\Delta r_r = r_{AC} - r_{DC} = \frac{4}{45} (\alpha_o d)^4 S^2 r_{DC} \quad (5.46)$$

so that

$$r_{AC} = r_{DC} + \Delta r_r \quad (5.47)$$

In the per phase equivalent circuit the equivalent rotor resistance is,

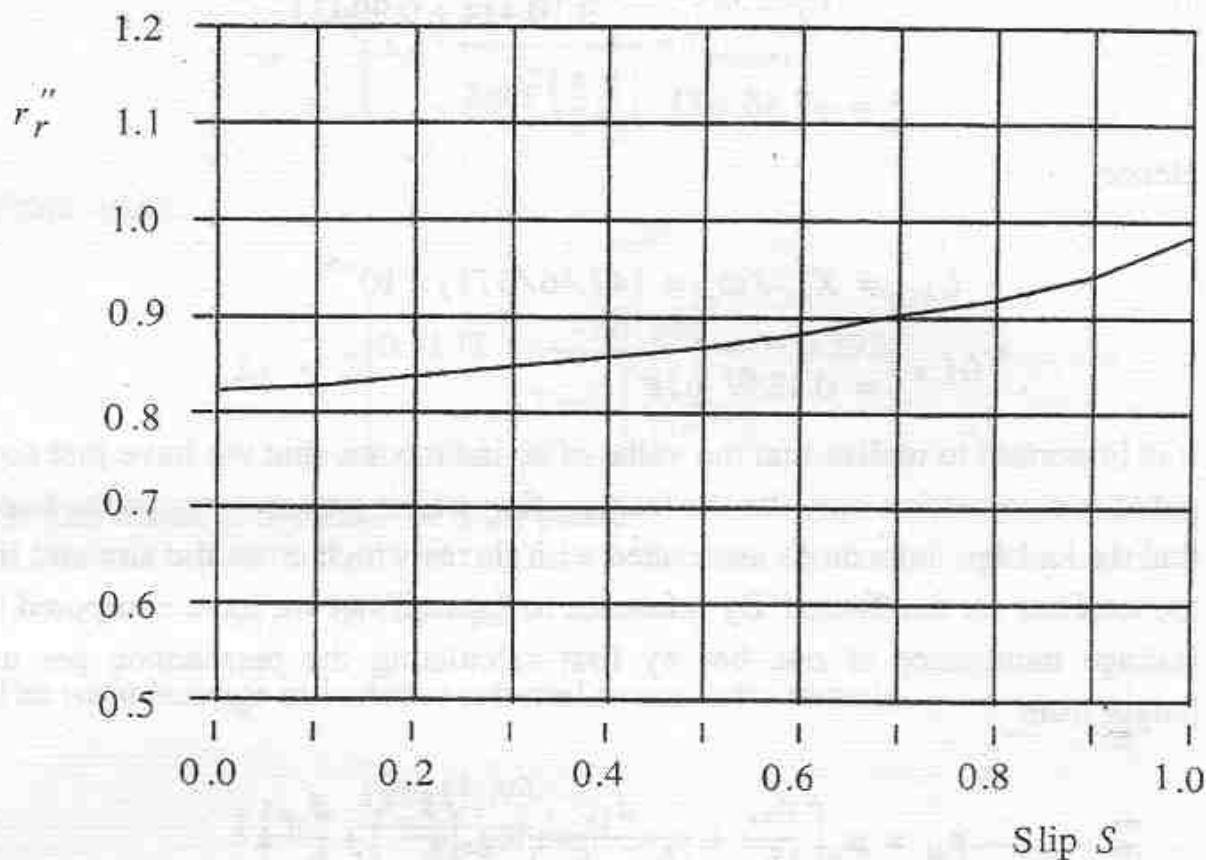


Figure 5.5 Variation of rotor resistance of 250 hp machine with slip due to deep bar effect.

$$\frac{r_{AC}}{S} = \frac{r_{DC}}{S} + \Delta r_{r0} S \quad (5.48)$$

where  $\Delta r_{r0}$  is the change in rotor resistance between  $S = 0$  and  $S = 1$ . That is,  $\Delta r_{r0}$  is obtained by simply setting  $S = 1$  in Eq. (5.46). In the case of our example 250 hp machine  $\Delta r_{r0} = (0.981 - 0.82) = 0.161$

Having completed the study of how stator and rotor resistance vary with frequency, it must be remembered that the rotor leakage inductance is also influenced by skin effect. The corresponding ac value of leakage inductance can be computed from Eq. (5.31) as

$$X_{AC} = (\alpha d)r_{DC} \left[ \frac{\sinh(2\alpha d) - \sin(2\alpha d)}{\cosh(2\alpha d) - \cos(2\alpha d)} \right]$$

$$\begin{aligned}
 &= (1.517)(34.79) \left[ \frac{10.366 - 0.1074}{10.414 + 0.9942} \right] \times 10^{-6} \\
 &= 47.46 \mu\Omega
 \end{aligned}$$

Hence

$$\begin{aligned}
 L_{AC} &= X_{AC}/\omega_e = (47.46/377) \times 10^{-6} \\
 &= 0.1259 \mu\text{H}
 \end{aligned}$$

It is important to realize that the value of ac inductance that we have just computed is a correction only for the leakage flux which passes through the bar so that the leakage inductance associated with fluxes which cross the slot and link the total bar are unaffected. By reference to Example #4 we have computed the leakage inductance of one bar by first calculating the permeance per unit length from

$$p_{sl} = \mu_o \left[ \frac{d_{3r}}{3b_{sr}} + \frac{d_{1r}}{(b_{sr} - b_{or})} \log_e \left( \frac{b_{sr}}{b_{or}} \right) + \frac{d_{or}}{b_{or}} \right]$$

Note that only the first term in this equation is associated with leakage fluxes which partially link the bar. The permeance for the remainder is

$$\begin{aligned}
 p_{sl(air)} &= (\mu_o) \left[ \frac{0.047}{0.385 - 0.09} \log_e \left( \frac{0.385}{0.09} \right) + \frac{0.040}{0.09} \right] \\
 &= 0.849 \times 10^{-6} \text{ H/m}
 \end{aligned}$$

The effective slot leakage per bar is therefore

$$\begin{aligned}
 L_b &= p_{ls(air)} l_e + L_{AC} \\
 &= \left[ (0.849) \left( \frac{8.896}{39.37} \right) + 0.1259 \right] \times 10^{-6} \\
 &= 0.3178 \mu\text{H}
 \end{aligned}$$

The effective leakage inductance per bar including the effect of the end ring and harmonic leakage is

$$L_{lr} = 2 \left( L_b + \frac{L_e}{2 \sin^2 \left( \frac{\pi P}{2 S_2} \right)} + L_{b(har)} \right)$$

From which

$$L_{lr} = 2 \left[ 0.3178 + \frac{0.01986}{2 \sin^2 \left[ \frac{\pi}{2} \left( \frac{8}{97} \right) \right]} + 0.292 \right] \times 10^{-6}$$

So that for an entire mesh or rotor phase

$$L_{lr} = 2.416 \mu\text{H}$$

The rotor leakage inductance referred to the stator turns is

$$\begin{aligned} L_{lr''} &= \frac{12 k_1^2 k_{s1}^2 N_s^2}{S_2} L_{lr} \\ &= \frac{(12)(0.91)^2 (0.9963)^2 (240)^2}{(97)} 2.41 \times 10^{-6} \\ &= 14.15 \text{ mH (starting value)} \end{aligned}$$

This result can be compared with our previous value of 14.6 mH in Example #5, corresponding to only a 4% reduction in the rotor leakage inductance.

For low values of  $\alpha d$  the ac reactance is related to the dc reactance by

$$X_{AC} = \omega L_{AC} = \omega L_{DC} \left[ 1 - \frac{8}{315} (\alpha d)^4 \right]$$

or

$$L_{AC} = L_{DC} \left[ 1 - \frac{8}{315} (\alpha d)^4 \right]$$

If we express  $\alpha d$  as a fraction of the  $\alpha d$  which occurs at starting as we did for the rotor resistance then

$$\alpha d = (\alpha_o d) \sqrt{S}$$

or

$$L_{AC} = L_{DC} \left[ 1 - \frac{8}{315} (\alpha_o d)^4 S^2 \right]$$

$$\frac{L_{AC} - L_{DC}}{L_{DC}} = -\frac{8}{315} (\alpha_o d)^4 S^2$$

Hence the deviation of the ac inductance from the dc inductance decreases as the square of the slip. A sketch of the equivalent circuit for the 250 hp motor without an iron loss term (to be discussed) is given in Figure 5.6. Note the

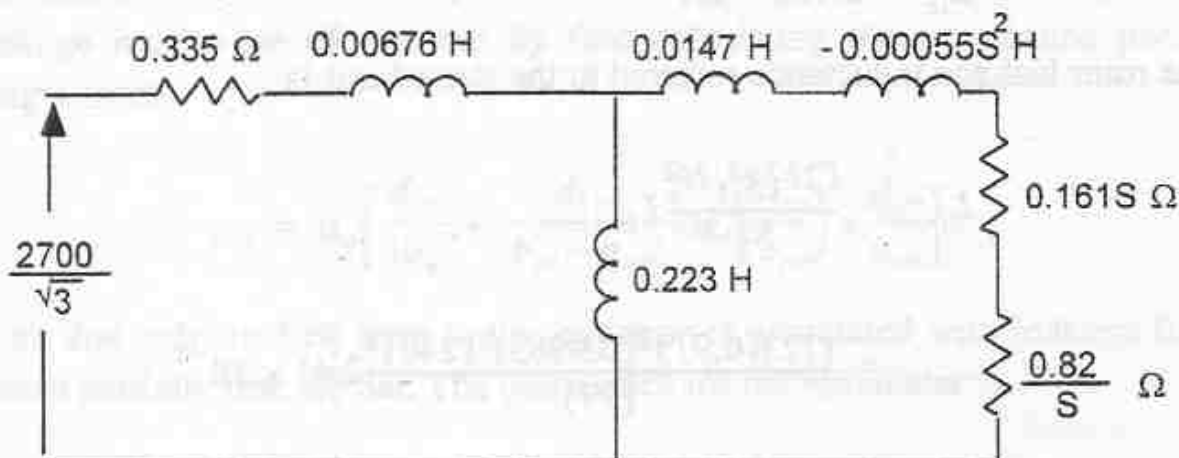


Figure 5.6 Per phase equivalent circuit for 250 hp machine example with  $2700 V_{L-L}$  excitation

presence of the slip dependant rotor parameters. The variation of rotor leakage inductance is clearly small and could have been neglected in this example but is included for the sake of completeness.

## 5.5 Rotor Parameters of Irregularly Shaped Bars

By examining the behavior of a rectangular bar placed in iron, it has been shown that skin effect in rotor bars has the effect of increasing equivalent resistance and decreasing equivalent inductance as the frequency of current increases. The increase of rotor resistance has a beneficial effect in aiding starting capability of squirrel cage machine and nearly all conventional machine

designs (NEMA Designs B, C and D) enhance motor starting capability by specially selected rotor bar shapes. Figure 5.3 shows a typical variety of such shapes.

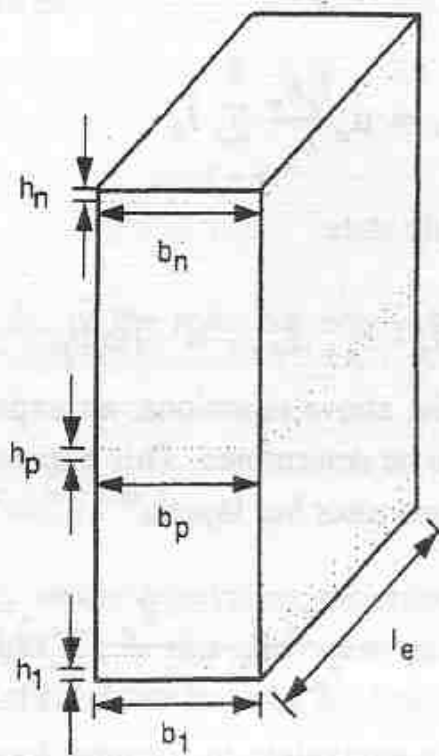


Figure 5.7      Rectangular bar broken into  $n$  sections. Rectangular bar is shown but methodology applies to any bar shape.

Although closed form solutions are usually impossible except for carefully selected exceptions, the following approach can be readily applied to rotor bars of arbitrary cross sectional shape. In this algorithm, the rotor bar is divided into  $n$  layers illustrated in Figure 5.7. All layers of the bar are assumed to have the same axial length. If sufficient number of layers are chosen the layers can be assumed to be essentially rectangular in which case each layer  $p$  has a unique resistance  $r_p$  determined by

$$r_p = \frac{\rho l_e}{h_p b_p} \quad (5.49)$$

Likewise, each layer has a unique reactance determined by the layer geometry,  $\mu_0$ , and the slip frequency.

$$X_p = S\omega_e \mu_o \frac{l_e h_p}{b_p} \quad (5.50)$$

If  $I_k$  is the current in layer  $k$  the flux linking the  $p^{th}$  layer can be expressed,

$$\tilde{\Phi}_p = \mu_o \frac{l_e h_p}{b_p} \sum_{k=1}^p \tilde{I}_k \quad (5.51)$$

where, in the steady state

$$r_p \tilde{I}_p - r_{p+1} \tilde{I}_{p+1} = -j\omega \tilde{\Phi}_p \quad (5.52)$$

Considering the above equations, an expression for the current in the  $p+1$  rotor bar layer can be determined. This expression utilized as information concerning the previous rotor bar layers,

$$\tilde{I}_{p+1} = \frac{r_p}{r_{p+1}} \tilde{I}_p + j \frac{X_p}{r_{p+1}} \sum_{k=1}^p \tilde{I}_k \quad (5.53)$$

This process is equivalent to forming loop equations of equivalent circuit as illustrated in Figure 5.8. The computation of all the reactance values

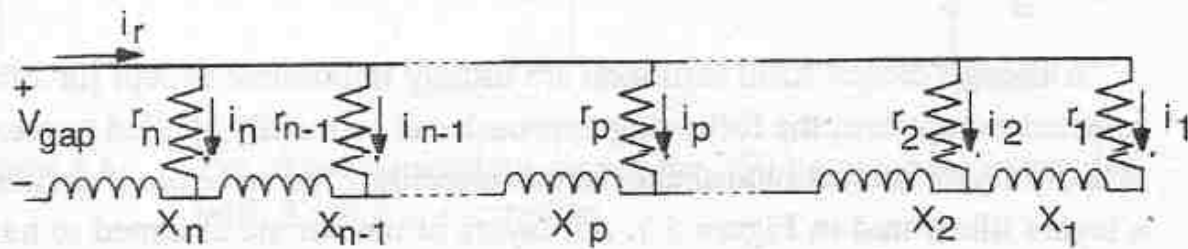


Figure 5.8 Rotor equivalent circuit with multilayer representation of rotor bar

requires an initial assumption about the current in the first rotor bar layer. It is assumed that an arbitrary current flows through the first rotor bar layer. A value of one ampere is convenient for calculation purposes. The values for all the reactances and resistances for the layers can then be determined. At the same time, the currents flowing through all the components is determined. The

voltage ( $\tilde{V}_{gap}$ ) seen at the "outer" terminals of the equivalent circuit can be determined by the following,

$$\tilde{V}_{gap} = r_n \tilde{I}_n + jX_{lr} \tilde{I}_r \quad (5.54)$$

where

$$\tilde{I}_r = \sum_{k=1}^n \tilde{I}_k \quad (5.55)$$

The equivalent impedance  $\tilde{Z}_{in}$  of the rotor bar equivalent circuit can now be determined,

$$\tilde{Z}_{in} = \frac{\tilde{V}_{gap}}{\tilde{I}_r} = r_{be} + jS\omega_e L_{be} \quad (5.56)$$

The real component of  $\tilde{Z}_{in}$  is the equivalent resistance of the rotor bar while the imaginary component of  $\tilde{Z}_{in}$  is the equivalent reactance of the rotor bar. The equivalent inductance of the rotor bar can be determined utilizing the slip frequency.

$$L_{be} = \frac{Imag(\tilde{Z}_{in})}{S\omega_e} \quad (5.57)$$

The equivalent resistance and inductance of a single rotor bar can now be computed for every value of slip. The values for the leakage inductance and resistance of an individual rotor bar permits the computation of the equivalent circuit parameters  $X_{lr}'$  and  $r_r'$  by the approach of Section 4.15. Items such as rotor end ring resistance, rotor end ring leakage inductance, harmonic leakage and effective rotor to stator turns ratio also need to be considered.

The skin effect algorithm can be simulated in Matlab code and the code is shown at the end of this chapter. The rotor bar of the 250 hp machine example was again used with this process. The stator resistance and leakage inductance, as well as the magnetizing inductances are assumed to be the same as Figure 5.6. In general, the number of layers subdividing the rotor bar must be increased until convergence is guaranteed. In this example at least 10 layers were found to be necessary.

The range of the calculated equivalent rotor resistance over the operating range of the motor was 0.82 to 0.946 ohms and highest at high slip frequencies as expected. The calculated rotor leakage inductance ranges from 0.0197 H under high slip conditions to 0.0198 under small slip conditions.

Steady state torque-speed curves were produced for three cases to determine the effectiveness of the skin effect algorithm. The rotor resistance and rotor leakage inductance is plotted versus slip for each case. The three cases are:

A) Base Case: Same as Figure 5.6.

B) Wide Case: Only the dimensions of the rotor bars are altered. The bars are twice as wide and half as deep compared with the base case. (This is an impractical case since no room is left for the rotor teeth but was chosen simply for purpose of illustration).

C) Deep Case: Only the dimensions of the rotor bars are changed. The bars are twice as deep and half as wide compared with the base case.

The cases were designed to provide the identical rotor resistance under very low slip conditions. The effects of skin effect dramatically increased as the relative depth of the rotor bars increased. The following three figures illustrate how the rotor resistance and rotor leakage inductance change with variations in the bar shape.

In general, the algorithm to incorporate the deep bar effect can be readily implemented in a machine design code since the computations involved for a specific bar shape are relatively straightforward. Alternatively, the computations can be done "off line" and the data inputted to the design program either as a table lookup or a functional polynomial fit to computed curves. The software MATHEMATICA is particularly convenient for computing a polynomial fit. A plot of two frequently used bar shapes are given in Figure 5.11 and Figure 5.12. They can also be used to approximate the frequency dependence for various other bar geometries. Note that skin effect is much more dominant for the coffin shaped bar of Figure 5.12 since the narrow portion of the bar is near the rotor surface. The solution for rotor leakage inductance is somewhat lower than the value predicted from the analytical solution since the effect of the slot leakage inductance in the portion above the bar was neglected in the analytical solution.

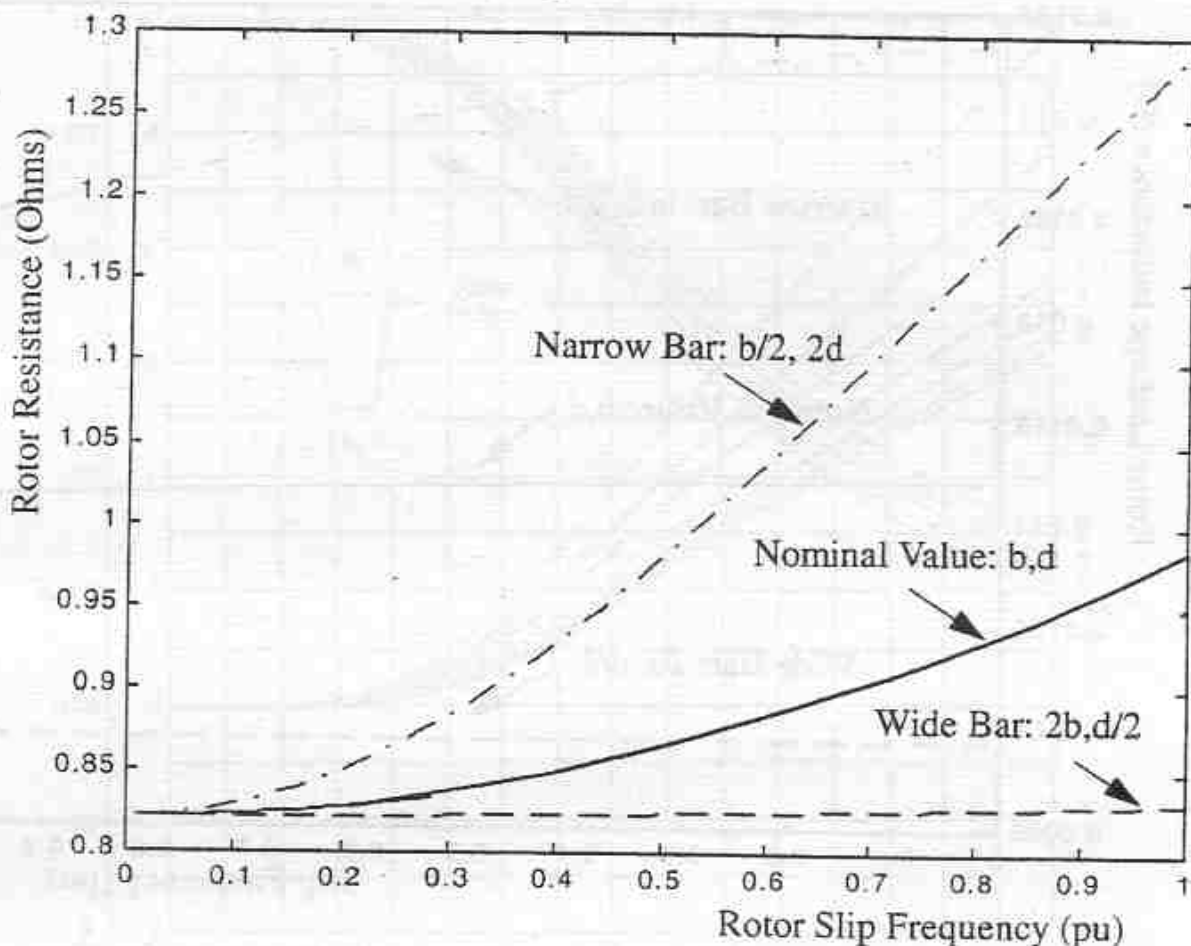


Figure 5.9 Rotor bar resistance vs. slip frequency for three different bar shapes

## 5.6 Categories of Electrical Steels

Electrical steels are generally divided into three categories a) grain oriented (GO) silicon, b) non-oriented (NO) silicon, and c) motor lamination quality (MLQ) steels. GO silicon steels have a strong preferred texture in the rolling direction. The preferred crystal orientation in the rolling direction gives the steel superior magnetic properties in that direction when compared with the transverse direction. This stems from the superior magnetic properties of iron along the crystal lattice cube edge. GO sheets are used in large high efficiency power and distribution transformers and large high speed generator segments.

NO silicon steels have essentially a random texture with nearly isotropic magnetic properties. These steels are used in rotating electric machines such as motors and generators. NO steels are available in semi-processed (SP) and

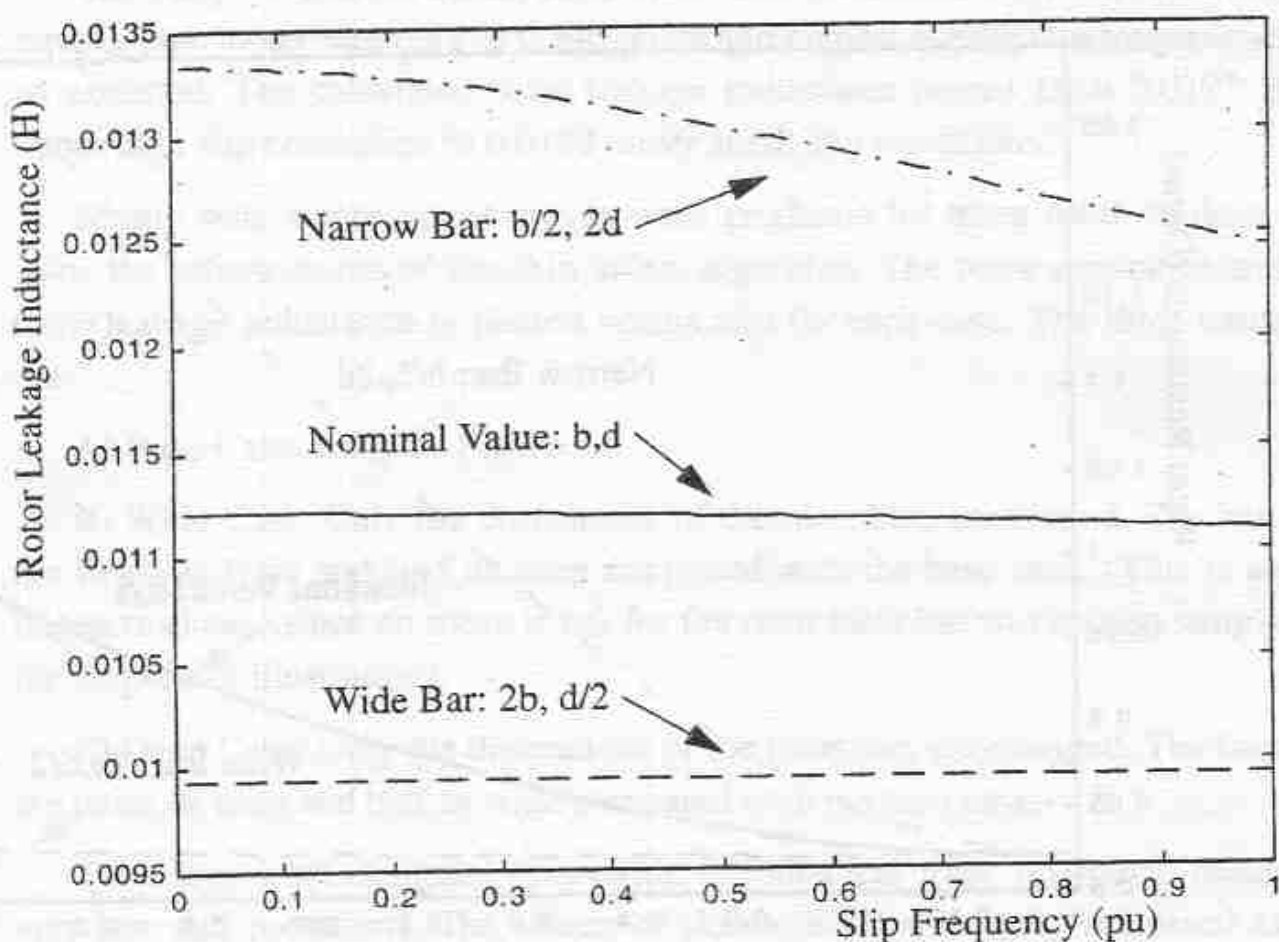


Figure 5.10 Rotor bar leakage inductance vs. slip frequency for three different bar shapes

fully processed (FP) form. End users must anneal SP steels in order to develop the desired magnetic properties. FP steels are shipped from the steel mill fully annealed with fully developed magnetic properties. NO steels generally contain silicon to increase the resistivity of the steel thereby reducing eddy current losses. They are also usually provided with an insulating coating to reduce eddy currents between laminations.

MLQ steels are a subgroup of NO steels. In the 1950s, cold rolled carbon (CRC) steels were used in the cores of fractional horsepower and intermittent duty motors. Use of expensive silicon steels was not justified, since low core losses and high electrical efficiencies, were not deemed important in the small motor industry at that time. Carbon steels had a relatively low cost in comparison to silicon steels, however, their magnetic properties were relatively poor. MLQ steels evolved from the need for an electrical steel that would cost less

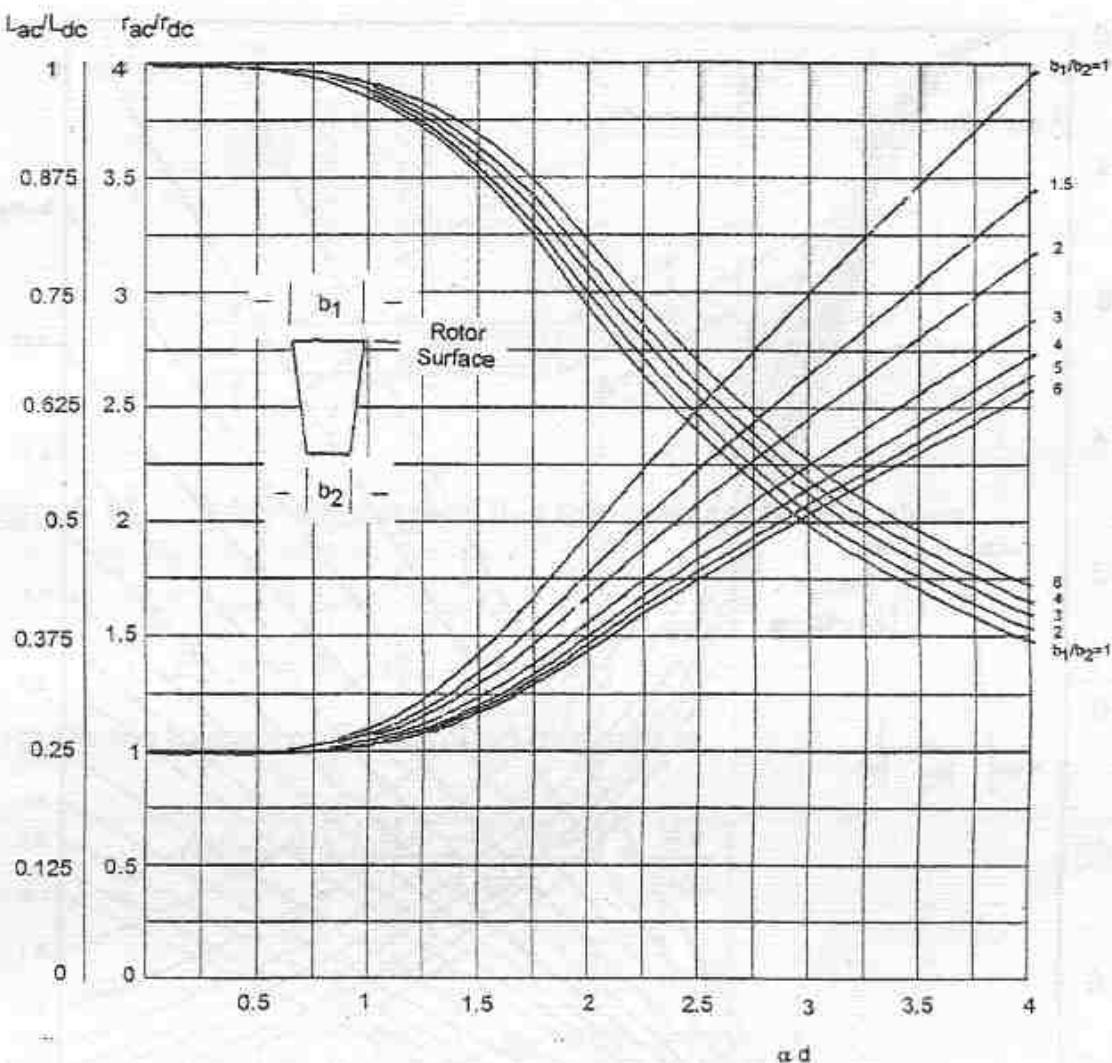


Figure 5.11 Variation of bar resistance and inductance for inverted coffin shaped bar with  $\alpha d$  where  $d$  is the bar depth and  

$$\alpha = \sqrt{(\omega \mu_o)/(2\rho)}$$

## 5.7 Core Losses Due To Fundamental Flux Component

If the magnetic flux density in the core of an ac machine is sinusoidal, two types of losses are produced; eddy current and hysteresis losses. The eddy current loss arises from precisely the same phenomena that results in eddy current losses in conductors. These losses account for the currents which circulate within the laminations of the stator and rotor. These currents are induced by the time varying magnetic field. These currents are again non-uniform and tend to be largest at the surface of the laminations.

The eddy current effect in iron laminations can be understood by reference to Figure 5.13 which shows a thin rectangular conductor impressed with a

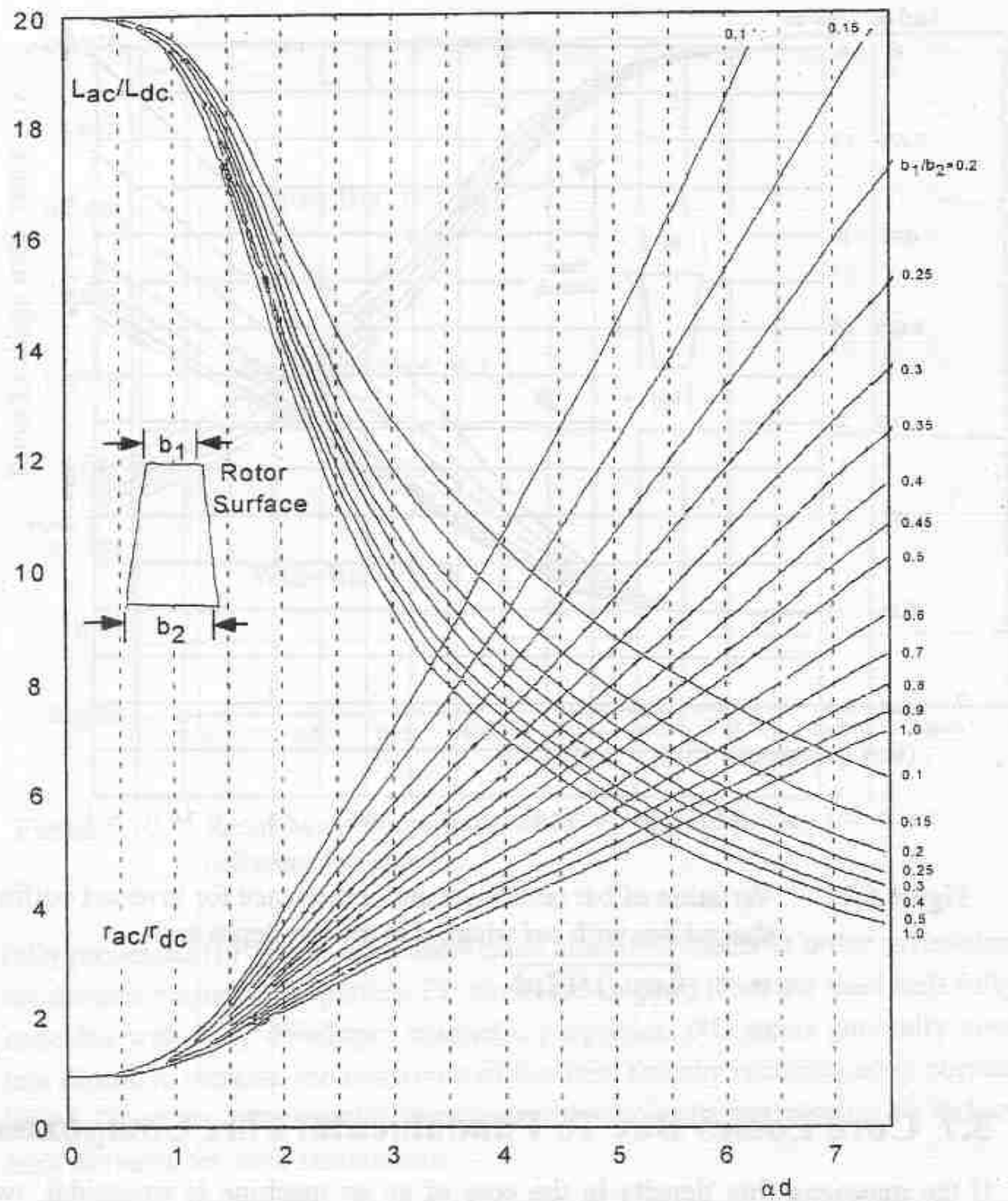


Figure 5.12 Variation of bar resistance and inductance for coffin shaped bar with  $\alpha d$  where  $d$  is the bar depth and  $\alpha = \sqrt{(\omega \mu_o)/(2\rho)}$

sinusoidal flux density  $B_m \sin \omega t$ . The flux enclosed within the current path shown at a distance  $x$  from the center is

$$\Phi(x) = 2x[L - 2(t-x)]B_m \quad (5.58)$$

The amplitude of the voltage induced within this current path is

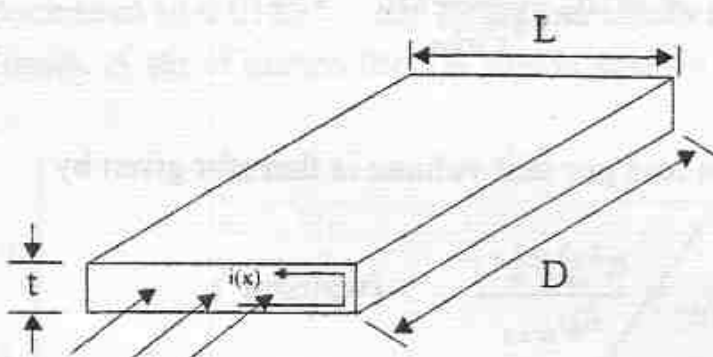


Figure 5.13 Eddy current path in a thin rectangular iron sheet

$$E_m = \omega B_m 2x [L - (t - 2x)] \quad (5.59)$$

The resistance to current flow around this path is

$$dR(x) = \rho \left( \frac{2[L - (t - 2x)]}{Ddx} + \frac{4x}{Ddx} \right) \quad (5.60)$$

or,

$$dR(x) = \rho \left( \frac{2L - t + 8x}{Ddx} \right) \quad (5.61)$$

The corresponding loss is therefore

$$dP_e = \frac{E_m(x)^2}{2dR(x)} = \frac{\omega^2 B_m^2 \{2x[L - (t - 2x)]\}^2 Ddx}{2\rho_{iron}(2L - t + 8x)} \quad (5.62)$$

If  $t$  and  $x$  are small compared to  $L$  then

$$dP_e = \frac{\omega^2 B_m^2 x D L}{\rho_{iron}} dx \quad (5.63)$$

The total eddy current loss in the lamination is

$$P_e = \int_0^t \frac{\frac{1}{2} \omega^2 B_m^2 x^2 D}{\rho_{iron}} dx \quad (5.64)$$

$$= \omega^2 B_m^2 \frac{t^3}{24\rho_{iron}} DL \quad (5.65)$$

The eddy current loss per unit volume is therefore given by

$$p_e = \frac{\pi^2 f_e^2 B_m^2 t^2}{6\rho_{iron}} \quad (\text{watts/m}^3) \quad (5.66)$$

where  $\rho_{iron}$  is the resistivity of the magnetic material,  $B_m$  is the peak flux density,  $f_e$  is the frequency and  $t$  is the thickness of the material. The thickness of the laminations  $t$  is clearly of considerable importance in limiting the eddy current losses since it appears in Eq. (5.66) as a squared term. The eddy current can be controlled by making the laminations very thin. However, the increased cost in assembly together with an increasing penalty in space factor  $k_i$  prevents widespread use of laminations thinner than 0.014" with the thinner laminations generally being preferred for the higher frequency machines such as 400 Hz alternators.

The second type of iron loss, hysteresis loss, accounts for the energy involved in continually reversing the molecular dipoles of the magnetic material. This loss is proportional to the area of the hysteresis loop of the material times the number of times this area is traversed per second, i.e. the frequency. These losses are usually expressed in the form

$$p_h = K_{hys} f_e B_m^{k_{hys}} \quad (5.67)$$

The exponent  $k_{hys}$  is called the Steinmetz coefficient and, during Steinmetz's era, was equal to 1.6. This coefficient of 2 is chosen for convenience for most modern magnetic materials.

The total iron loss is the sum of the hysteresis and eddy current loss and is generally expressed in the form

$$p_i = (K_{hys} f_e + K_f f_e^2) B_m^2 \quad \text{watts/m}^3 \quad (5.68)$$

where the value  $k_{hys}$  has been taken as 2. A plot of the eddy current and hysteresis losses in low carbon, cold rolled steel is given in Figure 5.14 and Figure 5.15. While given in English units recall that 1.0 T. = 64.5 Klines/in<sup>2</sup>. Also in 1 in<sup>3</sup> = 16.387 cm<sup>3</sup>. Note that when the lamination thickness is 0.025", the

eddy current loss is about 50% greater than the hysteresis loss. When the lamination thickness decreased to 0.0185" the hysteresis losses begin to exceed the eddy current losses. A set of curves for 3% silicon steel is given in Figure 5.16.

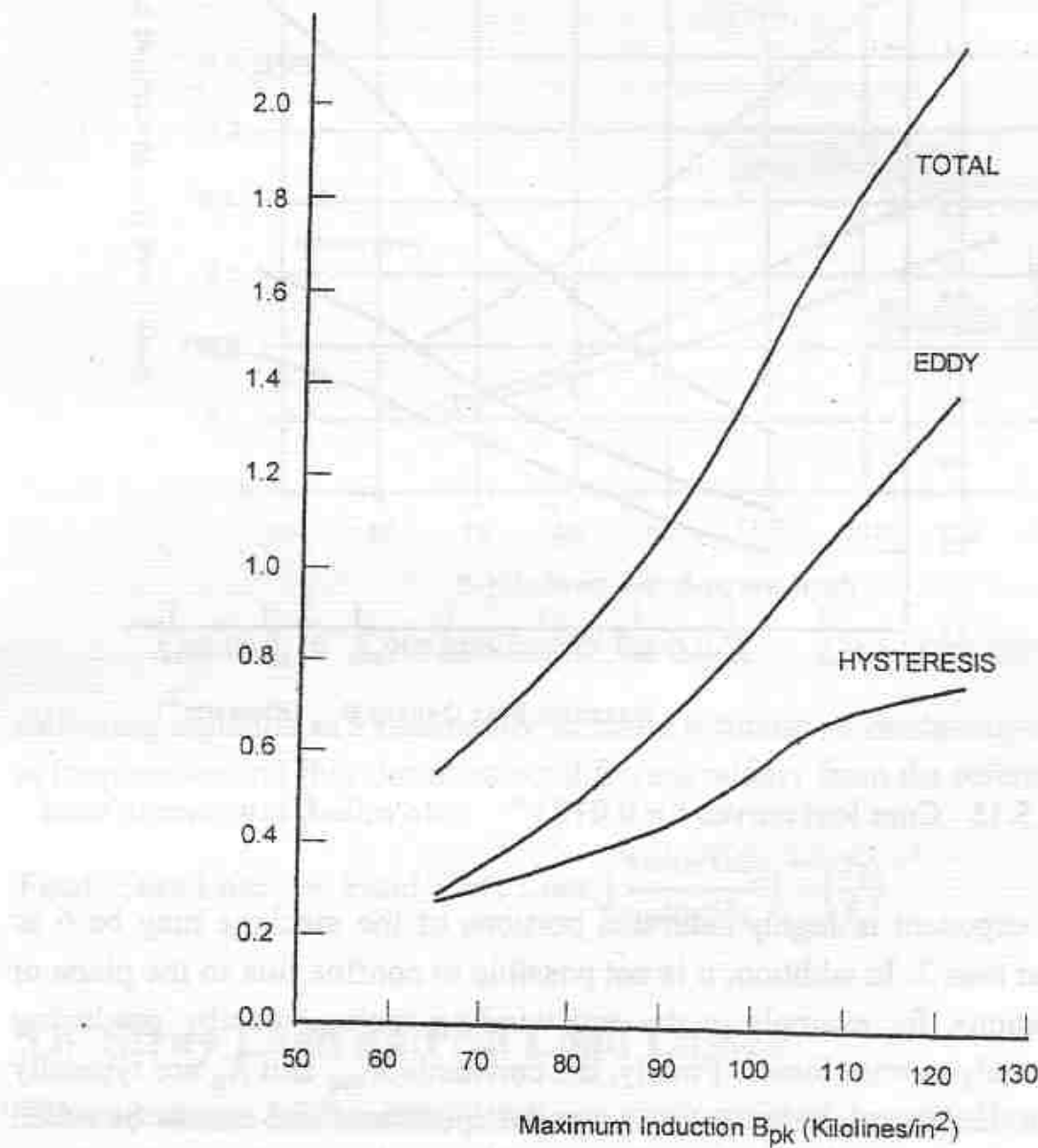


Figure 5.14 Core loss curves for 0.025" cold rolled, low carbon steel

Calculations of iron losses with the aid of Eq. (5.68) unfortunately give good values only in the case of transformers and the like and not in the case of electric machinery. The reason for this problem is that space harmonics produce flux densities whose rate of rise,  $dB/dt$ , is much greater than that of a sine wave of the same flux density. This causes the eddy current losses to rise much faster than simply the square of the fundamental component of flux density and

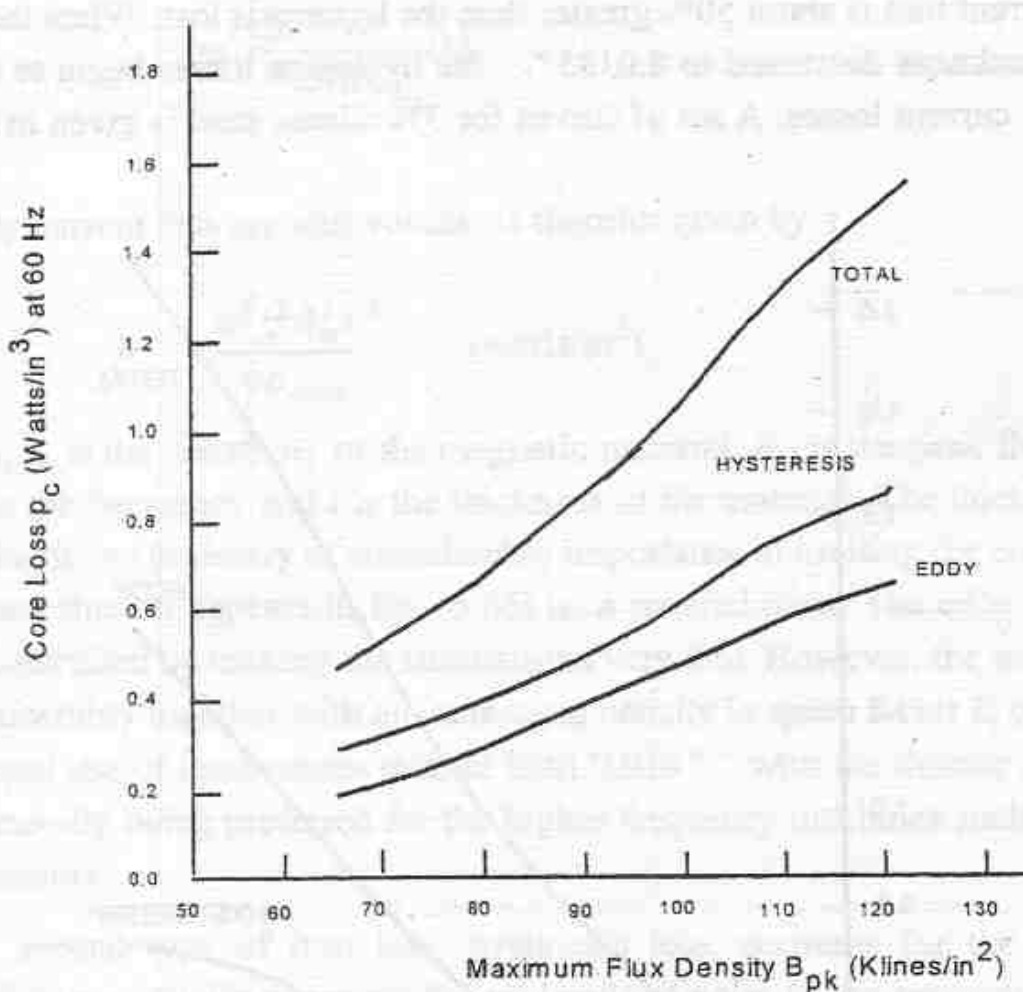


Figure 5.15 Core loss curves for 0.0185" cold rolled, low carbon steel.

the actual exponent in highly saturated portions of the machine may be 6 or more rather than 2. In addition, it is not possible to confine flux to the plane of the laminations, for example in the end winding region, thereby producing additional eddy current losses. Finally, the constants  $K_{hys}$  and  $K_e$  are typically obtained in the laboratory by testing prepared specimens and cannot be relied upon as the losses build up in cores of actual machines. Additional losses are encountered which include burrs on edges of stamping causing contact between lamination and attendant eddy current losses. Localized stresses in the lamination sheets, for example near bolt holes and at the surface of the teeth due to the punching process, cause increased hysteresis losses in these regions. These effects are generally accounted for by adding on an extra 30 to 40% to the losses measured from laboratory specimens. Additional losses can influence the efficiency of a small induction machine by as much as 2.5%. If accurate measurements are made at one level of flux density and frequency the

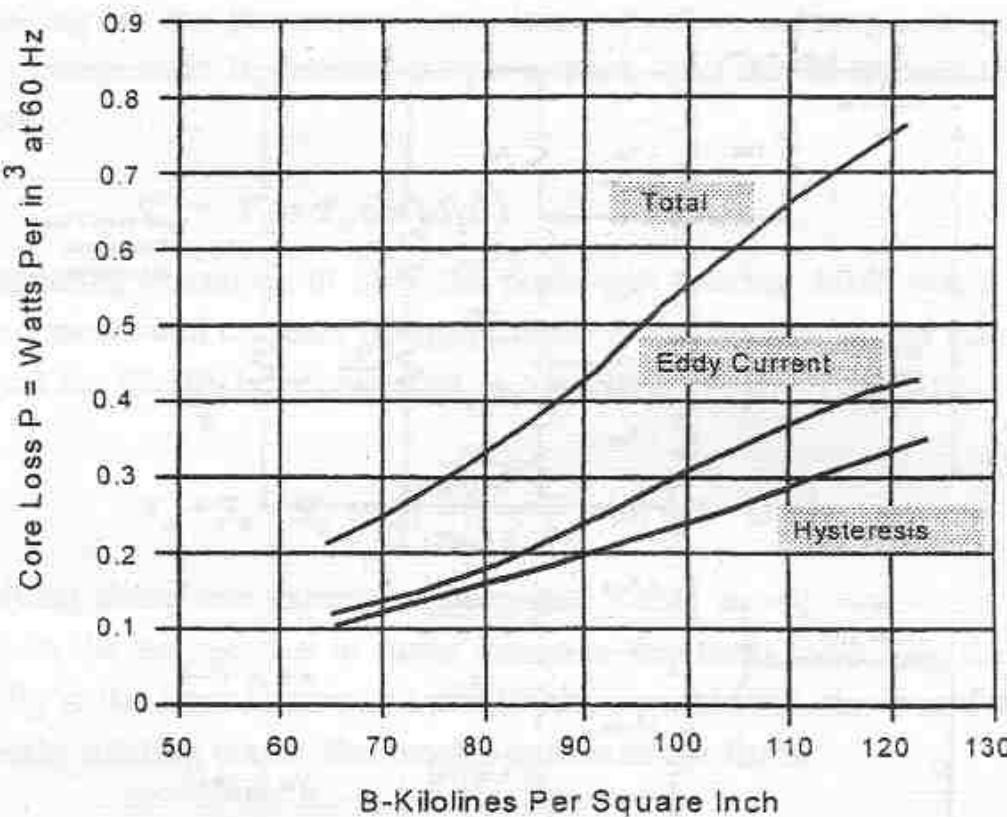


Figure 5.16 Core loss curves for 0.025 " 3% silicon steel.

following equation is a reasonably accurate estimate of fundamental core loss at frequencies and flux densities not differing widely from the reference value,

$$\text{Fund. Core Loss}_2 = \text{Fund. Core Loss}_1 \left( \frac{\text{volts/Hz}_2}{\text{volts/Hz}_1} \right)^{2.5} \left( \frac{f_2}{f_1} \right)^{1.4} \quad (5.69)$$

## 5.8 Stray Load and No Load Losses

The calculation of the stray load and stray no-load losses of an induction machine is a very complex problem which deals precisely with the issues that we have been so far able to avoid in our study, namely the fact that the rotor and stator surfaces are slotted and not smooth and also the fact that the windings are located in these slots and therefore result in *MMF* harmonics higher than the first harmonic. Calculation of such loss phenomena is typically done with the aid of a more detailed equivalent circuit than we are accustomed to, shown on Figure 5.17.

In order to gain an appreciation for the complexity involved let us discuss briefly the significance of the various terms in this equivalent circuit.

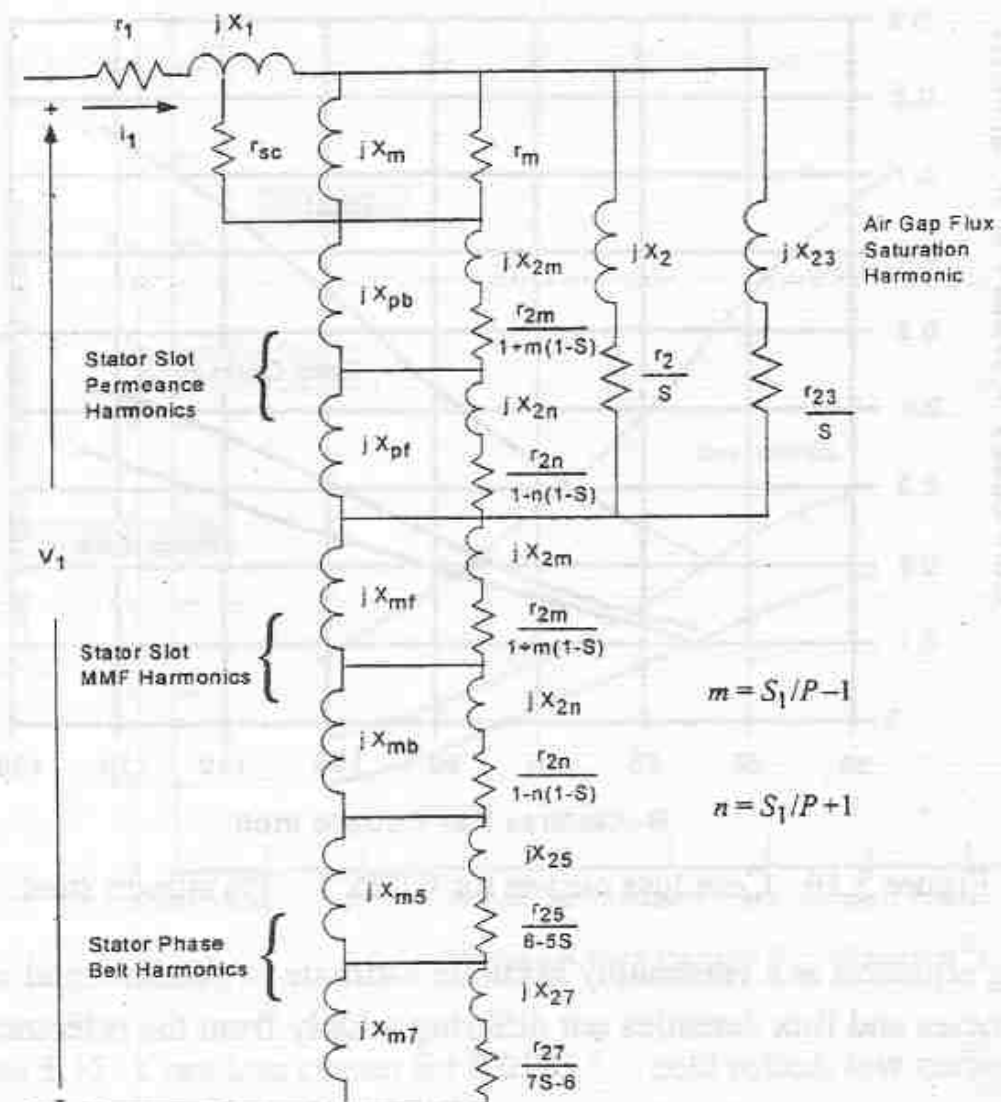


Figure 5.17 General equivalent circuit of a polyphase induction motor

a) *Permeance Variation Loss.* When two magnetic surfaces, one slotted and one smooth, with an MMF across the gap between them, move relative to each other, the smooth surface sees a locally varying magnetic field due to the periodic permeance variations caused by the slots in the opposite surface. The permeance amplitude variation is related to the geometry of the slots and the frequency from the speed of rotation. In particular, the stator slot openings causes a current to flow in the rotor bars which results in an ohmic loss. The current which flows in the rotor is limited primarily by the reactance of the rotor bars which is much larger than its resistance. In addition to the copper losses, the permeance variation of the stator slots also cause eddy currents to flow in the rotor iron laminations causing additional losses. When the rotor as well as the stator is slotted, these additional losses occur in both the stator and rotor teeth. The problem is represented in the circuit by two meshes obtained

by breaking up the permeance wave into a positive rotating and a negative rotating component. In general, the permeance wave can be represented by the function

$$\mathcal{P}_s = \mathcal{P}_0 + \mathcal{P}_1 \cos(S_1 \theta) \quad (5.70)$$

Restricting ourselves to only the positively rotating *MMF* wave, then, if balanced sinusoidal currents flow, the fundamental component of stator *MMF* can, from Eq. (2.70), be represented as a travelling wave of the form,

$$\mathcal{F}_a + \mathcal{F}_b + \mathcal{F}_c = \frac{3}{2} \left( \frac{4}{\pi} \right) \left( \frac{N_t I_m}{CP} \right) \sin \left( \frac{P}{2} \theta - \omega_e t \right) \quad (5.71)$$

Multiplying these two expressions together yields an expression for the flux rotating in the air gap due to stator currents. The term containing the permeance  $\mathcal{P}_0$  is the normal constant amplitude, sinusoidally distributed and synchronously rotating wave. The second term is of the form,

$$\Phi_p = \Phi_m \sin \left( \frac{P}{2} \theta - \omega_e t \right) \cos(S_1 \theta) \quad (5.72)$$

where

$$\Phi_m = \frac{3}{2} \left( \frac{4}{\pi} \right) \left( \frac{N_t I_m}{CP} \right) \mathcal{P}_1 \quad (5.73)$$

This expression can be expanded to form

$$\Phi_p = \frac{\Phi_m}{2} \left[ \sin \left( \frac{P}{2} \theta - \omega_e t + S_1 \theta \right) + \sin \left( \frac{P}{2} \theta - \omega_e t - S_1 \theta \right) \right] \quad (5.74)$$

The first term represents a wave which is travelling backward with respect to the synchronously rotating main flux wave but yet in the forward direction at an electrical angular speed of  $\omega_e / (1 + (2S_1)/P)$ . The second term corresponds to a wave which is travelling backwards at a speed of  $\omega_e / ((2S_1)/P - 1)$ . The slip corresponding to the forward travelling wave is

$$S_f = \frac{\omega_e / (1 + (2S_1)/P) - \omega_r}{\omega_e / (1 + (2S_1)/P)}$$

$$= 1 - \left( 1 + \frac{(2S_1)}{P} \right) (1 - S) \quad (5.75)$$

where  $S$  is the slip corresponding to the fundamental component. In a similar manner it can be readily determined that the slip for the backward travelling wave is

$$S_b = 1 + \left( \frac{2S_1}{P} - 1 \right) (1 - S) \quad (5.76)$$

The harmonic components of the pulsating gap flux density over each tooth can be found from the same conformal mapping solution used to obtain the Carter Factor discussed in Chapter 3. This theory assumes that each tooth is excited by an MMF which can be treated as essentially a constant over one tooth pitch. The appropriate constant can be taken as the average value of the flux density estimated at the center line of the slot in question after the fundamental component has been removed as shown in Figure 5.18. The presence of

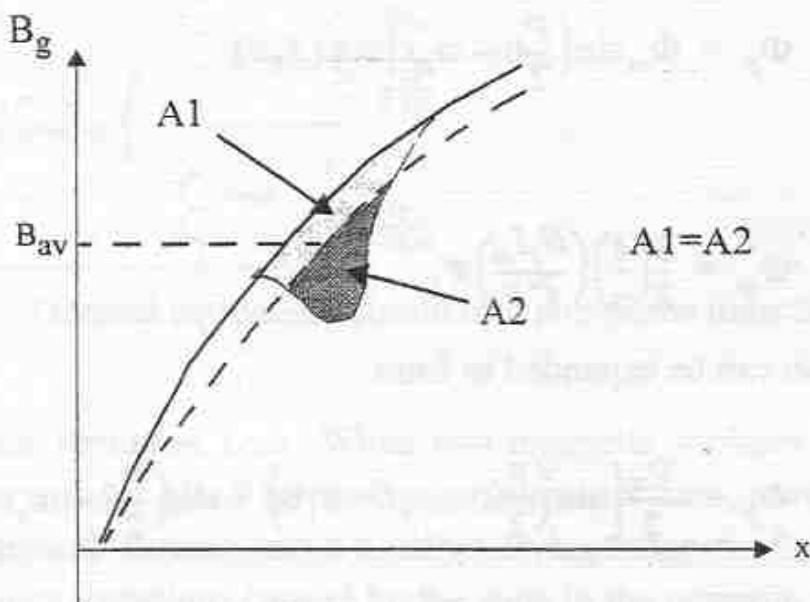


Figure 5.18 Illustrating method for choosing average flux density over each tooth span

the slot clearly causes the flux to dip over the center line of the slot opening causing harmonics in the flux waveform as well as the decrease in the average flux previously discussed. The first three slot harmonic components of flux in the gap are given in Figure 5.19 as a function of the slot opening to tooth pitch

ratio. The quantity  $\beta$  in this figure is one-half the peak to peak pulsation in the

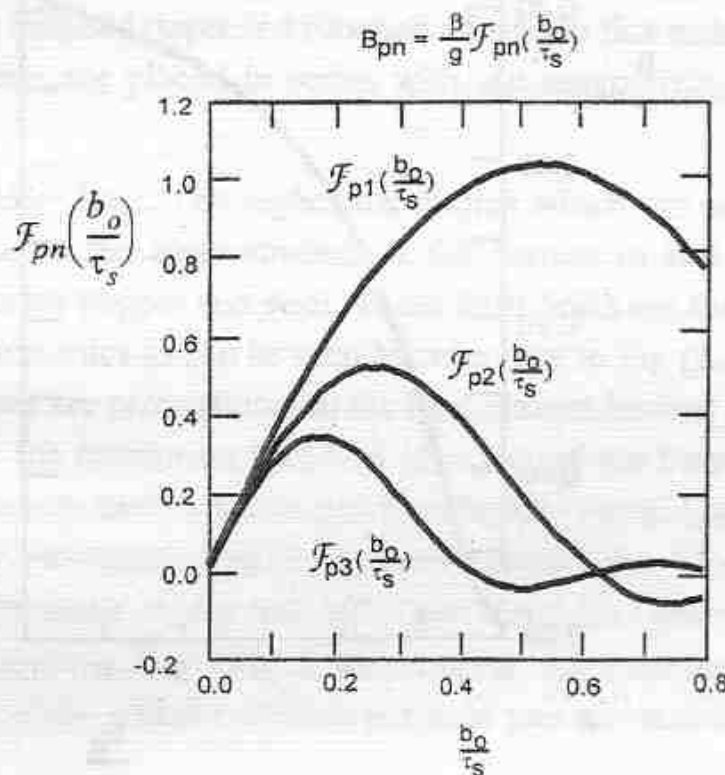


Figure 5.19 First three harmonics of slot ripple flux density

flux over one tooth divided by the maximum flux and is plotted in Figure 5.20. These harmonics relate to the Fourier coefficients of the slot pulsation and should not be confused with the fundamental component of the useful flux  $B_{gl}$ .

The permeance  $P_1$  in Eq. (5.70) can be obtained from Figure 5.19. Since the amplitude of the flux  $\Phi_m$  in Eq. (5.73) is, in general

$$\Phi_m = B_{p1} A_{s+t} = B_{p1} \tau_s l_e \quad (5.77)$$

and, from Figure 5.19,

$$\Phi_m = \frac{\beta}{g} F_{p1}\left(\frac{b_o}{\tau_s}\right) \tau_s l_e \quad (5.78)$$

whereupon,

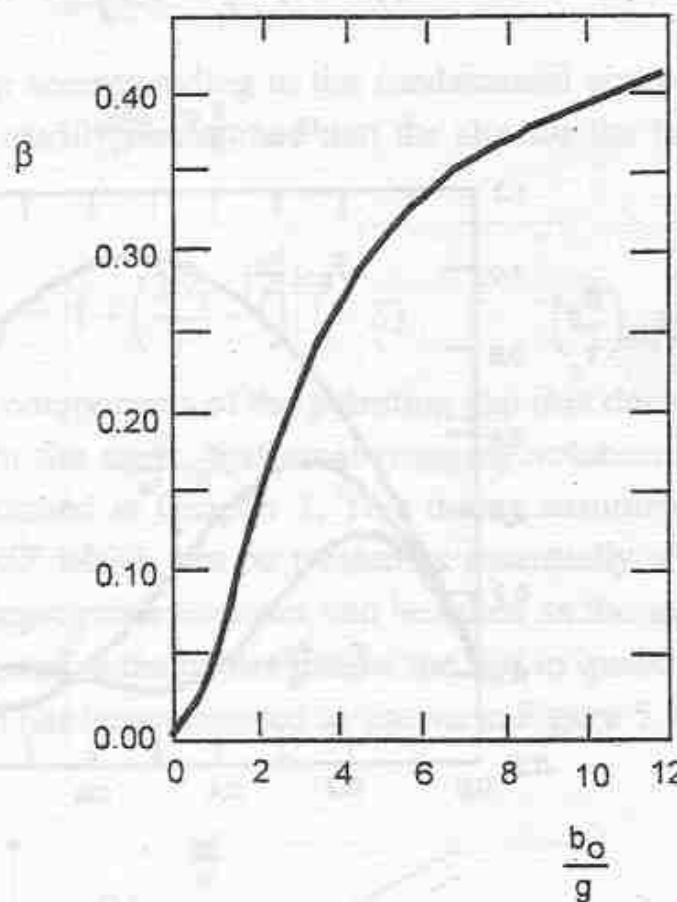


Figure 5.20 Parameter  $\beta$  as a function of the ratio of slot opening to the air gap length

$$\mathcal{P}_1 = \frac{\Phi_m}{\mathcal{F}_{p1}} = \beta \frac{\tau_s l_s}{g} \quad (5.79)$$

The effect of the slot permeance harmonics can be incorporated into the per phase equivalent circuit as shown in Figure 5.17. The quantity  $X_{pb}$  in Figure 5.17 represents the reactance corresponding to the voltage generated at the air gap by the backward traveling permeance harmonic ( $m = S_1/P - 1$ ). This reactance is obtained by converting the permeance of one slot to a phase inductance by the same procedure used to obtain the slot leakage inductance, Eq. (4.41). The elements acted upon by that voltage have values equal to the reactance  $X_{2m}$  and the resistance  $r_{2m}$ . The quantity  $X_{2m}$  is the reactance which limits the flow of current in the squirrel cage rotor. The resistance  $r_{2m}$  is the resistance in series with  $X_{2m}$  which is used to calculate the permeance harmonic loss. These two quantities are obtained in the same manner as used to

obtain  $X_2$  and  $r_2$  in Section 4.15. However, the frequency dependence due to deep bar effect as in Section 5.5 is clearly necessary. The quantities  $X_{pf}$ ,  $X_{2n}$  and  $r_{2n}$  have the same meaning for the forward traveling permeance harmonic. Since the slot induced ripple is a function of air gap flux rather than current, the circuit elements are placed in series with the magnetizing branch of Figure 5.17.

b) *Slot MMF Loss.* The higher harmonics which are present in the *MMF* waveform due to the concentration of the current in stator slots also cause losses in the rotor copper and steel. These harmonics are the same order as the permeance harmonics as can be seen by reference to Eq. (2.32). The slot *MMF* harmonic losses are proportional to the load current instead of the magnetizing current, since the harmonics involved arise out of the Fourier analysis of the *MMF* wave as opposed to the air gap flux density wave. Losses again occur in both the rotor conductors and in the rotor laminations. The problem is again analyzed by breaking up the slot *MMF* harmonic into positive and negatively rotating components. The result is very similar since the slot harmonic *MMFs* are multiples of the number of slots per pole pair as were the permeance harmonics.

The reactance  $X_{mb}$  represents the voltage which is generated by the backward traveling slot *MMF* harmonic ( $m = S_1 / P - 1$ ). The quantity  $X_{2m}$  is again the zigzag reactance which limits the flow of current acted upon by the *MMF* harmonic voltage. The term  $r_{2m}$  is the series resistance which accounts for the losses. The combination  $X_{2m}$  and  $r_{2m}$  are present in both cases since physically, the squirrel cage is acted upon by harmonics of the same order from two different sources, namely the permeance variations and the steps in the *MMF* wave. In this case the circuit elements must be placed in series with the stator resistance and inductance since these losses are clearly dependant on the amplitude of the stator *MMF*.

c) *Phase Belt Harmonic Losses.* It has been mentioned in Chapter 4 that a leakage reactance for higher harmonics of the stator *MMF* do not exist for squirrel cage machines since the cage acts to short out these harmonic fluxes. The flow of this current does, however, produce losses and account is taken of its effect in the form of phase belt harmonic losses. In Figure 5.17  $X_{m5}$  represents the fifth harmonic voltage generated by the stator phase belt. The quantity  $X_{m7}$  represents the seventh harmonic voltage generated. Because the phase belt harmonics fall off rapidly, *MMF* harmonics between the fifth and seventh

and the stator slot harmonic are typically neglected. The reactances  $X_{25}$  and  $X_{27}$  limit the current that flows due to the phase belt harmonics and  $r_{25}$  and  $r_{27}$  are used to calculate the phase belt harmonic losses. Since the wave travels backward and has five times the number of poles as the fundamental, the harmonic slip for the fifth harmonic is

$$\begin{aligned} S_5 &= \frac{\frac{\omega_e + \omega_r}{5}}{\frac{\omega_e}{5}} \\ &= 1 + 5 \frac{\omega_r}{\omega_b} \\ &= 6 - 5S \end{aligned}$$

The corresponding result is easily obtained for the positively rotating seventh harmonic wave. The relevant 5<sup>th</sup> and 7<sup>th</sup> harmonic inductances can be calculated from Eq. (4.116).

*d) Saturation Induced Loss* This loss occurs as a result of the fact that the air gap flux density is typically non-sinusoidal as a result of saturation, typically in the teeth. As a result, the flux density has a significant third harmonic component (and other odd harmonics) which, in turn, cause currents to flow in the rotor cage. Since these harmonics necessarily rotate synchronously with the fundamental component they are different from the slot harmonic which rotate at sub-synchronous speeds. A treatment of saturation induced losses and the equivalent circuit parameters for this case is discussed in Ref. [9].

## 5.9 Calculation of Surface Iron Losses Due to Stator Slotting

The problem concerned with loss in the iron due to the effect of slotting can be visualized by referring to Figure 5.21(a) in which the air gap flux density is plotted as a function of the gap periphery. The average value for each slot pitch associated with the dc offset in Figure 5.21(b) is accounted for by Carter's Coefficient. An approximation to the air gap slot ripple flux density using only the first harmonic of the ripple obtained from Figure 5.18 is sketched in Figure

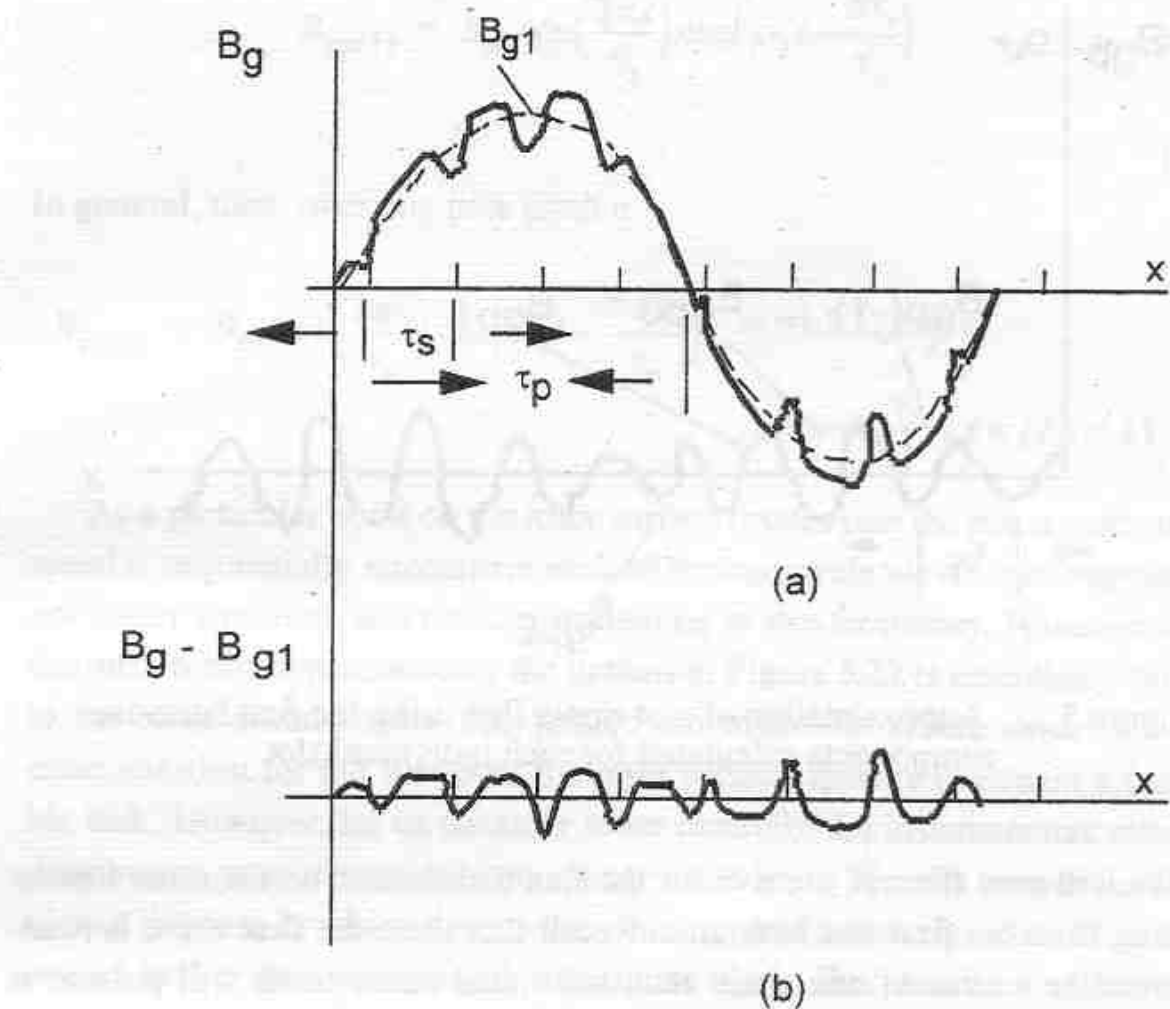


Figure 5.21 (a) Air gap flux density distribution along the air gap periphery neglecting the higher *MMF* harmonics, (b) flux density distribution with the fundamental component (useful component) removed.

5.22. The air gap flux is assumed to be essentially sinusoidal but perturbed by the effect of stator slotting. The rotor surface is assumed smooth initially. Note that the *MMF* harmonics have been neglected here since they will be accounted for separately. If we subtract the fundamental component from this waveform slot ripple field of Figure 5.21(b) results. It can be observed that the slot ripple field varies somewhat from slot to slot since the ripple component in a particular tooth is related to the average flux density over the tooth span encompassing that tooth. The waveform shown in Figure 5.21(b) is given for only one time instant and each tooth eventually takes on the slot ripple waveform of all the individual teeth shown in Figure 5.21 as the fundamental flux rotates around the air gap.

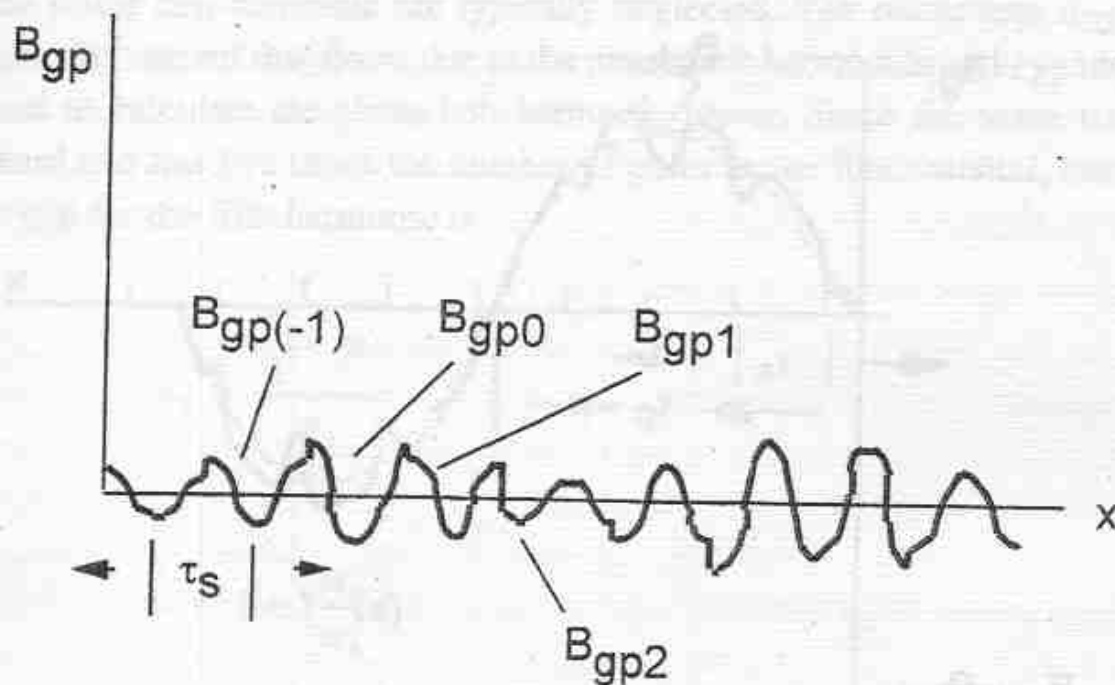


Figure 5.22 Approximation of slot ripple flux using the first harmonic components calculated for each individual slot

We will now attempt to solve for the flux distribution on the rotor surface resulting from the first slot harmonic. Recall that since the flux wave is rotating, over the course of one cycle each individual stator tooth will pulsate at each of the "half cycle" waveforms of Figure 5.21(b). In fact, this amplitude variation of the flux pulsation varies smoothly in time. The pulsating flux which occurs over one stator tooth pitch due to the first slot harmonic can therefore be written in the form

$$B_{gp0} = B_{p1} \cos\left(\frac{2\pi x}{\tau_s}\right) \cos(\omega_e t) \quad -\tau_s/2 < x < \tau_s/2 \quad (5.80)$$

where  $B_{p1}$  corresponds to the ripple flux density obtained over the slot having the peak gap fundamental flux density. Equation (5.80) states that the flux density in the gap is sinusoidally distributed in space but pulsates in time at line frequency. The pulsating component of flux density in the gap over any of the other stator teeth is the same as Eq. (5.80) but phase shifted in time by the appropriate number of slot pitches. For example the flux density over the adjacent tooth in the direction of flux rotation is

$$B_{gp(1)} = B_{p1} \cos\left(\frac{2\pi x}{\tau_s}\right) \cos\left(\omega_e t - \frac{\pi\tau_s}{\tau_p}\right) \quad \tau_s/2 < x < 3\tau_s/2$$

(5.81)

In general, then, over any pole pitch  $n$

$$B_{gp(n)} = B_{p1} \cos\left(\frac{2\pi x}{\tau_s}\right) \cos\left(\omega_e t - \frac{m\pi\tau_s}{\tau_p}\right) \quad m=1,2,\dots,2\tau_p/\tau_s$$

$$(2n-1)\frac{\tau_s}{2} < x < (2n+1)\frac{\tau_s}{2}$$

(5.82)

As a particular point on the rotor surface rotates past the stator teeth at rotor speed it sequentially encounters each of the one cycle waveforms representing one stator slot pitch at a rate corresponding to slip frequency. However should the rotor rotate synchronously the pattern of Figure 5.22 is essentially "locked" to the rotor surface since this pattern too rotates at synchronous speed. An exact solution for the flux over the rotor surface appears to remain a formidable task. However, let us consider more carefully the instantaneous rotor flux distribution considering only one stator tooth span. We will choose for convenience the case in which the rotor is rotating synchronously. We will select the region under the tooth having maximum ripple flux density (tooth 0 corresponding to Eq. (5.80)) as the region of interest.

At  $t = 0$  the location of a small rotor surface area is assumed to be centered under tooth 0 as shown in Figure 5.23(a). The harmonic ripple flux density is instantaneously a minimum at this point. At time  $t = \pi\tau_s / 2\omega_e\tau_p$  this increment of rotor surface has moved midway between teeth 0 and 1 as shown in Figure 5.23(b). The harmonic ripple flux density is clearly a maximum at this instant. When  $t = \pi\tau_s / \omega_e\tau_p$ , the increment of surface has moved under tooth #1 as in Figure 5.23(c). It appears as if the increment has moved onto another (somewhat lower) "cycle" of Figure 5.22. However, it can be recalled that the rotor is moving synchronously with the stator excitation. Therefore, at this instant the windings in slot #1 are loaded with precisely the same value of current as existed in slot #0 at time  $t = 0$ . The same argument holds for each progressive slot pair. For example, the current in slot #2 is now the same as what appeared in slot #1 at  $t = 0$ . Hence, the flux density penetrating the incremental surface area under consideration has therefore returned to the same value as what existed previously at  $t = 0$ . The flux density in effect continuously cycles over the same sinusoidal waveform as illustrated in Figure 5.24. Since the rotor

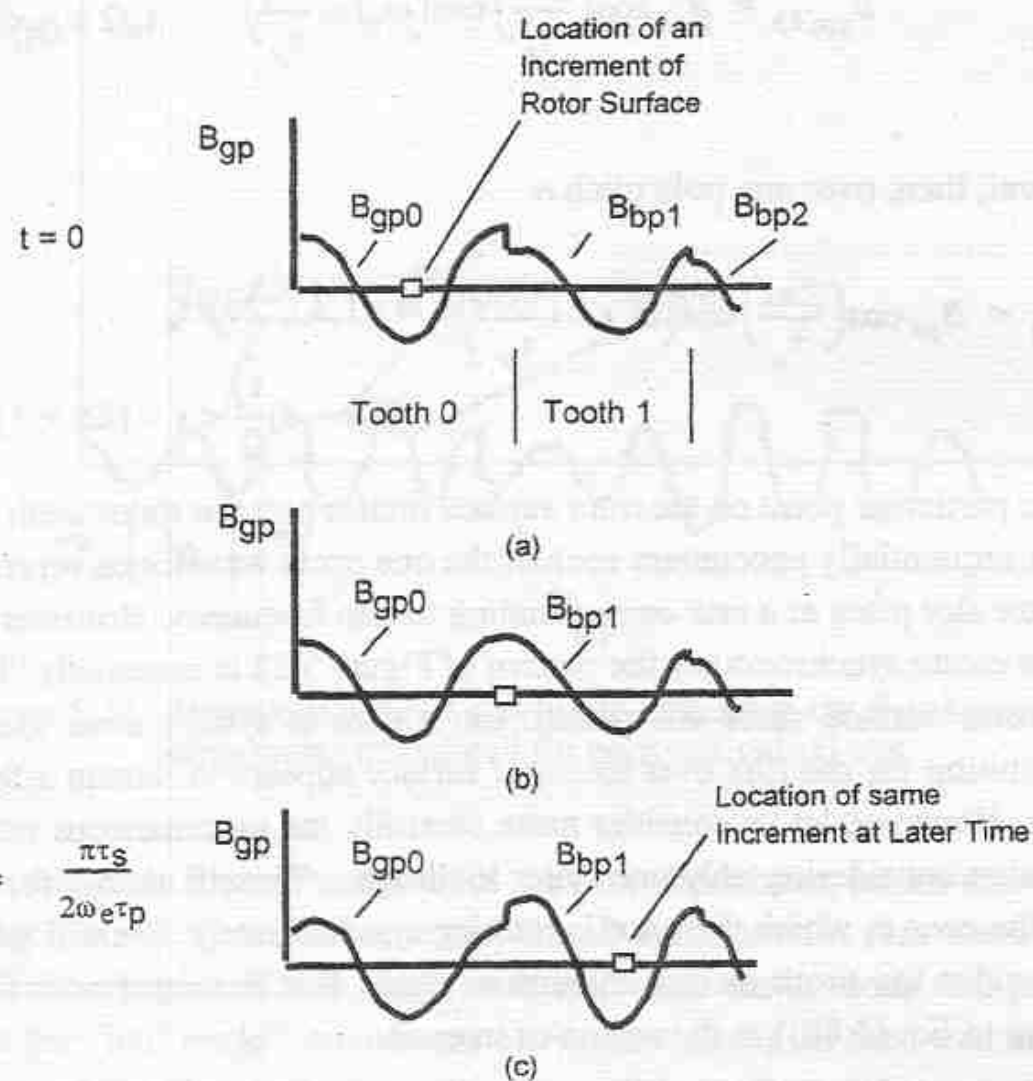


Figure 5.23 Increment of rotor surface moving between two stator slots.  
 (a) alignment at  $t = 0$  and corresponding flux density distribution, (b) alignment at an intermediate point, (c) alignment at  $t = (P\pi)/(ω_e S_1)$

surface immediately to the left of our sample increment experiences the same variation only slightly delayed in time it follows that this effect can be interpreted as a traveling wave impinging on the rotor surface of the form

$$B_{gp1} = B_{p1} \cos \left[ \frac{2S_1}{P} \left( \omega_e t - \frac{\pi x}{\tau_p} \right) \right] \quad (5.83)$$

Let  $x$ ,  $y$  and  $z$  denote the tangential, radial and axial directions of an equivalent cartesian coordinate system. The solution for the flux density in the rotor iron is described by the Maxwell Equation

$$\nabla \times \bar{B} = \bar{J}/\mu_i \quad (5.84)$$

Since  $B$  is directed radially, this would imply that a current density is induced in the axial direction. However, since the iron is laminated, current cannot flow in this direction (except for eddy currents which we will assume are sufficiently small that they do not materially affect the field). Hence, the  $z$  (axial) component of Eq. (5.84) becomes

$$\frac{\partial}{\partial y} B_{px} - \frac{\partial}{\partial x} B_{py} = 0 \quad (5.85)$$

Due to symmetry we can deduce that the  $z$  component of  $B$  is zero and, since the flux density is everywhere continuous

$$\nabla \cdot \bar{B} = 0$$

or

$$\frac{\partial}{\partial x} B_{px} + \frac{\partial}{\partial y} B_{py} = 0 \quad (5.86)$$

If we differentiate Eqs. (5.85) and (5.86) with respect to  $x$  and subtract the result, we can obtain the following

$$\frac{\partial^2}{\partial x^2} B_{px} + \frac{\partial^2}{\partial y^2} B_{px} = 0 \quad (5.87)$$

If Eqs. (5.85) and (5.86) are differentiated with respect to  $y$  and added, one obtains

$$\frac{\partial^2}{\partial x^2} B_{py} + \frac{\partial^2}{\partial y^2} B_{py} = 0 \quad (5.88)$$

The form of these equations clearly suggests a harmonic solution. Since the flux density must be continuous across the rotor surface, then if increasing  $y$  denotes penetration into the rotor

$$B_{py}(y)|_{y=0} = B_{py}(0) = B_{p1} \cos \left[ \frac{2S_1}{P} \left( \omega_e t - \frac{\pi x}{\tau_p} \right) \right] \quad (5.89)$$

We will therefore assume that for any point  $x, y$  within the rotor body

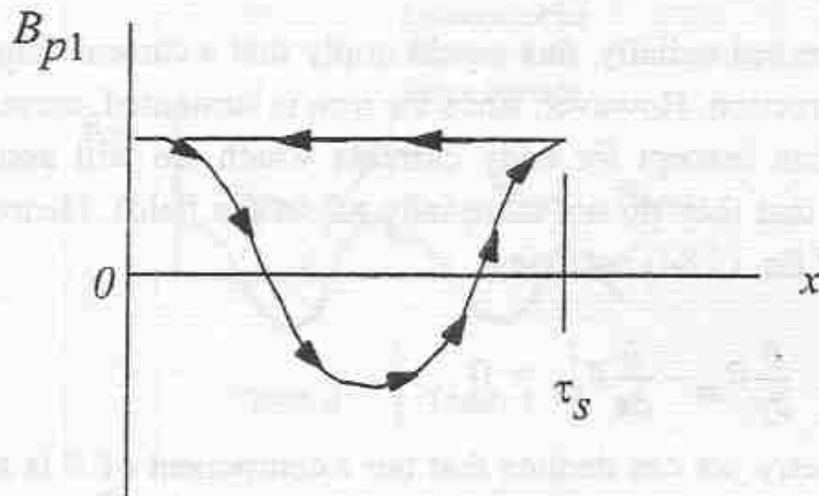


Figure 5.24 Illustrating cyclic motion of flux density over an increment of rotor surface

$$B_{py}(x, y) = B_{p1} b_y(y) \cos \left[ \frac{2S_1}{P} \left( \omega_e t - \frac{\pi x}{\tau_p} \right) \right] \quad (5.90)$$

Substituting this expression in Eq. (5.88), performing the indicated differentiation and simplifying we have

$$\frac{\partial^2}{\partial y^2} b_y(y) - \left[ \left( \frac{2S_1}{P} \right) \frac{\pi^2}{\tau_p^2} \right] b_y(y) = 0 \quad (5.91)$$

Since  $B_{py}(x, y) \rightarrow 0$  as  $y \rightarrow \infty$ , the solution of Eq. (5.91) is of the form

$$b_y(y) = e^{-\left(\frac{2S_1\pi}{P\tau_p}y\right)} \quad (5.92)$$

Hence,

$$B_{py}(x, y) = B_{p1} e^{-\left(\frac{2S_1\pi}{P\tau_p}y\right)} \cos \left[ \frac{2S_1}{P} \omega_e t + \frac{\pi x}{\tau_p} \right] \quad (5.93)$$

From Eq. (5.85) we can readily establish that

$$B_{px}(x, y) = B_{p1} e^{-\left(\frac{2S_1\pi}{P\tau_p}y\right)} \sin \left[ \frac{2S_1}{P} \omega_e t + \frac{\pi x}{\tau_p} \right] \quad (5.94)$$

It is useful to define the *penetration constant*

$$\begin{aligned} d_e &= \frac{\tau_p}{\pi} \frac{P}{2S_1} \\ &= \frac{\tau_s}{2\pi} \end{aligned} \quad (5.95)$$

It can be noted that the fields  $B_{px}$  and  $B_{py}$  are everywhere  $90^\circ$  out of phase. Therefore the amplitude of the field at a point  $x, y$  inside the rotor is

$$B_{r0}(x, y) = \sqrt{2} B_{p1} e^{-\frac{y}{d_e}} \quad (5.96)$$

which indicates that the flux density is everywhere uniform with  $x$  (tangential direction) but decreases exponentially with  $y$  (radial direction into the rotor). It can be recalled that when the rotor is rotating synchronously, Eq. (5.96) applies only over the stator slot pitch corresponding to maximum (and negative maximum) flux density. The subscript 0 in Eq. (5.96) is used to remind us that the solution applies to a stator slot pitch of the rotor material spanned by the pitch stator tooth 0 in Figure 5.24.

If  $d_e$  is used as an equivalent skin depth, the losses in the rotor can be written as the loss density times the rotor volume in question. Recall from Section 5.5 that the iron losses vary as the flux density squared. Hence, the loss for this particular portion of the rotor surface is

$$P_{r0} = \left( \frac{2\pi D_{or}}{S_1} \right) k_{ir} l_i d_e \left( \frac{B_{p1}}{B_{g1}} \right)^2 C_{ir} \quad (5.97)$$

where  $l_i$  is the length of rotor iron,  $k_{ir}$  is the packing factor for rotor iron,  $B_{g1}$  is the peak value of fundamental flux density in the gap and  $C_{ir}$  is the loss per unit volume of the rotor magnetic material measured at the value  $B_{g1}$  and at frequency  $(2S_1 / P)(\omega_e / 2\pi)$ .

The losses can be obtained over other stator pole pitches by the same manner. Since the average flux density over adjacent teeth vary sinusoidally, so also does the ripple flux density. The solution for the other teeth can be written by inspection. For example, for tooth #1

$$B_{r1} = \sqrt{2} B_{p1} \cos\left(\frac{\pi P}{S_1}\right) e^{\frac{-y}{d_e}} \quad (5.98)$$

The losses for this portion of the rotor are

$$P_{r1} = \left(\frac{2\pi D_{or}}{S_1}\right) k_{ir} l_i d_e \left(\frac{B_{p1}}{B_{g1}}\right)^2 \cos^2\left(\frac{\pi P}{S_1}\right) C_{ir} \quad (5.99)$$

The total rotor surface loss can be written as

$$P_{r(surf)} = \sum_{n=0}^{S_1/(P-1)} P \left(\frac{2\pi D_{or}}{S_1}\right) k_{ir} l_i d_e \left(\frac{B_{p1}}{B_{g1}}\right)^2 \cos^2\left(\frac{n\pi P}{S_1}\right) C_{ir} \quad (5.100)$$

which, after some factoring becomes

$$P_{r(surf)} = 2[\pi D_{or} k_{ir} l_i d_e] \left(\frac{B_{p1}}{B_{g1}}\right)^2 C_{ir} \sum_{n=0}^{S_1/(P-1)} \frac{\cos^2\left(\frac{n\pi P}{S_1}\right)}{(S_1/P)} \quad (5.101)$$

The coefficient inside the square brackets is recognized as the total rotor surface volume. It can be shown that the summation of Eq. (5.101) is identically equal to 0.5 regardless of the number of slots/pole whereupon

$$P_{r(surf)} = \pi D_{or} k_{ir} l_i d_e \left(\frac{B_{p1}}{B_{g1}}\right)^2 C_{ir} \quad (5.102)$$

It is convenient to replace the equivalent depth  $d_e$  in Eq. (5.102) by its equivalent in terms of the stator slot pitch. Also, we have thus far neglected the presence of possible rotor slot openings in our solution. Clearly, we must reduce the volume corresponding to surface losses by the ratio of the thickness of the rotor tooth to the rotor slot pitch to correct for this missing material. Hence, finally,

$$P_{r(surf)} = 0.5 D_{or} k_{ir} l_i \tau_s \left(\frac{t_{or}}{\tau_r}\right) C_{ir} \left(\frac{B_{p1}}{B_{g1}}\right)^2 \quad (5.103)$$

where  $t_{or}$  denotes the equivalent thickness of a rotor tooth top at the air gap surface.

Thus far we have considered only the first slot harmonic. Analogous solutions can be obtained readily for all higher harmonics since the form of the result, Eq. (5.103), is identical. An expression which considers all harmonics is

$$P_{r(surf)} = 0.5 D_{or} k_{ir} l_i \tau_s \left( \frac{t_{or}}{\tau_r} \right) \sum_{n=1}^{\infty} \left( \frac{C_{irn} B_{pn}}{B_{g1}} \right)^2 \quad (5.104)$$

Note that the loss coefficient  $C_{ir}$  is included in the summation since it is a function of frequency. The solution as written is inconvenient since the loss coefficient  $C_{ir}$  is now a function of two variables, the gap flux density  $B_{g1}$  as well as the frequency. From Eq. 5.44 it is evident that the losses vary with frequency (hysteresis loss) as well as frequency squared (eddy current loss). The relative weighting of the hysteresis and eddy current losses depends upon the thickness of the material but clearly the exponent associated with frequency dependent losses is between 1 and 2. If  $C_{ir}$  is assumed to vary with frequency to the  $v^{th}$  power, and since the slot harmonic frequencies are integer ratios of the fundamental, Eq. (5.104) can be written as

$$P_{r(surf)} = 0.5 D_{or} k_{ir} l_i \tau_s \left( \frac{t_{or}}{\tau_r} \right) C_{ir} \left( \frac{B_{p1}}{B_{g1}} \right)^2 \left[ 1 + 2^v \left( \frac{B_{p2}}{B_{p1}} \right)^2 + 3^v \left( \frac{B_{p3}}{B_{p1}} \right)^2 + \dots \right] \\ n = 1, \dots, \infty \quad (5.105)$$

It is conventional to define a pole face loss factor for stator slots as

$$K_{pfr} = \left( \frac{B_{p1}}{B_{g1}} \right)^2 \sum_{n=1}^{\infty} n^v \left( \frac{B_{pn}}{B_{p1}} \right)^2 \quad (5.106)$$

so that Eq. (5.105) becomes

$$P_{r(surf)} = 0.5 D_{or} k_{ir} l_i \tau_s \left( \frac{t_{or}}{\tau_r} \right) C_{ir} K_{pfr} \quad (5.107)$$

The quantity  $K_{pfr}$  is plotted in Figure 5.25 for three different values of  $v$  corresponding to lamination thicknesses of 0.025, 0.019 and 0.014 inches. The

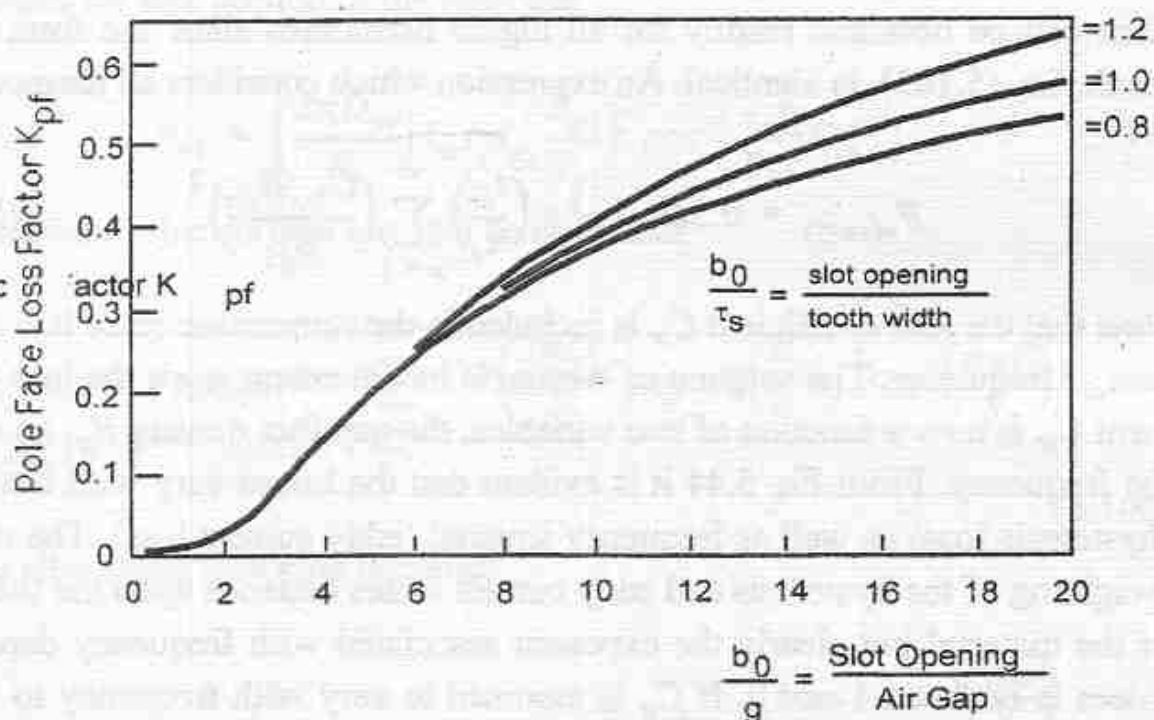


Figure 5.25 Pole face loss factor  $K_{pf}$  as a function of the ratio of slot opening to air gap length

subscript "r" has been dropped from Figure 5.26 since the curves are equally valid for the losses in stator as well as rotor teeth.

It can be recalled that the loss coefficient  $C_{ir}$  represents the rotor loss per unit volume at the frequency  $S_1 f_e / P$  and at the flux density  $B_{gl}$ . Since, the losses vary as  $B^2$  it is not necessary to measure  $C_{ir}$  at each value of gap flux density. Rather, Eq. (5.107) can be put in the form

$$P_{r(surf)} = 0.5 D_{or} k_{ir} l_i \tau_s \left( \frac{l_{or}}{\tau_r} \right) C_{ir} K_{pfr} \left( \frac{B_{gl}}{B_{ref}} \right)^2 \quad (5.108)$$

where  $C_{ir}$  is now measured at a reference value of flux density  $B_{ref}$ .  $B_{ref}$  is generally taken as 100 kJ/in<sup>2</sup>. A plot of  $C_{ir}$  as a function of frequency is shown in Figure 5.26 for three different lamination thicknesses. Here again the subscript "r" has been dropped since the curves can be used for stator as well as rotor tooth losses. When the rotor has slotting as well as the stator, losses also appear on the stator surface. The proper equation is simply obtained from Eq. (5.108) by inspection. The relevant equation is

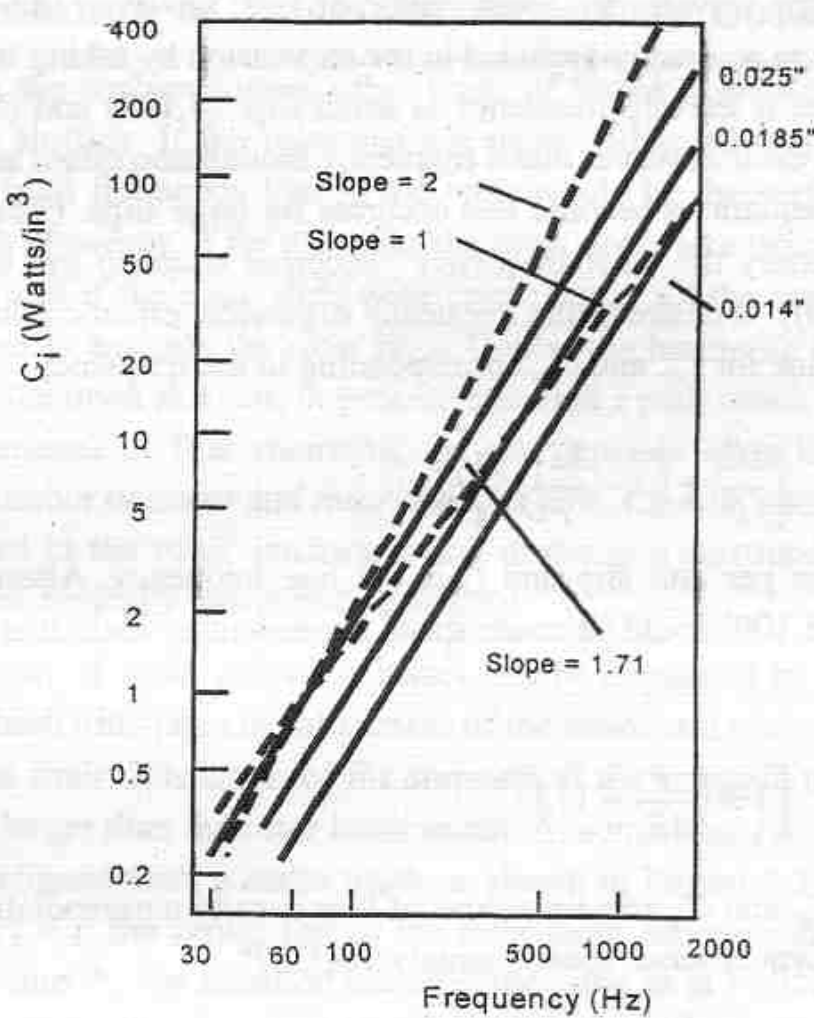


Figure 5.26 Loss coefficient  $C_i$  for silicon steel as a function of frequency, peak flux density maintained at 100 Klines/in<sup>2</sup> (1.55 T)

$$P_{s(surf)} = 0.5 D_{is} k_{is} l_i \tau_r \left( \frac{t_{os}}{\tau_s} \right) C_{is} K_{pfs} \left( \frac{B_{gl}}{B_{ref}} \right)^2 \quad (5.109)$$

Whereas Eqs. (5.108) and (5.109) can be considered as our final result, a short amount of additional discussion is useful. Recall that we have chosen to calculate the losses for the specific case of synchronous speed operation. It could be questioned whether the results change when the motor is loaded since synchronous speed operation implies an unloaded condition. Consider again the rotor material under one stator tooth pitch used for our previous derivation. As the motor begins to slip, the material begins to encounter the one cycle cosine-sinusoidal waveforms shown in Figure 5.23. A proper expression for the losses in this rotor material would now be a weighted average of the losses associated

with each of the waveforms. Examination of Eq. , however, indicates that just such an average is already included in the expression by taking the summation shown. Hence, if the slip frequency is small Eqs. (5.108) and (5.109) remain accurate. It is clear however that a frequency modulation effect actually occurs so that these equations become less accurate for large slips. Clearly, when the rotor is stationary the "slot frequency" becomes equal to the line frequency (see Eq. (5.80)). If desired, this frequency dependent effect could be corrected by using a value for  $C_{ir}$  and  $C_{is}$  corresponding to the frequency

$$\left[ \frac{2S_1}{P} + \left( 1 - \frac{2S_1}{P} \right) S \right] f_e \quad (5.110)$$

where  $S$  is the per unit slip and  $f_e$  is the line frequency. Alternatively, Eqs. (5.108) and (5.109) could be made speed dependent by including a term of the form

$$\left[ 1 + \left( \frac{P}{2S_1} - 1 \right) S \right]^v$$

In this case  $C_{ir}$  and  $C_{is}$  remain values of loss density corresponding to the slot frequency at synchronous speed, namely  $2S_1 f_e / P$ .

Since many machine designers choose to use the average rather than the peak value of gap flux density as a key parameter, Eq. (5.109) can be written alternatively as

$$P_{r(surf)} = (\pi^2/8) D k_{ir} l_i \tau_s \left( \frac{t_{or}}{\tau_r} \right) C_{ir} K_{pfs} \left( \frac{B_{g1(ave)}}{B_{ref}} \right)^2 \quad (5.111)$$

The coefficient  $\pi^2 / 8 = 1.234$ . This coefficient has variously appeared as 1.65 and 2.0 in other authors' works using different assumptions.<sup>1</sup> Because the gap of an induction machine is small, the surface losses tend to be the major contributor to stray losses, typically 20-30%.

1. P. L. Alger, G Angst, and E. J. Davies, "Stray-Load Losses in Polyphase Induction Machines", Trans AIEE, June, 1959, pp. 349-355.

## 5.10 Calculation of Tooth Pulsation Iron Losses

In addition to the surface losses, other types of losses also occur which are caused by the slotting. If the rotor and the stator had equal numbers of slots then the only high frequency loss in the rotor would be the surface iron loss just calculated. However, if for example, the rotor slots were twice the number of stator slots and if the rotor slots were open, nearly all the stator harmonic flux would tend to encircle the rotor slots. Hence, the harmonic flux which is interrupted by the open slot can, in general, also find a path which encircles the slot and the amount of flux encircling the slot depends upon the difference between the number of stator and rotor slots per pole. Clearly, additional losses are encountered in the rotor conductors and in the iron surrounding the slot. These losses are typically calculated separately.

The problem of tooth pulsation losses can be explained by reference to Figure 5.27 which illustrates the alignment of the stator and rotor teeth for two positions of the rotor. It is assumed for purposes of the example that the stator tooth width is larger than the rotor tooth width. At some time  $t = 0$  a particular rotor tooth is aligned with a stator tooth as shown in Figure 5.27(a). A short instant later at  $t = t_1$  the center line of the rotor tooth becomes aligned with a stator slot. At time  $2t_1$  the situation becomes the same as at  $t = 0$ . It is apparent by comparison of the first two cases that the flux entering the rotor slot at  $t = 0$  will be larger than  $t = t_1$ . The difference between these two cases constitutes a flux pulsation which passes down the tooth body and ultimately links one of the rotor conductors. Hence, additional rotor copper as well as iron losses in the stator and rotor are created.

In order to investigate this problem we will again assume that the rotor is rotating synchronously. We will again assume that the rotor surface is initially smooth. The value of pulsating flux that occurs for the rotor tooth in question is again proportional to the average flux linking the tooth in much the same manner as the previous problem. We will again choose the rotor tooth which follows the peak of the flux density wave  $B_{g1}$ . When the rotor tooth is lined up with a stator tooth the flux density over the tooth is equal to  $B_{g1}$ . The flux remains at this value until the edge of the stator slot begins to sweep over the rotor tooth. The flux linking the rotor tooth then abruptly drops to a smaller value which again remains fairly constant until the stator slot sweeps off of the other side of the rotor tooth. The flux penetrating the rotor tooth as a function of time is approximately a rectangular function as shown in Figure 5.28. The

average (negative) component of this waveform is again accounted for by Carter's Coefficient. Since the harmonic components of Figure 5.28 contribute to the losses it is apparent that the problem is most severe when the rotor slot pitch is exactly half the stator slot pitch (twice as many rotor slots as stator slots).

The flux change  $\Delta\Phi$  which occurs whenever a stator slot passes by the rotor slot is found by solving for the area  $\Delta B$  shown in Figure 5.27. Since the flux density distribution is complicated the relationship between the flux pulsation and the maximum flux across the slot must be determined numerically. It can be shown that the flux pulsation over a span of one rotor tooth can be written in the form<sup>2</sup>

$$\Delta\Phi = b_{os} l_{es} \beta \sigma B_{g1} \quad (5.112)$$

where  $B_{g1}$  is taken as the maximum flux density over the slot under consideration. The functions  $\beta$  and  $\sigma$  are plotted in Figure 5.20 and Figure 5.29 respectively.

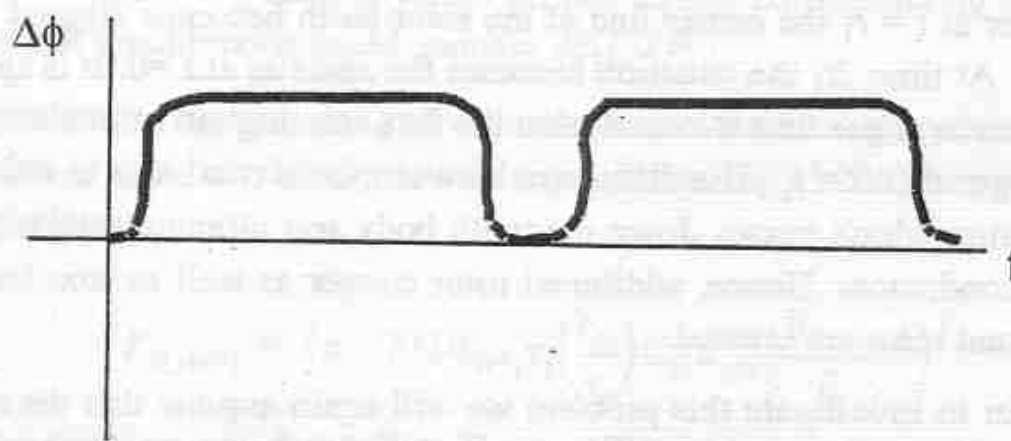


Figure 5.28 Waveform of slot flux pulsation as a function of time.

The fundamental component of the flux change can be found by taking the first Fourier harmonic of Figure 5.28. The result is

2. B. Heller and V. Hamata, "Harmonic Field Effects in Induction Machines", Elsevier Scientific Publishing Co., Amsterdam, 1977.

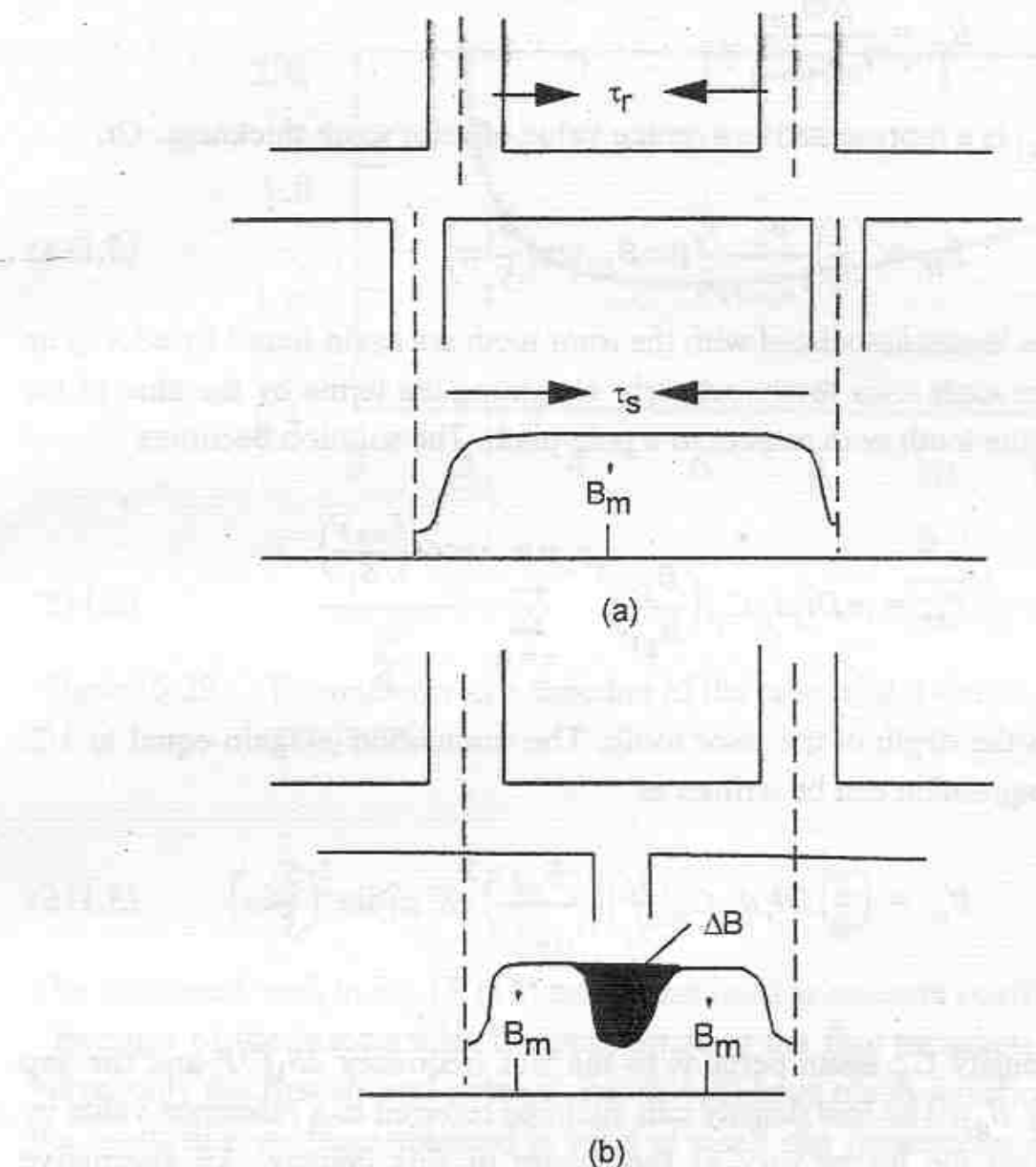


Figure 5.27 Illustration of slot flux pulsation showing two limiting alignments of stator and rotor teeth.

$$\Delta\Phi_{1p} = \left(\frac{2}{\pi}\right) b_{os} l_e \beta \sigma B_{g1} \sin\left(\frac{S_1}{S_2}\pi\right) \quad (5.113)$$

The frequency associated with the first harmonic is again equal to the stator slot frequency  $[(2S_1)/P]\omega_e$ .

The flux density in the slot itself is

$$B_{lt} = \frac{\Delta\Phi_{lp}}{l_{ir} t_{r(ave)}}$$

where  $t_{r(ave)}$  is a representative average value of rotor tooth thickness. Or,

$$B_{lt} = \left(\frac{2}{\pi}\right) \frac{b_{os}}{t_{r(ave)}} \frac{l_e}{l_i} \beta \sigma B_{g1} \sin\left(\frac{S_1}{S_2} \pi\right) \quad (5.114)$$

The iron losses associated with the rotor teeth are again found by adding up the losses in each rotor tooth, properly weighting the terms by the sine of the location of the tooth with respect to a pole pitch. The solution becomes

$$P_{tr} = \pi D l_i d_{tr} C_{ir} \left(\frac{B_{1t}}{B_{g1}}\right)^2 \sum_{n=0}^{S_2/(P-1)} \frac{\cos\left(\frac{n\pi P}{S_1}\right)}{\frac{S_2}{P}} \quad (5.115)$$

where  $d_{tr}$  is the depth of the rotor tooth. The summation is again equal to 1/2. The final expression can be written as

$$P_{tr} = \left(\frac{2}{\pi}\right) D l_e d_{tr} C_{ir} \left(\frac{l_e}{l_i}\right) \left(\frac{b_{os}}{t_{r(ave)}}\right)^2 \beta^2 \sigma^2 \sin^2\left(\frac{S_1}{S_2} \pi\right) \quad (5.116)$$

The loss density  $C_{ir}$  again pertains to the slot frequency  $2S_1 f/P$  and the gap flux density  $B_{g1}$ . The loss density can again be referred to a reference value by assuming that the losses vary as the square of flux density. An alternative expression is

$$P_{tr} = \left(\frac{2}{\pi}\right) D l_e d_{tr} C_{ir} \left(\frac{l_e}{l_i}\right) \left(\frac{b_{os}}{t_{r(ave)}}\right)^2 \beta^2 \sigma^2 \left(\frac{B_{g1}}{B_{ref}}\right)^2 \sin^2\left(\frac{S_1}{S_2} \pi\right) \quad (5.117)$$

Again  $B_{ref}$  is typically taken as 1.55 T (100 Klines/in<sup>2</sup>). An analogous expression can be written for the stator tooth pulsation loss should the rotor be slotted. Also, the tooth flux density can also be corrected for higher harmonics in the waveform. Since the harmonics of a square wave are inversely proportional to  $n$ , a more accurate version of  $B_t$  is

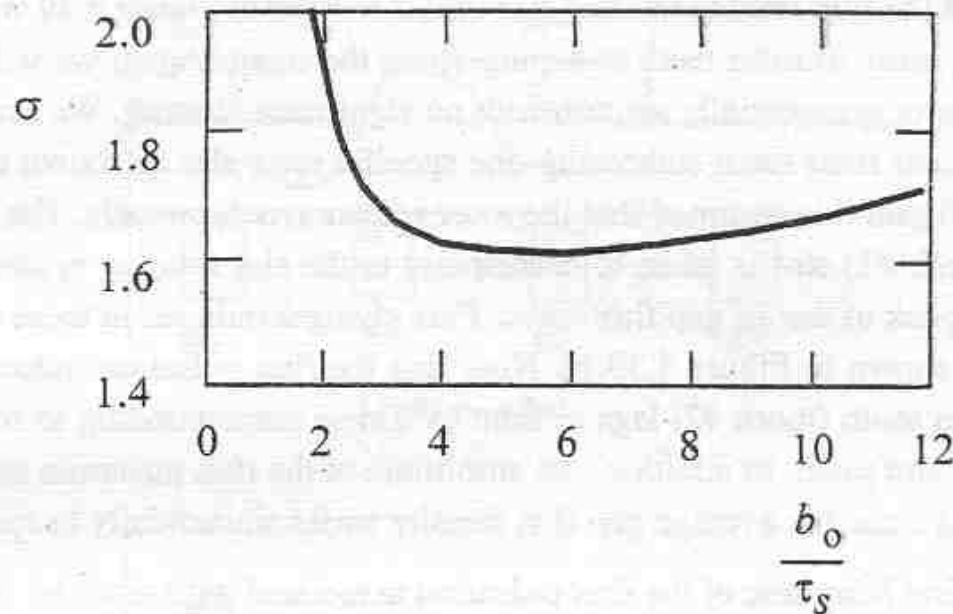


Figure 5.29 Parameter  $\sigma$  as a function of the ratio of slot opening to the air gap length.

$$B_t^2 = B_{1r}^2 \left[ 1 + \left(\frac{1}{3}\right)^{3-v} + \left(\frac{1}{5}\right)^{5-v} + \dots \right] \quad (5.118)$$

The bracketed term in Eq. (5.118) can be included as an extra coefficient in Eq. . Because of the inaccuracies in approximating the flux pulsation as a square wave, only the first several terms in Eq. (5.118) have much significance. Again the result that we have obtained is valid at small slip frequencies as well as at zero slip (synchronous speed). If desired the loss term can be corrected for frequency changes by the same factor as used in Section 5.9, that is Eq. (5.109).

The tooth pulsation iron loss is sometimes neglected by other authors since it is claimed that the currents which flow in the short circuited bar (to be computed) tend to cancel the flux pulsation. However, this occurs only for a purely inductive bar which is clearly not the case at slot ripple frequencies due to skin effect. In fact, it can be shown that when the pulsation frequency is sufficiently large such that the high frequency approximations are valid (Eqs.(5.36) and (5.37)), the tooth flux produced by the slot currents could in fact increase the net flux in the tooth.

As already mentioned the pulsating flux in the rotor teeth also results in harmonic losses in the short circuited rotor bars of a squirrel cage machine.

The current which flows in a given rotor bar is a result of the time rate of change of the flux linking the bar. It is useful to refer to Figure 5.30 which now shows an array of rotor teeth sweeping along the stator. Again we will assume that the rotor is essentially smooth with no significant slotting. We can identify two adjacent rotor teeth embracing one specific rotor slot as shown on Figure 5.30(a). Again it is assumed that the rotor rotates synchronously. The left hand tooth (tooth #1) slot is taken to correspond to the slot rotating synchronously with the peak of the air gap flux wave. Flux changes induced in these two rotor slots are shown in Figure 5.30(b). Note that the flux pulsation induced in the right hand tooth (tooth #2) lags in time by a time corresponding to rotation of one rotor slot pitch. In addition, the amplitude of the flux pulsation in tooth #2 is reduced since the average gap flux density varies sinusoidally in space.

The first harmonic of the flux pulsation associated with tooth #1 is

$$\Delta\Phi_1(t) = \Delta\Phi_{1p} \cos\left(\frac{2S_1}{P}\omega_e t\right) \quad (5.119)$$

where  $\Delta\Phi_{1p}$  is given by Eq.(5.113). The flux penetrating tooth #2 can be written as

$$\Delta\Phi_2(t) = \Delta\Phi_{1p} \cos\left(\frac{2S_1}{P}\omega_e t - 2\pi\frac{S_1}{S_2}\right) \cos\left(\frac{P\pi}{S_2}\right) \quad (5.120)$$

The pulsating flux linking the bar can be found by subtracting Eq. (5.120) from Eq. (5.119). After a certain amount of algebra the result can be written as

$$\begin{aligned} \Delta\Phi_1(t) - \Delta\Phi_2(t) &= \Delta\Phi_{1p} \left[ \sin\left(\frac{2S_1}{P}\omega_e t - \frac{S_1}{S_2}\pi + \frac{P\pi}{2S_2}\right) \sin\left(\frac{S_1}{S_2}\pi - \frac{P\pi}{2S_2}\right) \right. \\ &\quad \left. + \sin\left(\frac{2S_1}{P}\omega_e t - \frac{S_1}{S_2}\pi - \frac{P\pi}{2S_2}\right) \sin\left(\frac{S_1}{S_2}\pi + \frac{P\pi}{2S_2}\right) \right] \end{aligned} \quad (5.121)$$

Two terms appear because of the modulation of the slot frequency with the fundamental frequency.

The emf induced in the bar between slots #1 and #2, say bar #1, can be represented in phasor form as

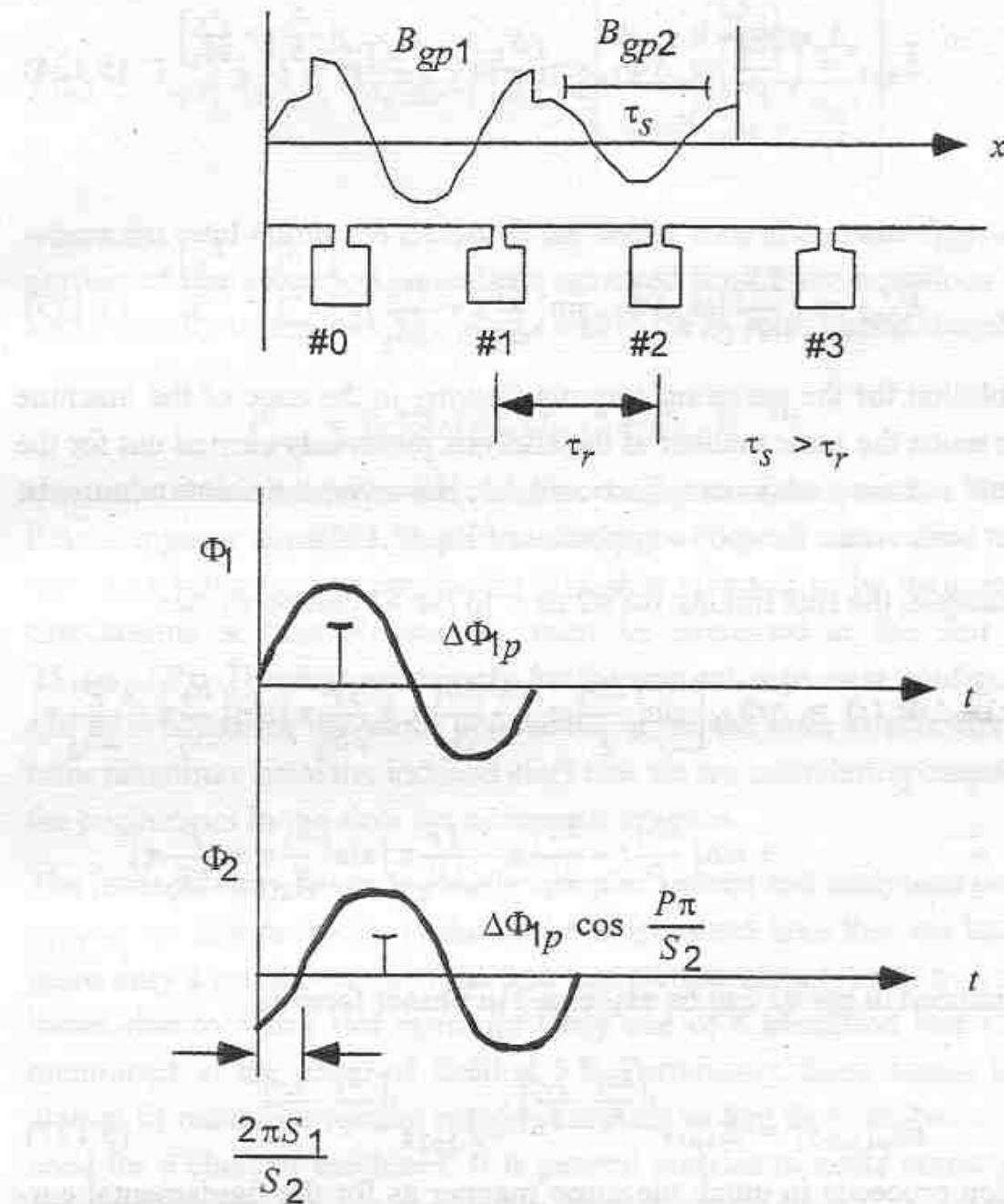


Figure 5.30 Flux pulsations of two adjacent teeth vs. time

$$\tilde{E}_{bp(bar1)} = j \left( \frac{2S_1}{P} \right) \omega_e (\Delta \tilde{\Phi}_1 - \Delta \tilde{\Phi}_2) \quad (5.122)$$

which can be written in terms of two voltage components

$$\tilde{E}_{bp(bar1)} = \tilde{E}_{bp1} + \tilde{E}_{bp2} \quad (5.123)$$

where

$$\tilde{E}_{bp1} = \left(\frac{2S_1}{P}\right)\omega_e \Delta\tilde{\Phi}_{1p} \sin\left(\frac{S_1}{S_2}\pi - \frac{P\pi}{2S_2}\right) e^{j\left[-\frac{S_1}{S_2}\pi + \frac{P\pi}{2S_2}\right]} \quad (5.124)$$

and

$$\tilde{E}_{bp2} = \left(\frac{2S_1}{P}\right)\omega_e \Delta\tilde{\Phi}_{1p} \sin\left(\frac{S_1}{S_2}\pi + \frac{P\pi}{2S_2}\right) e^{j\left[-\frac{S_1}{S_2}\pi - \frac{P\pi}{2S_2}\right]} \quad (5.125)$$

The solution for the pulsating currents flowing in the cage of the machine follows in much the same manner as the analysis previously carried out for the fundamental current component, Section 4.12. However, the solution must be carried out twice, once for each component of Eq. (5.123).

For example, the flux linking bar #2 next to bar #1 can be written

$$\begin{aligned} \Delta\Phi_2(t) - \Delta\Phi_3(t) &= \Delta\Phi_{1p} \left[ \sin\left(\frac{2S_1}{P}\omega_e t - \frac{3S_1}{S_2}\pi + \frac{3P}{2S_2}\pi\right) \sin\left(\frac{S_1}{S_2}\pi - \frac{P}{2S_2}\pi\right) \right. \\ &\quad \left. + \sin\left(\frac{2S_1}{P}t - \frac{3S_1}{S_2}\pi - \frac{3P}{2S_2}\pi\right) \sin\left(\frac{S_1}{S_2}\pi + \frac{P}{2S_2}\pi\right) \right] \end{aligned} \quad (5.126)$$

The emf induced in bar #2 can be expressed in phasor form as

$$\tilde{E}_{bp(bar2)} = \tilde{E}_{bp1} e^{j\left[\frac{3S_1}{S_2} - \frac{3P}{S_2}\right]} + \tilde{E}_{bp2} e^{j\left[\frac{3S_1}{S_2} - \frac{3P}{S_2}\right]} \quad (5.127)$$

The solution proceeds in much the same manner as for the fundamental currents except that a different expression is used for the phase shift. The effects of the end ring can be included in the same manner as before. After including the effects of the end ring, the equations which define the solution for the current that flows in the bar reduces to

$$\tilde{E}_{bp1} = \tilde{I}_{bp1} \left[ R_b + j\left(\frac{2S_1}{P}\right)\omega_e L_b \right] + \tilde{I}_{bp1} \left[ \frac{R_e + j\left(\frac{(2S_2)}{P}\right)\omega_e L_e}{2 \sin^2\left(\frac{S_1}{S_2}\pi - \frac{P\pi}{2S_2}\right)} \right] \quad (5.128)$$

$$\tilde{E}_{bp2} = \tilde{I}_{bp2} \left[ R_b + j \left( \frac{2S_1}{P} \right) \omega_e L_b \right] + \tilde{I}_{bp2} \left[ \frac{R_e + j \left( \frac{2S_2}{P} \right) \omega_e L_e}{2 \sin^2 \left( \frac{S_1}{S_2} \pi + \frac{P\pi}{2S_2} \right)} \right] \quad (5.129)$$

where the total current in the bar is the vector sum of  $I_{bp1}$  and  $I_{bp2}$ . The "(#1)" portion of the subscripts have been removed from these equations since they apply equally to any bar. The power loss in the  $S_2$  rotor bars is therefore,

$$P_{prc} = 0.5 Re[\tilde{E}_{bp1} \tilde{I}_{bp1}^* + \tilde{E}_{bp2} \tilde{I}_{bp2}^*] \quad (5.130)$$

where the asterisk denotes the complex conjugate of the quantity. The 0.5 coefficient appears since we have been dealing with peak rather than rms quantities. It is important to emphasize that skin effect is to be included in these calculations so that  $R_b$  and  $L_b$  must be evaluated at the slot frequency  $2S_1(\omega_e/P)$ . This loss exists only for the squirrel cage rotor configuration and can be omitted for the stator conductors or for the rotor conductors of wound rotor machines since the induced emfs that we are considering cancel out when the conductors in the slots are connected in series.

The issue of stray losses is clearly complex indeed and analytical work is continuing on this problem. It should be emphasized here that we have investigated only a small portion of the iron loss picture, namely rotor iron and copper losses due to stator slot openings (only one of 4 identified loss components mentioned at the onset of Section 5.8). Fortunately, these losses in different classes of machines remain roughly constant so that they can be measured and used for a class of machines. It is general practice to make corrections to the usual (fundamental component) iron and copper losses to account for these losses. If measured at one value of current and frequency, the stray losses can be converted to another pair of values by

$$\text{Stray Losses}_2 = \text{Stray Losses}_1 \left( \frac{I_2}{I_1} \right)^2 \left( \frac{f_2}{f_1} \right)^{1.4} \quad (5.131)$$

A tabulation of the stray load and no load losses for a variety of machines is given in Table 5.9.

**Table 5.9 Iron Loss Distribution in ac Machines**

	Fundamental Losses	Additional Losses Due to Non-Sinusoidal Waveform (Punching Stresses, Burrs, etc.)	Stray No-Load Losses	Stray Load Loss in% of Output Power
Induction Motor with Semi-Open Stator and Rotor Slots	100%	30% to 40%	50% to 70%	0.3 to 0.6%
Induction Motor with Semi-Open Stator Slots	100%	30% to 40%	120% to 160%	0.3 to 0.6%
Salient Pole Synchronous Machines	100%	40% to 60%	50% to 70%	0.1 to 0.2%
Round Rotor Turbogenerators (4 pole)	100%	30% to 40%	40% to 50%	0.05% to 0.15%
(2 pole)	100%	15% to 25%	25% to 35%	0.05% to 0.15%

## 5.11 Friction and Windage Losses

Bearing friction losses are an unavoidable loss in a rotating machine. The amount of the bearing friction losses depends upon the pressure on the bearing, the peripheral speed of the shaft at the bearing and the coefficient of friction between bearing and shaft. The windage losses are also produced by rotation and depend upon the peripheral speed of the rotor, the rotor diameter, the core length and generally upon the construction of the machine. While friction losses can be determined more or less accurately, the windage losses have to be determined on the basis of actual test. Figure 5.31 and Figure 5.32 show typical windage and friction losses for different classes of machines and were derived by tests on a large number of machines. They can be used to obtain an approximate estimate of these losses. As a rule of thumb the friction and windage losses can be converted from a known measured speed to another speed by the expression

$$F\&W_2 = F\&W_1 \left( \frac{\text{speed}_2}{\text{speed}_1} \right)^2 \quad (5.132)$$

## 5.12 Example #8 - Calculation of Iron Loss Resistances

The iron loss characteristic curves for 0.025", 3% Si steel was given in Figure 5.16. Note that these curves combine the effects of eddy current and hysteresis and are given in units of watts/lb rather than watts/in<sup>3</sup>. In order to convert to useful units the density of the laminations must be specified. This value can be taken as 0.276 lb/in<sup>3</sup>. First let us calculate the equivalent iron loss resistance which accounts for the loss in the stator teeth of the example 250 hp machine.

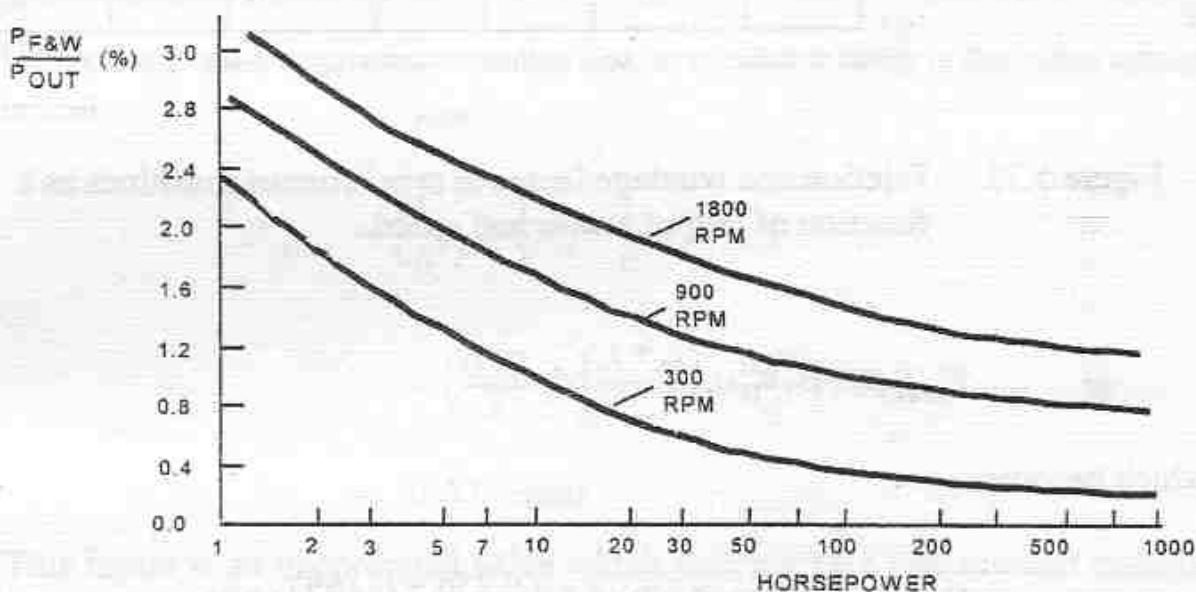


Figure 5.31 Friction and windage losses in synchronous machines as a function of output power and speed

The volume of iron used for the  $S_1$  stator teeth can be expressed as the following integral

$$V_{\text{teeth}} = S_1 k_{is} l_{is} \int_0^{d_s} \left[ t_t + \left( \frac{t_r - t_t}{d_s} \right) x \right] dx$$

The numerical values of the various quantities can be determined by reference to Figure 3.11. This integral can be evaluated as

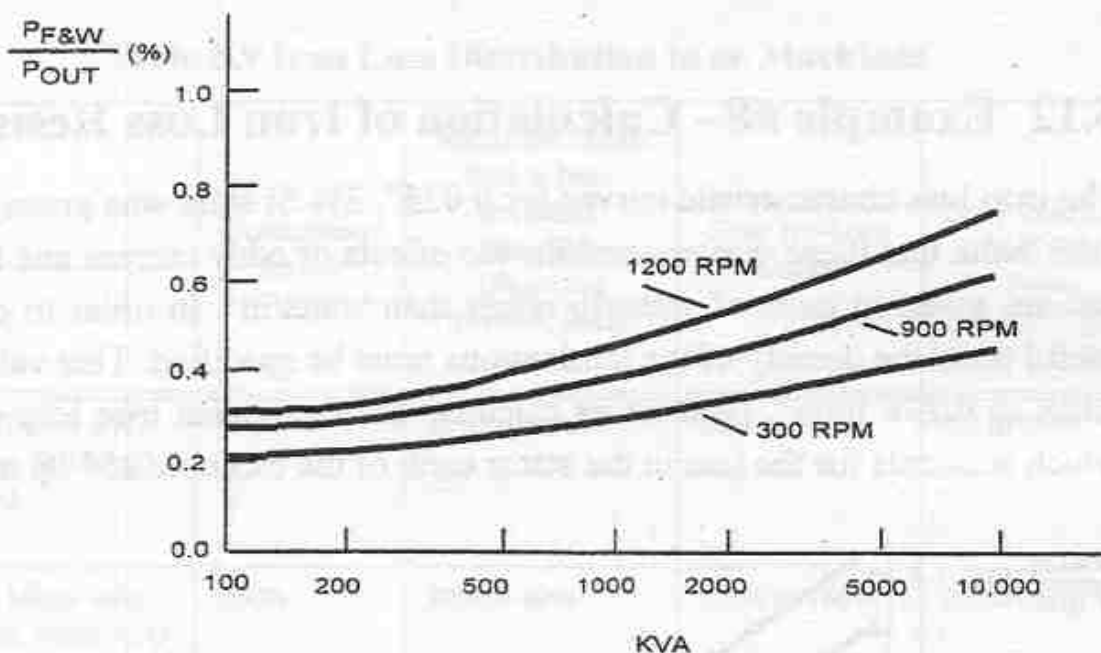


Figure 5.32 Friction and windage losses in synchronous machines as a function of output power and speed

$$V_{teeth} = S_1 k_{is} l_{is} \left( \frac{t_t + t_r}{2} \right) d_s$$

which becomes

$$\begin{aligned}
 V_{teeth} &= (120)(0.97)(8.5) \left( \frac{0.256 + 0.369}{2} \right) (2.2) \\
 &= 680.2 \text{ in}^3
 \end{aligned}$$

From Example #2 in Chapter 3 it was determined that for an air gap fundamental component of flux density of 0.775 T., the density in the top, the middle, and the root of the tooth are

$$B_t = 1.86 \text{ T} = 119,970 \text{ lines/in}^2$$

$$B_m = 1.52 \text{ T} = 98,040 \text{ lines/in}^2$$

$$B_r = 1.29 \text{ T} = 83,205 \text{ lines/in}^2$$

Note that these values relate to the flux density at a point  $30^\circ$  away from the maximum value of  $B_g$ . However, since the machine is heavily saturated for the condition that we are using to evaluate the parameters these values will also be taken as the maximum value of B in the teeth.

From Figure 5.16 the corresponding values of power density are

$$p_t = 0.72 \text{ watts/in}^3$$

$$p_m = 0.52 \text{ watts/in}^3$$

$$p_r = 0.38 \text{ watts/in}^3$$

Using Simpson's approximation the loss in the stator teeth is therefore approximately

$$\begin{aligned} P_{teeth} &= \left( \frac{1}{6}p_e + \frac{2}{3}p_m + \frac{1}{6}p_r \right) V_{teeth} \\ &= \left( \frac{0.72}{6} + \frac{2}{3}(0.52) + \frac{0.38}{6} \right) 680.2 \\ &= 360.5 \text{ watts} \end{aligned}$$

This figure is an uncorrected value which does not take into account manufacturing imperfections and non-sinusoidal waveform.

Reference to Table 5.9 indicates that for an induction machine with open stator slots and semi-closed rotor slots this value can be increased by 30-40% to account for these additional losses. The exact value clearly depends on a number of unknowns such as manufacturing processes, and would usually be determined for a particular line of machines by test. If we assume here a figure of 35% then a corrected value of power lost in the teeth is

$$P_{teeth} = (1.35)(360.5)$$

$$= 487 \text{ watts}$$

From Example #2 it was established that the voltage across the machine which results in a gap flux density of 0.775 T is 2700 volts, line-to-line. At no

load this voltage appears across the sum of the stator leakage inductance plus the magnetizing inductance if resistance is neglected. The stator tooth loss is roughly dependant on air gap flux since the slot leakage flux takes a short cut across the slot and the end winding leakage is not involved. Hence, the equivalent value of resistance which results in a power loss in the teeth of 773 watts is, from Example #3,

$$r_t = \frac{V_{gap}^2}{P_{teeth}} = \frac{(2700)^2}{487}$$

$$= 14,970 \text{ } \Omega$$

Consider now the loss which occurs in the stator core. The volume of iron which occupies the stator core is

$$V_{core} = k_{is} l_{is} \frac{\pi}{4} [D_{os}^2 - (D_{os} - 2h_{cs})^2]$$

$$= \frac{\pi}{4} k_{is} l_{is} h_{cs} (D_{os} - 2h_{cs})$$

which can be evaluated as

$$V_{core} = \left(\frac{\pi}{4}\right)(0.97)(8.5)(1.76)[32 - 2(1.76)]$$

$$= 324.6 \text{ in}^3$$

By reference to Example #2, the maximum value of flux density in the stator core is 1.49 T, or changing units,

$$B_{cs} = 96,487 \text{ lines/in}^2$$

which, from Figure 5.16 results in a loss density of

$$p_c = 0.5 \text{ watts/in}^3$$

If we again use a factor of 35% to correct for additional fundamental losses then

$$P_{core} = (1.35)p_c V_{core}$$

$$= (1.35)(0.5)(649.2) = 438 \text{ watts}$$

Because the stator slot leakage fluxes take a return path through the stator core, then, neglecting resistance, the total voltage also appears across the flux producing core loss which corresponds to both the core flux plus the slot leakage flux.. Hence, an equivalent value of resistance which results in a power loss in the core of 438 watts is

$$r_c = \left( \frac{L_m + L_{slot}}{L_{slot}} \right)^2 \frac{V_{l-l}^2}{P_{core}}$$

$$= \frac{(0.223 + 0.00347)(2700)^2}{(0.223)438}$$

$$= 17,166 \Omega$$

It should be noted that iron loss also exists for the rotor teeth and rotor core. However, during normal operation the frequency associated with this loss is much lower than 60 Hz and is therefore much smaller than the stator iron loss. This loss is effectively included in the 35% "imponderables" factor.

The final resistance to be calculated are to account for the stray losses. Let us first compute a value of resistance which accounts for the stray load losses. Reference to Table 5.9 indicates that for a machine with open stator slots and semi-open rotor slots the power dissipated due to stray load losses is between 0.3 and 0.6% of rated output. For the 250 hp machine under study we will use a figure of 0.4%. The rated current which flows under rated load conditions can be approximated by taking rated output power and dividing by rated voltage and an estimated power factor and efficiency, or

$$I_b = \frac{P_s}{\sqrt{3} V_{(I-I)} (\text{powerfactor})(\text{efficiency})}$$

$$= \frac{(746)(250)}{\sqrt{3}(2400)(0.93)(0.9)}$$

$$= 53.6 A$$

The resistance which accounts for load losses is a function of current and is therefore in series with the load current rather than in parallel across the terminal voltage. The equivalent resistance which produces a loss of 0.4% of rated power is

$$\begin{aligned} r_{sl} &= \frac{(0.004)(P_b)}{3I_b^2} \\ &= \frac{0.004(746)(250)}{(3)(53.6^2)} \\ &= 0.086 \Omega \end{aligned}$$

The final resistance to be calculated is to account for no-load losses. In this case a resistor is to be calculated which appears across the magnetizing inductance since this loss component results from fluxes in the air gap. It should be noted that the presence of the resistor to account for load losses is in series with the stator current and will already produce a loss at no load since magnetizing current must flow through this resistor as well as load current. Since the series resistances are small the magnetizing current of the machine is readily approximated by the expression

$$I_m = \frac{V_{l-l}}{\sqrt{3}(X_{ls} + X_m)}$$

where  $X_{ls}$  and  $X_m$  are the 60 Hz reactance corresponding to  $L_{ls}$  and  $L_m$ . This quantity can be evaluated as

$$\begin{aligned} I_m &= \frac{2700}{(\sqrt{3})(377)(0.00683 + 0.223)} \\ &= 17.9 A \end{aligned}$$

The power consumed by the resistor  $r_l$  at no load is therefore

$$\begin{aligned} P_l &= I_m^2 r_{sl} \\ &= (17.9)^2(0.463) \end{aligned}$$

$$= 148 \text{ watts}$$

Reference to Table 5.9 shows that for our machine with open stator and semi-closed rotor slots the no load losses as a per cent of fundamental losses is 120 to 160%. We will use a value of 140% in our calculations. The power loss due to stray loss at no load is therefore

$$P_{nl} = (1.4)(572.6 + 537.5)$$

$$= 1554 \text{ watts}$$

The losses which are thus far unaccounted for are

$$P_{nl} - P_t = 1554 - 148$$

$$= 1406 \text{ watts}$$

Hence, the resistance which will produce these losses when connected across the magnetizing branch is

$$r_{nl} = \left( \frac{V_{I-I}^2}{P_{nl} - P_t} \right) \left( \frac{X_m}{X_m + X_{ls}} \right)^2$$

$$= \frac{(2700)^2}{1406} \left( \frac{84.45}{87.02} \right)^2$$

$$= 4883 \Omega$$

Since the resistance  $r_c$  depends upon the total stator flux, it can logically be placed across the stator circuit so as to include the slot leakage portion of stator leakage reactance. However this refinement is rarely used since the slot leakage inductance is a very small fraction of the magnetizing inductance. The resistances  $r_{nl}$ ,  $r_c$  and  $r_t$  can then be combined in parallel to form one equivalent iron loss resistor  $r_i$  which accounts for the air gap flux dependant iron loss. This resistance is

$$r_i = \frac{1}{1/r_{nl} + 1/r_c + 1/r_t}$$

$$= 1/(1/4,883 + 1/17,166 + 1/14,970)$$

$$= 3031$$

A final version of the equivalent circuit per phase for the 250 hp example induction machine is shown in Figure 5.33. The small effect of the slip fre-

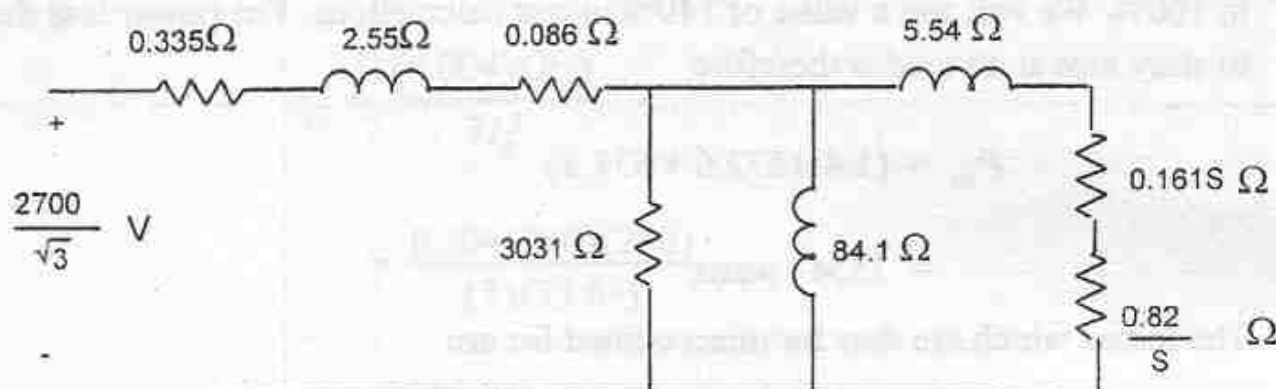


Figure 5.33 Per phase equivalent circuit of the 250 hp induction machine at 60 Hz including iron loss terms

quency on the rotor leakage inductance has been neglected. It is important to mention that the calculation have been based on an assumption of a gap flux density of 0.775 Tesla (Example #2). In Example #3 this value was determined to produce an air gap voltage of 12% above rated voltage ( $2400 V_{L1}$ ). In practice, the process must be repeated several times to account for a range of voltage  $\pm 10\%$  around rated voltage. The variation of magnetizing inductance with voltage is typically presented in terms of a plot of no-load (zero-slip) voltage versus magnetizing current.

## 5.13 References

- [9] Y. Liao and T.A. Lipo, "Effect of Saturation Third Harmonic on the Performance of Squirrel-Cage Induction Machines", Electric Machines and Power Systems, vol. 22, No. 2, March/April, 1993, pp. 155-172.

```
% Program for plotting speed/torque curves for an induction machine  
% utilizing the per-phase equivalent circuit model. The skin effect is  
% considered for calculation of referred rotor resistance and leakage  
% inductance parameters from the rotor bar geometry.
```

```
for index=1:3      % the index loop iterates the entire process for the  
                   % three cases of rotor dimensions.  
% Induction machine parameters  
r1 = 0.435;          % equivalent circuit stator resistance  
l1 = 3.32/377;        % equivalent circuit stator leakage  
reactance  
lm = 81.4/377 ;       % equivalent circuit magnetizing reactance  
re = 0.78e-06;        % resistance of end ring portion of one  
rotor  
slot pitch  
leff = 9.06*2.54;      % effective length of rotor bars under  
stator iron (cm)  
lgross = 13.95*2.54;    % gross bar length including extensions and  
% ducts (cm)  
xslots = 97.;           % number of rotor slots  
ns = 240;              % number of stator turns  
lend = 1.986e-08;       % leakage reactance of rotor ring  
lbhar = 0.259e-6;       % leakage inductance of rotor harmonics for  
% one bar  
lbtop = 0.947e-6;       % leakage inductance of top air portion of  
bar  
rho = 2.1e-06 ;          % resistivity of rotor bar material (ohm-  
cm)  
v = 2400/sqrt(3);        % applied voltage  
u = 4*pi*1.e-09;         % Henries per cm  
bardepthbase = .5625*2.54;    % rotor bar depth in cm  
barwidthbase = .375*2.54;     % rotor bar width in cm  
k = .91;                 % winding factor (pitch,distribution,skew)  
p = 8.;                  % number of machine poles  
fop=60;  
we = 2*pi*fop;  
slices = 100;  
  
bardepth = bardepthbase*index/2;  
barwidth = 2*barwidthbase/index;  
% Induction Machine Rotor Matrix, elements arranged (height, width )  
all  
% in cm  
for i=1:slices  
rm(i,1)=bardepth/slices;
```

```
rm(i,2)=barwidth;
end

% determine number of "slices" of the rotor bar
number=slices;

for count=1:100          % count iterates the calculation of rotor
parameters                % as well as equivalent circuit currents
and                      % machine output torque for slip ranging
from                     % 0.01 to 1.0

slip = 0.01*count;
s(count)=0.01*count;

% determine resistance for each "slice" of the rotor bar
for n= 1:number
resist(n)=(lgross*rho)/(rm(n,1)* rm(n,2));
end

% determine the leakages for each slice of the rotor bar
for n=1:number
leak(n)=2*pi*slop*u*leff*rm(n,1)/ rm(n,2);
end

% initial current is set to 0.001 amp, everything will eventually be
% scaled to the applied voltage.
current(1)=0.001;

currentsum=0.001;
for n=2:number
current(n)=resist(n-1)*current(n-1)/resist(n) + j*leak(n-
1)*currentsum/resist(n);
currentsum=currentsum+current(n);
end

% determine voltage seen at air gap
magvolts= resist(number)*current(number) +
j*(leak(number)+slip*we*lbtop)*currentsum;

% determine equivalent bar resistance and reactance
z = magvolts/currentsum;
resistbar = real(z);
reactbar = imag(z);
```

```
%final determination of rotor resistance reflected onto the stator
rbe = (resistbar + re/(2*(sin((pi*p)/(2*rslots)))^2));
rr(count) = 12*k*k*ns*ns*(2*rbe)/rslots;
rrref=rr(count);

% final determination of rotor reactance reflected onto the stator
llr= (reactbar/(2*pi*slip*fop)) + lend/(2*(sin((pi*p)/(2*rslots)))^2 +
lbar);
lr(count) = 12*k*k*ns*ns*(2*llr)/rslots;
lrref=lr(count);

% induction motor equivalent circuit model

% combine rotor and magnetizing reactances
zeq(count)=((j*we*lm*rr(count)/s(count))-(we*we*lr(count)*lm))/(
(rr(count)/s(count) +
j*we*(lm+lr(count))));

% determine stator current
is(count) = v / (rl + j*we*ll + zeq(count));

% determine voltage across the magnetizing reactance
vm(count) = v - is(count)*(rl + j*we*ll);

% determine rotor current
ir(count) = vm(count)/( j*we*lr(count) + rr(count)/s(count));

% determine mechanical shaft speed
speed(count) = 3600*(2/p) *(1-s(count));
power(count) = 3*abs(ir(count))^2*rr(count)*(1-s(count))/s(count);
powert(count) = p*power(count)/(2*we);

% determine output torque
torque(count) = 3*(abs(ir(count))^2)* rr(count) / (s(count)*2*we/p);
if index==1
    rout1 (count)=rr(count);
    lout1 (count)=lr(count);
    tout1 (count)=torque(count);
elseif index==2
    rout2(count)=rr(count);
    lout2(count)=lr(count);
    tout2(count)=torque(count);
else
    rout3(count)=rr(count);
    lout3(count)=lr(count);
```

```
tout3(count)=torque(count);  
end  
end  
  
end  
figure (1)  
plot(s,rout1,'--',s,rout2,'-',s,rout3,'-.')  
print  
save  
pause  
figure (2)  
plot(s,lout1,'--',s,lout2,'-',s,lout3,'-.')  
axis([0 1. 0.015 0.025])  
print  
pause  
figure (3)  
plot(speed,tout1,'--',speed,tout2,'-',speed,tout3,'-.')  
print
```

# Chapter 6

## Principles of Design

### 6.1 Introduction

The design of electrical machinery is both an art and a science. There are so many factors involved in the design process that it is not possible to work along rigid lines. Any design must be a compromise between a large number of conflicting requirements. Thus there is no unique solution to a design problem, and designs for the same specification will differ because of different emphasis *being placed on each requirement by the particular designer.*

To a great extent, design is an iterative process; that is parts of the design are repeated in order to obtain the desired solution. For instance, in the design of a motor of a given horsepower rating, an initial estimate has to be made of the efficiency. When the design has been completed, only then can the efficiency be checked. The initial and final values must agree to some desired tolerance. If they do not, the initial values and portions of the design must be adjusted as necessary. Similar iterations may be involved in optimizing other parts of the design. As a designer gains experience, he or she will be able to deal with the iterative process more quickly, generally because one makes better initial assumptions. This dependence on an iterative process has, to a large extent, led to the use of high speed digital computers for the design of electric machinery.

### 6.2 Design Factors

Those factors which influence the design of a machine may be categorized as follows.

(1) *Economic Factors.* In most cases this is the overriding consideration since, all other design factors being equal, this factor will decide who sells the

machine and who does not. Clearly, in order to be competitive, there must be an absolute minimum of material in the machine and the machine must be designed such that manufacturing cost is minimized. Design of the machine should always be compatible with the equipment available for machining and assembly already in place in the plant and with materials which are in stock without time consuming and costly special purchase. Better performance is nearly always possible at more cost but the best machine for the job is that in which the first cost plus the cost of losses and maintenance over the life expectancy is a minimum. The rising costs of electrical energy has recently prompted a resurgence of interest in the trade-off between first cost and running cost resulting in machines of much higher efficiency than customarily used in the past.

(2) *Material Limitations.* The technical and economic limits of materials generally determine the performance and dimensions of the machine. Progress in magnetic and insulating materials has been continuous. These new materials have had a dramatic affect on machine design in the past and will continue to do so in the future.

(3) *Specifications.* The design, performance and materials used are often subject to specifications issued by I.E.E.E. or similar bodies. In this country the motor manufacturers have banded together to form the National Electrical Manufacturers Association (NEMA) to set standards for size, performance and testing of AC and DC machines from 1.0 up to 450 HP. Also, standards of the individual motor manufacturer also plays an important role since there will often be standard wire sizes, insulation thicknesses etc. dictated by manufacturing economy. NEMA also sets standard diameters which sometimes may necessitate ingenuity in determining the best size for a given application.

(4) *Special Factors.* In some applications special considerations may exist which have an overriding concern. For example, design of aircraft generators requires a design of minimum weight with maximum reliability. For design of traction motors the emphasis is on reliability and ease of servicing. For type-writer motors the most important factor may be minimum noise. Motors for starting large compressors may have to deal with a large inertia in which the heating during starting is severe. Hence, the starting torque per ampere may be a major consideration for this application.

(5) *Theoretical Factors.* In this category are all the quantifiable details of electrical and mechanical design. These considerations are discussed in more detail in the subsequent sections.

## 6.3 Standards for Machine Construction

It might be said that rarely is the machine designer presented with a problem in which he is not confronted with geometric constraints. Frequently these constraints are application dependent, for example it is essential that a traction motor on a locomotive fit in the space available under the rail car. The need for standard shapes and sizes of motor and generators has resulted in NEMA standards. It is necessary for general purpose electrical machines to satisfy certain criterion in order to bear their stamp of approval. The most recent ANSI/NEMA standards is Publication MG1-1978 which includes a number of revisions. NEMA standards specify the power, speed voltage and frequency rating of machines for a number of applications. Standard designs are classified according to performance. Typical torque-speed curves for various NEMA Design Classes for squirrel-cage induction machines are shown in Figure 6.2.

Four classes of motors are identified. *Class A* motors are the "vanilla" flavor motor having normal starting torque and normal starting current. The motor is designed to have 200 to 250% pull out torque. Larger sizes usually require special starting equipment. This type of motor is frequently replaced by a *Class B* motor. *Class B* motors have a normal starting torque but a lower starting current. They can be started on-line up to 300 HP. These motors have slightly poorer efficiency and power factor than *Class A* motors as well as slightly lower pull out torque. They usually contain deep bars in the rotor. These motors are probably the most popular type of induction motor. *Class C* motors have a high starting torque and a low starting current. The machines usually employ a double squirrel cage. Starting torque is on the order of 175 to 200% while pull out torque is greater or equal to 185% of rated torque. The motor has low slip, high efficiency and is suitable for high starting torque applications. *Class D* motors are machines which have very high starting torque and are designed to operate with high slip. These motors are used for accelerating large inertia loads or which operate with a fly wheel (for example a punch press). The high resistance rotor cage is frequently accomplished by use of brass bars. Typical starting current and starting torque values for the most common type of machine, NEMA class A and B are summarized below

in Table 6.1 and Table 6.2. Figure 6.1 shows torque versus speed curves for a family of 1800 RPM, NEMA *Class B* machines.

HP = 1	2	3	5	10	25	200
I <sub>start</sub> =10.3	9	7.6	6.9	5.8	5.5	5.5

Table 6.1 Typical per unit starting current values (NEMA Class B).

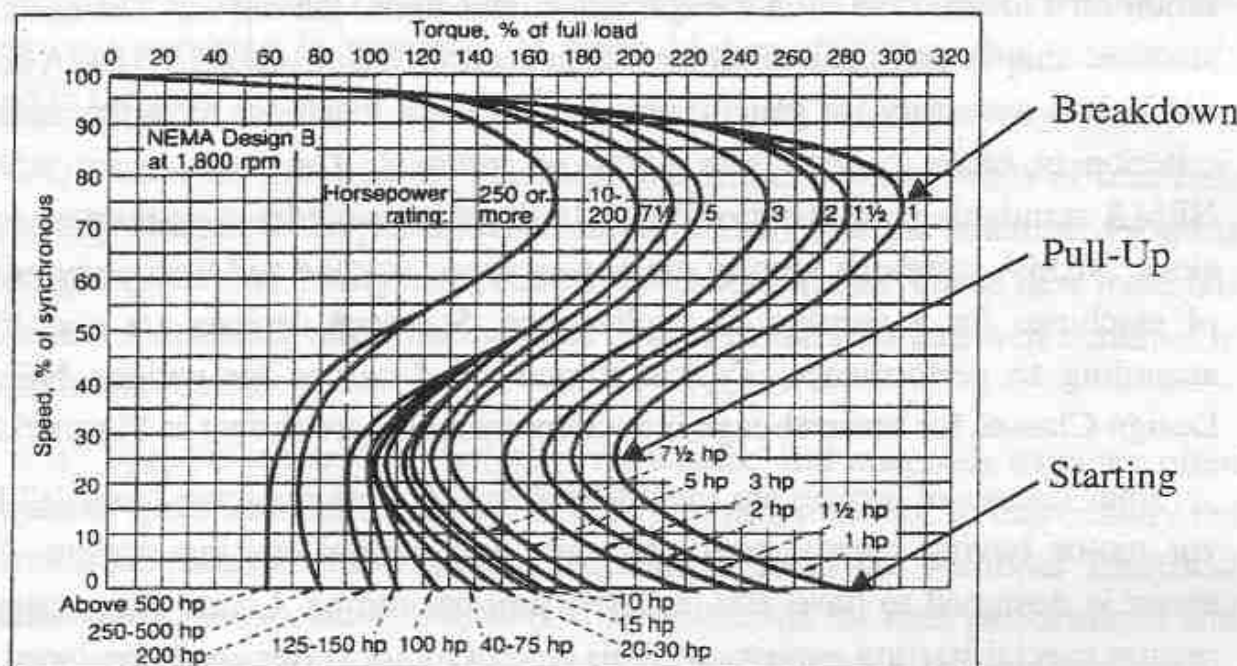


Figure 6.1 Speed vs. torque curves showing breakdown, pull-up and starting torques of 1800 RPM, NEMA Class B machines for various ratings

Motors are also designated according to their type of enclosure. Twenty types of enclosures are defined by NEMA in two major categories: Open Machines, which have ventilating openings which permits passage of external cooling air to the machine, and Totally Enclosed Machines in which the internal air is enclosed within the housing. The most popular type of Open Machine is the drip-proof machine which is protected from water or liquid falling essentially vertically on the machine (ODP). Other types of open machines are Weather Protected Type I and Type II machine which add extra screens or lou-

**Table 6.2 Typical Starting Torque Values in Per Unit of Rated Torque (NEMA Class A and B).**

HP	P=2	4	6	8	20	12
5	1.35	1.35	1.35	1.25	1.2	1.15
20	1.35	1.35	1.35	1.25	1.2	1.15
40	1.25	1.35	1.35	1.25	1.2	1.15
100	1.0	1.35	1.35	1.25	1.2	1.15
200	1.0	1.15	1.35	1.25	1.2	1.15

vers to the design and Splash-Proof which offers greater protection than drip proof but is still regarded as an indoor-type enclosure. The most frequently used Totally Enclosed Machine is the Totally Enclosed Fan Cooled Machine (TEFC) which is a machine equipped with exterior cooling by means of a fan integral within the machine but external to the enclosing parts. Special strengthening of the frames and special fittings are utilized to make some totally enclosed motors "explosion-proof" and "dust-explosion proof". Other types of enclosures include TEAAC (totally enclosed air to air cooled), TEFV (totally enclosed force ventilated), and TEWAC (totally enclosed water to air cooled) and TEPC (totally enclosed pipe cooled).

NEMA specifies the following horsepowers as standard: 0.5, 0.75, 1, 1.5, 2, 3, 5, 7.5, 10, 20, 25, 30, 40, 50, 60, 75, 100, 125, 150, 200, 250, 300, 350, 400, 450, and 500 horsepower. It can be noticed that there exists a rather logarithmic increase in horsepower sizes. From the point of view of a machine designer of NEMA machines, the major concern is to utilize the same laminations or the least number of laminations having the same outside diameter  $D_{os}$  to produce a family of induction machines. Standard voltages for NEMA machines as a function of size are summarized in Table 6.3.

One primary purpose of NEMA standards is to standardize the external dimensions of electrical machines according to "frame sizes" so that OEMs (original equipment manufacturers) as well as end point users can more easily select between various manufacturers without drastic changes in shaft couplings, mounting brackets, etc. A typical page from the NEMA standards showing standard letter designations of a drip proof type enclosure is shown in Figure 6.3. Most of the dimensions of Figure 6.3 are not specified by NEMA

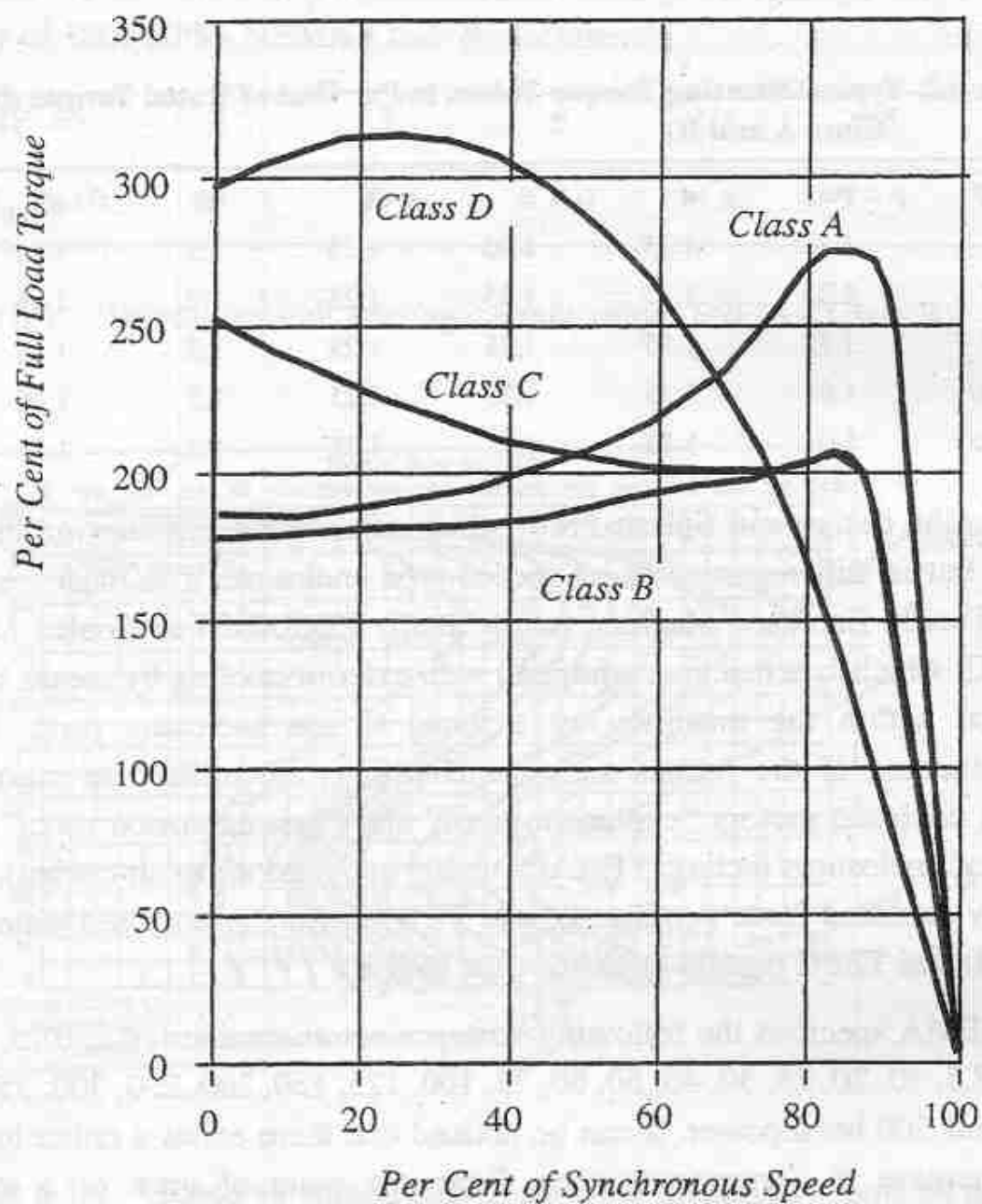


Figure 6.2      Torque-speed curves for NEMA squirrel cage induction machines

and most of those that do concern practical matters such as spacing of bolt holes, etc. The most important parameter from a designer's point of view is the shaft height since this quantity essentially fixes the diameter of the machine for a given frame size. A table showing the specific value of a number of this key dimension is given in Table 6.4. Note that the first two numbers of the frame size is exactly equal to four times the dimension  $D$  so that the diameter in inches of a machine of a given frame size is roughly equal to one-half the first two digits of the frame size.

**Table 6.3 Recommended voltages for electric motors**

Rated voltage, V	Recommended power range, hp
230 or 460	Up to 100
460 or 575	100-600
2,300	200-4,000
4,000	400-7,000
6,600	1000-12,000
13,200	3,500-25000

Frame	D	Frame	D
140	3.50	320	8.00
160	4.00	360	9.00
180	4.50	400	10.00
210	5.00	440	11.00
250	6.25	500	12.50
280	7.00	580	14.50
320	8.00	680	17.00

**Table 6.4 NEMA frame sizes and corresponding shaft height**

## 6.4 Main Design Features

The major theoretical factors in design of an electric machine can be broken into five areas, electrical, magnetic, dielectric, thermal, and mechanical.

1) *Electrical*. In order to make the machine compatible with the electrical supply the voltage, frequency and number of phases of the machine are specified. In addition, the minimum power factor at rated load may also be specified. From this data the designer must determine the type of connection (wye or delta), the type of winding (wave or lap, one or two layer, random or form wound, etc.) and winding factors. Other important electrical features are the current density in the windings, the copper losses, and the short circuit current.

DIMENSIONS—A-C AND D-C  
JUNE 1976  
PART II PAGE 7

Fig. 11-1. Lettering of Dimension Sheets for Foot-mounted Machines—Side View. A

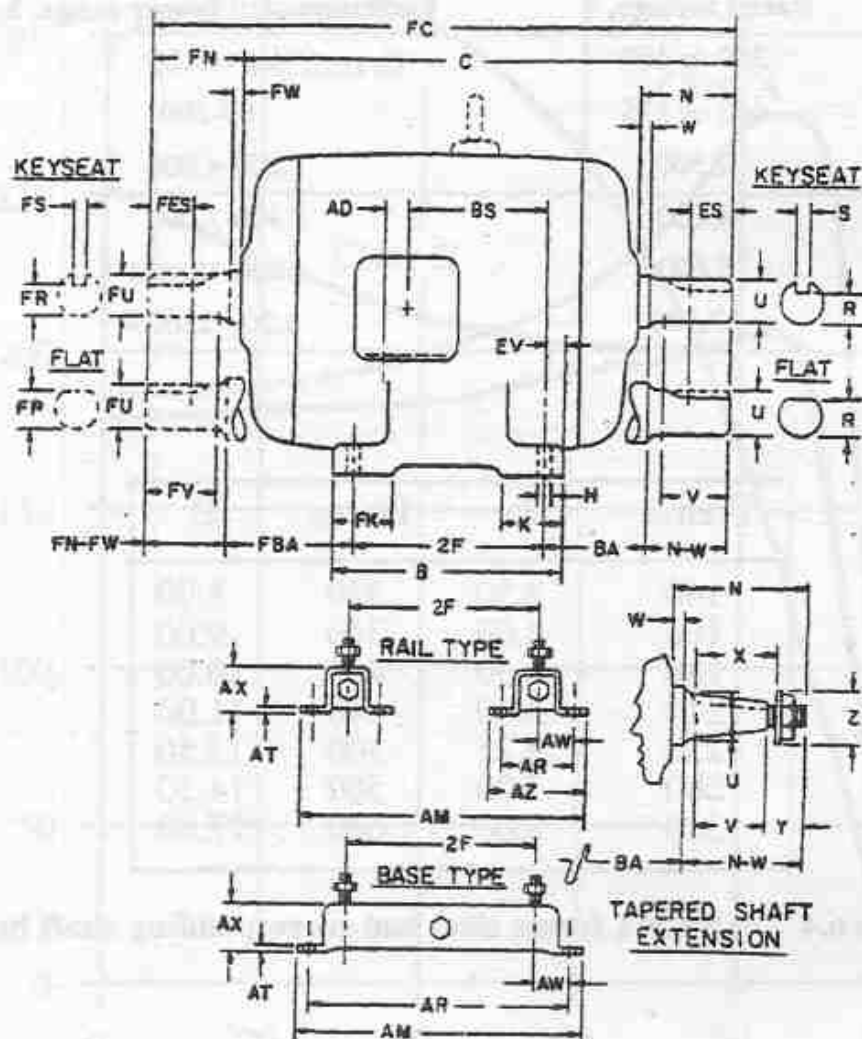


Figure 6.3 Standard designations for an open drip proof squirrel cage machine - side view

2) *Magnetic*. In the category of magnetic considerations are such factors as fixing maximum flux densities in the teeth and core, the resulting iron losses, the effect of saturation on prescribed overvoltages, calculation of magnetizing and leakage inductances, determination of slot and tooth shapes, calculation of harmonic effects (stray load and no load losses and harmonic torques).

3) *Dielectric*. The influence of the electric fields also have an important effect on the design of the machine. Important considerations involve selection of proper insulation thickness for strand to strand, coil to coil and coil to ground insulation to survive continuous as well as surge voltages (i.e. lightning

JUNE 1976  
PART II PAGE 2

DIMENSIONS—A-C AND D-E

Fig. 11-2. Lettering of Dimension Sheets for Foot-mounted Machines—Drive End View.

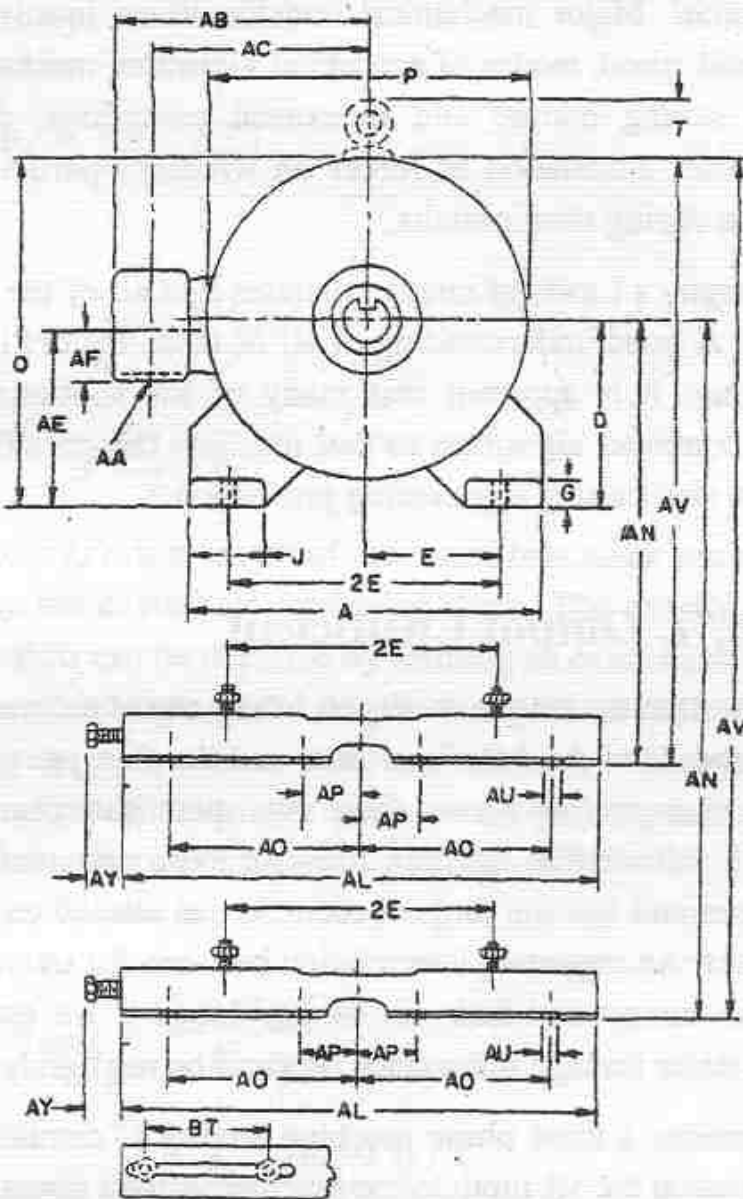


Figure 6.4 Standard designations for an open drip proof squirrel cage machine - end view

strokes). Other related considerations concern proper routing of the windings to the outside world and the selection of bushings to avoid flashovers.

4) *Thermal*. The heat produced within a machine will, without proper venting, cause the machine to self destruct. Although the considerations here intrigue mechanical rather than electrical engineers, the problems are no less important. Important considerations involve selection of the coolant (air, water, hydrogen), selection and spacing of ducts, design of centrifugal fan, calcula-

tion of temperature rise, and design of cooling tank and radiators (where applicable).

5) *Mechanical.* Major mechanical considerations involve calculation of critical rotational speed, modes of acoustical vibration, mechanical stresses on rotating shaft during normal and overspeed conditions, determination of moment of inertia, calculation of forces on windings particularly in the end winding portion during short circuits.

One of Murphy's Laws, of course, dictates that all of the above considerations interact. A good understanding of all of these factors is, indeed, a lifetime undertaking. It is apparent that many of the subtleties can never be relegated to a computer algorithm so that machine design will always remain stimulating and challenging engineering profession.

## 6.5 The $D_{is}^2 L$ Output Coefficient

It is well known that the torque produced in any electrical machine is proportional to the product of the *MMF* per pole and the flux per pole. Since, for a given amount of copper and iron, these two quantities cannot be increased without limit, it follows that the "densities" of these two quantities have definite upper values and that the torque produced can also be expressed in terms of these densities. An important interrelation between the output power and the densities of the current and flux can be developed if we assume that stator resistance and stator leakage inductance drops to be negligibly small.

Let us consider a three phase machine having  $C$  circuits per phase. For sinusoidal excitation the VA input to the machine is then given by

$$VA = \frac{3}{2} V_s I_s \quad (6.1)$$

where  $V_s$  and  $I_s$  are the rated peak per-phase values of stator voltage and current. If stator leakage inductance and resistance is neglected then the amplitude of voltage is related to the amplitude of the air gap flux linkages by

$$\begin{aligned} V_{gap} &= \omega_e \lambda_m \\ &= (2\pi f_e) k_1 N_s \Phi_p \end{aligned} \quad (6.2)$$

Hence, the VA input to the machine at the air gap can be expressed as

$$VA_{gap} = 3\pi f_e k_1 N_s \Phi_p I_s \quad (6.3)$$

The value of flux per pole is related to the peak fundamental air gap flux density in the gap by

$$\begin{aligned}\Phi_p &= \frac{2}{\pi} B_{g1} (\tau_p l_e) \\ &= \frac{2}{\pi} B_{g1} \left( \frac{\pi D_{is} l_e}{P} \right) \\ &= \frac{2 D_{is} l_e}{P} B_{g1}\end{aligned}\quad (6.4)$$

where, in Eq. (6.4)  $l_e$  is the length of the stator iron stack including the inter-laminar air space but excluding ventilation ducts. The density of the conductors in the stator slots can be depicted by forming an expression for the average RMS amperes per unit length of the air gap. Since the three phases are assumed balanced the average peak current is the same in each coil of the machine. We will neglect the effect of non-unity pitch which makes peak total current in some slots less than others. If the pitch is unity the RMS current per unit length of the stator circumference is

$$K_{s(rms)} = \frac{S_1 n_s (I_s / C)}{\sqrt{2} \pi D_{is}} \quad (6.5)$$

$$\begin{aligned}&= \frac{S_1}{\sqrt{2} \pi D_{is}} \left( \frac{6 C N_s}{S_1} \right) \left( \frac{I_s}{C} \right) \\ &= \frac{6 N_s I_s}{\sqrt{2} \pi D_{is}}\end{aligned}\quad (6.6)$$

Inserting Eqs. (6.4) and (6.6) into Eq. (6.3) we have the following expression for volt amperes

$$VA_{gap} = 3\pi f_e k_1 N_s \left( \frac{2 D_{is} l_e B_{g1}}{P} \right) \left( \frac{\sqrt{2} \pi D_{is} K_{s(rms)}}{6 N_s} \right)$$

or

$$VA_{gap} = \sqrt{2}\pi^2 \frac{f_e k_1}{P} (D_{is}^2 l_e) B_{g1} K_{s(rms)} \quad (6.7)$$

The frequency of the machine can be related to the rotational synchronous speed in RPM by

$$f_e = \frac{\Omega_s P}{120} \quad (6.8)$$

where  $\Omega_s$  is the synchronous speed of the machine in RPM, so that Eq. (6.7) becomes

$$VA_{gap} = \left( \frac{\sqrt{2}\pi^2}{120} \right) k_1 \Omega_s (D_{is}^2 l_e) B_{g1} K_{s(rms)} \quad (6.9)$$

The power at the gap of the machine is defined by

$$P_{gap} = VA_{gap} \cos \phi_{gap} \quad (6.10)$$

or at the output shaft,

$$P_{mech} = VA_{gap} \eta_{gap} \cos \phi_{gap} \quad (6.11)$$

where  $\eta_{gap}$  is the efficiency as seen from the air gap, i.e. including rotor iron and copper loss and stray losses. So that, finally,

$$P_{mech} = \left( \frac{\sqrt{2}\pi^2}{120} \right) k_1 k_{is} \Omega_s (D_{is}^2 l_e) B_{g1} K_{s(rms)} \eta_{gap} \cos \phi_{gap} \quad (6.12)$$

Equations (6.9) and express the volt-ampere input and power output of any AC or DC machine and is sometimes called *Essen's Rule* [1]. It is useful to examine these results carefully in order to note the effect of each term on the machine design. Clearly for a given volt ampere input, the output power is maximized by making  $\cos \phi_{gap}$  unity which can only be approximated by having very small rotor leakage inductance. This implies that the flux density  $B_{g1}$  and MMF per pole  $F_{p1}$  then act at right angles internally at the air gap of the machine. The input and output power can be also raised by increasing one of four quantities.

- (1) The rms surface current density  $K_{s(rms)}$ .

The surface current density is limited by the  $I^2R$  losses in the conductor, the effectiveness of the cooling media and the permissible temperature rise in the insulating materials.

- (2) The fundamental magnetic flux density  $B_{g1}$ .

The flux density is limited by the saturation point of the material used, the hysteresis and eddy current losses, the stray no load losses, and the effectiveness of the coolant.

- (3) The rotational synchronous speed in RPM  $\Omega_s$ .

The rotational speed is limited by rotational stresses in the rotating member, by brush problems in the cases of DC, synchronous or wound rotor induction machines, and by performance requirements of the machine for a given application.

- (4) The quantity  $D_{is}^2 l_e$ .

Without ducts  $l_e$  is essentially equal to  $l_i$  (length of actual iron) and this term differs from the volume of the portion of the machine occupied by the rotor only by the constant  $\pi/4$ . This quantity is also roughly proportional to the total active volume of the machine since the volume of the stator copper and iron is roughly equal to the volume used for rotor copper and iron.

Since  $K_{s(rms)}$ ,  $B_{g1}$  and  $\Omega_s$  have definite limits it is apparent that increased size is inevitably achieved by an increased volume of iron and copper. Equation can be written in the form

$$\frac{P_{mech}}{D_{is}^2 k_{is} l_e \Omega_s \eta_{gap} \cos \phi_{gap}} = \left( \frac{\sqrt{2} \pi^2}{120} \right) k_1 K_{s(rms)} B_{g1} = C_o \quad (6.13)$$

Since the right hand side varies over relatively small limits, the quantity expressed by the right hand side of Eq. (6.13) is called the *output constant* of a machine. In practice the output constant is not truly a constant but increases with rating. This fact is due to many factors including the use of better magnetic and insulating materials as size increases, the fact that large machine have a larger pole pitch for the same speed resulting in better cooling than a machine with a smaller rating and due to the larger extension of the end winding and larger air velocity in machines of higher rating. Also the voltage is important

since for higher the voltage the more space is necessary for the insulation and less space is left for the copper.

The torque as function of  $D_{is}^2 l_e$  is readily obtained from Eq. (6.12) by dividing by rotor speed. The result is,

$$T_e = \frac{P_{mech}}{(2\omega_e/P)} \quad (6.14)$$

$$= \left( \frac{\sqrt{2}\pi}{4} \right) k_1 k_{is} (D_{is}^2 l_e) B_{g1} K_{s(rms)} \eta_{gap} \cos \phi_{gap} \quad (6.15)$$

It is useful to note that the torque is fundamentally independent of the number of poles of the machine.

The dependence of the output "constant" of an induction machine on pole pitch is shown in Figure 6.5. In Figure 6.6 is an auxiliary curve which gives the ratio between the effective core length and the pole pitch, the so-called *aspect ratio*. This ratio cannot be chosen arbitrarily because it is of importance for the cooling of the machine. In order to demonstrate this fact it is first observed that thermal considerations specify that for a given amount of losses and cooling air, the bore surface area cannot be made smaller than a definite minimum value. Hence, we can state that

$$P\tau_p l_e = S \quad (\text{a constant}) \quad (6.16)$$

or

$$\pi^2 \frac{D_{is}^2}{P} \left( \frac{l_e}{\tau_p} \right) = S$$

It follows that the bore diameter

$$D_{is} = \frac{1}{\pi} \sqrt{PS \frac{1}{l_e/\tau_p}} \quad (6.17)$$

Hence the inner bore diameter varies inversely with the square root of the aspect ratio. A large  $l_e/\tau_p$  is desirable when weight is a major consideration since the rotor volume is

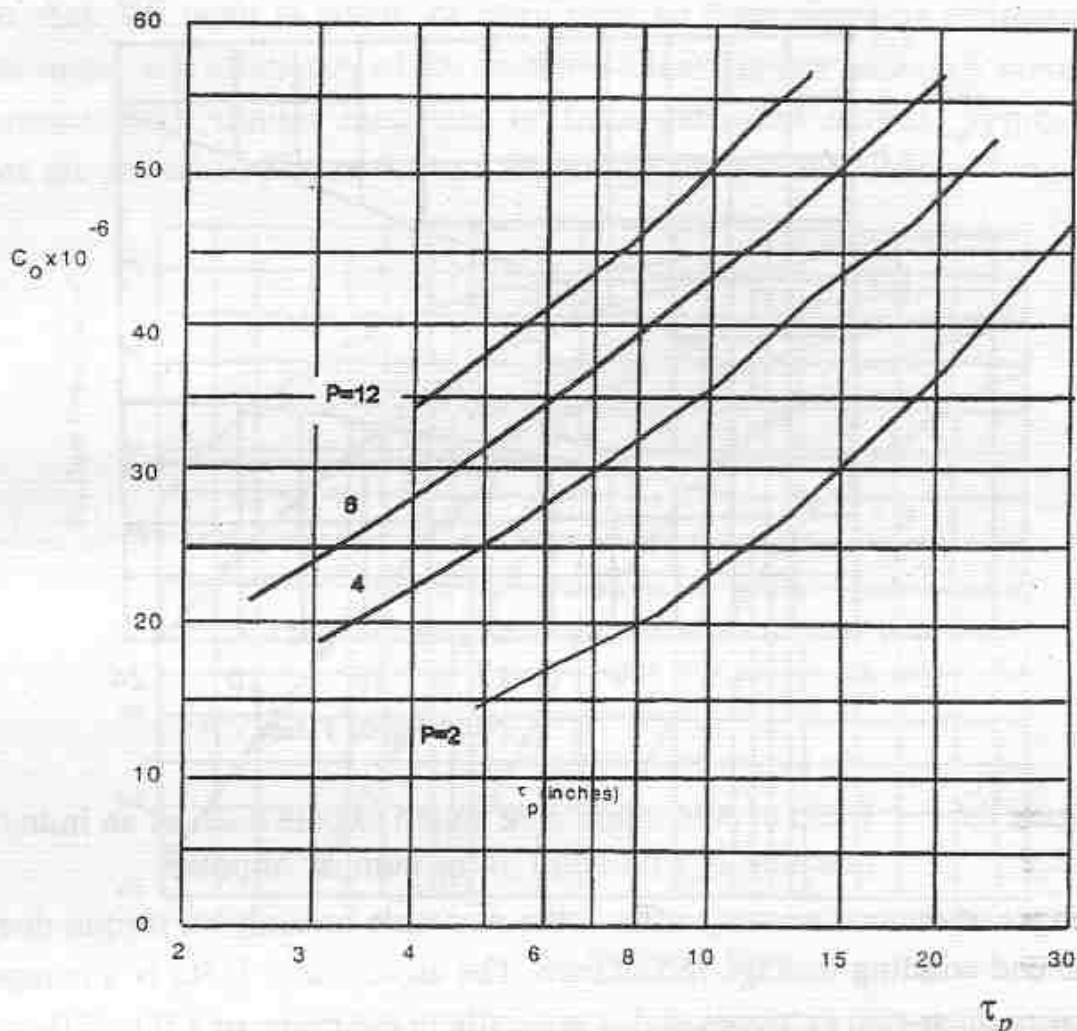


Figure 6.5 Output constant  $C_o$  of induction motor as a function of pole pitch  $\tau_p$  [2]

$$V_r = \frac{\pi}{4} D_{is}^2 l_e = S \frac{D_{is}}{4} \quad (6.18)$$

$$= \frac{\sqrt{P}}{4\pi} S^{3/2} \frac{1}{\sqrt{l_e/\tau_p}}$$

Therefore, for a given bore surface determined by thermal considerations, the weight (i.e. volume) and hence cost of the machine decreases with increasing  $l_e/\tau_p$ . Increasing the aspect ratio also clearly decreases the inertia of the rotor. This is especially useful for control and servo applications. The penalty paid for a large  $l_e/\tau_p$  is an increase in the surface current density  $K_{s(rms)}$ . If the aspect ratio is too large the machine is long and tubular and is difficult to cool whereas if the ratio is too small the machine is pillbox shaped. In this case

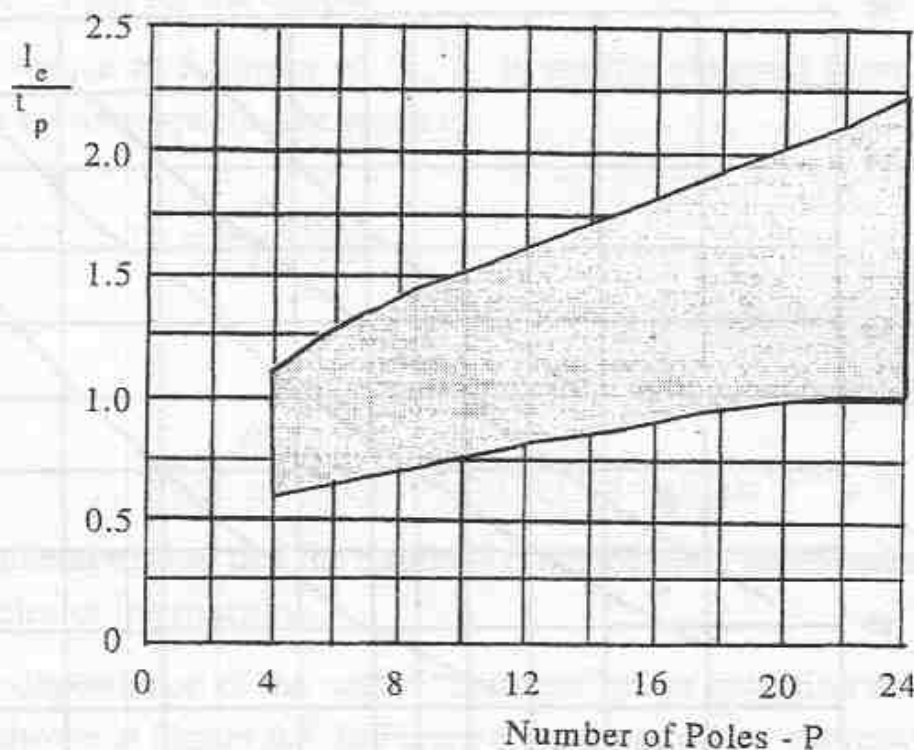


Figure 6.6 Ratio of equivalent core length to pole pitch of an induction machine as a function of the number of poles

leakage inductance severely affects the available breakdown torque due to the large end winding leakage inductance. The aspect ratio  $l_e/\tau_p$  is a compromise between these two extremes and is typically in the range of 1.0 to 2.0 as shown in Figure 6.6. As a guide to a first choice of aspect ratio, Schuisky[3] offers the following values shown in Table 6.5.

Poles $P$	Induction Machine	Synchronous Machine
2	0.6-1	1-4
4	1.26	1.26
6	1.44	1.44
8	1.59	1.59
12	1.81	1.81
24	2.29	2.29
48	2.88	2.88

Table 6.5 Aspect ratios for induction and synchronous machines with an increasing number of poles

Having selected the output coefficient  $C_o$ , it is possible to determine the required volume of the machine when the volt ampere input and speed are

given or the VA input when  $D_{is}$ ,  $I_i$  and  $\Omega_s$  are given. When the power output rather than VA input is given, its input must be determined by estimating the power factor and efficiency of the machine. These figures generally come from experience with similar machines or from published curves. Typical such curves are shown in Figure 6.7 and Figure 6.8 for a NEMA class B machines,

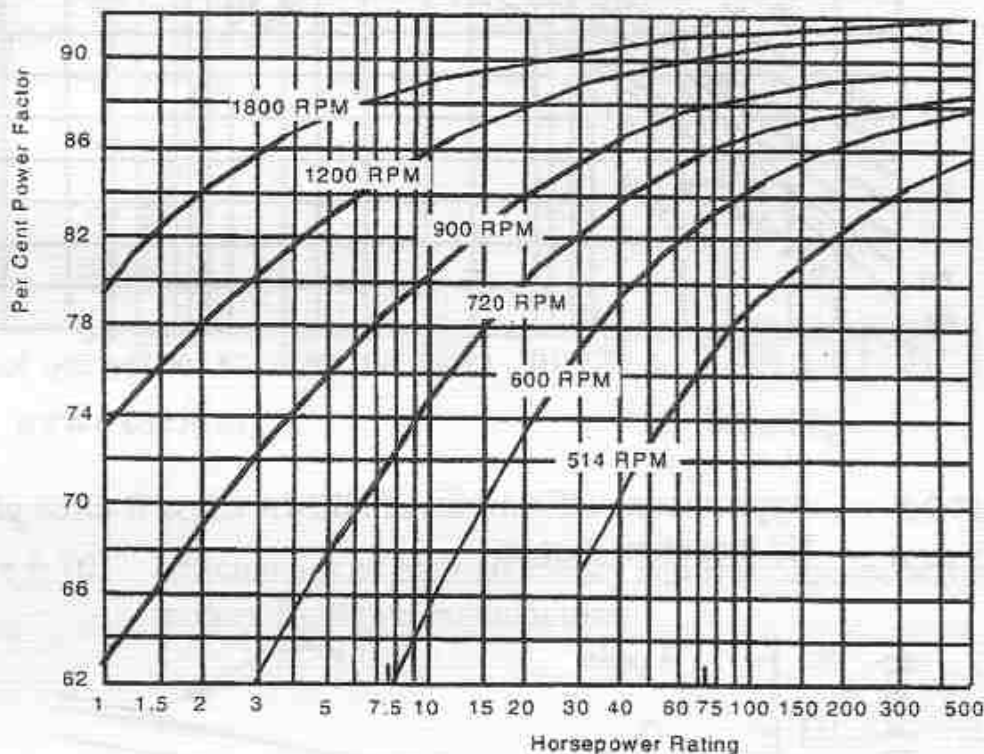


Figure 6.7 Approximate power factors of NEMA Class B three phase 60 Hz induction motors

corresponding to machines having starting torques between 115 and 150% rated and starting currents between 500 and 1000% rated. Similar curves exist for other NEMA classes.

Measured efficiency and power factors for a range of standard and high efficiency machines for a single manufacturer has been reported in [4]. Figure 6.9 to Figure 6.12 show these nominal results.

## 6.6 The $D_{os}^3 L$ Output Coefficient

While the  $D^2L$  equation has been used extensively to design electrical machines, it does not consider several key factors. For example, machine size is affected by the complete stator geometry which includes the relative proportions of the stator inner and outer diameters, slot and tooth dimensions, flux

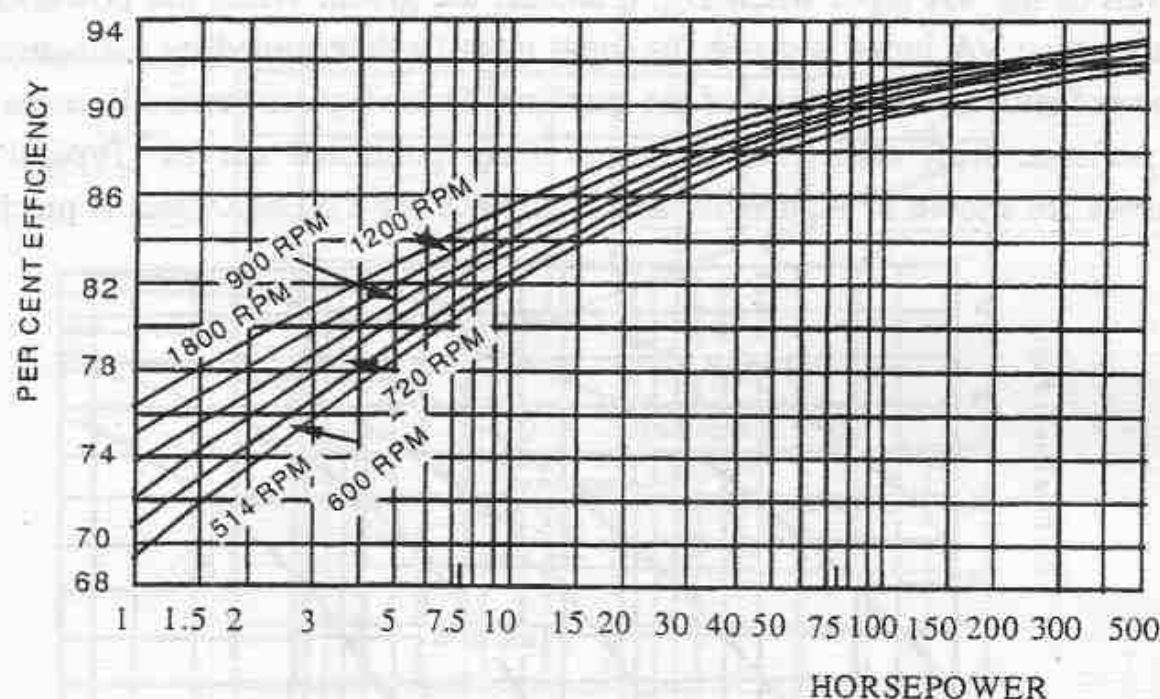


Figure 6.8 Approximate efficiencies of NEMA Class B three phase 60 Hz induction motors

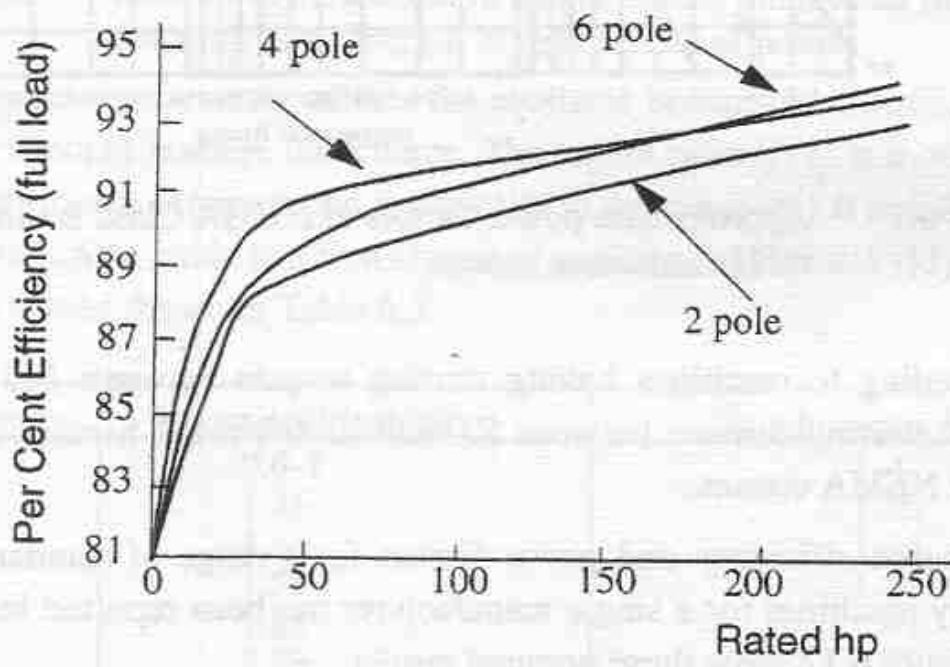


Figure 6.9 Efficiencies of standard class B squirrel cage induction machines of one manufacturer

densities in the iron parts as well as the gap and also the actual current densities in the conductor themselves. The output coefficient  $C_o$  contains only the air

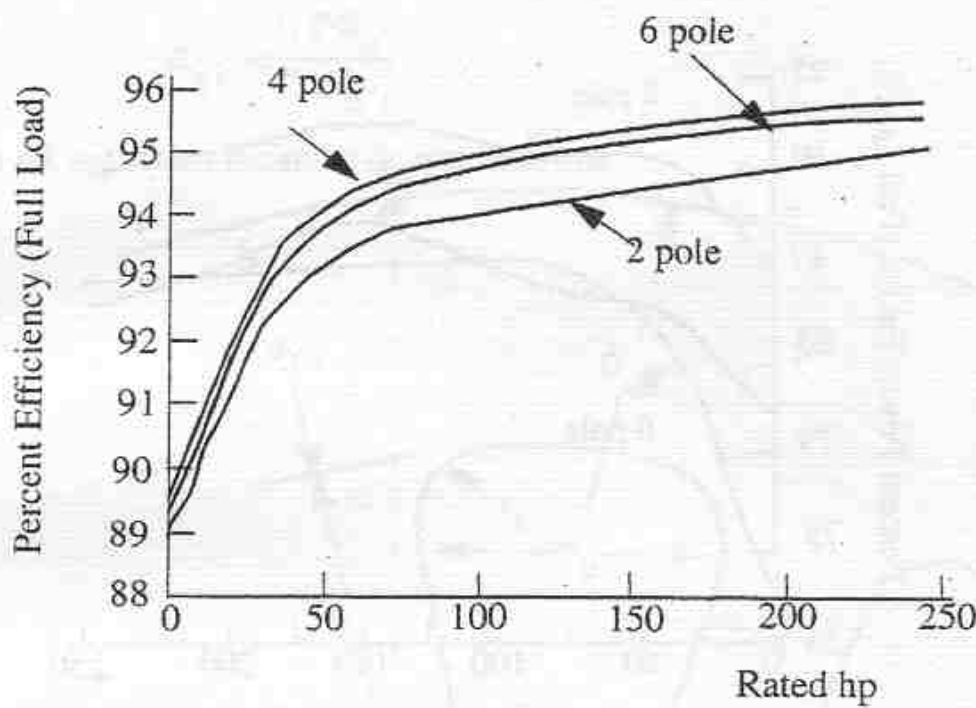


Figure 6.10 Efficiencies of high efficiency squirrel cage induction motors from one manufacturer

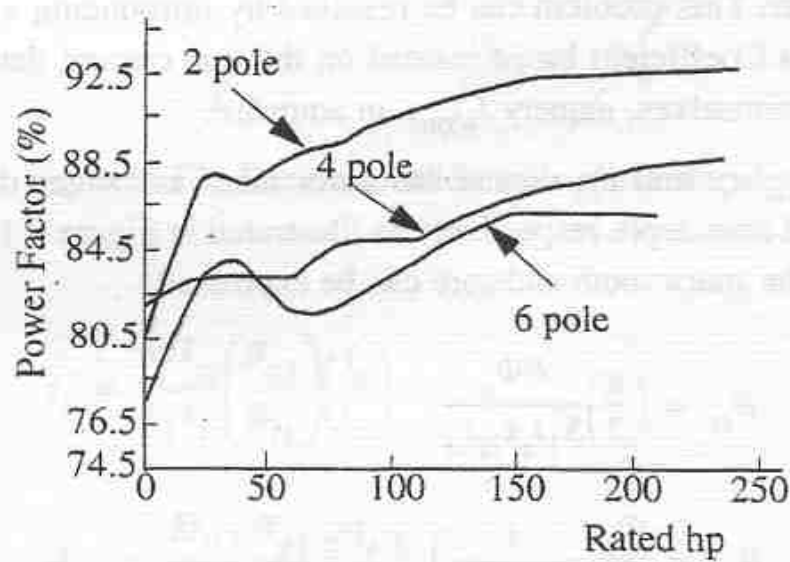


Figure 6.11 Power factors of standard class B induction machines corresponding to Figure 6.9

gap quantity  $B_{g1}$  and the surface current density  $K_{s(rms)}$ . There are additional relationships connecting these air gap quantities with the flux and current den-

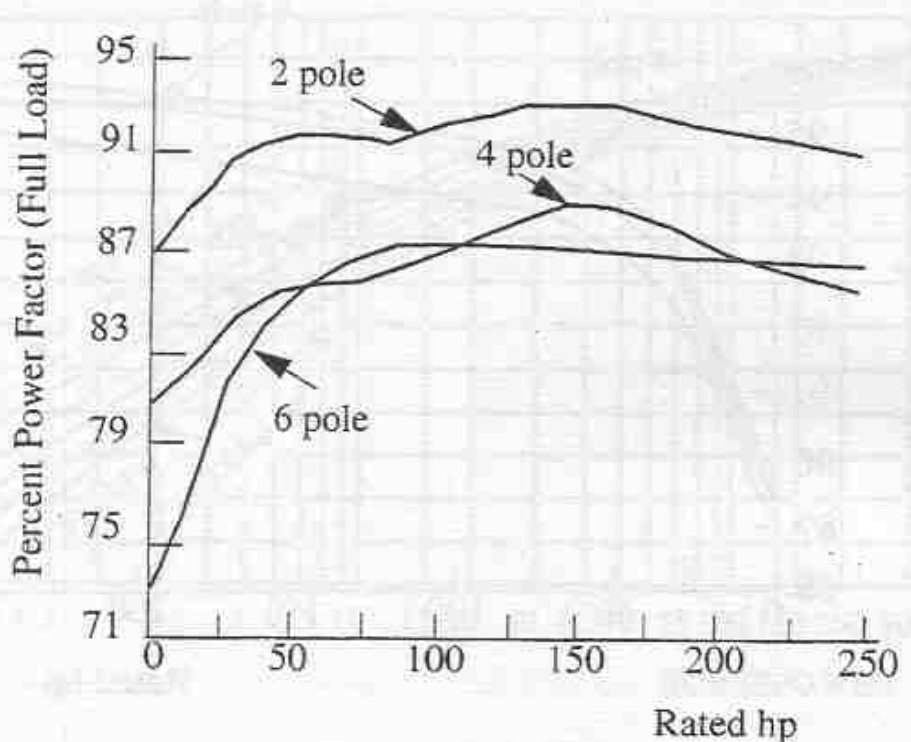


Figure 6.12 Power factor of high efficiency machines of Figure 6.10

sities existing within the machine's interior. Also, the value  $D^2L$  obtained from Eq. (6.13) only gives an estimate of the air gap diameter, rather than the machine's outer diameter, which is more often the constrained variable than the rotor diameter. This problem can be resolved by introducing a modified form of the Output Coefficient based instead on the true current density within the conductors themselves, namely  $J_{s(rms)}$  in amps/in<sup>2</sup>.

If  $D_{is}$ ,  $D_{os}$ ,  $t_s$ , and  $d_{cs}$  denote the stator inner and outer diameters, tooth thickness and core depth respectively as illustrated in Figure 6.13, then the flux densities in the stator tooth and core can be expressed,

$$B_{ts} = \left(\frac{\pi}{2}\right) \frac{P\Phi_p}{S_1 t_s k_{is} l_{is}} \quad (6.19)$$

$$B_{cs} = \frac{\Phi_p}{2} \left( \frac{1}{d_{cs} k_{is} l_{is}} \right) \quad (6.20)$$

where  $k_{is}$  represents the ratio between the actual length of stator iron (excluding ducts but including air space between lamination) and the physical length of stator iron  $l_{is}$ .  $\Phi_p$  denotes the flux per pole, in Eq. (6.3). In addition, from Eq.(6.4),

$$B_{g1} = \frac{P\Phi_p}{2D_{is}l_e} \quad (6.21)$$

Upon taking ratios it can be determined that

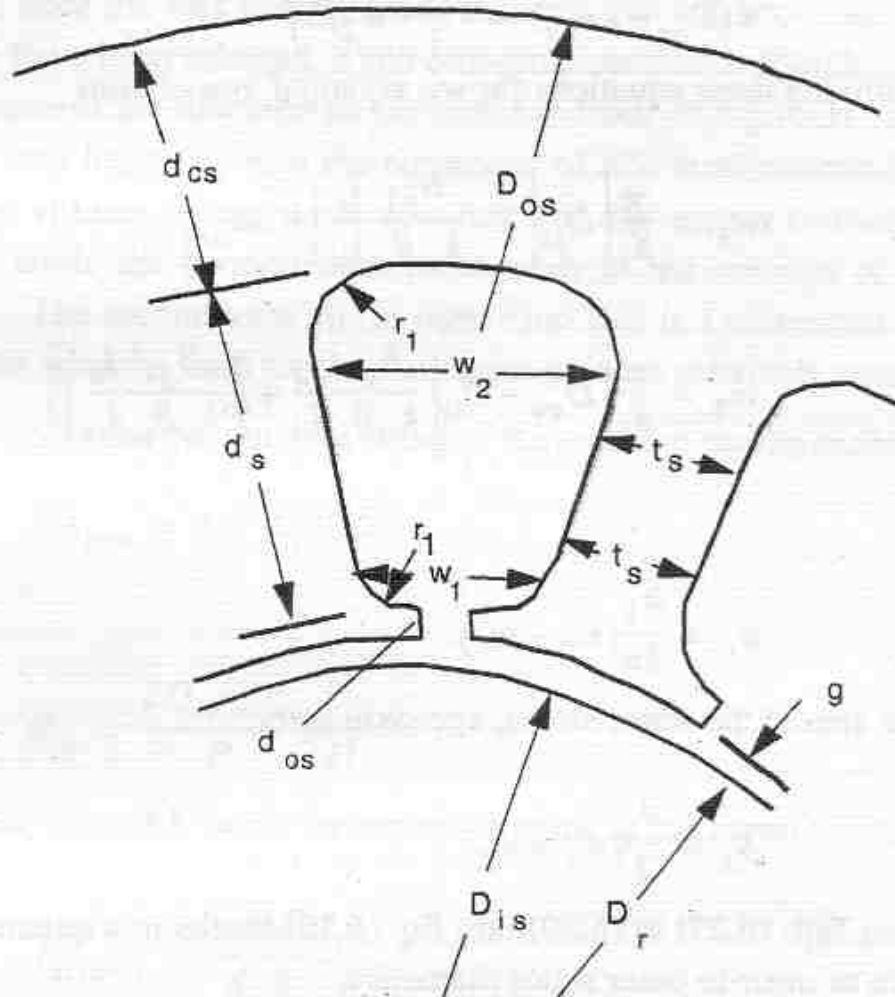


Figure 6.13 Dimensional data for stator slot shape

$$t_s = \frac{\pi D_{is}}{S_1 k_{is}} \left( \frac{B_{g1}}{B_{ts}} \right) \left( \frac{l_e}{l_{is}} \right) \quad (6.22)$$

$$d_{cs} = \frac{D_{is}}{Pk_{is}} \left( \frac{B_{g1}}{B_{ts}} \right) \left( \frac{l_e}{l_{is}} \right) \quad (6.23)$$

The stator outer diameter and slot depth can be introduced by means of the equation,

$$D_{os} = D_{is} + 2(d_{os} + d_s + d_{cs}) \quad (6.24)$$

and the slot widths core depth by

$$\pi(D_{is} + 2d_{os}) = (t_s + w_1)S_1 \quad (6.25)$$

$$\pi(D_{os} - 2d_{cs}) = (t_s + w_2)S_1 \quad (6.26)$$

Upon solving these equations for  $w_1$ ,  $w_2$  and  $d_s$  one obtains

$$w_1 = \frac{\pi}{S_1} \left[ D_{is} \left( 1 - \frac{B_{g1}}{k_{is} B_{ts}} \frac{l_e}{l_{is}} \right) + 2d_{os} \right] \quad (6.27)$$

$$w_2 = \frac{\pi}{S_1} \left[ D_{os} - D_{is} \left( \frac{B_{g1}}{k_{is} B_{ts}} \frac{l_e}{l_{is}} + \frac{2}{P} \frac{B_{g1}}{k_{is} B_{cs}} \frac{l_e}{l_{is}} \right) \right] \quad (6.28)$$

and

$$d_s = \frac{S_1}{2\pi} (w_2 - w_1) \quad (6.29)$$

The area of the stator slot is, approximately,

$$A_s = \frac{d_s}{2} (w_1 + w_2) \quad (6.30)$$

Inserting Eqs. (6.27) to (6.29) into Eq. (6.30) results in a quadratic in terms of the ratio of inner to outer stator diameters,

$$a \left( \frac{D_{is}}{D_{os}} \right)^2 - 2b \left( \frac{D_{is}}{D_{os}} \right) + 1 = \frac{S_1 A_s}{\pi D_{os}^2} + \frac{\delta_1}{D_{os}^2} \quad (6.31)$$

where

$$a = \left( \frac{B_{g1}}{k_{is} B_{ts}} \frac{l_e}{l_{is}} + \frac{2}{P} \frac{B_{g1}}{k_{is} B_{cs}} \frac{l_e}{l_{is}} \right)^2 - \left( 1 - \frac{B_{g1}}{k_{is} B_{ts}} \frac{l_e}{l_{is}} \right)^2$$

$$b = \left( \frac{B_{g1}}{k_{is} B_t} + \frac{2}{P} \frac{B_{g1}}{k_{is} B_{cs}} \right) \frac{l_e}{l_{is}}$$

$$\delta_1 = 4 \left[ d_{os}^2 + D_{is} d_s \left( 1 - \frac{B_{g1}}{k_{is} B_{ls}} \frac{l_e}{l_{is}} \right) \right]$$

Note that once the flux density ratios between gap and tooth and between gap and core have been selected,  $a$  and  $b$  become constants. If both numerator and denominator of the first term on the right hand side of Eq. (6.31) are multiplied by the iron length  $l_{is}$  then the numerator of this term essentially corresponds to the volume of the stator core reserved for copper (volume of the stator slots), while the denominator corresponds to the volume of the purchased steel. The second term on the right hand side is a correction factor to account for the material used for the slot opening and is relatively small.

From Eq. (6.3), the volt ampere rating of the machine can be expressed as

$$VA_{gap} = 3\pi f_e k_1 N_s \Phi_p I_s \quad (6.32)$$

where

$$\Phi_p = \frac{2D_{is} k_{is} l_{is}}{P} B_{g1}$$

The peak phase current  $I_s$  can be expressed in terms of the current density as

$$J_{s(rms)} = \frac{3\sqrt{2}N_s I_s}{S_1 A_{cu}} \quad (6.33)$$

where  $A_{cu}$  is the portion of the slot area occupied by copper. That is,

$$A_{cu} = k_{cu} A_s$$

In terms of the air gap flux density, current density and slot area, Eq. (6.32) can therefore be written,

$$VA_{gap} = \sqrt{2}\pi f_e k_1 \frac{D_{is} k_{is} l_{is}}{P} (S_1 k_{cu} A_s) B_{g1} J_{s(rms)} \quad (6.34)$$

Neglecting the second term on the right hand side of Eq. (6.31), solving for  $S_1 A_s$  and then inserting into Eq.(6.34) results in the expression

$$VA_{gap} = \frac{\sqrt{2}\pi^2}{4} f_e \frac{k_1 k_{is} k_{cu}}{P} \left[ a \left( \frac{D_{is}}{D_{os}} \right)^3 - 2b \left( \frac{D_{is}}{D_{os}} \right)^2 + \frac{D_{is}}{D_{os}} \right] (D_{os}^3 l_{is} \cdot B_{g1} J_{s(rms)})$$

which represents a sizing equation in terms of  $D_{os}^3 l_{is}$ . In terms of mechanical speed, from Eq. (6.8),

$$\frac{VA_{gap}}{\Omega_{mech}} = \frac{\sqrt{2}\pi^2}{480} (k_1 k_{is} k_{cu}) \left[ a \left( \frac{D_{is}}{D_{os}} \right)^3 - 2b \left( \frac{D_{is}}{D_{os}} \right)^2 + \frac{D_{is}}{D_{os}} \right] (D_{os}^3 l_{is}) [B_{g1} J_{s(rms)}]$$
(6.35)

The polynomial in the square brackets is clearly a function which should be maximized in order to produce a minimum value of  $D_{os}^3 l_{is}$  for a given volt ampere and speed requirement. Since the input volt amperes are related to the output power in watts by

$$P_{out} = VA_{gap} \eta_{gap} \cos \theta_{gap} \quad (6.36)$$

where  $\eta_{gap}$  is the efficiency measured at the air gap, that is neglecting stator copper and stator iron loss. In a similar manner  $\cos \theta_{gap}$  is the power factor when viewed at the air gap (i.e.  $\theta_{gap}$  is the phase angle of the stator current with respect to the air gap voltage). Eq. (6.35) can also be written in terms of the output power as

$$\frac{P_{out}}{\Omega_{mech}} = \frac{\sqrt{2}\pi^2}{480} (k_1 k_{is} k_{cu}) (\eta_{gap} \cos \theta_{gap}) \left[ a \left( \frac{D_{is}}{D_{os}} \right)^3 - 2b \left( \frac{D_{is}}{D_{os}} \right)^2 + \frac{D_{is}}{D_{os}} \right]$$

$$\times (D_{os}^3 l_{is}) (B_{g1} J_{s(rms)}) \quad (6.37)$$

$$(6.38)$$

or simply,

$$\frac{P_{out}}{\Omega_{mech}} = \xi_o D_{os}^3 l_{is} \quad (6.39)$$

The quantity  $\xi_o$  is called the  $D_o^3 L$  output coefficient. The quantity in square brackets in Eq. (6.38) is clearly important in the optimization of the machine design. Defining the function

$$f_o(D_{is}/D_{os}) = \left[ a \left( \frac{D_{is}}{D_{os}} \right)^3 - (2b) \left( \frac{D_{is}}{D_{os}} \right)^2 + \frac{D_{is}}{D_{os}} \right] \quad (6.40)$$

The function  $f_o(D_{is}/D_{os})$  is plotted in Figure 6.14 as a function of  $D_{is}/D_{os}$ . The peak of one of the curves represents an optimum (minimum) value of  $D_{is}/l_{is}$  for a given ratio of  $B_{cs}/B_{ts} = 0.8$  and a particular value of  $B_{g1}/B_{ts}$  and  $D_{os}$  [5]. The optimal value of  $D_{is}$  can be determined by differentiating Eq.

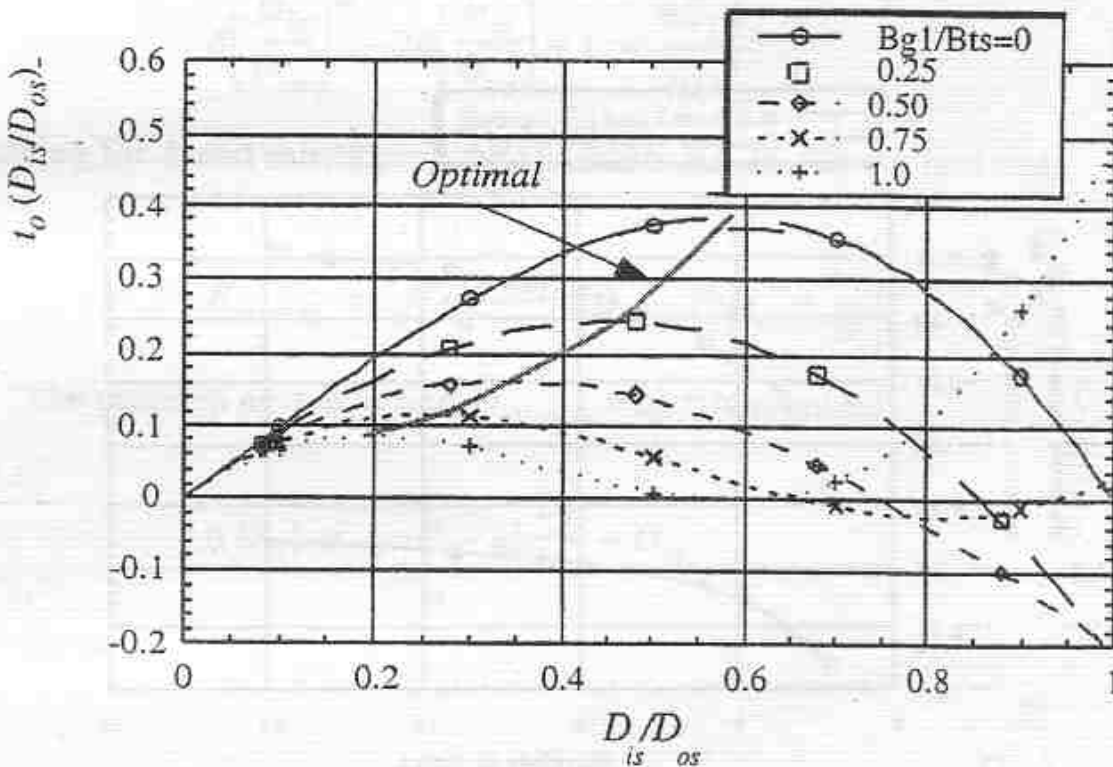


Figure 6.14 The output function  $f(D_{is}/D_{os})$  versus  $D_{is}/D_{os}$  for the case where  $B_{cs} = 0.8B_{ts}$  and  $P=4$

(6.40) with respect to  $D_{is}$  while holding  $D_{os}$  constant, and setting the result to zero. Hence,

$$\frac{\partial f_o(D_{is}/D_{os})}{\partial D_{is}} = 0 = 3a \frac{D_{is}^2}{D_{os}^3} - 4b \frac{D_{is}}{D_{os}^2} + \frac{1}{D_{os}} \quad (6.41)$$

so that

$$\left. \frac{D_{is}}{D_{os}} \right|_{optimal} = \frac{2b \pm \sqrt{4b^2 - 3a}}{3a} \quad (6.42)$$

Figure 6.15 shows how the optimal value of  $f_o(D_{is}/D_{os})$  varies with pole number. Note that the optimum value of  $D_{is}/D_{os}$  increases as the number of poles increase indicating a tendency toward a "ring shaped" stator. The maximum value of  $f_o(D_{is}/D_{os})$  also increases slowly beyond a pole number of 6 indicating that the amount of stator iron slowly decreases with pole number beyond six. This is primarily due to the fact that the flux per pole decreases with pole number thereby necessitating a progressively smaller core cross sectional area as the pole number increases.

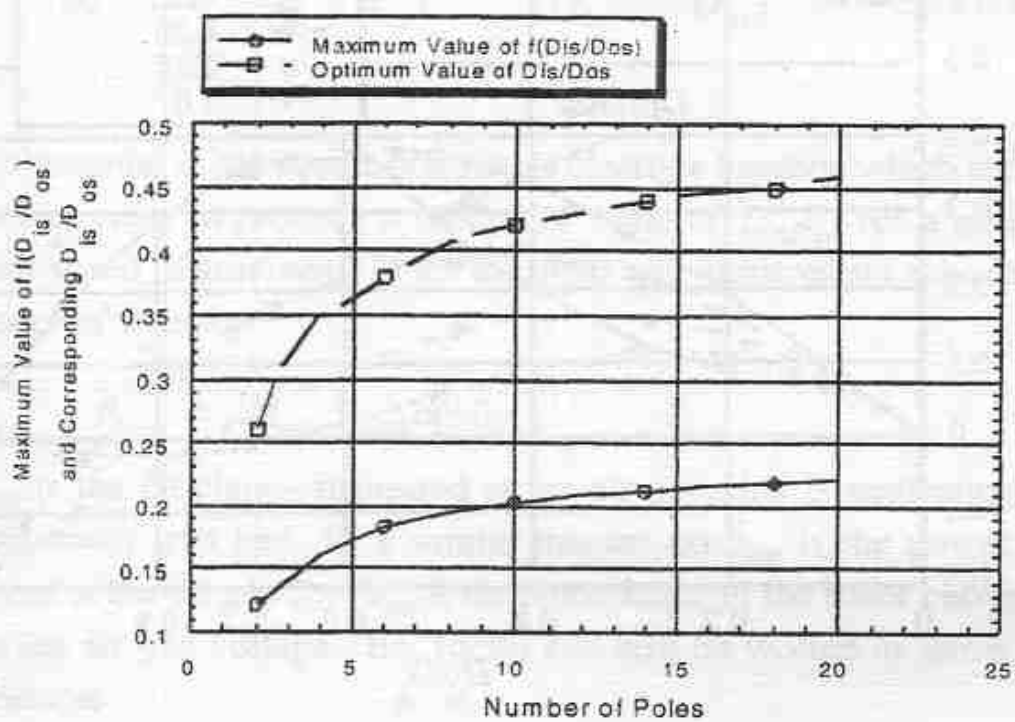


Figure 6.15 Effect of pole number on the output function  $f_o(D_{is}/D_{os})$ . Flux densities  $B_{cs} = 0.8 B_{ts}$ ,  $B_{g1}/B_{ts} = 0.5$

While the solution plotted in Figure 6.15 is optimal, it is optimal only when the current density  $J_{s(rms)}$  is held constant and not the surface current density  $K_{s(rms)}$ . In the case of machines of low pole number, the optimal values obtained from Eq. (6.42) are good designs. However, when the pole number increases, the values obtained from this result yield progressively poorer designs since the usual limitation on surface current density (heating) becomes exceeded. This problem can be overcome by introducing an inequality con-

straint in addition to Eq. (6.40). The surface current density is related to the current density by,

$$K_{s(rms)} = \frac{K_{cu} A_s S_1}{\pi D_{is}} J_{s(rms)} \quad (6.43)$$

and, from Eq. (6.31), neglecting  $\delta_1$ ,

$$a\left(\frac{D_{is}}{D_{os}}\right)^2 - 2b\left(\frac{D_{is}}{D_{os}}\right) + 1 = \frac{4S_1 A_s}{\pi D_{os}^2} \quad (6.44)$$

Solving for  $A_s$  and substituting the result into Eq. (6.43), we find that,

$$K_{s(rms)} = \frac{K_{cu} J_{s(rms)}}{4} \left( aD_{is} - 2bD_{os} + \frac{D_{os}^2}{D_{is}} \right) \quad (6.45)$$

The problem now is to find  $D_{is(opt)}$  which maximizes

$$f(D_{is}) = a\frac{D_{is}^3}{D_{os}^2} - 2b\frac{D_{is}^2}{D_{os}} + D_{is} \quad (6.46)$$

subject to

$$g(D_{is}) = K_{s(max)}^* - \frac{K_{cu} J_{s(rms)}}{4} \left( aD_{is} - 2bD_{os} + \frac{D_{os}^2}{D_{is}} \right) \geq 0 \quad (6.47)$$

where  $K_{s(max)}^*$  is a prescribed value of surface current density.

The problem involving the inequality can be converted into one with an equality constraint by the method of Lagrange multipliers [6]. In terms of this formulation, the problem is to solve,

$$\frac{\partial f(D_{is})}{\partial D_{is}} = \lambda \frac{\partial g(D_{is})}{\partial D_{is}} \quad (6.48)$$

satisfying

$$g(D_{is}) = 0 \quad (6.49)$$

Equations (6.48) and (6.49) can be written explicitly as

$$\frac{3a}{D_{os}^2} D_{is}^2 - \frac{4b}{D_{os}} D_{is} + 1 = -\lambda \frac{K_{cu} J_{s(rms)}}{4} \left( a - \frac{D_{os}^2}{D_{is}^2} \right) \quad (6.50)$$

satisfying

$$K_{s(max)}^* - \frac{K_{cu} J_{s(rms)}}{4} \left( a D_{is} - 2b D_{os} + \frac{D_{os}^2}{D_{is}^2} \right) = 0 \quad (6.51)$$

Multiplying Eq. (6.51) by  $D_{is}$  forms the quadratic equation,

$$\frac{K_{cu} J_{s(rms)}}{4} \left[ a \frac{D_{is}^2}{D_{os}^2} - 2b \frac{D_{is}}{D_{os}} + 1 \right] - \frac{K_{s(max)}^*}{D_{os}} \left( \frac{D_{is}}{D_{os}} \right) = 0 \quad (6.52)$$

which can be solved as

$$\frac{D_{is}}{D_{os}} = \frac{b}{a} + \frac{2K_{s(max)}^*}{a K_{cu} J_{s(rms)} D_{os}} \pm \sqrt{\left( \frac{b}{a} + \frac{2K_{s(max)}^*}{a K_{cu} J_{s(rms)} D_{os}} \right)^2 - \frac{1}{a}} \quad (6.53)$$

Solving Eq. (6.50) for  $\lambda$ ,

$$\lambda = \frac{3a \left( \frac{D_{is}}{D_{os}} \right)^2 - 4b \left( \frac{D_{is}}{D_{os}} \right) + 1}{\frac{K_{cu} J_{s(rms)}}{4} \left[ \left( \frac{D_{os}}{D_{is}} \right)^2 - a \right]} \quad (6.54)$$

The procedure for finding the optimal value of  $D_{is}/D_{os}$  is then to solve Eq. (6.53) for  $D_{is}/D_{os}$  and to insert this solution into Eq. (6.54). Since the plus sign in (6.53) yields a value of  $D_{is}/D_{os} > 1$ , the negative sign should be selected. If  $\lambda$  is negative then the solution for  $D_{is}/D_{os}$  is optimal. If  $\lambda$  is positive, then  $J_{s(rms)}$  must be reduced or  $D_{os}$  increased to obtain a feasible solution. Figure 6.16 compares the optimal values obtained with  $K_{s(rms)}$  as unconstrained and constrained, wherein  $B_t/B_{g1} = 0.5$ ,  $B_c/B_{g1} = 0.8$ ,  $K_{s(max)} = 5 \times 10^4$  A/m (1,270 A/in) and  $J_{s(rms)} = 5 \times 10^6$  A/m<sup>2</sup> (3,225 A/in<sup>2</sup>). Note that with the constraint  $D_{is}/D_{os}$  approaches 1.0 asymptotically rather than 0.5 indicating a ring shaped stator of small radial thickness when the surface current constraint is properly taken into account.

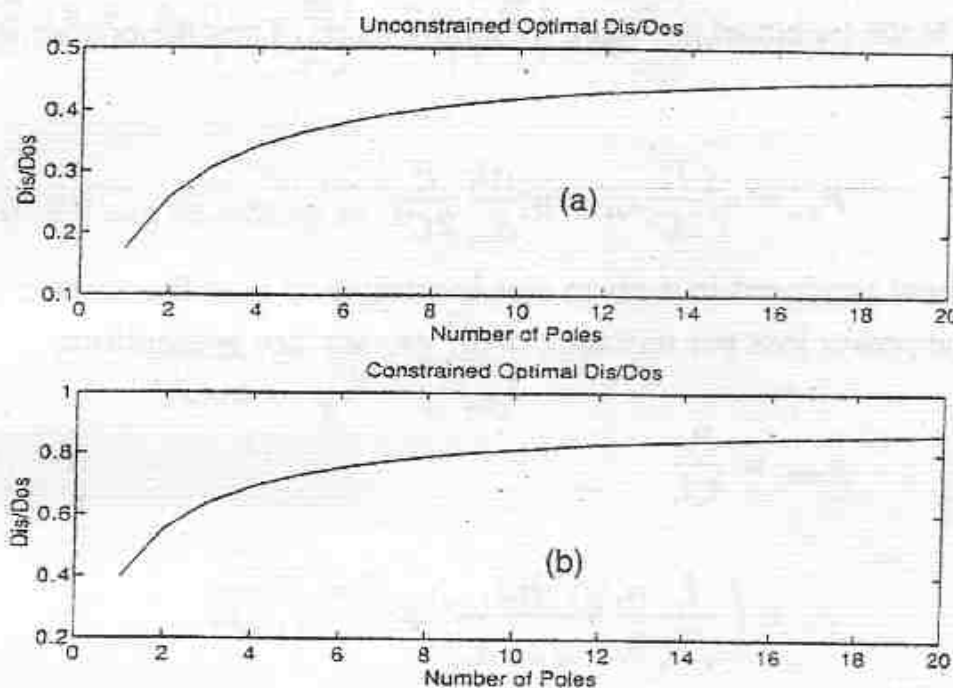


Figure 6.16 Comparison of diameter ratio  $D_{is}/D_{ox}$  (a) without and (b) with constraints on the surface current density  $K_{s(rms)}$

## 6.7 Power Loss Density

It has already been mentioned that limits must be imposed on the surface current density to prevent overheating. Since the cooling capability of a machine varies with the area, a convenient expression describing loss from the point of view of optimization is the power loss per unit area. From Eq. (6.5) the RMS current per unit length of stator circumference (surface current density) is

$$K_{s(rms)} = \frac{S_1 n_s (I_s/C)}{\sqrt{2} \pi D_{is}} = \frac{I_s}{\sqrt{2} C} \frac{n_s}{\pi (D_{is}/S_1)} \quad (6.55)$$

$$= \frac{I_s n_s}{\sqrt{2} C \tau_s} \quad (6.56)$$

The resistance of the slot portion of each conductor is

$$r_{sl} = \frac{\rho l_s}{A_{cu}}$$

where  $l_s$  is the length of the stack including ducts. Thus the copper loss in each slot is

$$P_{sl} = n_s^2 \frac{I_s^2}{2C^2} r_{sl} = n_s^2 \frac{\rho l_s}{A_{cu}} \frac{I_s^2}{2C^2} \quad (6.57)$$

The heat produced in a given slot is dissipated over the surface of one slot pitch. The power loss per unit area of air gap surface is therefore,

$$\begin{aligned} p_{diss} &= \frac{P_{sl}}{\tau_s l_s} \\ &= \left( \frac{I_s n_s}{\sqrt{2} C \tau_s} \right) \left( \frac{n_s I_s}{\sqrt{2} C A_{cu}} \right) \rho \\ &= K_{s(rms)} J_{s(rms)} \rho = \frac{K_{s(rms)} J_{s(rms)}}{\sigma} \end{aligned} \quad (6.58)$$

where  $K_{s(rms)}$  is defined by Eq. (6.6) and  $J_{s(rms)}$  is the current density per unit area of the conductor cross section, defined by Eq. (6.33).

## 6.8 The $D^{2.5}L$ Sizing Equation

Multiplication of the two sizing equations for  $D_{os}^3 l_s$  and  $D_{is}^2 l_s$  and taking the square root of the result yields another useful expression for the output torque of the machine

$$\frac{P_{out}}{\Omega_{mech}} = \sqrt{\xi_o \xi_r} \cdot \sqrt{D_{os}^3 D_{is}^2} \cdot l_{is} \quad (6.59)$$

where

$$\xi_r = \frac{\sqrt{2}\pi^2}{120} (k_1 k_{is} K_{s(rms)} B_{g1}) \eta_{ag} \cos \phi_{ag} = C_o (\eta_{ag} \cos \phi_{ag}) \quad (6.60)$$

and

$$\xi_0 = \frac{\sqrt{2}\pi^2}{480} (k_1 k_{cu} k_{is}) \left[ a \left( \frac{D_{is}}{D_{os}} \right)^3 - 2b \left( \frac{D_{is}}{D_{os}} \right)^2 + \frac{D_{is}}{D_{os}} \right] J_{s(rms)} B_{g1} (\eta_{ag} \cos \phi_{ag}) \quad (6.61)$$

Equation (6.59) can be written as

$$\frac{P_{out}}{\Omega_{mech}} = \sqrt{\xi_o \xi_r \left( \frac{D_{is}}{D_{os}} \right)^2 \cdot D_{os}^{2.5} l_{is}} \quad (6.62)$$

or simply

$$\frac{P_{out}}{\Omega_{mech}} = \xi_{o(2.5)} \cdot D_{os}^{2.5} l_{is} \quad (6.63)$$

where

$$\xi_{o(2.5)} = \frac{\sqrt{2}\pi^2}{240} (k_1 k_{is} B_{g1}) \eta_{ag} \cos \phi_{ag} \sqrt{k_{cu} K_{s(rms)} J_{s(rms)}} \left[ \frac{D_{is}}{D_{os}} \sqrt{f_o \left( \frac{D_{is}}{D_{os}} \right)} \right] \quad (6.64)$$

The function  $f_o(D_{is}/D_{os})$  is defined by Eq. (6.40). It has been shown in Section 6.7 that the quantity  $K_{s(rms)} J_{s(rms)}$  is proportional to the stator  $P R$  loss per unit surface area (neglecting the portion of the loss due to the end windings and hence is closely related to the temperature rise of the machine. Thus, if this product is kept constant the cooling capability is preserved as the machine dimensions are changed to satisfy other criteria. A plot of the function

$$\left( \frac{D_{is}}{D_{os}} \sqrt{f_o \left( \frac{D_{is}}{D_{os}} \right)} \right)$$

is shown in Figure 6.17.

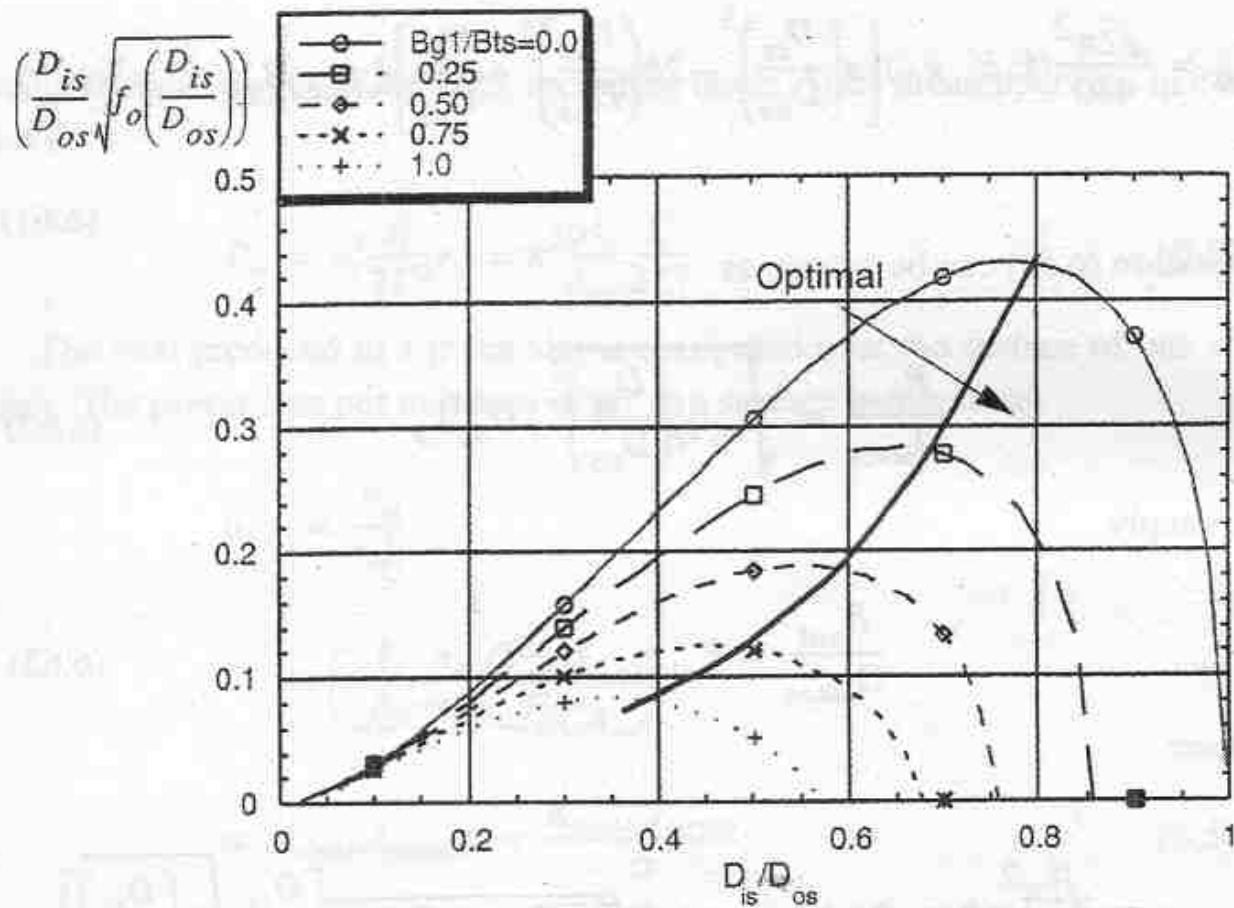


Figure 6.17 The output function  $\frac{D_{is}}{D_{os}} \sqrt{f_o\left(\frac{D_{is}}{D_{os}}\right)}$  versus  $D_{is}/D_{os}$  for the case where  $B_{cr} = 0.8$ ,  $B_{ts}$  and  $P = 4$

## 6.9 Choice of Magnetic Loading

The choice of magnetic loading is influenced by a number of factors which apply to all types of machines.

### 6.9.1 Maximum Flux Density in Iron

The maximum flux density in any iron component must clearly be kept below a well defined maximum to avoid saturation. In a well designed machine the highest flux density usually occurs in the teeth. The flux density entering a tooth is related approximately to the flux density in the gap by the ratio of tooth width to slot pitch, i.e.

$$B_0 = \frac{\tau_s}{t_o} B_{g1} \quad (6.65)$$

Clearly, if the flux density at the narrowest point in the teeth is to remain below a certain limit the maximum value of  $B_{g1}$  is also fixed. The maximum value for tooth flux density is typically in the range 100,000 to 130,000 lines/in<sup>2</sup> (roughly 1.55 to 2.0 Tesla) for common steel while the flux density in the core normally ranges over values from 90,000 to 110,000 lines/in<sup>2</sup> (roughly 1.4 to 1.7 Tesla). These values are for 60 Hz operation and must, of course, be adjusted for operation at higher frequencies. When the frequency reaches 500 Hz, tooth and core flux densities on the order of 1.2 T and 1.0 T are used respectively because of the increased losses.

In large machines which have large diameters the taper of teeth is not significant. However, in small machines which have smaller diameters the taper of the teeth is very pronounced and consequently saturates first at the tip of the stator teeth and the root of the rotor teeth. In addition, higher slot fill factors are possible for large machines. Therefore less space is lost to insulation resulting in a consequent increase in space available for the teeth. Hence, small machines typically have lower values of gap flux density than large machines. With ordinary electric steels the maximum value of  $B$  should not exceed the following levels at 60 Hz:

$$\text{Stator Core } B_{cs} = 110,000 \text{ lines/in}^2 \approx 1.7 \text{ T}$$

$$\text{Rotor Core } B_{cr} = 110,000 \text{ lines/in}^2 \approx 1.7 \text{ T}$$

$$\text{Stator Tooth } B_{ts} = 135,000 \text{ lines/in}^2 \approx 2.1 \text{ T}$$

$$\text{Rotor Tooth } B_{tr} = 142,000 \text{ lines/in}^2 \approx 2.2 \text{ T}$$

### 6.9.2 Magnetizing Current

The magnetizing current of a machine is directly proportional to the *MMF* required to force the flux through the air gap and iron portions of the machine. The *MMF* required for the air gap is simply proportional to the air gap flux density. However, the flux density in the iron depends upon the value of specific magnetic loading. If a small value of loading is chosen, the flux density in the iron is low and therefore these parts are worked on the linear portion up to the "knee" of the B-H curve. Operation in this region requires a small or even negligible value of *MMF*. However, such operation represents inefficient utili-

zation of the available iron. If larger values of magnetic loading (flux density) are assumed the *MMF* required rises rapidly. Thus a large value of magnetic loading results in increased values of magnetizing *MMF* and hence magnetizing current. A good compromise involves design of a mildly saturated machine with sufficient reserve to accommodate an overvoltage of 10% (NEMA standard).

The iron loss is also frequency dependent since the hysteresis and eddy current losses vary with frequency and frequency squared respectively. It follows that for high speed machines (high frequency machines) the magnetic loading must be reduced in order to obtain reduced iron losses so that reasonable value of efficiency may be achieved. Whereas a typical value of peak air gap flux density for a 60 Hz machine may be 40,000 lines/in<sup>2</sup> (0.62 Tesla) the corresponding value in a 400 Hz servo motor may be only half this value. The magnetic loading can be increased somewhat since the power output increases faster than the magnetic losses with increased dimension. This topic will again be discussed in Section 6.12. Figure 6.49 shows typical air gap flux densities for both standard and high efficiency induction machines for a range of ratings from 3 to 150 hp.

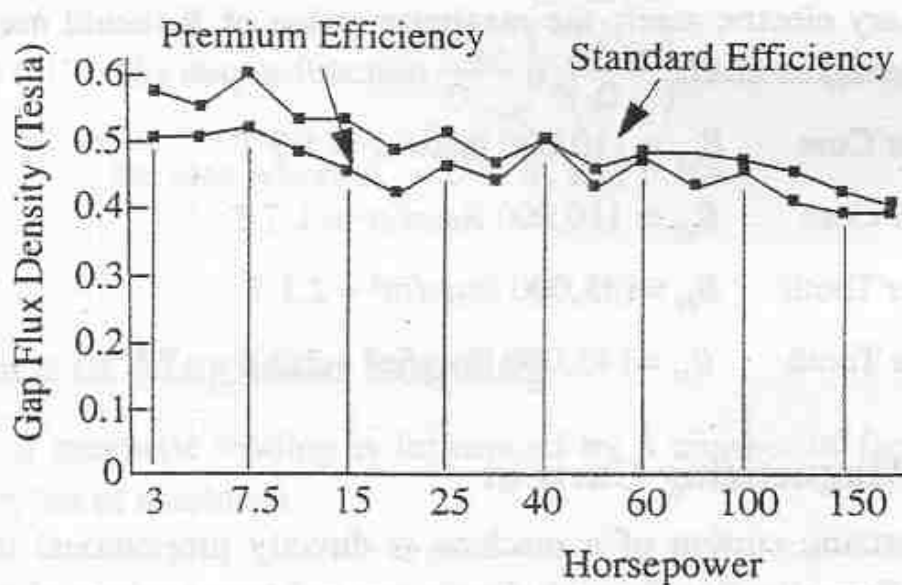


Figure 6.49 Air gap flux density for a range of motors from one manufacturer ( $64.5 \text{ klines/in}^2 = 1 \text{ Tesla}$ )

Without better available information the following equation may be used as a first guess for air gap flux density:

**Table 6.10 Table of round copper wire for random wound machines**

AWG	Bare Wire Diam- eter (in)					Wgt/ 1000 ft. @ 25°C (lb)	Ohms/ 1000 ft. ( $\Omega$ )
		Heavy (in)	Triple (in)	Qua- druple (in)	Glass (in)		
	0.0605	0.0634	0.0652	0.0662	0.0662	11.10	2.80
15	0.0517	0.0600	0.0617	0.0628	0.0628	9.87	3.24
	0.0538	0.0557	0.0585	0.0594	0.0594	8.76	3.65
16	0.0508	0.0537	0.0552	0.0563	0.0563	7.81	4.10
	0.0480	0.0508	0.0524	0.0534	0.0534	6.97	4.59
17	0.0453	0.0481	0.0498	0.0506	0.0506	6.21	5.15
	0.0427	0.0454	0.0470	0.0480	0.0480	5.52	5.80
18	0.0403	0.0430	0.0445	0.0455	0.0455	4.91	6.51
	0.0380	0.0406	0.0422	0.0432	0.0432	4.37	7.32
19	0.0359	0.0385	0.0399	0.0410	0.0410	3.90	8.21
	0.0339	0.0364	0.0379	0.0390	0.0390	3.48	9.20
20	0.0320	0.0345	0.0358	0.0370	0.0370	3.10	-
	0.0302	0.0326	0.0340	0.0352	0.0352	2.76	-
21	0.0285	0.0309	0.0322	0.0334	0.0334	2.46	-
22	0.0253	0.0276	0.0288	0.0301	0.0301	1.94	-
23	0.0226	0.0248	0.0260	0.0273	0.0273	1.55	-
24	0.0201	0.0222	0.0230	0.0243	-	1.22	-
25	0.0179	0.0199	0.0212	0.0219	-	0.97	-

$$B_{g1} = 0.464 \tau_p^{1/6} \quad (6.66)$$

where  $\tau_p$  is given in centimeters and  $B_{g1}$  in teslas.

## 6.10 Choice of Electric Loading

Although the saturation phenomena of magnetic circuits does not exist in the case of electric circuits the losses associated with the conductors again play a major role in fixing the electric loading. Major factors in limiting the electric loading of the machine are the following.

### 6.10.1 Voltage Rating

Contrary to what one might expect, more of the slot is typically occupied more by air than by the copper conductor. In addition to assembly problems which dictate that some "play" remain in order to slip the coils in the slots, the conductors must be insulated between strands, between separate coils and with respect to ground, i.e. the core. The insulation required with respect to ground is, in itself, a major portion of the available slot area since this insulation must withstand surges due to lightning and line switching in addition to normal overvoltage conditions. Standard IEEE tests require that the machine withstand for one minute a voltage of two times the rated phase voltage plus 1000 volts at its normal working temperature. The amount of copper cross sectional area expressed as a per unit of the available cross sectional area of a stator slot is typically in the range 0.2 to 0.4. The amount of available conductor area decreases as the voltage rating of the machine increases since groundwall and coil separator insulation as well as the insulation buildup on the conductor wires increases as shown in Table 6.10.

Modern pulse width modulated inverters to vary the speed of ac motors has presented the motor designer with new challenges in the area of insulation. In such cases the motor insulation system is subjected to voltage step changes at a rate of up to 20,000 times per second. These changes are, in reality, very oscillatory indicating resonance with the capacitance of the motor insulation system. Over-shoots of double the DC bus voltage can occur. Hence, when a nominal 460 V AC supply is replaced by a similarly rated inverter the rectified 650 V DC can result in over 1200 volts across the motor winding from line to line. The magnitude of this transient combined with the high repetition rate can reduce the life of the insulation system by as much as 90% statistically increas-

ing rapidly when the inverter switching rate exceeds 5,000 Hz. NEMA standard MG1 defines the acceptable wavefronts for a general purpose motor as  $V_{peak} \leq 1000$  V with rise time  $\geq 2\ \mu s$  and for an "inverter grade" motor as  $V_{peak} \leq 1600$  V with rise time  $\geq 0.1\ \mu s$ .

A new magnet wire has been developed that adds a shield coat between the original base coat and the topcoat on the wire. This style of coating of three different materials achieves a greatly improved protection from rapid rise time, high frequencies and elevated voltages while maintaining good flexibility and processability. Accelerated laboratory testing has indicated that this new wire is up to 200 times more resistant to inverter transient damage than normal magnet wire [8].

### 6.10.2 Performance Under Stalled Conditions

Although the stalled condition is usually an abnormal mode of operation, when it does occur there are many unusual stresses are involved which must be factored into the design. Failure of many components both inside and outside the motor can cause such operation. For example, any faulty connection within the motor or in a feed line to the motor which opens a phase will result in the disappearance of starting torque and high current the remaining two windings. Broken end rings or rotor bars can sometimes reduce starting torque sufficiently to stall the motor. Since the torque of an induction motor varies as the square of the voltage, performance is sensitive to line voltage. Low line voltage or poor regulation of line voltage due to high starting current are a frequency cause of starting problems.

When a motor becomes stalled, the resulting high currents can quickly cause damage if the protection scheme is not adequate. Stalled motor currents are of the order of four to seven times full load current. Consequently, depending upon the design, current densities under stalled conditions may be as much as 40,000 Amps/in<sup>2</sup>. Since all of the heat generated by the rotor current is stored within the bars during such a short period of time we can write

$$\text{energy stored} = \text{energy dissipated}$$

$$C_p \frac{d\Theta}{dt} = \rho J_{s(rms)}^2 \quad (6.67)$$

where  $\rho$  is the resistivity,  $J_{s(rms)}$  is the current density in rms, and  $C_p$  is the heat capacity of the conductor material and is equal to the product of the specific heat times the bar density. This equation can be written as

$$\frac{d\Theta}{dt} = \frac{J_{s(rms)}^2}{C_p/\rho} \quad (6.68)$$

Table 6.6 shows values of  $C_p/\rho$  for a number of conductor materials. From this table it can be determined that if the stator current density is 15,000 Amps/in<sup>2</sup> the rate rise of temperature is 3 1/2 °C/second resulting in a smoking temperature of 150 °C in 35 seconds. If the current density is increased to 40,000 Amps/in<sup>2</sup>, the rate of rise of temperature increases to 25 °C/second producing a smoking temperature of 150 °C in only 5 seconds. Generally speaking, small, lightweight, well ventilated motors are designed with a relatively high starting current density and the problem of coordination of protection is a major concern.

Material	$C_p/\rho^*$
Copper	$63.1 \cdot 10^6$
Cast Aluminum	$20.0 \cdot 10^6$
Cast Zinc	$12.9 \cdot 10^6$
Brass	$15.6 \cdot 10^6$
Cast Bronze	$10.6 \cdot 10^6$

\*Values of  $C_p/\rho$  are for 100° C

Table 6.6 Transient heating coefficient for several materials

Representative values of stator surface current density  $K_{s(rms)}$  and stator current density  $J_{s(rms)}$  for Open Drip Proof and Totally Enclosed Fan Cooled Machines are given in Table 6.7 and Table 6.8 respectively. Without information available from similar designs the following equation may be used as a starting point to select  $K_{s(rms)}$

$$K_{s(rms)} = 220\tau_p^{2/3} \quad (6.69)$$

where  $\tau_p$  is given in inches and  $K_{s(rms)}$  expressed in rms amps/in.

In squirrel cage rotors the current in the bars and the end ring segments are normally limited to 5,000 A(rms)/in<sup>2</sup>. For a slip ring machine the current density in the rotor windings is typically allowed to be 20 to 30% higher than in the stator winding.

HP	P=2		P=4		P=6	
	$K_{s(rms)}$	$J_{s(rms)}$	$K_{s(rms)}$	$J_{s(rms)}$	$K_{s(rms)}$	$J_{s(rms)}$
1	350	3100	350	2800	350	2600
5	530	2800	530	2600	530	2400
10	610	2800	610	2600	610	2400
50	800	2800	710	2600	690	2400
100	850	2800	785	2600	710	2400
500	900	2800	800	2600	715	2400

Table 6.7 Current Densities  $K_{s(rms)}$  and  $J_{s(rms)}$  in rms amps/in and rms amps/in<sup>2</sup> respectively for Open Drip Proof Machines of NEMA Design.

HP	$K_{s(rms)}$	$J_{s(rms)}$			
		P=2	P=4	P=6	P=8
1	290	3500	2900	2400	2200
5	530	3300	2800	2300	2100
10	600	3200	2700	2300	2000
50	660	2000	2400	2200	1900
100	660	1500	1500	1600	1700
500	660	1500	1500	1300	1300

Table 6.8 Current densities  $K_s(rms)$  and  $J_s(rms)$  in rms amps/in and rms amps/in<sup>2</sup> respectively for totally enclosed, fan cooled machines for NEMA Design.

It should be mentioned that the values of current density given here are only representative value. The amount in which the current density can be pushed is entirely dependant on the type of cooling used. Generally speaking, in totally enclosed machines with no external cooling, designs can be made with current densities on the order of 3,000 to 3,500 Amps(rms)/in<sup>2</sup>. Machines with forced air cooling over the stator surface can tolerate a current density of 5,000 to 6,000 Amps(rms)/in<sup>2</sup>. When the air cooling is done through the use of ducts or vents embedded either axially or radially in the stator (and, perhaps rotor) laminations the current density can be increased to about 9-10,000 Amps(rms)/in<sup>2</sup>. Finally, if liquid cooling is employed (using water, oil, WEG (water, ethylene, glycol) either in ducts or by spraying on the end windings) the current density can be increased to values between 15,000 and 20,000 Amps/in<sup>2</sup> or even higher. The value of surface current density is correspondingly increased in each case.

If Eqs. (6.66) and (6.69) are used as representative values for air gap flux and surface current respectively, the pole pitch can be found as function of output horsepower directly from Eq. (6.9) if the efficiency, power factor and aspect ratio are assumed. Figure 6.19 shows the result if the efficiencies and power factors of Figure 6.7 and Figure 6.8 are used and if the aspect ratio  $l_e / \tau_p$  is taken as the dashed line of Figure 6.6.

It is interesting to observe how the rating of the machine increases if the rules that we have set down for flux density and current density (Eqs. (6.66) and (6.69)) are observed. From Eq. (6.9) it is apparent that the volume of the machine increases with pole pitch squared so that if the pole pitch (i.e. diameter) is increased while the length is held constant then

$$T = \frac{HP}{\Omega_s} \propto \tau_p^{(2+1/6+2/3)} = \tau_p^{17/6} \quad (6.70)$$

or nearly as the cube of pole pitch or diameter. On the other hand if the machine length is increased while the pole pitch (i.e. diameter) is held constant then since  $B_{g1}$  and  $K_{s(rms)}$  remain constant,

$$T = \frac{HP}{\Omega_s} \propto l_e \quad (6.71)$$

so that a linear variation results. Equations (6.70) and (6.71) can be used as scaling rules in order to arrive at a satisfactory design.

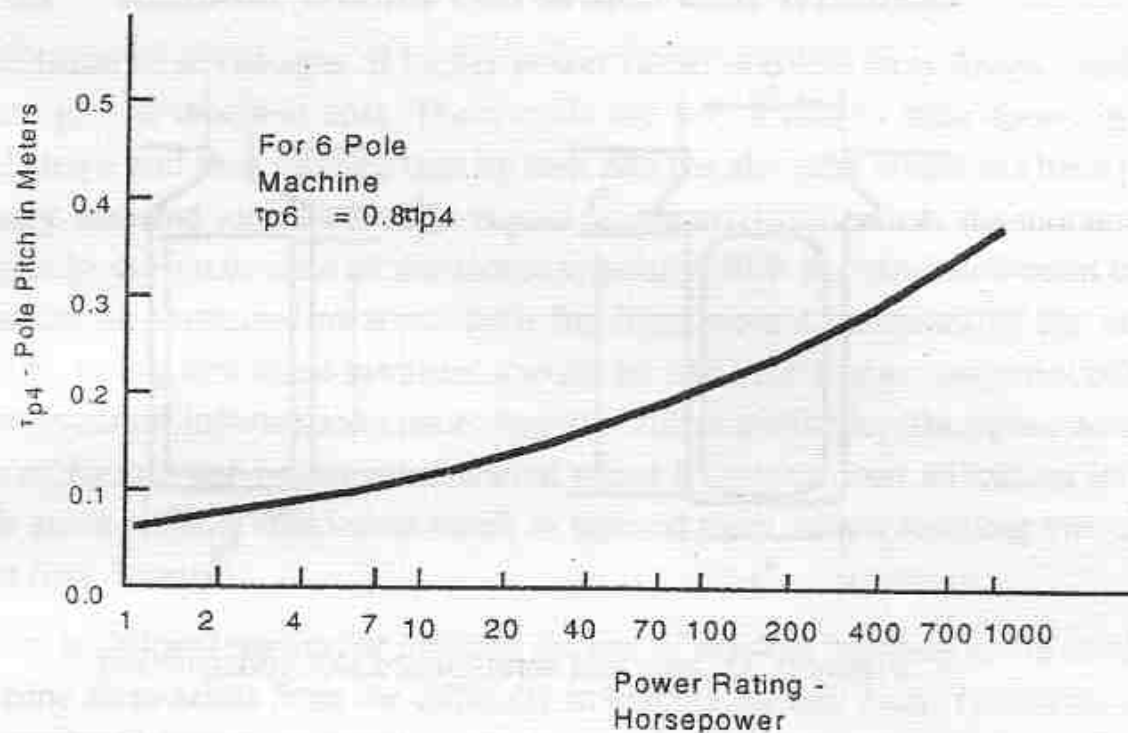


Figure 6.19 Estimate for pole pitch as a function of horsepower output

## 6.11 Practical Considerations Concerning Stator Construction

In general two types of stator slots in widespread use; open and semi-closed slots. An open slot, shown in Figure 6.19 is designed to be used with form wound coils whereas the semi-closed slot is used with random wound coil construction. The open slot construction is generally used on larger machine, approximately 100 HP or larger, particularly when the number of turns per coil is low or where the voltage is high, 2300 V. and up. Considerations for high voltages necessitate application of the ground insulation prior to insertion of the coil in the slot. Hence, the need for open slot construction. The open slot arrangement significantly increases the effective air gap, resulting in a smaller magnetizing reactance and a relatively lower power factor compared with the closed slot. The open slot construction may also accentuate the importance of slot and permeance harmonics and their influence on torque pulsations and stray losses. A further advantage of the open slot is that it permits use of a

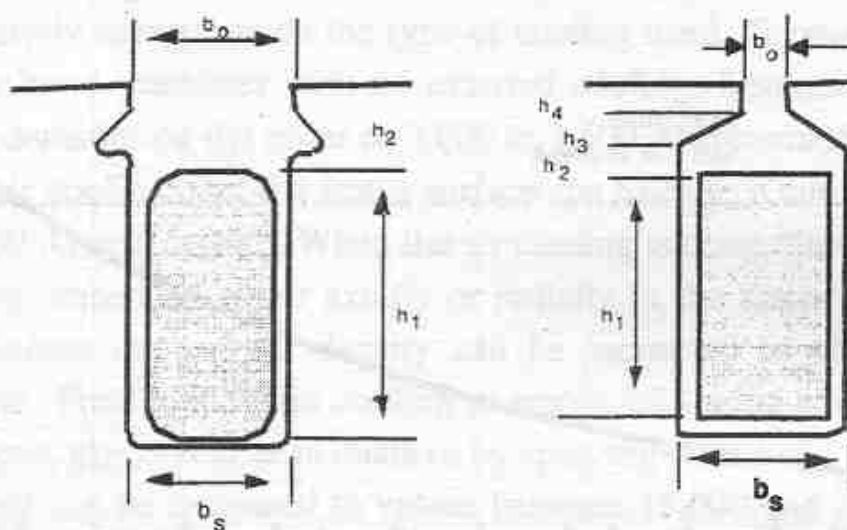


Figure 6.20 Open and semi-closed slot construction

recessed wedge away from the air gap, thereby allowing an additional path for ventilating air.

The closed slot construction is quite limited as to creepage or insulation thickness since it is approximately the thickness of the slot wedge to ground and also the thickness of the phase insulation between phases in the slot. Accordingly, closed slot construction is seldom used for applications above 550 volts. By virtue of its limited creepage in the slot, random wound coils are usually not built with large creepages in the end turn region also. For example, slot tubes usually extend only 1/4" beyond the end of the core and even this nominal value may be reduced if the tubes are not centered. Sometimes a cuff is used on the end of the tube which can be effective in providing some additional insulation. However, if moisture exposure is to be expected, random wound motors of open construction are a risky application and it is better to use the totally enclosed, fan cooled (TEFC) design. The slot opening of the open slot bears an important relation to the insulated diameter of the wire to be used. In general, the opening should be over twice this diameter to avoid crossed wires from being damaged during insertion and to materially reduce the insertion time.

### 6.11.1 Random Wound vs. Formed Coil Windings

In addition to advantages of higher power factor and less stray losses, random windings are lower in cost. These coils are preformed to their approximate final shape and then inserted turn by turn into the slot tube which has been previously inserted into the slot. In regard to material utilization, the amount of copper in the gross area of the slot is typically 30% for random wound construction as compared to about 50% for form wound machines of the same voltage rating and these numbers should be used for design purposes unless more accurate information concerning slot fill is available. The space advantage of form wound coils is somewhat offset by poorer iron utilization in the teeth since parallel sided slots result in tapered teeth with a resulting non-uniform flux density.

An additional reason for limiting the use of random winding to the smaller machine sizes arises from the difficulty in bracing the coil ends. The forces due to inrush currents or short circuit currents may be quite high in larger machines. Tying alone is insufficient to support random windings, particularly in two pole machine, since the motion of even one wire may result in loosening of the coil bundle. As a result, varnish dip must be relied upon to anchor the end turns rigidly. This, in turn, places a limit upon the time for which a random wound machine may remain stalled before the overload protection removes power since the varnish softens as it becomes heated. Even with form wound coils in large machines, bracing of the end windings is often a serious problem, particularly for machines with a small number of poles. In this case the end winding length is large and the ampere turns per pole and consequent forces between coils are likely to be large. In addition to the usual interleaved tying which is done on all machines, additional bracing in the form of one or more supporting rings is often used to provide additional reinforcement for tying cords and to enhance structural rigidity. The cords themselves are glass fiber tape treated with permafil epoxy which is subsequently cured by baking.

Still another difference between random wound and form wound stators is in the method of connection. In the former, particularly in sizes up to 25 HP, an entire phase of a number of coils may be wound without cutting the wire. Such an assembly of coils, together with other assemblies for the other phases, may then be inserted coil by coil without the necessity of any wire cutting. The resulting wound stator is then free from many of the connections which must

otherwise be made resulting in greater yield. On the other hand, for wound coils require a separate connection operation for all the coils in the machine.

### 6.11.2 Delta vs. Wye Connection

Machines of both delta and wye or star connection are in widespread use. In general, the choice usually depends upon which connection results in the optimum number of turns per coil. This consideration becomes more important as machines become larger since the turns per coil become smaller so that the options available from series or parallel connection of phase belts become restricted. Textbooks often make a point of the fact that third harmonic voltages are induced in a delta connection which can result in the corresponding currents circulating in the phases of a delta connection. While this is the case, careful choice of pitch factor and control of saturation can keep these losses to a negligibly small value. One major advantage of wye connected machines, however, involve applications where the overload protection may be marginal. If a motor is stalled due to an open circuit of one line, the line current of a wye connected machine will be the same as the equivalent delta connected machine. However, in the delta connected machine the phase across the line will have twice the current of the other two phases which are connected in series across the line. The net result is that the delta connected machine will have 15% more current density in the phase across the line than the equivalent wye connected has in its two phase across the line. This will result in a rate of temperature rise which is 33% greater in a delta wound machine as compared to the wye connected machine. Overload protection must be adjusted accordingly if this aspect is at all critical.

### 6.11.3 Lamination Insulation

Insulation between laminations is of considerable importance in induction machines as it is with any type of motor. In general, flux densities and frequencies are such that the voltage induced across the laminations are in the order of 1 1/2 volts per inch for two pole, 60 Hz motors. Short core length motors, six inches length or less, can usually rely upon the oxide coating of the steel laminations which occur during the annealing process. However, when core lengths reach 12 inches or more, a more reliably controlled insulation system is warranted and core plate enamel should be considered. As to the rotor, the inter-lamination voltage is very small due to the small slip frequencies. However,

insulation may still be necessary or harmonic fluxes will produce significant increases in load loss. For example, the effect of skewing the rotor slots will be essentially nullified if the insulation between laminations and that from the rotor bars to the laminations is not effective.

#### 6.11.4 Selection of Stator Slot Number

The number of stator slots  $S_1$  for a given size of punching is usually determined by the requirements of the motor including breakdown torque, starting current, allowable temperature rise and so forth. With small motors and with few poles an integral number of slots per pole per phase invariably chosen in order to maintain balance between phases. The numbers 24, 36, 48, 54, 60 and 72 slots are very commonly used.

In general, it might be imagined that it is desirable to keep the number of slots as small as possible since manufacturing costs clearly rise with the number of slots and therefore coils to be inserted. However, many factors tend to favor a large number of slots. First, and perhaps most important, is the fact that the breakdown torque varies inversely with the leakage reactance of the machine. Since the slot leakage and zig-zag leakage reactances vary inversely with the number of stator slots it is desirable to keep the number of stator slots large. In addition, a large number of slots permits the design of a winding distribution which has a small *MMF* harmonic content, thereby reducing the belt leakage as well as the stray load losses. Finally, concentration of coils into a small number of slots results in a concentration of heat in these slots leading to cooling problems.

On the other hand, the number of slots cannot increase arbitrarily due to structural problems arising from narrow stator teeth. Also, it is more difficult to load the slots to the same current loading  $K_{s(rms)}$  since the space lost to insulation, slot opening, packing factor etc. increases as the slots become smaller. The thickness of the stator teeth also depends upon the breadth of the slot selected relative the available slot pitch. Clearly narrow teeth relative to the slot pitch tends to result in teeth which are highly saturated. In addition, problems with end turns arise since the angle  $\alpha$  which defines the angle of departure of the end turns from the stack is directly related to the ratio of slot breadth to slot pitch (see Figure 4.13). As a result, the number of stator slots are usually chosen such that the thickness of the stator teeth lies between 1/4" and 1". The

ratio of slot breadth to slot pitch generally lies in the range 0.4 to 0.6 with 0.5 taken as a recommended starting point.

### 6.11.5 Choice of Dimensions of Active Material for NEMA Designs

Although special designs may permit the choice of motor diameter and length purely from application considerations, the motor designer is more often restricted to designs which conform to the NEMA standard frame sizes. However, the NEMA standards only specify the overall length and width of the machine and shed little light on the working dimensions important to a machine designer, namely air gap diameter and active iron length. The table below can be used as a guide for selection important motor active dimensions which will allow for a frame, cooling fan, standard shafts, etc. and usually result in a machine of acceptable design. The duct lengths, if any, are not considered.

Frame Size	Poles	Max Stator OD - $D_{os}$	Min Rotor ID - $D_{ir}$	Max Iron Length $l_i$	Air Gap
250	2	10 - 1/2	1 - 7/8	4 - 1/2	0.025
	4	10 - 1/2	1 - 7/8	5 - 1/4	0.017
	6/8	10 - 1/2	1 - 7/8	4	0.018
280	2	11 - 3/4	2 - 1/4	5 - 1/2	0.027
	4	11 - 3/4	2 - 1/4	6 - 1/2	0.018
	6/8	11 - 3/4	2 - 1/4	7	0.020
320	2	13 - 1/2	2 - 5/8	6	0.030
	4	13 - 1/2	2 - 5/8	8	0.020
	6/8	13 - 1/2	2 - 5/8	8	0.022
360	2	15 - 1/4	3 - 1/4	6 - 3/4	0.033
	4	15 - 1/4	3 - 1/4	7 - 1/4	0.028
	6/8	15 - 1/4	3 - 1/4	7 - 1/2	0.024

Table 6.9 Recommended diameters, maximum lengths and air gaps for NEMA standard machines

**Table 6.10 Recommended diameters, maximum lengths and air gaps for NEMA standard machines**

Frame Size	Poles	Max Stator OD- $D_{os}$	Min Rotor ID - $D_{is}$	Max Iron Length $l_i$	Air Gap
400	2	17	3 - 7/8	7 - 1/2	0.045
	4	17	3 - 7/8	8 - 1/4	0.032
	6/8	17	3 - 7/8	8 - 1/4	0.025
440	2	18 - 3/4	4 - 3/8	10 - 1/2	0.050
	4	18 - 3/4	4 - 3/8	14	0.035
	6/8	18 - 3/4	4 - 3/8	14	0.028

### 6.11.6 Selection of Wire Size

Even the largest motor manufacturing plant is confronted with an inventory problem so that the motor designer must frequently make imaginative use of the available stock in order to realize a good design. Frequently when the desired wire size is not available the required cross sectional area is achieved by using two or more conductors of the same or dissimilar diameters. Conductors used in parallel in this manner are usually called strands and the process of using such parallel conductors termed "wires in hand". While not all of the following wire diameters and insulation thicknesses may be available in a given situation the following table, Table 6.10, can be considered as representative. The symbol AWG denotes a standard size (American Wire Gauge) but as can be observed, copper wire is not necessarily made only in standard AWG sizes. Heavy insulated wire is typically used with stators with *B* and *F* insulation up to approximately 100 HP while quadruple coated wire is used for stators of machines larger than 100 HP and in most wound rotors. Triple coated wire is used in stators with class *H* insulation and in wound rotors with class *H* insulation. Glass fiber insulated wire is frequently used for high voltage (2300 volt) machines. Classes *A* and *B* consist mainly of organic materials such as silk, cellulose, asbestos and mica whereas classes *F* and *H* consist of inorganic materials such as fiberglass, teflon and silicon compounds.

### 6.10.7 Selection of Air Gap

Figure 6.21 shows a plot of recommended air gaps for induction machines hav-

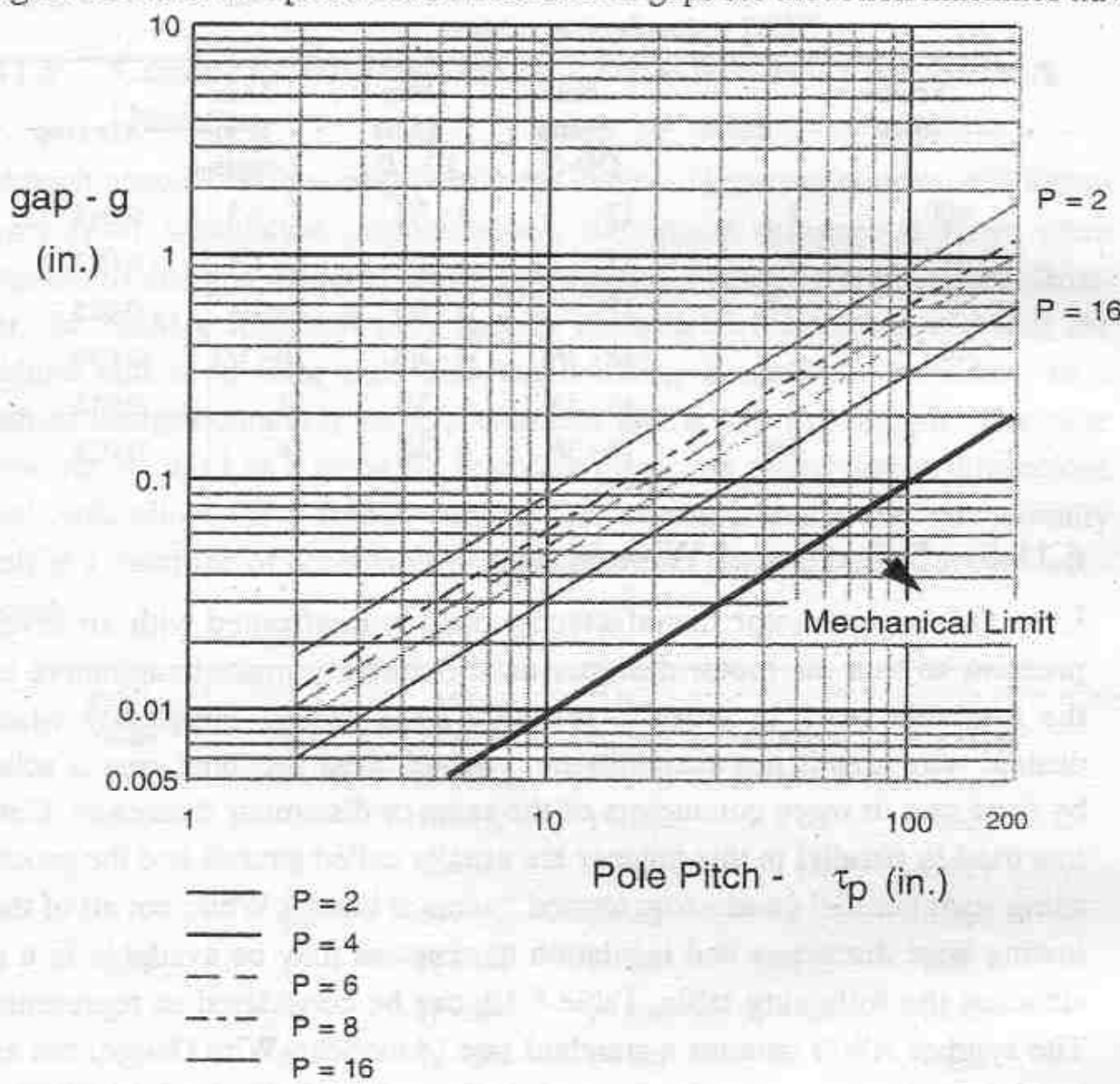


Figure 6.21 Airgap length of squirrel cage induction machines vs. pole pitch and number of poles

ing poles between 2 and 16 [9]. Also shown is the mechanical limit below which it is not possible to maintain the required spacing between stator and rotor due to mechanical tolerances. Air gaps for high efficiency motors are often somewhat greater than for standard motors, as shown in order to reduce the stray loss. This often results in a slightly poorer power factor since the magnetizing is necessarily reduced. The variation in the air gap as a function of pole pitch and number of poles can be approximated by

$$g = 3 \times 10^{-3} \left( \sqrt{\frac{P}{2}} \right) \tau_p \quad (6.72)$$

A plot showing air gaps machines designed over a range from 3 to 150 hp is given in Figure 6.22.

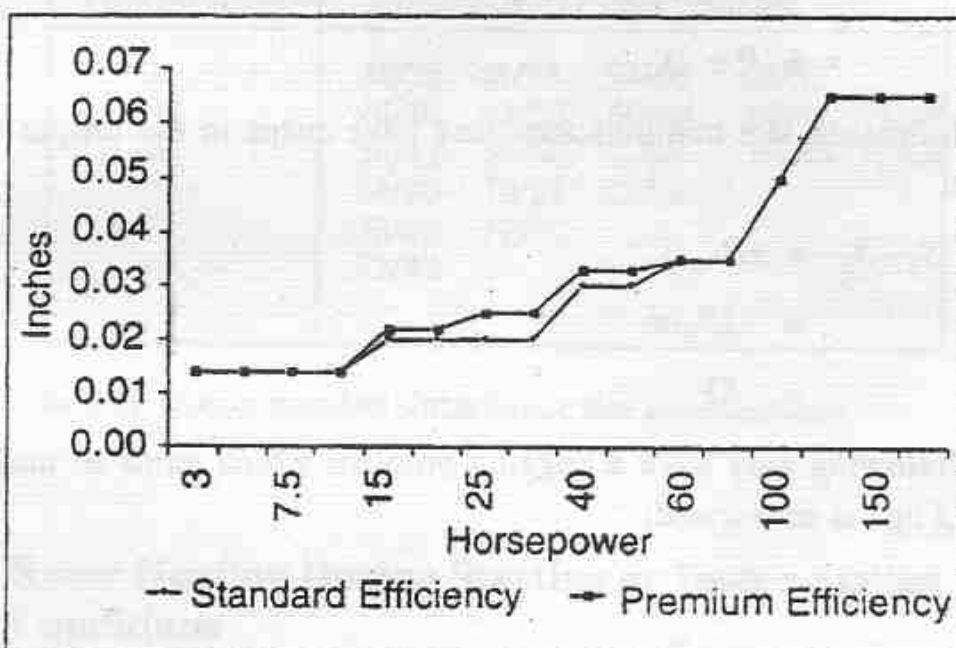


Figure 6.22 Air gap in inches for standard and high efficiency machines

## 6.11 Rotor Construction

The major problem concerned with rotor construction centers around the selection of the number of rotor slots  $S_2$ . Literature on this subject abounds. In many cases, the rules are based on qualitative appraisals of the results of harmonic analysis, but when they are put to test the assumptions inherent in many of these analyses loose significance. It is unfortunate but true that it is extremely difficult to make quantitative calculations. Rules for the choice of rotor slot number can only be classified as good or bad when specifically related to some attribute of interest. Frequently a choice categorized as good for one purpose is bad for another. The following information has been culled from the writings of Alger, Kuhlman and Veinott [10]–[12].

### 6.11.1 Slot Combinations to Avoid

The following slot combinations have been shown to be noisy or to produce vibrations; \

$$\begin{aligned} S_1 - S_2 &= \pm 2 \\ &= \pm (P \pm 1), \text{ and} \\ &= \pm (P \pm 2). \end{aligned}$$

The following slot combinations may have cusps in the torque versus speed curve;

$$\begin{aligned} S_1 - S_2 &= \pm P \\ &= -2P, \text{ or} \\ &= -5P \end{aligned}$$

The following may have a cogging problem which tends to make the motor "hang up" at zero speed;

$$\begin{aligned} S_1 - S_2 &= 0 \text{ or} \\ &= \pm mP \end{aligned}$$

where  $m$  is an integer. Problems associated with cogging indicate a problem associated with a torque component a function of angular position whereas cusps result from torques produced by a function of speed. Cusps therefore are essentially induction motor torques arising from a magnetic pole number different than the fundamental component (*MMF harmonics*) while cogging is a result of synchronous motor type torques arising from reluctance variation.

In general if  $S_2$  meets the criterion above and is divisible by the number of poles, motor noise is a minimum but some cogging difficulties may result. Quietness is also helped if  $S_2$  differs from  $S_1$  by 20% or more. If  $S_2$  is larger than  $S_1$  the rotor leakage inductance and resistance when referred to the stator are reduced and vice versa resulting in relatively high breakdown torque and starting current. On the other hand, the manufacturing cost increases with the number of rotor slots particularly for cast rotors. For cast rotors, or when rotor bar insulation may be a problem, stray load losses can be reduced if  $S_2$  is smaller than  $S_1$ . The amount of reduction, however, is only on the order of 15%. The most usual combinations found today in smaller sizes have  $S_1 - S_2 = \pm 2P$  and the rotor slots are skewed one rotor slot in order to reduce the torque cusps

inherent in this combination. A table showing desirable stator/rotor slot combinations for various pole numbers is given in Table 6.11.

Pole Number	Stator/Rotor Slot Number			
2	36/28	48/38	54/46	60/52
4	48/40	48/56	60/44	60/76 72/58
6	54/42	54/66	72/88	72/54 72/84
8	54/70	72/58	72/88	
10	72/88	72/92		
12	72/92			

Table 6.11 Recommended stator/rotor slot combinations

### 6.11.2 Rotor Heating During Starting or Under Stalled Conditions

It may be just as likely that limiting thermal stresses will be reached first in the rotor of the machine than in the stator. Blow holes in case aluminum rotors may cause localized high current densities which may melt like a fuse under abnormal stalled conditions. Double cage rotors in particular, by the nature of their design, have most of the current flowing in the top bar of the cage which is typically a much smaller area than the bottom bar. Such windings are quite vulnerable to failure. Modern designs provide for a thermal path for heat to easily flow from the top cage to the lower one by means of an integrally cast connection between the two windings as shown in Figure 6.23. Note that the connection between the top and bottom bars is "off center". By reversing rotor punchings every half inch or so, a poor electrical connection is made to exist axially in order to produce the beneficial effects of a double cage machine. However, a good radial connection is maintained thermally in order to carry the heat to the bottom bar.

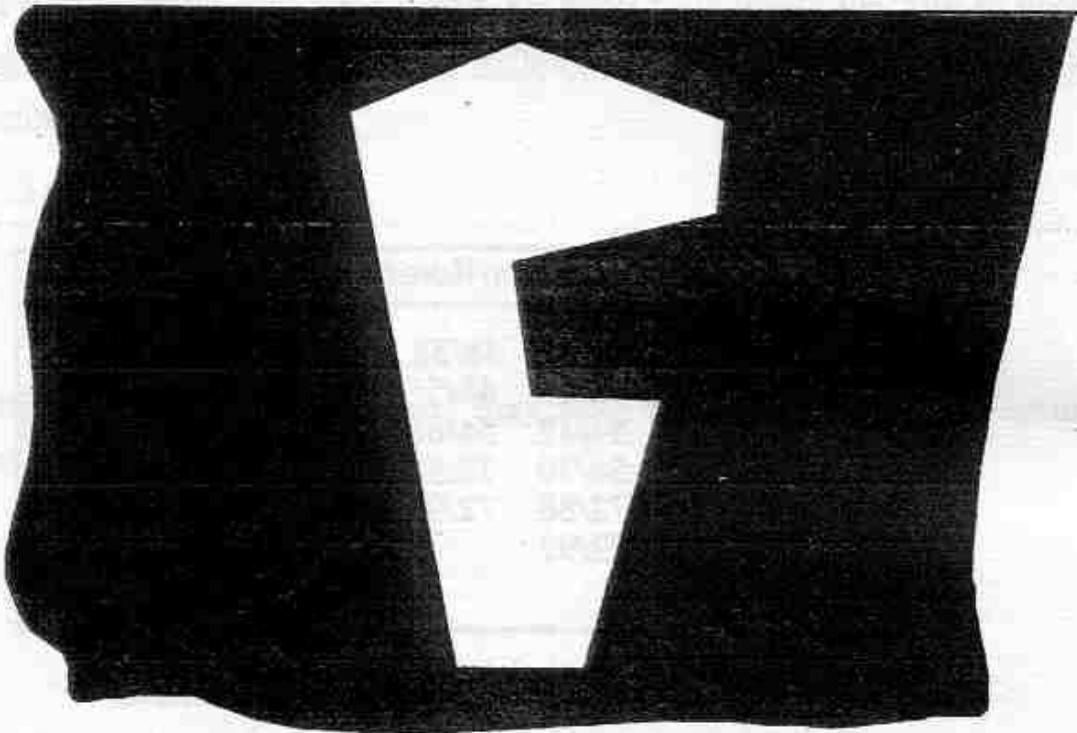


Figure 6.23 Asymmetric rotor slot construction for double cage machine with good thermal heat capacity

## 6.12 Effect of Machine Performance by a Change in Dimension

Because of the considerable effort involved, design of a line of machines is often accomplished by a detailed design of one machine, then a design of similar machines but different rating by simple scaling. Consider two machines of the same design with all dimensions in the ratio  $k:1$  and having the same speed, flux density and current density.

- 1) Weight. Clearly since the linear dimension of both the iron and copper parts has increased by  $k$  the weight of the second machine will increase by  $k^3$ .
- 2) Terminal Voltage. The core area, the flux per pole increases by  $k^2$ , and therefore if the number of turns is not changed, the voltage will increase by a factor of  $k^2$ . In most cases, the number of turns must be changed to satisfy a given terminal voltage constraint. In this case the number of stator turns must decrease inversely by  $k^2$ .
- 3) Load Current. The current carrying capacity of the machine, assuming adequate ventilation increases in proportion to the area of the conductors, or by

a factor of  $k^2$ . When the stator turns are reduced by  $k^2$  and the amount of copper is kept the same, the current carrying capacity of the machine increases by a factor of  $k^4$ .

4) Input KVA. Since the current and voltage increase as  $k^2$  the power input will increase by a factor of  $k^4$ . This factor remains the same when the number of turns are adjusted to keep the voltage rating the same.

5) Resistance. The copper cross section will increase by a factor of  $k^2$  when the turns are not changed. However, the conductor length will increase by  $k$ , so that the resistance will decrease by a factor of  $k$ . When the number of turns are reduced by  $k^2$  the cross section will increase by an overall factor of  $k^2 \cdot k^2 = k^4$  while the conductor length will change by an overall  $k/k^2 = 1/k$ . Hence, when the voltage rating of the new machine is held constant the resistance will decrease by a factor of  $k^5$ .

6) Copper Loss. Since the current squared goes up by  $k^4$  and the resistance goes down by  $k$ , the copper loss will increase by a factor of  $k^3$ . When the voltage is maintained constant, the current squared goes up by  $k^8$  while the resistance goes down by  $k^5$  making the copper loss increase by the same factor of  $k^3$ .

7) Iron Loss. Since the flux density in the iron remains constant and the volume of iron increases by  $k^3$ , the iron loss will also increase by a factor of  $k^3$ . The iron loss will not change with changes in the number of turns if the resulting flux density remains unchanged.

8) Power Output. Since power input increases by  $k^4$  and the losses increase by  $k^3$  the power output increases as  $k^4 - ak^3$  where  $a$  is the per unit losses at the design  $k=1$ . Hence, the power output increases at a rate slightly less than  $k^4$ . Note that this is essentially the same result as would be indicated by Eq. (6.70) if both  $\tau_p$  and  $I_i$  are changed by the same amount.

9) Efficiency. Since the efficiency is the ratio of power output to power input, then efficiency varies as  $(k^4 - ak^3) / k^4 = 1 - a/k$ . Hence, as  $k$  becomes larger the efficiency approaches unity. This result clearly shows that, with electric and magnetic loading held constant, an increase in size will always improve the efficiency of the machine. This also explains in part why fractional horsepower machines have an efficiency on the order of 60% while the efficiency of a large turbo-alternator is about 98%. Note that efficiency and power output remains nominally unchanged with a change in the number of stator turns.

10) Inductance. Since the area of the magnetic circuit will increase by the factor  $k^2$  while its length increases by  $k$ , the inductances of the machine increase by  $k$  whereas the resistances have been shown to decrease by  $k$  when the number of turns are held constant. When the stator turns are changed by  $1/k^2$  to keep the rated voltage constant, the inductances of the machine will decrease rather than increase by a factor of  $k$ .

11) Magnetizing Current. If the gap flux density is kept constant the *MMF* required to drive the flux across the air gap is proportional to the gap  $g$ . Thus the magnetizing *MMF* varies with  $k$  whereas the load current varies with  $k^2$  so that the magnetizing current as a percentage of load current decreases with  $1/k$ . This helps explain why induction machines get better as they get larger. It also helps explain why permanent magnet motors becomes less desirable as the size of the machine becomes larger since the magnetizing current penalty which affects the no-load losses become relatively unimportant as the machine becomes large.

12) Stored Magnetic Energy. Since magnetizing current increases linearly with the dimension and the inductance also increases to the first power, the stored energy increases with  $k^3$ . The stored energy remains unchanged with a modification in the number of turns. This points to the problem involved with protection of large machines.

13) Power Factor. Neglecting the effect of leakage inductance, the power factor can be estimated from the ratio  $I_{load}/(\sqrt{I_{load}^2 + I_{mag}^2})$ . Since  $I_{load}$  varies as  $k^2$  and  $I_{mag}$  as  $k$  the power factor varies as

$$pf = \cos\left(\frac{k^2}{\sqrt{k^4 + k^2}}\right) = \cos\left(\frac{k}{\sqrt{1 + k^2}}\right)$$

which slowly increases as the size increases.

14) Time Constants. Since the resistance decreases and the inductance increases, the electrical time constants of the machine (transient, subtransient, etc.) will increase by a factor  $k^2$ . When the stator turns ratio is changed and the amount of copper is kept constant, the electrical time constant remains changed by the same factor,  $k^2$ . This fact has an important bearing on the transient behavior of a given machine and explains why a large machine is more difficult to control than a small machine.

15) Breakdown Torque. Since the voltage increases as  $k^2$  and the inductance as  $k$ , the breakdown torque increases as  $k^3$ . However, since power output increases nearly as  $k^4$ , this points to a reduction in the overload capability of the machine. This conclusion indicates that simple scaling will ultimately lead to an unsatisfactory design if  $k$  is too large. The problem remains the same if the stator turns are changed.

Control of leakage reactance is an important aspect of any type of machine design and in general means must be found to maintain the leakage inductance constant as the size of the machine increases. This is typically accomplished by increasing the number of slots in a manner roughly proportional to the air gap diameter.

16) Power Density. Since the volume increases by  $k^3$  and the power input increases by  $k^4$  the power density increases by  $k$ . This result indicates that large machines are more effective in utilizing the available magnetic material and explains the trend toward ever larger turbo-generators.

17) Temperature. Since the losses increase as  $k^3$  whereas the available surface area for cooling increases only as  $k^2$ , the temperature will increase by a factor  $k$ . Hence, a simple scale of all dimensions by  $k$  will not necessarily result in a satisfactory thermal design since the temperature limits of the machine may be exceeded. This result points to the need for improved cooling techniques as the rating of the machines increase.

Frequently design modifications involve changing only the length or the diameter of a previous design but not both. Table 6.12 shows how the same parameters previously discussed vary explicitly with length  $l$  and diameter  $D$  when  $N$  is held constant and when  $N$  is changed to keep the terminal voltage constant.

Table 6.12 Trend of motor quantities as a function of  $l$  and  $D$  with constant  $B$  and  $J$

Parameter	Symbol and/or Proportionality	Constant $B$ , $J$ and $N$	Constant $B$ , $J$ and $V$
Voltage	$V \propto N \cdot D \cdot l$	$l \cdot D$	1
Turns	$N$	1	$1/(l \cdot D)$
Current	$I \propto D^2/N$	$D^2$	$l \cdot D^3$

Table 6.12 Trend of motor quantities as a function of  $l$  and  $D$  with constant  $B$  and  $J$

Parameter	Symbol and/or Proportionality	Constant B, J and N	Constant B, J and V
Power	$V \cdot I$	$l \cdot D^3$	$l \cdot D^3$
Resistance	$R \propto N^2 \cdot l/D^2$	$l/D^2$	$1/(l \cdot D^4)$
Losses	$I^2 R$	$l \cdot D^2$	$l \cdot D^2$
Power Out	$V \cdot I - I^2 R$	$l \cdot D^3$	$l \cdot D^3$
Mag. Inductance	$L_m \propto N^2 \cdot A_m / l_{mpath}$	$l$	$1/(l \cdot D^2)$
Leak. Inductance	$L_l \propto N^2 \cdot A_l / l_{lpath}$	$l$	$1/(l \cdot D^2)$
Mag. Field Energy	$W_m \propto L \cdot I^2$	$l \cdot D^2$	$l \cdot D^2$
Mag. Current	$I_m \propto V/L_m$	$D$	$l \cdot D^2$
Elec. Time Constant	$\tau_e \propto L_m/R$	$D^2$	$D^2$
Breakdown Torque	$T_{pk} \propto V^2/L_l$	$l \cdot D^2$	$l \cdot D^2$
Power Density	$(VA)/(Vol)$	$D$	$D$
Temperature Rise	$\Theta \propto (I^2 R)/A_{surf}$	$D$	$D$
Power Factor	$I/I_m$	$D$	$D$

## 6.13 References

- [1] W.B. Essen, "Notes on the Design of Multipolar Dynamos," Journal IEE, vol. 20, no. 93, 1891, pp. 265-93.
- [2] M. Liwschitz-Garik and C.C. Whipple, "Electric Machinery, vol. 2 AC Machines", Van Nostrand Publishers, 1946.
- [3] W. Schuisky, "Induktionsmaschinen", Springer-Verlag, Vienna, 1957 (in German).

- [4] P. Pillay, "Applying Energy-Efficient Motors in the Petrochemical Industry", IEEE Industry Applications Magazine, vol. 3, No. 1, Jan/Feb 1997, pp. 32-40.
- [5] V.B. Honsinger, "Sizing Equations for Electrical Machinery", IEEE Trans. on Energy Conversion, vol. EC-2, No. 1, March 1987, pp. 116-121.
- [6] J.C. Hsu and A.U. Meyer, "Modern Control Principles and Applications", (book), McGraw-Hill Book Company, New York, 1968.
- [7] A.H. Bonnett, "Quality and Reliability of Energy-Efficient Motors", IEEE Industry Applications Magazine, January/February 1997, pp. 22-31.
- [8] D. Van Son, J.C. Kauffman, "Inverter-Fed Motors Improved with Transient Resistant Windings", Advanced Motor Drive News, Vol. 3, No. 3, Summer 1996, pp. 4-5.
- [9] H. De Jong, "AC Motor Design - Rotating Magnetic Fields in a Changing Environment", Hemisphere Publishing Co. 1989.
- [10] P.L. Alger, "Induction Machines - Their Behavior and Uses", Gordon and Breach Science Publishers, New York, 2nd Edition, 1965.
- [11] J.H Kuhlman, "Design of Electrical Apparatus", John Wiley and Sons, Inc., New York, 2nd Edition, 1940.
- [12] C. G. Veinott, "Theory and Design of Small Induction Motors", McGraw-Hill Book Co., Inc., New York, 1959.